ΠΑΝΕΠΙΣΤΗΜΙΟ ΚΡΗΤΗΣ
UNIVERSITY OF CRETE

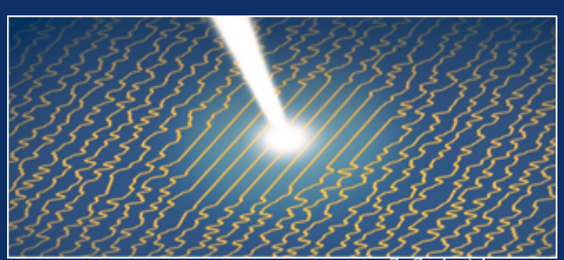

G. Goslovich

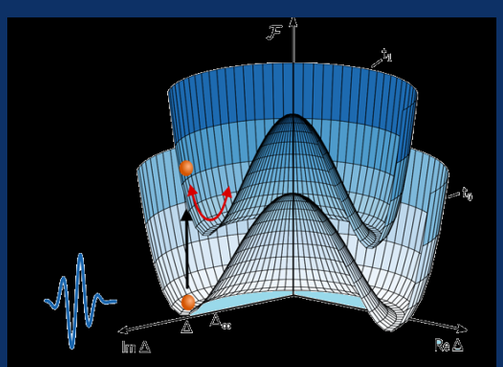

D. Manske

Abstract Proceedings

ULTRAFAST DYNAMICS & METASTABILITY

ULTRAFAST BANDGAP PHOTONICS

2023

X Symposium

COHERENT®

Professor Michael K.Rafailov

University of Alberta

Professor Ilias E Perakis

The Foundation Research & Technology – HELLAS
University of Alabama at Birmingham

Abstract Proceedings comprising summaries of research papers prepared for two closely related Conferences – Ultrafast Bandgap Photonics and Ultrafast Dynamics and Metastability of Transient States, forming the Symposium. The Symposium builds a bridge between cutting edge modern physics and emerging applications which are desperately in need. Symposium is vertically integrated, covering the area of interaction of high intensity and relatively low energy pulses with condensed matter, from fundamental physics to practically applicable energy sources, devices and technologies.

This workshop is the 10th in a series of International symposia, conferences and workshops on Ultrafast Dynamics and closely related and application technology driven Ultrafast Bandgap Photonics which we are running from 2016. University of Crete and Foundation for Research and Technology - FORTH are hosting the 10th Symposium on the island of Crete.

The Symposium is organized by sections that are focused either on research field or on phenomena. The division is pretty much conditional, while providing direct access to general topics of interest for the research community and applications as well. Phenomenology topics, like ultrafast dynamic in hterostructures and spin-and orbital ultrafast phenomena may overlap areas of studies like photoinduced high temperature superconductivity and ultrafast magnetism, creating multiple entries into the Proceedings General reviews of Ultrafast Dynamics and Ultrafast Bandgap Photnics progresss are provided in 7 Plenary papers, while the most interesting recent discoveries are presented here as the keynote papers. Each section begins with the plenary and keynote papers, where results and considerations of most common interests are presented, while the Astract Proceedings is compiled based alphaetic list of the speakers in Program -as it was presented at the Symposium. Plus to Table of Contents the Abstract Prosceeding has list of authors where the authors of submitted papers are listed with their papers associated page numbers.

The Abstract Proceeding is actually a snapshot of most interesting and noticeable research results in Ultrafast Transient Phenomena and Ultrafast Bandgap Photonics which one can get in 2023. a snapshot of up to date research results and progress in Ultrafast Dynamics and Metastability and the applications in Ultrafast Bandgap Photonics. It is an Encyclopedia of Ultrafast Dynamics, Metastability and Ultrafast Bandgap Photonics that presents the status quo in the disciplines ranging from Theoretical Physics to Ultrafast Laser and covering practically all phenomena of interests in interaction of ultrashort high intensity-low energy interaction with condensed matter .

In Loving Memory of Elena

Contents

Observation of Pines' demon in Sr_2RuO_4

A. A. Husain[1], E. W. Huang[2], M. Mitrano[3], M. S. Rak[1],S. I. Rubeck[1,] X. Guo[1,] H. Yang[4], C. Sow[5]
Y. Maeno[5], B. Uchoa[6], T.C. Chiang[1], P.E. Batson[7], P. W. Phillips[2], P. Abbamonte[1]
[1] *University of Illinois, Urbana, IL, 61801, USA*
[2] *Institute for Condensed Matter Theory, Urbana, IL, 61801, USA*
[3] *Harvard University, Cambridge, MA, 02138, USA*
[4]*Rutgers University, Piscataway, New Jersey, 08854, USA*
[5]*Kyoto University, 606-8502 Kyoto, Japan*
[6] *University of Oklahoma, Norman, OK, 73019, USA*
[7] *Rutgers University, Piscataway, NJ, 08854, USA*

The characteristic excitation of a metal is its plasmon, which is a quantized collective oscillation of its electron density. In 1956, David Pines predicted that a distinct type of plasmon, dubbed a "demon," could exist in three-dimensional metals containing more than one species of charge carrier [1]. Consisting of out-of-phase movement of electrons in different bands, demons are acoustic, electrically neutral, and do not couple to light, so have never been detected in an equilibrium, three-dimensional metal. Nevertheless, demons are believed to be critical for diverse phenomena including phase transitions in mixed-valence semimetals [2], optical properties of metal nanoparticles[3] , soundarons in Weyl semimetals[4], and high temperature superconductivity in, for example, metal hydrides[3,5,6,7]. Here, we present evidence for a demon in Sr_2RuO_4 from momentum-resolved electron energy-loss spectroscopy (M-EELS). Formed of electrons in the β and γ bands, the demon is gapless with critical momentum q_c = 0.08 reciprocal lattice units and room temperature velocity v = (1.065 ± 0.12) × 10^5 m/s, which undergoes a 14% renormalization upon cooling to 20 K due to coupling to the particle-hole continuum. The momentum dependence of the intensity of the demon confirms its neutral character.

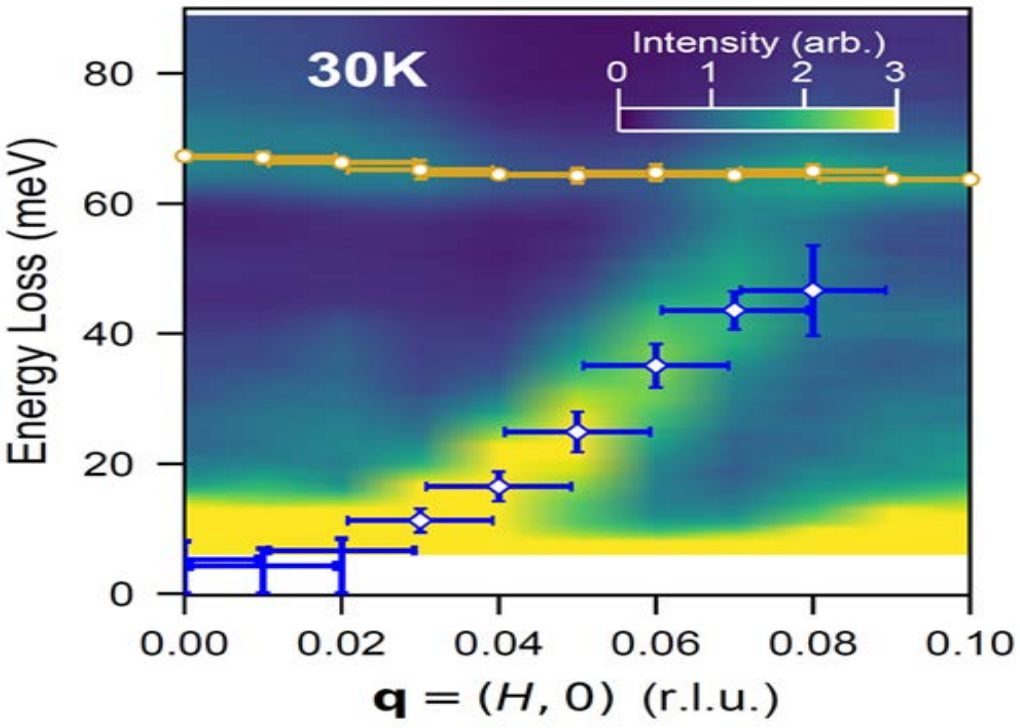

Fig. 1: *Dispersion curve of the demon in Sr_2RuO_4 observed with omentum-resolved* ***EELS.***

Our study confirms a 66-year old prediction and suggests that demons may be a pervasive feature of multiband metals[8].

References

[1] D. Pines, *Canadian Journal Physics* **34**, 1379 (1956).
[2] C. M. Varma, *Review of Modern Physics* **48**, 219 (1976).
[3] R. Akashi, R. Arita, *Journal of Physical Society of Japan* **83**, 061016 (2014).
[4] A. N. Afanasiev, A.A. Greshnov, D. Svintsov, *Physical Review B* **103**, 205201 (2021).
[5] J. Ihm, M.L Cohen, S.F. Tuan, *Physical Review B* **23**, 3258 (1981).
[6] J. Ruvalds, *Advances in Physics* **30**, 677 (1981).
[7] E.A. Pashitskii, V.I. Pentegov, A.V. Semenov, *Low Temperature Physics* **48**, 26 (2022).
[8] A. A. Husain, E. W. Huang, M. Mitrano, M. S. Rak, S. I. Rubeck, X. Guo, H. Yang, C. Sow, Y. Maeno, B. Uchoa, T. C. Chiang, P. E. Batson P. W. Phillips, P. Abbamonte, arxiv:2007.06670.

Conductivity dynamics in THz driven spin-ladders

J. Dössegger[1], T. Suter[1], L. Lanini[1], M. Glantschnig[1], P. Puphal[2], E. Pomjakushina[3], S. L. Johnson[1]
E. Abreu[1]
[1]*ETH Zürich, 8093 Zürich, Switzerland*
[2]*Max-Planck Institute for Solid State Research, 70569 Stuttgart, Germany*
[3]*Paul Scherrer Institut, 5232 Villigen, Switzerland*

The nature of the superconducting state in unconventional superconductors, in particular high temperature superconducting cuprates, remains to be fully understood. The fundamental building blocks in cuprates are two-dimensional CuO_2 layers. One approach to simplifying the problem consists in lowering the dimensionality of the system. $Sr_{14-x}Ca_xCu_{24}O_{41}$ (SCCO) compounds have a quasi-one-dimensional structure characterized by alternating layers of Cu_2O_3 ladders and CuO_2 chains. These spin-ladder systems exhibit a rich phase diagram, where conductivity, charge order and magnetic order can be controlled by varying temperature, external pressure and the level of Sr substitution by Ca, x. In particular, a superconducting phase arises for temperatures below 15 K, an applied pressure of 3-10 GPa and x > 11.5. The conductivity in these inherently hole doped materials, and in particular the superconducting phase, is believed to be controlled by the distribution of holes between the chains and the ladders. [1]

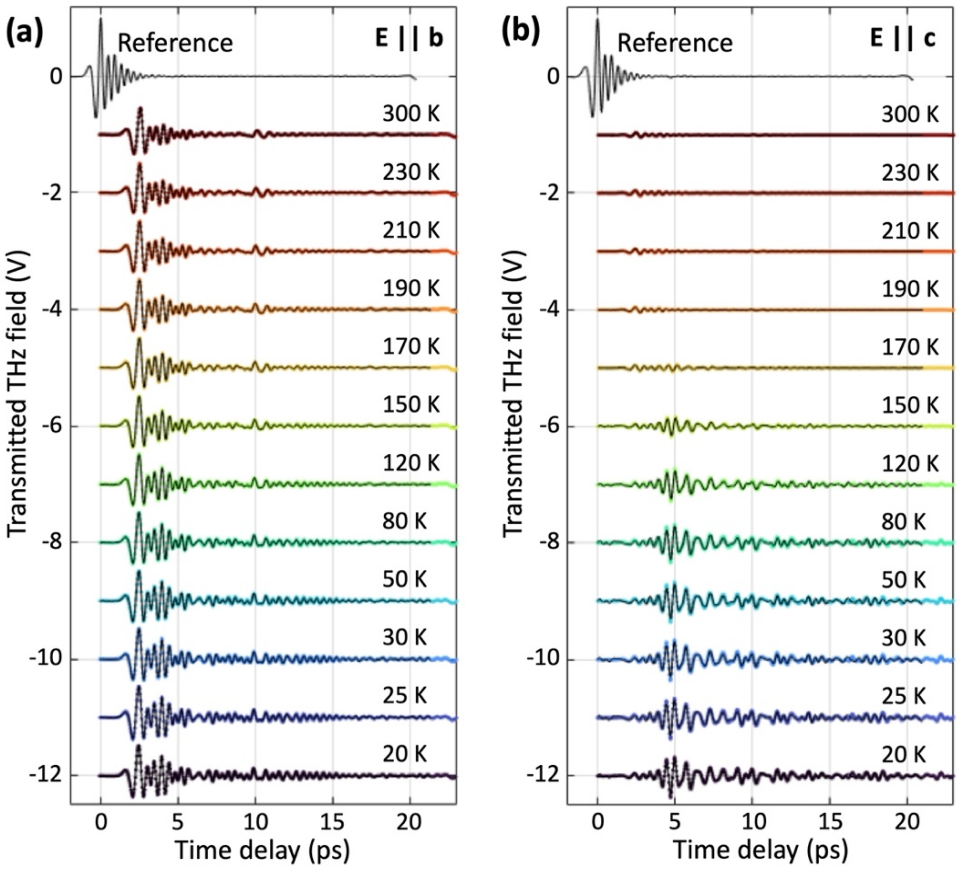

Fig. 1. *Temperature dependence of the THz transmission through an a-cut sample of $Sr_{14}Cu_{24}O_{41}$ (x = 0), with the THz electric field E aligned along* ***(a)*** *the b-axis and* ***(b)*** *the c-axis of the material.*

We investigate the low frequency response of bulk single crystal SCCO samples with Ca contents x = 0, 7 and 12. I will first present our characterization of the temperature and doping dependent anisotropic conductivity response, obtained using THz time domain spectroscopy in the 0.3-2.7 THz range. [2] I will then discuss the ultrafast nonlinear conductivity transient that arises following excitation by a strong THz field pulse, and how this behavior depends on the intensity and polarization of the pump and on the temperature and doping level of the sample. [2]

References

[1] T. Vuletić, B. Korin-Hamzić, T. Ivek, S. Tomić, B. Gorshunov, M. Dressel, J. Akimitsu, *Physics Reports* **42**, 169 (2006).
[2] J. Dössegger, T. Suter, L. Lanini, M. Glantschnig, P. Puphal, E. Pomjakushina, S. L. Johnson, E. Abreu, *(to be submitted)* (2023).
* Acknowledgement(s): JD and EA acknowledge support from the Swiss National Science Foundation through Ambizione Grant PZ00P2_179691.

Ultrafast dynamics of charge carriers in energy and momentum space. Ultrafast control of spin-dependent energy level alignment of molecular/WSe_2 heterostructures

M. Aeschlimann
University of Kaiserslautern-Landau, 67663 Kaiserslautern, Germany

One of the great challenges in information technology is the development of novel concepts to control charge and spin carriers in active functional units at ever shorter lengths and faster timescales. The easiest way to realize such nanoscale devices is to use intrinsic two-dimensional (2D) materials such as transition metal dichalcogenides (TMDCs) and to design their spin-dependent band structure by chemical functionalization or optical engineering. For TMDCs, this is mainly achieved by forming 2D heterostructures with either other TMDCs or 2D honeycomb materials. While this approach has been successfully used to tune the interfacial properties of 2D heterostructures, it still shows limitations in the tunability of the interfacial energy level alignment as well as in the lateral dimensions of the heterostructures. In this contribution, we present an alternative way to functionalize the properties of TMDCs by adsorption of molecular materials. As an exemplary case, we focus on a heterostructure consisting of the TMDC bulk crystal WSe_2 and the prototypical molecule C_{60}. Both were chosen because of their interesting optical and spin-dependent electronic properties. On the one hand, the valence band structure of WSe_2 shows an overall vanishing spin polarization in spite of the layer- and valley-dependent spin polarization of the individual tri-layers (see Fig. 1a). On the other hand, the excited state dynamics of C_{60} and other fullerenes is dominated by charge transfer excitons (as shown in the sketch in Fig. 1b), which can transiently manipulate the energy level alignment of the surrounding material [1,2].

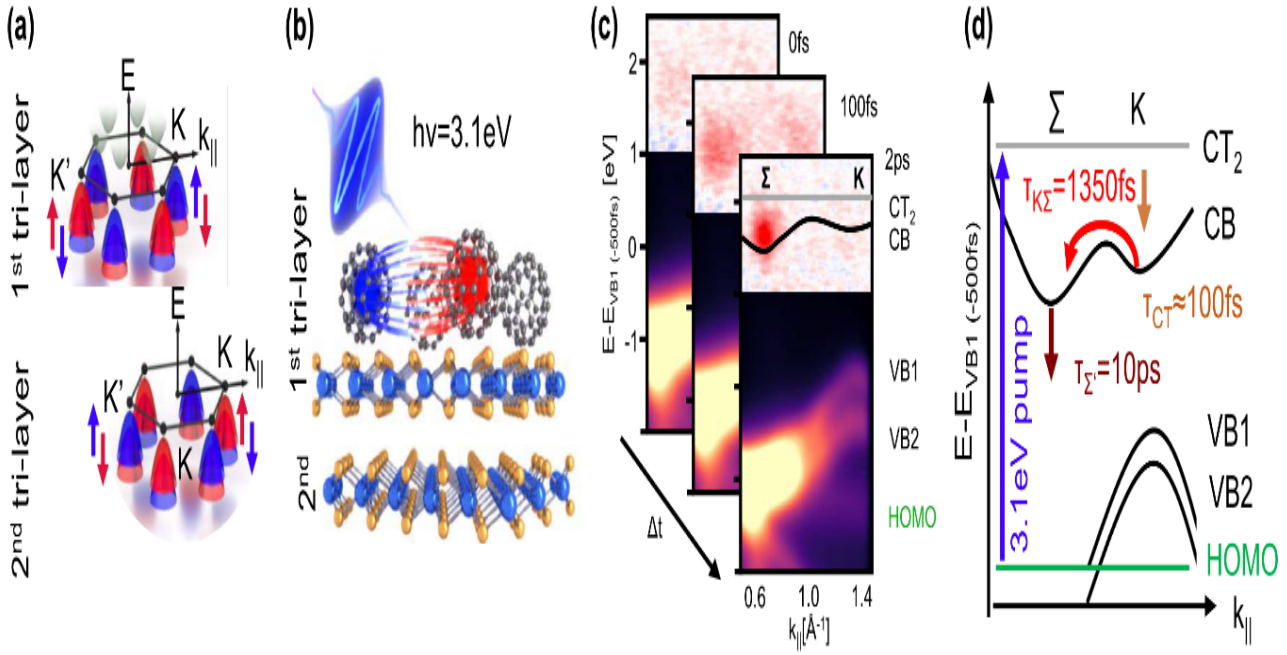

Fig.1 (a) *Sketch of the layer- and valley-dependent local valence band structure of the first two WSe_2 tri-layers. Bands with opposite spin character are marked in red and blue.* ***(b)*** *Illustration of the investigated C_{60}/WSe_2 heterostructure and of the resonant optical exaction of the C_{60} layer.* ***(c)*** *Exemplary energy vs. momentum cuts of the tr-ARPES data set along the* ***K-Σ-*** *high symmetry direction. The photoemission yield of the excited states is illustrated as difference map with intensity accumulation in red and depletion in blue. Energy level alignment, optical excitation scheme and scattering processes of the ultrafast dynamics of the C_{60}/WSe_2 heterostructure.*

The studied material system of a single C_{60} layer on a 2H-WSe_2 bulk crystal is shown in Fig. 1b. For a resonant optical excitation of the C_{60} layer with 3.1eV photons, we uncovered the existence of a highly efficient interfacial charge transfer process that can transiently lift the spin degeneracy of the bulk WSe_2 band structure near the interface. Our conclusions are based on spin-, time-, and momentum-resolved fs-XUV photoemission spectroscopy experiments performed along the Σ-K high symmetry direction of the WSe_2 crystal. This particular high symmetry direction reveals the characteristic hole-like valence bands (VB) and electron-like conduction bands (CB) of WSe_2, as

well as the non-dispersive highest occupied molecular orbital (HOMO) and excitonic states of C_{60}. An exemplary time and momentum resolved photoemission (tr-ARPES) data set is shown in Fig. 1c, the corresponding energy level alignment in Fig. 1d. We will show that optical excitation of the C_{60}/WSe_2 heterostructure with 3.1eV photons leads to a resonant optical transition from the C_{60} HOMO into the manifold of excitonic C_{60} states and to the formation of charge transfer excitons (CT_2). These CT_2 excitons decay within 100fs leading to electron transfer into the K-valley of the first WSe_2 tri-layer. This interlayer scattering is followed by interlayer scattering from the K to the Σ valley of the WSe_2 CB. These scattering processes together with the extracted scattering times are summarized in Fig. 1d. For example, we will provide evidence for a significant increase of the interval scattering time between the K- and the Σ-valley upon adsorption of C_{60} [3] and demonstrate a depopulation time of the Σ-valley of about 10ps.The most important observation, however, is the absence of any interlayer hole transfer between the C_{60} layer and the WSe_2 bulk crystal. This allow us to confirm that only electrons are transferred across the interface. This electron transfer leads to a transient charging of the C_{60} (positive charges) and the first WSe_2 layer (negative charges) as illustrated in the sketch in Fig. 2a. This charge distribution results in an interfacial dipole at the C_{60} and WSe_2 interface and causes the transient shifts with different signs of the C_{60} and WSe_2 valence states observed in our tr-ARPES experiments, see Fig. 2b.

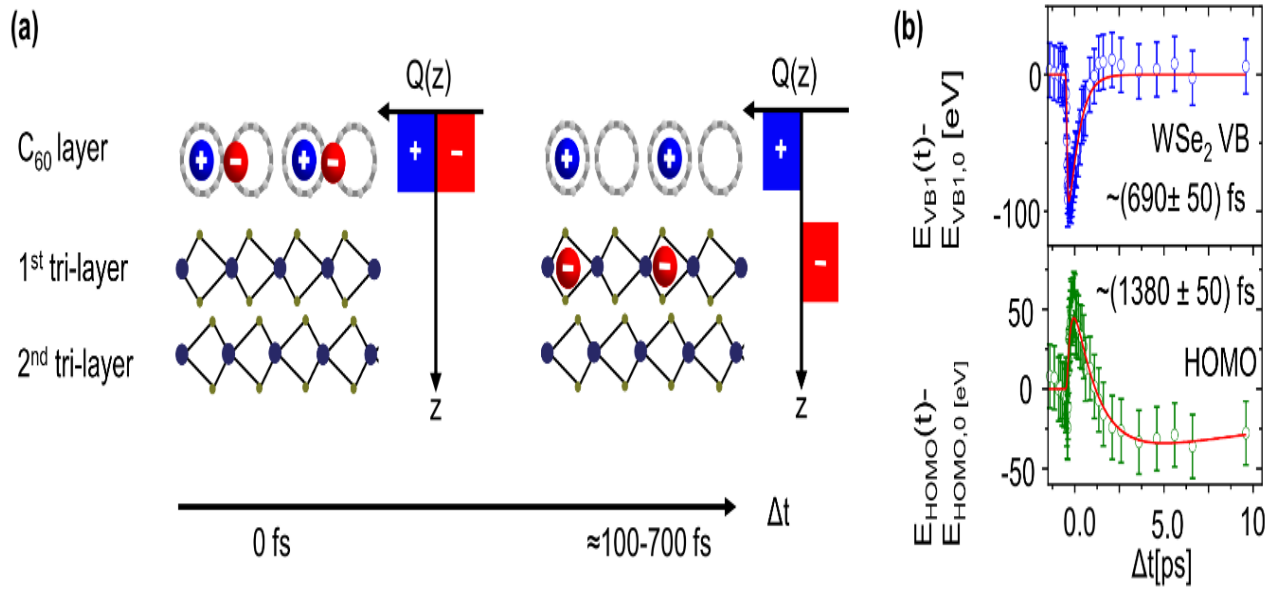

Fig.2. ***(a)*** *Sketch of the charge transfer process across the C_{60}/WSe_2 interface and the resulting charge distributions for two characteristic time steps.* ***(b)*** *Transient energy shifts of the C_{60} (HOMO) and WSe_2 valence band structure after optical excitation with 3.1eV photons.*

Finally, we will turn to our spin-, time-, and momentum-resolved photoemission spectra that were recorded at the K-point of the WSe_2 valence band structure for characteristic time delays after the optical excitation. These spectra contain characteristic signatures of the spin polarization of the WSe_2 valence bands that can be unambiguously attributed to the first and second WSe_2 tri-layer. In this contribution, we discuss the spectral line shape of our spin-resolved tr-ARPES data in details and demonstrate different energy shifts for the valence band of the first and second WSe_2 tri-layer. The layer dependent magnitude of these valence band shifts can be attributed to the strength of the interfacial dipole field, which decreases towards the bulk of the WSe_2 crystal. In conclusion, our study of C_{60}/WSe_2 heterostructures has revealed an ultrafast charge separation at the C_{60}/WSe_2 interface. This results in an interfacial dipole responsible for a layer-dependent (Stark-like) shift of the spin-polarized WSe_2 valence band structure. This layer-dependent shift transiently lifts the spin-degeneracy of the WSe_2 crystal valence band structure. Thus, our results provide a clear pathway to manipulate the spin functionalities of a molecular/TMDC heterostructure by optical excitation on the ultrafast timescale.

References

[1] B. Stadtmüller, S. Emmerich, D. Jungkenn, N. Haag, M. Rollinger, S. Eich, M. Maniraj, M. Aeschlimann, M. Cinchetti, S. Mathias, *Naure Communications* **10**, 1470 (2019).

[2] S. Emmerich, S. Hedwig, M. Cinchetti, B. Stadtmüller, M. Aeschlimann, *Journal of . Electron Spectroscopy and Related Phenomena* **252**, 147110 (2021).

[3] R. Bertoni, C. W. Nicholson, L. Waldecker, H. Hübener, C. Monney, U. De Giovannini, M. Puppin, M. Hoesch, E. Springate, R. T. Chapman C. Cacho, M. Wolf, A. Rubio, R. Ernstorfer, *Phyics Reiew Letters* **117**, 277201 (2016).

Hybrid phonons in the structures with van der Waals nanolayers

W. Yan[1], V. E. Gusev[2], D. D. Yaremkevich[3] T. L. Linnik[3], S. M. Kukhtaruk[3]
A. Patanè[1], A. J. Kent[1]A. Nadzeyka[4], M. Bayer[5], A. V. Scherbakov[5]
A. V. Akimov[1]
[1]*University of Nottingham, Nottingham NG7 2RD, UK*
[2]*Le Mans Université, 72085 Le Mans, France*
[3]*V.E. Lashkaryov Institute of Semiconductor Physics, 02000 Kyiv, Ukraine.*
[4]*Raith GmbH, 44263 Dortmund, Germany*
[5] *Technische Universität Dortmund, 44227 Dortmund, Germany.*

Two-dimensional van der Waals crystals (2D-vdW) consist of chemically bonded atomic layers held together by weak vdW forces. They provide the perfect atomic-size "Lego-type" toy models for the exploration of new classical and quantum phenomena in solid state physics. Their versatile homo- and heterostructures created by stacking, twisting, stretching and bending of vdW layers provide means of manipulating optical, electrical, magnetic, piezoelectric and spin properties. Coherent THz and sub-THz phonons, which carry dynamical strain, could become an instrument to control classical and quantum phenomena in the unexplored picosecond temporal and nanometer spatial regimes.Coherent phonons in vdW nanolayers fabricated from different materials and heterostructures are intensively studied during the last decade (for a review see Ref.[1]). The experiments use the picosecond ultrasonics pump-probe technique which allows measurement of the vibrations of nanolayers with sub-picosecond resolution. In the present talk we describe a series of experiments where different phonon modes are studied in various vdW nanolayers [2-4]. Special attention is paid to the role of elastic interaction with the substrate and between the vdW layers of different materials. The frequencies of breathing phonon modes are strongly dependent on the nanolayer/substrate coupling, which allows us to estimate the stiffness of the contact with the substrate [2]. Figure 1 demonstrates this method for obtaining the image of the elastic contact between InSe layer and sapphire substrate [3].

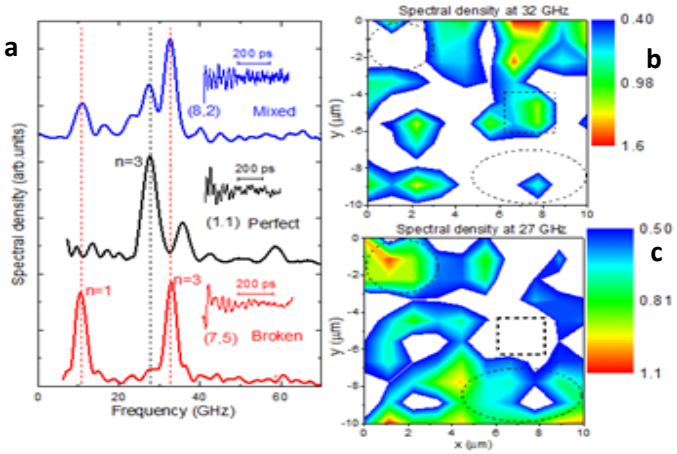

Fig.1. *Images of elastic contact InSe nanolayer/ sapphire substrate [3].*
a. *Temporal evolutions* ***(insets)*** *and their fast Fourier transforms measured at three different positions on an InSe/InSe homojunction on a sapphire substrate. Position coordinates inside brackets are in microns. The lowest* ***red*** *spectrum corresponds to a broken interface; the* ***black*** *middle spectrum corresponds to a perfect interface; the top* ***blue*** *spectrum corresponds to a position where both broken and perfect interfaces coexist.*
b-c. *Spectral density images at frequencies of 32 GHz and 27 GHz corresponding to the phonon resonances for broken* ***(b)*** *and perfect* ***(c)*** *interfaces. The areas marked by dashed squares and ovals indicate homogeneous regions of broken and perfect interfaces, respectively.*

In another experiment, we study in-plane coherent phonon modes in MoS_2 nanolayers transferred on a nanograting - Fig. 2 [4].

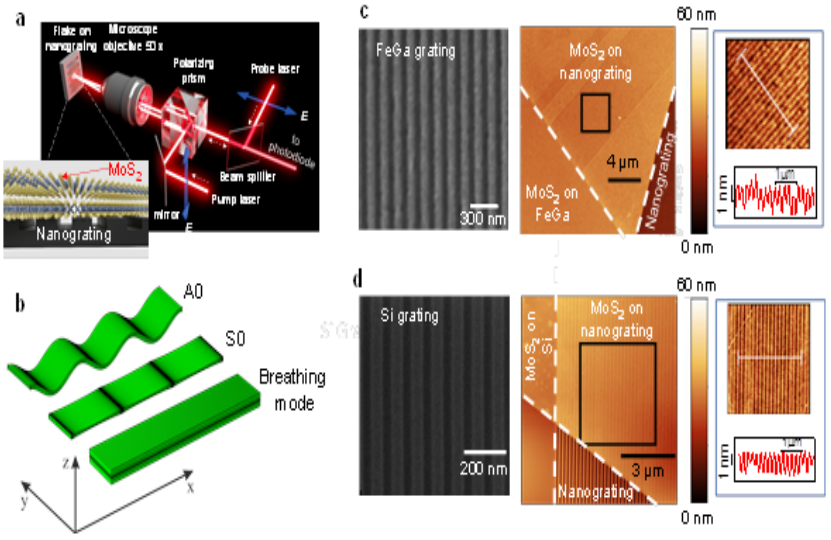

Fig. 2. *Picosecond acoustics of van der Waals layers on nanogratings [4]*
a, *Schematic illustration of the pump-probe setup and the MoS_2 layer on the grating.*
b, *Fundamental antisymmetric (**A0, top**), symmetric (**S0, middle**) and breathing modes (bottom) of the free standing layer.*
c, *Scanning electron microscopy (SEM) image of the FeGa grating with 150 nm period (**left**), AFM image of a 200 nm period nanograting with a 13 nm thick MoS_2 (**middle**). A zoomed image of the area enclosed by the black square is shown to the right, and the height profile of the layer on the grating along a white line is shown below.* ***d,*** *The same as in **c** but for the Si grating: SEM (period 100 nm); AFM (layer thickness 8.3 nm on grating with period 200 nm).*

We can generate and detect coherent phonons propagating with the LA sound velocity with frequency up to 40 GHz and hybrid flexural phonons with frequencies up to 10 GHz (Fig. 3 and 4).

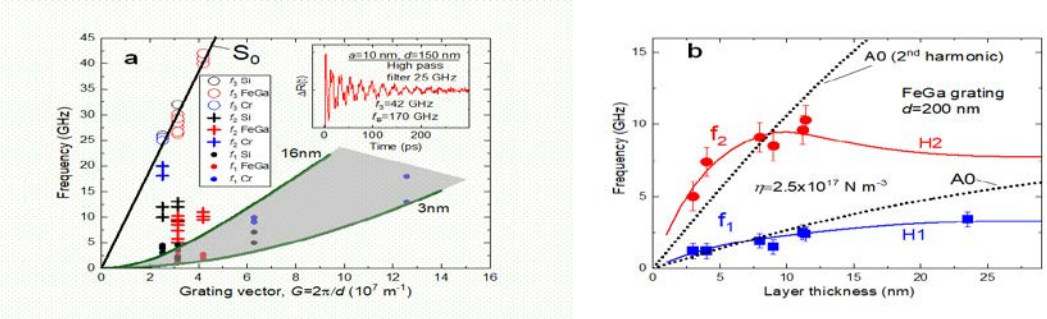

Fig. 3. *Phonon modes in hybrid nanostructures [4].* ***a.*** *The measured frequencies of phonon modes as a function of grating vector for various hybrid nanostructures (**symbols**). The correspondence of different symbols to the frequency group (f_1, f_2 and f_3) and grating material (FeGa, Si, and Cr) are shown in the inset table. The solid lines are the calculated dispersion curves for S0 (black straight line) and A0 modes (**green curved lines**) for the free standing MoS_2 layers. The shaded area includes phonon modes calculated for A0 modes in the layers with thethicknesses between 3 and 16 nm. The inset shows the temporal evolution of the measured $\Delta R(t)$ after high pass filtering which emphasizes the detection of high frequency S0 and breathing modes.* ***b.*** *The dependence of frequencies f_1 and f_2 on the vdW layer thickness measured in FeGa grating with a period d = 200 nm (**symbols**) and the corresponding theoretical dependences H1 and H2 (**lines**) calculated by Comsol Multiphysics software. The dotted lines are the calculated thickness dependences for A0 modes with $q_x = G$ and $q_x = 2G$ in a free-standing layer.*

The latter arise from the periodic modulation of the elastic coupling of the vdW layer at the grooves and ridges of the nanograting. The simulation of hybrid phonons is demonstrated in Fig. 4. This creates a new type of a tailorable 2D periodic phononic nanoobject, a *flexural phononic crystal*, offering exciting prospects for the ultrafast manipulation of states in 2D materials.

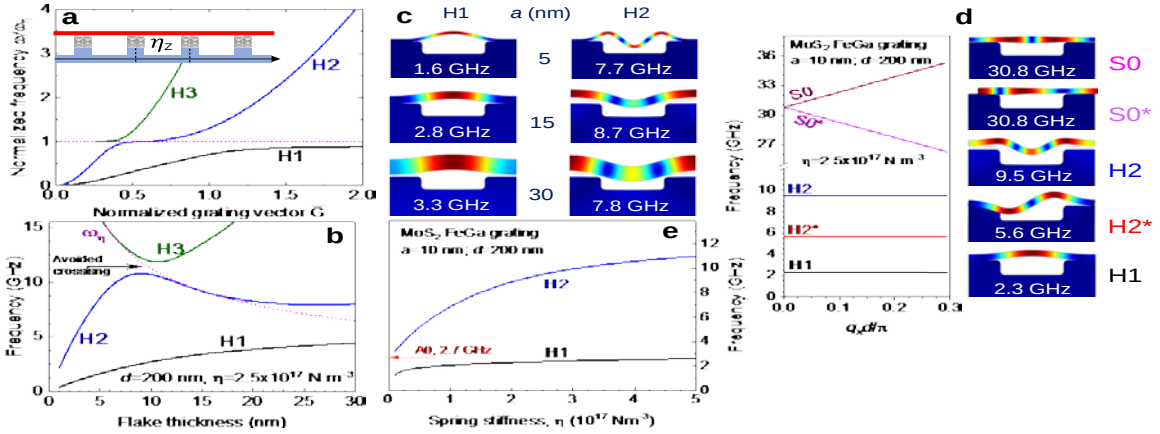

Fig. 4. *Theory of phonon mode hybridization [4]* ***a.*** *The dependence of normalized frequencies of the experimentally relevant hybrid eigen modes on the normalized grating vector $\bar{G}$ in the hybrid nanostructure. Inset: the scheme of the spring model.* ***b.*** *Calculated dependence of the mode frequencies on the layer thickness. The avoided crossing of modes H2 and H3 is highlighted by an arrow. The dotted line corresponds to the mass-on-spring type oscillation.* ***c.*** *The layer motion for H1 and H2 hybrid modes displayed for three layer thicknesses.* ***d.*** *The dispersion curves and layer motion for the phononic crystal showing even (S0, H1 and H2) and odd (S0* and H2*) phonon modes near the centre of the Brillouin zone.* ***e****, The dependences of the frequencies for H1 and H2 modes on the spring stiffness. The arrow indicates the frequency of A0 resonance for free-standing MoS_2 layer.* ***a*** *and* ***b*** *are the results of analytical calculations for infinitively rigid grating and $q_x a << 1$; other panels are numerical calculations performed by COMSOL Multiphysics for FeGa grating with d=200 nm.*

The experiments with coherent phonons in vdW nanolayers pave a way to control strain--induced processes in 2D-vdW materials on a picosecond time scale. Based on static and low frequency strain-induced effects, high frequency phonons could be used in a similar way as done in epitaxial nanostructures to manipulate light emission[5], conductivity[6] magnetization[7] and plasmons [8].

References

[1] F. Vialla, N. Del Fatti, *Nanomaterials* **10**, 2543 (2020).
[2] J. Greener,A.Akimov,V.Gusev,Z.Kudrynskyi,P.Beton,Z.Kovalyuk,T.Tanigichi,K.Watanabe,A.Kent,A.Patane,*Physical Review* B**98**,075408 (2018)
[3] J..G.Greener,E.De Lima Savi,A.Akimov,S.Raetz, S.Kudrynskyi, S.Kovalyuk, N.Chigarev, A.Kent, A.Patane,V.Gusev, *ACS Nano* **13**,11530 (2019).
[4] W. Yan, A.Akimov, M.Barro-Burilla, M. Bayer, J. Bradford, V. Gusev, L. Hueso, A Kent, S. Kuktaruk, A.Nadzeika, *Nano Letters* **22**, 6509 (2022).
[5] A. V. Akimov, A. V. Scherbakov, D. R. Yakovlev, M. Bayer, *Ultrasonics* **56**, 122 (2015).
[6] A. V. Akimov, C. L. Poyser, A. J. Kent, *Semiconductor Science and Technology* **32**, 1 (2017).
[7] J. Jager. A.Scherbakov, B. Glavin, A.Salasyuk, R.Campion, A.Rushforth, D.Yakovlev, A.Akimov, M. Bayer,*Physical Review B* **92**, 020404 (2015).
[8] V. V. Temnov, *Nature Photonics* **6**, 728 (2012).

Observation of giant nonlinearities and photon bound-states using a single artificial atom

N. O. Antoniadis[1], N. Tomm[1], S. Mahmoodian[2], M. Janovitch[1], M. Brunelli[1], R. Schott[3], S. R. Valentin[3], A. D. Wieck[3], A. Ludwig[3], P. P. Potts[1], A. Javadi[1], R. J. Warburton[1]
[1]*University of Basel, 4056 Basel, Switzerland*
[2]*The University of Sydney, AU-2006 Camperdown, Australia*
[3]*Ruhr-Universität Bochum, DE-44780 Bochum, Germany*

A coherent and efficient light-matter interface at the level of single emitters and single photons is the main requirement for photonic quantum gates. The β-factor determines the efficiency of the light-matter interface. Here, we use a semiconductor quantum dot in an open microcavity (Fig. 1a) to realise a one-dimensional atom [1]. We achieve an extinction of 99.2% in the transmission at low input power. This demonstrates that the β-factor is high, in this case 92%. The transmission dip depends strongly on the input laser power and in fact vanishes at "high" powers (Fig. 1b). This nonlinearity is provided by the atom and means that the light-matter interaction depends strongly on the number of photons interacting with the two-level system within its emission lifetime. The tunable nature of the microcavity allows the β-factor to be tuned, which enables control over the photon statistics from strong bunching (g(2)(0)=587) to anti-bunching [2]. In the nonlinear regime, photon bound states can arise, strongly correlated quasi-particles of the system. We probe the bound states in a direct way by using pulsed excitation (pulse width comparable to the radiative decay time). We observe a photon-number-dependent time delay in the scattering from the quantum dot-cavity system. By scattering a weak coherent pulse and measuring the time-dependent output power and correlation functions, we show that single photon, two- and three-photon components incur different time delays of 144.02 ps, 66.45 ps and 45.51 ps respectively (Fig.1c) [3].

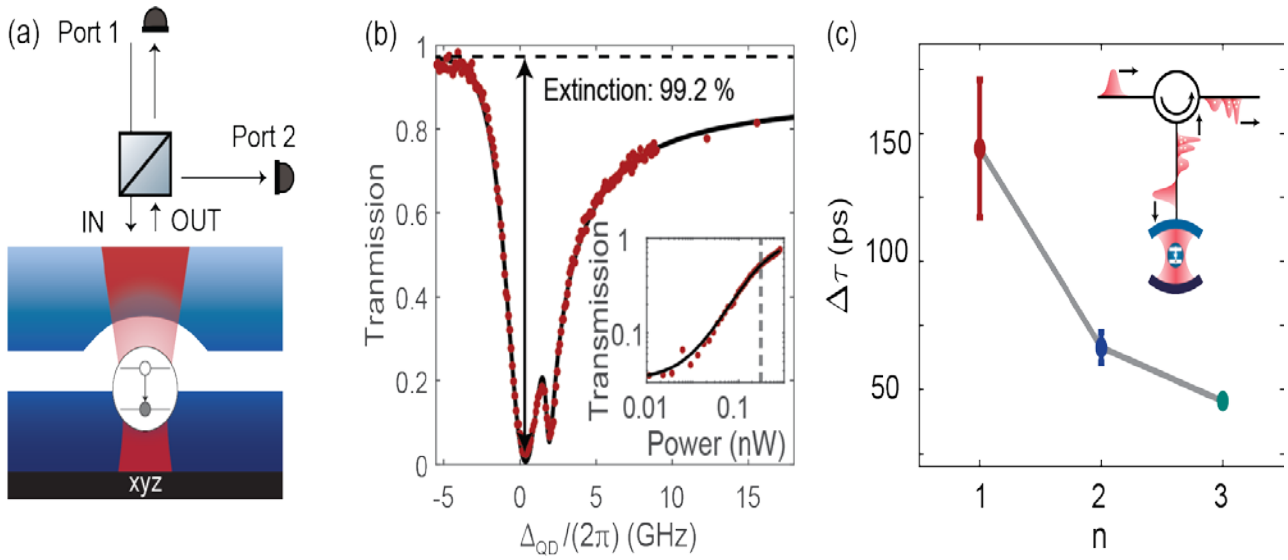

Fig. 1. (a) *Schematic of the open microcavity. A quantum dot is embedded in the bottom mirror. We can either measure the transmission (port 1 to port 2) or the back-reflection (port 1 to port 1).* ***(b)*** *Transmission through the system as a function of quantum dot detuning. We observe an extinction as high as 99.2 %.* ***(c)*** *Delay of scattered single-, two- and three-photon components for back-reflected light.*

The reduced time delay of the two-photon component with respect to the one-photon component is a fingerprint of the celebrated example of stimulated emission, where the arrival of two photons within the lifetime of an emitter causes one photon to stimulate the emission of the other. Furthermore, at the optimal pulse width we show that the two-photon scattering results in the efficient creation of two-photon bound states with a temporal wave function that matches theoretical predictions very precisely.

References

[1] N. Tomm, A. Javadi, N. O. Antoniadis, D. Najer, M. C. Löbl, A. R. Korsch, R. Schott, A. D. Wieck, A. Ludwig, R. J. Warburton, *Nature Nanotechnology* **16**, 399 (2021).
[2] N. O. Antoniadis, N. Tomm. T. Jakubczyk. R. Schott. A. D. Wieck. A. Ludwig.R. J. Warburton. A. Javadi. *npj Quantum Information* **8**, 27 (2022).
[3] N. Tomm, S. Mahmoodian, N. O. Antoniadis, R. Schott, A. D. Wieck, A. Ludwig, A. Javadi, R. J. Warburton, *Naure. Physics (in print)* (2023).

Spin-Photon Quantum Interfaces and their Applications

M. Atatüre
University of Cambridge, Cambridge CB3 0HE, UK

Optically active spins in solids are often considered prime candidates for scalable and feasible quantum-optical devices. They are formed by a confined spin in a solid-state matrix coupled to optical transitions using higher-lying orbital states. These transitions typically have energies significantly smaller than the bandgap energy, so the host material acts as a natural trap for holding a quantum object isolated. This sets a great advantage over the atomic counterparts of such light-matter interfaces requiring complex trapping and isolation infrastructure. This advantage can thus be leveraged towards miniaturization, on-chip integration, and scalability using a plethora of material host platforms. Choice of host material will also be influenced by the intended applications straddling the broad areas from quantum networks and communication to the development of quantum sensors. There are numerous forerunning material platforms including diamond, semiconductors, and atomically thin 2d materials today [Fig. 1]. Each promising material platform brings its own advantages along with their challenges. Semiconductors are arguably the most investigated candidate material and offer great in-depth knowledge on how to design, fabricate and scale quantum-enabled devices. Layered materials offer immense opportunities in integration and feasible heterostructure device design, yet material quality has been an apparent limitation until today. Diamond comes across as a material platform that can deliver acceptable performance both as a host for spin-photon quantum interfaces and a material suitable for heterogeneous on-chip integration. The substantially weaker spin noise due to the only 1.1% nuclear-spin-active carbon isotope is a great advantage for the confined spins in color centers, while the large bandgap energy and the high stiffness of the material renders the optical properties equally attractive.

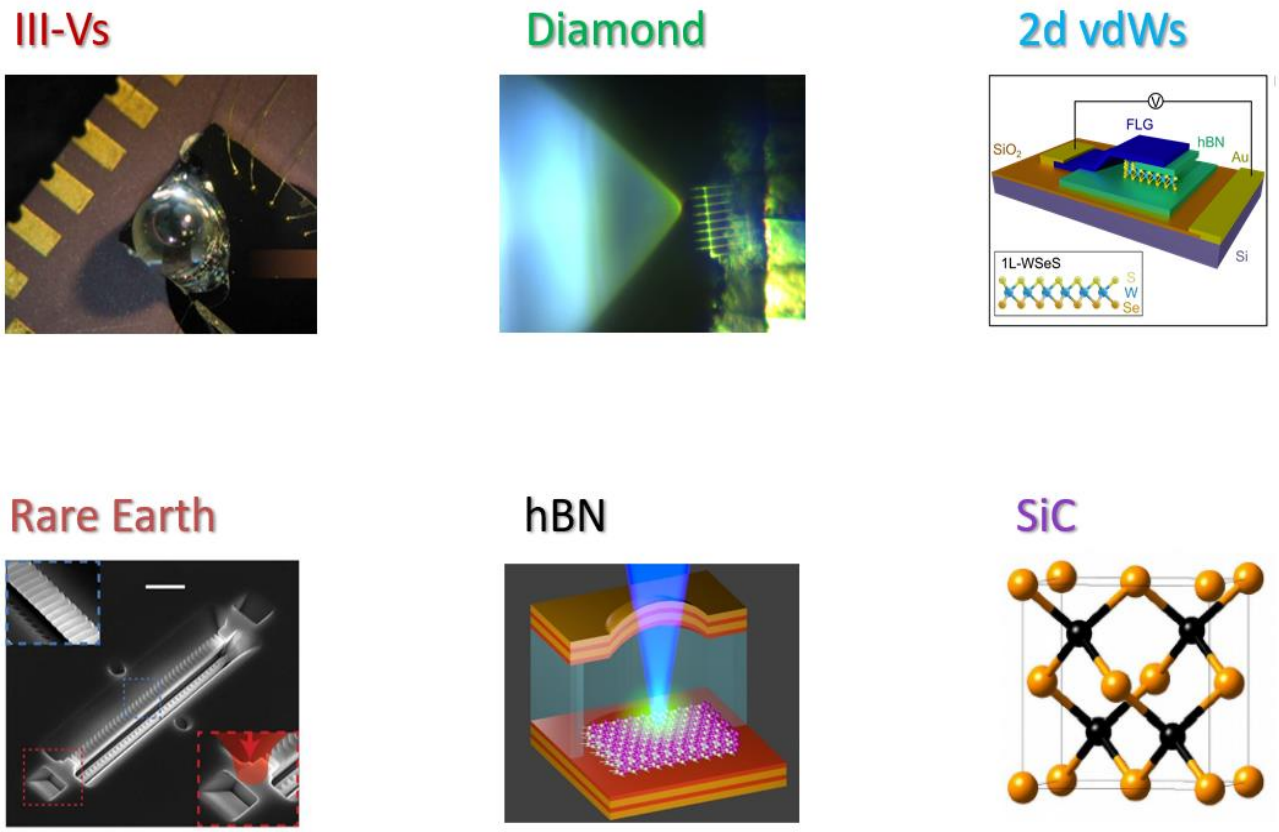

Fig. 1. *Forerunning material systems that can host quantum devices linking single spins and single photons.*

While none of the forerunning material platforms is a clear winner in this pursuit of scalable quantum technologies [1], diamond makes the most appearance across different applications. It is thus worth investigating diamond colour centres in detail as a platform with a strong focus on the family of group-IV color centres for quantum networks and nitrogen-vacancy centers for sensing.

References

[1] M. Atature, D. Englund, N. Vamivakas, S.-Y. Lee, J. Wrachtrup, *Nature Reviews Materials* **3**, 38 (2018).

Entangled photon factories and multinuclear gates for quantum networks and computing

E. Barnes
Virginia Tech, Blacksburg, VA 24061, USA

Multi-photon entangled graph states are a fundamental resource in quantum communication networks, distributed quantum computing, and sensing. These states can in principle be created deterministically from quantum emitters such as optically active quantum dots or defects, atomic systems, or superconducting qubits. However, finding efficient schemes to produce such states has been a long-standing challenge. I will present an algorithm that, given a desired multi-photon graph state, determines the minimum number of quantum emitters and precise operation sequences that can produce it. The algorithm itself and the resulting operation sequence both scale polynomially in the size of the photonic graph state, allowing one to obtain efficient schemes to generate graph states containing hundreds or thousands of photons. Among the most mature and promising platforms for multi-photon entangled graph state generation are nitrogen-vacancy (NV) centers in diamond and other color centers in solids. One of the challenges in using these systems for graph state generation and networking applications is to controllably manipulate entanglement between the electron and the nuclear spin register despite the always-on nature of the hyperfine interactions, which makes this an inherently many-body quantum system. I will present a general formalism to quantify and control the generation of entanglement in an arbitrarily large nuclear spin register coupled to a color center electronic spin. I will describe a reliable measure of nuclear spin selectivity, by exactly incorporating into our treatment the dynamics with unwanted nuclei. I will also show how to realize direct multipartite gates through the use of dynamical decoupling sequences, drastically reducing the total gate time compared to protocols based on sequential entanglement with individual nuclear spins. We quantify the performance of such gate operations in the presence of unwanted residual entanglement links, capturing the dynamics of the entire nuclear spin register.

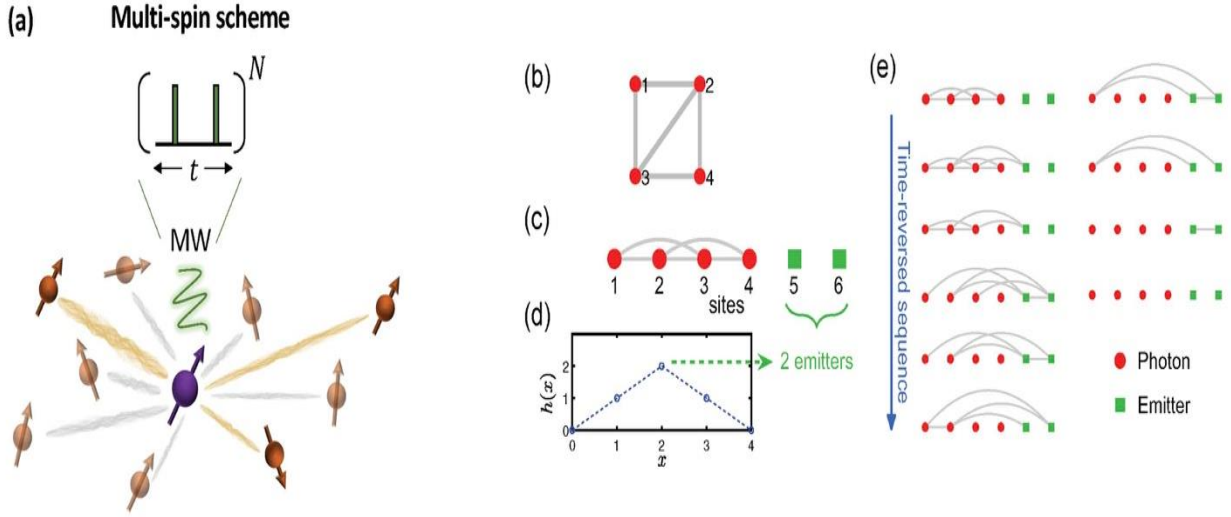

Fig. 1. (a) *Schematic of a defect spin (purple) hyperfine-coupled to a nuclear spin register (orange) and driven by a dynamical decoupling sequence with 2N pulses and pulse spacing t.*
(b) *An example four-photon graph state. Each red dot corresponds to a photonic qubit, and lines represent CZ gates;*
(c) *Arranging the graph state in a 1D array and computing the entanglement entropy as a function of the bipartition point x;*
(d) *reveals that two quantum emitters (green squares) are needed to produce the four-photon state in* ***(b)****;*
(e) *Time-reversed sequence of operations that systematically absorb all photons into the emitters. Reversing this sequence gives a precise protocol for generating the graph state in* ***(b)*** *from the two emitters.*

Finally, using experimental parameters of a well-characterized 27 nuclear spin register device, we show how to prepare with high-fidelity entangled states for quantum error correction. While in this analysis we focus on a particular NV-diamond-based register, our framework is completely general and applicable to other defects in diamond and in SiC.

References

[1] B. Li, S. E. Economou, E. Barnes, *npj Quantum Information* **8**, 11 (2022).
[2] E. Takou, E. Barnes, S. E. Economou, *Physical Review X* **13**, 011004 (2023).
[3] E. Takou, E. Barnes, S. E. Economou, *arXiv:2302.05580* (2023).

* Acknowledgments: This work was supported by the National Science Foundation (grant nos. 1741656 and 2137953).

Emergence in out of equilibrium systems: Theoretical treatment of complex out-of-equilibrium dynamics and the ensuing phenomena

M. Battiato
Nanyang Technological University, Singapore 639798, Singapore

Emergence is the phenomenon by which a system with many heterogeneous degrees of freedom develops behaviours that are qualitatively different from its simpler parts. A famous example is life. Describing and predicting emergence requires handling the system in its full complexity: if simplified, or if degrees of freedom are removed, entire behaviours will simply not happen. Femtosecond laser pulse-generated out-of-equilibrium states of materials are a very fertile ground for emergence, as being away from the rather strict requirements of equilibrium or near equilibrium conditions frees up a large number of degrees of freedom. Spectacular examples of emergence in these cases are, among others, the super-diffusive spin transport, [1-4] spintronic THz emitters [4] and the giant spin injection in semiconductors [5, 6].Such effects are the results of the complex interplay of the far-from-equilibrium state of the system, spin-, band- and momentum-dependent thermalization, transport of excited quasiparticles and interaction with electromagnetic fields. To address the cull complexity of the situation without losing the emergent behaviours, one has to move beyond usual treatments. We have developed the, so far, only available numerical algorithm to solve the full Boltzmann transport and scattering equation for realistic band structures, and, for the first time, no close to equilibrium approximation, as well as several essential computational properties (see left panel of Fig. 1) [7-9].

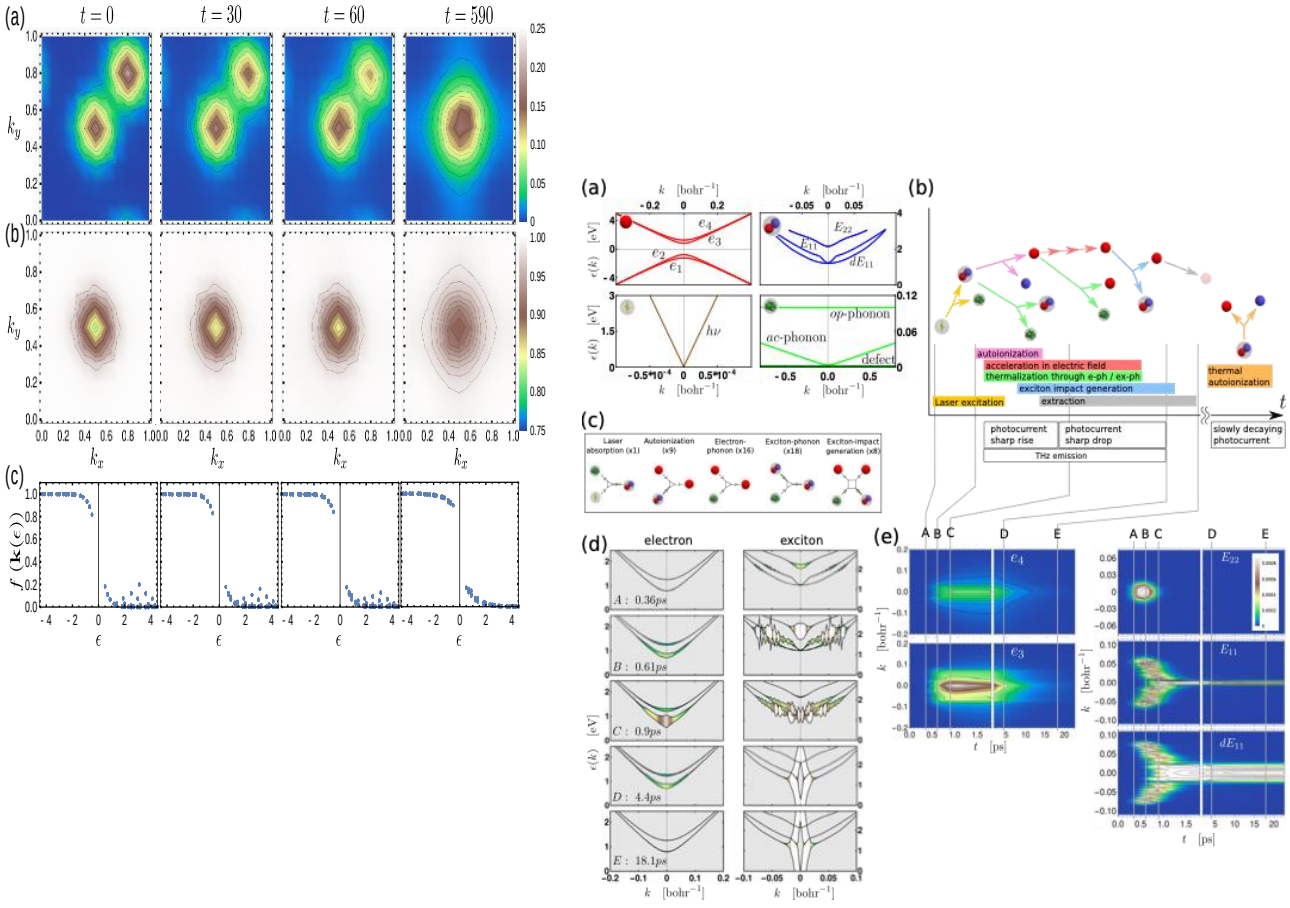

Fig. 1. Left: *Snapshots of thermalizing population through electron-electron scatterings is semiconductor.*
Top and middle left*: momentum-resolved population in the conduction and valence band.*
Bottom left*: energy resolved population [7].*
Right*: Schematics of the theoretical treatment of laser excitation and thermalization under bias of CNTs [10].*

More recently we have shown how disorder in carbon nanotubes can dramatically impact the thermalization dynamics [11].
Interestingly the same numerical method can be employed to produce spectra and, in connection with time-resolved Boltzmann simulations, time- resolved spectra (see left panel of Fig. 2) [12].
The developed approach allows us to tackle the thermalisation dynamics of different types of quasiparticles: we managed to describe and identify the unconventional thermalisation pathways in GeTe driven by spin-selective electron-electron and electron-phonon scatterings (see right panel of Fig. 2). [10]

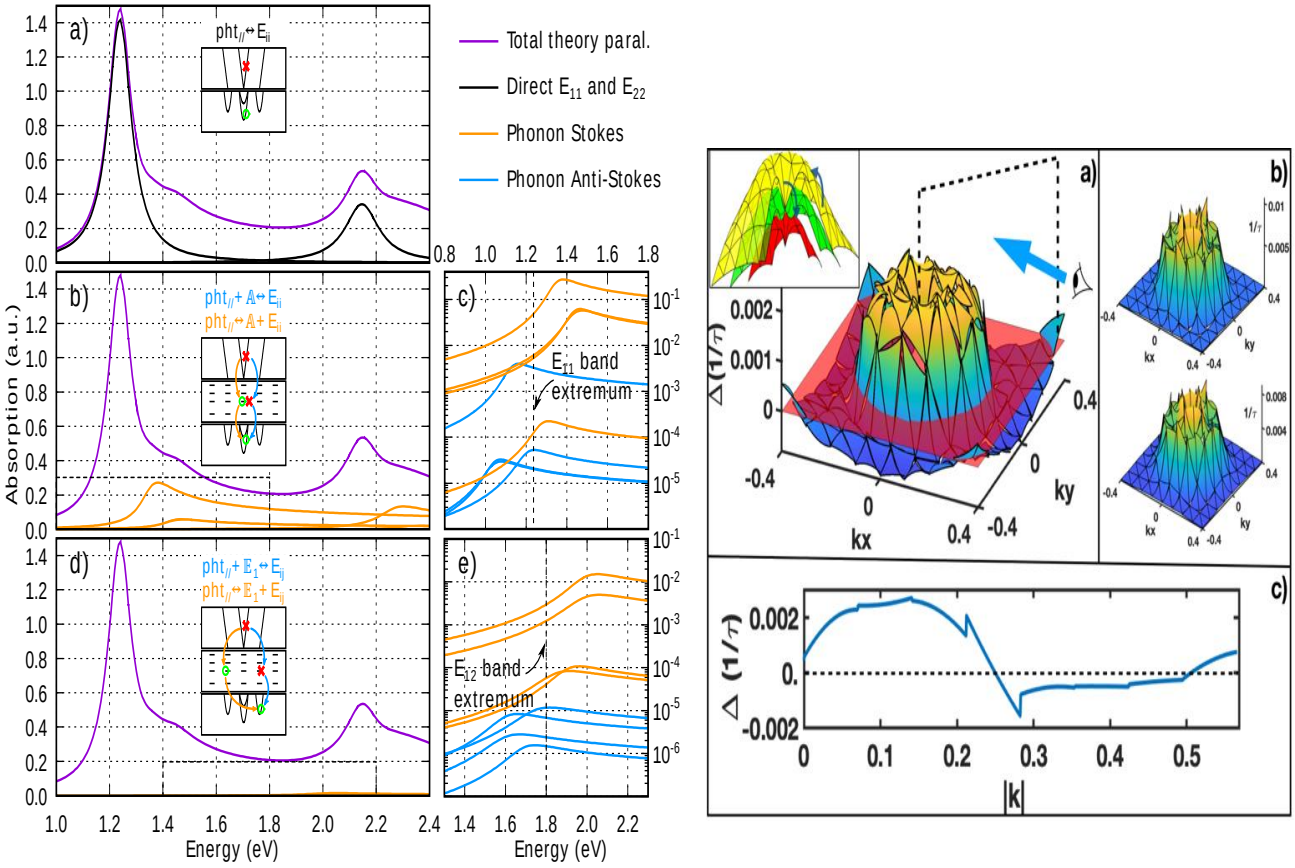

***Fig.2. Left**: Absorption spectrum for light parallel to the CNT's axes. Each panel shows a different process contributing to the total spectrum [12]. **Right**: Change with temperature of the scattering rate (inverse lifetime) due to electron-electron scattering in GeTe [10].*

Finally, more recently, we have been able to address the failure of generating lasing with carbon nanotubes. We showed that reaching the population inversion necessary for lasing to start at the main E11 exciton transition is not achievable. We have however shown that at frequencies corresponding to anti-Stokes phonon-assisted optical generation of excitons, lasing can be triggered way below the population inversion threshold.

References

[1] M. Battiato, K. Carva, P.M. Oppeneer, *Physical Review Letters* **105**, 027203 (2010).
[2] D. Rudolf, C. La-O-Vorakiat, M. Battiato, R. Adam, J. M. Shaw, E. Turgut, P. Maldonado, S. Mathias, P. Grychtol, H. T. Nembach, T. J. Silva M. Aeschlimann, H. C. Kapteyn, M. M. Murnane, C. M. Schneider, P. M. Oppeneer, *Nature Communications* **3,** 1037 (2012).
[3] A. Eschenlohr, M. Battiato, P. Maldonado, N. Pontius, T. Kachel, K. Holldack, R. Mitzner, A. Fohlisch, P. M. Oppeneer, C. Stamm, *Nature Materials* **12**, 332 (2013).
[4] T. Kampfrath, M. Battiato, P. Maldonado, G. Eilers, J. Notzold, S. Mahrlein, V. Zbarsky, F. Freimuth, Y. Mokrousov, S. Blugel, M. Wolf, I. Radu, P. M. Oppeneer, M. Munzenberg, *Nature Nanotechnology* **8**, 256 (2013).
[5] M. Battiato, K. Held, *Physical Review Letters* **116**, 196601 (2016).
[6] L. Cheng, X. Wang, W. Yang, J. Chai, M. Yang, M. Chen, Y. Wu, X. Chen, D. Chi, K. E. J. Goh, J.-X. Zhu, H. Sun, S. Wang, J. C. W. Song M. Battiato, H. Yang, E. E. M. Chia, *Nature Physics* **15**, 347(2019).
[7] M. Wais, K. Held, M. Battiato, *Computer Physics Communications* **264**, 107877 (2021).
[8] I. Wadgaonkar, R. Jain, M. Battiato, *Computer Physics Communications* **263**, 107863 (2021).
[9] I. Wadgaonkar, M. Wais, M. Battiato, *Computer Physics Communications* **271**, 108207 (2022).
[10] F. R. Bagsican, M. Wais, N. Komatsu, W. Gao, L. Weber, K. Serita, H. Murakami, K. Held, F. A. Hegmann, M. Tonouchi, J. Kono, I. Kawayama, M. Battiato, *Nano Letters* **20**, 3098 (2020).
[11] M. Wais, F. R. Bagsican, N. Komatsu, W. Gao, K. Serita, H. Murakami, K. Held, I. Kawayama, J. Kono, M. Battiato,M. Tonouchi, under review
[12] S. Dal Forno, N. Komatsu, M. Wais, A. Mojibpour, I. Wadgaonkar, S. Ghosh, Y. Yomogida, K. Yanagi, K. Held, J. Kono, M. Battiato *Carbon* **186**, 465 (2022).
[13] O. J Clark, I. Wadgaonkar, F. Freyse, G. Springholz, M. Battiato, J. Sánchez Barriga, *Advanced Materials* **34,** (2022).

* Acknowledgements: M.B. acknowledges financial support from the Nanyang Technological University, for the grant NAP-SUG, and MOE Singapore for the grants Tier 1 RG75/22, Tier 1 RT13/22, and Tier 2 T2EP50222-0047.

Non-equilibrium carrier dynamics and carrier-phonon interaction in 2D quantum materials

M. Bauer
Kiel University, 24098 Kiel, Germany

Electron-phonon interaction is one of the most fundamental quasiparticle interaction in solids governing for instance transport and thermodynamic properties of materials, but being also responsible for unconventional phenomena such as low-temperature superconductivity and the formation of charge-ordered phases. In this presentation I will discuss the results of two time- and angle resolved photoemission (trARPES) studies of our group that addressing electron-phonon interactions and there effect on electron and spin degrees of freedom on ultrafast timescales in two different types of 2D transition metal dichalcogenides (TMDC). In a singly oriented film of single-layer WS_2 deposited on a Au(111) surface we studied the spin- and valley-selective photoexcitation and decay of free carriers at the K and K'-points (Fig. 1) [1]. The results reveal that in the valence band (VB) maximum an ultimate valley polarization of free holes of 84% can be achieved upon excitation with circularly polarized light at room temperature. For the photoexcited free electrons in the conduction band (CB) minimum, we observe a significantly smaller valley polarization. Clear differences in the carrier dynamics between electrons and holes imply intervalley scattering processes into dark states being responsible for the efficient depolarization of the excited electron population. The observed characteristic timescale for this process match very well values predicted by theory for the formation of momentum forbidden intervalley dark excitons in tungsten-based single-layer TMDCs due to electron-phonon interaction [2].

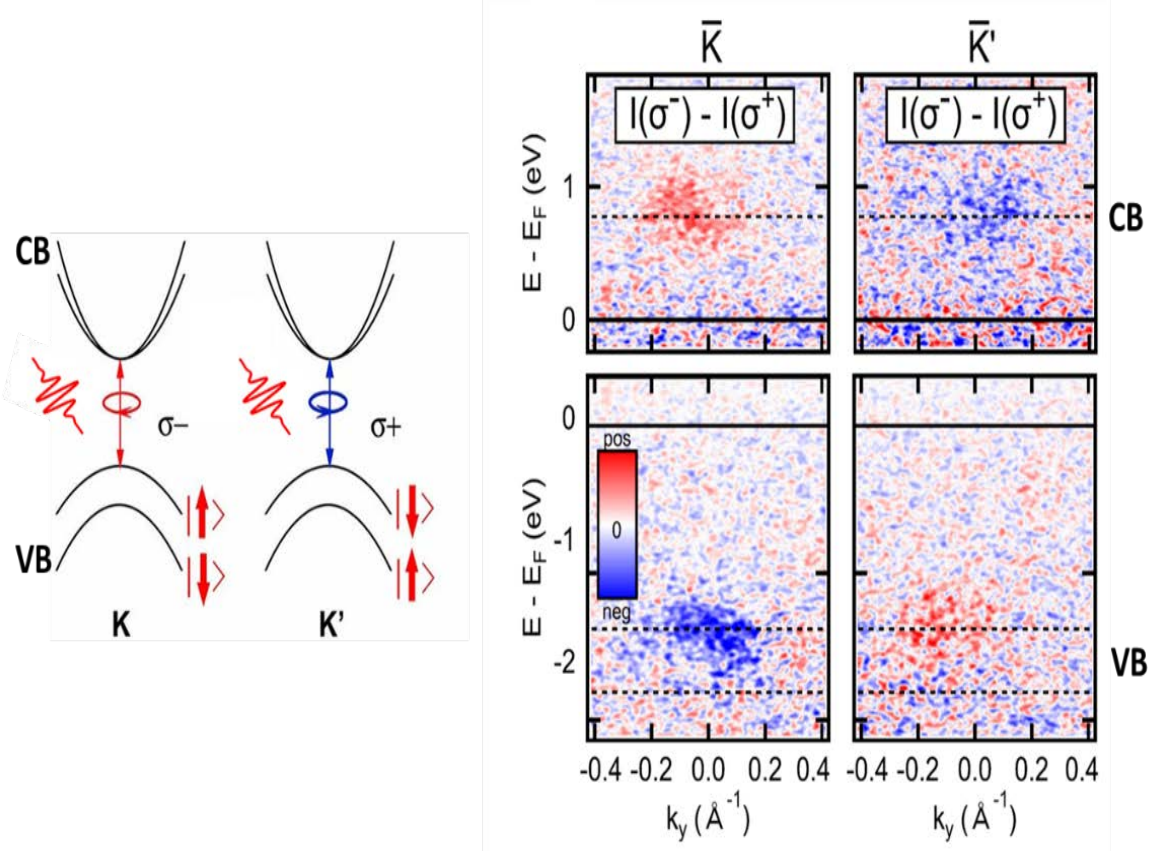

***Fig. 1. Left**: Illustration of the optical excitation at K and K' in WS_2 using circularly polarized pump pulses. **Right**: Transient valley-selective VB and CB) populations created by band gap-resonant absorption of circular polarized light as probed in a trARPES experiment. The figure displays the photoemission signal contrast observed at the K and the K' point upon excitation with left (σ^-) and right (σ^+) circularly polarized pump pulses, respectively. The contrast inversion between K and K' indicates the valley selectivity of the excitation process with respect to the pump polarization.*

In the second example I will discuss results on the electron-phonon interaction in the Weyl-semimetal *Td*-WTe_2 as probed in a trARPES experiment following the excitation of coherent phonons using NIR pump pulses [3].

We can show that a phonon-frequency selective analysis of the experimental data provide high-resolution information on strengths and types of couplings of the individual modes to the electronic bands (Fig. 2). I particularly will focus on the observation of a transient modulation of a Dresselhaus-type spin splitting of electronic bands driven by the selective coupling of an interlayer shear mode of the layered compound. The latter results reveal real-time insights into electron-phonon coupled processes that are of vital importance for a light-driven topological phase transition in *Td*-WTe_2 [4].

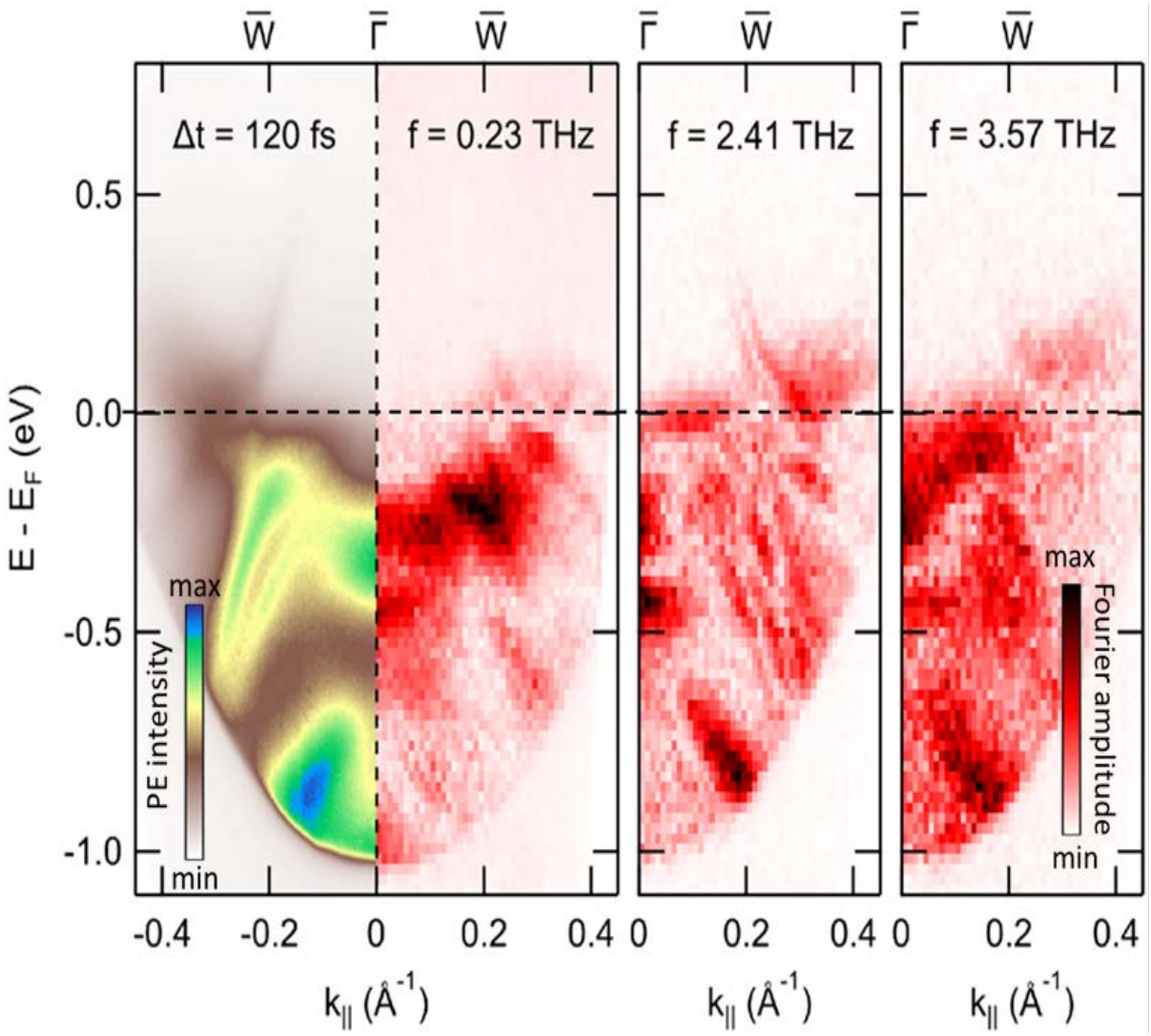

Fig. 2. Left*: trARPES snapshot of Td-WTe_2 at a NIR-pump UV-probe temporal delay of 120 fs (left spectrum) in comparison to energy-momentum maps derived from a Fourier-analysis of a complete trARPES scan. Here, f denotes the frequencies of coherent phonon peaks identified in the Fourier-spectrum of the pump-probe scans. The Fourier amplitude is a measure for the coupling strength of the respective phonon mode to the electronic bands of WTe_2.*

In summary, the examples illustrate the potential of trARPES in providing relevant information on electron-phonon couplings in quantum materials. In particular, the concept of a frequency-domain analysis of trARPES data, which are modulated due to the excitation of coherent phonons, may provide in the future quantitative and electronic band- and phonon mode-resolved views onto electron phonon interactions in general [5, 6].

References

[1] H. Beyer, G. Rohde , A. Grubišić Čabo , A. Stange, T. Jacobsen, L. Bignardi , D. Lizzit , P. Lacovig, C. E. Sanders, S. Lizzit, K. Rossnagel, P. P. Hofmann, M. Bauer, *Phyical Review Letters* **123**, 236802, (2019).

[2] M. Selig, G. Berghäuser, A. Raja, P. Nagler,C.Schüller,T.F.Heinz,T.Korn,A.Chernikov,E.Malic,A. Knorr, *Nature Communications* **7**, 13279 (2016).

[3] P. Hein, S. Jauernik, H. Erk, L. Yang, Y. Qi, Y. Sun, C. Felser, M. Bauer, *Nature Communications* **11**, 2613, (2020).

[4] E.J. Sie, C.M. Nyby, C.D. Pemmaraju, S.J. Park, X. Shen, J. Yang, M.C. Hoffmann, B.K. Ofori-Okai, R. Li, A.H. Reid, S. Weathersby, E. Mannebach, N. Finney, D. Rhodes, D. Chenet, A. Antony, L. Balicas, J. Hone, T.P. Devereaux, T.F. Heinz, X. Wang, A.M. Lindenberg, *Nature* **565**, 61 (2019).

[5] T. Suzuki, et al., *Physical. Review B* **103**, L121105 (2021).

[6] U.D. Giovannini, H. Hübener, S.A. Sato, A. Rubio, *Physical Review Letters* **125**, 136401 (2020).

* Acknowledgement(s) : M. Bauer acknowledges support DFG, (grants 239392151, 266380790, and 389191527).

Quantumness in a tight space: Randomness, n-reconfigurability and multiparty entanglement on chip

N. Belabas
Université Paris-Saclay, 91120 Palaiseau France

Quantum-dot based semiconductor sources offer unprecedented brightness. Feeding synchronized indistinguishable photons emitted by such an efficient single photo source (figure, left) into integrated reconfigurable photonic chips (figure, middle column) enables the implementation of multiphoton protocols. These on-chip protocols harness quantumness with remarkable performances and represent small-scale quantum computation in the "noisy intermediate scale" regime with linear optical gates. We detail three instances and associated protocols:

1. **N-indistinguishability** is required for N-photon quantum information protocols and is non-trivial to measure beyond N=2. We proposed a method to measure multi-photon N-indistinguishability on chip and implemented a N=4 demonstration (top blue row of figure) [1].
2. We generated with high fidelity a 4-photon entangled state, $|GHZ_4\rangle$**,** a state of the class of the graph states useful for quantum information. Owing to the high photon rate of our demonstration, we could perform a 4-photon state full tomography on chip and achieved a record generation rate for integrated generation of $|GHZ_4\rangle$ (medium green row in figure) [2].
3. Harnessing quantumness on chip also comes at the cost of the sacrifice of space-like separation that is typically relied upon for certification of randomness.

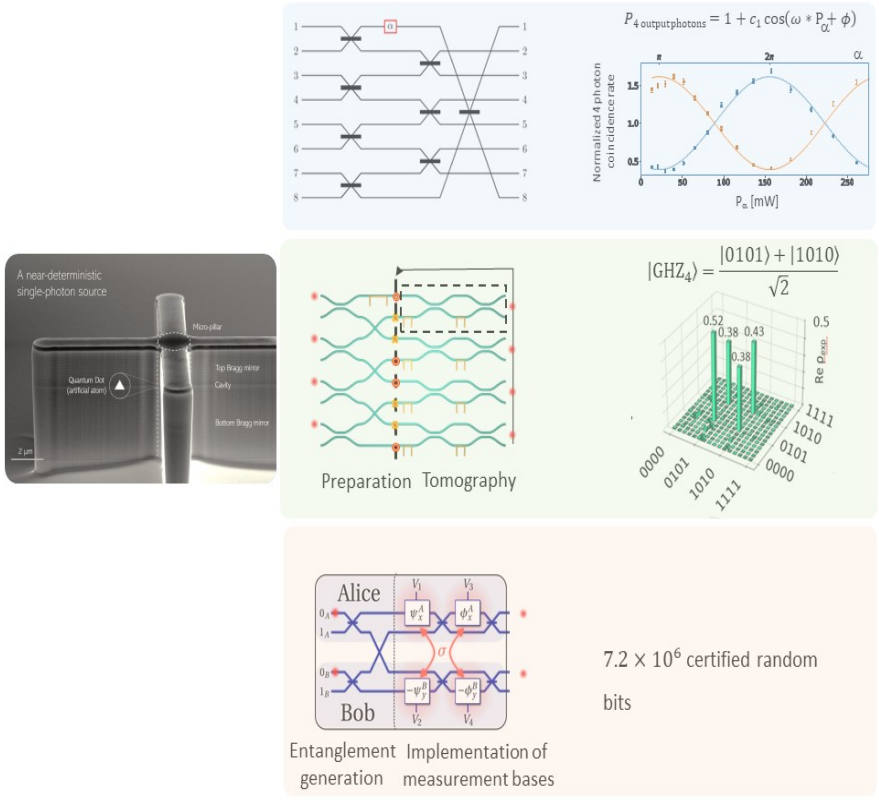

***Fig.1. Left**: A semiconductor quantum-dot-based quasi-deterministic efficient source of photons.* ***Blue top** – 4-photon indistinguishability as measured by the contrast of interference at the output of a 2-layer-interferometer as a function of a single phase [1].*
***Green middle** – Post-selected $|GHZ_4\rangle$ preparation and full characterization with a reconfigurable glass circuit, here the real part of the density matrix we achieve a Fidelity to $|GHZ_4\rangle$ of $\mathcal{F}_{exp}$ = 86.0±0.4%. and a purity of the generated state $\mathcal{P}_{exp}$ = 76.3±0.6%. [2].*
***Red bottom** – Alice and Bob play a contextual game (equivalent to CHSH inequality testing) to guarantee randomness. On-chip and thus without space-like separation, the crosstalk σ between the devices enabling the change of bases for both parties prevent the application of this framework. We introduce a new metrics and protocol to certify randomness in this context that is close to real-world applications [3].*

By introducing a dedicated protocol which is based on witnessing contextual correlations, and metrics that account for an amount of signaling in the absence of space-like separation, we could for the first time certify randomness in a tight space (bottom orange row in Fig.1) [3].

References

[1] M. Pont, G. Corrielli, A. Fyrillas, I. Agresti, G. Carvacho, N.Maring, P.-E. Emeriau, F. Ceccarelli, R.Albiero, P.H. D. Ferreira, N. Somaschi J. Senellart, I. Sagnes, M.Morassi, A. Lemaitre, P. Senellart , F. Sciarrino, M. Liscidini, N. Belabas R.Osellame, *arXiv quant-ph 2211.15626*
[2] M. Pont, R.Albiero, S.E. Thomas, N. Spagnolo, F.Ceccarelli, G. Corrielli, A.Brieussel, N.Somaschi, H. Huet, A.Harouri, A.Lemaître, I.Sagnes N. Belabas, F. Sciarrino, R. Osellame, P.Senellart, A. Crespi, *Physical Review* X **12**, 031033 (2022)
[3] A. Fyrillas, B.Bourdoncle, A.Maïnos, P.-E. Emeriau, K.Start, N. Margaria, M.Morassi, A.Lemaître, I.Sagnes, P.Stepanov, T. H.Au, S. Boissier N. Somaschi, N. Maring, N. Belabas, S. Mansfield, *arXiv:2301.03536.*

* Acknowledgements: This work is partly supported the European Union's Horizon 2020 FET OPEN project PHOQUSING (Grant ID 899544), the European Union's Horizon 2020 Research and Innovation Programme QUDOT-TECH under the Marie Sklodowska-Curie Grant Agreement No. 861097, the French RENATECH network, the Paris Ile-de-France Region in the framework of DIM SIRTEQ. Fabrication of one of the photonic chips was partially performed at PoliFAB - www.polifab.polimi.it

Time-resolving multi-body dynamics in materials with attosecond soft x-rays

T.P.H. Sidiropoulos[1], N. Di Palo[1], D.E. Rivas[1], S. Severino[1], M. Reduzzi[1], B. Nandy[1], B. Bauerhenne[2] S. Krylow[2], T. Vasileiadis[3], T. Danz[4], P. Elliott[5], S. Sharma[5], K. Dewhurst[6], C. Ropers[4], Y. Joly[7], M. E. Garcia[2], M. Wolf[3], R. Ernstorfer[3], J. Biegert[1]

[1] *Barcelona Institute of Science and Technology,08860 Castelldefels, Spain*
[2] *Universität Kassel, 34132 Kassel, Germany*
[3] *Fritz Haber Institute of the Max Planck Society, 14195 Berlin, Germany*
[4] *University of Göttingen, 37073 Göttingen, Germany*
[5] *Max-Born-Institut für Nichtlineare Optik und Kurzzeitspektroskopie, 12489 Berlin, Germany*
[6] *Max-Planck-Institut für Mikrostrukturphysik, 06120 Halle, Germany*
[7] *Université Grenoble Alpes, 38000 Grenoble, France*

We show that core-level x-ray absorption near edge structure (XANES) spectroscopy with attosecond soft x-ray (SXR) pulses [1] can image the flow of energy inside a material in real time [2]. We photoexcite graphite with a 11 ± 1 fs pump pulse at 1850 nm, or with a 15 ± 1 fs pulse at 800 nm, for various pump fluences between 2.8 ± 0.2 mJ/cm^2 and 81 ± 5 mJ/cm^2. Figure 1(a) shows the measured differential x-ray absorption ΔA(E) (pumped minus unpumped) from which striking changes of up to 15% are immediately apparent. We identify these features as π bonding state and as π* and σ* antibonding states. Attosecond-resolved measurement with a pump-probe delay step size of 0.6 fs show the buildup of coherent charge oscillations, i.e., polarization of the material. These oscillations occur at occupied states below and unoccupied states above the Fermi level predominantly at the pump carrier frequency. We identify the incoherent background due to the dephasing of coherent charge oscillation. This background rises within a few oscillations of the light field, signifying the ultrafast transfer of energy from the light field into the electron and hole excitation of the material.

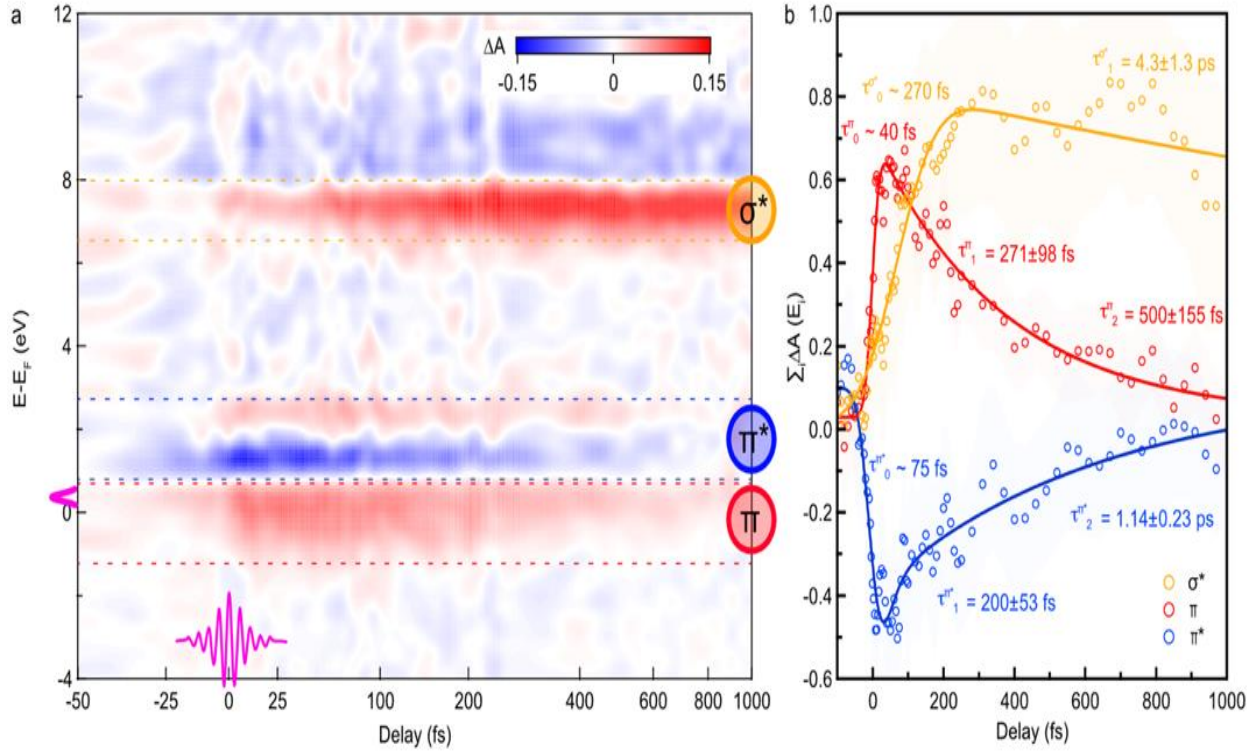

Fig. 1 Time-dependent XANES measurement. *(a) Shown is the differential absorption ΔA(E) between the XANES spectrum with and without pump pulse. The observed features are identified as arising from electrons at the bottom of the CB (π^*), holes at the top of the valence band (π), and predominately from optical phonons (σ^*); note that the material is n-doped to 650 meV. The pump pulse bandwidth and duration are indicated in pink. (b) Sum of the differential absorption $\sum_i \Delta A(E_i)$ over the respective energy range for π (red), π^* (blue), and σ^*(yellow). The curves are fitted with a double exponential convolved with a Gaussian.*

Further, we find that ultrafast dephasing of the coherent carrier dynamics is governed by impact excitation (IE) for electrons, while holes exhibit a switchover from impact excitation to Auger heating (AH) already during the 11-fs duration of the infrared light field.

We further analyze the coherent phonon signal (see Fig. 2) by analyzing the oscillatory pattern (Fig. 2b) exhibited by the σ* d*a*ta with a short-time Fourier transform (STFT) analysis (Fig. 2c-e).

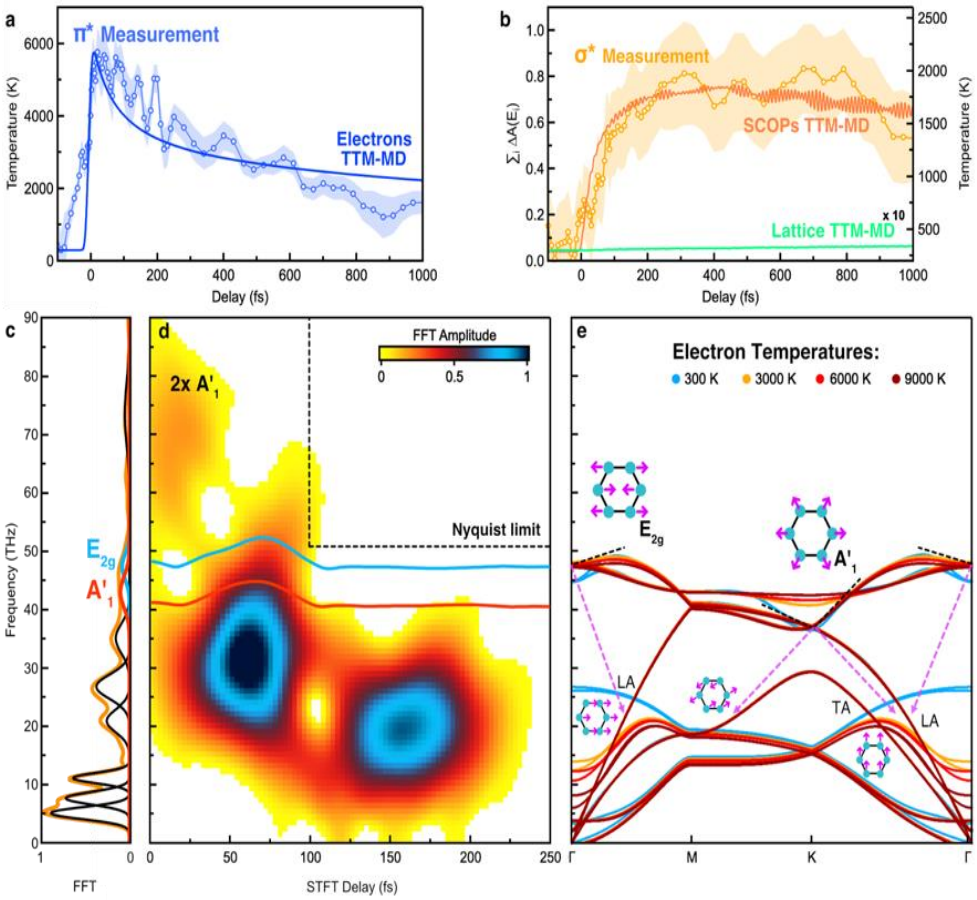

Fig. 2 Phonon dynamics retrieved from attosecond-XANES. ***(a)*** *and* ***(b)*** *show results from the TTM-MD simulation (**solid lines**) together with experimental data from Fig. 1. The evolution of the electronic temperature is shown in* ***(a)*** *while* ***(b)*** *shows the SCOPs and lattice subsystems;*
(c) *shows results from a Fourier analysis of the experimental σ data (shown in* ***(b)***). *A multi-peak fit reveals the predominant modes; positions of the A_1' E_{2g} are shown in red and blues, respectively.*
(d) *Short-Time Fourier Transform (STFT) of the σ data* ***(b)*** *over a time range of 250 fs, visualizing coherent phonon contributions. A comparison with the calculated phonon dispersion* ***(e)***, *for different electronic temperatures (see SI), allows to identify the phonon modes, their main branches (dashed lines), and their dispersion (dashed arrows). Striking are the high frequency oscillations at twice the phonon frequency of A_1', the simultaneous and fast rise of the coherent Raman active E_{2g} mode, concomitantly with the non-Raman-active A_1', mode, and the rapid decay into coherent low-frequency phonons and their temporal dynamics.*

The STFT analysis shows that already during and shortly after the laser excitation, coherent motion emerges over a broad range of frequencies. A comparison with the phonon dispersion from two-temperature-model molecular dynamics (TTM MD) simulations [4] [Fig. 1b] identifies them as the Raman-active $\Gamma - E_{2g}$ and the non-Raman-active $K - A'_1$ SCOPs at 46.4 ± 2.7 and 42.7 ± 1.1 THz, respectively. The surprising early contribution from the (non-Raman-active) A'_1 mode originate from the very strong electron-SCOPs coupling, thus acting almost impulsively. We demonstrate the ability to track energy flow upon light absorption between electrons, holes, and phonons in real-time. We applied the method to graphite and demonstrate its capability by disentangling the coherent and incoherent contribution to the multi-body dynamics. We expect that the general applicability of the method will prove valuable to address questions such as, for instance, the energy dissipation in light-harvesting, organic electronic and energy storage systems, or to re-examine long-standing questions in non-equilibrium multi-body physics such as phase-transitions and superconductivity.

References

[1] S. M. Teichmann, F. Silva, S. L. Cousin, M. Hemmer, J. Biegert, *Nature Communications* **7**, 11493 (2016).
[2] T.P.H. Sidiropoulos, N. Di Palo, D.E. Rivas, S. Severino, M. Reduzzi, B. Nandy, B. Bauerhenne, S. Krylow, T. Vasileiadis, T. Danz, P. Elliott S. Sharma, K. Dewhurst, C. Ropers, Y. Joly, K. M. E. Garcia, M. Wolf, R. Ernstorfer, J. Biegert, *Physical Review X*. **11,** 041060 (2021).
[3] B. Buades, D. Moonshiram, T. P. H. Sidiropoulos, I. Leon, P. Schmidt, I. Pi, N. Di Palo, S. L. Cousin, A. Picon, F. Koppens, J. Biegert *Optica* **5**, 502 (2018).
[4] S. Krylow, F. Valencia Hernandez, B. Bauerhenne, M. E. Garcia, *Physical Review* B **101**, 205428 (2020).

The polaritonic Bardeen-Cooper-Schrieffer state

R. Binder, M. Spotnitz, N.H. Kwong
University of Arizona, Tucson, AZ 87721, USA

Exciton-polaritons in semiconductor microcavities are well known for their ability to undergo Bose-Einstein condensation (BEC) as a consequence of the bosonic character of polaritons in the low-density regime. One of the signatures for BEC is the emergence of coherent emission as a form of spontaneous symmetry breaking. There are, however, other forms of condensation possible. One is the conventional semiconductor lasing, sometimes called 'photon lasing', in which Coulomb interaction effects can be largely ignored, and the lasing process is driven by fermionic gain. In-between the two is the regime of the Bardeen-Cooper-Schrieffer (BCS) state, where the interaction is important, but the pairing does not lead to tightly bound bosonic quasi-particles. In the BCS state the electron-hole pairs are not well separated, and understanding the spontaneous symmetry breaking requires a theory that contains the fermionic degrees of freedom of the electrons and holes, since the polariton BCS laser is a hybridized state between bosonic cavity photons and Cooper-pair fermions (electrons and holes). It is the purpose of this talk to discuss the conceptual foundation of the polaritonic BCS state and to present a microscopic theory that helps understand the physical properties of the polaritonic BCS state. In particular, we have developed a comprehensive theory of the fluctuation modes, from which we obtain information of the frequencies of the linear excitations of that state. This knowledge, in turn, can help us develop experimental proposals for spectroscopic approaches to the linear excitations of the polaritonic BCS state and to predict measurable quantities, such as absorption spectra, that can probe those excitations.

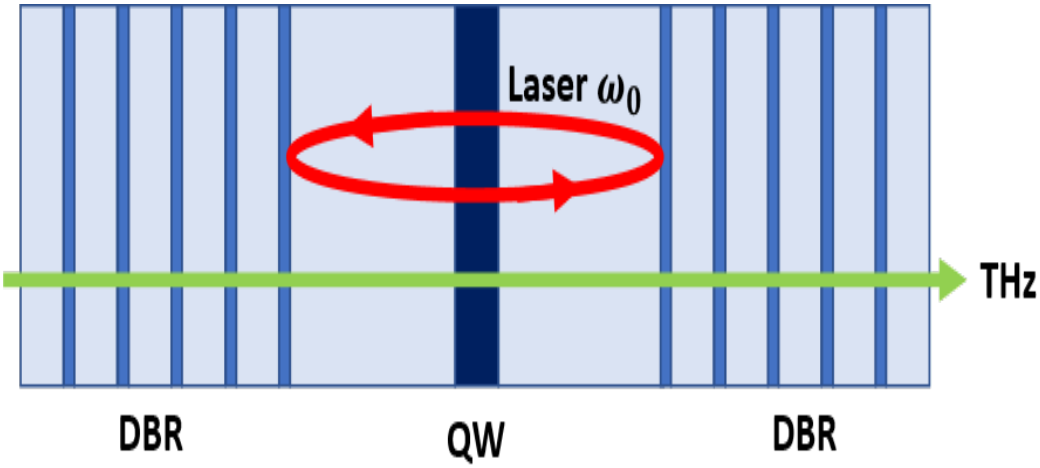

Fig. 1 *Schematic of the cavity indicating the cavity confinement of the laser radiation in the near-infrared, and the absence of cavity effects in the THz regime.*

Experimental demonstration of a polariton laser operating in the BCS regime has been achieved only recently [1] in the group of Hui Deng, Univ. Michigan. For the theoretical analysis of that experiment, we used a microscopic many-particle theory to compute experimental observables such as emission frequency. The observation of fermionic gain enabled us to rule out BEC, and the large detuning of the emitted light from the cavity resonance enabled us to rule out photonic lasing. We have since extended the theoretical analysis and studied linear response and fluctuation modes of the polariton laser, i.e., a driven-dissipative quantum many-particle system prepared in a spontaneous broken-symmetry steady state, using optical frequencies (interband transitions) [2] and terahertz (THz) frequencies (intraband transitions) [3,4]. In this talk, we focus mainly on the rich landscape of optical fluctuation modes, that exhibits discrete and continuum soft modes in a two parameter (pump density and cavity decay rate) space. Since we obtain a complete set of eigenvalues and eigenvectors of the linear response including discrete states and spectral continua, our analysis gives unprecedented insight into the microscopic physics of a polariton laser and its excitation spectrum. For example, as the external parameters such as cavity decay rate and pump power are varied, we find that collective modes can 'collide' at exceptional points, and that there is a continuum of exceptional points in the two-dimensional plane of pump density and cavity decay rate.

Fig. ***2*** shows an example of the eigenvalues of the fluctuation modes when excited by THz radiation (a) and near-infrared radiation (b).

The modes shown in (b) contain the Goldstone mode G_0, as well as various collective (spectrally discrete) modes and spectral continua. A detailed analysis of the collective modes reveals that these collective modes are not pure Higgs modes [4].

All modes in (b) involve only interband transitions where the photon angular momentum of $\pm 1\hbar$ is transferred to the electrons that undergo transitions from the valence to the conduction band with angular momentum difference of the lattice-periodic part of the Bloch wavefunctions of $\pm 1\hbar$. Hence, the orbital angular-momentum of the modes in (b) is the same as that of the Goldstone mode, namely zero (s-wave solutions).

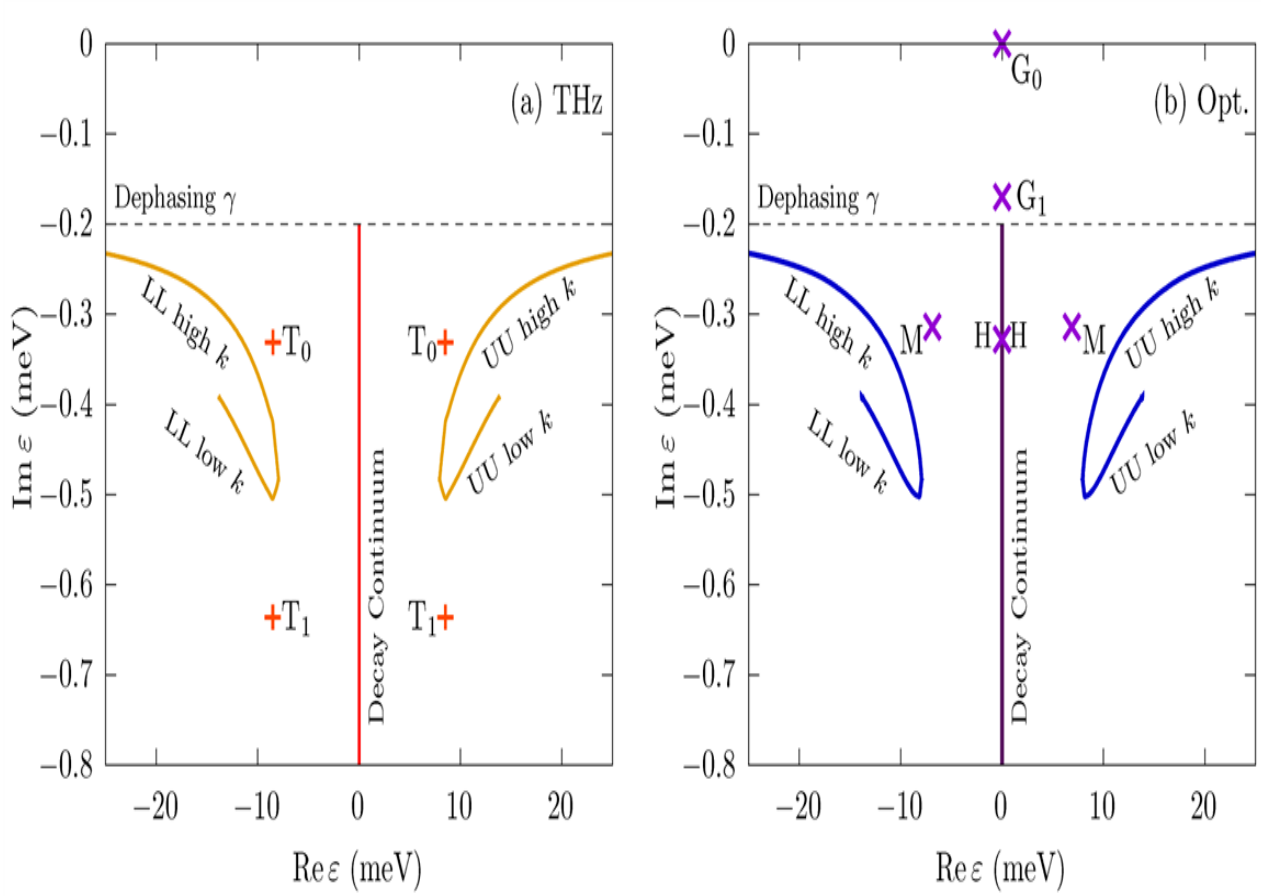

***Fig. 2 (a) & (b)**. The eigenvalues of the fluctuation matrix of a polariton laser in the BCS regime, showing spectral continua and discrete modes (collective states). The modes can be triggered by THz radiation **(a)** or near-infrared radiation **(b)**. The fluctuation modes of the light field and the interband polarization oscillate at frequencies close to the fundamental band gap of GaAs, i.e., the near infrared. The fluctuation modes of the carrier distributions and carrier density oscillate at THz frequencies in both cases. From Ref. [4].*

In contrast, the modes in (a) have orbital angular momentum of $\pm 1\hbar$, since these are related to intraband transitions where the intraband photon angular momentum is transferred to the angular momentum of the electrons and holes that is related to the envelope motion (the plane-wave part) of the Bloch states (the angular momentum related to the lattice-periodic part of the Bloch states remains unchanged) and thus to the relative motion of the electron-hole pairs. It is interesting to note that the modes in (a), triggered by THz probes, contain collective modes (called T_0 and T_1 here), which is a pure Coulomb correlation effect. The gaps in the continuum energies relative to the energy of the Goldstone mode correspond to the gaps in the excitation spectrum of the BCS state in superconductors. We note, however, that that the polaritonic system is an open-pumped-dissipative system and therefore not equivalent to a superconductor in thermal equilibrium.

In addition to GaAs microcavities, we are also studying analogous effects in microcavities containing two-dimensional materials such as $MoSe_2$.

References

[1] R. Binder, N.H. Kwong, *Physical Review* B **103**, 085304 (2021).

[2] J. Hu, Zh. Wang, S. Kim, H. Deng, S. Brodbeck, Ch. Schneider, S. Hoefling, N.H. Kwong, R. Binder, *Physical Review* X **11** 011018 (2021).

[3] M. Spotniz, N.H. Kwong, R. Binder, *Physical Review*. B **104**, 115305 (2021).

[4] M. Spotniz, N.H. Kwong, R. Binder, *Physical Review* B (accepted for publication) (2023).

* We gratefully acknowledge financial support from NSF under grant number DMR 1839570, and CPU time at HPC University of Arizona.

Advances in time-resolved photoemission spectroscopy with high-intensity mid-IR excitation at ALLS

J.M. Parent, G. Jargot, B. Frimpong, A. Longa, F. Légaré, F. Boschini
Institut national de la recherche scientifique, Varennes, QC J3X 1P7, Canada

The Advanced Laser Light Source (ALLS) laboratory at the Institut national de la recherche scientifique (INRS), Montreal (QC, Canada), is a national user facility offering a coherent rainbow of ultrashort light pulses spanning seven orders of wavelength, from the THz to the hard X-rays, coupled to several endstations. After a brief summary of ALLS' experimental capabilities, I will discuss the new time- and angle-resolved photoemission (TR-ARPES) endstation that will enable novel investigations of light-induced electron dynamics in quantum materials [1-3]. At the moment, the TR-ARPES endstation relies on a low photon energy UV probe (6 eV) with ~10 meV bandwidth, but an HHG-based beamline, comprising a time-preserving monochromator operating in the 10-40 eV energy range, is under construction and will soon enable comprehensive studies of mid-IR-induced electron dynamics over the entire momentum space of quantum materials. Intense near- and mid-infrared optical pulses are generated via a home-build three-stage optical parametric amplifier followed by difference frequency generation (see scheme in Fig. 1).

Here I will present some preliminary 6-eV probe TR-ARPES data acquired at ALLS. In particular, I will show how mid-IR light (in the 150-300 meV photon energy range) transiently modifies the dispersion of the topological surface state of Bi_2Te_3, prototypical 3D topological insulator. Figure 2 displays iso-energy contour maps in the k_x-k_y momentum space at zero pump-probe delays above the equilibrium Fermi level (E=0 eV).

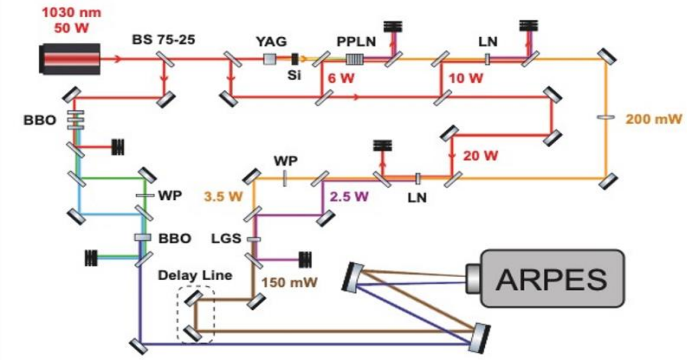

Fig. 1. *Sketch of the optical modules for the generation of near- and mid-infrared pump and 6-eV probe at the TR-ARPES endstation of ALLS.*

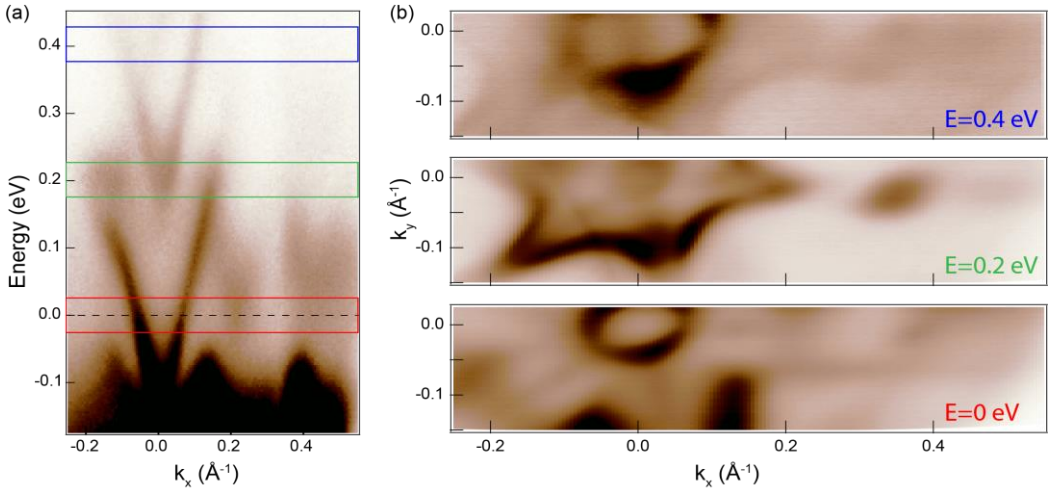

Fig. 2. (a)*: ARPES map of Bi_2Te_3 at zero pump-probe delay upon 300-meV pump excitation.* ***(b)****: Iso-energy contour maps at 0, 0.2, and 0.4 eV above the Fermi level (as highlighted in a), at zero pump–probe delay.*

I will also discuss the capabilities of our state-of-the-art hemispherical analyzer (ASTRAIOS 190, SPECS) that enables the detection of photoelectrons within a 60-degree emission cone without the need of mechanically move the sample.

References

[1] D. Golež, S.K.Y. Dufresne, M.-J. Kim, F. Boschini, H. Chu, Y. Murakami, G. Levy, A.K. Mills, S. Zhdanovich, M. Isobe, H. Takagi, S. Kaiser P. Werner, D.J. Jones, A. Georges, A. Damascelli, A.J. Millis, *Physical Review B* **106,** L121106 (2022).
[2] M. Michiardi, F. Boschini, H.-H. Kung, M.X. Na, S.K.Y. Dufresne, A. Currie, G. Levy, S. Zhdanovich, A.K. Mills, D.J. Jones, J.L. Mi, B.B. Iversen, Ph. Hofmann, A. Damascelli, *Nature Communications* **13**, 3096 (2022)
[3] M. Zonno, F. Boschini, A. Damascelli, *Journal of Electron Spectroscopy and Related Phenomena* **251**, 147091 (2021)
* Acknowledgements: F. Boschini acknowledges support from the Fonds de recherche du Québec – Nature et technologies (FRQNT) and the Natural Sciences and Engineering Research Council of Canada (NSERC)

Ultrafast dynamics and applications of type II Semiconductor heterostructures

Markus Stein[1], Felix Schäfer[1], Daniel Anders[1], K. Volz[2], T. Meier[3], S. Chatterjee[1]
[1] *Justus Liebig University Giessen,35392 Giessen, Germany*
[2] *Philipps University Marburg, 35043 Marburg, Germany*
[3]*Paderborn University, 33098 Paderborn, Germany*

Low-dimensional quantum structures of compound semiconductors such as type-I quantum wells are the backbone of the established optoelectronic devices. Their fundamental properties have been intensely studied for more than half a century [1]. The accompanying immense development in materials quality are indispensable for reliable long term device performance and true scalability, presumably the two prime advantages of semiconductor technology. These developments have been accompanied by stringent development of microscopic theories such as the Semiconductor Bloch Equations [2]. The interplay of experimental and theoretical research has successfully fostered design and understanding of this class of quantum structures. Regardless, even more than two decades old predictions remain discussed as they have not been demonstrated experimentally [3].
More recently, heterostructures featuring type-II band offsets offer additional degrees of freedom in tailoring their optoelectronic response. From a fundamental stand point, these type-II heterostructures offer the potential to investigate charge-transfer-like excitations. Their nonlinear optical response is investigated experimentally using polarization resolved four wave mixing, optical-pump optical-probe, and optical-pump Terahertz-probe spectroscopy. The four-wave mixing data reveal clear signatures which are consistent with of coherent biexcitons obeying the suitable polarization selection rules. Type-I quantum well reference samples show the well-known beating signatures in the transients as well as clear spectral signatures [4]. The latter are also present in type-II samples. However, the smaller exciton and biexciton binding energies infer longer beating times which are not observable due to faster dephasing of type-II exciton coherences.

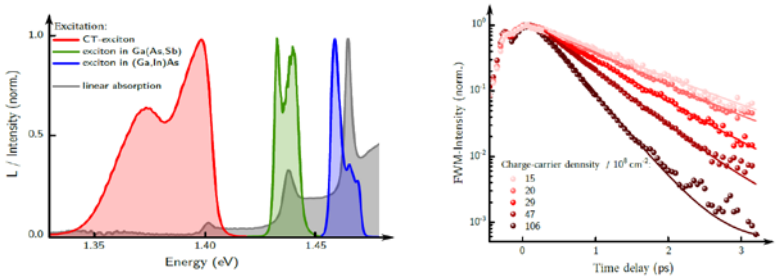

***Fig. 1. Left**: linear absorption spectrum (grey) and shaped pulses tuned resonantly to the CT exciton resonance (red), as well as the Ga(As,Sb) and the (Ga,In)As quantum well exciton resonances, show in green and blue, respectively. **Right**: degenerate transient four-wave mixing (FWM) data for excitation resonant to the CT exciton.*

For applications, such type-II active devices combine the advantages of a spectrally broad, temperature stable efficient gain with the potential for electrical injection pumping. The intrinsic charge-carrier relaxation dynamics limit the feasible repetition rates beyond constraints of cavity design and heat removal. Here, we investigate the initial buildup of gain after optical excitation as well as its recovery after a stimulated emission process in a (Ga,In)As/GaAs/Ga(As,Sb) heterostructure optimized for the near infrared. This experimentally simulates the operation condition of a pulsed laser or semiconductor optical amplifier which are ideally limited by the materials charge-carrier dynamics. The gain bandwidth in these heterostructures exceeds 50 meV full-width-at-half-maximum and should support very temperature stable operation as well as ultrafast pulsing. We use an optical pump - optical probe setup where a first optical pulse injects hot charge carriers that eventually build up spectral gain in the sample. The energies are chosen such to mimic typical electrical injection surplus energies. Subsequently, a second laser pulse tuned to the broad spectral region in which gain is observed is used to stimulate emission and thus eliminate the gain. Analysis of the absorption spectra after stimulated emission reveals gain recovery times in the vicinity of 5 ps [5], which defines a physical limit for the highest laser repetition rate possible with this material system in the range of 100 GHz under a direct electrical injection scheme. The understanding of the ultrafast dynamics of such type-II heterostructures is important for designing and optimizing next generation mid-infrared light sources. Tailoring the band offsets will reduce the emission energies of active devices and is envisioned to reduce if not eliminate any Auger losses. Furthermore, such structures area ideal model systems to study the structure and dynamics of excitations across internal interfaces.

References

[1] J. Shah, Ultrafast Spectroscopy of Semiconductors and Semiconductor Nanostructures, *Springer Series in Solid-State Sciences* **115**, (2013)
[2] M. Lindberg, S. W. Koch, *Physical Review B* **38**, 3342, (1988).
[3] C. Ciuti, C. Piermarocchi, V. Savona, P. E. Selbmann, P. Schwendimann, A. Quattropani. *Physical Review Letters* **84**, 1752 (2000).
[4] M. Fey, M. Stein, C. Fuchs, W. Stolz, K. Volz, S. Chatterjee *Physical Review B* **106** 165303, (2022)
[5] F. Schäfer, M. Stein, J. Lorenz, F. Dobener, C. Ngo, J. T. Steiner, C. Fuchs, W. Stolz, K. Volz, T. Meier, J. Hader, J. V. Moloney, S. W. Koch S. Chatterjee, *Applied Physics Letters* **122**, 082104 (2023).
* Acknowledgment: Financial support from the Deutsche Forschungsgemeinschaft via the Collaborative Research Center No. 223848855-SFB 1083 and European Regional Development Fund (ERDF) through FPG990 0005/2018 is gratefully acknowledged.

Observation of a longer decay time constant and deviation from the Supercollision model of the carriers' cooling in bilayer graphene

A. I. Chatzakis
Texas Tech University, Lubbock, TX 79409, USA

Optical-pump THz-probe spectroscopy is employed to investigate the cooling dynamics of hot carriers in quasi-free standing bilayer epitaxial graphene with hydrogen intercalation. The epitaxial graphene layer on SiC is sitting on top of a graphene-like layer called the buffer layer (BL). About 30% of the carbon atoms in BL are covalently bound with the Si atoms on the SiC surface, which

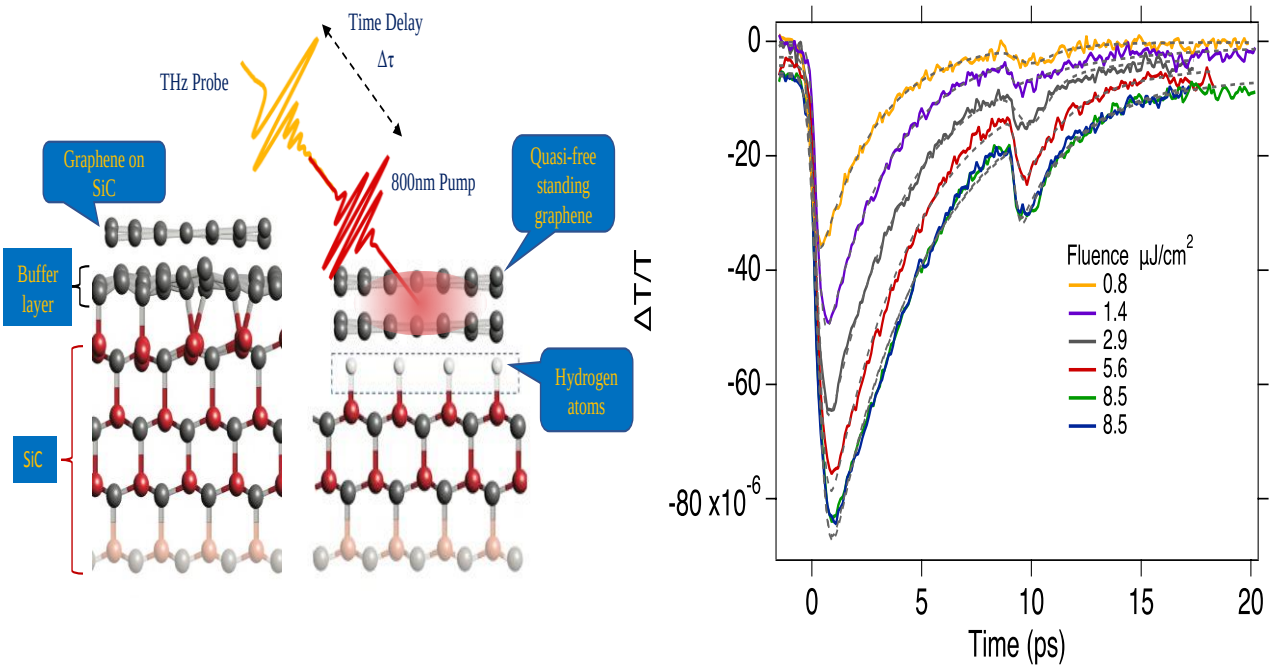

heat diffusion, cooling via optical phonons, and interactions with the substrate phonons. We identify the dominant cooling mechanism of hot carriers and demonstrate (i) that the predictions of the supercollision cooling model significantly deviate from the experimental data and, (ii) that the relaxation of the hot carriers primarily occurs due to electron–optical phonon interactions. Furthermore, the observed experimental dynamics exhibit the expected longer timescales, in the range of 2.6 to 6.4 ps, which increase nonlinearly with excitation intensity. The increased relaxation times are due to the decoupling of the graphene layer from the SiC substrate after hydrogen intercalation which increases the distance between graphene and substrate [3]. In addition, we observe an increase in pump-induced conductivity.

References

[1] C. Riedl, C. Coletti, T. Iwasaki, A. A. Zakharov, U. Starke, *Physical Review Letters* **103**, 246804 (2009).
[2] J. C. W. Song, M. Y. Reizer, L. S. Levitov, *Physical Review Letters* **109**, 106602 (2012).
[3] M. T. Mihnev, F. Kadi, C. J. Divin, T. Winzer, S. Lee, C.-H. Liu, Z. Zhong, C. Berger, W. A. de Heer, E. Malic, A. Knorr' T. B. Norris *Nature Communications* **6**, 8105 (2015).

Controlling THz emission in topological materials

E. E. M. Chia
Nanyang Technological University, Singapore 637371, Singapore

In this talk I will show terahertz (THz) emission data on a few topological materials. In the ferromagnet-semiconductor Co/MoS_2 heterostructure, by making use of the strongly out-of-equilibrium character of the injected spins, we demonstrate a highly-efficient spin injection from a ferromagnet into a semiconductor, thus overcoming the crippling problem of impedance mismatch. Astonishingly, we measure a giant spin current that is orders of magnitude larger than typical injected spin current densities using currently available techniques [1]. In thin polycrystalline films of the centrosymmetric Dirac semimetal $PtSe_2$, we observe a giant and highly tunable THz emission that is rapidly turned on at oblique incidence. Strikingly, we find the THz emission to be locked to both the in-plane photon momentum and polarization state of the incident pump beam, where the THz sign and amplitude are fully controlled by the incident pump polarization, helicity and photon momentum. Moreover, the emitted THz efficiency is two orders of magnitude larger than that of the standard THz-generating nonlinear crystal ZnTe, and approaches that of the record-setting topological material TaAs.

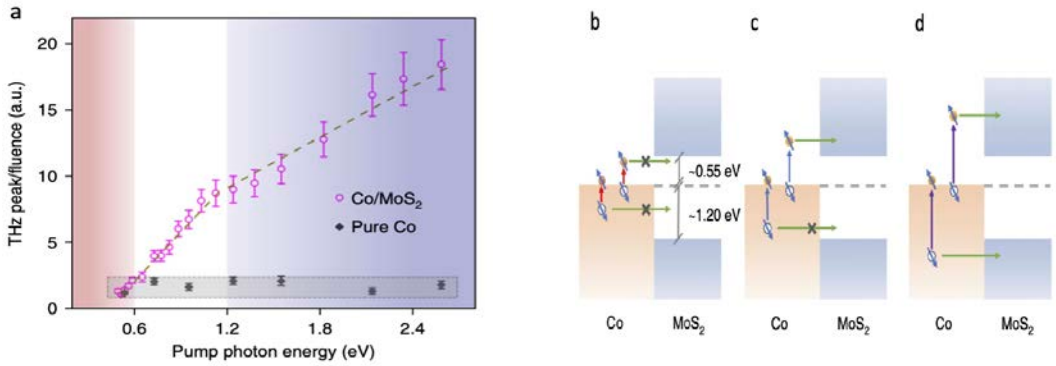

Fig. 1 (a) *(THz peak)/(absorbed fluence) of Co/MoS_2 under different pump wavelengths. The red, white and purple regions represent different spin injection processes illustrated in panels* ***(b), (c)*** *and* ***(d),*** *respectively [1].*

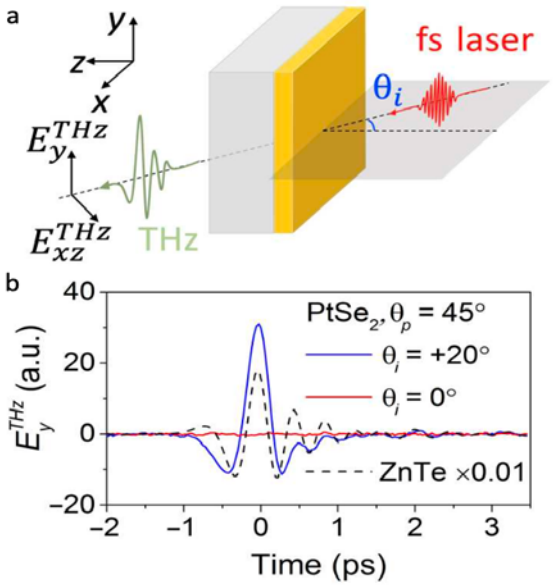

Fig. 2 (a) *Schematic of THz emission setup for Dirac semimetal $PtSe_2$.* ***(b)*** *THz emission amplitude for different incident pump angle [2].*

Our work demonstrates how photon drag activates a rich and pronounced directional optical linearity that are available even in centro-symmetric and polycrystalline Dirac materials [2].

References

[1] L. Cheng, X. Wang, W. Yang, J. Chai, M. Yang, M. Chen, Y. Wu, X. Chen, D. Chi, K. E. J. Goh, J.-X. Zhu, H. Sun, S.Wang, J. C. W. Song M. Battiato, H. Yang, E. E. M. Chia, *Nature Physics* **15**, *347* (2019).
[2] L. Cheng, Y. Xiong, L. Kang, Q. Chang, M. Chen, J. Qi, H. Yang, Z. Liu, J. C. W. Song, E. E. M. Chia, *Science Advances* **9,** 7856 (2023).

Light-enhanced charge density wave coherence in High-temperature superconductor

G. Coslovich
SLAC National Accelerator Laboratory, Menlo Park, California 94720, USA

The use of ultrashort optical and X-ray pulses offers new opportunities to study fundamental interactions in materials exhibiting unconventional quantum states, such as stripes, charge density waves and high-temperature superconductivity. To understand the microscopic interdependence between these order parameters, a probe capable of discerning their interaction on its natural length and time scales is necessary. In this talk, I will focus on high temperature superconductors and recent ultrafast resonant soft x-ray scattering results tracking the transient evolution of charge density wave correlations in $YBa_2Cu_3O_{6+x}$ [1]. In this study, ultrashort infrared pulses produce a non-thermal quench of the superconducting state while X-ray pulses detect the reaction of charge density waves. The response happens on a picosecond timescale and is characterized by a large enhancement of spatial coherence of charge density waves, nearly doubling their correlation length, accompanied by a smaller increase of their amplitude (Fig.1). Such behavior can be reversed at higher fluences and at higher temperatures (above T_C, 65 K) where the photo-induced CDW melting process takes place instead.

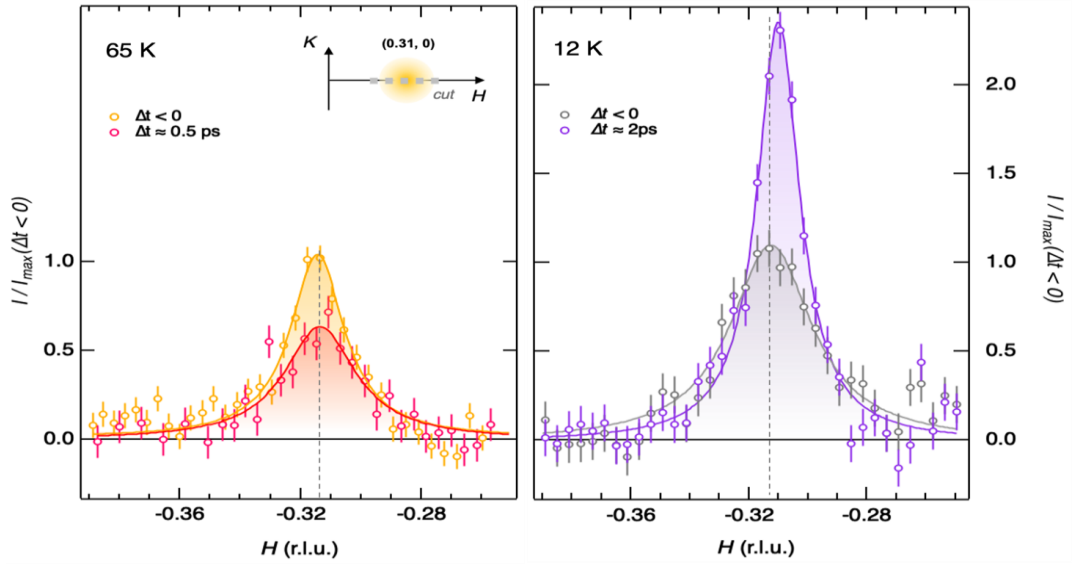

***Fig. 1. Left**: X-ray scattering profile of the CDW along the H direction in reciprocal space at 65 K before (**orange**) and after (**red**) laser excitation. The data show the well-known melting dynamics of the CDW order. **Right**: X-ray scattering profile at 12 K before (**grey**) and after (**purple**) laser excitation, highlighting the light-induced enhancement of CDW correlations. See Ref. [1] for further details.*

This ultrafast snapshot directly reveals the coupling between superconductivity and charge density waves on its natural timescale. It demonstrates that their competition manifests inhomogeneously at the nanoscale level, as disruption of spatial coherence, indicating the role of superconductivity in stabilizing topological defects within charge density waves domains. The study highlights a path for enhancing spatial coherence (order) by using light pulses changing the balance between intertwined orders (Fig.2).

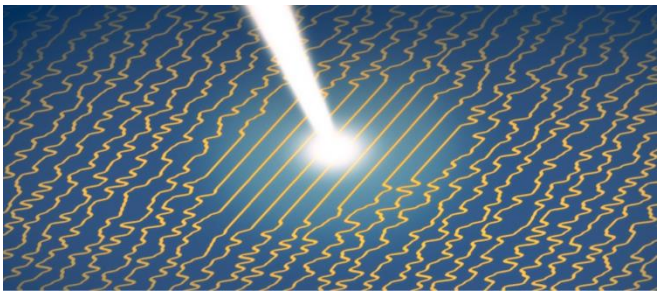

***Fig.2.**Illustration of the light-induced enhanced coherence in a CDW system.(Image credit: Greg Stewart, SLAC)*

In conclusion, I will also discuss ongoing developments at the LCLS to further expand on these results and unlock novel capabilities to control and observe quantum materials with light pulses.

References

[1] S. Wandel, F.Boschini, E. H. da Silva Neto, L. Shen, M. X. Na, S. Zohar, Y. Wang, S. B. Welch, M. H. Seaberg, J. D. Koralek, G. L. Dakovski W. Hettel, M.-F. Lin, S. P. Moeller, W. F. Schlotter, A. H. Reid, M. P. Minitti, T.Boyle, F. He, R. Sutarto, R. Liang, D. Bonn,W. Hardy R. A. Kaindl, D. G. Hawthorn, J.-S. Lee, A. F. Kemper, A. Damascelli, C. Giannetti, J.J. Turner, G. Coslovich, *Science* **376**, 860 (2022).

* Use of the Linac Coherent Light Source (LCLS), SLAC National Accelerator Laboratory, is supported by the U.S. Department of Energy, Office of Science, Office of Basic Energy Sciences under Contract No. DE-AC02-76SF00515.

Ultrafast magnetization reversal driven by circularly-polarized Optical phonons

C.S. Davies[1], F.G.N. Fennema[1], A. Tsukamoto[2], I. Razdolski[3], A.V. Kimel[1], A. Kirilyuk[1]
[1] *Radboud University, 6525 Nijmegen, the Netherlands*
[2]*Nihon University, 101-8360 Tokyo, Japan*
[3]*University of Bialystok, 15-328 Bialystok, Poland*

All-optical switching (AOS) of magnetization – the process through which ultrashort optical pulses reverse magnetic ordering without any bias magnetic fields – offers a promising and potentially disruptive paradigm for future data-storage technologies operating at ultrafast speeds with high efficiency. Multiple avenues for AOS have emerged in recent years [1] ranging from thermal single-shot exchange-driven switching in ferrimagnets [2] and helicity-dependent switching in ferromagnets [3] to non-thermal switching mechanisms driven by the resonant excitation of electronic [4] or phononic [5] subsystems. Here, we explore further how the resonant excitation of infrared-active optical phonons can switch magnetization. Specifically, using narrow-band transform-limited infrared optical pulses delivered by the free-electron laser facility FELIX, with frequency ranging between 6 THz and 40 THz (wavelength 7.5-50 μm) [6], we drive transverse optical phonons at resonance in different systems. We have recently discovered that optical phonons in paramagnetic substrates can, when driven at resonance by circularly-polarized infrared pulses, realize directional AOS in an adjacent film [7]. In our experiments, we irradiate thin GdFeCo films mounted on fused-silica, sapphire and silicon substrates with circularly-polarized optical pulses. The resulting helicity-dependent magnetic switching scales in efficiency with the transverse optical phonon spectrum characteristic not of the metal but rather the substrate (see Fig. 1).

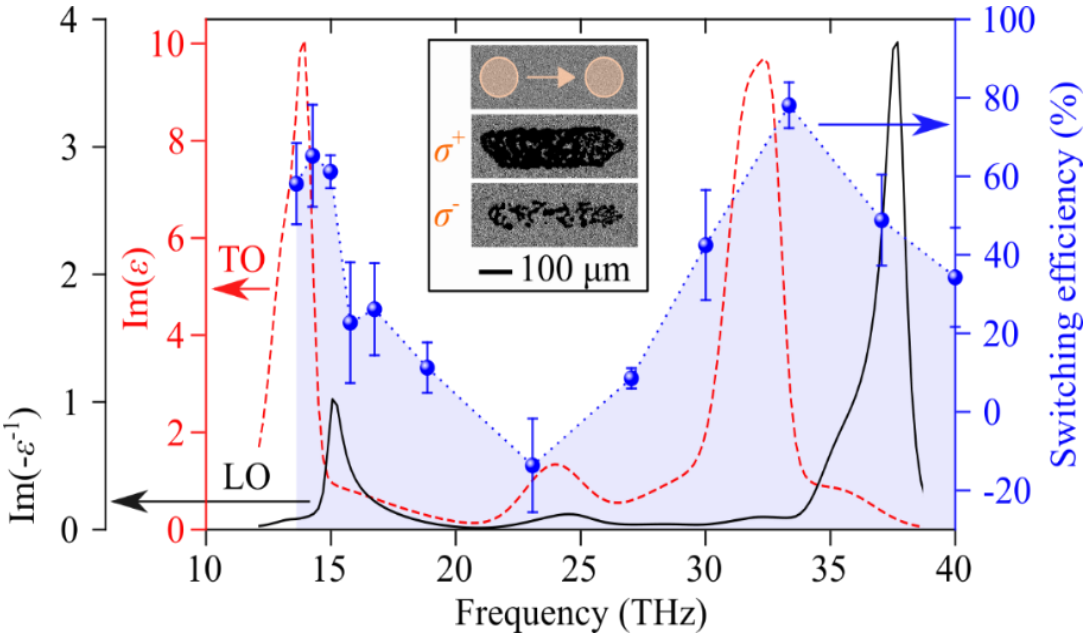

Fig. 1 *Spectral dependence of helicity-dependent switching of magnetization in a nanolayer of GdFeCo mounted on a fused-silica substrate (**blue line,** typical images shown in inset). Also overlaid is the spectrum of longitudinal and transverse optical phonons characteristic of the fused-silica substrate (**black** and **red lines** respectively).*

Since this approach is based on the excitation of phonons in a dissimilar material, it could be universally applied to manipulate magnetic ordering in any conceivable system.

References

[1] A. Kirilyuk, A.V. Kimel, T. Rasing, *Review of Modern Physics* **82**, 2731 (2010).
[2] C. S. Davies, T. Janssen, J. H. Mentink, A. Tsukamoto, A. V. Kimel, A. F. G. van der Meer, A. Stupakiewicz, A. Kirilyuk, *Physical Review Applied* **13**, 024064 (2020).
[3] C.-H. Lambert, S. Mangin, B. S. D. Ch. S. Varaprasad, Y. K. Takahashi, M. Hehn, M. Cinchetti, G. Malinowski, K. Hono, Y. Fainman, M. Aeschlimann, E. E. Fullerton, *Science* **345**, 1337 (2014).
[4] A. Stupakiewicz, K. Szerenos, D. Afanasiev, A. Kirilyuk, A. V. Kimel, *Nature* **542**, 71 (2017).
[5] A. Stupakiewicz, C. S. Davies, K. Szerenos, D. Afanasiev, K. S. Rabinovich, A. V. Boris, A. Caviglia, A. V. Kimel, A. Kirilyuk *Nature Physics* **17**, 489 (2021).
[6] G. M. H. Knippels X. Yan, A. M. MacLeod, W. A. Gillespie, M. Yasumoto, D. Oepts, A. F. G. van der Meer, *Phyical Review Letters* **83**, 1578 (1999).
[7] C. S. Davies, F. G. N. Fennema, A. Tsukamoto, I. Razdolski, A. V. Kimel, A. Kirilyuk, *submitted* (2022).

Effects of Floquet engineering on the coherent exciton Dynamics in monolayer WS_2

M.A. Conway[1], S.K. Earl[1], T.-H.-Y. Vu[2], M.S. Fuhrer[2], M.T. Edmonds[2], J.A. Davis[1]
[1]*Swinburne University of Technology, Hawthorn VIC3122, Australia*
[2] *Monash University, Clayton VIC3800, Australia*

Coherent light-matter interactions offer a versatile means to optically control nonlinear phenomena [1, 2]. In particular, Floquet-engineering can utilise the periodicity of a light-field to alter the properties of quantum-matter. In 2D materials, interactions between the n-photon-dressed band replicas, called Floquet-Bloch bands, can facilitate ultrafast manipulation of excitonic properties. A simple example of this for a two-level system is the AC-Stark effect(Fig. 1(a)) [3, 4]. Semiconducting monolayer transition metal dichalcogenides (TMDCs) are ideal platforms for band structure engineering as they possess an optically accessible bandgap with intrinsic, but opposite, Berry phase at the K and K′-valleys. Combining the nontrivial Berry phase with appreciable spin-orbit splitting of atomic orbitals, these time-reversal symmetric valleys couple to different optical selection rules: K-valley excitons (X_K) are dressed by left-circularly polarized light (σ^-), while K′-valley excitons ($X_{K'}$) are dressed by right-circularly polarized light (σ^+). When excited by linearly polarized light, the superposition of σ^+ and σ^- polarized components that comprise the light-field prepare a coherent superposition of excitons in the K- and K′-valley [5]. Optical manipulation of this inter-valley exciton coherence, $|X_K\rangle\langle X_{K'}|$, has been indicated in experiments driving a valley selective AC-Stark shift to break the valley degeneracy. This causes the phase of the inter-valley exciton coherence to rotate, resulting in a measurable rotation of polarization of the measured photoluminescence[6]. However, there are ambiguities in these time-integrated photoluminescence measurements; whether or not the process proceeds adiabatically cannot be resolved; and subsequent investigations of a Bloch-Siegert effect (Fig. 1(b)) suggest there is a counteracting shift induced in the opposite valley which is not separable from the dominant AC-Stark effect (Fig. 1(a)) [7]. Here we utilise multidimensional coherent spectroscopy (MDCS) [8] to directly measure the pump induced changes to the amplitude and phase of a coherence in monolayer WS_2. To isolate the influence of the AC-Stark and Bloch-Siegert effects on the signal phase, φ_{sig}, we can measure a pump induced phase rotation of the 1Q coherence during t_1, wherein $\varphi_{sig} \propto -\omega_1 t_1$: After the arrival of the σ^+-polarized first pulse (labelled k_1) a 1Q-coherence between the ground state, g, and the K'-valley exciton state, $X_{K'}$, will be created. This $|g\rangle\langle X_{K'}|$ 1Q-coherence evolves with a frequency given by the A-exciton energy in monolayer WS_2 of 2.07 eV, over the t_1 time period, until the second pulse arrives. Placing a red-detuned optical pump during t_1 that is co- or cross-circularly polarized relative to k_1, we can induce an additional phase rotation of the signal due to the energy shift induced by the AC-Stark or Bloch-Siegert effect, respectively. The evolution of the measured phase difference as a function of t_1, obtained by taking a slice at the exciton energy, is shown in Fig. 1(c). For a σ^+ polarized pump during t_1 we induce an appreciable change in the phase of the $|g\rangle\langle X_{K'}|$ coherence up to a π phase shift (red lines). With a σ^- polarized pump a much smaller phase shift is observed (blue lines). In the case of the σ^+ polarized pump the polarization is the same as the $|g\rangle\langle X_{K'}|$ coherence induced by k_1. In this configuration, the AC-Stark effect will blue-shift the $X_{K'}$ state [3, 4], which causes the phase to shift over the pulse duration, as measured. Conversely, with the σ^- polarized pump the Stark shift is occurring in the X_K state, which should not affect the measured phase. The Bloch-Siegert effect will, however, cause a blue-shift of the X_K state [7], and is the source of the phase shift observed in this case. For $250 < t_1 < 400$ the measured phase shift increases as the k_1 pulse is moved through the pump pulse. The rate of change of the phase is determined by the induced energy shift, i.e. the coherence evolves as $e^{i\Delta\omega t_1}$. The time dependent energy shift can thus be determined by differentiating the measured phase shift with respect to t_1. This is shown in Fig. 1(d) for a σ^+ polarized pump in t_1. A Gaussian fit to the instantaneous Stark shift (red lines) closely resembles the temporal profile of the measured cross-correlation between the pump and the MDCS excitation beams (black line). This indicates that within the temporal resolution afforded by the 31 fs k_1 pulse the AC-Stark effect follows the instantaneous intensity of the pump. The peak Stark shift measured is > 16meV for the highest pump fluence of 751.7 $\mu J/cm^2$.

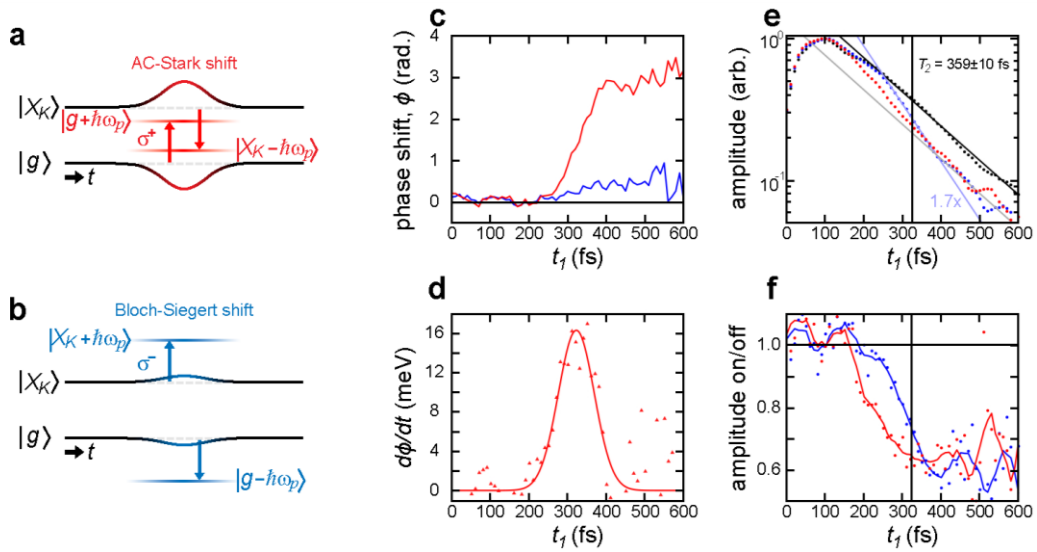

Fig. 1. (a) *and* ***(b)*** *schematically represent an energy diagram of the K'-valley as a function of time t, upon arrival of the red-detuned σ^+ and σ^- polarised pump an AC-Stark or Bloch-Siegert blue-shift is induced, respectively. (c) Phase dynamics at the exciton energy driven by a σ^+ and σ^- circularly polarized pump arriving during t_1;* ***(d)*** *derivative of the phase shift φ for the σ^+ pump case in* ***(c)*** *yields the instantaneous Stark shift, dφ/dt* ***(e)*** *signal amplitude integrated around the exciton energy as a function of t_1 with a log y-axis. Over pump duration the amplitude decreases due to power broadening to which we can fit a slope with a decay rate 1.7 times the unpumped decay;* ***(f)*** *signal amplitude in* ***(e)*** *of the pumped data divided by the unpumped reference highlights the flat region beyond the pump duration. The lines follow the smoothed data points.*

The smooth evolution of the phase through the pump-induced Stark shift suggests the process is adiabatic. On the other hand, however, Fig. 1(e) shows the normalized signal amplitude integrated around the exciton energy, as a function of t_1, in which a decrease in the signal amplitude can be seen over the pump duration, suggesting the pump causes a loss of coherence. After the pump pulse, the decay rate once again matches the unpumped data, as indicated by the slope of the data and fits in Fig. 1(e). We rule out the possibility that the loss of coherence is due to the red-detuned pump exciting carriers through two-photon absorption as the increased scattering and faster decoherence would persist as long as the photoexcited carriers remain, which is expected to be well beyond the measurement time. Thus, we conclude that the decrease of the macroscopic coherence is a field driven effect persisting only over the finite pump duration.

Varying the intensity of the pump pulse shows that the magnitude of the added coherence loss is linearly proportional to the pump fluence and is quantitatively consistent with power broadening. In the case of short pulses, where the pulse duration is less than the decoherence time, quantifying the power broadening can be more challenging [10]. An experimental estimate of the average power broadening throughout the pulse is obtained from the data in Fig. 1(e). A linear fit to the data (on the semi-log axes) over the duration of the pulse yields a decay rate that is 1.7 times faster than the unpumped decay. This suggests an average power broadened linewidth of ≈5 meV.

By using multidimensional coherent spectroscopy (MDCS) to create excitonic coherences in monolayer WS_2 we have been able to measure the changes to the amplitude and phase induced through a process of Floquet engineering. While the average phase evolves smoothly, and follows what would be expected from Floquet theory, even though the pulses are short, there is a loss in macroscopic coherence due to power broadening caused by the electric field of the pump pulse. This places some limitations on the possible use of this approach for applications requiring adiabatic control, but also points to means by which the effects can be minimized. The experiments described here will provide a valuable tool to quantify the effectiveness of such approaches, including suggestions for inducing proposals to induce spectral narrowing with shaped pump pulses.

References

[1] J. W. McIver, B. Schulte, F.-U. Stein, T. Matsuyama, G. Jotzu, G. Meier, A. Cavalleri, *Nature Physics.* **16**, 38 (2020).
[2] Y. Kobayashi, C. Heide, A.C. Johnson, V. Tiwari, F. Liu, D.A. Reis, T.F. Heinz, S. Ghimire, *Nature Physics* **19**, 171 (2023).
[3] J. Kim, X. Hong, C Jin, S-F Shi, C-Y.S. Chang, M-H Chiu, L-J Li, F. Wang, *Science* **346**, 1205 (2014).
[4] E.J. Sie, J.W. McIver, Y-H. Lee, L. Fu, J. Kong, N. Gedik, *Nature Materials* **14**, 290-294 (2015).
[5] A. M. Jones, H. Yu, N.J. Ghimire, S. Wu, G. Aivazian, J.S. Ross, B. Zhao, J. Yan, D.G. Mandrus, D. Xiao, W. Yao, X. Xu, *Nature Nanotechnology* **8**, 634 (2013).
[6] Z. Ye, D. Sun, T. F. Heinz, *Nature Physics*. **13**, 36 (2017).
[7] E.J. Sie, C H Lui, Y-H Lee, L. Fu, J Kong, N. Gedik, *Science* **355**, 1066 (2017).
[8] J. O. Tollerud, J. A. Davis, *Progress in Quantum Electronics* **55**, 1 (2017)
[9] M.A. Conway, S.K. Earl, J.B. Muir, T-H-Y Vu, J.O. Tollerud, K. Watanabe, T. Taniguchi, M.S. Fuhrer, M.T. Edmonds, J.A. Davis, *arXiv:10.48550/arXiv.*2301.12599 (2023)
[10] N.V. Vitanov, B.W. Shore, L. Yatsenko, K. Böhmer, T. Halfmann, T. Rickes, K. Bergmann, *Optics Communications* **199**, 117-126 (2001).
[11] I.I. Boradjiev, N.V. Vitanov, *Optics Communications* **288**, 91(2013).

Ultrafast dynamics from the perspective of resonant inelastic X-ray scattering

M. P. M. Dean
Brookhaven National Laboratory, Upton, NY 11973, USA

Resonant inelastic x-ray scattering (RIXS) is a state-of-the-art spectroscopic technique with unique capabilities for probing a wide variety of electronic excitations in quantum materials [1]. The advent of x-ray free electron lasers has opened new opportunities to apply this technique to transient states, as demonstrated by pioneering experiments that measured the short-range magnetic correlations in photo-excited iridates [2, 3]. It has long been recognized that very strong mixing or "hybridization" between Cu and O orbitals, coming from small charge-transfer energy Δ, is crucial for the physics of cuprates. Controllably modifying Δ represents an attractive potential means to modify the properties of correlated materials. In this talk, I will address the prospects of using RIXS to probe the charge transfer properties of quantum materials. Figure 1 illustrates the use of O K-edge RIXS to probe the charge-transfer energy and hybridization in quantum materials and shows the different regimes of a charge-transfer insulator, a mixed charge-transfer/Mott-Hubbard insulator, and a Mott-Hubbard insulator.

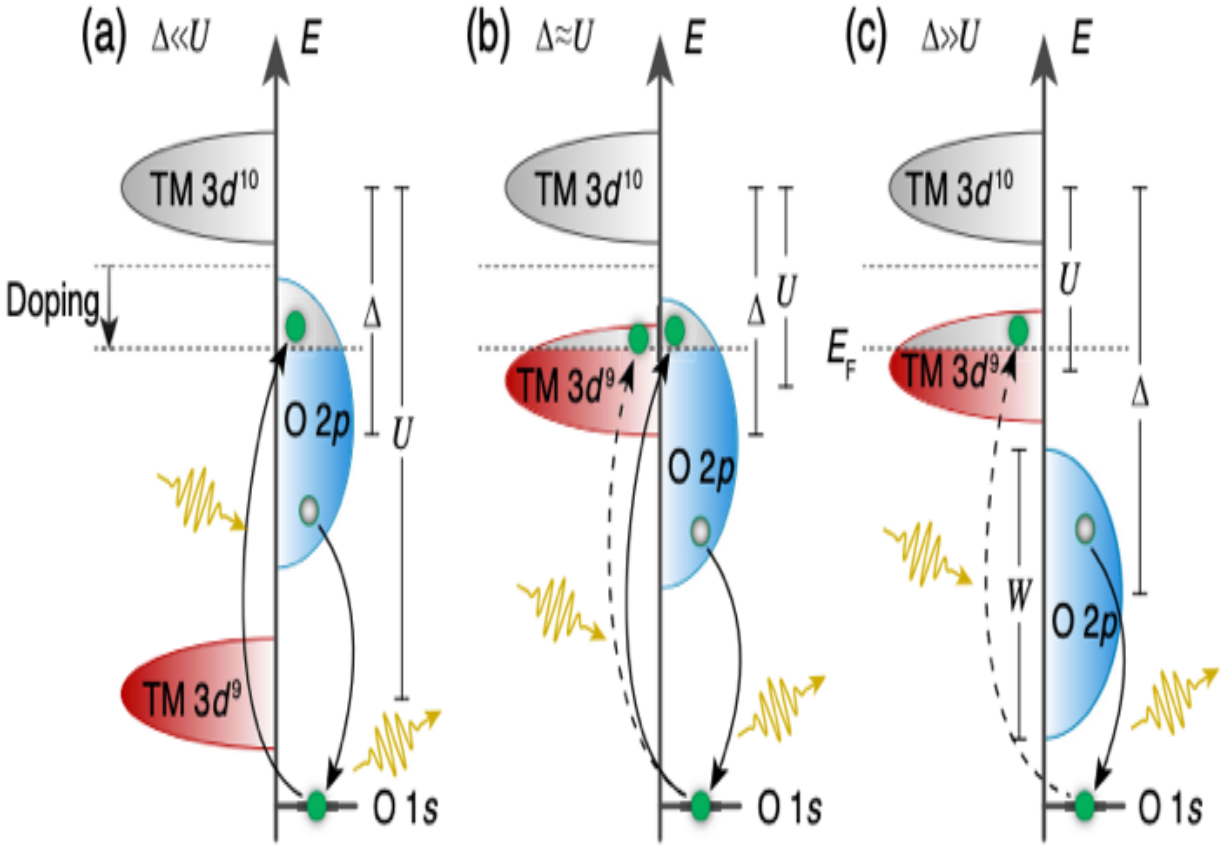

Fig. 1. *Schematic of the O K edge RIXS process.* ***(a)–(c)****RIXS processes for different values of the Hubbard U and charge-transfer energy Δ. For a charge-transfer insulator (Δ ≪ U), the doped holes are mostly in the oxygen 2p orbitals, while in a Mott-Hubbard insulator (Δ ≫ U), the doped holes mainly occupy the TM 3d state. In the mixed charge-transfer/Mott-Hubbard regime (Δ ∼ U), the doped holes are spread among both the TM and oxygen sites. Arrows show examples of x-ray transition pathways, which, because of x-ray dipole selection rules, can involve either O states or TM-O hybridized states, making this process ideal to distinguish situations* ***(a)–(c)****.*

Thus far, we have managed to apply RIXS to study charge transfer properties in equilibrium and have used it to solve several open problems in the physics of the recently discovered low valence superconductors nickelates and how they relate to cuprates. Some important questions include: Do these materials have appreciable oxygen charge-transfer character and superexchange akin to the cuprates or are they in a distinct Mott-Hubbard regime where oxygen plays a minimal role and superexchange is negligible?

Figure 2 illustrates the use of O K-edge RIXS to quantify the role of oxygen in these materials in which we compare the low valence nickelate $La_4Ni_3O_8$ to prototypical cuprate $La_{2-x}Sr_xCuO_4$. As expected, the cuprate lies deep in the charge-transfer regime of the Zaanen-Sawatzky-Allen (ZSA) scheme. The nickelate, however, is not well described by either limit of the ZSA scheme and is found to be of mixed charge-transfer–Mott-Hubbard character with the Coulomb repulsion U of similar size to the charge-transfer energy Δ. Nevertheless, the transition-metal-oxygen hopping is larger in $La_4Ni_3O_8$ than in $La_{2-x}Sr_xCuO_4$, leading to a significant superexchange interaction and an appreciable hole occupation of the ligand O orbitals in $La_4Ni_3O_8$ despite its larger Δ [4]. This explains our prior direct measurements of magnetic exchange in this material [5].

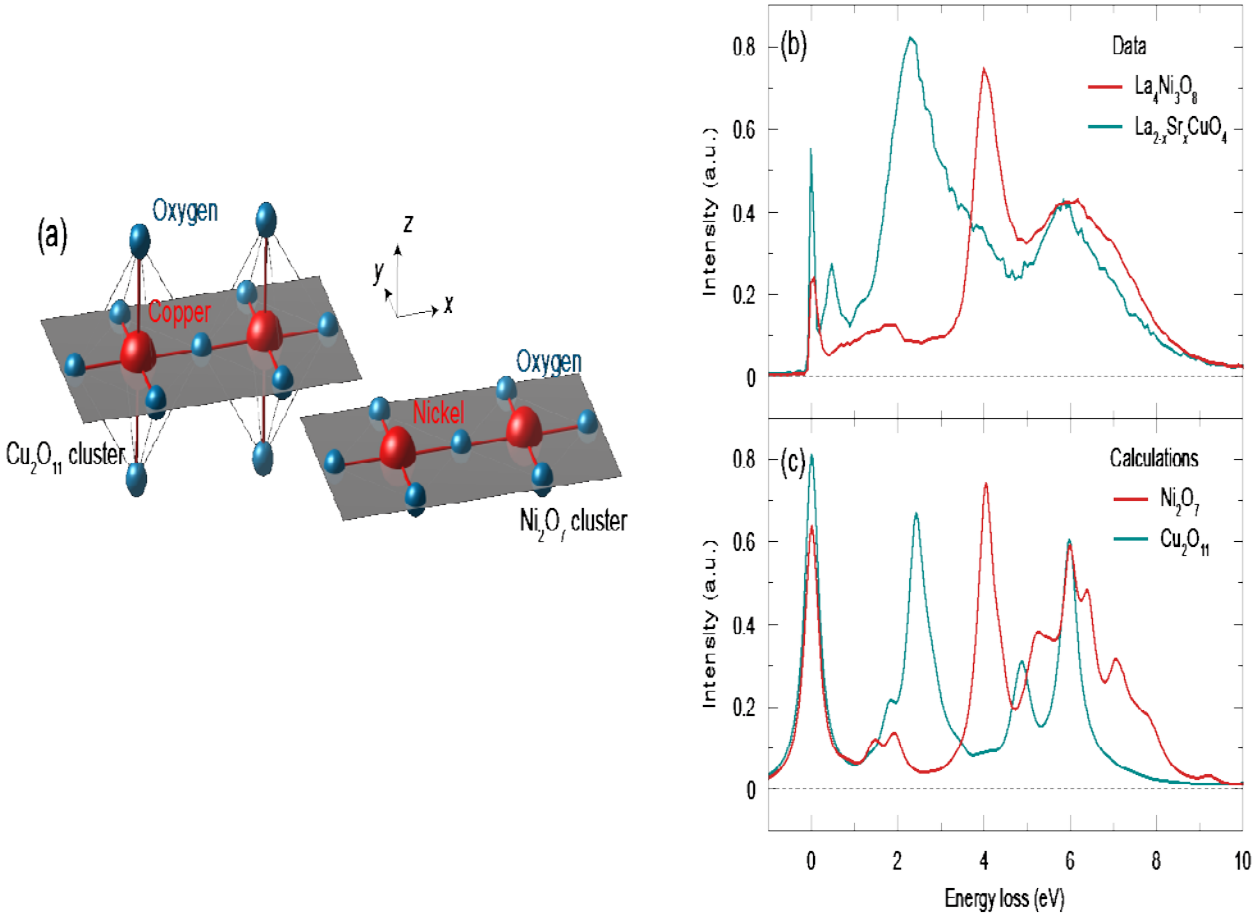

Fig. 2. *Cluster exact diagonalization results.* ***(a)*** *Sketch of the clusters used in the case of the cuprates and nickelates.* ***(b)*** *Measured O K-edge RIXS spectra for $La_{2-x}Sr_xCuO_4$ and $La_4Ni_3O_4$.* ***(c)*** *Calculated spectra for these materials. The feature at 0.5 eV in the $La_{2-x}Sr_xCuO_4$ sample is known to come from a plasmon, so is not expected to appear in our model calculations.*

I will end the talk by discussing how to extend this approach to study charge density waves in these materials [6] and prospects to ultrafast pump-probe measurements of this type.

References

[1] Y. Cao, D.G. Mazzone, D. Meyers, J.P. Hill, X. Liu, S. Wall, M.P.M. Dean, *Philosophical Transactions of the Royal Society* A **377**, 2145 (2019).

[2] M. P. M. Dean, Yue Cao, X. Liu, S. Wall, D. Zhu, R. Mankowsky, V. Thampy, X. M. Chen, J. G. Vale, D. Casa, J. Kim, A. H. Said P. Juhas, R. Alonso-Mori, J. M. Glownia, A. Robert, J. Robinson, M. Sikorski, S. Song, M. Kozina, H. Lemke, L. Patthey, S. Owada T. Katayama, M. Yabashi, Y. Tanaka, T. Togashi, J. Liu, C. R. Serrao, B. J. Kim, L. Huber, C.-L. Chang, D. F. McMorrow, M. Först J. P. Hill, *Nature Materials* **15**, 601(2016).

[3] D. G. Mazzone, D. Meyers, Y. Cao, J. G. Vale, C. D. Dashwood, Y.Shi, A. J. A. James, N. J. Robinson, J. Lin, V. Thampy, Y. Tanaka A. S. Johnson, H. Miao, R.Wang, T. A. Assefa, J. Kim, D. Casa, R. Mankowsky, D.Zhu, R. Alonso-Mori, S. Song, H. Yavas, T.Katayama, M. Yabashi, Y. Kubota, S. Owada, J. Liu, J. Yang, R. M. Konik, I. K. Robinson, J. P. Hill, D. F. McMorrow, M. Först, S. Wall, X. Liu M. P. M. Dean, *Proceedings of the National Academy of Sciences* **118**, e2103696118 (2021).

[4] Y. Shen, J. Sears, G. Fabbris, J. Li, J. Pelliciari, I. Jarrige, Xi He, I. Bozovic, M. Mitrano, Junjie Zhang, J. F. Mitchell, A. S. Botana, V. Bisogni M. R. Norman, S. Johnston, M. P. M. Dean, *Physical Review* X **12**, 011055 (2022)

[5] J. Q. Lin, P. Villar Arribi, G. Fabbris, A. S. Botana, D. Meyers, H. Miao, Y. Shen, D. G. Mazzone, J. Feng, S. G. Chiuzbaian, A. Nag A. C. Walters, M. Garcia-Fernandez, Ke-Jin Zhou, J. Pelliciari, I. Jarrige, J. W. Freeland, Junjie Zhang, J. F. Mitchell, V. Bisogni, X. Liu M. R. Norman, M. P. M. Dean, *Physical Review Letters* **126**, 087001 (2021)

[6] Y. Shen, J. Sears, G. Fabbris, J. Li, J. Pelliciari, M. Mitrano, W. He, Junjie Zhang, J. F. Mitchell, V. Bisogni, M. R. Norman, S. Johnston M. P. M. Dean, *Physical Review* X **13**, 011021 (2023).

Non-equilibrium superconductivity in a prototype two-band Superconductor MgB_2 driven by narrow-band THz pulses

S. Sobolev[1], A. Lanz[1], T. Dong[1,2], A. Pokharel[1], A. Pashkin[3], S. Winnerl[3], M. Helm[3], V.V. Kabanov[2]
T-Q. Xu[4], Y. Wang[4], Z. Z. Gan[4], L.Y. Shi[2], N-L. Wang[2], J. Demsar[1]
[1] *Johannes Gutenberg-University Mainz, 51099 Mainz, Germany*
[2] *Peking University, Beijing 100871, China*
[3] *Jozef Stefan Institute, 1000 Ljubljana, Slovenia*
[4] *Helmholtz-Zentrum Dresden-Rossendorf, 01328 Dresden, Germany*

Excitation of a superconductor (SC) with a low energy electromagnetic pulse may lead to a non-equilibrium state, which may profoundly differ from a quasi-thermal one, driven by optical excitation. Such a non-equilibrium may be especially pronounced in multi-band superconductors, such as MgB_2. Here, we report on studies of the dynamics of the SC order in ultra-clean thin films of MgB2 [1], the prototype two-band SC with two distinct superconducting gaps opening in the two bands with weak interband coupling [2,3]. We performed systematic time-resolved studies of gap dynamics following excitation with intense narrow-band THz pulses with photon energies tuned between the two superconducting gaps. We demonstrate that the temperature and excitation density dependent dynamics qualitatively follows the behavior predicted by the phenomenological Rothwarf-Taylor model for dynamics in a single gap BCS superconductor [4]. This implies strong coupling between the two condensates on the ps timescale. Tracking the dependence of the amplitude of the THz driven gap suppression, however, displays a pronounced minimum near ~ 0.6 T_c (see Fig. 1). This cannot be accounted by the phenomenological model.

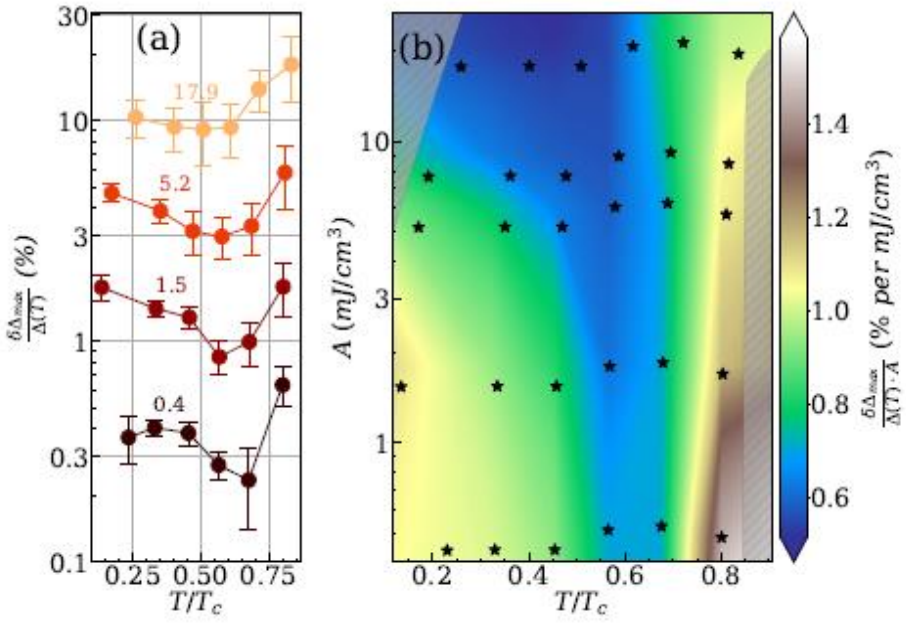

Fig. 1. (a)*: The amplitude of photoinduced suppression of the effective gap (D) as a function of temperature and absorbed energy density, A (mJ/cm^3), when pumping with 2.7 THz narrow-band THz pulses.* ***(b)*** *Photoinduced suppression amplitudes normalized to A presented in the contour plot. Star-like marks in the color plot represent the data points. Areas that could not be accessed in the experiment are masked with grey.*

Comparison of the results to those obtained by excitation with near-infrared pulses suggests that excitation with narrowband THz pulses results in long-lived (100 ps timescale) non-thermal quasiparticle distribution, which gives rise to Eliashberg-type enhancement of superconductivity [5,6], competing with pair-breaking.

References

[1] S. Kovalev, T. Dong, L-Y. Shi, C. Reinhoffer, T-Q. Xu, H-Z. Wang, Y. Wang, Z-Z. Gan, S. Germanskiy, J-C. Deinert, I. Ilyakov P.H.M. van Loosdrecht, D. Wu, N-L. Wang, J. Demsar, Z. Wang, *Physical Review B* **104**, L140505 (2021).
[2] A.Y. Liu, I.I. Mazin, J. Kortus, *Physical Review Letters* **87**, 087005 (2001).
[3] S. Souma, Y. Machida, T. Sato, T. Takahashi, H. Matsui, S.-C. Wang, H. Ding, A. Kaminski, J. C. Campuzano, S. Sasaki, K. Kadowaki, *Nature* **423**, 65-67 (2003).
[4] V.V. Kabanov, J Demsar, D Mihailovic, *Physical Review Letters* **95**, 147002 (2005).
[5] G.M. Eliashberg, *Journal of Experimental and Theoretical Physics-JETP Letters* **11**, 114 (1970).
[6] M. Beck, I. Rousseau, M. Klammer, P. Leiderer, M. Mittendorff, S. Winnerl, M. Helm, G. N. Gol'tsman, J. Demsar, *Physical Review Letters.* **110**, 267003 (2013).

* Acknowledgement(s): This work was funded by the Deutsche Forschungsgemeinschaft (DFG, German Research Foundation) Grant No. TRR 173-268565370 (project A05) and TRR 288−422213477 (project B08). T.D. acknowledges support by the Alexander Humboldt Foundation.

Atomic layer-controlled nonlinear THz valleytronics in Semi-metal and semiconductor $PtSe_2$

S. S. Dhillon
Paris-Sorbonne Université, 75005 Paris, France

Platinum diselenide (PtSe2) is a promising two-dimensional (2D) material for the terahertz (THz) range as, unlike other transition metal dichalcogenides (TMDs), its bandgap can be uniquely tuned from a semiconductor in the near-infrared to a semimetal with the number of atomic layers. This gives the material unique THz photonic properties that can be layer-engineered. Here, we demonstrate that a controlled THz ultrafast nonlinearity - tuned from monolayer to bulk $PtSe_2$ - can be realised in $PtSe_2$ through the generation of ultrafast photocurrents and the engineering of the bandstructure valleys. Further, we show layer dependent circular dichroism, where the sign of the ultrafast currents can be controlled through the excitation of different bandstructure valleys. As well as showing that PtSe2 is a promising material for THz generation through layered optical nonlinearities, this work opens up new class of circular dichroism materials, beyond the monolayer limit that has been the case of traditional TMDs, and impacting a range of domains from THz valleytronics, THz spintronics to harmonic generation. Over the past few years, a large number of 2D transition metal dichalcogenides (TMDs) semiconductors have been studied, with unique bandstructures and distinct properties from their bulk counterparts [1]. The terahertz (THz) spectral region, however, remains relatively unexplored for novel TMD applications since most TMDs have tunable bandgap energies residing in the optical region. However, a newly discovered TMD material, platinum diselenide ($PtSe_2$), has sparked considerable interest. Unlike other TMDs, its bandgap can be tuned from a semiconductor in the near-infrared to a semimetal depending on the number of atomic layers, making it an attractive THz candidate [2]. Although THz emission time-domain spectroscopy (TDS) has provided valuable insights into transport phenomena in 2D materials, the transition between semiconductor and semimetal behavior and their effects on THz photocurrents and nonlinearities has not been studied in a single material system. These phenomena can be explored in $PtSe_2$ owing to its layer-controlled bandgap, large electronic mobilities, and tunability from a semiconductor to a Dirac semimetal [3]. This also opens perspectives for functionalizing THz emission properties with number of Atomic Layers. Very recent studies have investigated THz photocurrents in $PtSe_2$ but only for a specific thickness, limiting the understanding of the effect of the bandstructure. Further, these studies have assumed an entirely centrosymmetric nature and neglected the effect of the substrate [4]. The latter is primordial to consider in 2D materials, such that the origin of the generated photocurrents can be understood in the context of the layer-dependent bandstructure. Figure 1a,b shows the principle of our approach, where we exploit the layer-dependent energy gaps and the valley properties of $PtSe_2$.

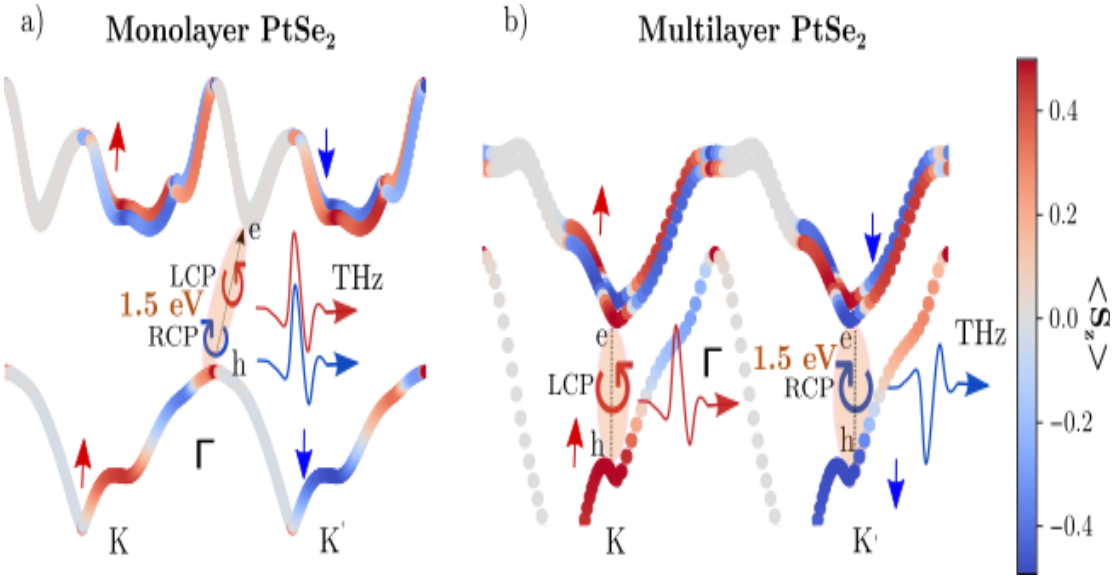

***Fig. 1**: **Schematic of helicity-dependent generation of THz photocurrents in substrate-coupled $PtSe_2$.** Simulated spin-resolved band structure (**red** for spin up and **blue** for spin down) of **a)** ML and **b)** multilayer $PtSe_2$ on a substrate under the circular **right** (RCP) and **left** (LCP) femtosecond excitation pulse at 1.5 eV. For the ML, indirect interband excitations around Γ point (**orange**) are possible, whilst, for multilayer $PtSe_2$, direct interband transitions in the vicinity of K(K') under the circular left (**right**) polarized light can be excited.*

It shows the simulated spin-resolved bandstructure for the two extremes of monolayer (ML) and multilayer $PtSe_2$ on a substrate. The $PtSe_2$ is excited with an optical pulse at 1.5 eV, generating ultrafast THz photocurrents that radiate as a short THz pulse. In the ML case, the states at the K points are not accessible for photon energies of 1.5 eV, and the interband response is governed by (indirect) transitions around the Γ point. Here the bands are not spin-polarized and thus the optical absorption is not selective to a specific circular polarization (LCP or RCP) of the incident light. However, this situation changes drastically with multilayer $PtSe_2$ since the material slowly becomes semi-metallic with an increasing number of layers, and the interband transitions at the K points become accessible for photon energies of 1.5 eV, dominating the optical response. Through symmetry breaking owing to the substrate, K and K′ points have a strong and opposite spin nature that results in a strong circular dichroism (CD) in $PtSe_2$ i.e. interband transitions in the vicinity of the K(K′) points couple exclusively to LCP (RCP) light. We show that this results in the generation of THz photocurrents and the resulting THz emission with opposite signs when excited with LCP or RCP light [5]. To highlight the observed trends for different $PtSe_2$ thicknesses under circularly polarized light, the linear effects were extracted as $(E_{\circlearrowleft} + E_{\circlearrowright})/2$ and the circular effects as $(E_{\circlearrowleft} - E_{\circlearrowright})/2$ from the experimental measurements of the THz electric field (E) with LCP ($\circlearrowleft$) and RCP ($\circlearrowright$) excitations. These are shown in Figure 2 for 3.85 nm and 38.5 nm $PtSe_2$ for TE polarizations. As expected a circular effect is only observed for the thickest films. This further highlights the strong effect of the $PtSe_2$ bandstructure on the THz properties.

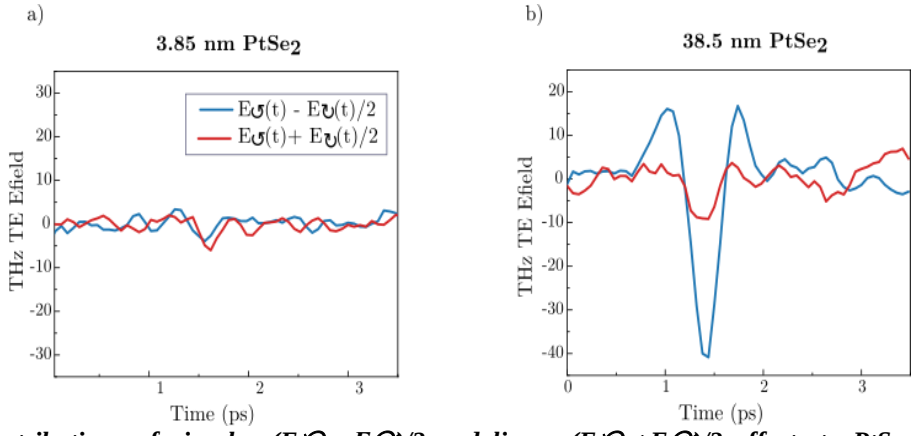

Fig 2*: Contributions of circular ($E_{\circlearrowleft} - E_{\circlearrowright}$)/2 and linear ($E_{\circlearrowleft} + E_{\circlearrowright}$)/2 effects to $PtSe_2$ THz emission.** *Circular and linear effects for THz TE emission for* ***a) *3.85 nm $PtSe_2$ and* ***b)*** *38.5 nm $PtSe_2$ shown by blue and red lines, respectively, are obtained from measurements in THz-TDS reflection geometry with LCP and RCP excitations.*

This work has investigated the first observation of layer-dependent, polarization and valley-selective excitation of ultrafast photocurrents in ML to multilayer $PtSe_2$. We show the amplitude and phase-resolved THz emission from this 2D material under optical femtosecond excitation, permitting access to the processes of ultrafast photocurrent generation. We demonstrate that this is a result of a second-order nonlinear response with the THz pulse generated from the ultrafast photocurrents induced by the nonlinear conductivity of $PtSe_2$. In particular, we show the critical role of the environment, with the substrate inducing a structural asymmetry in the inherent centrosymmetry of $PtSe_2$. This is strongly illustrated by THz photocurrents that show an opposite phase change with left and right circular polarization (LCP and RCP) optical excitation for semi-metal multi-layer $PtSe_2$ but remain the same for the few layers semiconducting cases. These results are corroborated theoretically through extensive DFT simulations of the layer-dependent bandstructure showing important circular dichroism (CD) for semimetal $PtSe_2$ owing to the excitation of opposite valleys and the strong interaction with the substrate. This work shows that CD is not limited to the ML limit as in other TMDs with natural non-centrosymmetry, and can be finely controlled in the novel layer-dependent bandstructure of $PtSe_2$ [5].

References

[1] S. Manzeli, D. Ovchinnikov, D. Pasquier, O. V. Yazyev, A. Kis, *Nature Reviews Materials* **2**, 17033(2017).
[2] Y. Wang, L. Li, W. Yao, S. Song, J. T. Sun, J. Pan, X. Ren, C. Li, E. Okunishi, Y. Wang, E. Wang, Y. Shao, Y. Y. Zhang, H. Yang, E. F. Schwier H. Iwasawa, K. Shimada, M. Taniguchi, Z. Cheng, S. Zhou, S. Du, S. Pennycook, S. Pantelides, H. Gao, *Nano Letters* **15**, 6 4013(2015).
[3] L. Ansari, S. Monaghan, N. McEvoy, C. Coileain, C. P. Cullen, J. Lin, R. Siris, T. Stimpel-Lindner, K. F. Burke, G. Mirabelli, R. Duffy E. Caruso, R. E. Nagle, G. S. Duesberg, P. K. Hurley, F. Gity, *npj 2D Materials and Applications* **3**, 1 33(2019).
[4] L. Zhang, D. Zhang, F. Hu, X. Xu, Q. Zhao, X. Sun, H. Wu, Z. Lu¨, X. Wang, Z. Zhao, *Advanced Optical Materials* **10**, 2201881(2022).
[5] M. Hemmat,(submitted).

* Acknowledgement: The authors acknowledge funding from European Union's Horizon 2020 research and innovation program under grant agreement No 964735 (FET-OPEN EXTREME-IR).

Few-cycle pulses for optical frequency comb Spectroscopy from the ultraviolet to mid-infrared

S. A. Diddams
University of Colorado, Boulder, CO 80309 USA

Optical frequency combs are a unique spectroscopic tool, providing an unparalleled combination of frequency accuracy, high-resolution and broad spectral coverage. The field of frequency comb spectroscopy has grown rapidly to encompass multiple spectroscopic scenarios, ranging from trace gas detection for atmospheric sensing to fundamental spectroscopy in chemistry, physics and biology. In this talk, I will highlight our recent development of frequency comb spectroscopy tools and techniques that span from the ultraviolet (~200 nm) to the infrared (~25 microns).

Our typical frequency comb spectroscopic system start with a straightforward approach to generate few-cycle optical pulses with robust 1550 nm Er:fiber laser frequency comb technology [1,2]. With modest average power, we generate >0.5 MW pulses at 100 MHz rate. The high peak power allows us to exploit the second-order nonlinearities in infrared-transparent, nonlinear crystals (LiNbO3, GaP, GaSe, and CSP) to provide a robust source of phase-stable infrared ultrashort pulses with simultaneous spectral brightness exceeding that of an infrared synchrotron. Additional cascaded second-order nonlinearities in $LiNbO_3$ lead to comb generation with four octaves of simultaneous coverage (0.350 to 5.6 μm). With a free-running comb-tooth linewidth of 10 kHz at 193 THz, we realize a notable spectral resolving power exceeding 10^{10} across 0.86 PHz of bandwidth. Recently, we have also been exploring non-perturbative harmonic generation in ZnO to produce light at even shorted wavelengths—at and below 200 nm [3]. This is achieved with very tight focusing of the few-cycle pulse in the ZnO to peak intensities exceeding 1 TW/cm^2. Spectroscopic scenarios we have been exploring with this unique frequency comb source include trace gas and atmospheric sensing, spectroscopy of biologically relevant proteins and hyperspectral microscopy [1,4,5]. Readout of spectral information imprinted on the infrared frequency comb is enabled by either dual-comb spectroscopy or dual-comb electro-optic sampling [4]. In this later case, a second comb at a wavelength of 1550 nm, and a slightly different repetition rate, stroboscopically samples and upconverts the mid-infrared comb to the near-infrared. This approach has the benefit of shot-noise limited detection with robust 1550 nm detectors that have significantly greater efficiency, and spectral and electrical bandwidth when compared to mid-infrared detectors.

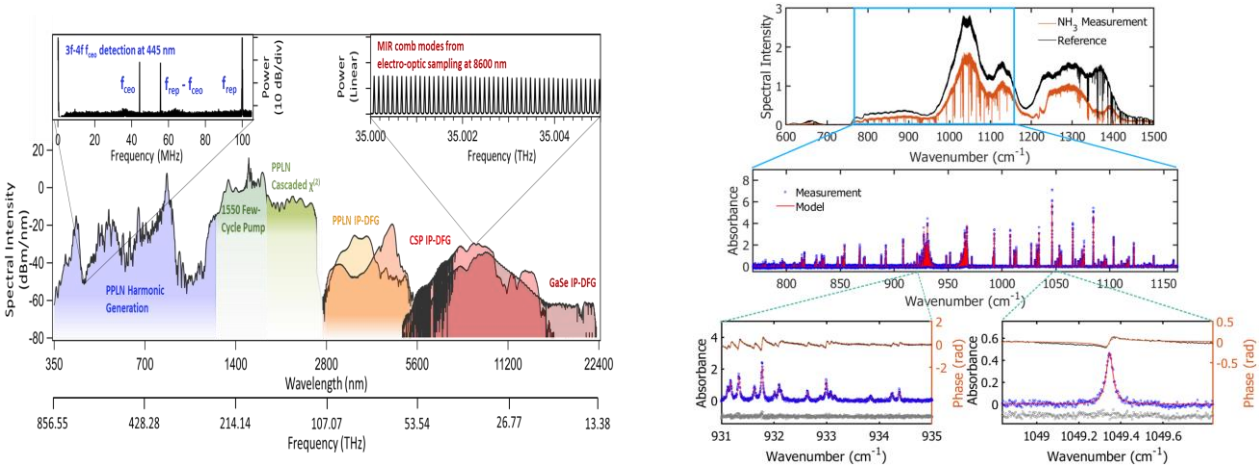

Fig. 1: ***(Left)*** *An erbium fiber mode-locked laser comb at 1550 nm seeds the generation of a few-cycle pulse to drive frequency conversion in second-order $\chi^{(2)}$ nonlinear crystals. The resulting composite spectrum, generated in three nonlinear crystals, spans six octaves [2].* ***(Right)*** *Example of using the mid-IR portion of this comb for high-resolution gas phase spectroscopy of NH_3 with dual-comb electro-optic sampling [4].*

Finally, a new direction involves the direct heterodyne of incoherent thermal light with the frequency comb itself, thereby bringing the power of telecommunications photonics and the precision of frequency comb metrology to laser heterodyne radiometry, with implications for solar and astronomical spectroscopy, remote sensing, and precise Doppler velocimetry [6].

References

[1] H. Timmers, A. Kowligy, A. Lind, F. C. Cruz, N. Nader, M. Silfies, G. Ycas, T. K. Allison, P. G. Schunemann, S. B. Papp S. A. Diddams, *Optica* **5**, 727 (2018).
[2] D. M. B. Lesko, H. Timmers, S. Xing, A. Kowligy, A. J. Lind, S. A. Diddams, *Nature Photonics* **15**, 281 (2021).
[3] D. M. B. Lesko, K. F. Chang, S. A. Diddams, *Optica* **9**, 1156 (2022).
[4] A. S. Kowligy, H. Timmers, A. J. Lind, U. Elu, F. C. Cruz, P. G. Schunemann, J. Biegert, S. A. Diddams, *Sci Adv* **5**, eaaw8794 (2019).
[5] H. Timmers, A. Kowligy, A. J. Lind, N. Nader, J. Shaw, D. Zalvidea, J. Biegert, S. A. Diddams, *OSA Technical Digest* , SF1E.4(2019) .
[6] E. Tsao, A. Lind, P. Chang, C. Fredrick, N. Hoghooghi, F. Quinlan, S. Diddams, Optica Publishing Group, JW3A.17(2022).

Ultrafast manipulation of the magnetic order in Correlated insulators via sub-gap optical excitation

H.A. Dürr
Uppsala University, 751 20 Uppsala, Sweden.

Strongly correlated magnetic insulators provide a unique opportunity to investigate the interaction between different degrees of freedom in a system possessing several exciting interaction mechanisms, including spin-orbit coupling and coulomb correlations. This talk will provide an overview how time-resolved optical and x-ray spectroscopy methods can contribute to our understanding of several such materials systems.For wide-band-gap insulators such as NiO theoretical predictions promise the coherent manipulation of electronic correlations with strong optical fields [1]. Contrary to metals where rapid dephasing of optical exci- tations via electronic processes occurs, the sub-gap excitation in charge-transfer insulators has been shown to couple to low-energy bosonic excitations such as phonons and magnons [2]. We use the prototypical charge-transfer insulator NiO to demonstrate that sub-gap excitation does not lead to a renormalization of electronic correlations up to peak electrical field strengths of 0.3 V/Å (see Fig. 1). However, when the excitation becomes resonant with a phonon-assisted dd-excitation we find a renormalized NiO band-gap in combination with a significant reduction of the antiferromagnetic order. We employ element-specific x-ray absorption spectroscopy at the FLASH free electron laser [4] to demonstrate the reduction of the upper band-edge at the O 1s-2p core-valence resonance whereas the antiferromagnetic order is probed via x-ray magnetic linear dichroism (XMLD) at the Ni 2p-3d resonance. Comparing the transient XMLD spectral lineshape to ground-state measurements allows us to extract a spin temperature rise of more than 60 K for time delays longer than 400 fs. At earlier times a non-equilibrium state is formed characterized by O 2p mid-gap states. These results can be understood in terms of a transient Ni-O charge transfer during the optical driving field. CrI_3 is a prototype of a new class of 2D magnetic insulator materials displaying ferromagnetic order down to the monolayer limit with a potential for device applications [5]. The optical and magneto-optical properties are proposed to be dominated by the presence of several excitonic dd-transitions characterized by spin polarized electron and hole pairs [6] with evidence of strong coupling to optical phonons [7].

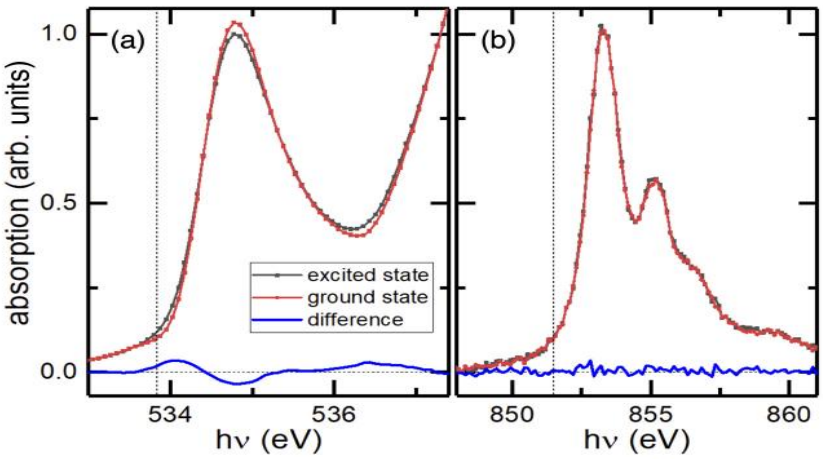

Fig. 1: ***(a)*** *Measured XAS spectra for O 1s-2p transitions and* ***(b)*** *for Ni 2p-3d transitions. [3] Measurements were obtained at the LCLS free electron laser using 2mm optical radiation as pump. While the more itinerant O 2p orbitals respond to laser excitation as indicated by the change in transient absorption in the excited state in* ***(a)****, Ni 3d levels remain unchanged indicating a negligible change of electron correlations up to the employed pump electric field strengths of 0.3 V/Å* ***(b)****.*

We will show how time resolved spectroscopic techniques can be used to investigate the optical and magneto-optical response of CrI_3 to understand their origin. This could open up the exciting prospect to extend sub-bandgap opto-magnetism down to the monolayer limit.

References

[1] N. Tancogne-Dejean, M. A. Sentef, A. Rubio, *Physical Review Letters* **121**, 097402 (2018).
[2] F. Novelli, G. De Filippis, V.Cataudella, M.Esposito, I.Vergar, F.Cilento, E. Sindici, A. Amaricci, C. Giannetti, D. Prabhakaran, SWall, A. Perucchi S. Dal Conte, G.Cerullo, M.Capone, A. Mishchenko, M. Grüninger, N.Nagaosa, F. Parmigiani, D. Fausti, *Nature Communications* **5**, 5112 (2014).
[3] O. Grånäs, I. Vaskivskyi, X. Wang, P. Thunström, S. Ghimire, R. Knut, J. Söderström, L. Kjellsson, D. Turenne, R. Y. Engel, M. Beye, J. Lu D. J. Higley, A. H. Reid, W. Schlotter, G. Coslovich, M. Hoffmann, G. Kolesov, C. Schüßler-Langeheine, A. Styervoyedov, N. Tancogne-Dejean M. A. Sentef, D. A.Reis, A. Rubio, S. S. P.Parkin, O Karis, J.-E.Rubensson, O.Eriksson, H. A.Dürr, *Physical Review Research* **4**, L032030 (2022).
[4] X. Wang, R. Y Engel, I. Vaskivskyi, D.Turenne, V.Shokeen, A.Yaroslavtsev, O. Grånäs, R.Knut, J. O. Schunck, S. Dziarzhytski, G. Brenner R.-P. Wang, M.Kuhlmann, F.Kuschewski, W.Bronsch, C. Schüßler-Langeheine, A. Styervoyedov, S. SP Parkin, F. Parmigiani, O. Eriksson M.Beye, H. A Dürr, *Faraday Discussions* **237**, 300 (2022).
[5] B. Huang, G. Clark, E.Navarro-Moratalla, D.R. Klein, R. Cheng, K.L. Seyler, D. Zhong, E.Schmidgall, M. A. McGuire, D. H. Cobden, W.Yao D. Xiao, P.Jarillo-Herrero, X. Xu, *Nature* **546**, 270 (2017).
[6] M. Wu, Z. Li, T. Cao, S. G. Louie, *Nature Communications* **10**, 1 (2019).
[7] P. Padmanabhan, F. L. Buessen, R. Tutchton, K. W. C. Kwock, S. Gilinsky, M. C. Lee, M. A. McGuire, S. R. Singamaneni, D. A. Yarotski A. Paramekanti, J.-X. Zhu, R. . Prasankumar, *Nature Communications* **13**, 4473 (2022).

Theoretical investigations on ultra-fast demagnetization using Ab-initio and simulation methods

E. Hubert[1], J. Braun[1], S. Mankovsky[1], S. Polesya[1], H. Lange[1],
M. Weißenhofer[2], U. Nowak[2]

[1] *Ludwig Maximilian University of Munich, 80539 Munich, Germany*
[2] *University of Konstanz, 78464 Konstanz, Germany*

The field of ultra-fast demagnetization started with the pioneering work of Beaurepaire *et al.* [1] who demonstrated the rapid decay of the magnetization of Ni after a short laser pule via the magneto-optical Kerr effect (MOKE). Similar experimental work was done later using for example the transverse MOKE [2], the X-ray magnetic circular dichroism (XMCD) [3] or the spin and angle resolved photo emission spectroscopy (ARPES) [4]. Theoretical investigations on ultra-fast demagnetization were first performed on a model level followed by simplified quantum-mechanical studies. A great step forward could be made by using an implementation of a scheme based on time-dependent density functional theory (TD-DFT) that allowed to describe in an ab-initio or parameter-free way the demagnetization after a strong laser pulse [5]. As electronic spectroscopies sensitive to the magnetization play a crucial role to monitor ultra-fast demagnetization processes the scheme has been extended in the meantime to calculate spectroscopic properties directly and to make this way direct contact with experiment. As an alternative to this all-in-one approach, we use the time and spin dependent potential and occupation functions from TD-DFT calculations as an input to our own programs that work on a fully relativistic level within the Green function formalism implemented by means of multiple scattering theory. This approach allows us to calculate spectroscopic and many other magnetic properties in a time-resolved but quasi-static way. Concerning spectroscopy first applications have been made for time-resolved XMCD calculations. As will be shown, the resulting sequence of spectra reflect in a one-to-one manner the decay of the magnetization with the connection between spectra and magnetization as suggested by the so-called XMCD sum rules. Another application is the calculation of spin resolved ARPES spectra on the basis of the one-step model of photo emission. Fig. 1 shows a corresponding sequence for ferromagnetic Fe that reflect in particular the diminishing of the exchange splitting that was observed in experiment.

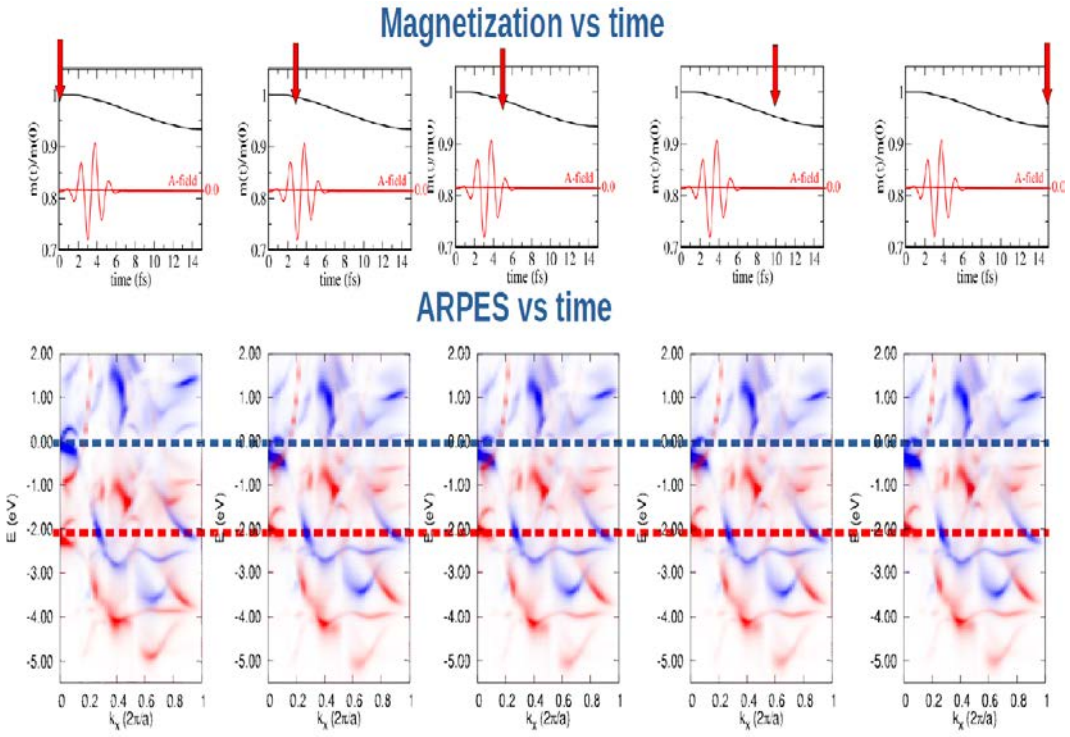

Fig. 1. ***Top****: Magnetization m(t) versus time with five time markers.* ***Bottom****: photo emission spectra from ferromagnetic Fe for normal emission along the path G-X calculated via the one-step model using the TD-DFT based potential for the marked times. The dashed lines mark the exchange splitting at the G-point at t=0.*

As will be shown, using the two-time Keldysh non-equilibrium Green function formalism [6] allows to go beyond the quasi-static approach concerning a description of the XMCD but also ARPES. First results of corresponding applications of this very powerful and flexible scheme will be presented for two-photon photo emission experiments involving surface states. Because of the large computational

costs and other restrictions of TD-DFT calculations they allow only to cover the time window of the demagnetization and the first stage of the subsequent relaxation of the system. For that reason, simulations that are based on simplified parametrized models are and will always be indispensable tools for studies that account at the same time for the electronic, magnetic and lattice degrees of freedom. So far such studies used either empirical parameters or parameters derived from the electronic ground state. Using TD-DFT based potentials and occupation functions, on the other hand, should lead to more realistic parameters. Fig. 2 shows as an example the exchange coupling parameters J_{ij} (middle row) of ferromagnetic Co as a function of the distance R_{ij} calculated for a sequence of times when a laser pulse is applied (top row together with the time dependent magnetic moment). These parameters have been used for subsequent Monte Carlo simulations to get the effective time dependent critical temperature T_c that is shown in the bottom row of Fig. 2

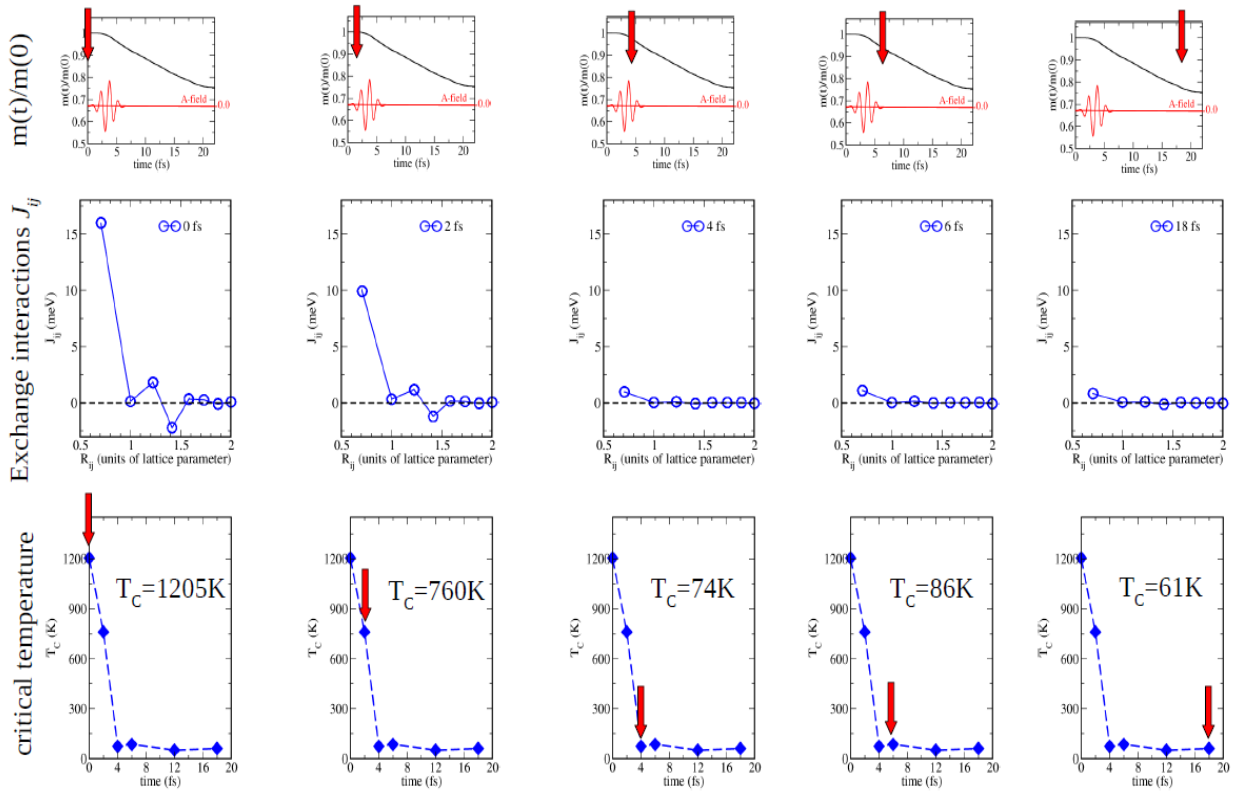

***Fig. 2**. Exchange coupling parameters J_{ij} of ferromagnetic Co as a function of the distance R_{ij} of 2 moments on site i and j (**middle**) and resulting effective critical temperature T_c (**bottom**) for a sequence of times.*

The data show obviously a very pronounced diminishing of T_c due to the laser pulse as it is exploited in heat-assisted magnetic writing. Similar results have been obtained and will be shown for the magneto-crystalline energy.

An important aspect in this context and for the magnetization dynamics in general is the coupling of the electronic system carrying the magnetization and the lattice. As will be shown, the corresponding spin-lattice coupling parameters J_{ijk} as well as higher order terms can be obtained in a similar manner as the conventional exchange parameter J_{ij} by a generalization of the so-called Lichtenstein formula. Using TD-DFT based potentials and occupation functions, again the time-dependence of the parameters J_{ijk} as well as of any other parameters entering the model Hamiltonians or equations of motion used within magnetization dynamics simulations can be accounted for. An interesting aspect of corresponding combined spin lattice dynamics simulations based on the parameters J_{ijk} that will be addressed is the angular momentum transfer between the spin and lattice systems.

References

[1] E. Beaurepaire, J.-C. Merle, A. Daunois, J.-Y. Bigot, *Physical Review Letters* **76** 4250 (1996)
[2] S. Mathias, C. La-O-Vorakiat, P. Grychtol, P. Granitzka, E. Turgut, J. M. Shaw, R. Adam, H. T. Nembach, M. E. Siemens, S. Eich C. M.Schneider, T. J.Silva, M.Aeschlimann, M. M.Murnane, H. C.Kapteyn, *Proceedings of National Academy of Sciences-PNAS***109**, 4792 (2012).
[3] I. Radu, C. Stamm, A. Eschenlohr, F. Radu, R. Abrudan, K. Vahaplar, T. Kachel, N. Pontius, R. Mitzner, K. Holldack, A. Föhlisch, T. A. Ostler J.H. Mentink, R. F. L. Evans, R. W. Chantrell, A. Tsukamoto, A. Itoh, A. Kirilyuk, A. V. Kimel, Th. Rasing, *SPIN* **5**, 1550004 (2015).
[4] S. Eich, M. Plötzing, M. Rollinger, S. Emmerich, R. Adam, C. Chen, H. C. Kapteyn, M. M. Murnane, L. Plucinski, B. Stadtmüller, M. Cinchetti M. Aeschlimann, C. M. Schneider, S. Mathias, *Science Advances* **3,** e1602094 (2017).
[5] K. Krieger, J. K. Dewhurst, P. Elliott, S. Sharma, E. K. U. Gross, *Journal of Chemical Theory & Computations* **11**, 4870 (2015).
[6] J. Braun, H. Ebert, *Physical Review B* **98**, 245142 (2018).
[7] S. Mankovsky, S. Polesya, H. Lange, M. Weißenhofer, U. Nowak, H. Ebert, *Physical Review Letters* **129**, 067202 (2022).

Ultrafast optical parametric oscillators spanning the Ultraviolet to mid-infrared

M. Ebrahim-Zadeh
ICFO-Institut de Ciencies Fotoniques, 08860 Castelldefels, Spain

The latest developments in ultrafast wavelength conversion sources based on optical parametric oscillators covering spectral regions from the ultraviolet to deep-infrared, and temporal domains from the continuous-wave to few-cycle pulses are described. The advent of novel nonlinear optical materials over the past decade combined with progress in solid-state and fiber laser technology has had a tremendous impact on frequency conversion sources, enabling their advancement to new spectral and temporal domains. The developments have led to the realization of a new generation of advanced solid-state sources of tunable coherent radiation providing unprecedented capabilities with regard to wavelength coverage, output power and efficiency, spatial, spectral and temporal quality, and operating in all time scales from the continuous-wave (cw) to the ultrafast few-cycle pulses. In particular, optical parametric oscillators (OPOs) are now firmly established as truly viable and practical sources of broadly tunable coherent radiation capable of accessing extended spectral regions from the ultraviolet (UV) to the deep-infrared (deep-IR), not available to conventional solid-state lasers. Harnessing the superior linear and nonlinear optical properties of new birefringent and quasi-phase-matched (QPM) crystals and advanced laser pump sources, together with the application of innovative design concepts, OPOs have transformed solid-state laser technology in new directions and towards new frontiers. The exploitation of birefringent crystals such as BiB_3O_6 (BIBO) and $CdSiP_2$ (CSP), and QPM materials such as MgO-doped periodically-poled $LiNbO_3$ (MgO:PPLN), stoichiometric $LiTaO_3$ (MgO:sPPLT), $KTiOPO_4$ (PPKTP), orientation-patterned GaAs (OP-GaAs) and GaP (OP-GaP), combined with ultrafast solid-state and fiber pump lasers, have enabled tunable ultrashort pulse generation across vast spectral regions from ~250 nm in the UV up to ~12 μm in the deep-IR, with pulses down to a few-cycle duration [1-6]. In the femtosecond time-scale, operation of synchronously-pumped OPOs into deep-IR at wavelengths as long as ~8 μm has been realized by exploiting internal cascaded parametric generation based on MgO:PPLN and CSP using the KLM Ti:sapphire laser as pump source [4] or by external cascaded pumping [5] using a commercial near-IR femtosecond OPOs as the intermediate stage, as shown in Fig. 1. At the same time, by employing ultrashort pump pulses of ~20 fs duration, with careful control of dispersion, operation of femtosecond OPOs has been extended to new temporal limits, providing broadband mid-IR pulses with as few as 3.7 optical cycles and bandwidths spaning over ~500 nm [6].

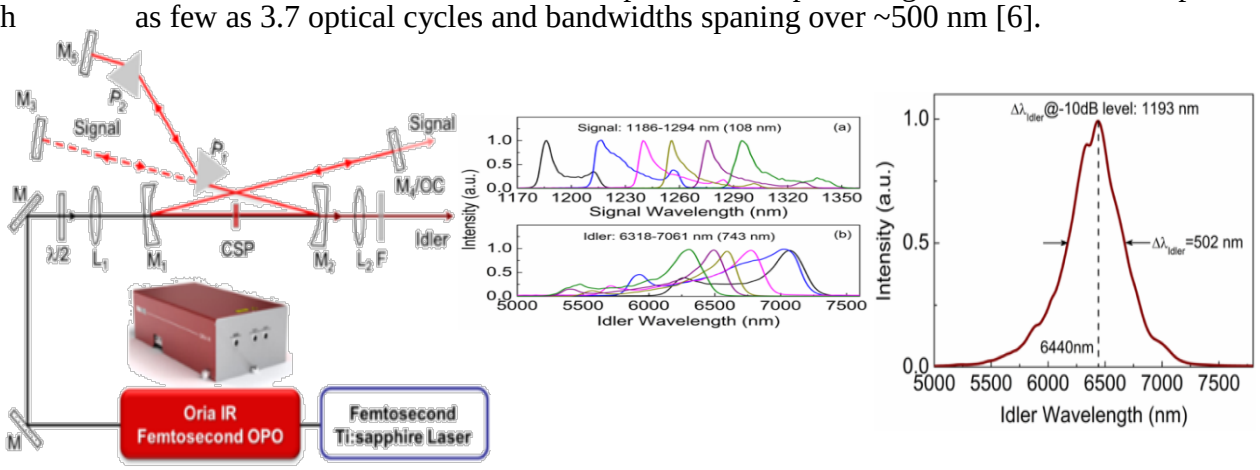

***Fig. 1. (Left)**: Schematic of the cascaded CSP femtosecond OPO tunable in the deep-IR. **(Middle)**: Corresponding **(a)** signal, and **(b)** idler spectra across the tuning range. **(Right)**: Representative idler spectrum centered at 6440 nm [5].*

Successful operation of femtosecond OPOs has been further extended to wavelengths beyond 8 μm in the deep-IR by direct pumping with the KLM Ti:sapphire laser, and without the need for intermediate cascaded step [7,8]. The configuration of such an OPO is shown in Fig. 2. By exploiting type-I (*e*→*oo*) critical phase-matching in combination with angle-tuning in CSP, the high-repetition-rate femtosecond OPO can provide continuous wavelength coverage across 7306–8329 nm (1201–1369 cm^{-1}) in the deep-IR. The oscillator delivers up to 18 mW of idler average power at 7306 nm and >7 mW beyond 8 μm at 80.5 MHz repetition rate, with spectra exhibiting bandwidths of >150 nm across the tuning range. With an equivalent spectral brightness of ~5.6×10^{20} photons s^{-1} mm^{-2} sr^{-1} 0.1% BW^{-1}, this OPO represents a viable alternative to synchrotron and supercontinuum sources for

deep-infrared applications in spectroscopy, metrology and medical diagnostics. In another development, the advent of the new QPM nonlinear material, OP-GaP, has enabled femtosecond pulse generation across 3.6–8 μm in the deep-IR from a single OPO system [9], as shown in Fig. 3. Average output powers of 54 mW at ~3.8 μm in the mid-IR signal, with >10 mW across the entire deep-IR idler tuning range, was obtained. The measured quantum conversion efficiency of 28.9% from pump to idler at 3.8 μm is the highest recorded from any OPO based on OP-GaP or CSP.

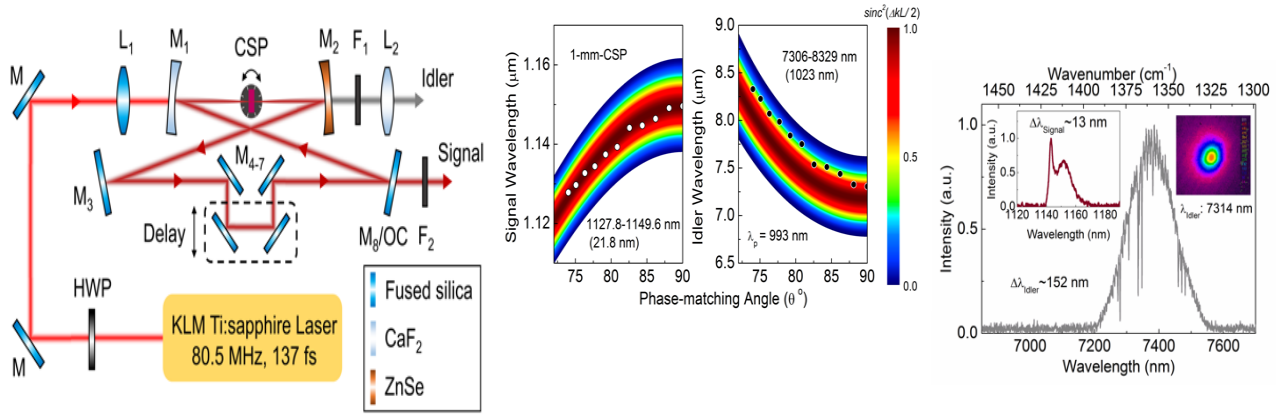

***Fig. 2. (Left)**: Schematic of the experimental setup for the Ti:sapphire-pumped CSP femtosecond OPO. **(Middle)**: Idler and signal tuning as a function of the internal phase-matching angle in the CSP crystal, for a pump wavelength of 993 nm, superimposed on the parametric gain map. **(Right)**: Deep-IR idler spectrum centered on 7387 nm with a FWHM bandwidth of 152 nm. Insets: Corresponding signal spectrum centered at ~ 1150 nm with FWHM bandwidth of 13 nm, TEM_{00} beam profile at 7314 nm [7, 8].*

In another development, the advent of the new QPM nonlinear material, OP-GaP, has enabled femtosecond pulse generation across 3.6–8 μm in the deep-IR from a single OPO system [9], as shown in Fig. 3. Average output powers of 54 mW at ~3.8 μm in the mid-IR signal, with >10 mW across the entire deep-IR idler tuning range, was obtained. The measured quantum conversion efficiency of 28.9% from pump to idler at 3.8 μm is the highest recorded from any OPO based on OP-GaP or CSP.

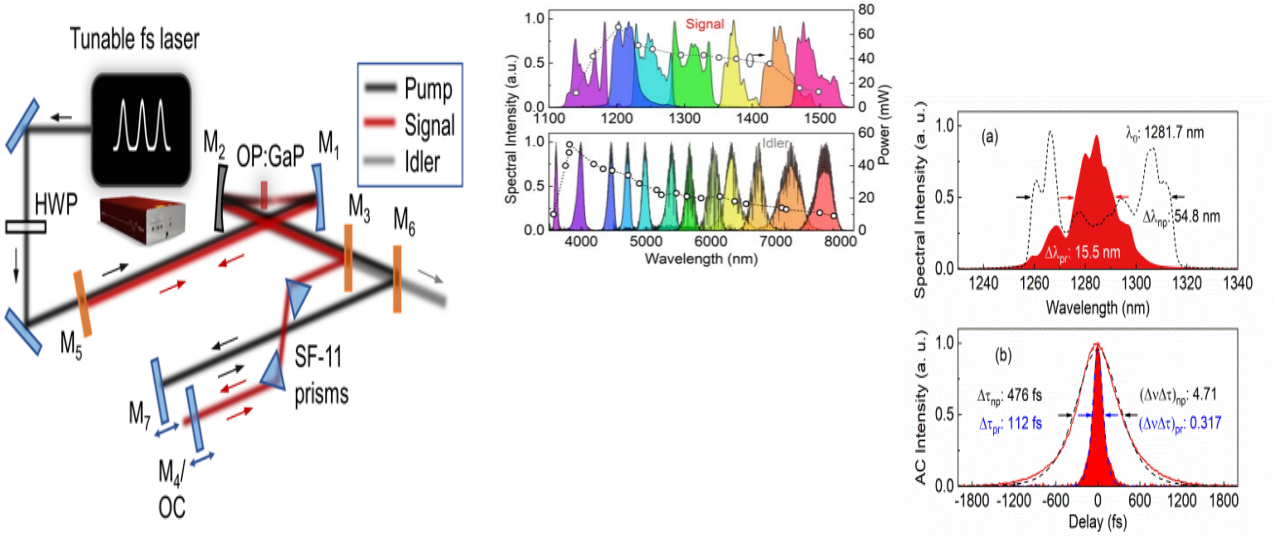

***Fig. 3. (Left)**: Schematic of femtosecond OPO based on OP-GaP. **(Middle)**: Signal and idler average power and optical spectra across the tuning range. **(Right)**: Signal spectra at a central wavelength of 1281.7 nm measured with (**filled area**) and without (**dashed line**) prisms in the cavity. **(b)** Corresponding intensity autocorrelations with (**filled area**) and without (**red line**) prisms [9].*

In the picosecond time scale, has also become possible into the deep-IR spectral range by direct pumping using Yb-fiber lasers at 1.064 μm. The major improvements in the optical quality of the CSP crystal with low transmission loss over long interaction lengths have made it possible to overcome the low nonlinear gains under low pumping intesities, thus enabling the realization of high-repetition-rate picosecond OPOs at wavelegnths out to 6.7 μm [10]. The configuration of such an OPO is shown in Fig. 4.

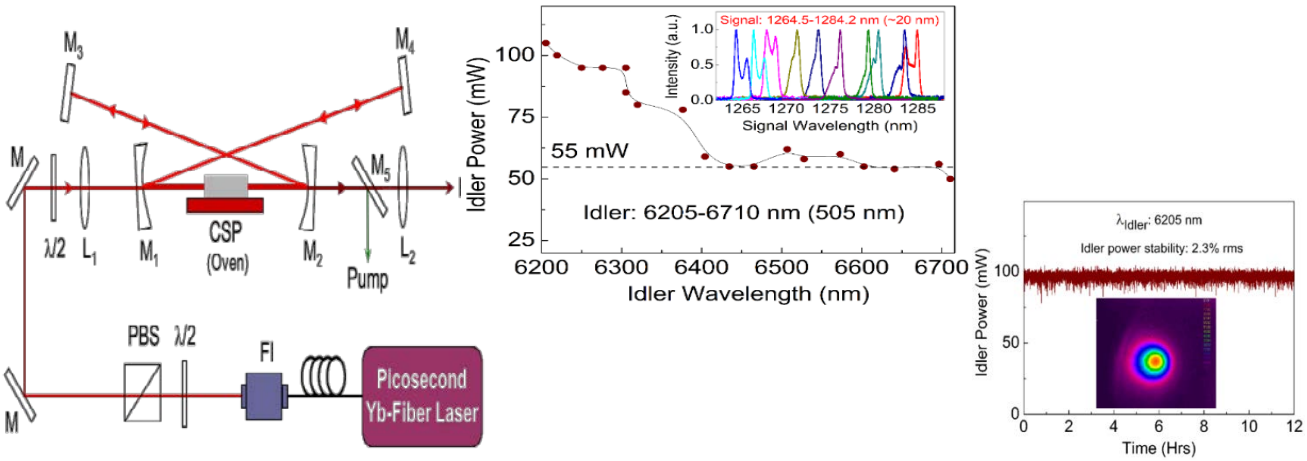

***Fig. 4. (Left)**: Schematic of the experimental setup for the Yb-fiber laser pumped high-average-power deep-IR picosecond OPO. **(Middle)**: Power across the idler tuning range of the picosecond CSP OPO. **Inset:** Signal spectra across the temperature tuning range. (**Right**): Long-term power stability of the deep-IR idler from the picosecond CSP OPO. **Inset**: deep-IR idler beam profile at an operating wavelength of 6205 nm [10].*

The OPO is based on a 16.3-mm-long CSP crystal cut at θ=90º (ϕ=45º) for type-I ($e \rightarrow oo$) noncritical phase-matching and synchronously pumped by ~20 ps pulses from a mode-locked Yb-fiber laser 79.5 MHz repetition rate. The OPO is tunable across 6205-6710 nm in the idler, providing as much as 105 mW of average power at 6205 nm, with >55 mW over nearly the entire tuning range. The deep-IR idler output exhibits a passive power stability better than 2.3% rms over 12 hours in high beam quality. With the extended wavelength coverage, practical average powers, high beam quality, and good passive stability, this OPO represents an attractive source of high-repetition-rate picosecond pulses in the deep-IR for many applications including spectroscopy and imaging. The latest progress in picosecond OPOs include broadband phase-locked pulse generation[11], see Fig. 5.

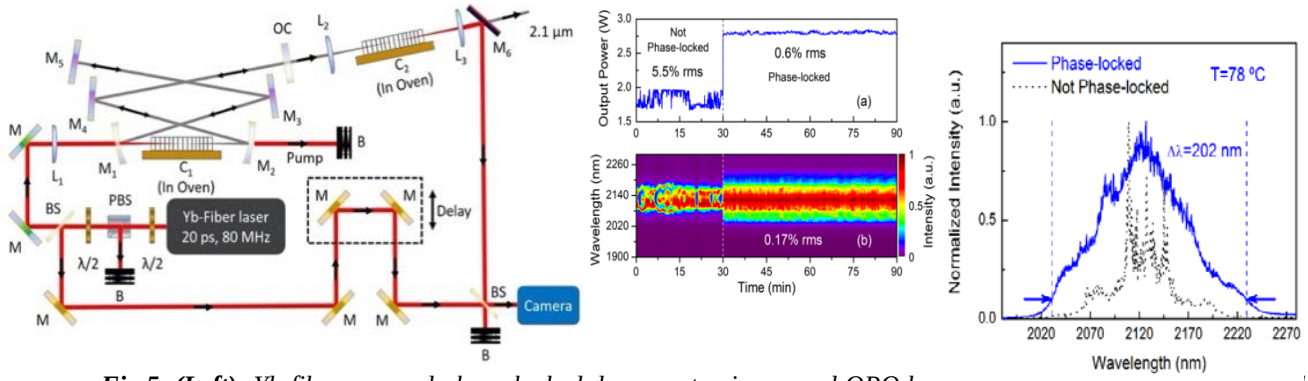

***Fig.5. (Left)**: Yb-fiber-pumped phase-locked degenerate picosecond OPO based on MgO:PPLN for broadband generation in the near-infrared. **(Middle)**: **(a)** Output power and stability in transition from unlocked to phase-locked regime; **(b)** spectral stability of ps-OPO output in transition from unlocked to phase-locked regime. **(Right)**: OPO output spectrum in the absence of phase-locking and in degenerate phase-locked state [11].*

This talk will provide an overview of the latest progress at the forefront of OPO technology, enabled by new nonlinear materials, advanced solid-state and fiber laser pump sources, and novel desing concepts. Some emerging applications of OPO sources in optical microscopy, imaging and spectroscopy will also be highlighted.

References

[1] M. Ebrahim-Zadeh, S. C. Kumar, *IEEE Journal of Selected Topics in. Quantum Electronics* **20**, 7600519 (2014).
[2] M. Ebrahim-Zadeh, S. C. Kumar, K. Devi, *IEEE Journal of Selected Topics in Quantum Electronics* **20**, 0902823 (2014).
[3] S. C. Kumar, P. G. Schunemann, K. T. Zawilski,M. Ebrahim-Zadeh, *Journal of Optical Society of America-JOSA* B **33**, D44 (2016).
[4] V. R. Badarla, S. C.Kumar, A. Esteban-Martin, K. Devi, K. T. Zawilski, P. G. Schunemann, M. Ebrahim-Zadeh, *Optics Letters* **41**, 1708 (2016).
[5] S. C. Kumar, A. Esteban-Martin, A. Santana, K. T. Zawilski, P. G. Schunemann, M. Ebrahim-Zadeh, *Optics Letters* 41, 3355 (2016).
[6] S. C. Kumar, A. Esteban-Martin, T. Ideguchi, M. Yan, S. Holzner, T. W. Hänsch, N. Picqué, M. Ebrahim-Zadeh, *Laser & Photonics Review* **8** 86 (2014).
[7] C. F. O'Donnell, S. C. Kumar, K. T. Zawilski, P. G. Schunemann, M. Ebrahim-Zadeh, *Optics Letters* **43**, 1507 (2018).
[8] C. F. O'Donnell, S. C. Kumar, K. T. Zawilski, P. G. Schunemann, M. Ebrahim-Zadeh, *IEEE Journal of Selected Topics in. Quantum Electronics* **24**, 1 (2018).
[9] C. F. O'Donnell, S. C. Kumar, P. G. Schunemann, M. Ebrahim-Zadeh, *Optics Letters* **44**, 4570 (2019).
[10] S. C. Kumar, K. T. Zawilski, P. G. Schunemann, M. Ebrahim-Zadeh, *Optics Letters* **42**, 3606 (2017).
[11] B. Nandy, S. Chaitanya Kumar, M. Ebrahim-Zadeh, *Optics Letters* **45,** 3981 (2020).

* *Acknowledgments: Spanish Government through Project Nutech PID2020-112700RB-I00 (MCIN/AEI/10.13039/501100011033), and "Severo Ochoa" Center of Excellence, CEX2019-000910-S) – Funded by the Spanish State Research Agency; Generalitat de Catalunya (CERCA); Fundación Cellex; Fundació Mir-Puig.*

Theory of ultrafast disordering in photo-induced phase transitions

M. Eckstein
University of Hamburg, 22607 Hamburg, Germany

Using ultrashort laser pulses, it has become possible to probe the dynamics of long-range order in solids on microscopic timescales. In the conventional description of symmetry-broken phases within time-dependent Ginzburg-Landau theory, the order parameter evolves coherently along an average trajectory. Recent experiments, however, indicate the profound effect of order parameter fluctuations on the dynamics. An extreme scenario is ultrafast inhomogeneous disordering [1], where the average order parameter is no longer representative of the state on the atomic scale. While this has a profound effect on the dynamics, a theoretical approach which takes into account atomic scale inhomogeneities of both the electronic structure and the order parameter is challenging. In my talk, I will report on results for the Holstein model, which are based on a nonequilibrium generalization of statistical dynamical mean-field theory, coupled to stochastic differential equations for the order parameter [3]. The results show that ultrafast disordering can occur already in this minimal model for the Peierls charge-density wave transition (Fig. 1) [2].

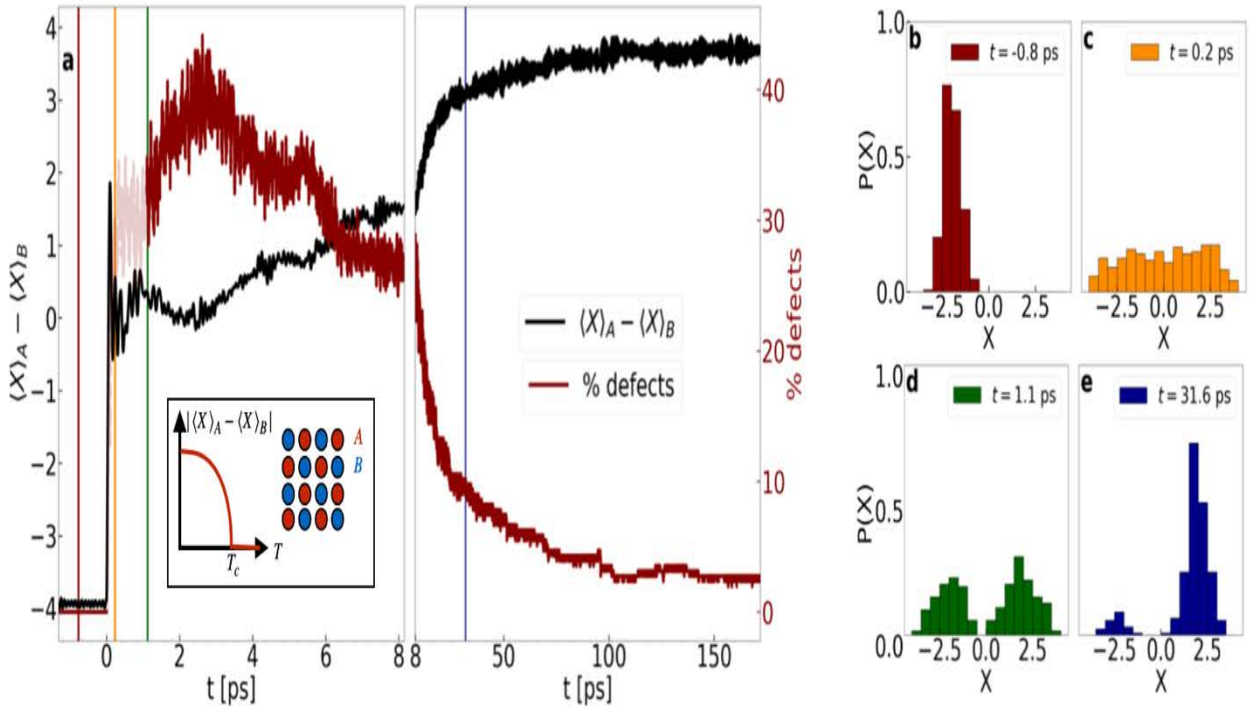

Fig. 1 (a): *Dynamics of the order parameter X_A-X_B for the charge density wave transition in the Holstein model after a sudden excitation of the electrons. The order parameter is the difference of an atomic displacement between two sublattices A and B of a bipartite lattice (see inset). After the excitation, the CDW order is quenched, and recovers on a timescale of 100ps. The figure shows a strong excitation, in which the sign of the order can be reversed.* ***(b)*** *to* ***(e)*** *Probability distribution of the local lattice displacement on the A sublattice at four representative times (see vertical lines in* ***(a)****: Already at an early time when the average order parameter is still close to zero, one finds a bimodal distribution* ***(c)****: The order parameter is locally restored, while the system is still in a disordered state, which is the hallmark of ultrafast disordering.*

Similar techniques may help in future to solve the coupled electron lattice dynamics for strongly interacting electrons.

References

[1] S. Wall, S. Yang, L. Vidas, M. Chollet, J. Glownia, M. Kozina, T. Katayama, T. Henighan, M. Jiang, T. Miller, D. Reis, L. Boatner O. Delaire, M. Trigo, *Science* **362**, 572 (2018).
[2] A. Picano, F. Grandi, M. Eckstein, *arXiv:2112.15323*.
[3] A. Picano, F. Grandi, Ph. Werner, M. Eckstein, *arXiv:2209.00428*.
* Acknowledgement(s): We acknowledge financial support from the ERC starting grant No. 716648.

State of the art in soft x-ray lab sources: Probing magnetization dynamics with atomic selectivity in the femto- to picosecond range

S. Eisebitt
Max Born Institute for Nonlinear Optics and Short Pulse Spectroscopy, 12489 Berlin, Germany

Soft x-rays are a unique tool to study magnetism due to presence of circular and linear x-ray dichroism, allowing to quantitatively access the spin (S) and orbital (L) magnetic moments in an element specific fashion via the exploitation of suitable resonant and polarization dependent electronic transitions. Furthermore, the short wavelength as compared to visible radiation allows to access magnetic ordering on the nanometer scale spatial scale. Scattering and imaging approaches are exploited to access order from the unit cell range to the mesoscale. With magnetization dynamics on these spatial scales typically covering the few femtosecond to picosecond temporal scale, pulsed sources in the soft x-ray spectral range are key to interrogate dynamical processes in pump-probe experiments. So far, experiments of this kind have almost exclusively been performed at large scale, accelerator-based facilities. However, with many synchrotron radiation sources upgrading to higher brightness with associated electron bunch length exceeding 100 ps, shorter pulses of soft x-rays are available only at free electron x-ray lasers (FELs) and a few synchrotron beamlines.

Laser-based secondary sources of soft x-rays have started to fill this gap. Sources based on high harmonic generation (HHG) provide < 50 fs pulses, allowing to access ultrafast magnetization phenomena. Their dominant use in magnetism research has been in the photon energy range up to about 100 eV (λ=12.4 nm), predominantly in spectroscopy (see e.g. [1, 2]) but also with a few proof-of-principle scattering and diffractive imaging experiments reported. [3,4] While HHG to photon energies in the water window and even above have been reported, applications in magnetism research have been very sparse so far, due to the very strong decrease in photon flux for increasing photon energies. In particular, the "workhorse photon energies" allowing to exploit the transitions form the $2p_{3/2,1/2}$ levels of the 3d transition metals could not be exploited for the study of ultrafast magnetization dynamics at laser based soft x-ray sources yet. With the photon flux demands typically increasing from spectroscopy via resonant scattering to resonant imaging, the more photon hungry methods are so far practically limited to photon energies below 100 eV, with the notable exception of two recent resonant magnetic scattering experiments with HHG sources at around 150 eV photon energy, i.e. accessing 4d to 5f transitions in lanthanides. [5, 6]

We report on a development of a high-flux HHG source based on an OPCPA system providing a 2 µm HHG driver at 10 kHz repetition rate, extending up to 600 eV photon energy with sub-25 fs pulses as shown in Fig. 1 [7]. First experiments on magnetization dynamics on this system are discussed. Exploiting the magneto-optical Kerr effect with soft x-rays in angle resolved measurements, we monitor (transient) spectral changes in the entire broad spectrum at an absorption resonance. These changes encode depth information on the (transient) magnetization profile which can be extracted in conjunction with scattering simulations [8]. In this fashion we are able to trace the transient magnetization depth profile during ultrafast demagnetization after laser excitation, demonstrated in a prototypical FeGd thin film system with seed and cap layers [6]. Developments to extend these capabilities to the photon energy range up to 800 eV using a 3 µm-driver system with similar architecture of the laser system are under way.

To reach the photon energies up to 900 eV with suitable photon flux in order access 3d elements at their L-edges or even up to 1500 eV to reach the M-edges of lanthanides is of large importance in the study of magnetic materials via x-ray dichroism in spectroscopy and scattering - but also a formidable challenge, in particular via HHG. Such work has so far been the exclusive domain of large scale facilities. For studies where fs temporal resolution is not required, laser-driven plasma x-ray sources (PXS) provide an alternative. We report on the development of such a soft x-ray source specifically for studies in magnetism with a pulse duration of slightly below 10 ps, together with soft x-ray optics and endstations to measure x-ray absorption and resonant magnetic scattering [9]. The driver for the PXS is an in-house-developed double-stage Yb:YAG-based thin-disk amplified laser, producing pulses with a duration of 2 ps full width at half-maximum at a wavelength of 1030 nm with a pulse energy of 150 mJ at 100 Hz repetition rate [10]. Soft x-rays are produced in the plasma generated when the pulses hit a tungsten target. A flux curve of the source is included in Fig. 1. Note that such a source is intrinsically unpolarized.

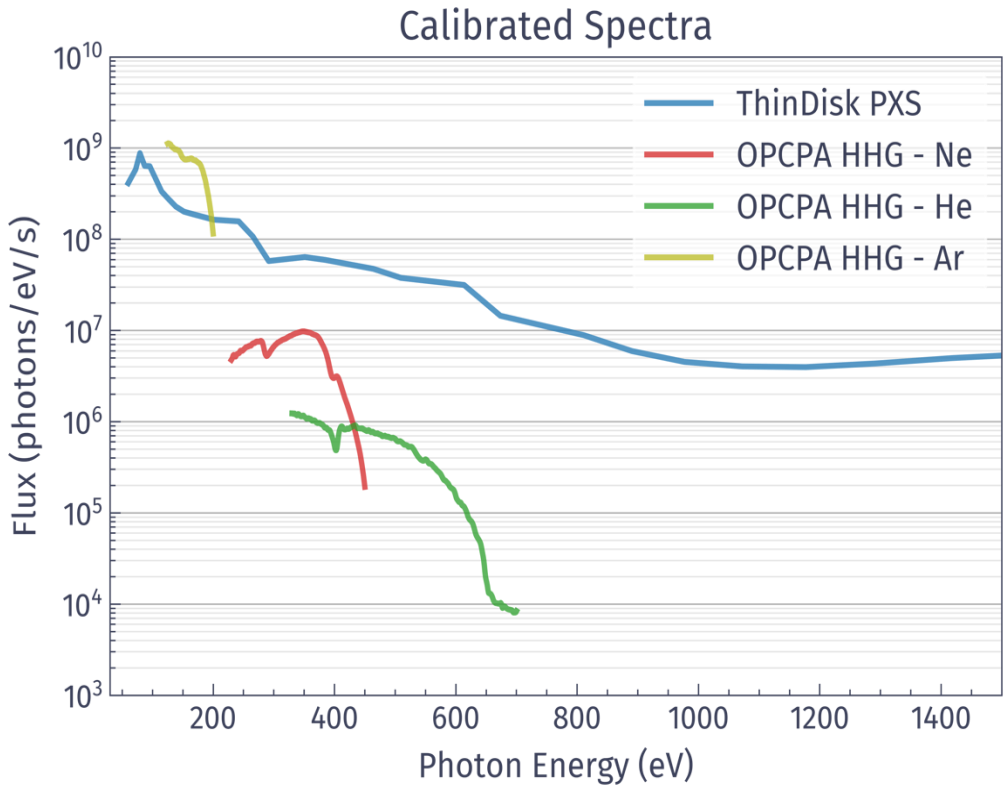

Fig. 1 *Photon flux curves of the 2µm-driven OPCPA-based HHG source (yellow, red and green lines for the use of different gases in the HHG process) [7]. Photon flux curve of the laser-driven plasma x-ray source, operated with a tungsten target [12]. In both cases, only the photon flux corresponding to the solid angle actually accepted by the subsequent optical elements in the beamline is shown. All photon flux measurements were carried out with a detector calibrated by the German national metrology institute Physikalische Technische Bundesanstalt (PTB).*

Nevertheless, we demonstrate for the first time the ability to measure (i) x-ray magnetic circular dichroism absorption spectra (Fe L_3, 707 eV) [11], (ii) resonant magnetic scattering from antiferromagnetic order in Fe/Cr superlattices (Fe L_3, 707 eV) [12], (iii) small angle scattering from ferromagnetic domains in Fe/Gd multilayers (Fe L_3, 707 eV and Gd M_5, 1189 eV) [13] at such elevated photon energies with a laboratory source.
Not only does such a source allow for the static characterization of magnetic samples during competitive data acquisition times, but in all three modes we are able to acquire transients of magnetization dynamics after laser excitation in pump-probe-experiments with a temporal resolution of slightly below 10 ps.
The source and instrument developments will be discussed together with the new capabilities to probe magnetization dynamics with atomic selectivity and reciprocal space information in a laboratory setup, detailing and extrapolating from the first demonstration experiments.

References

[1] C. La-O-Vorakiat, M. Siemens, M. M. Murnane, H. C. Kapteyn, S. Mathias, M. Aeschlimann, P. Grychtol, R. Adam, C. M. Schneider, J. M. Shaw H. Nembach, T. J. Silva, *Physical Review Letters* **103,** 257402 (2009).
[2] F. Willems, C. V. Schmising, C. Struber, D. Schick, D. W. Engel, J. K. Dewhurst, P. Elliott, S. Sharma, S. Eisebitt, *Nature Communications* **11** 871 (2020).
[3] B. Vodungbo, J. Gautier, G. Lambert, A. B. Sardinha, M. Lozano, S. Sebban, M. Ducousso, W. Boutu, K. Li, B. Tudu, M. Tortarolo, R. Hawaldar R. Delaunay, V. Lopez-Flores, J. Arabski, C. Boeglin, H. Merdji, P. Zeitoun, J. Luning, *Nature Communications* **3**, 999 (2012).
[4] O. Kfir, S. Zayko, C. Nolte, M. Sivis, M. Moller, B. Hebler, S. S. P. K. Arekapudi, D. Steil, S. Schafer, M. Albrecht, O. Cohen, S. Mathias C. Ropers, *Science Advances* **3,** (2017)
[5] G. Fan, K. Legare, V. Cardin, X. Xie, R. Safaei, E. Kaksis, G. Andriukaitis, A. Pugzlys, B. E. Schmidt, J. P. Wolf, M. Hehn, G. Malinowski, B. Vodungbo, E. Jal, J. Luning, N. Jaouen, G. Giovannetti, F. Calegari, Z. Tao, A. Baltuska, F. Legare, T. Balciunas, *Optica* **9**, 399 (2022).
[6] M. Hennecke, D. Schick, T. Sidiropoulos, F. Willems, A. Heilmann, M. van Moerbeck-Bock, L. Ehrentraut, D. Engel, P. Hessing, B. Pfau M. Schmidbauer, A. Furchner, M. Schnuerer, C. von Korff Schmising, S. Eisebitt, *Physical Review Research* **4**, L022062 (2022).
[7] M. van Mörbeck-Bock, T. Feng, A. Heilmann, L. Ehrentraut, H. Stiel, M. Hennecke, T. Sidiropoulos, C. von Korff Schmising, S. Eisebitt, M. Schnürer, *Proceedings SPIE* **11777**, 117770C (2021); doi: 10.1117/12.2591309.
[8] D. Schick, *Computer Physics Communications* **266,** (2021).
[9] M. Borchert, J. Braenzel,1 R. Gnewkow, L. Lunin,1 T. Sidiropoulos, J.Tümmler, I. Will, T. Noll, O. Reichel, D. Rohloff, A. Erko, T. Krist C. von Korff Schmising, B. Pfau, S. Eisebitt, H. Stiel, D. Schick, (submitted), (2023).
[10] R. Jung, J. Tümmler, I. Will, *Optics Express* **24**, 883(2016).
[11] M. Borchert, D. Engel, C. von Korff Schmising, B. Pfau, S. Eisebitt, D. Schick, *Optica* (accepted), (2023). *DOI: 10.1364/OPTICA.480221*
[12] D. Schick, M. Borchert, J. Braenzel, H. Stiel, J. Tummler, D. E. Burgler, A. Firsov, C. V. Schmising, B. Pfau, S. Eisebitt, *Optica* **8**, 1237 (2021).
[13] L. Lunin, M. Borchert, N. Schneider, K. Korell, D. Sommer, S. Eisebitt, B. Pfau, D. Schick, (to be submitted), (2023)

***** *Acknowledgement: I am indebted to all authors of Refs. 6,7,9,11,12,13 who have significantly contributed to the results discussed in this presentation.*

Search for the ultrafast Meissner effect in driven $YBa_2Cu_3O_{6.48}$

S. Fava[1], G. Jotzu[1], M. Buzzi[1], G. De Vecchi[1], T. Gebert[1], Y. Liu[2], S. Nakata[2], B. Keimer[2], A. Cavalleri [3]

[1] *Max Planck Institute for the Structure and Dynamics of Matter, 22761 Hamburg, Germany*
[2] *Max Planck Institute for Solid State Research, 70569 Stuttgart, Germany*
[3] *University of Oxford, Oxford OX1 3PU, UK*

Resonant excitation of certain phonon modes in high-T_c cuprates has been shown to induce transient properties reminiscent of superconductivity at temperatures far above equilibrium T_c [1-3]. These out-of-equilibrium superconducting-like states have been investigated in time-domain terahertz spectroscopy experiments, that revealed the dissipation-less nature of the electronic transport. A fundamental question remains open: do these non-equilibrium superconducting-like states also feature an ultrafast Meissner effect and expel a statically applied magnetic field? To address this question, we developed an experimental technique based on the Faraday effect in a magneto-optic crystal adjacent to the sample. Tracking the polarisation changes in an ultrashort near-infrared pulse reflected off this crystal, allows us to reconstruct the strength of the magnetic field surrounding the photo-excited region (Fig. 1). We make use of this technique to investigate the possible expulsion of a statically applied magnetic field in the photo-induced superconducting-like state of $YBa_2Cu_3O_{6.48}$, a response that would amount to an ultrafast Meissner effect.

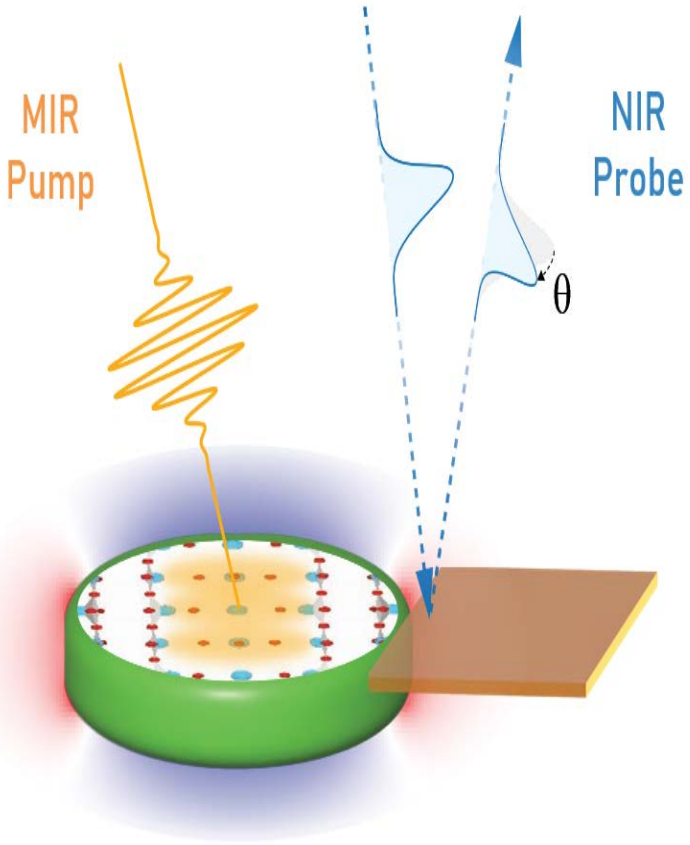

Fig. 1*: Schematic representation of the experimental setup. The $YBa_2Cu_3O_{6.48}$ sample (**green puck at the center**) is embedded in an external magnetic field (not shown) and the Cu-O apical phonon mode is driven resonantly by a mid-infrared laser pulse (**orange**). The local magnetic field changes due to the superconducting diamagnetic response are encoded in a red or blue shading for positive and negative values, respectively. These changes are measured in close proximity of an edge of the sample in a GaP crystal (**orange slab**) by virtue of the Faraday effect using a near-infrared probe beam (**blue pulse**).*

We discuss how the measured field expulsion depends on temperature and external magnetic field, leading to a more complete understanding of this exotic state of matter.

References

[1] W. Hu, S. Kaiser, D. Nicoletti, C.R.Hunt, I.Gierz, M.C.Hoffmann, M.Le Tacon, T. Loew, B. Keimer, A.Cavalleri, *Nature Materials* **13,** 705(2014).
[2] B. Liu, M. Först, M. Fechner, D. Nicoletti, J. Porras, T. Loew, B. Keimer, A. Cavalleri, *Physical Review* X **10**, 011053 (2020).
[3] A. von Hoegen, M. Fechner, M. Först, N. Taherian, E. Rowe, A. Ribak, J. Porras, B. Keimer, M. Michael, E. Demler, A. Cavalleri, *Physical Review* X **12**, 031008 (2022).

Ultrafast electrical switching and charge state control of silicon Vacancy centers in diamond

M. Rieger, V. Villafañe, L. Todenhagen, S. Appel, M. Brandt, K. Mueller
J. J. Finley
Technical University of Munich, 85748 Garching, Germany

Optically-active point defects in diamond feature atomic-sized two-level systems, constituting a promising solid-state platform for the development of novel quantum technologies. Example applications are the generation of non-classical light, such as single photons and photonic cluster states, and nodes in quantum networks [1, 2]. One of the most intensively studied color centers in diamond is the nitrogen vacancy complex (NV), which exhibits a remarkable coherence time and a spin-selective dark shelving state that proves useful for non-resonant spin pumping and readout [3]. However, NVs lack efficient emission into the zero-phonon line (ZPL), and are susceptible to external environmental noise due to their inherent symmetry, leading to instability of the optical transition energy. Conversely, group IV vacancy complexes in diamond (G4V) (with silicon, germanium, tin or lead) show excellent optical properties due to their crystallographic symmetry which favors emission into ZPL [4]. In this group, the silicon vacancy (SiV−) has been so far the most studied complex and T2 spin coherence times exceeding ~10ms have been demonstrated at low operation temperatures (T~100mK) [5]. Even though the energy levels of the G4V, forming a double-lambda system with spin S=1/2, can be used to store and process quantum information, the lack of optical spin selection rules makes their optical readout difficult and inefficient. In this contribution, we present our efforts towards controlling and understanding the SiV− charge state mechanisms towards implementing spin-to-charge conversion protocols. By means of voltage pulses applied from a pair of interdigital metal contacts on the diamond surface we develop a method to dynamically manipulate the charge state of SiV− centers and demonstrate that they can be switched reversibly between SiV^0 and SiV− at MHz-rates (see Fig. 1).

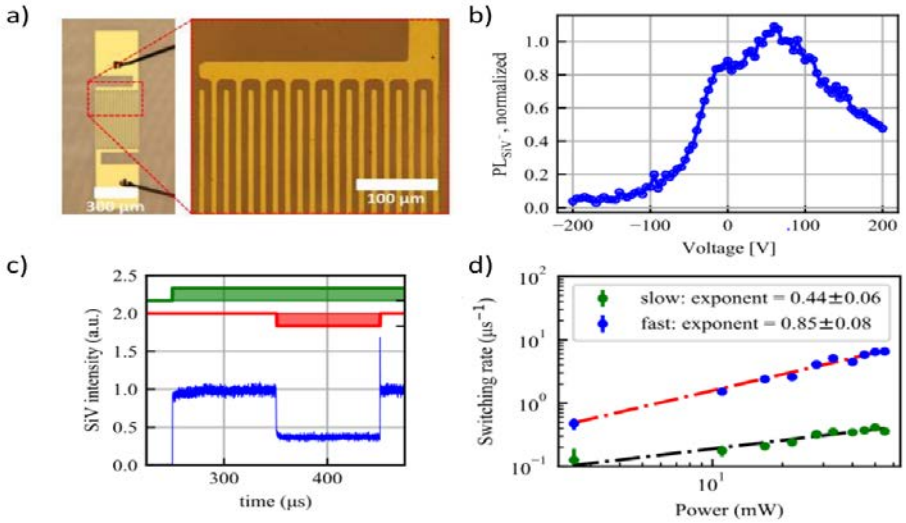

Fig. 1. a) *Optical micrograph of the diamond in planar-interdigital configuration.* ***b)*** *SiV- photoluminescence intensity upon changes in the applied voltage between V=±200 V.* ***c)*** *Time-resolved photoluminescence during an optical and electrical sequence depicting the change of the SiV- charge state.* ***d)*** *SiV- switching rate as a function of the applied optical power.*

We furthermore fully explore the charge cycle of the SiV− center spectroscopically and find that it is aided by the presence of P1 and divacancy centers in the host lattice. Our results shed light on the charge cycle mechanisms on G4V and elucidate the potential for realizing an opto-electronic readout of their spin state.
Finally, we will discuss current strategies to enhance the SiV− spin coherence times beyond the conventionally used ~mK temperatures. Specifically, 1D optomechanical structures containing single SiV- centers can be engineered to achieve optical cooling of the host diamond lattice and therefore extend the SiV− spin coherence time. Such a hybrid physical platform for coherent cavity acousto-optics (AO) is based on SiV− in diamond and confined GHz phonons. The strong AO coupling in these structures will be exploited to perform unconventional spin initialization techniques in SiV− centers while cooling down the host lattice and thus increase the spin coherence time at higher temperatures.

References

[1] M. Ruf, N.H. Wan, H. Choi, D. Englund, R. Hanson, *Journal of Applied Physics* **130**, 070901 (2021).
[2] S. Prawer, A.D. Greentree, *Science* **320**, 1601(2008).
[3] N. Bar-Gill, L. M. Pham, A. Jarmola, D. Budker, R.L. Walsworth, *Nature Communications* **4**, 1743 (2013).
[4] B. Pingault, D.D. Jarausch, C. Hepp, L. Klintberg, J.N. Becker, M. Markham, C. Becher, M. Atatüre, *Nature Communications* 8, 15579 (2017).
[5] D D. Sukachev, A. Sipahigil, C.T. Nguyen, M.K. Bhaskar, R.E. Evans, F. Jelezko, M.D. Lukin, *Physical Review Letters* **119**, 223602 (2017).

The Effect of Disorder on the Thermalization of Correlated Quantum Systems under an Interaction Quench

H. F. Fotso
University at Buffalo SUNY, Buffalo, NY 14260, USA

To enable the investigation of the nonequilibrium dynamics of interacting systems in the presence of disorder, we recently introduced the nonequilibrium DMFT+CPA method [1]. An embedding scheme that combines the nonequilibrium extensions of both the dynamical mean field theory (DMFT) [2] and the coherent potential approximation (CPA) [3,4]. This framework enables investigations of the important interplay of interaction and disorder on the nonequilibrium dynamics of quantum systems. The approach was previously benchmarked on the equilibrium solution of the Anderson-Hubbard model revealing among other features the disorder-induced insulator to metallic phase transition that occurs for strong interactions when the disorder strength is increased. Here, we employ this framework to analyze the effect of disorder on the nonequilibrium dynamics of a correlated system, described by the Anderson-Hubbard model, under an interaction quench. The system, initially in equilibrium at a given temperature, $T_{initial} = 1/\beta_{initial}$, has the interaction abruptly switched from zero to a finite value at a given time. To investigate the role of disorder, we use our effective medium approach to calculate, through the nonequilibrium Green's functions, for different values of the final interaction and for different disorder strengths, the distribution functions as the system evolves in time. This allows us to determine the effective temperature after the quench and to analyze the effects of disorder on the thermalization for various interaction strengths.

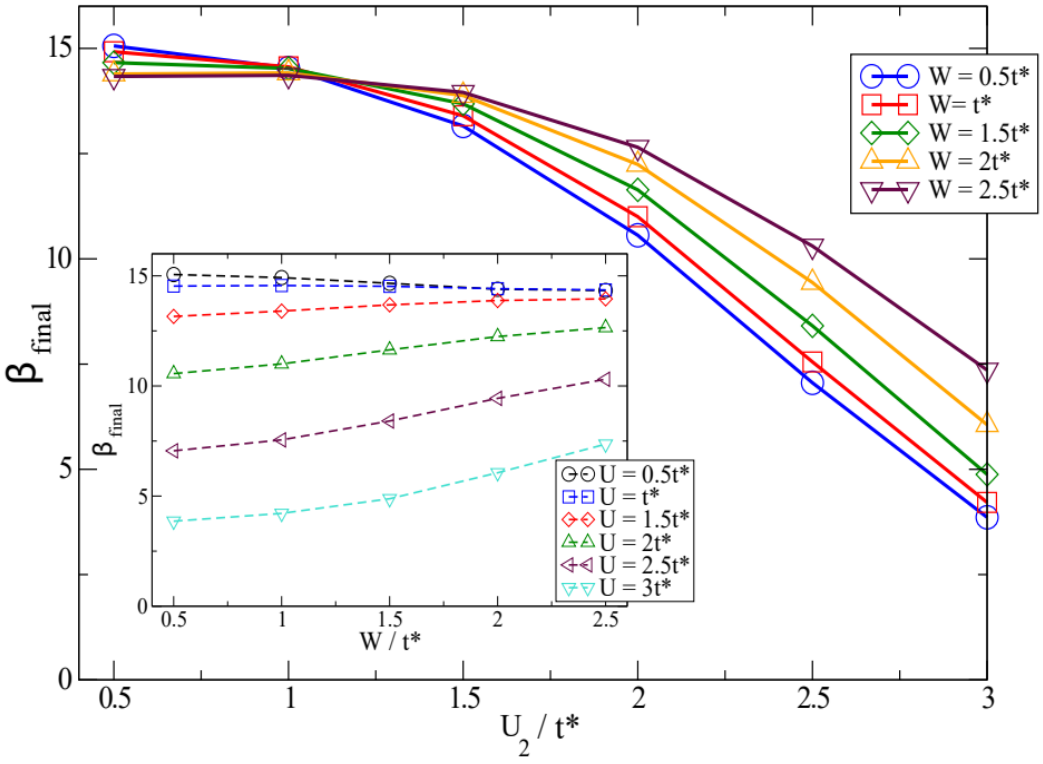

Fig. 1: *Inverse effective temperature as a function of the final interaction strength (U_2) for different disorder strengths (W). The systems is initially at a temperature such that $\beta_{initial} = 15$.* ***Inset****: Effective inverse temperature β as a function of the disorder strength for different interaction strengths. Increased disorder strength for moderate interaction strengths leads to a lower long-time temperature.*

The analysis shows that, for moderate interaction strengths after the quench, disorder can tune the final temperature of the system across a broad range of values; With increased disorder strength leading to lower effective temperature [5].

References

[1] E. Dohner, H. Terletska, K.-M. Tam, J. Moreno, H. F. Fotso, *Physical Review* B **106**, 195156 (2022).
[2] J. K. Freericks, *Physical Review* B **77**, 075109 (2008).
[3] Y. Zhu, L. Liu, H. Guo, *Physical Review* B **88**, 205415 (2013).
[4] A. V. Kalitsov, M. G. Chshiev, J. P. Velev, *Physical Review* B **85**, 235111 (2012).
[5] E. Dohner, H. Terletska, H F Fotso, *arXiv:2303.06495* (2023).

* Acknowledgement(s) : We acknowledge support from National Science Foundation under Grant No. PHY-2014023.

Time-crystalline behavior in central spin models with Heisenberg interactions

R. Frantzeskakis[1], J. Van Dyke[2], L. Zaporski [3], D. A. Gangloff [4], C. Le Gall [5], M. Atatüre[3]
S. Economou [2], E. Barnes [2]
[1] University of Crete, Heraklion, 71003 Greece
[2] Virginia Tech, Blacksburg, VA 24061 USA
[3] University of Cambridge, Cambridge, CB3 0HE, United Kingdom
[4] University of Oxford, Oxford, OX1 3PJ, United Kingdom
[5] Microsoft Research, Cambridge, CB1 2FB, United Kingdom

Time crystals have been experimentally realized recently [1, 2]. Different physical non-equilibrium-driven systems can create a time crystal phase. Quantum dots have been proposed as one of the best candidates to protect quantum information [3]. In addition, color centers are well known for their enormous dephasing times and the stabilization of their quantum states [2,4]. We study how we can take advantage of nuclear-electron spin/defect hyperfine interactions to create a time crystal phase in a central-spin model. This nuclear hyperfine interaction is unavoidable in spin systems [5-7]. We focus on stabilizing multi-qubit computational basis pure quantum states in the presence of Heisenberg hyperfine interactions.We propose applying a strong enough on-site magnetic field on electron spin/defect (central spin) to create a time crystal phase in the central-spin model. An on-site constant magnetic field can effectively decouple the Heisenberg interactions, achieving the subharmonic response which can be seen through a phase diagram (Figure 1a). However, an on-site magnetic field may not be applicable in different spin systems, so we propose another way to stabilize multi-qubit states (Figure 1b). We focus on applying a sequence of π pulses in the electron spin to observe subharmonic behavior. This sequence of H2I π pulses (Heisenberg-to-Ising pulses) can make a Heisenberg Hamiltonian behave like an Ising one [8]. Electrons/defects and nuclear spins can be stabilized by quantum control of the central spin (magnetic field or Heisenberg to Ising pulses) and periodic driving of electrons and nuclei.

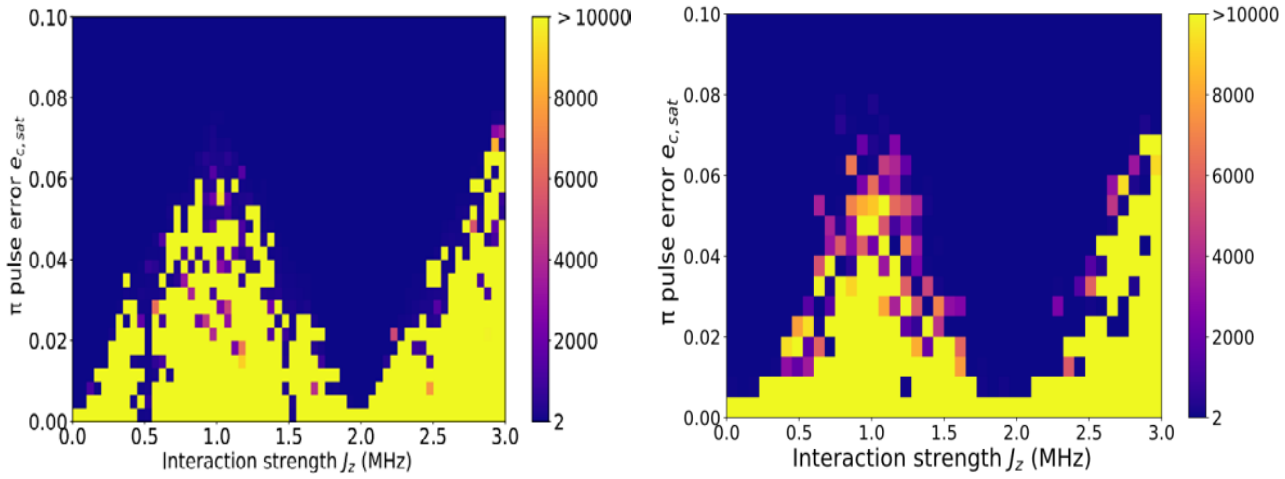

***Fig. 1. Left (or a)**: Phase diagram with an on-site constant central spin magnetic field; **Right (or b)**: Phase diagram with application of H2I π pulses.*

This may be beneficial for using physical central spin systems with hyperfine interactions like color centers (defect coupled to nuclei), multi-dots systems opening the road of using quantum dots, and color centers in protecting quantum information. More details can be found in our recent arXiv preprint [9].

References

[1] J. Zhang, P.W. Hess, A. Kyprianidis, P. Becker, A. Lee, J.Smith, G. Pagano, I. D. Potirniche, A.C. Potter, A. Vishwanath, N.Y. Yao, *Nature* **543**, 217 (2017).
[2] J. Randall, C.E. Bradley, F.V. van der Gronden, A. Galicia, M.H. Abobeih, M.Markham, D. J. Twitchen, F. Machado, N.Y. Yao, TH. Taminiau *Science* **374**, 1474 (2021).
[3] J.S. Van Dyke, Y.P. Kandel, H. Qiao, J.M. Nichol, S.E. Economou, E. Barnes, *Physical Review B* **103**, 245303 (2021).
[4] E. Bauch, C.A. Hart, J.M. Schloss, M.J. Turner, J.F. Barry, P. Kehayias, S. Singh,R. L. Walsworth, *Physical Review X* **8**, 031025 (2018).
[5] L.V. Assali,H.M. Petrilli, R.B. Capaz, B. Koiller, X. Hu, S.D. Sarma, *Physical Review B* **83**, 165301 (2011).
[6] G. Gillard, I.M. Griffiths, G. Ragunathan, A. Ulhaq, C. McEwan, E. Clarke, E.A. Chekhovich, E.A., *npj Quantum Information* **7**, 43 (2021).
[7] S. Pezzagna, J. Meijer, *Applied Physics Reviews* **8**, 011308 (2021).
[8] E. Barnes, J.M. Nichol, S.E. Economou, *Physical Review B* **99**, 035311 (2019).
[9] R. Frantzeskakis, J. Van Dyke, L. Zaporski, D.A. Gangloff, C.L. Gall, M. Atatüre, S.E. Economou, E. Barnes, *arXiv:2303.00893*.

* This work was supported by DARPA (grant no. D18AC00025), by NSF grant no. 1847078 and by EU Horizon 2020 programme (GA 862035 QLUSTER).

Theoretically describing pump-probe experiments in Electron-Phonon coupledsystems out to ps time scales

J. K. Freericks[1] M. Petrovic[1],Manuel Weber[2]
[1] *Georgetown University, Washington, DC 20003, USA*
[2] *Max Planck Institute for the Physics of Complex Systems, 01187 Dresden, Germany*

In this talk, we describe coupled nonequilibrium electron-phonon systems semiclassically—using Ehrenfest dynamics for the phonons and quantum mechanics for the electrons—via a classical Monte Carlo approach that determines the nonequilibrium response to a large pump field. The semiclassical approach is quite accurate, because the phonons are excited to average energies much higher than the phonon frequency, eliminating the need for a quantum description of their behavior. The energy for the electrons is still in a quantum-degenerate regime, so quantum mechanics is critical to describe their behavior. The numerical efficiency of this method allows us to perform a self-consistent time evolution out to very long times (tens of picoseconds) enabling us to model pump-probe experiments of a charge density wave (CDW) material. Our system is a half-filled, one-dimensional (1D) Holstein chain that exhibits CDW ordering due to a Peierls transition. The chain is subjected to a time-dependent electromagnetic pump field that excites it out of equilibrium, and then a second probe pulse is applied after a time delay. By evolving the system to long times, we capture the complete process of lattice excitation and subsequent relaxation to a new equilibrium, due to an exchange of energy between the electrons and the lattice, leading to lattice relaxation at finite temperatures. We employ an indirect (impulsive) driving mechanism of the lattice by the pump pulse due to the driving of the electrons by the pump field. We identify two driving regimes, where the pump can either cause small perturbations or completely invert the initial CDW order. Our work successfully describes the ringing of the amplitude mode in CDW systems that has long been seen in experiment, but never successfully explained by microscopic theory. We also describe the fluence-dependent crossover that inverts the CDW order parameter and changes the phonon dynamics.

We work with a Holstein model, which involves a coupling of the local electronic charge density to the phonon coordinate at each lattice site. We work with spinless electrons on a one-dimensional lattice with nearest neighbor hopping γ. The phonons are local Einstein modes with a frequency given by $\Omega = 0.01\ \gamma/\hbar$. The system has a charge-density-wave ground state at $T=0$, but does not display long-range order for any finite temperature. However, because we work in a finite system, once the correlation length is larger than the system size the system appears ordered. We always work with a proper superposition of the two translationally invariant charge-density-wave states, so our system only displays broken symmetry when we look at correlation functions. Using this code, we can compute Green's functions and from that we can extract the photoemission spectroscopy (PES). As observed in experiments (see, e.g., Ref. 1), the lattice motion causes the gap energy to oscillate, which isreflected in the computed PES at low temperatures in Fig. 1. The equilibrium spectrum before the pump isgapped (due to the Peierls distortion), which implies that only the lower band is populated. After excitation, the system will stabilize to a new equilibrium with a reduced gap energy. Increasing the temperature of the lattice has two major effects on the computed PES. The first is the evident damping of the gap oscillations, so the system relaxes faster to a new equilibrium PES for higher initial temperatures. The second effect is the "washing out" of the finer details in the spectrum at higher temperatures, increasing at longer times. The period of initial PES oscillations in Fig. 1(a) is much larger (around 1000 $\hbar/\gamma$) than what one would expect for $\Omega = 0.01\ \gamma/\hbar$ which is a clear sign that electron-phonon interaction significantly modifies the intrinsic phonon frequency. The advantage of our self-consistent MC approach is evident from the time scale of Fig. 1, where the time resolution must be kept at $0.1\ \hbar/\gamma$ to capture the electron dynamics, still the fast evolution scheme allows us to average over 3000 MC configurations. Translating these units to the ones in experiments, for $\gamma = 1$ eV, the time step is $\Delta t \approx 0.07$ fs, while the simulation time is around 7 ps. Most other methods can only approach maximal times on the order of 10s to 100s of fs.

As one can see in Fig. 1, exciting the electron impulsively excites the amplitude mode phonon as well, whose oscillation is damped as a function of time. The band edges of the PES oscillate with the frequency of the amplitude mode (which is renormalized from its bare value)

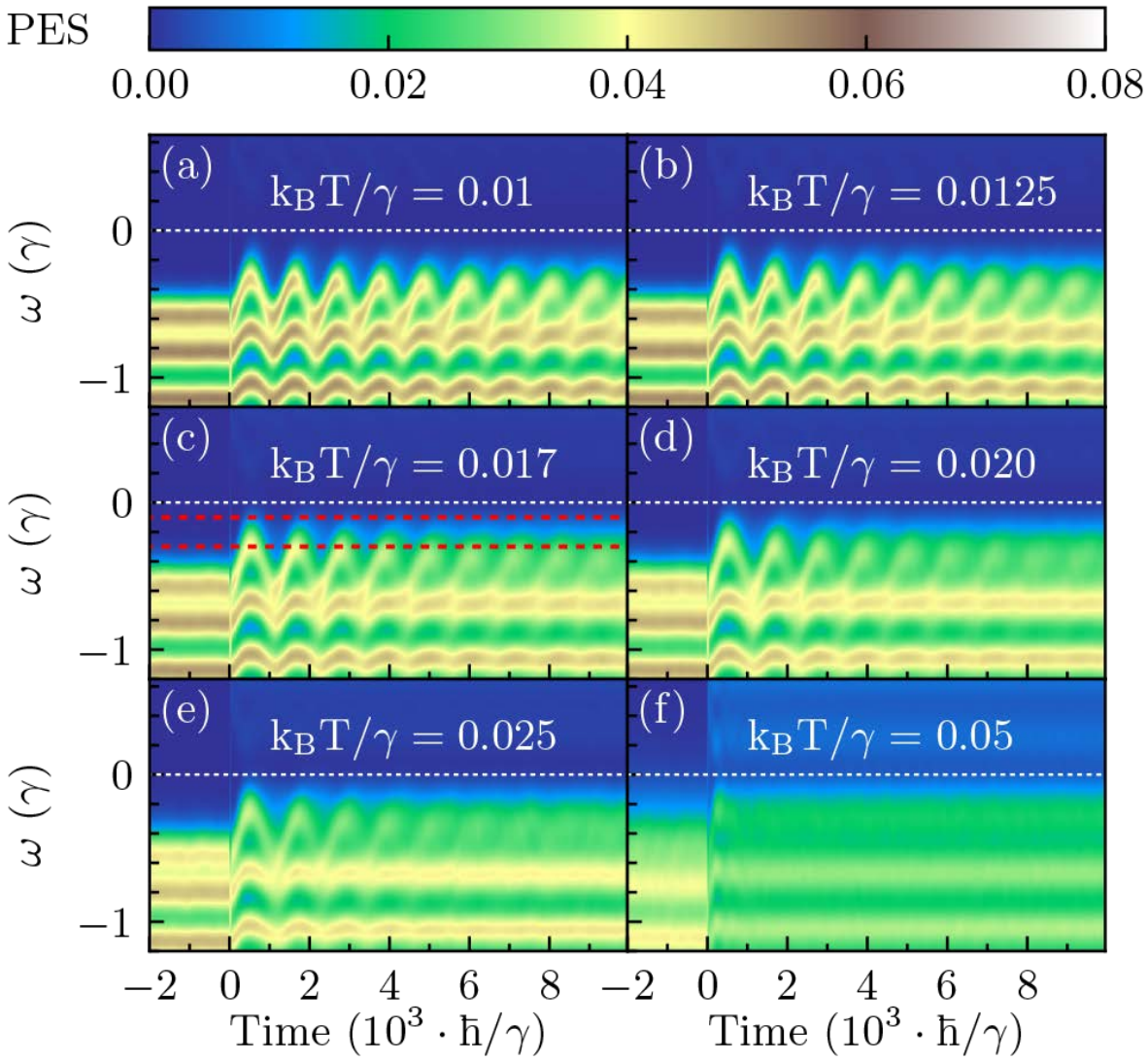

Fig. 1. *Photoemission spectra for a chain of L = 30 sites at different temperatures. The electron-phonon coupling is* $\lambda = 0.6$ *and the phonon frequency is* $\Omega = 0.01\ \gamma/\hbar$. *The pump parameters are* $E_0 = 0.33$, $\sigma_p = 10\ \hbar/\gamma$, *and* $\omega_p = 0.1\ \gamma/\hbar$.

As the initial temperature is raised, the damping is more rapid. In the talk, I will discuss this phenomenon and describe more pump/probe experiments on electron-phonon coupled systems.

References

[1] F. Schmitt, P. S. Kirchmann, U. Bovensiepen, R. G. Moore, L. Rettig, M. Krenz, J.-H. Chu, N. Ru, L. Per- fetti, D. H. Lu, M. Wolf, I. R. Fisher, Z.-X. Shen, *Science* **321**, 1649 (2008).

* Acknowledgements: This work was supported by the U.S. Department of Energy (DOE), Office of Science, Basic Energy Sciences (BES) under Award DE-FG02-08ER46542. J.K.F. was also supported by the McDevitt bequest at Georgetown University. This research used resources of the National Energy Research Scientific Computing Center (NERSC), a U.S. Department of Energy Office of Science User Facility operated under Contract no. DE-AC02-05CH11231.

Attosecond chronoscopy of correlations between conducting electrons in quantum materials

J. Freudenstein[1], M. Meierhofer[1], M. Borsch[2], D. Afanasiev[1], M. Liebich[1], M. Knorr[1], M. Kira[2], R. Huber[1]
[1] *University of Regensburg, 93040 Regensburg, Germany*
[2] *University of Michigan, Ann Arbor, Michigan 48109, USA*

Correlations between delocalized Bloch electrons are the driving force behind key properties of solids as well as intriguing phase transitions [1]; to directly follow how many-body interactions affect intrinsic electron motion, sub-femtosecond temporal resolution is desirable [2]. Multi-terahertz (THz) photon energies are perfectly matched to resonantly probe millielectronvolt (meV) correlation-induced excitations [3] and THz fields have been used to control charge carriers on subcycle time scales [4]. Yet, resolving the influence of correlations on the attosecond dynamics of delocalized Bloch electrons has remained an open challenge.

Here we directly reveal the effect of many-body interactions on the motion of delocalized electrons, in the time domain, by combining attosecond resolution with meV energy selectivity, for the first time [5]. Our clocking concept (Fig. 1a) employs the force of an intense few-cycle THz pulse (dark-grey shaded area). At a tunable delay time, t_{ex}, a 9-fs near-infrared excitation pulse creates electron–hole (*e*–*h*) pairs by resonant interband transitions. As the freshly generated *e*–*h* pairs are separated by the THz field, their relative momentum, $\hbar k$, and their relative coordinate, x, increase. Upon reversal of the polarity of the THz field, both $\hbar k$ and x decrease. For a favorable excitation time, the *e*–*h* pairs can recollide at $x = 0$ (blue trajectory), generating high-order sideband (HSB) radiation. For less optimized t_{ex}, the *e*–*h* pairs will not recollide, yielding weak HSB emission.

Whereas quasi-free *e*–*h* pairs follow ballistic trajectories governed by the single-particle band structure (Fig. 1a), strong many-body correlations (Fig. 1b), such as excitonic binding (purple field lines) and interactions with other carriers modify the trajectories and, thus the optimal excitation time. Coulomb attraction, for instance, acts as a restoring force. In order to reach large relative momenta and therefore enable highly energetic recollisions, an enhanced action of the THz field during the separation phase of the *e*–*h* pair is needed. This can be achieved by optical excitation at earlier t_{ex} (Fig. 1b, blue trajectory). Overall, the different dynamics for quasi-free versus correlated charge carriers should manifest in a measurable shift, Δt, of the optimum injection time t_{ex}.

The vastly different strength of Coulomb interactions in bulk and monolayer WSe_2 offer a perfect benchmark to test this concept. By actively stabilizing our setup [6], even shifts as small as 300 as of

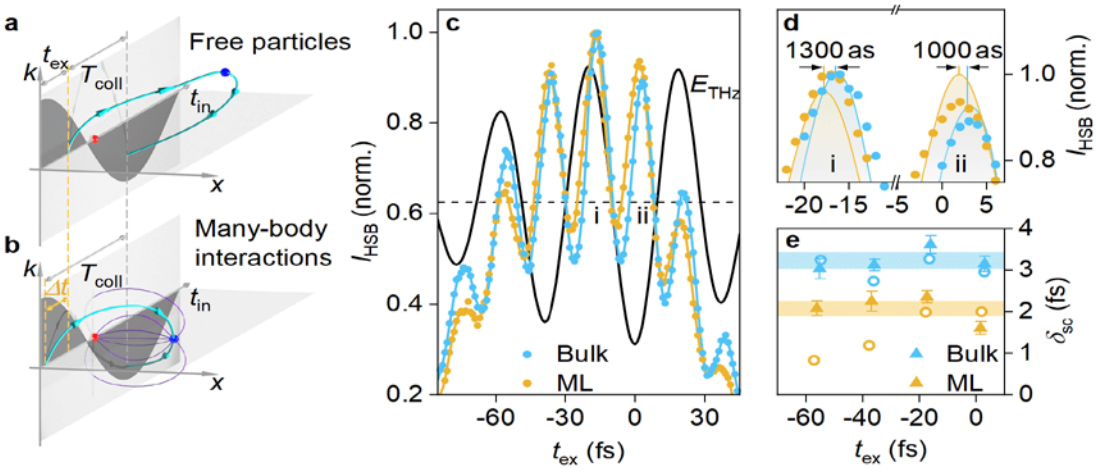

***Fig. 1. a**, **b**, Attosecond correlation clocking. An e–h pair created at excitation time t_{ex} is accelerated by the force of an intense THz waveform (**dark-grey shaded area**), changing e–h distance x and relative crystal momentum $\hbar k$. Uncorrelated e–h pairs (**a**) generated shortly after a THz field crest ballistically recollide at a delay time T_{coll} (**blue trajectory**), emitting HSB radiation. Many-body interactions (**b**), such as excitonic e–h pair correlations (**purple field lines**) modify trajectories and reduce T_{coll}. Δt indicates the difference between optimum t_{ex} with and without many-body interactions. **c**, Experimental THz driving field centered at 25 THz. **d**, Experimentally recorded HSB intensity, I_{HSB}, from bulk (**blue**) and monolayer WSe_2 (**orange**). **e**, Close-up of two I_{HSB} maxima compares experiment (**spheres**) with QDCE-computations (solid lines). The timing differences extracted from measurements are labelled. **f**, Measured subcycle delay δ_{sc} in bulk (blue) and monolayer (**orange**) WSe_2. Shaded areas indicate peak-averaged values $\langle \delta_{sc}^{bulk} \rangle = 3.2 \pm 0.2$ fs and $\langle \delta_{sc}^{ML} \rangle = 2.1 \pm 0.2$ fs.*

the optimal t_{ex} can be detected, corresponding to 0.7% of the driving field's oscillation period. In a first set of experiments, a peak THz field of E_{peak} = 4.9 MV cm^{-1} (Fig. 1c) was used. Both monolayer and bulk show a strongly modulated high-order sideband emission as a function of t_{ex}. Close inspection of the peaks of the HSB generation reveals a small temporal shift between the bulk and monolayer case. For a quantitative analysis, the subcycle delay δ_{sc}, which is the timing difference between the HSB emission peaks and the nearest THz field crest, is extracted. Figure 1d shows the measured HSB emission (data points) for two distinct peaks. Full quantum dynamic cluster expansion (QDCE) computations (solid lines) corroborate the temporal shape of the HSB emission and link the significant reduction of $\langle\delta_{sc}^{bulk}\rangle = 3.2 \pm 0.2$ fs to $\langle\delta_{sc}^{ML}\rangle = 2.1 \pm 0.2$ fs between bulk and monolayer (Fig. 1e) to enhanced excitonic correlations in the monolayer case [5].
To explore how excitonic attraction competes with lightwave-driven charge separation, we measure the average subcycle delay in bulk and monolayer WSe_2, for various fields E_{peak}. (Fig. 2a).

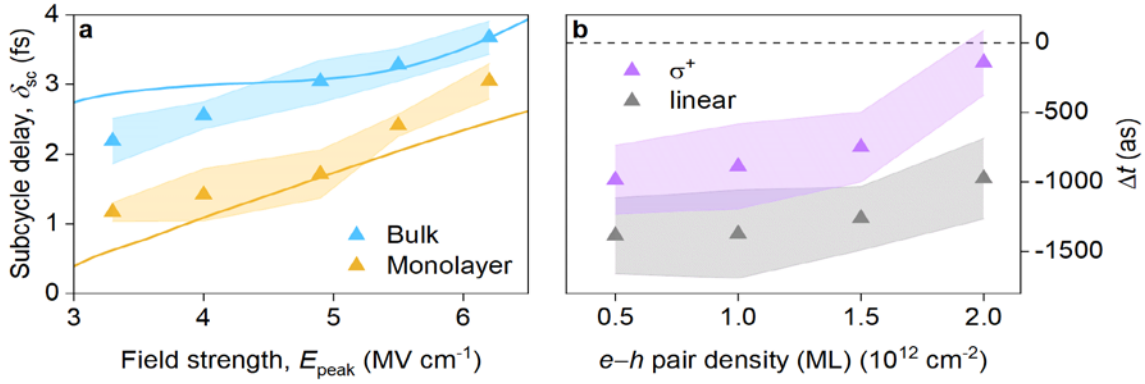

***Fig. 2. a**, Measured (triangles and shaded areas) and QDCE-computed (solid lines) subcycle delay δ_{sc} and their respective standard error (areas) for bulk (blue) and monolayer WSe_2 (orange) as a function of the peak THz field strength E_{peak}. **b**, Averaged subcycle delay difference, $\Delta t = \delta_{sc}^{ML} - \delta_{sc}^{bulk}$ and their respective standard error (areas), measured between bulk and monolayer for linearly (grey triangles) and right circularly polarized excitation (purple triangles) as a function of the e–h pair density in the monolayer.*

The monotonic increase of δ_{sc} confirmed by our QDCE computations (solid lines); strong fields ionize the excitonic coherence faster, which reduces the probability of recollision in the subsequent THz half-cycle. Thus maximum I_{HSB} is reached for coherent excitons excited closer to a field zero-crossing (i.e. larger t_{ex}), explaining the observed δ_{sc} trend.
Additionally, even the valley pseudospin can be exploited to switch the strength of the Coulomb interaction $V_{\mathbf{k},\mathbf{k}'}$ between electrons at wave vectors **k** and **k**'. Specifically, the presence of electrons at **k** effectively reduces $V_{\mathbf{k},\mathbf{k}'}$ via Pauli blocking. Such a reduction is expected to be particularly strong in monolayer samples when circularly polarized light excites *e*–*h* pairs and blocks **k** states only in a single valley. Indeed, we find that $\Delta t = \delta_{sc}^{ML} - \delta_{sc}^{bulk}$, which ranges from -150 as to -1.4 fs, is significantly less negative (Fig. 2b), corresponding to a stronger reduction of $V_{\mathbf{k},\mathbf{k}'}$ for circular than for linear polarization. For large excitation fluences, Δt approaches zero – the quasi-free limit for the bulk. Our computations predict that δ_{sc} could even resolve correlation changes associated with the Mott transition from excitons to an electron–hole plasma. In conclusion, attoclocking delocalized Bloch electrons reveals many-body correlations in a completely new way – directly in the time domain – as demonstrated by correlation tuning in transition metal dichalcogenide monolayers and bulk crystals. Deciphering tailored correlation dynamics in artificial van-der-Waals heterostructures or naturally occurring correlated states in quantum materials could revolutionize our understanding of unexpected phase transitions and emergent quantum-dynamics for future electronic, optoelectronic, and quantum information technologies.

References

[1] I. A. Perakis, M. K. Rafailov, J. M. Auxier, *Proceedings "VII Ultrafast Dynamics and Metastability & Ultrafast Bandgap Photonics"* (2022).
[2] A. L. Cavalieri, N. Müller, T. Uphues, V. S. Yakolev, A. Baltuška, B. Horvath, B. Schmidt, L. Blümel, R. Holzwarth, S. Hendel, M. Drescher U. Kleineberg, P. M. Echenique, R. Kienberger, F. Krausz, U. Heinzmann, *Nature* **449**, 1029 (2007).
[3] T. Kampfrath, K. Tanaka, K. A. Nelson, *Nature Photonics* **7**, 680 (2013).
[4] J. Reimann, S. Schlauderer, C. P. Schmid, F. Langer, S. Baierl, K. A. Kokh, O. E. Tereshchenko, A. Kimura, C. Lange, J. Güdde, U. Höfer R. Huber, *Nature* **562**, 396 (2018).
[5] J. Freudenstein, M. Borsch, M. Meierhofer, D. Afanasiev, C. P. Schmid, F.Sandner, M. Liebich, A. Girnghuber, M. Knorr, M. Kira, R. Huber *Nature* **610**, 290 (2022).
[6] M. Meierhofer, S. Maier, D. Afanasiev, J. Freudenstein, J. Riepl, J. Helml, C. P. Schmid, R. Huber, *Optics Letters* **48**, 1112 (2023).

* The work in Regensburg has been supported by the Deutsche Forschungsgemeinschaft (DFG, German Research Foundation) through Project ID 422 314695032-SFB 1277 (Subproject A05) as well as Research Grant HU1598/8. Work in Ann Arbor has been supported by ARO through Award W911NF1810299, W.M. Keck Foundation and College of Engineering Blue Sky Research Program.

Time, energy and momentum resolved probing of charge order Dynamics in a Kagome metal

D.Azoury[1], A. von Hoegen[1], Y.Su[1], K.H. Oh[1], T. Holder[3], H. Tan[3], B. R. Ortiz[2], A. C. Salinas[2], S. D. Wilson[2]
B. Yan[3], N. Gedik[1]
[1]*Massachusetts Institute of Technology, Cambridge, MA02139, USA*
[2]*University of California, Santa Barbara, CA 93106, USA*
[3]*Weizmann Institute of Science, Rehovot 7610001, Israel*

The recently discovered group of superconducting kagome metals, AV_3Sb_5 (A = K, Rb, Cs) exhibit a variety of intertwined unconventional electronic phases, which emerge from a puzzling charge density wave (CDW) phase[1-3]. Understanding of this parent charge order is crucial for deciphering the entire phase diagram. However, the mechanism of the CDW is still controversial, and its primary source of fluctuations – the collective modes – have not been experimentally observed. Here, I will present recent results in which we used time- and angle- resolved photoemission spectroscopy to investigate the CDW phase of CsV_3Sb_5 (see Figure 1 top). After excitation with an ultrafast laser pulse, we obtained momentum resolved tomographic images of the CDW gap which shows the melting of the charge order within 250 fs (see Figure 1 bottom). Furthermore, we detect coherent oscillations at various high symmetry points across the electronic band-structure, and identify these modes as CDW induced phonons, in good agreement with recent Raman measurements[4]. In contrast, measuring the in-gap intensity dynamics reveals two new modes that were not previously detected by any other spectroscopic method. Our experimental results distinguish these modes from the phonon modes, and using DFT calculations, we show that they correspond to the collective excitations of the order parameter.

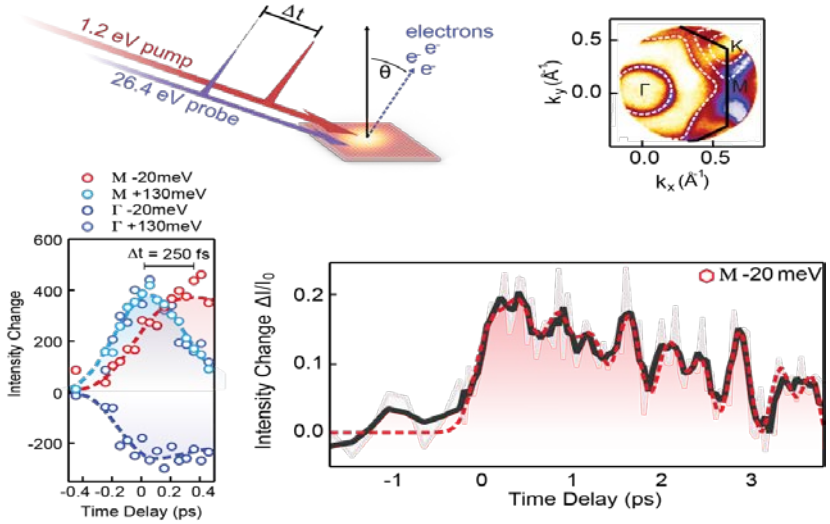

***Fig. 1. Top**: Schematic of the pump-probe high-harmonic angle-resolved photoemission experiment next to a false-color plot of the Fermi surface of CsV_3Sb_5 in the charge density phase. **Bottom**: Time-resolved intensity change at the **Γ** and **M** bands, the latter hosts the CDW, for two energies above (+130 meV) and below (-20 meV) the Fermi energy. The dynamics at the M band show a delay of 250 fs with respect to the dynamics at the Γ band. The dynamics at the M band are superimposed with coherent oscillations with frequencies of 1.6 THz and 2.4 THz. The faded line is the raw data, the black line is the data smoothed by a three-point average (provided as a guide to the eye) and the dashed line is a fit to the data.*

These observations together with ab-initio calculations provide clear evidence for a structural rather than electronic mechanism of the charge density wave. Our findings pave the way for better understanding of the unconventional phases hosted on the kagome lattice.

References

[1] B. R. Ortiz, L. C. Gomes, J. R. Morey, M. Winiarski, M. Bordelon, J. S. Mangum, I W. H. Oswald, J. A. Rodriguez-Rivera, J. R. Neilson S. D. Wilson, E. Ertekin, T. M. McQueen, E. S. Toberer, *Physical Review Materials* **3**, 094407 (2019)
[2] H. Zhao, H. Li, B. R. Ortiz, S. M. L Teicher, T. Park, M. Ye, Z. Wang, L. Balents, S. D. Wilson, I. Zeljkovic, *Nature* **599**, 216 (2021).
[3] H. Chen, H. Yang, B. Hu, Z. Zhao, J. Yuan, Y. Xing, G. Qian, Z. Huang, G. Li, Y. Ye, S.Ma, S. Ni, H. Zhang, Q. Yin, C. Gong, Z. Tu H. Lei, H. Tan, S. Zhou, C. Shen, X. Dong, B. Yan, Z. Wang, H.-J. Gao, *Nature* **599**, 222 (2021).
[4] S. Wu, B. R. Ortiz, H. Tan, S. D. Wilson, B. Yan, T. Birol, G. Blumberg, *Physical Review* B **105**, 155106 (2022).

* Acknowledgement(s) : Alexander von Hoegen acknowledges support from the Alexander von Humboldt foundation. We acknowledge support from the US Department of Energy and Gordon and Betty Moore Foundation's EPiQS Initiative grant GBMF9459. *B.Y. acknowledges the financial support by the European Research Council (ERC Consolidator Grant "NonlinearTopo", No. 815869) and the ISF - Personal Research Grant (No. 2932/21). S.D.W., B.R.O., and A.C.S. gratefully acknowledge support via the UC Santa Barbara NSF Quantum Foundry funded via the Q-AMASE-i program under award DMR-1906325.*

Ultrafast time-reversal symmetry breaking: Magnetism and entropy production

R.M. Geilhufe
Chalmers University of Technology, 41296 Gothenburg, Sweden

High intensity THz lasers allow for the coherent excitation of individual phonon modes. The ultrafast control of emergent properties by means of phonons opens up new tuning mechanisms for functional materials. Such properties are often related to the targeted breaking of symmetries. Here, we focus on the breaking on time-reversal symmetry, connected to two phenomena. First, the emergence of magnetism due to chiral phonons. Second, the process of entropy production for laser induced phonons. Chiral phonons are lattice excitations with finite angular momentum. As individual ions in a crystal are charged, a circular ionic motion induces a magnetic field. However, the expected field strength due to an ionic motion is tiny and of the order of the nuclear magneton [1,2]. Astonishingly, recent experiments show the opposite effect [3-5]. Independently of the material class, a huge phonon magnetic moment has been observed, being in the order of the Bohr magneton, i.e., 4-5 orders of magnitude larger than predicted for an ionic effect. Hence, a coupling and angular momentum transfer to electrons should be involved. The linear coupling of phonon angular momentum and spin angular momentum is a consequence of inversion and time-reversal symmetry. However, the exact coupling constant is unknown. A part of this coupling constant is related to the spin-orbit interaction of electrons combined with conventional electron-phonon coupling. Here, we show that an additional effect emerges, based on the accelerating ionic motion. In fact, inertial effects on electrons couple the ionic angular momentum to the electron spin, in a quantum version of the classical Coriolis force. We derive this contribution and estimate its effect on the spin-polarization of electronic states in KTaO3 (see Fig 1 left).In the second part of the talk we pay attention towards ultrafast thermodynamic processes connected to the laser excitation. Even though, it is known that an intense laser field induces heat in a sample, the microscopic mechanisms for heat or entropy production connected to a laser excitation have only sparsely been discussed. In particular the dynamics of heat and entropy production during the excitation process is unknown in most cases.

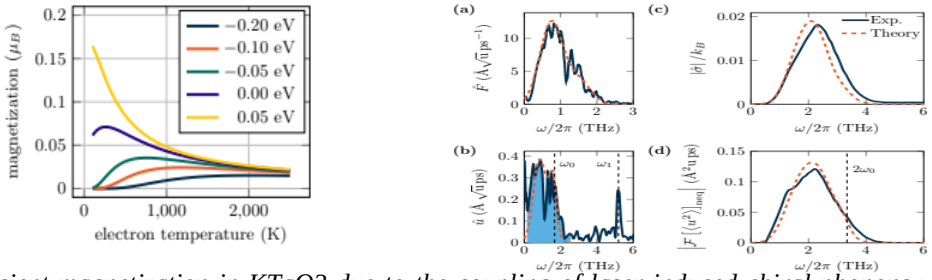

***Fig. 1. Left**: Transient magnetization in KTaO3 due to the coupling of laser induced chiral phonons with the electron spin. The magnetization depends on the doping level (colored lines in units of fermi level energy against conduction band edge) and the electronic temperature due to the laser excitation. **Right**: Entropy production in SrTiO3 obtained using the formalism of Ref [8] and experimental data from Ref [9]. Comparison of theoretical and experimental laser profile **(a)** and phonon amplitude **(b)**. The computed entropy production is shown in (c), the displacement-displacement correlation in **(d)**.*

To make progress in this direction, I will introduce a model to calculate the entropy production in a pump-probe experiment. While entropy has been known for almost 200 years, it cannot be measured directly. Here, we show that tracking the ionic motion, e.g., in a time-resolved X-ray scattering experiment allows us to reproduce the process of entropy production in the presence of an applied laser field. This opens the prospect for an ultrafast thermodynamics approach to nonequilibrium quantum materials.

References

[1] D. M. Juraschek, N. A. Spaldin, *Physical Review Materials* **3**, 064405 (2019).
[2] R. M. Geilhufe, V. Juričić, S. Bonetti, J.-X. Zhu, A. V. Balatsky, *Physical Review Research* **3**, L022011 (2021).
[3] B. Cheng, T. Schumann, Y Wang, X. Zhang, D. Barbalas,S. Stemmer,and N. P. Armitage , *Nano Letters* **20**, 5991 (2020).
[4] F. G. G. Hernandez, A. Baydin, S. Chaudhary, F. Tay, I. Katayama, J. Takeda, H. Nojiri, A. K. Okazaki, P. H. O. Rappl, E. Abramof M. Rodriguez-Vega, G. A. Fiete, J. Kono, *arXiv:2208.12235* (2022).
[5] M. Basini, M. Pancaldi, B. Wehinger, M. Udina, T. Tadano, M. C. Hoffmann, A. V. Balatsky, S. Bonetti, *arXiv:2210.01690* (2022).
[6] R. M. Geilhufe, *Physical Review Research* **4,** L012004 (2022).
[7] R. M. Geilhufe, W. Hergert. *Physical Review* B **107**, L020406 (2023).
[8] L. Caprini, H. Löwen, R. M. Geilhufe, *arXiv:2302.02716* (2023).
[9] M. Kozina, M Fechner, P. Marsik, T. van Driel, J. M. Glownia, C. Bernhard, M. Radovic, D. Zhu, S. Bonetti, U. Staub, M. C. Hoffmann, *Nature Physics* **15**, 387 (2019).

* Acknowledgement(s) : RMG acknowledges support from the Swedish Research Council (VR starting grant No. 2022-03350) and Chalmers University of Technology. Computational resources were provided by the Swedish National Infrastructure for Computing (SNIC) via the National Supercomputer Centre (NSC).

Direct observation of few-femtosecond Spin currents across metallic layers

R. Géneaux[1], H.-T. Chang[2], A. Guggenmos[2], F. Légaré[3], K. Légaré[3], J. Lüning[4], T. Parpieev[2]
B. R. de Roulet[2], M. W. Zürch[2], S. Sharma[6], M. Schultze[7], S.R. Leone[2]
[1] *Université Paris-Saclay, 91191 Gif-sur-Yvette, France*
[2]*University of California, Berkeley, CA 94720, USA*
[3]*Institut National de la Recherche Scientifique, Varennes, QC J3X 1P7, Canada*
[4]*Sorbonne Université, 75005 Paris, France*
[5] *Lawrence Berkeley National Laboratory, Berkeley, CA 94720, USA.*
[6]*Max-Born-Institut für Nichtlineare Optik und Kurzzeitspektroskopie, 12489 Berlin, Germany*
[7]*Graz University of Technology, 8010 Graz, Austria*

Femtosecond laser pulses are able to act on the magnetic moments of solids, as amply demonstrated by magneto-optical experiments [1, 2]. However, the vast majority of control schemes make use of incoherent interactions (scattering, diffusion) between electrons, spins and phonons. On the contrary, the observation of direct and coherent interactions between light and spins has been scarce, despite first hints discovered more than ten years ago [3].Here we examine the ultrafast spin response of Co/Pt multilayers when driven by 4 fs laser pulses. The material response is captured by magnetic circular dichroism (MCD) using broadband attosecond pulses, an extension of the well-developed attosecond transient absorption method [4]. This recently developed approach [5] is extended here by measuring MCD across both the Pt $O_{2,3}$ and the Co $M_{2,3}$ edges in a spectrally continuous way, as shown in Figure 1. The method thus combines outstanding time resolution and element-specificity, providing a layer-resolved probe of electronic and spin dynamics. Importantly, the experiment can unambiguously separate electronic and magnetic contributions to both the absorption and MCD of the sample. We observe that the electronic excitation is simultaneous in Pt and Co layers (within an uncertainty of 1.5 fs). However, the rise time of carrier signal differs between the two elements, with the rise time in Pt being systematically 1.5 times faster than in Co. This rise time can be ascribed to electron thermalization times, and thus this difference can be interpreted as different pre-thermal (sub-15 fs) electron processes in either metal. This is possibly linked to different screening environment in each metals [6].The spin response of each layer uncovered by attosecond magnetic circular dichroism is markedly different. The system shows a sub-5 fs spike of magnetization in the platinum layer, simultaneously with a strong magnetization decrease in cobalt (see right of Fig. 1).

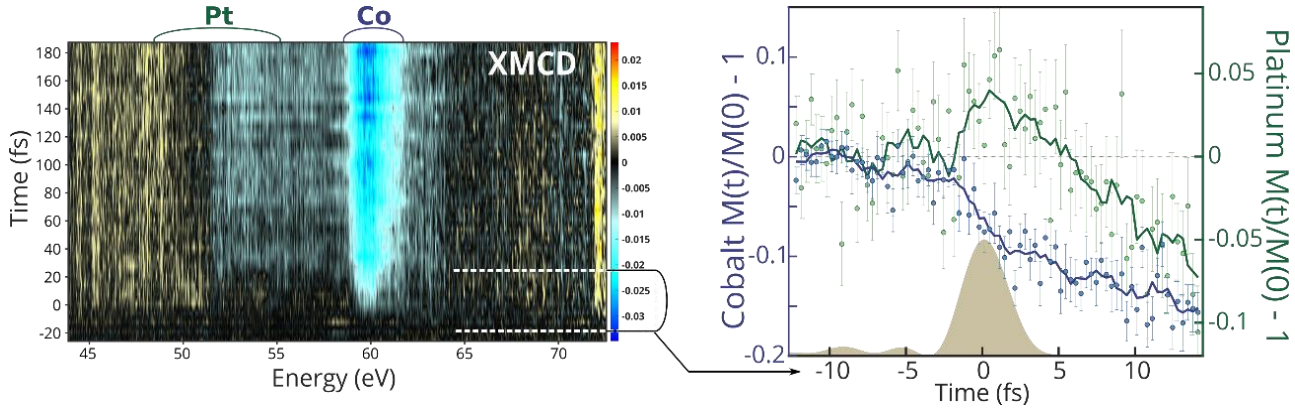

***Fig. 1. Left**: Broadband magnetic circular dichroism measured across both Pt and Co edges **(indicated on top)**. **Right**: Measured dynamics of the Co and Pt magneto-optical index at very early time delays. The **brown** shaded area indicates the measured pump pulse intensity profile.*

After that, both magnetic moments begin to decay with two distinct timescales, ascribed to coherent and incoherent demagnetizing processes. Simulations in the framework of fully noncollinear time-dependent density functional theory (TD-DFT) [7] reproduce this behavior. We interpret our observations as a coherent light-driven spin injection across the metallic layers of the junction, making it one the shortest spin current ever observed. Our findings suggests that our ability of shaping light fields in refined ways could be translated into the shaping of spin currents in materials.

References

[1] E. Beaurepaire, J.-C. Merle, A. Daunois, J.-Y. Bigot, *Physical Review Letters* **76**, 4250 (1996).
[2] C.D. Stanciu, *Physical Review Letters* **99,** 047601 (2007).
[3] J.-Y. Bigot, M. Yomir, E. Beaurepaire, *Nature Physics* **5**, 515 (2009).
[4] R. Geneaux, H.J. B. Marroux, A. Guggenmos, D. M. Neumark, S.R. Leone, *Philosophical Transactions Royal Society A* **377, 20170463 (2019).**
[5] F. Siegrist, J. A. Gessner, M. Ossiander, C. Denker, Y.-P. Chang, M. C. Schroder, A. Guggenmos, Y. Cui, J. Walowski, U. Martens, J. K. Dewhurst, U. Kleineberg, M. Munzenberg, S. Sharma, M. Schhultze, *Nature* **571,** 240 (2019).
[6] B.Y. Mueller,B. Rethfeld, *Phyical. Review B* **87,** 035139 (2013).
[7] J. K. Dewhurst, P. Elliott, S Shallcross, E. K. U. Gross, S. Sharma, *Nano Letters* **18,** 1842 (2018).

First results of high-resolution pp-RIXS on Correlated materials from the European XFEL

G. Ghiringhelli[1], L. Adriano[2], A. Alic[3], D.R. Baykusheva[13], R. Carley[2], G.S. Chiuzbaian[3]
M.P.M. Dean[4] ,O. Duros[3], A. Foelisch[5], M. Först[6], B.K. Freelon[7], N. Gerasimova[2], X. Jiang[8], D. Jost[9]
M. Kusch[5], T. Laarman[10], V. Lebedev[1], W.S. Lee[9], C.Y. Liu[5], L. Martinelli[1], L. Mercadier[2], G. Merzoni[1]
M. Minola[12], M. Mitrano[13], S. Molodtsov[2], C.S. Pathiraja[7], S. Parchenko[2], J.N. R. Pelige[7], Y.Y. Peng[8]
Q. Qiu[7], T. Schmitt[14], J. Sears[4], A. Scherz[2], S. S. N. Lalithambika[10], S. Techert[10], M. Teichmann[2]
S.F.R. TenHuisen[13], B. van Kuiken[2], Z. Yin[2], J. Schlappa[2]
[1] *Politecnico di Milano, 20133 Milano, Italy*
[2] *European XFEL, 22869 Schenefeld,, Germany*
[3] *Sorbonne University, 75252 Paris, France*
[4] *Brookhaven National Laboratory, Upton, NY 11973, USA*
[5] *Helmholtz-Zentrum Berlin für Materialien und Energie, 12489 Berlin, Germany*
[6] *Max-Planck-Institut für Struktur und Dynamik der Materie, 22761 Hamburg, Germany*
[7] *University of Houston, Houston, TX 77021, USA*
[8] *Peking University, Beijing 100871, China*
[9] *Stanford University, Menlo Park, CA 94305, USA*
[10] *Deutsches Elektronen-Synchrotron DESY, 22607 Hamburg, Germany*
[11] *University of Limerick, V94 T9PX, Ireland*
[12] *Max Planck Institute for Solid State Research, 70569 Stuttgart, Germany*
[13] *Harvard University, Cambridge, MA 2138, USA*
[14] *Paul Scherrer Institut, 5232 Villigen, Switzerland*

Pump-probe spectroscopy has a rich tradition in the optical regime but is quite a novelty in the x-rays. X-ray free electron lasers (XFEL) provide brilliant sources of ultrashort x-ray pulses that offer new opportunities in this direction. In the first generation of XFELs the low repetition rate has been the main limiting factor when dealing with photon hungry techniques such as photoelectron spectroscopy and inelastic scattering. The constraints are even more stringent when working with solid samples that can easily be damaged by very energetic x-ray pulses, thus further reducing the useable average flux. Moreover, some difficulties in scanning the x-ray photon energy and in changing their polarization have slowed down even the simplest of all x-ray spectroscopies, i.e., x-ray absorption spectroscopy (XAS). Among the spectroscopic techniques available at synchrotron x-ray sources, resonant inelastic x-ray scattering (RIXS) spectra are particularly rich in information about the electronic and magnetic properties of materials, because they host several excitations, of orbital, charge spin and vibrational character. In particular, the current state of the art RIXS instruments at synchrotrons (20-40 meV total linewidth) allow resolving not only the crystal field excitations, but also magnons and paramagnons, optical phonons, particle-hole pairs and charge density fluctuations. Two decades of instrumentation development have therefore boosted RIXS to be the most innovative x-ray spectroscopy for the study of quantum materials, in which different degrees of freedom are all relevant and multiply entwined. Therefore, RIXS is probably the most promising spectroscopy for XFELs, if sufficient resolution can be achieved both in energy and in time. So far the pioneering work realized with low repetition rate x-ray FELs [1,2,3] suffered from low resolution and low statistical quality. In this context, the availability of the hRIXS spectrometer at the spectroscopy and coherent scattering (SCS) instrument of the European XFEL in Hamburg [4] is a major step forward. Thanks to the high repetition rate, the average flux on the sample is comparable if not larger than the typical one at storage ring x-ray sources, even when the number of photons per pulse stays below the damaging threshold. The necessary flux reduction is obtained not only with gas attenuators, but also by the action of the beam line monochromator that selects a very narrow bandwidth in energy. In the first months of 2022, thanks to hRIXS we could measure, for the first time, pump probe (pp) RIXS in the soft x-ray range, combining time resolution around 100 fs and energy resolution around 100 meV at Cu and Ni L_3 edges. This achievement was possible thanks to the joint efforts of the SCS staff and of the hRIXS User Consortium who designed and realized the beam line and the spectrometer in close collaboration. The commissioning runs were open to the broad RIXS community, who could thus provide help while directly learning how to operate the instrument. For this very first high-resolution pp-RIXS experiment, we selected two charge transfer antiferromagnetic insulators based on divalent Ni and Cu, the cubic NiO and the layered perovskite La_2CuO_4 (LCO). We used an optical pump able to promote electrons across the Mott gap, as longer wavelength pulsed sources in the far IR and THz range, more suitable for the fine tuning of some transport properties [5,6] were not available. The temporal resolution was about 100 fs and the energy resolution 93 meV for Cu L_3 (931 eV) and ≈ 80 meV for Ni L_3 (853 eV) edges. We acquired spectra changing the pump delay between -0.2 ps and 50 ps, and the laser fluence on the sample between 1 mJ/cm^2 up to 35 mJ/cm^2.Although issued from a technical commissioning, where the priority was on the instrumentation, the results are extremely exciting. First, the static RIXS spectra

taken at EuXFEL are in all consistent with those measured with similar resolution at synchrotrons. This means that the short pulses do not influence the RIXS process itself and the high power peak does not damage the sample. Second, a few ps dynamics is detected at the elastic, quasi-elastic (phonon envelope) and magnon peaks in both samples. Also, the *dd* excitations get modified by the optical pump over a longer timescale of tens of ps, more related to the thermalization from the electronic bath to the lattice. Moreover, in NiO a transient excitonic state is populated by the optical pump, which is clearly detected in XAS and leads in RIXS to new spectral features, both in the energy-loss and energy-gain sector of the spectrum. The data analysis is still ongoing, also with the theoretical support by several groups. These results demonstrate the huge potential of high-resolution pp-RIXS for the study of quantum matter: the superior specificity and sensitivity of RIXS with respect to more established pp-techniques can be exploited in multiple ways. Moreover, when lower photon-energy pump pulses will be available pp-RIXS will also be an exceptional tool for the exploration of transient metastable states in complex materials. We note that the hRIXS spectrometer can be used also to study molecular systems thanks to an in vacuum liquid-jet system, therefore providing access to the dynamics of photo-dissociation and of charge transfer mechanisms in molecules.

References

[1] M. P. M. Dean, Y. Cao, X. Liu, S. Wall, D. Zhu, R. Mankowsky, V. Thampy, X. M. Chen, J. G. Vale, D. Casa, J. Kim, A. H. Said, P. Juhas R. Alonso-Mori, J. M. Glownia, A. Robert, J. Robinson, M. Sikorski, S. Song, M. Kozina, H. Lemke, L. Patthey, S. Owada, T. Katayama M. Yabashi, Yoshikazu Tanaka, T. Togashi, J. Liu, C. Rayan Serrao, B. J. Kim, L. Huber, C.-L. Chang, D. F. McMorrow, M. Först J. P. Hill *Nature materials* **15,** 601 (2016).

[2] M. Mitrano, S. Lee, A. A. Husain, L.Delacretaz, M. Zhu, G. De La Peña Munoz, S. X.-L. Sun, Y. I. Joe, A. H. Reid, S.F. Wandel, G.Coslovich W. Schlotter, T.Van Driel, J.Schneeloch, G. D. Gu, S. Hartnoll, N. Goldenfeld,P. Abbamonte, *Science Advances* **5,** 3346 (2019).

[3] E. Paris, C. W. Nicholson, S. Johnston, Y. Tseng, M. Rumo, G. Coslovich, S. Zohar, M. F. Lin, V. N. Strocov, R. Saint-Martin, A. Revcolevschi A. Kemper, W. Schlotter, G. L. Dakovski, C. Monney, and T. Schmitt, *NPJ Quantum Materials* **6,** 51(2021).

[4] N. Gerasimova, D. La Civita, L. Samoylova, M. Vannoni, R. Villanueva, D. Hickin, R. Carley, R. Gort, B.E. Van Kuiken, P. Miedema, L. Le Guyarder, L. Mercadier, G. Mercurio, J. Schlappa, M. Teichmann, A. Yaroslavtsev, H. Sinn, A. Scherz, *Journal of Synchrotron Radiation.* **29**, 1299 (2022)

[5] D. Fausti , R.I.Tobey, N.Dean, S. Kaiser, A. Dienst, M.C.Hoffmann, S. Pyon,T. Takayama, H. Takagi, A. Cavalleri, *Science* **331**, 6014 (2011).

[6] R. Mankowsky, A.Subedi, M. Först, S.O Mariager, M.Chollet, H.T Lemke, J.S Robinson, J.M Glownia, M. P Minitti, A.Frano, M. Fechner N.A Spaldin, T. Loew, B.Keimer, A.Georges, A.Cavalleri, *Nature* **516**, 71 (2014).

* Acknowledgement(s) : the hRIXS project was funded by Helmoltz Association (Germany), European X-FEL, European Research Council, Italian Ministry of Research (Italy), FIRI (Finland) and supported by University of Potzdam, HZB and DESY (Germany), Politecnico di Milano .

Influence of twist angle on ultrafast charge separation in WS_2-Graphene heterostructures

N. Hofmann[1], J. Gradl[1], N. Mishra[2], G. Orlandini[2], S. Forti[2], C. Coletti[3], A. Kleiner[4], S. Refaely-Abramson[4], I. Gierz[1]

[1] *University of Regensburg, 93053 Regensburg, Germany*
[2] *Istituto Italiano di Tecnologia, 56127 Pisa, Italy*
[3] *Istituto Italiano di Tecnologia, 16163 Genova, Italy*
[4] *Weizmann Institute of Science, Rehovot 7610001, Israel*

Since the discovery of graphene in 2004 the family of 2D materials has been growing steadily such that, by now, a whole zoo of high-quality 2D materials with a broad range of electronic properties is readily available. These 2D crystals can be stacked at will allowing for the fabrication of novel artificial materials with tailored electronic properties. Crucially, due to interlayer interactions, new electronic properties emerge that go beyond the sum of the electronic properties of the individual layers. One commonly encountered example with great relevance for optoelectronic applications is ultrafast charge separation following photoexcitation. The main driving force for charge separation is the band alignment (see Fig. 1). Provided that the band alignment is favorable, charge transfer occurs at those points in the Brillouin zone where the bands of the two participating layers hybridize and the wave function is delocalized over both layers. [1].

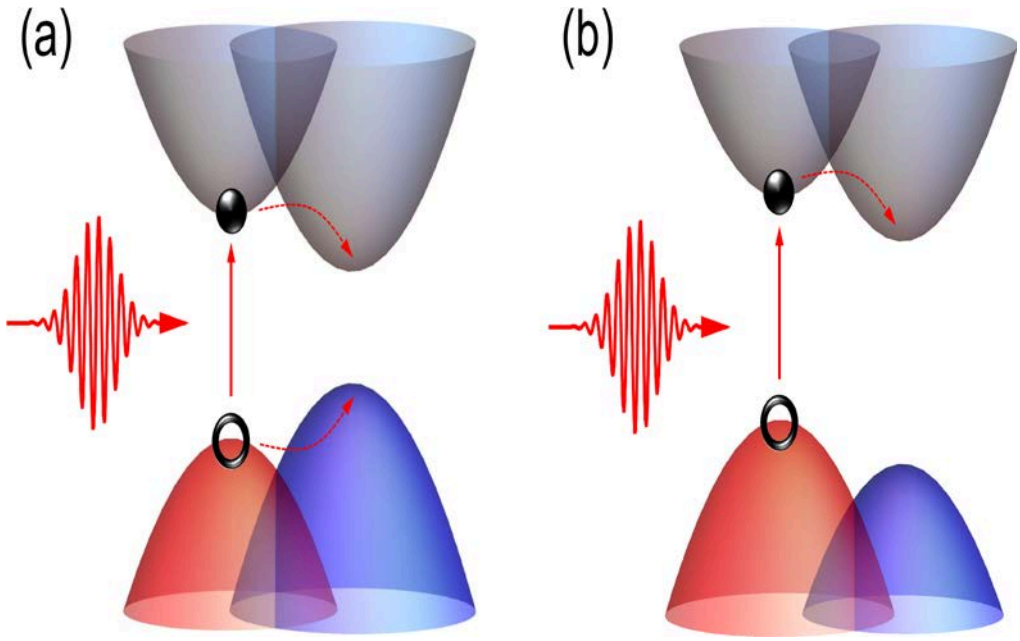

Fig. 1. *Ultrafast charge transfer in vdW heterostructures with type I* ***(a)*** *and type II* ***(b)*** *band alignment.*

Recently, is has been realized that the twist angle between the layers is a crucial parameter for controlling the band structure and therefor the electronic properties of various 2D van-der-Waals (vdW) stacks [2, 3]. The twist angle determines the orbital overlap between adjacent layers and thereby directly affects interlayer hybridization and – likely – non-equilibrium charge transfer.
We investigated the influence of the twist angle on ultrafast charge separation and recombination in WS_2-graphene vdW heterostructures using time- and angle-resolved photoemission spectroscopy (trARPES). We observe pronounced differences in the momentum- and energy-dependent non-equilibrium carrier and band structure dynamics for twist angles of 0° and 30°, that we interpret with the help of density functional theory band structure calculations. Our findings suggest that adjusting the twist angle in a vdW heterostructure can be used to tailor electron and hole transfer rates for specific applications.

References

[1] N. Hofmann, L. Weigl, J. Gradl, N. Mishra, G. Orlandini, S. Forti, C. Coletti, S. Latini, X. Lian, A. Rubio, D. Perez Paredes, R. Perea Causin, S. Brem, E. Malic, I. Gierz, *arXiv:2303.11856* (2023).
[2] Y. Cao, V. Fatemi, S. Fang, K. Watanabe, T. Taniguchi, E. Kaxiras, and P. Jarillo-Herrero, *Nature* **556**, 43 (2018).
[3] D. M. Kennes, M. Claassen, L. Xian, A. Georges, A. J. Millis, J. Hone, C. R. Dean, D. N. Basov, A. N. Pasupathy, A. Rubio, *Nature Physics* **17**, 155 (2021).

Atomic-level design and ultrafast THz *E*-field control of the emergent Ferromagnetism at oxide interfaces

A. X. Gray
Temple University, Philadelphia, PA 19122, USA

Interfacial charge transfer in oxide heterostructures gives rise to a rich variety of emergent electronic and magnetic phenomena [1]. As an example, epitaxial superlattices consisting of antiferromagnetic $CaMnO_3$ and paramagnetic $LaNiO_3$ exhibit emergent ferromagnetism that can be tailored by suppressing such charge transfer across the interface [2]. The ability to switch and tune this phenomenon enables precise control of the ferromagnetic state and, thus, has far-reaching consequences on the future strategies for the design of next-generation spintronic devices.
Here, we report a direct observation of the tunable character of interfacial charge transfer in $LaNiO_3/CaMnO_3$ superlattices using a combination of the depth-resolved soft x-ray standing-wave photoelectron spectroscopy [3], angle-resolved photoemission, and resonant magnetic x-ray scattering. Our results establish a connection between the depletion of the Ni 3*d* e_g states resulting in the metal-insulator transition in $LaNiO_3$, a charge-transfer-induced valence-state change of the interfacial Mn cations, and the concomitant suppression of the interfacial ferromagnetic state in $CaMnO_3$.We then use a combination of time-resolved magneto-optic Kerr effect, optical reflectivity, and transmissivity spectroscopies of variable-thickness $LaNiO_3/CaMnO_3$ superlattices to disentangle multiple interrelated electronic and magnetic processes driven by ultrafast high-field THz electric-field pulses.

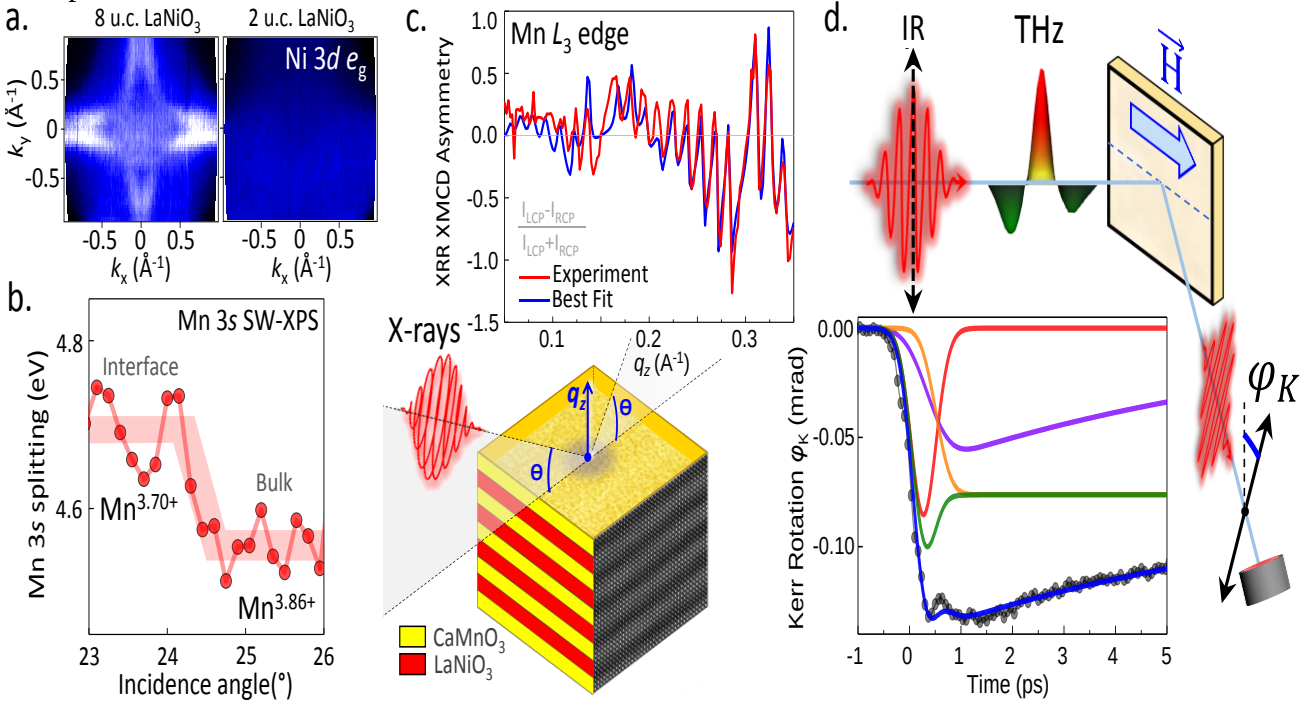

***Fig. 1. (a)**: Angle-resolved photoemission measurements of the $LaNiO_3$ layers in the $LaNiO_3/CaMnO_3$ superlattices grown in situ. Fermi-surface maps show depletion of the Ni 3d e_g states resulting in the metal-insulating transition in ultrathin (2 u.c.) $LaNiO_3$. **(b)**: Standing-wave x-ray photoelectron spectroscopy measurements of the Mn 3s core-level multiplet splitting show charge-transfer-induced valence-state change (by 0.16 e^-) of the interfacial Mn cations in $CaMnO_3$. **(c):** Specular angle-dependent soft x-ray reflectivity XMCD and the best fit to the experimental data measured at T = 20 K at the resonant Mn L_3 absorption threshold energy. The best fit model yields the magnetic interface thickness of 3.41 Å. **(d):** Schematics and the delay trace of the THz-pump IR MOKE probe response of the magnetic interface decomposed into several electronic and magnetic dynamical components.*

Our findings provide a new recipe for designing next-generation spintronic devices using charge-transfer and ultrafast external stimuli for efficient tuning and switching of low-dimensional electronic and magnetic states at interfaces.

References

[1] H. Chen, A. J. Millis, *Journal of Physics: Condensed Matter* **29**, 243001 (2017).
[2] R. U. Chandrasena, C. L. Flint, W. Yang, A. Arab, S. Nemšák, M. Gehlmann, V. B. Özdöl, F. Bisti, K. D. Wijesekara, J. Meyer-Ilse, E. Gullikson E. Arenholz, J. Ciston, C. M. Schneider, V. N. Strocov, Y. Suzuki, A. X. Gray, *Physical Review* B **98**, 155103 (2018).
[3] C.-T. Kuo, G. Conti, J. E. Rault, C. M. Schneider, S. Nemšák, A. X. Gray, *Journal of Vacuum Science & Technology* A **40**, 020801 (2022).
* Acknowledgements: authors acknowledge support from the U.S. Department of Energy, Office of Science, Office of Basic Energy Sciences, Materials Sciences and Engineering Division, under Award No. DE-SC0019297.

High energy few-cycle pulses around 12 µm for nonlinear Spectroscopy in the longwave-infrared

U. Griebner, P. Fuertjes, M. Bock, T. Elsaesser
Max Born Institute for Nonlinear Optics and Short Pulse Spectroscopy, 12489 Berlin, Germany

Few-cycle pulses at wavelengths beyond 10 µm are important for fundamental studies of the non-equilibrium properties of condensed matter, i.e., solids and liquids, and exhibit a high application potential, for example in optical materials processing. Our particular interest is on the study of molecular vibrations and/or for performing time resolved two-dimensional infrared spectroscopy [1]. The comparably small vibrational absorption cross sections require ultrashort pulses of sufficient energy in order to induce a nonlinear vibrational response. A technological challenge, however, is the limited availability of nonlinear crystals being transparent for the pump and the idler pulses and exhibiting high damage threshold. Thus, there has been limited improvement of ultrashort pulse longwave-infrared (LWIR) sources over the last two decades [2, 3]. Here we present a new light source that delivers femtosecond pulses beyond 10 µm wavelength with record parameters. The extremely compact system is based on the concept of optical parametric chirped pulse amplification (OPCPA). The LWIR source combines a novel type of front-end with the technology of picosecond 2-µm Ho:YLF regenerative amplifiers. The achieved idler peak power of 0.35 GW at 11.4 µm wavelength was sufficient to demonstrate the potential of this source for ultrafast spectroscopy beyond 10 µm in a nonlinear transmission experiment with liquid water.The OPCPA front-end consists exclusively of a commercial Cr:ZnS oscillator (IPG) operating at a repetition rate of 79 MHz. The oscillator provides pulses as short as 30 fs with a spectrum spanning from 1.9 µm up to 2.6 µm (30 dB-level) and 12.5 nJ energy. The emitted spectrum is sufficiently broad to seed the pump and the OPCPA at its signal frequency in parallel. The spectral components below 2.1 µm are separated with a dichroic mirror and seed the 2-µm pump, whereas the part above 2.1 µm is used directly as the signal input. The pump is a Ho:YLF regenerative amplifier providing pulses of a 3 ps duration and 13 mJ energy at a 1 kHz repetition rate [4]. Prior to amplification, the signal pulses of 46 fs duration are stretched in sapphire and phase shaped by an acousto-optic programmable dispersive filter (AOPDF). The first amplification stage is equipped with a 2 mm thick GaSe crystal, the second and the third with a 1 mm thick crystal. GaSe exhibits a high second order nonlinearity and a comparably high damage threshold. In all stages, the type II parametric process is phase matched at an internal angle of 12.2° (external angle: 36°). In total, only 6 mJ of the available pump is used for the three OPA stages in GaSe. All stages are pumped with a fluence of about 50 GW/cm^2. In the first stage, the signal pulses are amplified to 14 µJ. The second collinear stage generates idler pulses of 15 µJ energy at 11.4 µm, subsequently seeding the third stage. In the last amplification stage, the non-collinearity allows for a clean separation of the pump and the idler pulses.

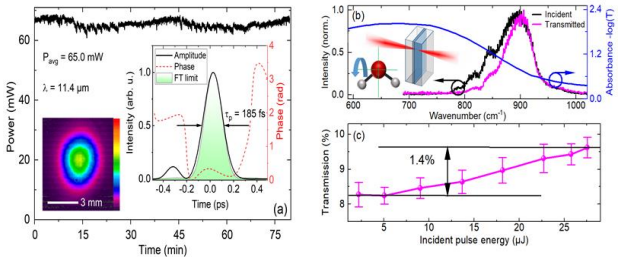

Fig. 1. (a) *Characterization of the LWIR OPCPA pulse performance, long-term pulse stability measurement.* ***Left inset****: Far-field intensity distribution.* ***Right inset****: Retrieved temporal pulse shape of the few-cycle pulse.* ***(b, c)*** *Nonlinear transmission of liquid water (12 µm thick film held between two transparent BaF_2 windows) at the librational (L2) band (vibration indicated by the blue circular arrow).* ***(b)*** *L2 absorption of water (blue line) and incident (black line) and transmitted (magenta line) spectra of the 11.4 µm pulses (energy: 25 µJ).* ***(c)*** *Transmission of the water sample as a function of incident pulse energy, showing a nonlinear transmission increase.*

The idler pulses are amplified to an energy exceeding 70 µJ.The spectrum has its center at 11.4 µm (877 cm^{-1}) and a full width at half maximum (FWHM) of 74 cm^{-1} (Fig. 1b) supporting a pulse duration of 172 fs. In principle, type II phase matching supports amplification beyond 12 µm. However, the spectral part above 13 µm is not accessible due to the group velocity mismatch in GaSe between the involved pulses. The idler pulses are characterized by the second-harmonic generation frequency-resolved optical gating technique. After compression in ZnSe and additional phase shaping with the AOPDF, we retrieve an idler pulse duration of 185 fs which corresponds to less than five optical cycles of the light wave (Fig. 1a, right inset). The compressed idler pulses have an energy of 65 µJ, corresponding to a peak power of 0.35 GW. In the 1 kHz train the pulses are highly stable with a rms-value of 1.9% and of excellent optical beam quality (Fig. 1a) [5]. The potential of this unique source for nonlinear spectroscopy was demonstrated. A fundamental and so far unaddressed problem of liquid water research is studied, the nonlinear response of librational excitations. These hindered rotations of water molecules were excited to such an extent that their optical absorption decreased significantly (Fig. 1b,c). The analysis of this absorption saturation suggests a lifetime of the librational excitation of 20 to 30 fs [5].

References

[1] A. Ashihara, N. Huse, A. Espagne, E. T. J. Nibbering, T. Elsaesser, *Journal of Physical Chemistry* A **111**, 743 (2007).
[2] M. Duda, L. von Grafenstein, M. Bock, D. Ueberschaer, P. Fuertjes, L. Roškot, M. Smrž, O. Novák, U. Griebner, *Optics Letters* **47**, 2891 (2022).
[3] A. Dubietis, A. Matijošius, *Opto-Electronic Advances* **6**, 2200460 (2023).
[4] P. Fuertjes, L. von Grafenstein, C. Mei, M. Bock, U. Griebner, T. Elsaesser, *Optics Express* **30**, 5142 (2022).
[5] P. Fuertjes, M. Bock, L. von Grafenstein, D. Ueberschaer, U. Griebner, T. Elsaesser, *Optica* **9**, 1303 (2022).

Quantum analog of vibration isolation, hidden order and high T Superfluorescence in lead-halide perovskites

K. Gundogdu
North Carolina State University, *Raleigh, NC 27695, USA*

As the demand for quantum approaches in computing, communication, and cryptology continues to soar, the quest for discovering new "quantum materials" has become an unparalleled necessity. While we possess an understanding of the required quantum properties for most applications, the guidelines for designing these materials still remain unclear, and the existence of quantum materials that function at room temperature remains scarce. A significant challenge we encounter is the limited lifespan of quantum coherent states at temperatures that are practically relevant. The fragility of the quantum phase, attributed to thermal scattering events, presents a fundamental obstacle. This prompts us to inquire: Do thermal processes inherently impede the design of quantum materials with extended coherence? Is there a means to safeguard quantum coherence despite the occurrence of thermal scattering? Remarkably, we have recently made an astonishing observation of room-temperature superfluorescence in lead-halide perovskites [1,2]. Superfluorescence (SF) arises from the macroscopic quantum state of optically excited dipoles, resulting in collective emission. Previously, SF has solely been observed in materials with discrete electronic transitions, such as two-level systems like quantum dots [3,4], defects in solids [5], or transitions between Landau levels formed under high magnetic fields (>10T) [5]. In all these instances, SF is confined to low temperatures due to the rapid thermal dephasing of electronic excitations. Thus, the discovery of room temperature SF in hybrid perovskites with extended electronic states (bands) is highly unexpected. This observation suggests the existence of a mechanism that protects the quantum phase of a system against thermal disturbances in lead-halide perovskites. Here, I will introduce the Quantum Analog of Vibration Isolation (QAVI) model, which we have proposed as a mechanism to protect the quantum phase of dipole oscillators from thermal dephasing. This model facilitates the phase transition of electronic dipoles into a superradiant state. In lead-halide perovskites, electronic excitations give rise to polaronic lattice distortions. These distortions manifest as low-energy lattice modes with LO-phonon characteristics. In such a configuration, the oscillations of polarons due to thermal phonon interactions depend on the frequency of the polaron and the thermal phonon involved. When a low-frequency thermal phonon scatters with the polaron, the polaron responds in phase. Conversely, when a high-frequency thermal phonon scatters with the polaron, the polaron responds out of phase.

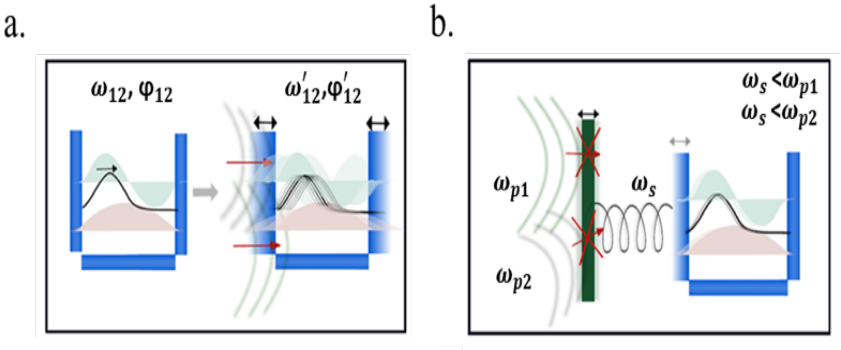

Fig. 1 (a) *Energy levels of a particle in a box simulates the quantum oscillator. The black line is a superposition state that oscillates within the box. The fluctuations in the box potential due to thermal phonons is illustrated as waves scattering off the walls and lead to dephasing of the quantum oscillator.* ***(b)*** *Once the polaron forms, electronic oscillator and the lattice distortion oscillator are strongly bound. This situation is illustrated as a spring that modulates the left wall in the box. Since incoming scattering phonons are molecular vibrations, they will impact the lattice distortion mode. This situation is a quantum analogue of vibrational isolation.*

This behavior effectively isolates the dipole from high-frequency thermal modes. In this presentation, I will share our studies conducted on lead-halide perovskites with different halide compositions.

References

[1] M. Biliroglu, G. Findik, J. Mendes D. Seyitliyev, L. Lei,Q. Dong,Y. Mehta,V.V. Temnov,F. So, K. Gundogdu, *Nature Photonics* **16,** 324 (2022).
[2] M. Findik, M. Biliroglu, D.Seyitliyev, J.Mendes, A. Barrette, H. Ardekani, L. Lei,Q. Dong, F. So, K.Gundogdu, *Nature Photonics* **15,** 676 (2021).
[3] G. Rainò, M.A. Becker, M.I. Bodnarchuk, R.F. Mahrt, M.V. Kovalenko, T.Stöferle, *Nature* **563,** 671 (2018).
[4] L. Phuong, K. Miyajima, K. Maeno, T. Itoh, M. Ashida, *Journal of Luminescence* **133,** 77 (2013).
[5] G. T. Noe II, J.-H. Kim, J. Lee, Y. Wang, A.K. Wójcik, S.A. McGill, D.H. Reitze,A.A. Belyanin, J.Kono, *Nature Physics* **8,** 219(2012).

Multi-photon absorption in direct-gap and indirect-gap Semiconductors

N. Cox, S. Faryadras, E. W. Van Stryland, D. J. Hagan
University of Central Florida, Orlando FL 32816, USA

Semiconductors have long been known to exhibit large two photon absorption (2PA) coefficients. It has also been shown that for extremely nondegenerate pairs of photons (energy ratios of approximately 10:1) the 2PA in direct gap semiconductors (e.g. GaAs, CdTe, ZnSe, ZnO, GaN) is enhanced over the degenerate value by up to 3 orders of magnitude [1]. This large nondegenerate (ND) 2PA has been shown be desirable for mid infrared detection, providing sensitive Mid-IR detection with uncooled, large bandgap semiconductors [2]. Large 2PA coefficients also correspond to large two-photon gain coefficients under population inversion, enabling the possibility of two-photon gain and lasing [3]. This nondegenerate enhancement has been shown to be even larger in quantum well systems, as demonstrated experimentally by Cox, et. al., [4]. In that paper, a waveguide geometry was used to allow propagation of TM waves, with electric field transverse to the waveguide, this allowing for allowed inter-subband transitions. In figure 1, we show theory and experimental results for a GaAs/AlGaAs quantum well structure using pump radiation at 1960 nm and a probe tunable between 1176 and 1326 *nm.*

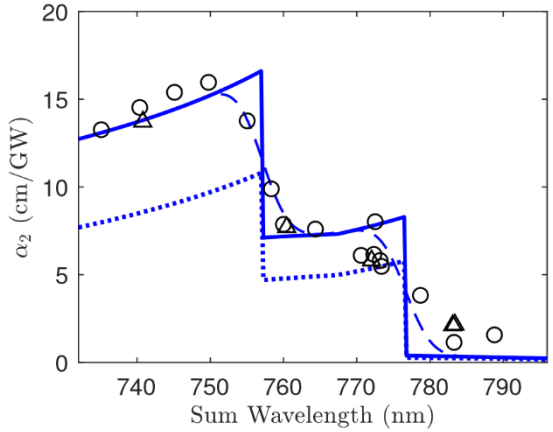

Fig. 1. *TM-TM ND-2PA coefficients vs sum wavelength (nm). Black circles: measured coefficients with total pulse energy* 3.5 *pJ. Black triangles: measured coefficients with pulse energy* 4.9 *pJ. Solid line: theory with 14-band basis. Dashed line: theory convolved with 4 nm Gaussian to approximate bandwidth effects.*

The ND2PA coefficients measured in Fig. 1 are not particularly large, but this particular experiment is not strongly nondegenerate. More nondegenerate experiments, with much longer pump wavelengths, are underway, but these are rater challenging due to the need to guide two waves of very different wavelength. Experiments with These results simply provide experimental proof of the theory. For much larger nondegeneracy, as the smaller photon energy approaches the inter-subband resonance, we anticipate that the ND2PA coefficients will grow rapidly, as shown in Fig. 2.

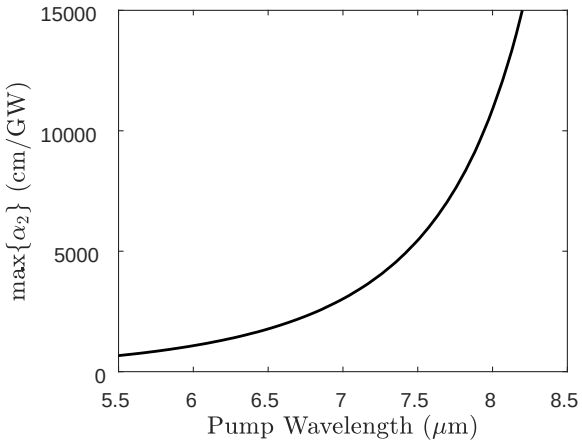

Fig. 2. *Maximum calculated TM-TM ND-2PA coefficient vs pump wavelength (nm) for the same quantum well structure used for Figure 1.*

With quantum well structure, we anticipate an enhancement of the 2PA coefficient of approximately a factor of 10 compared to bulk, and approximately a factor of 1000 over the degenerate case. While direct gap semiconductors have many advantages in photonics, Silicon is of practical interest for photonics applications due to its low cost and possibility for integration with electronics. However, its indirect bandgap provides a challenge in theoretical modeling since 2PA requires a phonon scattering process. This additional process means that there are many more possible transition schemes for 2PA in an indirect gap semiconductor, than for the direct-gap case.

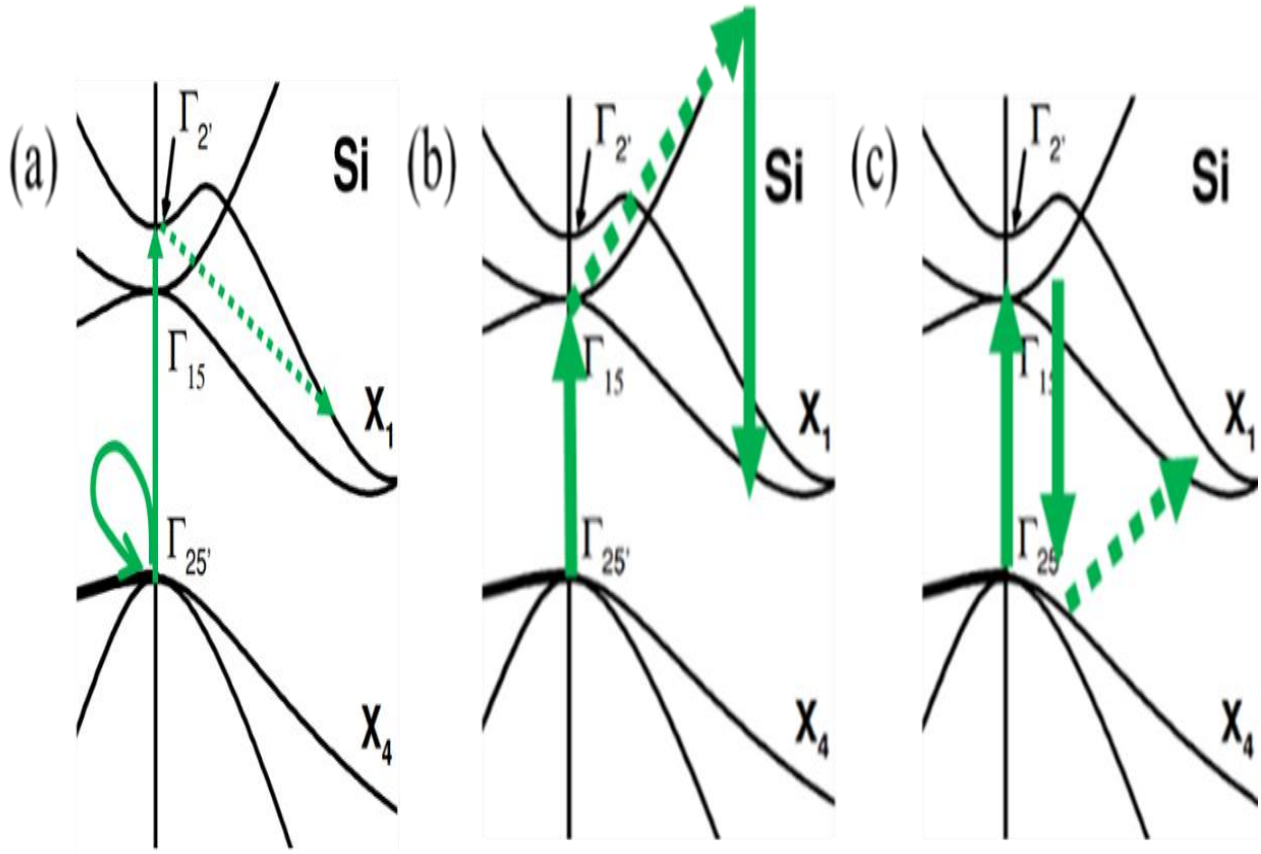

Fig. 3. *Diagrams for different transitions across the band structure of silicon, including, (a) allowed-forbidden, (b) allowed-allowed, and (c) another allowed-allowed transition.*

Despite this, the degenerate 2PA scaling in Silicon has been shown to be comparable to that of direct gap semiconductors with similar band gap energy. [5] As with direct gap semiconductors, these enhancements indicate the applicability of using nondegenerate 2PA as possible method for ultrafast, gated mid-IR detection using off-the-shelf Silicon photodiodes. It has also been shown that Mid-IR imaging can be achieved via ND2PA in Silicon cameras. [6] We present a model for nondegenerate 2PA (ND-2PA) in indirect semiconductors that is nearly identical to the direct gap theory with a phonon transition added as a perturbation step. We also experimentally investigate the enhancement of ND-2PA in Silicon for the extremely nondegenerate case using a femtosecond pump-probe arrangement, with several different Mid-IR pump wavelengths. In these experiments, the transmittance of a tunable near infrared probe pulse is monitored in the presence of a mid-IR pump pulse generated by difference frequency generation while varying the relative delay between pump and probe pulses. Our experimental results reveal that the 2PA enhancements due to nondegeneracy are similar to those seen in direct-gap semiconductors. However, the very low density of states near the indirect band edge is likely to restrict the enhancement for highly nondegenerate cases. Additionally, this nondegenerate 2PA data sheds light on which of the many transition schemes are dominant in the 2PA process in Silicon, something which up until now has remained somewhat unknown.

References

[1] C. M. Cirloganu, L. A. Padilha, D. A. Fishman, S. Webster, D. J. Hagan, E. W. Van Stryland, *Optics Express* **19**, 22951 (2011).
[2] D. A. Fishman, C. M. Cirloganu, S. Webster, L. A. Padilha, M. Monroe, D. J. Hagan, E. W. Van Stryland, *Nature Photonics* **5**, 561 (2011).
[3] M. Reichert, A. L. Smirl, G. Salamo, D. J. Hagan, E. W. Van Stryland, *Physical Review Letters* **117**, 073602 (2016).
[4] N. Cox, J. Wei, H. Pattanaik, T. Tabbakh, S.-P. Gorza, D. Hagan, E. W. Van Stryland, *Physical Review Research* **2**, 013376 (2020).
[5] A. D. Bristow, N. Rotenberg, H. M. VanDriel, *Applied Physics Letters* **90**, 191104 (2007).
[6] D. Knez, A. M. Hanninen, R. C. Prince, E. O. Potma, D. A. Fishman, *Light: Science and Applications* **9**, 125 (2020).

Ultrafast spectroscopic studies of topological quantum matter

M. Z. Hasan, I. Belopolski, S.-Y. Xu, M. Neupane, T. A. Cochrane, B. Kim
Princeton University, Princeton, NJ 08544, USA

Over the last decade, ultrafast techniques have been crucial to gain fundamental insights into the topological properties of quantum materials. We employed ultrafast time-resolved angle-resolved photoemission spectroscopy to probe and elucidate surface electronic structure and electron dynamics of Z_2 topological insulators, Dirac-Weyl semimetals, knotted quantum matter and exotic spin-orbit superconductors [1, 2, 3].

In this talk, I plan to present a few recent examples where ultrafast techniques have been crucial to discover the topological behavior: **(1)** It was long been speculated that $Mo_xW_{1-x}Te_2$ materials may realize Lorentz violating topological Weyl fermions. In order to explore its topology, we first showed theoretically that it is crucial to access the full electron dynamics to reveal a non-Lorentz electronic Weyl state in $Mo_xW_{1-x}Te_2$. Then, we experimentally explored $Mo_xW_{1-x}Te_2$ materials by a suite of pump-probe time-resolved ARPES techniques. By comparing our pump-probe results with *ab initio* simulations, we concluded that the materials indeed features topological states associated with non-trivial Berry curvature field which is the generator of the non-Lorentz Weyl topology and non-trivial Chern quantized numbers [4]. **(2)** In candidate topological semimetal class $TaIr(Te/Se)_4$, the Weyl points and Fermi arcs live entirely above the chemical potential level, making them inaccessible to conventional ARPES. We utilized ultrafast ARPES to directly access the electronic states above the Fermi level in $TaIrTe_4$. We observe signatures of Berry curvature singularity nodes and correspondingly coupled spin textured Fermi arcs states. A full map reveals, for the first time, that $TaIrTe_4$ is a topological metal (doped semimetal) with the minimum number of four Weyl nodes allowed by time-reversal symmetry [3]. **(3)** The third example would be on the possibility of novel phenomena induced by light. Here, we used pump-probe photoemission spectroscopy to explore the optically excited Dirac surface states in the bulk-insulating topological insulator Bi_2Te_2Se.

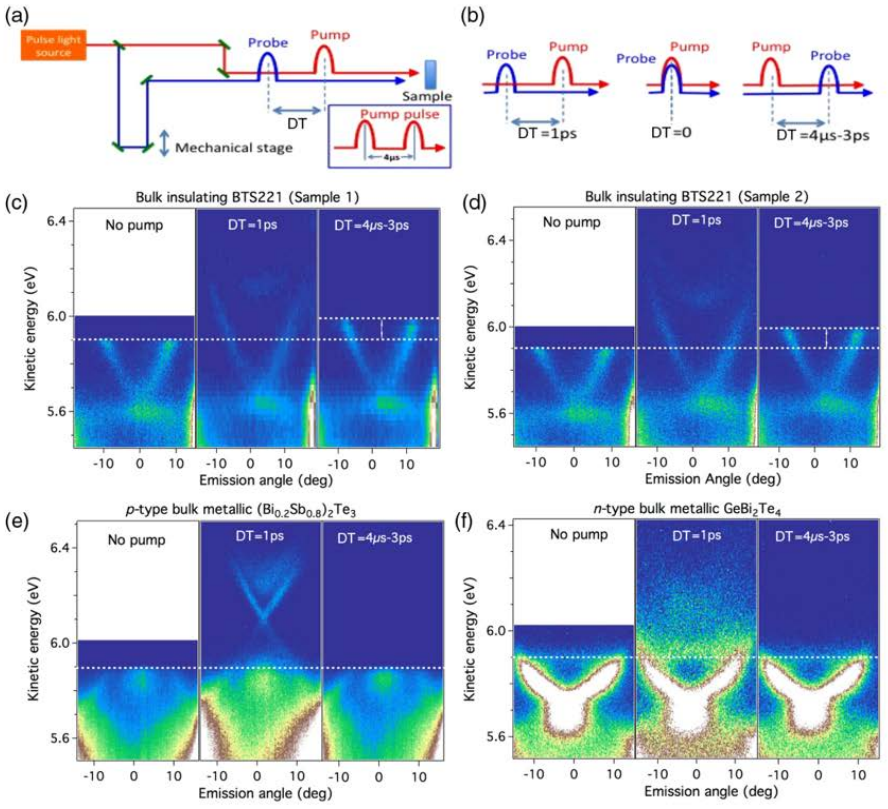

FIG. 1 (color online). Generation of photovoltage in a bulk insulating TI. (a),(b) Schematic view of the pump-probe ARPES experimental setup. The delay time is defined in (b). The inset in (a) shows the frequency of the pump pulse. (c) ARPES band dispersion of bulk insulating Bi_2Te_2Se (sample 1) near $\bar{\Gamma}$ point measured with no pump (left-hand panel), with pump (middle and right-hand panel). The delay time is noted on the spectra. (d) Similar measurement in (c) for Bi_2Te_2Se (sample 2). From (c) and (d) the generation of photovoltage (~100 mV) is evident in the bulk insulating sample. Similar measurement as in (d) for (e) *p*-type bulk metallic $(Bi_{0.2}Sb_{0.8})_2Te_3$ TI and (f) *n*-type bulk metallic $GeBi_2Te_4$ TI. No generation of the photovoltage is obtained for the bulk metallic topological insulators [see (e) and (f)]. The native Fermi level (Fermi level with the absence of pump pulse) is marked by the white dashed line in the spectra.

Our results revealed optical and ultrafast properties that are in sharp contrast to those of bulk-metallic (self-doped) topological insulators. We observed a gigantic optical lifetime exceeding **4 μs** for the surface states in Bi_2Te_2Se, whereas the lifetime in most topological insulators, such as Bi_2Se_3, has been limited to a few picoseconds. Moreover, we discovered a surface photovoltage, a shift of the chemical potential of the topological surface states, as large as 100 mV. Our results demonstrate a rare quantum platform to explore charge excitation and relaxation in energy and momentum space in two-dimensional systems [5]. **(4)** Finally, (time permitting) I will

talk about electronic structure and relaxation dynamics in a superconducting topological material. Topological superconductors host new states of quantum matter which show a pairing gap in the bulk and gapless surface states providing a platform to realize Majorana zero modes. Recently, alkaline-earth metal Sr intercalated Bi_2Se_3 has been reported to show superconductivity with a $T_c \sim 3$ K and a large shielding fraction. We report systematic electronic structure studies of $Sr_{0.06}Bi_2Se_3$ ($Tc \sim 2.5$ K). Using ARPES, we observed a quantum well confined two-dimensional state coexisting with a topological surface state in $Sr_{0.06}Bi_2Se_3$. Furthermore, our time-resolved ultrafast ARPES reveals the relaxation dynamics showing different decay mechanism between the excited topological surface states and the two-dimensional states. Our experimental observation is understood by considering the intra-band scattering for topological surface states and an additional electron phonon scattering for the 2D states, which is likely responsible for the superconductivity and topological phenomena [5-7].These ultrafast studies and their future extensions will be helpful in understanding low temperature superconducting states realized in these topological materials [6, 7].

References

[1] M. Z. Hasan, C. L. Kane, *Review of Modern Physics* **82**, 3045 (2010).
[2] D. N. Basov, R. D. Averitt, D. Hsieh, *Nature Materials* **16**, 1077 (2017).
[3] I. Belopolski, P. Yu, D. Sanchez, Y. Ishida, T. Chang, S. Zhang, S. Xu, H. Zheng, G. Chang, G. Bian, H.-T. Jeng, T. Kondo, H. Lin Z. Liu, S. Shin, M. Z. Hasan, *Nature Communications* **8,** 942 (2017).
[4] I. Belopolski, S. Xu, Y. Ishida, X. Pan, P. Yu, D. Sanchez, H. Zheng, M. Neupane, N. Alidoust, G. Chang, T. Chang, G. Bian, S. Huang,C. Lee D. Mou, L. Huang, Y. Song, B. Wang, G. Wang, Y. Yeh, Nan Yao, J. Rault, P. Le Fèvre, F. Bertran, H. Jeng, T. Kondo, A. Kaminski, H. Lin Z. Liu, F. Song , S. Shin, M. Z. Hasan, *Physical Review* B **94,** 085127 (2016).
[5] M. Neupane, S.-Y. Xu, Y. Ishida, S. Jia, B. Fregoso, C. Liu, I. Belopolski, G. Bian, N. Alidoust, T. Durakiewicz, V. Galitski, S. Shin, R. J. Cava M. Z. Hasan, *Physical Review Letters* **115,** 116801 (2015).

K-dependent band gap renormalization in a WS_2-graphene Heterostructure

N. Hofmann[1], A. Steinhoff[2], J. Gradl[1], N. Mishra[3], G. Orlandini[3], S. Forti[3], C. Coletti[4], S. Refaely-Abramson[5] T. Wehling[6], I. Gierz[1]

[1]*University of Regensburg, 93053 Reaensburg, Germany*
[2] *University of Bremen, 28359 Bremen Germany*
[3]*Istituto Italiano di Tecnologia, 56127 Pisa, Italy*
[4]*Istituto Italiano di Tecnologia, 16163 Genova, Italy*
[5]*Weizmann Institute of Science, Rehovot 7610001, Israel*
[6]*Institute for Theoretical Physics, University of Hamburg, Germany*

Monolayer transition-metal dichalcogenides show strong enhancement of Coulomb interactions due to their reduced dimensionality with immediate effects on both the optical as well as the single-particle band gap. Photogenerated electron-hole pairs have been shown to result in a giant band gap renormalization that has been attributed to efficient screening of the Coulomb interaction [1]. The corresponding band structure changes are predicted to show a pronounced momentum dependence [2] that we resolve using time- and angle-resolved photoemission spectroscopy (trARPES) on monolayer WS_2 supported by a graphene substrate (see Fig. 1).

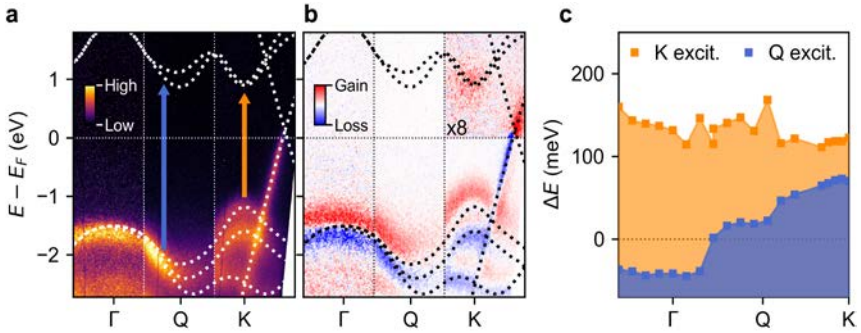

Fig. 1 *Momentum-dependence of bandgap renormalization of monolayer WS_2 on epitaxial graphene on SiC(0001) investigated by trARPES.* ***(a)*** *Equilibrium band structure.* ***(b)*** *Pump-induced changes of the photocurrent 240fs after photoexcitation with 2eV pump pulses.* ***(c)*** *Momentum-dependent shift of upper valence band of WS_2 for excitation at K (**orange**) and Q (**blue**), respectively.*

We find good agreement with *ab initio* calculations for excitation across the direct band gap at the K point. When excited close to the Q valley, however, we observe a strong k-dependence of the valence band shift that is not reproduced by theory. This implies that correlations beyond the GW approximation are at play.

References

[1] M. M. Ugeda, A. J. Bradley, S.-F. Shi, F. H. da Jornada, Y. Zhang, D. Y. Qiu, W. Ruan, S.-K. Mo, Z. Hussain, Z.-X. Shen, F. Wang, S. G. Louie, M. Crommie, *Nature Materials* **13**, 1091 (2014).
[2] D. Erben, A. Steinhoff, C. Gies, G. Schönhoff, T. O. Wehling, F. Jahnke, *Physical Review* B **98**, 035434 (2018).

Birth, rise, and collapse of Floquet-Bloch bands on Subcycle time scales

U. Höfer
Philipps-University of Marburg, 35032 Marburg, Germany

Strong light fields offer spectacular opportunities to tailor novel functionalities of solids. Floquet-Bloch states can form under periodic driving of electrons and enable exotic quantum phases. On subcycle time scales, lightwaves can simultaneously drive intraband currents and interband transitions and pave the way towards ultrafast electronics. Yet, the interplay of intra- and interband excitations as well as their relation with Floquet physics have been the key to open questions as dynamical aspects of Floquet states that have remained elusive. By monitoring the ultrafast build-up of Floquet-Bloch bands with time- and angle-resolved photoemission spectroscopy, we succeeded in providing this pivotal link.For this purpose, we extend our subcycle ARPES experiment [1] to the strong-field regime. We drive surface states of the topological insulator Bi_2Te_3 with MIR pump pulses of 25-40 THz and electric field strengths in the MV/cm range. Under these conditions, the carrier wave of the light ballistically accelerates the electrons in the Dirac cone back and forth, which gives rise to high-harmonic generation [2]. Our subcycle ARPES experiment reveals how Floquet-Bloch sidebands build up in the Dirac state in this regime. Starting with strong intraband currents, we observe that Floquet replicas emerge already in the second optical cycle, and that electrons in high-order sidebands scatter into bulk states and dissipation destroys the Floquet bands. Quantum nonequilibrium calculations confirm this behavior and explain the simultaneous occurrence of Floquet states with intra- and interband dynamics [3].On the experimental side, several challenges have to be overcome in order to obtain results as the ones depicted in Fig. 1. Firstly, the oscillating electric field of the lightwave does not only accelerate electrons in the material but also interacts with photoelectrons and results in momentum streaking of up to 0.1 A^{-1}. Analysis of the photoelectron streaking enables *in situ* reconstruction of the MIR electric field (Fig. 1b). Streaking compensated ARPES spectra then reveal the intrinsic electron dynamics of the Dirac state. Secondly, the driving frequency corresponds to optical cycles between 25 and 40 fs; thus ultrashort probe pulses which inevitably broaden the ARPES spectra are necessary to achieve subcycle resolution. By utilizing curvature-based image processing, we have succeeded in extracting the fine signatures induced by light under these conditions.

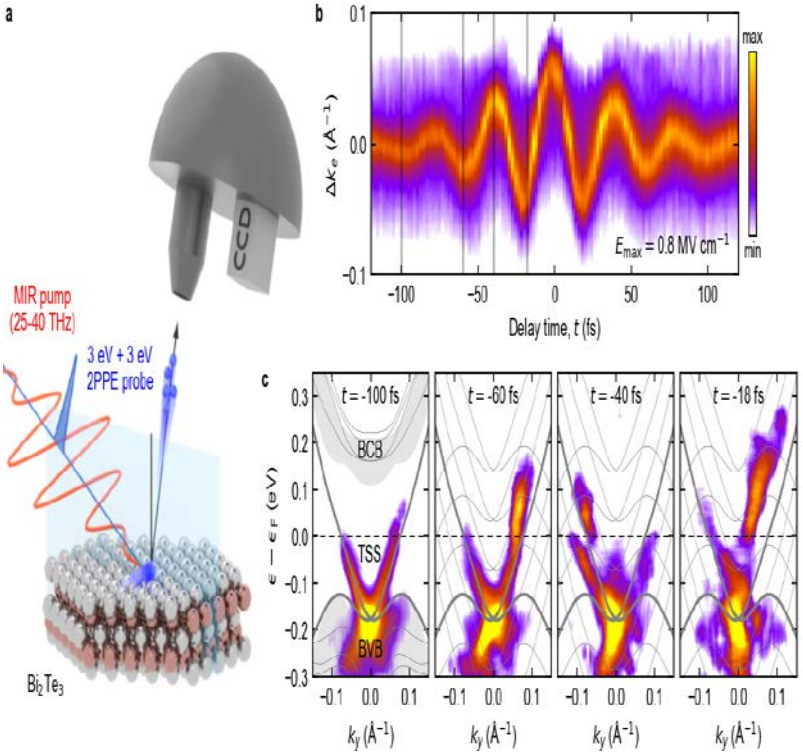

Fig. 1. a**: Schematics of subcycle ARPES with the MIR pump field and the ultrashort 3-eV 17-fs 2PPE probe pulse. **b**: Photoelectron momentum-streaking trace of the 25 THz driving field; thin vertical lines indicate temporal positions of the ARPES maps displayed in c. **c**: Curvature-filtered lightwave ARPES maps recorded before the arrival of the MIR field (t = -100 fs) and at selected delay times during the first half of the driving pulse; the images are compensated for the streaking shifts in b. The electronic distributions are initially accelerated along the ground-state band dispersion, but subsequently divert from it, splitting into multiple branches that follow approximately the TSS band structure shifted by integer multiples of the driving frequency (thin grey curves).Up to 100 fs before the maximum field crest, the effect of the MIR lightwave on the TSS is negligible. The ARPES image shows a partially filled Dirac cone (Fig. 1c). 40 fs later (t = -60 fs), the electric field has induced a strong asymmetry in the electronic distribution along the momentum axis, the hallmark of lightwave-driven currents. Most remarkably, a distinct splitting of electronic populations into multiple branches appears only one half of an oscillation cycle later (t = -40 fs). Simultaneously, the electron population oscillates back and forth along the momentum axis while the driving field evolves. The split bands notably follow the ground-state band structure shifted by integer multiples of $\hbar\Omega_{MIR}$= 0.1 eV (Fig. 1c, thin grey curves). As the field increases, the band splitting becomes more prominent and the probability to find the electrons shifts entirely to the upper branch near the field crest (**Fig. 1c, t = -18 fs).

Our observation is surprising because the conventional Floquet picture assumes multi-cycle lightwaves to form sidebands by coherent superposition of electronic states, whereas our sub-cycle experiments identify Floquet-Bloch states already within the first two cycles of the MIR pulse. Quantum nonequilibrium calculations are in excellent agreement with this behavior and describe the simultaneous occurrence of Floquet states with intraband dynamics very well [3].Close to the maximum of the field crest (t = -12 fs, not shown) and beyond, we observe transition of electrons into the bulk conduction band via its hybridization with split-off bands. The interplay between the intraband currents and the non-perturbative interband transition underlies various strong-field phenomena such as HHG. Our subcycle ARPES in the strong-field regime marks the first experimental visualization of the microscopic processes in momentum space.In conclusion, we truly visualized the birth, rise, and collapse of Floquet-Bloch states in a topological insulator. By introducing subcycle ARPES in the MIR, we directly monitor in momentum space how the lightwave-driven surface state of Bi_2Te_3 crosses over from an initial regime of deterministic quantum trajectories to a Floquet-Bloch band structure resulting from multi-path quantum interference. The dynamics unify the particle aspect of electrons describing subcycle acceleration with the wave-like interference of electrons forming light-induced sidebands.

References

[1] J. Reimann, S. Schlauderer, C. P. Schmid, F. Langer, S. Baierl, K. A. Kokh, O. E. Tereshchenko, A. Kimura, C. Lange, J. Güdde, U. Höfer R. Huber, *Nature* **562**, 396 (2018).

[2] C. P. Schmid, L. Weigl, P. Grössing, V. Junk, C. Gorini, S. Schlauderer, S. Ito, M. Meierhofer, N. Hofmann, D. Afanasiev, J. Crewse, K. A. Kokh O. E. Tereshchenko, J. Güdde, F. Evers, J. Wilhelm, K. Richter, U. Höfer, R. Huber, *Nature* **593**, 385 (2021).

[3] S. Ito, M. Schüler, M. Meierhofer, S. Schlauderer, J. Freudenstein, J. Reimann, D. Afanasiev, K. A. Kokh, O. E. Tereshchenko, J. Güdde M. A. Sentef, U. Höfer, R. Huber, "Build-up and dephasing of Floquet-Bloch bands on subcycle timescales", *Nature* (in print), (2023) DOI: 10.1038/s41586-023-05850-x.

Ultrafast X-ray photoelectron spectroscopy

P. Hofmann
Aarhus University, 8000 Aarhus C, Denmark

X-ray photoelectron spectroscopy (XPS) is an experimental tool capable of accurately determining the core level binding energies of atoms. This energy is not only element-specific but also provides detailed information on the atoms' oxidation state and chemical environment, making XPS an essential tool for studying catalytic processes. Indeed, the technique is so important that recent experimental developments have pushed it into regimes for which it was long deemed unsuitable, e.g., the presence of near-ambient-pressure gases or liquids. Due to the relative simplicity of the core level photoemission process, XPS line shapes have attracted considerable theoretical interest and many-body theories to study the solid's electronic and vibrational many-body response to the removal of the photoelectron have been developed since the 1970s [1]. Finally, the core level photoemission intensity can be interpreted as a diffraction pattern that gives access to the emitting atom's local geometrical environment in an experimental approach called X-ray photoelectron diffraction. The increasing availability of ultrafast X-ray sources at free electron lasers now opens the opportunity to take XPS into the ultrafast time domain and this talk will give recent examples: The extension of the conventional line shape model to account for the electronic temperature in laser-excited graphene [2], the excitonic Mott transition in WSe_2 [3], and preliminary data for excited WTe_2. The graphene case is briefly presented in this abstract for illustrative purposes.

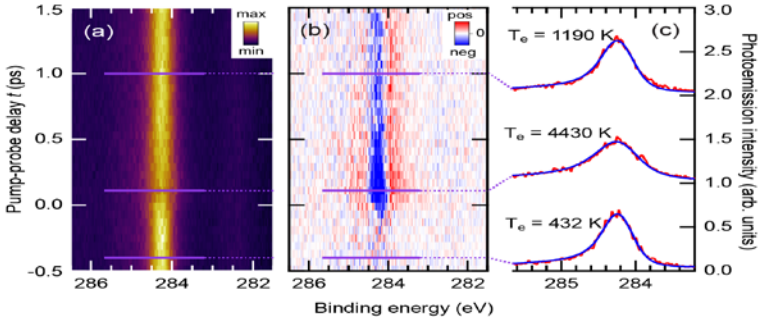

Fig. 1: (a) *C 1s photoemission intensity as a function of pump-probe delay and binding energy.* ***(b)*** *Same as in (a) but with the average spectrum before excitation subtracted. Red and blue indicate an increase and decrease in electron counts, respectively.* ***(c)*** *Selected spectra (cuts at specific time delays) along with best fit to a model taking into account the electronic temperature (blue line). The electronic temperatures resulting from the fit are noted close to the spectra. [2].*

For graphene, it is shown that the time-dependent XPS line shape can reveal detailed insight into the excitation of the system, directly giving access to parameters such as the electronic temperature [2]. After excitation with an optical pump pulse, the electronic temperature can rise to several thousand Kelvin and this is usually probed directly by the broadening of the Fermi edge in the valence band [4]. In the core level spectra, an ultrafast laser excitation gives rise to a time-dependent broadening, as shown in Fig. 1. It turns out that the origin of this broadening is an increased scattering with the hot electron gas and, upon expanding the conventional linewidth expression for XPS, data from the C 1s peak can be used to track the time-dependent electronic temperature. This is illustrated in Fig. 2 which shows a comparison of the electronic temperature determined by XPS and by the Fermi edge in the valence band.

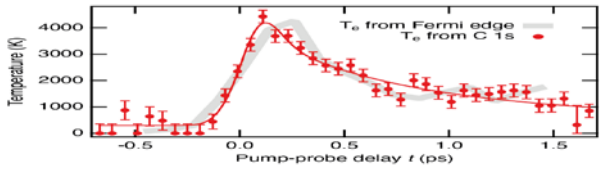

Fig.2*:Electronic temperature in graphene as a function of delay time between an optical pump pulse and an X-ray probe pulse. The markers show the results from the C 1s XPS line shape. The grey line shows the temperature obtained from the width of the Fermi edge in the valence band [2].*

Temperature-induced broadening effects are very common in core level spectra and usually caused by phonon scattering [1]. Broadening and line shape change due to a high electronic temperature, on the other hand, have been predicted a long time ago [5] but never observed because for samples in thermal equilibrium, the phonon-induced effects are usually much larger than the electronic effects. The ultrafast time scale, however, now offers a window on completely new mechanisms affecting XPS line shapes.

References

[1] P. H. Citrin, G. K. Wertheim, Y. Baer, *Physical Review* B **16**, 4256 (1977).
[2] D. Curcio, S. Pakdel, K. Volckaert, J. A. Miwa, S. Ulstrup, N. Lanatà, M. Bianchi, D. Kutnyakhov, F.Pressacco, G. Brenner, S. Dziarzhytski H. Redlin, S. Agustsson, K. Medjanik, D. Vasilyev, H.-J. Elmers, G. Schönhense, C. Tusche, Y.-J. Chen, F. Speck, T. Seyller, K. Bühlmann R. Gort, F. Diekmann, K. Rossnagel, Y. Acremann, J. Demsar, W. Wurth, D. Lizzit, L. Bignardi, P. Lacovig, S. Lizzit, C. E. Sanders, P. Hofmann, *Physical Review* B **104**, L161104 (2021).
[3] M. Dendzik, R. P. Xian, E. Perfetto, D. Sangalli, D. Kutnyakhov, S. Dong, S. Beaulieu, T. Pincelli, F. Pressacco, D. Curcio, S. Y. Agustsson M. Heber, J. Hauer, W. Wurth, G. Brenner, Y. Acremann, P. Hofmann, M. Wolf, A. Marini, G. Stefanucci, L. Rettig, Ralph Ernstorfer *Physical Review Letters* **125**, 096401 (2020).
[4] J. C. Johannsen, S. Ulstrup, F. Cilento, A. Crepaldi, M. Zacchigna, C. Cacho, I. C. E. Turcu, E. Springate, F. Fromm, C. Raidel, T. Seyller F. Parmigiani, M. Grioni. P. Hofmann, *Physical Review Letters* **111**, 027403 (2013).
[5] S. Satpathy, J. D. Dow, *Solid State Communications* **42**, 637 (1982).

Cavity-enhanced optical single-shot readout of a quantum dot Spin state on nanosecond timescales

M.R. Hogg[1], N.O. Antoniadis[1], W.F. Stehl[1], A. Javadi[1], N. Tomm[1], R. Schott[2], S.R. Valentin[2], A.D. Wieck[2] A. Ludwig[2], R.J. Warburton[1]

[1] *University of Basel, Klingelbergstrasse 82, 4056 Basel, Switzerland*

[2] *Ruhr-Universität Bochum, 44780 Bochum, Germany*

The ability to perform a projective measurement of a quantum state in a single measurement iteration (single-shot readout) is an enabling technique in quantum technologies. Single-shot readout is necessary in quantum computation protocols for extracting information at the end of the computation, as well as error detection and correction as the quantum processor runs [1]. Single-shot qubit readout is also essential to close the fair sampling loophole in fundamental tests of quantum non-locality [2]. Achieving single-shot readout within the qubit dephasing time enables experiments such as measurement-based quantum feedback [3]. The spin states of optically active III-V semiconductor quantum dots (QDs) are a promising resource for quantum technologies; however single-shot readout has proven challenging due to low photon collection efficiencies and back-action induced by the readout laser. Of the small number of previous experiments to achieve single-shot readout of InAs QD spin states, the most rapid to date achieved a fidelity of 82% in a readout time of 800 ns [4], significantly longer than the maximum spin T_2* times achieved to date (125 ns [5]).

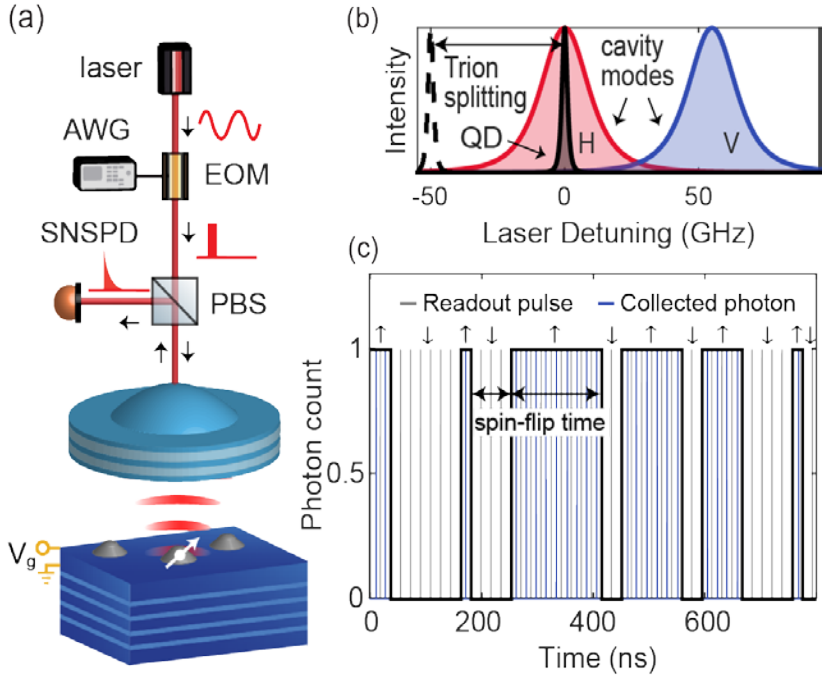

Fig. 1. *Tunable microcavity and single-shot spin readout.*
(a) *Experimental setup. Fast optical readout pulses are created using an electro-optic modulator (EOM) driven by an arbitrary waveform generator (AWG).*
(b) *Spin-selective cavity enhancement of quantum dot emission.*
(c) *Repeated single-shot measurements of the quantum dot spin state, showing bright and dark periods due to quantum jumps in the QD spin state.*

Here we achieve single-shot readout of an InAs quantum dot spin state with a fidelity of 95.2% in only 3 nanoseconds [6], an improvement of more than two orders of magnitude and well within the achievable T_2* time. Our approach uses a miniaturised Fabry-Perot microcavity to significantly enhance the spin readout signal. To the best of our knowledge, this is the fastest single-shot readout of a matter qubit ever achieved. Together with the recent demonstration of an on-demand single-photon source with a record 57% efficiency [7], our work provides a promising pathway towards the generation of high-rate spin-photon entanglement and photonic cluster states.

References

[1] A. G. Fowler, M. Mariantoni, J.M. Martinis, A.N. Cleland, *Physical Review A* **86**, 032324 (2012).
[2] B. Hensen, H. Bernien, A. Dréau, *Nature* **526**, 682 (2015).
[3] P. Campagne-Ibarcq, E. Flurin, N. Roch, D. Darson, P. Morfin, M. Mirrahimi, M. H. Devoret, F. Mallet, B. Huard, *Physical Review X* **3**, (2013).
[4] A. Delteil, W. Gao, P. Fallahi, J. Miguel-Sanchez, A. Imamoğlu, *Physical Review Letters* **112**, 116802 (2014).
[5] D. M. Jackson, U. Haeusler, L. Zaporski, J. H. Bodey, N. Shofer, E. Clarke, M. Hugues, M. Atatüre, C. Le Gall, D. A. Gangloff, *Physical Review X* **12**, 031014 (2022)
[6] N. O. Antoniadis, M. R. Hogg, W. F. Stehl, A. Javadi, N. Tomm, R. Schott, S. R. Valentin, A. D. Wieck, A. Ludwig, R. J. Warburton, *arXiv*:2210.13870 (2022)
[7] N Tomm, A. Javadi, N. O. Antoniadis, *Nature Nanotechnology* **16**, 399 (2021)

* Acknowledgement(s) : We acknowledge financial support from Horizon-2020 FET-Open Project QLUSTER, Swiss National Science Foundation project 200020 204069, and NCCR QSIT. A.J. acknowledges support from the European Union Horizon 2020 Research and Innovation Programme un- der Marie Sklodowska-Curie grant agreement no. 840453 (HiFig). S.R.V., R.S., A.L. and A.D.W. gratefully acknowledge support from DFH/UFA CDFA05-06, DFGTRR160, DFG project 383065199 and BMBF Q.Link.X.

Nonthermal melting of a charge density wave in atomic wires at the Quantum limit

M. Horn von Hoegen
Duisburg-Essen University,47057 Duisburg, Germany

In this talk, we present experimental results on the structural dynamics in the prototypical indium atomic wire system formed by self-assembly on Si(111). This surface system under-goes a Peierls-like symmetry breaking at T_c = 130 K resulting in the formation of a surface charge density wave. During this thermally driven first-order structural phase transition the system doubles the periodicity along and perpendicular to the wires resulting into a (8×2) reconstructed ground state [1]. The symmetry breaking is accompanied by the opening of a band gap of 0.2 eV and thus constitutes a metal to insulator transition. The insulating (8×2) ground state is composed of isolated distorted In hexagons which transform in parallel zig-zag chains of In atoms in the high temperature (4×1) state as is sketched in Fig. 1(a, c).

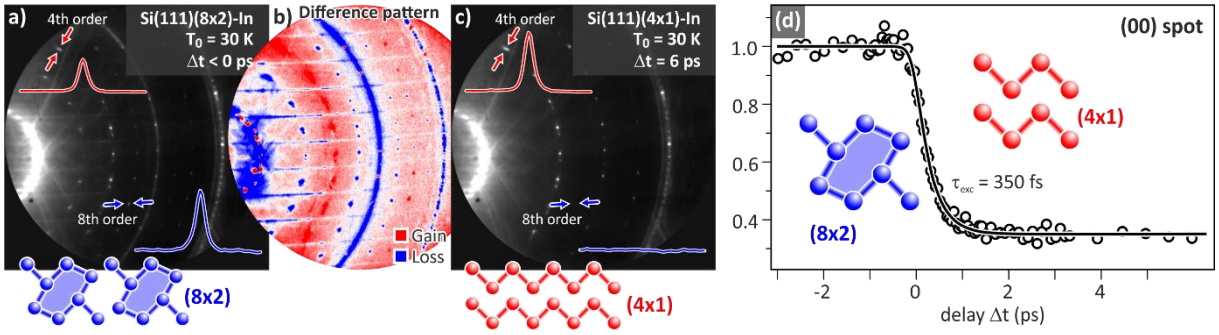

Fig. 1: (a,c) *RHEED patterns at negative time delay prior to and 6 ps after excitation, respectively. Diffraction spots indicative for the ground (8×2) and (4×1) excited state are marked. Spot profiles show the intensity loss and gain for (8×2) and (4×1) spots, respectively.* ***(b)*** *The difference pattern clearly depicts the systematic intensity losses (blue) for the features indicative for the (8×2) ground state, i.e., spots and streaks, and gains (red) for the features indicative for the (4×1) excited state.* ***(d)*** *The intensity evolution of the (00) spot for the transition from (8×2) ground to (4×1) excited state occurring in only 0.7 ps. No ringing of the intensity is observed.*

The non-equilibrium structural dynamics of these arrays of In atom wires upon impulsive excitation by fs-IR laser pulses is probed through ultra-fast time resolved reflection high energy electron diffraction (RHEED) under grazing incidence at a temporal resolution of 350 fs [2]. The sample is held in the (8×2) ground state at 30 K, i.e., way below T_c . The optical excitation through the 80 fs laser pulse at an incident laser fluence higher than $\Phi > 2$ mJ/cm^2 results in a non-equilibrium population of the electronic surface states which causes transient changes of the potential energy surface [3] as is sketched in Fig. 2. As a result, an accelerated displacive structural transition to the (4×1) excited state is driven. Since we do not observe any oscillatory behavior of the diffracted intensity we assume a critically damped behavior which is completed in only 700 fs [3,4]. The large surface unit cell together with the dynamically changing phononic band structure lead to an extremely effective coupling of the degrees of freedom for the kinetic energy of the In atoms towards the unexcited and cold Si substrate.

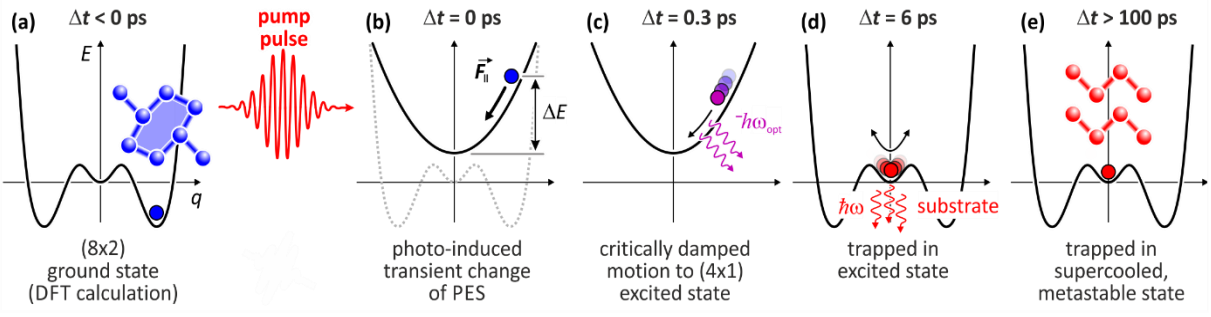

Fig. 2: (a,b) *Transient change of 3-valley potential energy landscape upon optical excitation through fs-laser pulse.* ***(b,c)*** *Accelerated displacive transition to excited state in less than a ps.* ***(d)*** *Energy dissipation through phonon emission into the substrate at 6 ps.* ***(e)*** *Trapped in metastable supercooled state for ns.*

Transient heating of the In atoms from 30 to 60...80 K occurs delayed at 6 ps [5]. Thus, the phase transition is driven by electronic entropy and not thermally. A weak energy barrier of 60 meV for the atoms collective motion from the excited (4×1) state to the (8×2) state hinders the immediate recovery of the ground state: the In layer remains for many nanoseconds in a super cooled metastable (4×1) state, which is not accessible under equilibrium conditions. The relaxation into the (8×2) ground state happens through the nucleation of the (8×2) at pre-existing defects like adsorbates [6] or step edges [7] which act as seeds and trigger a recrystallization front. This front propagates 1-dimensionally at a speed of ~100 m/s as determined from a correlation of the step morphology to recovery time constant [7].

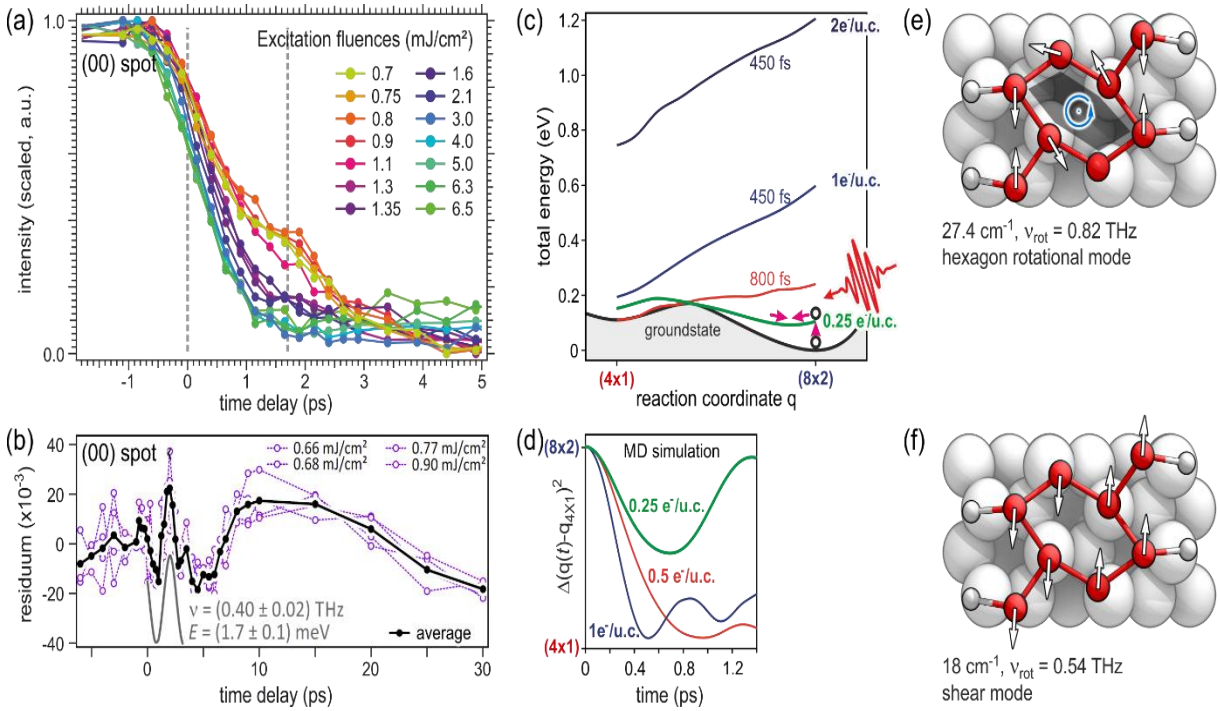

Fig. 3: ***(a)*** *Intensity drop of the (00) diffraction spot at various fluences.* ***(b)*** *The residuum after subtraction of an exponential decay from (a) clearly exhibits one oscillation maxima at* $t_{(8\times2)}$ *= 1.7 ps.* ***(c)*** *Under weak excitation conditions* $\Phi < 2$ *mJ/cm*^{2} *the amplitudon mode of the CDW is excited.* ***(d)*** *Ab initio molecular dynamics simulations show, that the system does overcome the reaction barrier and consequently not reach the excited (4×1) state.* ***(e,f)*** *Sketch of the two soft phonon modes transferring the surface system from (8×2) to (4×1), i.e., the hexagonal rotation mode at 0.82 THz and the shear mode at 0.54 THz.*

Under weak excitation conditions at a fluence lower than $\Phi < 2$ mJ/cm^2 only part of the surface is transformed to the excited high temperature (4×1) state. The recovery to the ground state then occurs in ~50 ps independent of density of adsorbates or step edges. From this and transient broadening of the (8×2) diffraction spots we can conclude, that the surface is composed of small patches of excited (4×1) units with a length of ~10 nm embedded in the (8×2) reconstructed groundstate surface.
From the untransformed (8×2) patches we observe one single intensity oscillation at $t_{(8\times2)}$ ~ 1.7 ps of the (00)-spot which we attribute to the excitation of the amplitudon mode of the surface charge density wave at the characteristic frequencies 0.82 THz and 0.54 THz of the surface localized hexagonal rotational and shear soft-phonon modes facilitating the transformation from (8×2) to (4×1) [8,9].

References

[1] F. Klasing, T. Frigge, B. Hafke, S. Wall, A. Hanisch-Blicharski, M. Horn-von Hoegen, *Phyical Review B* **89**, 121107(R) (2014)
[2] T. Frigge, B. Hafke, T. Witte, C. Brand, M. Horn-von Hoegen, *Review of Scientific Instruments* **90**, 045119 (2019).
[3] T. Frigge, B. Hafke, T. Witte, B. Krenzer, C. Streubühr, A. Samad Syed, V. Mikšić Trontl, I. Avigo, P. Zhou, M. Ligges, D. von der Linde U. Bovensiepen, M. Horn-von Hoegen, S. Wippermann, A. Lücke, S. Sanna, U. Gerstmann, W. G. Schmidt, *Nature* **544**, 207 (2017).
[4] C.W. Nicholson A Lücke, W G Schmidt, M Puppin, L Rettig, R Ernstorfer, M Wolf, *Science* **362**, 821 (2018).
[5] T. Frigge, B. Hafke, T. Witte, M. Horn-von Hoegen, *Structural Dynamics* **5**, 025101 (2018)
[6] S. Wall, B. Krenzer, S. Wippermann, S. Sanna, F. Klasing, A. Hanisch-Blicharski, M. Kammler, W.G. Schmidt, M. Horn-von Hoegen, *Physical Review Letters* **109**, 186101 (2012)
[7] B. Hafke, T. Witte, T Frigge, D. Janoschka, P. Dreher, M. Horn von Hoegen, *Structural Dynamics* **6**, 045101 (2019)
[8] E. Speiser, N. Esser, S. Wippermann, W. G. Schmidt, *Physical Review B* **94**, 075417 (2016)
[9] S. Wippermann, W.G. Schmidt, *Physical Review Letters* **105**, 126102 (2010).

* Acknowledgement: M. Horn von Hoegen acknowledges financial support from DFG through project B02 of Collaborative Research Center SFB616 "Energy dissipation at surfaces" and project C03 of Collaborative Research Center SFB1242 "Nonequilibrium dynamics of condensed matter in the time domain" (Project-ID 278162697).

Transient gap generation in $BaFe_2As_2$ driven by Coherent lattice vibrations

J. A. Warshauer[1], D. A. B. Lopez[1], Q. Dong[2], G. Chen[3], W. Hu[1]
[1]*Boston University, Boston, MA 02215, USA*
[2] *Institute of Physics Chinese Academy of Sciences, Beijing 100190, China*
[3] *University of Chinese Academy of Sciences, Beijing 101408, China*

Iron-based superconductors provide a rich platform to investigate the interplay between unconventional superconductivity, nematicity and magnetism. The electronic structure and the magnetic properties of iron-based superconductors are highly sensitive to the pnictogen height. Coherent excitation of the A_{1g} phonon by femtosecond laser directly modulates the pnictogen height, which has been used to control the physical properties of iron-based superconductors. Previous studies show that the driven A_{1g} phonon resulted in a transient increase of the pnictogen height in $BaFe_2As_2$, favoring an enhanced Fe magnetic moment. However, there are no direct observations on either the enhanced Fe magnetic moments or the enhanced spin-density wave (SDW) gap. Here, we use time-resolved broadband terahertz spectroscopy to investigate the dynamics of $BaFe_2As_2$ in the A_{1g} phonon driven state. Below the SDW transition temperature, we observe a transient gap generation at early time delays. A similar transient feature is observed in the normal state up to room temperature.

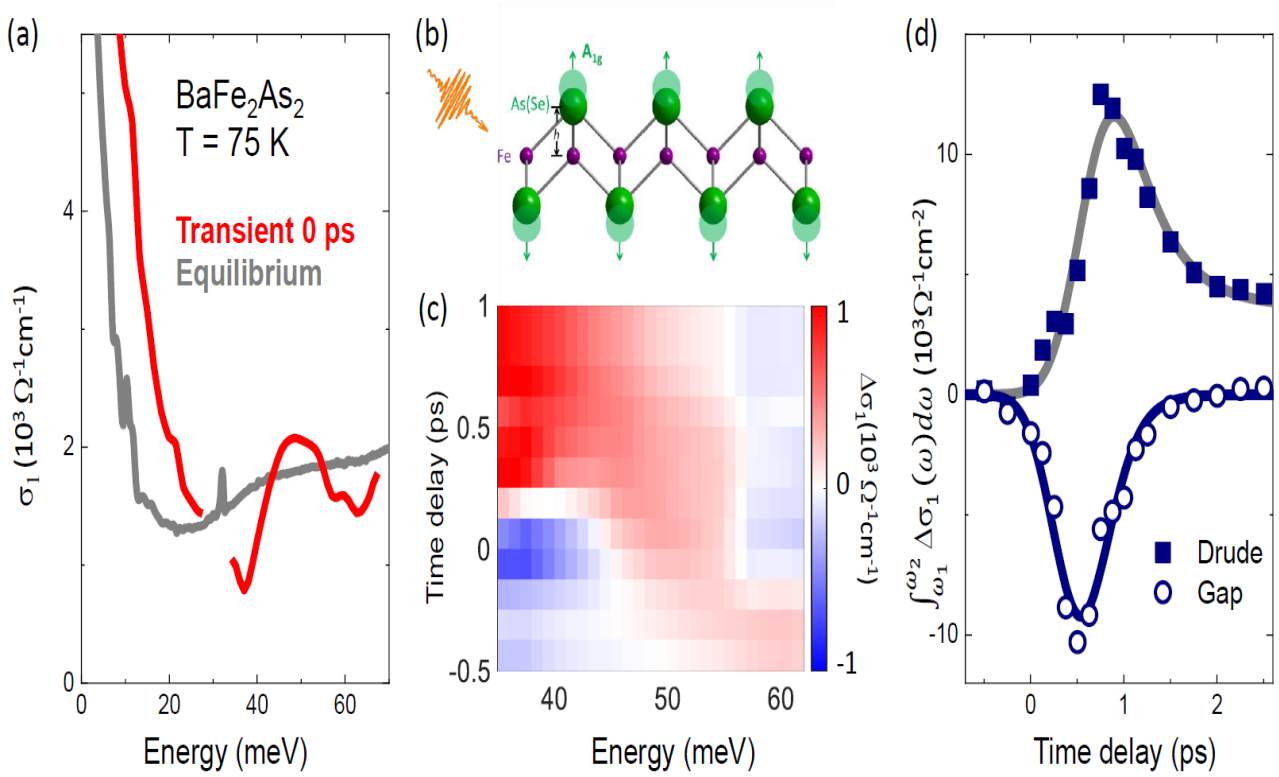

***Fig. 1. (a)**: The real part of optical conductivity $\sigma_1(\omega)$ at equilibrium (grey) and the photo-excited state (red) at T = 75 K. The transient $\sigma_1(\omega)$ shows a broadened Drude component and a gap formation near 50 meV, which takes the spectral weight from the equilibrium SDW gap at 45 meV. **(b)** Coherent excitation of the A_{1g} phonon modulates the pnictogen height h_{As}. **(c)**: Transient change in optical conductivity $\Delta\sigma_1(\omega)$ at T = 75 K. The transient gap is seen as the blue region at around 40 meV at early time delays. **(d)**: Different time scales for the light-induced Drude component (solid squares) and the transient gap (open circles) are evidenced by the time evolution of the transient change in spectral weight. Solid lines are exponential fits. Figures are from Ref. [1].*

Below the SDW transition temperature, we observe a transient gap generation at early time delays. A similar transient feature is observed in the normal state up to room temperature.

References

[1] J. A. Warshauer, D. A. B. Lopez, Q. Dong, G. Chen, W. Hu, *arXiv:2212.03337* (2022).

* Acknowledgement(s) : authors J. A. W. and W. H. acknowledge support from the National Science Foundation under Grant No. 1944957. D. A. B. L. was supported by the US Department of Energy under Award Number DE-SC-0021305. Q. D. and G. C. were supported by the National Natural Science Foundation of China (Grant Nos. 11874417, 12274440), the Strategic Priority Research Program (B) of Chinese Academy of Sciences (Grant No. XDB33010100) and the Ministry of Science and Technology of China (Grant No. 2022YFA1403903).

Linking high-harmonic generation and strong-field Ionization in bulk crystals

A. Husakou[1], P. Jürgens[1] S. D.C. R. Abbing[2], M. Mero[1], M. J.J. Vrakking[1]
A. Mermillod-Blondin[1], P. M. Kraus[3]
[1]*Max-Born-Institute for Nonlinear Optics and Short Pulse Spectroscopy, 12489 Berlin, Germany*
[2]*Advanced Research Center for Nanolithography (ARCNL, 1098XG Amsterdam, the Netherlands*
[3]*Vrije Universiteit, 1081 HV Amsterdam, the Netherland*

High-order harmonic generation in gases marked the birth of attosecond science. Transferring the concept of HHG to solid-state systems has opened up several research avenues ranging from fundamental investigations of strong-field-driven carrier dynamics to petahertz electronics. In solids, three main sources of nonlinearity have been identified with regards to harmonic generation. First is the traditional Kerr-type nonlinearity [1] which is based on the anharmonic motion of bound electrons in the valence band. Second, high-order harmonics have been associated with three-step-like [2] interband recollisions and intraband currents where the nonlinearity enters through the non-parabolic shape of the bands [3]. Third, the nonlinearity that is inherent to the process of photoionization was proposed as a possible origin for harmonic generation [4] and was recently identified as the dominant source of low-order wave-mixing in amorphous fused silica [5].

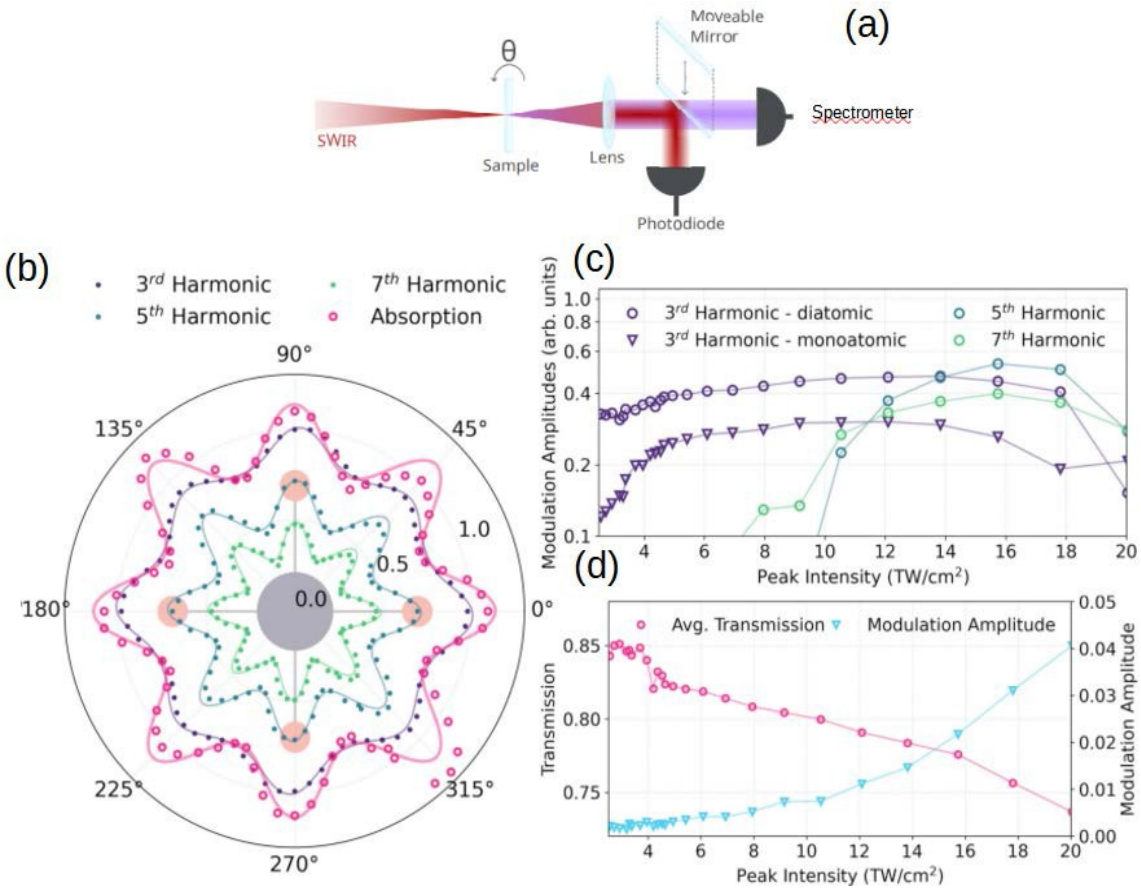

Fig. 1. *Experimentally determined high harmonic generation and absorption in MgO.* ***(a)*** *Experimental setup,* ***(b)*** *dependence of the emitted harmonics strength and pump absorption on the crystal orientation for 200-μm-thick MgO crystal and intensity of 18 TW/cm², **(c)** dependence of the diatomic and monoatomic harmonic emission strength on the intensity, **(d)** dependence of the average transmission and harmonic modulation amplitude on intensity.*

For crystals, the connection between carrier excitation and harmonic emission and its impact on the anisotropic angular dependence has not yet been fully understood. While photoionization is often a key factor, there has been no investigation of its angular dependence with regards to harmonic generation. In this contribution we combine measurements of the angular dependence of nonlinear absorption and high-order harmonic generation to identify the relation between high-harmonic emission and laser-induced ionization. An unambiguous correlation between the emission of harmonics and laser-induced ionization is found, which is supported by numerical solutions of the semiconductor Bloch equations and calculations of orientation-dependent ionization rates using

maximally localized Wannier functions.In Fig. 1(a), the experimental setup is shown along with obtained results for the MgO crystal. For low intensities the nonlinearity is dominated by third-order response with fourfold symmetry (not shown). With higher intensity, third harmonics response starts to show eight-fold symmetry, as shown in Fig. 1(c), simultaneously, 5^{th} and 7^{th} harmonics start to appear in the signal, characterized by almost perfect eight-fold symmetry, as can be seen in Fig. 1(b). The preferred directions of the emission are associated with the crystal orientation, with maximum emission occurring when the field is along the monoatomic (O-O) or diatomic (O-Mg) bond. The eight-fold anisotropic harmonic emission is accompanied by, and strongly correlated to, the anisotropy in absorption, as shown in Fig. 1(d). This establishes a definite link between the harmonic emission in the considered regime and the photoionization process, which leads to harmonic emission predominantly through injection current [5]. We have also performed similar measurements using Al_2O_3 crystal (not shown). While the clear correlation between the photoionization and harmonic emission was also established, for Al_2O_3 we observe a surprising change of the preferred direction from diatomic at lower intensities to monoatomic at higher intensities. To gain a deeper understanding of the photoionization and emission processes, we have performed numerical simulations using semiconductor Bloch equations as well as simulated ionization using maximally localized Wannier functions. In Fig. 2(a) we illustrate the possible transitions from the valence band to conduction band in MgO. While same-site transitions and transitions to interatomic space are not expected to show a strong degree of orientation dependence, the Wannier jumping to the nearest-neighbor (and next-nearest-neighbor) atoms do show significant orientation dependence, as indicated in Fig. 2(b).

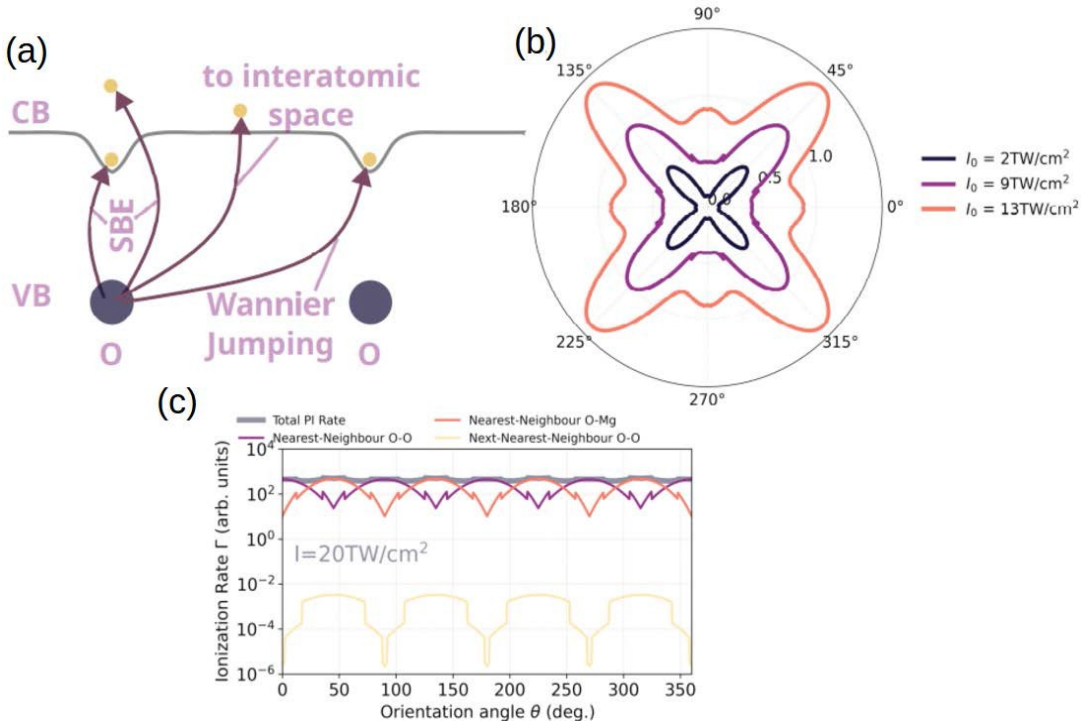

Fig. 2. *Results of numerical simulations.* ***(a)*** *Scheme of the possible transition from the valence zone to the conduction zone,* ***(b)*** *orientational dependence of the ionization rate for MgO crystal and different intensities,* ***(c)*** *contribution of different Wannier jumpings to the ionization rate for the intensity of 20 TW/cm^2.*

In addition, this dependence changes with intensity, illustrated by transition from fourfold symmetry to eight-fold symmetry in Fig. 2(b), in agreement with the experiment and in the intensity range corresponding to the experimental values. In addition, for still higher intensities the strong electric field starts to "dress" the states in the valence and conduction bands, inducing further modifications to the orientation dependence of the photoionization, as shown in Fig. 2(c), where at higher intensities 12- fold symmetry starts to emerge.

References

[1] P. A. Franken, A. E. Hill, C. W. Peters, G. Weinreich, *Physical Review Letters* **7**, 118 (1961).
[2] M. Lewenstein, P. Balcou, M. Y. Ivanov, A. L'Huillier, P. B. Corkum, *Physical Review* A **49**, 2117 (1994).
[3] E. Goulielmakis, T. Brabec, *Nature Photonics* **16**, 411 (2022).
[4] F. Brunel, *JOSA B* **7**, 521 (1990).
[5] P. Jürgens, B. Liewehr, B. Kruse, C. Peltz, D. Engel, A. Husakou, T. Witting, M. Ivanov, M. Vrakking, T. Fennel, A. Mermillod-Blondin, *Nature Physics* **16**, 1035 (2020).

* Acknowledgement(s) : It is our pleasant duty to thank M. Ivanov and T. Fennel for discussion of our experimental results and the numerical methods. A.H. acknowledges support from 823897 (ATLANTIC) RISE project funded by European Commission.

Highly efficient stimulated Raman conversion in gas-filled photonic Crystal fibers

A. A. Ishaaya
Ben-Gurion University of the Negev, Beer-Sheva 8410501, Israel

Gas-filled hollow-core optical fibers provide an excellent platform for stimulated Raman scattering (SRS), thanks to their long interaction lengths and inherent field confinement. Here, we review our investigations on SRS in SF_6- and CF_4-filled photonic bandgap fibers using ns-pulsed 1 μm laser sources. With relatively short fiber lengths, we were able to achieve ~70% conversion efficiency to the first Stokes order, with low peak power and low gas pressure. Moreover, we observed polarization-dependent Raman conversion, which we related to slight asymmetry in the fiber structure that affected wavelengths on the "red" side of the bandgap. Currently, we are pursuing similar investigations with ps sources. Wavelength conversion in gas-filled hollow-core fibers (HCFs) has been an active research field over the past two decades. The tight light confinement, the long interaction length, and the ability to guide very high peak powers make them an ideal platform for nonlinear light-matter interactions. First, efficient wavelength conversions via stimulated Raman scattering (SRS) were performed in H_2-filled hollow-core Kagome' photonic crystal fibers [1]. These Kagome' fibers have a relatively wide transmission band and can transmit both the pump and Stokes wavelengths for various gases. In this feature, they are similar to the relatively new class of hollow core fibers, the anti-resonant (ARF) or negative curvature fiber. These new-generation fibers have a simple microstructure cladding and, thus, are relatively easy to fabricate. The unique cladding facilitates low-loss guidance over a broad spectrum (100's of nm) and is lossy for high-order modes resulting in single-mode guidance. The typical mode field diameters are relatively large, 20-50 μm, and hence can sustain high power transmission. In hollow-core photonic bandgap fibers (PBGFs), where the low-loss transmission bandgap is limited to only ~100 nm, only gases with a small vibrational or rotational Raman shift can be exploited. In this case, a self-filtering effect of the higher Stokes lines will facilitate higher conversion efficiency to the first Stokes line [2]. As evident, with the above-noted HCFs, one can reach great conversion efficiencies with low pump peak powers relative to free-space large gas cells. In the PBGFs, the conversion is limited to wavelengths close to the pump wavelength, while in Kagomé and ARFs, the energy is typically transformed to multiple Stokes orders. This general principle is elegantly demonstrated in [3], with two hydrogen-filled hollow-core photonic crystal fibers, a broad, phase-locked, purely rotational frequency comb was established. A clean first Stokes seed pulse was generated using a narrowband photonic bandgap fiber via SRS coupled resonantly with a pump in a second broadband guiding kagomé- fiber. Using a spectral interferometric technique based on sum frequency generation, they show that the comb components are phase-locked. Finally, in both Kagomé and PBG fibers, only relatively low average-power pulsed pump lasers were used. In this regard, ARFs potentially pave the way for higher average-power conversions. Recently, the ARFs surpassed the gold standard of SMF in terms of lower transmission losses [4] and are expected to be further developed and incorporated into practical applications. We have been pursuing wavelength conversions in gas-filled hollow-core PBGFs for almost a decade and a half. We began by investigating fs pulse propagation in PBGF filled with Tetrafluoromethane (CF_4) and Sulphur Hexafluoride (SF_6) gases and observed self-phase modulation broadening [5]. Next, we obtained relatively high SRS conversion efficiency in CF_4-filled PBG fibers demonstrating 36% conversion from 532 nm to 559 nm in a 35 cm long fiber at low gas pressures and with low input peak power ns pulses [6,7]. Recently [8], we experimentally studied the SRS conversion process of ns-duration pulses as a function of gas, fiber length, input power, and gas pressure. For SF_6 pumped at 1030 nm and 1065 nm wavelengths, the first Stokes was observed at 1119 nm and 1161 nm, respectively. Fiber lengths of 5 m, 6 m, and 15 m produced maximum conversion efficiencies of 11.9%, 34.3%, and 55.7%, respectively, with the 1030 nm pump. The highest conversion efficiency for the 1065 nm pump reached 52.2% with a 15 m fiber, though it required double the peak power of the 1030 nm pump. Lastly, we optimized the SRS conversion, and the conversion efficiency to the first Stokes reached up to 70% in a 6 m fiber with a 1065 nm pump [9]. This indicates twice as much enhancement over the previous study. The increase is mainly due to a non-trivial correlation between the vibrational Raman conversion efficiency and the input pump beam's angle of linear polarization (AoLP). Also, the pump pulse dynamics (i.e., the rise and fall time relative to the pulse duration) were better adjusted for topping the conversion efficiencies. The experimental setup for the optimized SRS conversion is portrayed in Fig. 1a. The pump source is a high peak power Q-switched Ytterbium-doped PCF laser with a pulse duration of ~25 ns, a wavelength of 1065 nm, and a bandwidth of 0.2 nm. The pump beam is attenuated and linearly polarized via two perpendicularly oriented linear polarizers and a half-wave plate placed in between. These are followed by an additional rotatable half-wave plate to control the AoLP of the .

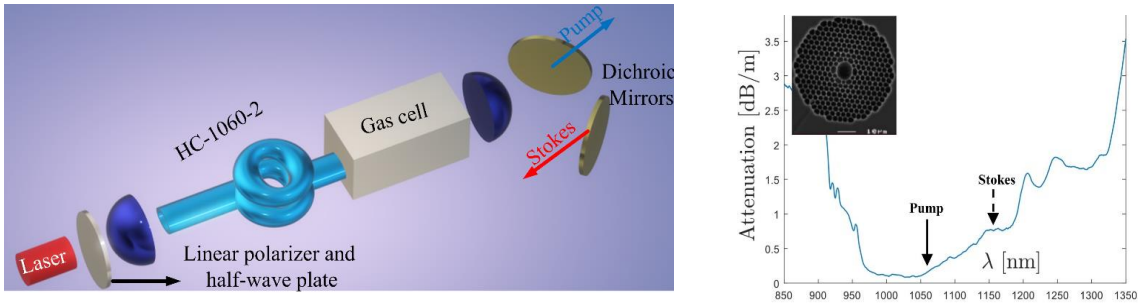

Fig. 1. (a) *The experimental setup.* ***(b)*** *SEM of the transverse microstructure of the NKT Photonics HC-1060-02 fiber and its measured attenuation in the relevant spectrum.*

beam. The beam is focused using a short focal length aspherical lens into the bare end of the HC-PBG fiber, which is open to the air. The opposite end of the HC-PBG fiber is mounted inside a gas cell, pointing at an antireflection-coated window. The cell is first vacuum-pumped, except for a minor leakage of the open-aired fiber tip, and then pressurized up to 12 bar, measured by a pressure gauge. The fiber is gradually filled with the gas to the state of a steady differential pressure distribution throughout the fiber (with a very slow flow of gas out of the fiber). The output beam, comprising both the pump and the converted Stokes signal, is collimated after the cell window and reflected off two dichroic mirrors to separate the first Stokes signal from the pump. The pump and Stokes beams are measured at the transmission of the first and the reflection of the second dichroic mirrors, respectively. The HC fiber is a commercially available NKT Photonics HC-1060-02 designed for single-mode operation in the transmission range. Fig. 1b displays a scanning electron micrograph of the transverse microstructure of the fiber and its measured attenuation at the relevant spectrum. We visualize in Fig. 2a the average powers of the pump and Stokes signal measured at the exit of a 6 m long SF_6-filled fiber versus the AoLP of the input pump beam.

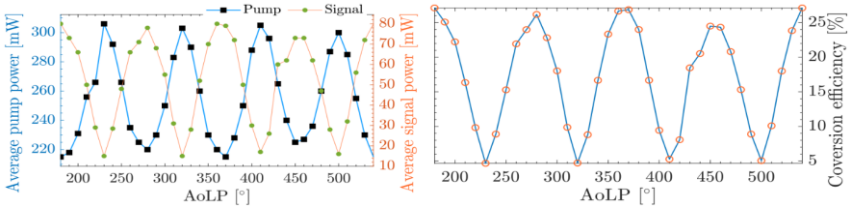

Fig. 2*. The average powers of the pump and Stokes signal* ***(a)*** *and the conversion efficiency* ***(b)****, measured at the exit of a 6 m long SF_6-filled fiber, versus the AoLP of the input pump beam.*

The Stokes signal power experience significant variations of ~±68.5%, whereas the pump shows ~±17.5%. We experimentally verified that the input AoLP does not affect the transmitted pump power for peak powers below the SRS threshold. Consequently, the pump variations in Fig. 2a are primarily due to corresponding stimulated Raman losses. The conversion efficiency, measured ratio of first Stokes to total coupled power, is plotted in Fig. 2b. The efficiency strongly depends on the AoLP with up to ~±70.6% peak variation, minima are clearly $\pi/2$ periodic, and the maxima seem similar though less sharp. Vibrational SRS in a perfectly circular symmetric fiber with a seedless configuration is independent of the AoLP of the pump beam. Thus, we hypothesized and experimentally verified that the significant variations of the conversion efficiency stem from the polarization sensitivity of the fiber and that the fiber's imperfection is more significant at the Stokes wavelength as it is out of the fiber's bandgap and has a larger mode field diameter and deeper penetration into the microstructured cladding than the pump. Due to the nonlinear nature of SRS and the long interaction length inside the fiber, slight asymmetries which result in variations in the field distributions can yield significant SRS polarization sensitivity. Consequently, with the optimized AoLP of the input pump beam, we reached ~ 70% conversion efficiency in a 6 m SF_6-filled HC-PCF. This is more than double the efficiency reported in [8]. To the best of our knowledge, it also shows a record conversion efficiency to a single Stokes order in SF_6 gas.

References

[1] F. Benabid, J. C. Knight, G. Antonopoulos, P. St. J. Russell, *Science* **298**, 399 (2002).
[2] F. Benabid, G. Bouwmans, J. C. Knight, P. St. J. Russell, F. Couny, *Physical. Review Letters* **93**, 123903 (2004).
[3] A. Abdolvand, A. M. Walser, M. Ziemienczuk, T. Nguyen, P. St. J. Russell, *Optics Letters* **37**, 4362 (2012).
[4] H. Sakr, Y.Chen, G.T.Jasion, T.D.Bradley, J.R.Hayes, H.C.H.Mulvad, I.A.Davidson, E.N.Fokoua, F. Poletti, *Nature Communications* **11**, (2020).
[5] A. Gilad, A. A. Ishaaya, *OSA Annual Meeting*, Rochester, NY, USA (Oct. 2010).
[6] L. Ben Yehud, D. Belker, G. Ravnitzki, A. A. Ishaaya, *Optics Letters* **39**, 1026 (2014).
[7] L. Ben-Yehud, A. A. Ishaaya, *CLEO/QELS 08*, San Jose, CA, USA (June 2014).
[8] S. Edelstein, A. A. Ishaaya, *Optics Letters* **44**, 5856(2019).
[9] R. Avrahamy, D. Belker, A. Halstuch, A. A. Ishaaya, "Polarization controlled, ultra-efficient Raman conversion to the first Stokes in gases-filled hollow-core photonic crystal fibres," (to be submitted), (2023).

Ultrafast coherent charge dynamics in Strongly correlated systems

S. Iwai[1], T. Amano[1], Y. Kawakami[1], H. Itoh[1] and K. Yonemitsu[2]
[1]*Tohoku University, 980-8578, Sendai, Japan*
[2]*Chuo University, 112-8551, Tokyo, Japan*

Recent advances of ultrafast laser technologies on attosecond time scale and quantum materials open coherent manipulations of correlated electron systems [1-3]. Thus, a strong light-field enables us to expect realization of a new class of photoinduced symmetry breaking which is different from the conventional regime on slower time scales, i.e., breaking of space inversion symmetry in ferroelectric compounds and that of time reversal symmetry in antiferromagnets. Here, we would like to discuss i) second harmonic generation (SHG) induced by non-scattering light-currents in a centrosymmetric organic superconductor [4, 5] and ii) ultrafast and large helicity-dependent polarization rotation in a Kitaev-type spin liquid candidate α-$RuCl_3$[6] as new examples of photoinduced symmetry breaking. i) An electromagnetic oscillation of light cannot directly access space inversion symmetry breaking because of its symmetric nature on the time axis (i. e., the time average of the oscillation is zero). However, recent developments of ultrashort laser technologies enable us to control the direction of charge motion by carrier-envelope phase (CEP) control of a strong light field. Considering non-scattering light-induced current, we can expect petahertz control of the space inversion symmetry in solids. Here, in a layered organic superconductor (κ -$(ET)_2Cu[N(CN)_2]Br$), SHG is observed by using a single-cycle 6 femtosecond near infrared pulse, which is in contrast to the perturbation theory where even harmonics are forbidden in centrosymmetric systems. The SHG shows a CEP sensitive nature and an enhancement near the superconducting temperature. The result and its quantum many-body analysis indicate that a polarized current is induced by non-dissipative acceleration of charge, which is amplified by superconducting fluctuations. ii) In a honeycomb-lattice spin-orbit assisted Mott insulator α-$RuCl_3$, an ultrafast magnetization is induced by circularly polarized excitation below the Mott gap. A helicity dependent light-induced polarization rotation in spin-liquid phase is 400 times [7] (20 times [8]) larger than that of a conventional paramagnet TGG (antiferromagnet NiO). Photo-carriers play an important role, which are generated by turning down the synergy of the on-site Coulomb interaction and the spin-orbit interaction realizing the insulator state. An ultrafast 6- fs measurement of photo-carrier dynamics and a quantum mechanical analysis clarify the mechanism, according to which the magnetization emerges from a coherent charge motion between different t_{2g} orbitals (d_{yz}-d_{xz}-d_{xy}) of Ru^{3+} ions. This ultrafast magnetization is weakened in the antiferromagnetic (AF) phase, which is opposite to the general tendency that the inverse Faraday effect is larger in AF compounds than in paramagnetic ones.

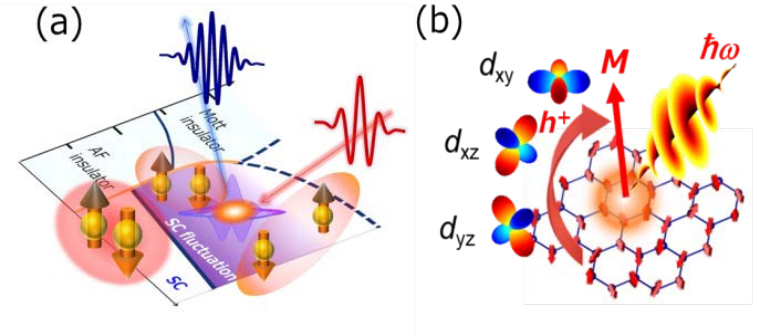

Fig. 1 *Schematic illustrations of* ***(a)*** *SHG induced by a light-induced non-scattering current in an organic superconductor and* ***(b)****light-induced magnetization in a Kitaev-type spin-liquid system.*

This temperature dependence indicates that the interorbital charge motion is affected by pseudo-spin rotational symmetry breaking in the AF phase.

References

[1] T. Ishikawa, Y. Sagae, Y. Naitoh, Y. Kawakami, H. Itoh, K. Yamamoto, K. Yakushi, H. Kishida, T. Sasaki, S. Ishihara, Y. Tanaka, K. Yonemitsu S. Iwai, *Nature Communications* **5**, 5528(2014).
[2] Y. Naitoh, Y. Kawakami, T. Ishikawa, Y. Sagae, H. Itoh, K. Yamamoto, T. Sasaki, M. Dressel, S. Ishihara, Y. Tanaka, K. Yonemitsu, S. Iwai *Physical Review* **B93**, 165126(2016).
[3] Y. Kawakami, T. Amano, Y. Yoneyama, Y. Akamine, H. Itoh, G. Kawaguchi, H. M. Yamamoto, H. Kishida, K. Itoh, T. Sasaki, S. Ishihara Y. Tanaka, K. Yonemitsu, S. Iwai, *Nature Photonics* **12**, 474 (2018).
[4] Y. Kawakami, T. Amano, H. Ohashi, H. Itoh, Y. Nakamura, H. Kishida, T. Sasaki, G. Kawaguchi, H. M. Yamamoto, K. Yamaomto, S. Ishihara K. Yonemitsu S. Iwai, *Nature Communications* **11**, 4138(2020).
[5] S. Iwai, Y. Kawakami, H. Itoh, and K. Yonemitsu, *Faraday Discussions* **237**, 353(2022).
[6] T. Amano, Y. Kawakami, H. Itoh, K. Konno, Y. Hasegawa, T. Aoyama, Y. Imai, K. Ohgushi, Y.Takeuchi, Y.Wakabayashi, K. Goto, Y. Nakamura H. Kishida, K. Yonemitsu, S. Iwai, *Physical Review Research* **4**, L032032(2022).
[7] R. V. Mikhaylovskiy, E. Hendry, V. V. Kruglyak, *Physical Review* **B86**, 100405(R)(2012).
[8] T. Satoh, S-J. Cho, R. Iida, T. Shimura, K. Kuroda, H. Ueda, Y.Ueda, B. A.Ivanov, F. Nori, M. Fiebig., *Physical Review Letters* **105**, 077402(2010).

***** Acknowledgement(s) :These studies have been performed in collaboration with T. Sasaki (IMR, Tohoku Univ.), Y. Nakamura, H. Kishida (Nagoya Univ.), G. Kawaguchi, H.M. Yamamoto (IMS), K. Yamamoto (Okayama Univ. Sci.).
These works are supported by JPMXS0118067426(Q-Leap) and JP19198318(JST-CREST).

Ultrafast loss of lattice coherence in the photoinduced Structural phase transition of V_2O_3

A. S. Johnson[1], D. Moreno-Mencía[2], E. B. Amuah[3], M. Menghini[1], J.-P. Locquet[4], C. Giannetti[5]
E. Pastor[6], S. E. Wall[3]
[1]*IMDEA Nanoscience, 28049 Madrid, Spain*
[2]*ICFO—Institut de Ciencies Fotòniques, 08860 Castelldefels, Barcelona, Spain*
[3]*Aarhus University, Ny Munkegade 120, 8000 Aarhus C, Denmark*
[4]*Katholieke Universiteit Leuven, 3001 Leuven, Belgium*
[5]*Universita Cattolica, 25121 Brescia, Italy*
[6]*Université de Rennes, 35000 Rennes, France*

Coherent phononic motion is one of the most distinctive behaviour of solids when photoexcited on the ultrafast timescale. Characteristic phonon oscillations have been used extensively to track when a material is driven through a phase transition [1, 2], and have been manipulated in multiple-pulse sequences to enable coherent control of structural phase transitions [3]. However, the question of whether and how this coherent motion, especially in zone centre modes, is sustained across a structural phase transition remains largely unexplored. This is because in many systems only the initial low-symmetry phase has appreciable Raman active phonon modes which can be observed using ultrafast spectroscopy [4], preventing direct measurement of coherent lattice motion in the final high-symmetry phase. Here, we present coherent phonon spectroscopy measurements of the light-induced phase transition in V_2O_3 [5]. V_2O_3 is notable as it hosts Raman-active modes readily observable through coherent phonon generation in both its low-symmetry monoclinic phase and high-symmetry corundum phase, thus making it an ideal testing ground for tracking the transfer of coherence across a light-induced phase transition. The low-symmetry phase has three characteristics phonon modes at 7, 8.3 and 9.8 THz, unfold through the structural phase transition leaving a single Raman-active mode in the high-symmetry phase at 7.5 THz (Fig. 1).

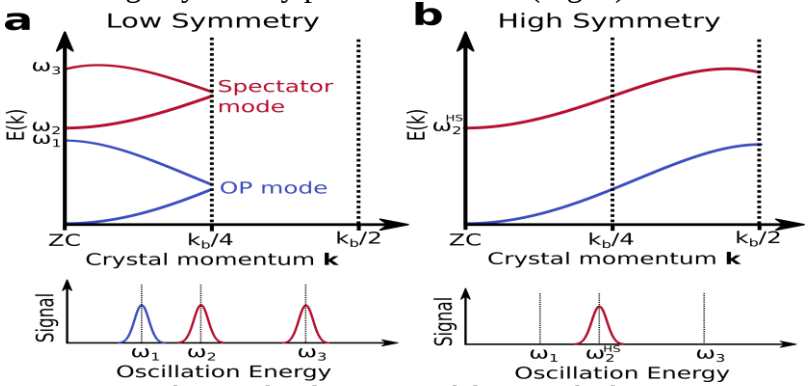

Fig. 1. *Representative phononic band structure exhibiting multiple Raman active modes in the low symmetry phase* ***(a)*** *and a single Raman active mode in the high symmetry phase* ***(b)****.*

When exciting across the phase transition, if coherence were preserved, we would expect to see the characteristic mode of the high symmetry phase emerge. Instead we observe a complete loss of oscillations and lattice coherence. This is particularly interesting as, by focusing on Raman-active modes, we are observing modes which do not undergo a significant change in momentum through the zone-folding in the phase transition, and which may be expected to be more resilient than modes which change from zone-center to zone-edge as have been studied in previous phonon spectroscopy experiments. Our results suggest that V_2O_3 undergoes an order-disorder style transition when photoexcited, adding it to the growing family of identified photoinduced order-disorder transitions [4,6]. In contrast to previous systems however, we can uniquely associate the disordering to the transition itself, rather than to significant disorder in the high-symmetry phase. We speculate this disordering may be due to mixing of the low-symmetry modes across the transition or due to anomalously strong phonon-anharmonicity due to the effective compression of the high-symmetry phase immediately following photoexcitation [7].

References

[1] S. Wall, D. Wegkamp, L. Foglia, K. Appavoo, J. Nag, R.F. Haglund Jr, J. Stähler M. Wolf , *Nature Communications* **3**, 721 (2012).
[2] A. Tomeljak, H. Schäfer, D. Städter, M. Beyer, K. Biljakovic, J. Demsar,. *Physical Review Letters* **102**, 1 (2009).
[3] J. G. Horstmann, H. Böckmann, B. Wit, F. Kurtz, G. Storeck, C. Ropers, *Nature* **583**, 232(2020).
[4] D. Perez-Salinas, A. S. Johnson, D. Prabhakaran, S.Wall, *Nature Communications* **13**, 8 (2022).
[5] A. S. Johnson, D. Moreno-Mencía, E. B. Amuah, M. Menghini, J.-P. Locquet, C. Giannetti, E. Pastor, S. E. Wall, *Physical Review Letters* 129, 255701 (2022).
[6] S.W. Wall, S. Yang, L. Vidas, M. Cholett, J.M. Glownia, M. Kozina, T. Katayama, T. Henighan, M. Jiang, T.A. Miller D.A. Reis, L.A. Boatner O. Delaire, , M. Trigo, *Science* **362**, 572(2018).
[7] A. S. Johnson,D. Perez-Salinas,K.M. Siddiqui,S. Kim,S. Choi,K.Volckaert, P.E. Majchrzak, S. Ulstrup, N. Agarwal, K. Hallman R. F. Haglund Jr, C.M. Günther, B.Pfau, S. Eisebitt, D.Backes, F.Maccherozzi, A. Fitzpatrick, S. S. Dhesi, P.Gargiani, M.Valvidares, N.Artrith F.de Groot, H. Choi, D. Jang, A. Katoch, S. Kwon, S.H. Park, H. Kim, S. E. Wall, *Nature Physics* **19**, 215 (2023).

Ultrafast dynamics and control of structure in Charge-density-waves

R. Winkler[1], L. Boie[1], M. Savoini[1], V. Ovuka[1], Y. Deng[2], S. Zerdane[2], A. Nag[2], S. Gurung[1], E. Abreu[1]
S. Biasco[1], D. Soranzio[1], T. Suter[1], J. Dössegger[1], M. Bosch[1], B. Strudwick[2], M. Sander[2], E. Divall[2]
P. Beaud[2], R. Mankowsky[2], A. Oggenfuss[2], C. Arrell[2], D. Babich[2], H. Lemke[2], M. Chollet[4], T. Sato[4]
V. Esposito[4], B. Liu[2], V. Krapivin[4], G. Orenstein[4], Y. Huang[4], P. Bhattacharyya[7], D. Zhu[4], P. Zalden[5]
F. Ardana-Lamas[5], Y. Uemura[5], H. Yousef[5], M. Biednov[5], C. Milne[6], U. Staub[3]
S. Teitelbaum[6], J. Demsar[7], M. Trigo[4]
S. L. Johnson[1]
[1] *ETH Zurich, 8093 Zurich, Switzerland*
[2] *Paul Scherrer Institute, 5232 Villigen, Switzerland*
[3] *Swiss Light Source, 5232 Villigen, Switzerland*
[4] *SLAC National Accelerator Laboratory, Menlo Park, CA 94025, USA*
[5] *European XFEL GmbH, 22761 Hamburg, Germany*
[6] *Arizona State University, Tempe, AZ 8528, USA*
[7] *Johannes Gutenberg-University Mainz, 51099 Mainz, Germany*

With strong connections to BCS-type superconductivity, the phenomenon of charge-density-waves (CDWs) in low-dimensional metallic systems is an important example of a second-order structural phase transition driven by electron-phonon coupling. In this talk I will present the current status of our work on $K_{0.3}MoO_3$, a material with a highly anisotropic structure (see Fig. 1) that results in a nearly 1-D conductivity. Below 183 K, this structure becomes unstable with respect to an incommensurate lattice distortion with wavevector $\mathbf{q}_{CDW}$ = (1 q_b 0.5), where $q_b \approx 0.748$ is a weak function of temperature. Time-resolved x-ray diffraction measurements have directly measured coherent structural dynamics of the charge density wave distortion in this material over a range of excitation levels driven by a femtosecond laser [1, 2]. The sudden laser-driven suppression of the interatomic potential that stabilizes the CDW is thought to cause coherent dynamics that transiently invert the phase of the CDW, a finding that is at least thematically consistent with optically based studies which show evidence of CDW domain formation with a phase that depends on the local excitation level of the material [3].

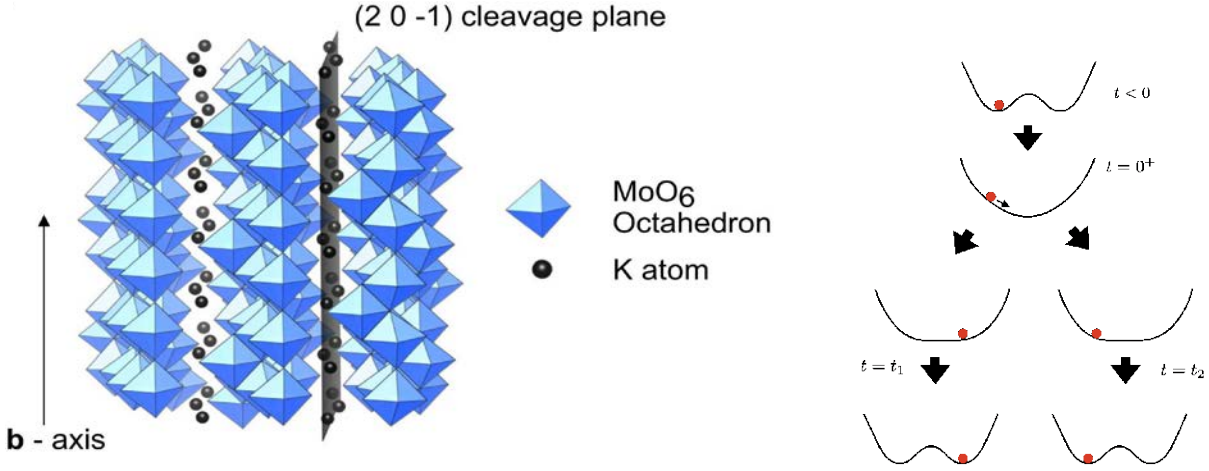

***Fig. 1. Left**: High-temperature structure of $K_{0.3}MoO_3$. The conductivity along the b-axis is significantly higher than in other directions, making this system a quasi-1D conductor that undergoes a charge-density-wave transition below approximately 183 K. **Right**: Proposed scenarios for femtosecond laser-driven melting and domain reformation, where the domain phase is determined by the relaxation time of the excitation relative to the coherent dynamics [3].*

Here I discuss recent results using x-ray free electron lasers to both better characterize the structural dynamics of the coherent phonon driven at low excitation levels, and to investigate the excitation regime where transient CDW melting and phase reversal are expected. I will also discuss future perspectives for making such control more general for second-order-like phase transitions.

References

[1] T. Huber, S. O. Mariager, A. Ferrer, H. Schäfer, J. A. Johnson, S. Grübel, A. Lübke, L. Huber, T. Kubacka, C. Dornes, C. Lauhe, S. Ravy G. Ingold, P. Beaud, J. Demsar, S. L. Johnson, *Physical Review Letters* **113**, 026401 (2014).
[2] M. Neugebauer, T. Huber, M. Savoini, E. Abreu, V. Esposito, M. Kubli, L. Rettig, E. M. Bothschafter, S. Grübel, T. Kubacka, J. Rittmann G. Ingold, P. Beaud, D. Dominko, J. Demsar, S. L. Johnson, *Physical Review* B **99**, 220302 (2019).
[3] R. Yusupov, T. Mertelj, V. V. Kabanov, S. Brazovskii, P. Kusar, J.-H. Chu, I. R. Fischer, D. Mihailovic, *Nature Physics* **6**, 681 (2010).
** This work was supported by the Swiss National Science Foundation under grant 200020_192337.*

Infrared spectroscopy of 2D moiré Superlattice materials

J. Yang[1], T. Han[1], T. Han[1], G. Chen[2], D. Rodan-Legrain[1], J. M. Park[1], Q. Zhang[1], L. Jiang[2], B. Lyu[4] , H.Li[2]
K. Watanabe[5], T. Taniguchi[5], Z. Shi[4], Y. Zhang[6], P. Jarillo-Herrero[1], F.Wang[2] , L. Ju[1]

[1]*Massachusetts Institute of Technology, Cambridge, MA 02135, USA*
[2]*Lawrence Berkeley National Laboratory, Berkeley, CA 94720, USA*
[3]*University of California at Berkeley, Berkeley, CA 94720, USA*
[4] *Shanghai Jiao Tong University, Shanghai, 200231China*
[5]*National Institute for Materials Science, Tsukuba 305-0047, Japan*
[6]*Fudan University, Shanghai, 200437 China*

Moiré superlattices of two-dimensional materials have emerged as a new material platform to engineer and study electron correlation and topology. So far, experimental progresses have been dominated by electron transport measurements which do not provide spectroscopy evidence of correlation or the relevant energy scales directly. Due to their ~micron lateral size, atomic thickness, and complicated device structures involving encapsulating layers and metallic gates, spectroscopy measurements of moiré superlattices have been very challenging.

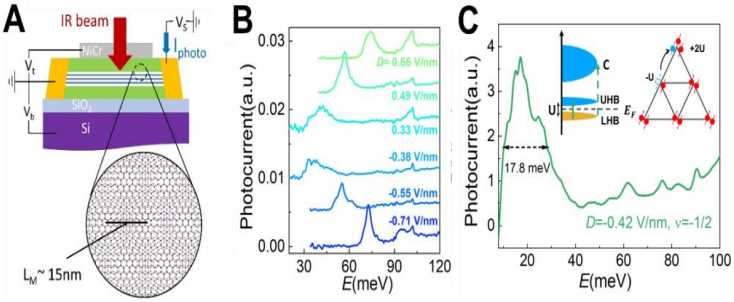

Fig. 1. *Device structure and optical transitions in ABC TLG/hBN moire superlattice.* ***A.*** *Illustration of dual-gated TLG device with a moiré wavelength of ~15 nm.* ***B.*** *Interband optical transitions between moiré bands at various displacement fields. Flatband formation can be visualized as the sharp transition peak emerges in the photocurrent spectrum.* ***C.*** *Photocurrent spectrum when the flat moire band is half-doped, featuring a strong resonance at ~18 meV that corresponds to optical transition across the correlated insulating gap.*

In this talk, I will introduce our recent efforts on FTIR photocurrent spectroscopy measurements of dual-gated ABC trilayer graphene/hBN moiré superlattice, which is a representative moiré superlattice material to study correlated and topological electron physics. We observed strong gate-tunable optical transitions that originated from the moire flat band. At half-filling of the valence flat band, a broad absorption peak emerges at ~18 meV, indicating direct optical excitation across an emerging Mott gap. Furthermore, I will talk about a unique moire-enabled interlayer electron-phonon coupling phenomenon in this system.

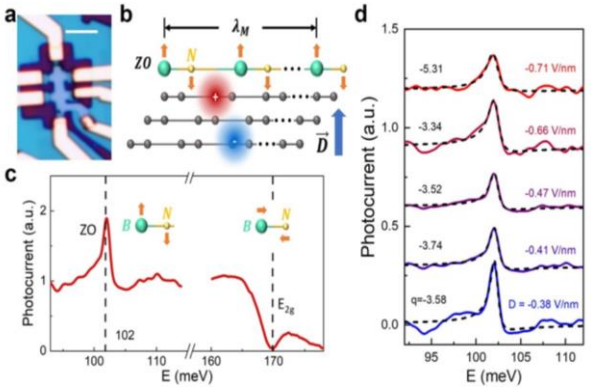

Fig. 2. *Moiré-enabled interlayer electron-phonon coupling in ABC trilayer graphene/hBN.* ***a.*** *Optical micrograph of the ABC TLG/hBN device. Scale bar: 3 micro-meters.* ***b.*** *Illustrattion of the interlayer EPC in TLG/hBN with a moiré wavelength λ_M. The hBN ZO phonon hybridizes with electron-hole pairs in graphene to gain electrical dipole.* ***c.*** *Photocurrent spectrum of TLG. The ZO phonon appears as a peak while the E_{2g} phonon appears as a dip due to light absorption.* ***d.*** *Photocurrent spectra at different gate displacement fields D. The asymmetric line-shape is due to interference of the renormalized ZO phonon with electron-hole pairs at the immediate vicinity in spectrum, which can be well-described by a Fano line-shape represented byt the dashed curves.*

The ZO phonon in hBN hybridizes with electron-hole excitations in trilayer graphene and appear as an asymmetric peak in the photocurrent spectrum. This Fano line-shaped peak evolves continuously as we tune the displacement field. I'll talk about the implications of this phenomenon to engineering the physics of moire quantum matters.

References

[1] J. Yang, G. Chen, T. Han, Q. Zhang, Y.H. Zhang, L. Jiang, B. Lyu, H. Li, K. Watanabe, T. Taniguchi, Z. Shi, S. Todadri, Y. Zhang, F. Wang, L. Ju, *Science* **375**, 1295 (2022).
[2] T. Han, J. Yang, Q. Zhang, L.Wang, K. Watanabe, T. Taniguchi, P.L. McEuen, L. Ju, *Physical Review Letters* **126**, 146402(2021).
[3] L. Ju, L. Wang, T. Cao, T. Taniguchi, K. Watanabe, S.G. Louie, F. Rana, J. Park, J Hone, F. Wang, P.L McEuen, *Science* **358**, 907(2017).
[4] L. Ju, L.Wang, X.Li, S.Moon, M.Ozerov, Z.Lu, T.Taniguchi, K.Watanabe, E.Mueller, F. Zhang, D. Smirnov, *Nature Communications* **11**, (2020).

* This work was supported by the STC Center for Integrated Quantum Materials, NSF Grant No. DMR-1231319. K.W. and T.T. acknowledge support from the Elemental Strategy Initiative conducted by the MEXT, Japan, Grant Number JPMXP0112101001, JSPS KAKENHI Grant Number JP20H00354 and the CREST(JPMJCR15F3), JST. B.L. and Z.S. acknowledges support from the National Key R & D Program of China (2016YFA0302001) and the National Natural Science Foundation of China (11774224 and 12074244). The electron-phonon coupling experiment was supported by NSF Grant No. DMR-2225925. L. J acknowledge the support from Sloan Fellowship.

Magnetic resonances of chiral phonons

D. M. Juraschek,[1] M. Fechner[2]
[1] *Tel Aviv University, Tel Aviv 6997801, Israel*
[2] *Max Planck Institute for the Structure and Dynamics of Matter, 22761 Hamburg, Germany*

Circularly polarized lattice vibrations, also known as chiral phonons, produce orbital motions of the atoms around their equilibrium positions in a solid. Due to this orbital motion, chiral phonons carry angular momentum (real or pseudo) and can therefore interact with the angular momentum of light and with the spin and orbital angular momentum of electrons [1,2]. The investigation of angular momentum coupling between chiral phonons and electrons has seen a tremendous increase of activity in recent years, including demonstrations of the existence of phonon analogs to the Hall Einstein-de Haas effects [3,4]. In dielectric materials, where the atoms possess ionic charges, an intriguing implication arises: circularly and elliptically polarized phonons can carry magnetic moments, induced by the orbital charge currents that the ions produce when moving along the eigenvectors of chiral phonon modes [5,6]. These charge currents are proportional to the ratio of the ionic charges and the ionic masses of the ions in the material, and the resulting magnetic moments usually lie on the order 1-10% of a nuclear magneton (μ_N) per phonon quantum. During the past year, theoretical predictions and experimental measurements have indicated that the magnitude of the phonon magnetic moment can be drastically enhanced by the means of electron-phonon, spin-phonon, and orbit-phonon coupling, where the phonon "borrows" part of the magnetic moment from the electron [7-10]. Through these mechanisms, much larger effective magnetic moments on the order fractions of or even several Bohr magnetons (μ_B) can be achieved, orders of magnitude larger than those expected from purely ionic charge currents. Here, we demonstrate that the presence of a (effective) phonon magnetic moment leads to resonances in the second-order nonlinear magnetoelectric and linear magnetic susceptibilities [11]. We show that the second-order nonlinear magnetoelectric susceptibility enables the excitation of chiral phonons through circularly polarized infrared absorption, as illustrated in Fig. 1(a), in agreement with recent experimental and theoretical studies [7,9,10].

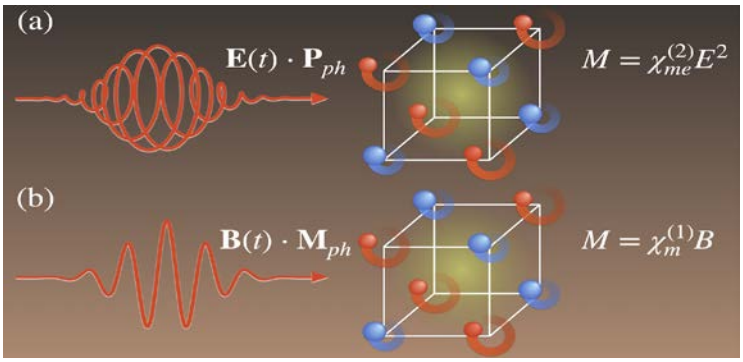

Fig.1: Chiral phonon excitation. (a) *The electric field component of a circularly polarized THz pulse, $\boldsymbol{E}(t)$, can couple to the electric dipole moment of the two orthogonal components of a chiral phonon mode, $\boldsymbol{P}_{ph}$. This leads to a contribution to the second-order nonlinear magnetoelectric susceptibility, $\chi_{me}^{(2)}$.* **(b)** *The magnetic field component of a linearly polarized THz pulse, $\boldsymbol{B}(t)$, can couple to the magnetic moment of a chiral phonon mode, $\boldsymbol{M}_{ph}$. This leads to a contribution to the linear magnetic susceptibility, $\chi_{m}^{(1)}$.*

The linear magnetic susceptibility, in contrast, comes from a Zeeman-type coupling of the magnetic field component of light with the phonon magnetic moment, as shown in Fig. 1(b)
We demonstrate that the mechanism described by the linear magnetic susceptibility leads to a multitude of novel phenomena: it enables the excitation of circularly polarized phonons with linearly polarized light, it can be utilized for phononic frequency up-conversion covering several orders of magnitude, and it makes the excitation of Raman-active phonons possible without Raman scattering. We use a combination of first-principles methods and phenomenological modeling to describe the chiral phonon dynamics that arise from the excitations by ultrashort laser pulses, and we propose candidate materials in which the mechanism can potentially be detected.

References

[1] L. Zhang, Q. Niu, *Physical Review Letters* **112**, 085503 (2014).
[2] H. Zhu, J. Yi, M.-Y. Li, J. Xiao, L. Zhang, C.-W. Yang, R. A. Kaindl, L.-J. Li, Y. Wang, X. Zhang, *Science* **359**, 579 (2018).
[3] G. Grissonnanche, S. Thériault, A. Gourgout, M.-E. Boulanger, E. Lefrançois, A. Ataei, F. Laliberté, M. Dion J.- S. Zhou, S.Pyon, T.Takayama, H. Takagi, N. Doiron-Leyraud and L. Taillefer, *Nature Physics.* **16**, 1108 (2020).
[4] S. R. Tauchert, M. Volkov, D. Ehberger, D. Kazenwadel, M. Evers, H. Lange, A. Donges, A. Book W. Kreuzpaintner, U. Nowak, P. Baum, *Nature* **602**, 73 (2022).
[5] T. F. Nova, A. Cartella, A. Cantaluppi, M. Först, D. Bossini, R. V. Mikhaylovskiy, A. V. Kimel R. Merlin, A. Cavalleri, *Nature Physics* **13**, 132 (2017).
[6] D. M. Juraschek, M. Fechner, A. V. Balatsky, N. A. Spaldin, *Physical Review Materials* **1**, 014401 (2017).
[7] D. M. Juraschek, T. Neuman, P. Narang, *Physical Review Research* **4**, 013129 (2022).
[8] A. Baydin, F. G. G. Hernandez, M. Rodriguez-Vega, A. K. Okazaki, F. Tay, G. T. Noe II, I. Katayama, J. Takeda H. Nojiri, P. H. O. Rappl, E. Abramof, G. A. Fiete, J. Kono, *Physical Review Letters* **128**, 075901 (2022).
[9] M. Basini, M. Pancaldi, B. Wehinger, M. Udina, T. Tadano, M. C. Hoffmann, A. V. Balatsky, S. Bonetti, *arXiv:2210.01690* (2022).
[10] C. S. Davies, N. Fennema, A. Tsukamoto, A. Kirilyuk, *IRMMW-THz* 43035 (2022).
[11] D. M. Juraschek, M. Fechner, *in preparation* (2023).

Field-resolved metrology for Attosecond-scale carrier dynamics

N. Karpowicz
Max Planck Institute of Quantum Optics, 85748 Garching, Germany

For decades, attosecond science has been giving us new insight into light-matter interaction by allowing time-resolved access to events lasting only a fraction of an optical cycle. The first generation of attosecond experiments made use of the high harmonic generation process to produce short bursts of extreme ultraviolet radiation, which were then used in a variety of experimental geometries to excite and observe laser-induced dynamics. As we learned about these physical processes, one thing became clear: the electric field of light often leaves its own imprint behind in a way that makes it possible to extract it directly from the measurement. We will show that this has surprisingly opened a door to a new generation of attosecond experiments, where charge carriers inscribe their motion directly into an electromagnetic wave that we can record with sub-fs resolution.

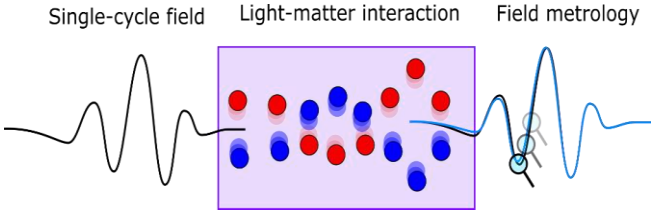

***Fig. 1. The framework of field-resolved attosecond metrology. Left**: a single-cycle pulse of light enters a medium. **Center**: The field induces time-dependent dynamics in the system (center). **Right:** The dynamics are encoded into subtle modifications of the electromagnetic wave. Field metrology allows us to obtain these traces of the interaction and relate them back to the underlying microscopic dynamics.*

There are a few things that need to be established for this class of experiment, sketched in Fig. 1, to work: 1) What are the physical origins of our “gate” that allows us to turn a rapidly-oscillating optical field into a nearly-constant signal suitable for electronics? 2) Can we model this gate precisely enough to invert its influence on the recorded waveform? 3) How is information embedded into the electric field, and how can we get it out?There are several solutions to the first question, which we can divide into two categories: electronic and photonic. Electronic methods make use of carrier-excitation dynamics in the detector to, for example, rapidly change the conductivity of a solid [1, 2, 3], resulting in a relatively long-lived current that will, as its time delay relative to the field under study is changed, allowing the waveform to be recorded electronically. Alternatively, photonic techniques [4], such as electro-optic sampling [5], translate the electric field present in a nonlinear medium into a modification of a measurable aspect of a second pulse.Once an electric field measurement has been implemented, there is still an important question to answer: what is the relationship between this measured trace and the true electric field within or impinging on the detector? And how does it relate to the electric field inside of a sample under study? This question can be highly non-trivial, and one must not forget that the electric field is not only a function of time, but also of space; sometimes untangling it will require techniques that capture the spatiotemporal evolution of the waveform [6]. Addressing this not only from the experimental side, we have developed a robust open-source nonlinear optics simulation platform that will be briefly discussed, with the goal of lowering barriers between experimentalists and deep and detailed views of the evolution of electric fields inside optical media [7]. Finally, how does the signal from the carriers get embedded into the electric field? There are a few experimental geometries where changes in electric field waveforms may be related back to the microscopic nonlinear polarization in the sample [8], which is an observable closely related to many other physical properties of interest, such as the energy exchanged between the medium and the sample.Finally we will provide an overview of the underlying technology that drives these experiments and of new ultrashort sources that are coming online. Optimally performing field driven metrology requires a rethinking of the ideal source, favoring phase and amplitude stability over the high intensities required to drive high harmonic generation.In summary, the field of attosecond metrology is undergoing a revolution in how data is acquired and insight is obtained, based on recording and interpreting the waveform of light. Understanding and controlling all aspects of the dynamics responsible for giving this unprecedented access to the electromagnetic field will be an essential component of the future of this ever-evolving field of study.

References

[1] A. Schiffrin, T. Paasch-Colberg, N. Karpowicz, V. Apalkov, D. Gerster, S. Mühlbrandt, M. Korbman, J. Reichert, M. Schultze, S. Holzner, J. V. Barth, R. Kienberger, R. Ernstorfer, M. I. Stockman, F. Krausz, *Nature* **493**, 70 (2013).
[2] S. Sederberg, D. Zimin, S. Keiber, F. Siegrist, M.S. Wismer, V.S. Yakovlev, I. Floss, C. Lemell, J. Burgdoerfer, M. Schultze, F. Krausz N. Karpowicz, *Nature Communications* **11**, 430 (2020).
[3] M. Ossiander, K. Golyari, K. Scharl, L. Lehnert, F. Siegrist, J.P. Bürger, D. Zimin, J.A. Gessner, M. Weidman, I. Floss, V. Smejkal, S. Donsa, C. Lemell, F. Libisch, N. Karpowicz, J. Burgdoerfer, F. Krausz, M. Schultze, *Nature Communications* **13**, 1620 (2022).
[4] D. Zimin, V.S. Yakovlev, and N. Karpowicz, *Science Advances* **8**, eade1029 (2022).
[5] S. Keiber, S. Sederberg, A. Schwarz, M. Trubetskov, V. Pervak, F. Krausz, and N. Karpowicz, *Nature Photonics* **10**, 159 (2016).
[6] M. Mamaikin, Y. Li, E. Ridente, W.Chen, J. Park, A. Y.Zhu, F.Capasso, M.Weidman, M.Schultze, F.Krausz, N.Karpowicz, *Optica* **9**, 616 (2022).
[7] https://www.github.com/NickKarpowicz/LightwaveExplorer
[8] A. Sommer, E. M. Bothschafter, S. A. Sato, C. Jakubeit, T. Latka, O. Razskazovskaya, H. Fattahi, M. Jobst, W. Schweinberger, V. Shirvanyan, V. S. Yakovlev, R. Kienberger, K. Yabana, N. Karpowicz, M. Schultze, F. Krausz, *Nature* **534**, 86 (2016).

New pathways for ultrafast structural control via Nonlinear phononics

G. Khalsa, J. Zheng, J. Moses
Cornell University, Ithaca, New York, 14853, USA

The strong coupling between structure, symmetry, and function is a broad reaching paradigm guiding all levels of science and technology from the discovery of new fundamental physical phenomena to the design of new technologies. The development of bright, tunable, mid- and far-infrared light sources has enabled transient ultrafast control of crystal structure and symmetry, unveiling new and hidden physics and functionality in crystalline materials [1]. Through the resonant excitation of infrared-active phonons with contemporary light sources the optical energy in the laser field is quickly converted to mechanical energy in the crystal, pushing it to a far-from-equilibrium state where symmetry and the local chemical environment can be dramatically altered. To enable access to new symmetries and new far-from-equilibrium and hidden phenomena in crystalline materials, new routes for structural and symmetry control on ultrafast timescales are sought.

To explain existing ultrafast structural and functional changes in this field, termed *nonlinear phononics*, the anharmonic lattice energy coupling between the resonantly excited infrared-active phonons and indirectly driven Raman-active phonons has been invoked and investigated. Recent theoretical work has suggested that nonlinear contributions to the lattice polarizability should be held on equal footing with the anharmonic lattice potential energy, predicting an induced broad frequency dielectric response in the infrared 7-orders-of-magnitude larger than silica[2]. Can the combination of the conventional anharmonic lattice potential pathway and the nonlinear lattice polarizability enable new pathways for control of symmetry, structure, and function on ultrafast timescales?

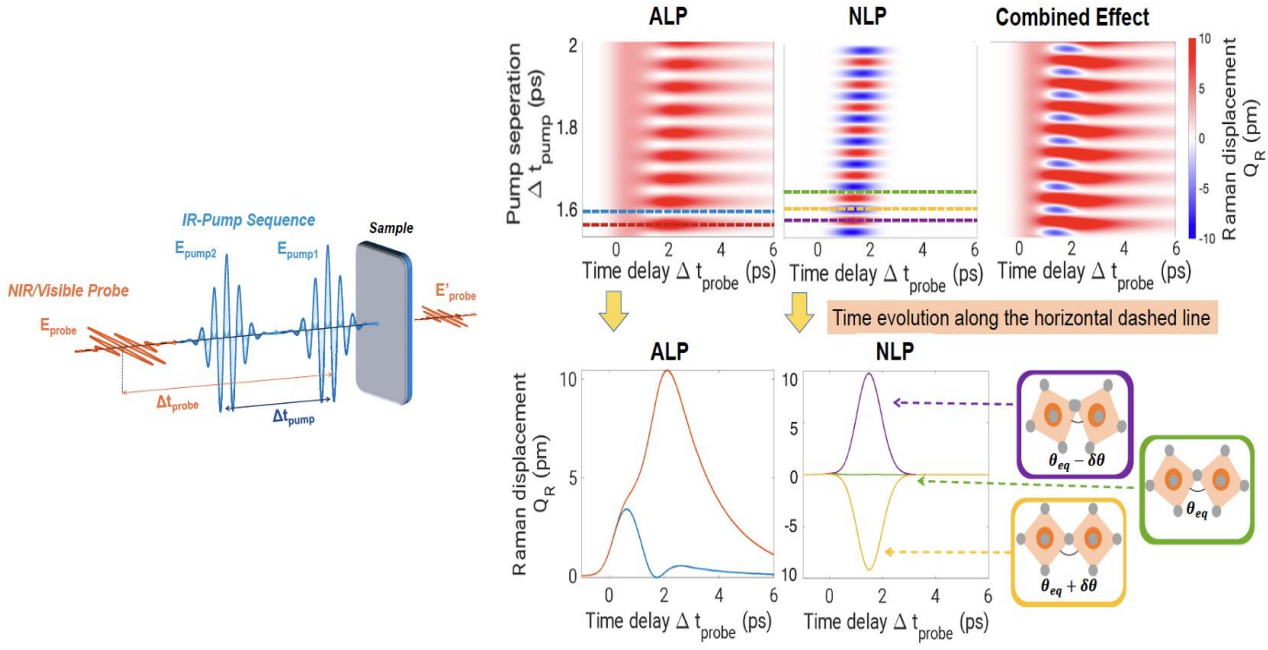

***Fig. 1.**: Coherent structural control through a two-THz-pulse scheme (**left**) enabled by the combination of the anharmonic lattice potential (ALP) and the nonlinear lattice polarizability (NLP). (**Top-right**) The ALP rectifies a Raman active phonon with a direction defined by intrinsic microscopic materials physics (red), while the NLP is sensitive to the relative phase between the ringing IR phonon excited by the first pulse and the electric field of the second pulse (red and blue). The combination of the ALP and NLP leads to control of the direction and duration of the rectified Raman response (Combined Effect) with pulse separation. (**Bottom-right**) Simulated dynamics of Raman phonon rectification through the ALP and NLP pathways for two-IR-pulse excitation along with schematic structural changes.*

Here we show theoretically that careful preparation of infrared-resonant light through, for example, the control of frequency, ellipticity, pulse shape, and pulse sequencing (Fig. 1), can enable control of structure and symmetry that are inaccessible by other means when the anharmonic lattice potential energy and nonlinear lattice polarizability are treated on equal footing.

References

[1] A. S. Disa, T. F. Nova, A. Cavalleri, *Nature Physics* **17**, 1087 (2021).
[2] G. Khalsa, N. A. Benedek, J. Moses, *Physical Review* X **11**, 021067 (2021).

* Acknowledgement(s): his work is supported by the Cornell Center for Materials Research with funding from the NSF MRSEC program (Grant No. DMR-1719875).

Ultra low loss silicon nitride integrated photonics: Frequency agile low noise lasers

T. J. Kippenberg
Swiss Federal Institute of Technology, 1015Lausanne, Switzerland

Recent advances in attaining ultralow loss, highly confining silicon nitride waveguides with loss in the dB/meter range [1] have opened up novel applications that benefit not only from scalable manufacturing, compact form factor and low power, but crucially have now reached a point where the performance is on par and even exceeding that of legacy optical systems. However, Si_3N_4 is a purely passive optical material with only a thermal and Kerr nonlinearities and hence must be endowed with pivotal capabilities such as light amplification, fast modulation, etc. through advanced integration techniques. I will describe a range of novel advances based on ultra-low loss Si_3N_4 and advanced photonic integration, including photonic integrated circuit based frequency agile lasers with fiber laser phase noise[2], parametric traveling wave amplifiers[3], Erbium amplifiers on chip[4] as well as soliton frequency combs[5], with applications from coherent communications[6], LiDAR [7,8] to cryogenic quantum interconnects[9] (cf Fig. 1) Erbium doped amplifiers are pivotal components for modern communication networks. Their unique property to achieve high gain, continuous, low-noise and high-power amplification is unmatched in long haul communication systems. Yet, their photonic integration has been compounded by high waveguide propagation losses. We demonstrate a hi waveguide amplifier based on erbium ion implantation into ultra-low loss Si3N4 with more than 30 dB net-gain and output power up to 142 mW[4]. Another paradigm for amplification are parametric amplifiers based on the optical Kerr effect. Having been pioneered in silicon photonics more than a decade ago [10], it was not possible to achieve time-continuous operation due to two photon absorption in silicon. Here we overcome this outstanding challenge and demonstrate time-continuous net gain fiber-to-fiber in a 2 m long photonic Damascene Si_3N_4 waveguide spiral [3].

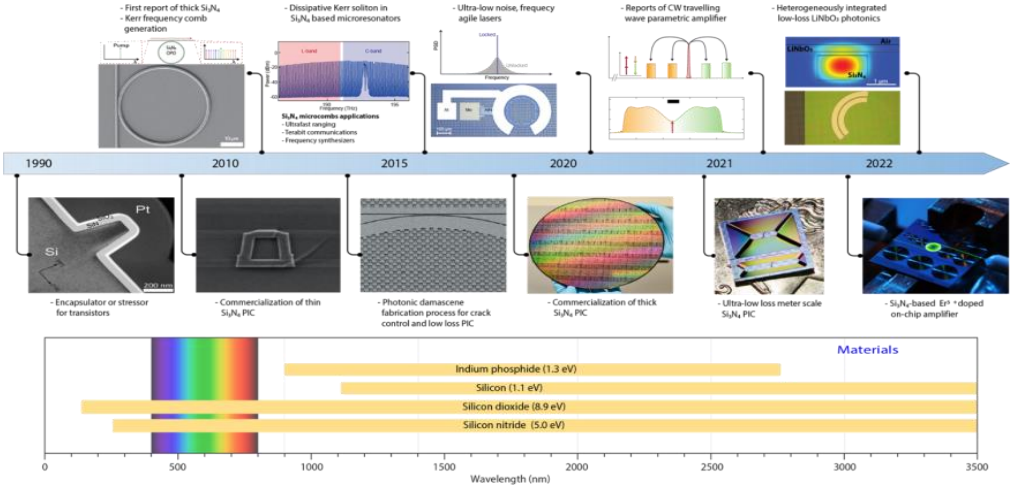

Fig.1*.Applications of ultra-low loss silcon nitride based photonic integrated circuits.*

Using monolithic integration of piezoelectric actuator ubiquitous in MEMS foundries [11] we can endow photonic Damascene Si_3N_4 circuits with fast, low power and hysteresis free non-thermal tuning capability without impairing propagation loss. Based on this platform we demonstrated the first ultra-fast tunable hybrid integrated laser, that combines the low noise of a fiber laser with unprecedented frequency modulation speed and linearity. We demonstrate proof-of principle applications in frequency modulated continuous wave LiDAR[2]. Electro-optical tuning via the optical Pockels effect is the fastest and most powerful modulation technique. Here we present a hybrid silicon nitride (Si_3N_4)–$LiNbO_3$ photonic platform and demonstrate its use for coherent laser ranging. Our platform is based on heterogeneous integration of ultralow-loss Si_3N_4 photonic integrated circuits with thin-film $LiNbO_3$ through direct bonding at the wafer level, in contrast to previously demonstrated chiplet-level integration, featuring low propagation loss of 8.5 dB/m[12], enabling narrow-linewidth lasing (intrinsic linewidth of 3 kilohertz) by self-injection locking to a laser diode[13].

References

[1] J. Liu, G. Huang, R. N. Wang, J. He, A. S. Raja, T. Liu, N. J. Engelsen, T. J. Kippenberg. *Nature Communications* **12**, 2236 (2021).
[2] G. Lihachev, J. Riemensberger, W. Weng, J. Liu, H. Tan. A. Siddharth, V. Snigirev, V. Shadymov, A. Voloshin, R. N. Wang, J. He, S. A. Bhave, T. J. Kippenberg. *Nature Communications* **13**, 3522 (2022).
[3] J. Riemensberger, N. Kuznetsov, J. Liu, J. He, R. N. Wang, T. J. Kippenberg. *Nature* **612**, 56 (2022).
[4] Y. Liu, Z.Qiu, X. Ji, A.Lukashchuk, J. J.He, J.Riemensberger, M.Hafermann, R. N.Wang, J.Liu, C.Ronning, T. J.Kippenberg.*Science* **376**, (2022)
[5] T. J. Kippenberg, A. L. Gaeta, M. Lipson, M. L. Gorodetsky. Dissipative Kerr solitons in optical microresonators. *Science* **361**, eaan8083 (2018).
[6] P. Marin-Palomo, J. N. Kemal, M. Karpov, A.Kordts, J.Pfeifle, M. H. P. Pfeiffer, P.Trocha, S. Wolf, V. Brasch, M. H. Anderson, R. Rosenberger, K. Vijayan, W. Freude, T. J. Kippenberg, C. Koos. *Nature* **546**, 274 (2017).
[7] P. Trocha, M. Karpov, D. Ganin, M. H. P. Pfeiffer, A. Kordts, S. Wolf, J. Krockenberger, P. Marin-Palomo, C.Weimann, S. Randel, W. Freude, T. J. Kippenberg, C. Koos. *Science* **359**, 887 (2018).
[8] J. Riemensberger, A. Lukashchuk, M. Karpov, W. Weng, E. Lucas, J. Liu, T. J. Kippenberg. *Nature* **581**, 164 (2020).
[9] A. Youssefi, I. Shomroni, Y. J. Joshi, N. R. Bernier, A. Lukashchuk, P. Uhrich, L. Qiu, T. J. Kippenberg. *Nature Electronics* **4**, 326 (2021).
[10] M. A. Foster, A. C. Turner, J. E. Sharping, B. S. Schmidt, M. Lipson, A. L. Gaeta. *Nature* **441**, 960 (2006).
[11] H. Tian, J. Liu, B. Dong, J. C. Skehan, M. Zervas, T. J. Kippenberg, S. A. Bhave. *Nature Communications* **11**, 3073 (2020).
[12] M. Churaev, R. N. Wang, V. Snigirev, A. Riedhauser, T. Blésin, C. Möhl, M. A. Anderson, A. Siddharth, Y. Popoff, D. Caimi, S. Hönl, J. Riemensberger, J. Liu, P. Seidler, T. J. Kippenberg. *arXiv:2112.02018* (2021).
[13] V. Snigirev, A.Riedhauser, G.Lihachev, M.Churaev, J.Riemensberger, R. N. Wang, A. Siddharth, G. Huang, C. Moehl, Y. Popoff, U. Drechsler, D. Caimi, S. Hoenl, J. Liu, P. Seidler, T. J. Kippenberg. *Nature* **615**, 411 (2023).

Floquet topological superconductivity induced by Chiral many-body interaction

S. Kitamura[1], H. Aoki[2]
[1] *The University of Tokyo, Tokyo 113-8656, Japan*
[2] *Advanced Industrial Science and Technology (AIST), Ibaraki 305-8568, Japan*

Light irradiation is a new means of controlling the quantum phase and properties of materials, with which various novel properties including nontrivial band topology can be achieved in a dynamical manner. Floquet theory enables us to describe such nontrivial modulation from the viewpoint of the effective static Hamiltonian, nevertheless the original system irradiated with an intense laser light is far from equilibrium. In particular, when the circularly-polarized laser light is applied, the effective static Hamiltonian acquires interaction terms with broken time-reversal symmetry (TRS), which is difficult to realize in conventional approaches [1,2].
While this idea triggered various attempts to control topology of superconductivity, especially with broken TRS, it turns out to be much more nontrivial than controlling band topology of normal states, because the superconducting gap does not couple to electromagnetic field directly due to its inherent particle-hole symmetry. Previous studies mainly focused on the topological superconductivity via the modulation of the normal band structure without changing the pairing symmetry [3].
As a new perspective, in this study, we focus on strongly-correlated superconductors, and propose an approach that combines control of topology and control many-body interaction [4]. We show that topologically-nontrivial chiral ($d+id$ wave) superconductivity can be achieved in the doped Hubbard model on the square lattice, due to the modulation of the effective pairing interaction induced by the circularly-polarized light, as sketched in Fig. 1.

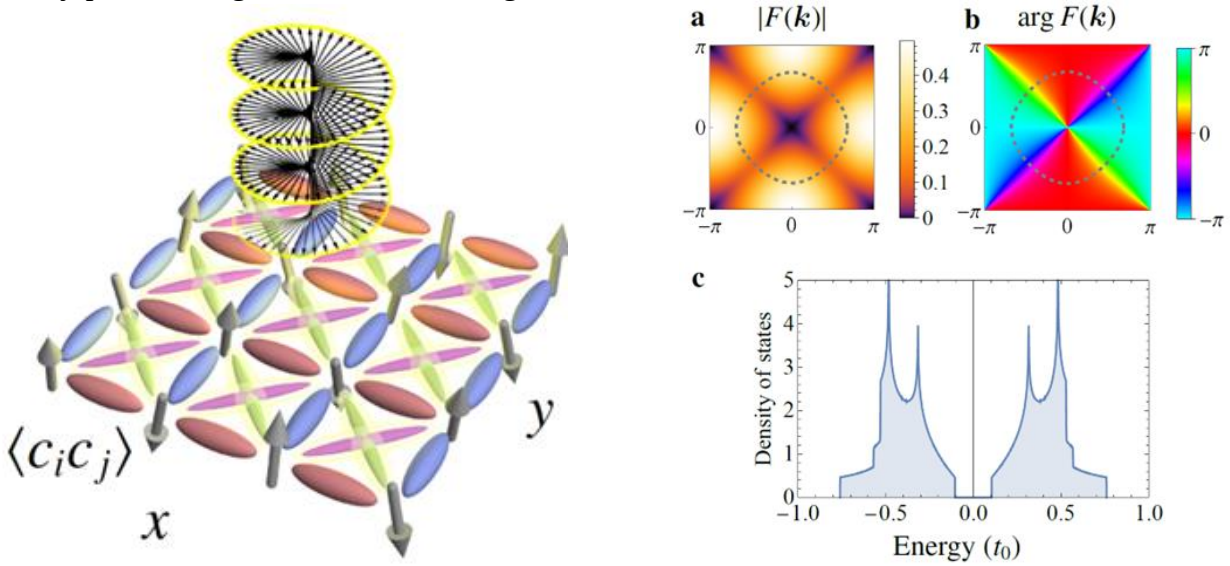

***Fig. 1. Left**: Sketch of the present proposal. The d-wave superconductivity on cuprates is depicted with red and blue bonds, which have positive and negative pairing amplitude, respectively. Illuminating an intense circularly-polarized light induces imaginary pairing amplitude (colored by magenta and green) in diagonal directions, which makes superconductivity chiral (d+id-wave). **Right**: Numerical results on the ground state of Floquet effective Hamiltonian of the t-J form. (a,b) Amplitude and phase of gap function F(**k**). The dashed lines represent the Fermi surface (at the critical temperature). (c) The density of states in the unit of hopping amplitude t_0, showing the full-gap nature of the d+id-wave.*

We first derive the Floquet t–J model by combining the Floquet theory and the Schrieffer-Wolff transformation. The obtained Hamiltonian has chiral many-body interactions with broken time-reversal symmetry, i.e., the scalar spin chirality term and so-called three-site terms with complex amplitudes. Then we show that these emergent interactions indeed modulate the pairing symmetry within the framework of Gutzwiller approximation, and demonstrate it by numerically calculating the phase diagram and transient dynamics.

References

[1] T. Oka, H. Aoki, *Physical Review B* **79**, 081406, (2009).
[2] T. Kitagawa, T. Oka, A. Brataas, L. Fu, E. Demler, *Physical Review B* **84**, 235108, (2011).
[3] K. Takasan, A. Daido, N. Kawakami, Y. Yanase, *Physical Review B* **95**, 134508, (2017).
[4] S. Kitamura, H. Aoki, *Communications Physics* **5**, 174, (2022).
* This work was supported by JSPS KAKENHI Grant (20K14407 and JP17H06138), and CREST (Core Research for Evolutional Science and Technology; Grant number JPMJCR19T3 and JPMJCR18T4).

Spectroscopy of Cavity Vacuum-Driven Materials

J. Kono
Rice University, Houston, TX 77005, U.S.A.

There is currently much interest in studying solids placed in cavities to uncover exotic new phases and phenomena in "strongly driven" materials in the complete absence of any external fields other than the fluctuating vacuum, or zero-point, electromagnetic fields. Judicious engineering of the quantum vacuum surrounding the matter inside the cavity can lead to significant and nonintuitive modifications of electronic states, producing a vacuum-dressed material with novel properties. Recent stimulating theoretical predictions include cavity-enhanced, cavity-induced, and cavity-mediated enhancement of electron-phonon coupling and superconductivity, electron pairing, anomalous Hall effect, ferroelectric phase transitions, quantum spin liquids, and photon condensation. Figure 1 highlights the opportunities in the cavity–matter interactions leading to several exotic phenomena ranging from the formation of polaritonics to nonlinear optics.

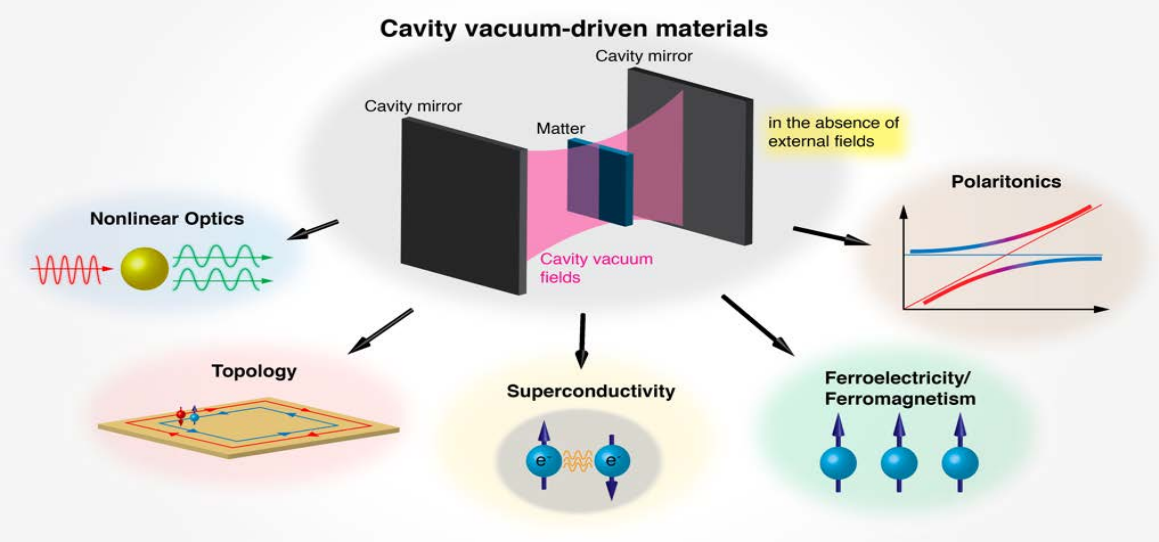

Fig. 1. *Various solid-state cavity quantum electrodynamics (QED) systems have recently emerged, opening up exciting new opportunities for studying the interaction of quantized vacuum fields with quantum many-body systems. Driven by some pioneering experimental developments, there have been many theoretical proposals for manipulating material properties and inducing new phases of matter with cavity-enhanced quantum vacuum, or zero-point, electromagnetic fields.*

The so-called ultrastrong coupling (USC) regime arises when the interaction energy becomes a significant fraction of the bare frequencies of light and matter [1]. Most intriguingly, when a material is ultrastrongly coupled with cavity-enhanced vacuum electromagnetic fields (or zero-point fields), its ground-state properties can be considerably modified. This nonperturbative virtual driving without any external field can lead to novel equilibrium phases with exotic properties.

This talk will describe our recent studies of USC phenomena in various solid-state systems in search of such vacuum-induced phases of matter [2–9]. We employ the quantum optics concept of Dicke cooperativity [10], i.e., many-body enhancement of light–matter interaction, to explore new states and phenomena in condensed matter systems in the USC regime. These results provide quantum optical strategies for creating, controlling, and utilizing novel phases in condensed matter systems enabled by the quantum vacuum.

References

[1] N. Marquez Peraca, A. Baydin, W. Gao, M. Bamba, *Semiconductors and Semimetals* **105** , 89 (2020).
[2] Q. Zhang, M. Lou, X. Li, J. L. Reno, W. Pan, J. D. Watson, M. J. Manfra, J. Kono, *Nature Physics* **12**, 1005 (2016).
[3] X. Li, M. Bamba, Q. Zhang, M. Lou, J. D. Watson, K. Yoshioka, M. J. Manfra, J. Kono, *Nature Photonics* **12**, 324 (2018).
[4] W. Gao, X. Li, M. Bamba, J. Kono, *Natures Photonics* **12**, 362 (2018).
[5] X. Li, M.Bamba, N. Yuan, Q. Zhang, Y. Zhao, M. Xiang, K. Xu, Z. Jin, W. Ren, G.Ma, S.Cao, D.Turchinovich, J. Kono, Science **361**, 794 (2018).
[6] T. Makihara, K. Hayashida, G. T. Noe II, X. Li, N. Marquez Peraca, X. Ma, Z. Jin, W. Ren, G. Ma, I. Katayama, J. Takeda, H. Nojiri, D. Turchinovich, S. Cao, M. Bamba, J. Kono, *Nature Communications* **12**, 3115 (2021).
[7] M. Bamba, X. Li, N. Marquez Peraca, J. Kono, *Communications Physics* **5**, 3 (2022).
[8] K. Hayashida, T. Makihara, N. Marquez Peraca, D. Fallas Padilla, H. Pu, J. Kono, M. Bamba, *Scientific Reports* **13**, 2526 (2023).
[9] N. Marquez Peraca, X. Li, J. M. Moya, K. Hayashida, X. Ma, K. J. Neubauer, D. Fallas Padilla, C.-L. Huang, P. Dai, A. H. Nevidomskyy, H. Pu E. Morosan, S. Cao, M. Bamba, J. Kono, *arXiv:2302.06028.*
[10] K. Cong, Q. Zhang, Y. Wang, G. T. Noe II, A. Belyanin, J. Kono, *Journal of Optical Society of America* B **33**, C80 (2016).
* Acknowledgements: The author acknowledges support from the U.S. Army Research Office (Grant No. W911NF2110157), the Gordon and Betty Moore Foundation (Award No. 11520), and the W. M. Keck Foundation (Award No. 995764).

Unraveling optically induced ultrafast dynamics of Nanoscale magnetic textures

R. Kukreja
University of California, Davis, CA 95616, USA

Ultrafast optical control of magnetization has emerged as a new paradigm for the next generation memory and data storage devices. Numerous studies have been performed to understand the mechanism of transfer of angular momentum at such fast timescales. However, it has been recently recognized that spatial domain pattern and nanoscale heterogeneities can play a critical role in dictating the ultrafast behavior [1-4]. These experimental findings have been possible due to recent advances in x-ray and extreme ultraviolet sources which combine the power of coherent x-rays with femtosecond (fs) temporal resolution [5]. I will discuss some of the key studies performed at x-ray free electron lasers (XFELs) sources in the recent years which have shed light on the magnetic behavior at ultrafast and ultrasmall frontier. I will also describe some of our recent experimental results at European XFEL and FERMI where we uncovered symmetry-dependent behavior of the ultrafast response [6, 7]. Our results on the same sample with the same experimental conditions but different ground state (isotropic labyrinth domains vs anisotropic stripe domains) shows that the symmetry of magnetic texture dictates the magnitude and timescale of the ultrafast response (see Fig. 1).

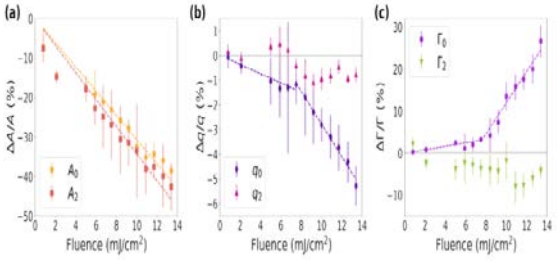

Fig. 1. *Laser pump fluence dependence of magnetic scattering obtained from isotropic labyrinth and anisotropic stripe domains:* ***(a)*** *Amplitude,* ***(b)*** *ring position, and* ***(c)*** *ring width for magnetic scattering diffraction pattern obtained from isotropic labyrinth (**A_0, q_0, Γ_0**) and anisotropic stripe domains (**A_2, q_2, Γ_2**). The magnetization quench amplitude for both of the domain pattern behave similarly, and shows linear dependence with the pump fluence. Ultrafast distortions of diffraction pattern (**ring width and ring position**) behave strikingly different for labyrinth and stripe domain pattern. A fluence threshold is observed for the ultrafast distortions of diffraction pattern.*

These results clarify the previous controversy in the literature for time-resolved magnetic studies for different samples showing distinct responses. We also utilized time-resolved magnetic scattering to test recent predictions of >10 km/s domain wall speeds. We observed fluence threshold dependence for distortions of diffraction pattern which are not seen for magnetization quenching, consistent with a picture of domain wall motion with pinning sites (see Fig.1). Supported by simulations, we show that a speed of 66 km/s for highly curved domain walls can explain the experimental data (see Fig. 2) [7].

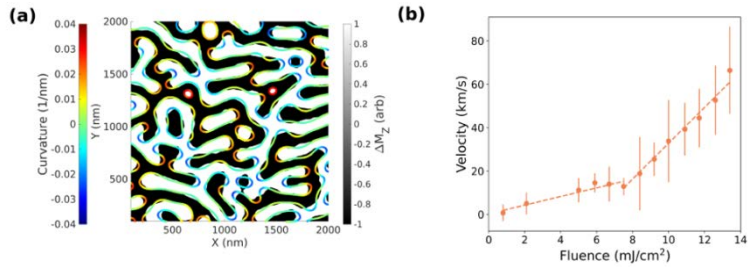

Fig. 2. *Simulated modification of domain pattern and calculated domain wall velocity: (a) Simulated modified domain pattern (**black and white domains**) and initial state (**colored outline**). The comparison clearly shows that regions with high curvature (**dark red or blue**) undergo noticeable domain wall motion,* ***(b)*** *Fluence dependence of calculated domain wall velocity for curved domain walls for labyrinth domain pattern.*

We thus show that these intriguing observations suggest preferential texture-dependent paths for the spin transport and provide us with a unique way to manipulate spin degrees of freedom.

References

[1] D. Z. E. Iacocca, L. Le Guyader, A. H. Reid, W.F. Schlotter, T.-M. Liu, D. J. Higley, G. Coslovich, S. F. Wandel, P. M. Tengdin, S.K. K. Patel, A. Shabalin, N.Hua, S.B. Hrkac, H.T. Nembach, J. M. Shaw, S.A. Montoya, A. Blonsky, C. Gentry, M. A. Hoefer, M.M. Murnane, H. C. Kapteyn
E. E. Fullerton, O. Shpyrko, H. A. Dürr, T. J. Silva, *Physical Review* B **106**, 144422 (2022).
[2] M. Hennes, A. Merhe, X. Liu, D. Weder, C. Von Korff Schmising, M. Schneider, C. Günther, Mahieu, B., Malinowski, G., Hehn, M., Lacour, D. Capotondi, F., Pedersoli, E., Nikolov, I. P., Chardonnet, V., Jal, E., Lüning, J., & Vodungbo, B, *Physical Review* B **102**,174437 (2020).
[3] B. Vodungbo, J.Gautier,G. Lambert,A.B, Sardinha, M. Lozano, S. Sebban, M. Ducousso, W.Boutu, K.Li, B. Tudu, M. Tortarolo, R. Hawaldar R. Delaunay, V. López-Flores, J. Arabski, C. Boeglin, H. Merdji, P. Zeitoun, J. Lüning, *Nature Communications* **3**, 999 (2012).
[5] B. Pfau, S.Schaffert, L. Müller,C. Gutt, A. Al-Shemmary, F.Büttner, R.Delaunay, S Düsterer, S.Flewett, R.Frömter, J. Geilhufe, E.Guehrs, C. Günther,
R. Hawaldar,M. Hille,N. Jaouen, A. Kobs, K. Li, J. Mohanty, S. Eisebitt, Nature Communications. **3**, 1100 (2012).
[6] J. Spencer, R. Kukreja. *APL Materials* **9**, 100702 (2021).
[7] N.Z. Hagström, R. Jangid, T.D. Meera, J. Brock, E.S. Lamb, B. Stoychev, J. Schlappa, N. Gerasimova, B.Van Kuiken, R. Gort, L. Mercadier, L. Le.Guyader, A. Samartsev, A. Scherz, G. Mercurio, H.A. Dürr, A.H. Reid, M. Arora, H.T. Nembach, J.Shaw, E. Jal, E. Fullerton, M.W. Keller,
R. Kukreja, S. Bonetti, T.J. Silva. E. Iacocca, *Physical Review* B **106**, 224424(2022).

Time resolved studies of ultrafast dynamics in Wide band-gap materials

P. Lample[1], M. Weis[1], S. G. Mizrahi[2], E. Peronne[2], D. Boschetto[2], R. Geneaux[1]
S Guizard[1]
[1] *Université Paris-Saclay, 91191 Gif-sur-Yvette, France.*
[2] *Ecole Polytechnique, 91120 Palaiseau, France.*

The interaction of intense light pulses with transparent materials is a domain of research with a long history which is however more active than ever, and this revival concerns both applied science and fundamental research. In this work, our aim is to explore the relaxation dynamics in wide band gap dielectrics, namely SiO_2 and Al_2O_3. Recently we have shown that time resolved studies are ideal tools to get new insights in the different electronic relaxation, trapping and avalanche mechanism that occur during and just after the interaction [1].
We intend now to investigate the interaction of excited carriers with the lattice, and how electronic excitation can influence the relaxation and lifetime of phonons. For this purpose, we have built at LOA an experimental set-up, which allows measuring simultaneously the change in transmission and reflectivity, induced by a pump pulse. This exciting pulse is the second harmonic of a Ti-Sa laser which delivers 40 fs pulse at a repetition rate of 1 KHz, and the probe pulse is the fundamental at 800 nm. In this poster, we wish to present the first set of results.
In SiO_2, (see Figure 1), we observe different mechanism depending on the pump intensity: first Kerr effect, followed by the coherent excitation of phonon, and finally photoexcitation of carriers in the conduction band, which is followed by a fast trapping of electron hole pairs.

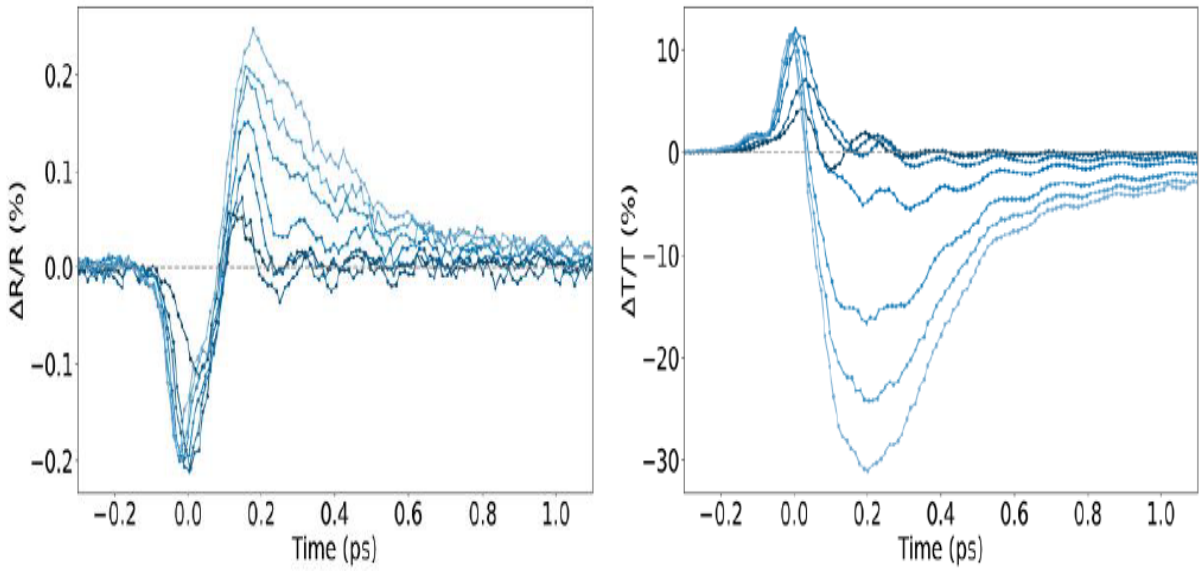

Fig. 1. *Variation of reflectivity (**left**) and transmission (**right**), for various pump intensity, as a function of time.*

It can be seen that a modulation, due to coherent excitation of phonon, is visible in both reflectivity and transmission change. For the highest pump intensity, this modulation vanishes, indicating that carrier excitation and the following electron-phonon collisions lead to a much faster damping of the phonons. A numerical model currently under development will be presented, which allows simulating these different mechanisms and the change of optical properties that we measure.
In Al_2O_3, we measure a much longer lifetime of excited carriers, in the range of tens of picosecond, showing that no self-trapping mechanism is occurring in this material. We have also studied the variation of both signal as a function of the orientation of the crystalline sample. Surprisingly a strong modulation is observed in the reflectivity signal, while the transmission is only weakly influenced by the orientation of the crystal. We give a possible interpretation of this unexpected behavior, in terms of surface phonons. This first set of experiments will be completed by measuring the polarization modulation induced for instance by coherent phonon excitation, and also by using a different probe wavelength domain, in the VUV in the Attolab facility at CEA- LIDYL.

References

[1] A. Bildé, K. Redeckas, A. Melninkaitis, M. Vengris, S. Guizard, *Journal of Physics. Condensed Matter* **33**, 315402 (2021).

* Acknowledgements: this work is supported by the ANR program TOCYDYS, contract ref. ANR-19-CE30-0015.

Electron-phonon coupling and electronic thermal transport across a Metal-semiconductor interface: a structural study

E. C. Landahl[1], W. Jo[3], B. Griffiths[1], J. Grammich[1], S. Lee[2]
[1] *DePaul University, Chicago, IL 60614 USA*
[2] *Korean Research Institute of Standards and Science, 305-340 Daejon, South Korea*
[3] *European X-ray FEL GmbH, 22869 Shenfield, Germany*

Understanding the interactions between energetic charge carriers and lattice vibrations (phonons) is crucial for optimizing the performance of optoelectronic devices, photovoltaics, and photocatalysts. The electron-phonon coupling coefficient, which characterizes the strength of these energy exchanges, is challenging to measure due to the involved microscopic time and length scales. In this study, we present an alternative approach to determine the coupling coefficient, thermal boundary resistance, and electron conductivity. We employ high angular-resolution time-resolved X-ray diffraction to examine lattice deformation after laser excitation of a nanoscale polycrystalline metal film on a semiconductor substrate.

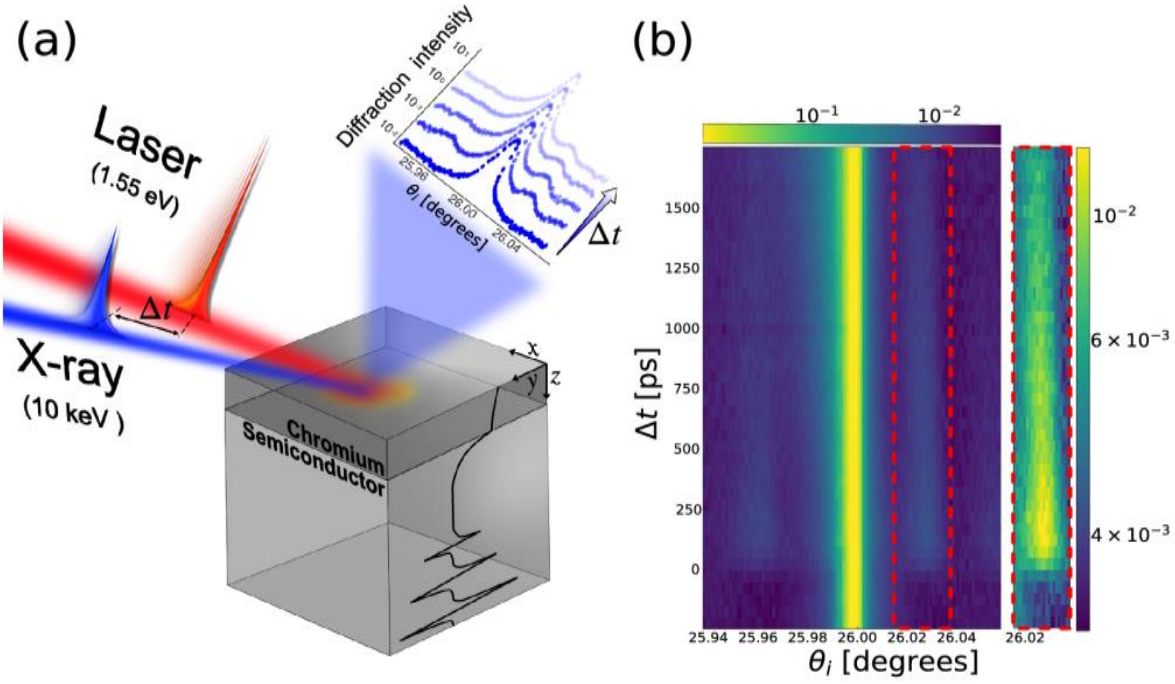

Fig. 1. ***(a)*** *Schematic of the TRXD experiment of metal layered semiconductor, and* ***(b)*** *time- and angle-resolved intensity profiles of the obtained GaAs (0 0 4) Bragg diffraction peak. The red dashed box indicates the region of interest where the intensity modulation along the angular axis is detected due to X-ray Brillouin scattering.*

Our results provide direct experimental evidence for differentiating between ballistic and diffusive transport components at the interface, with only the latter participating in thermal diffusion. This novel technique offers a robust method for investigating microscopic energy transport processes in various solid-state materials, advancing our understanding of their underlying mechanisms and potential applicationsLight-matter interactions involving energetic electrons and quasiparticles are of fundamental interest in condensed matter physics [1,2] and are also critical to the development of next-generation microelectronics. In particular, the interaction between electronic states and the lattice in excited solids stands out as one of the dominant scattering processes that determine various material properties, ranging from charge carrier and thermal transport, high-temperature superconductivity [3,4] and charge density waves [5]. Despite such importance, characterization of electron-phonon coupling (EPC) is challenging, especially when the system is driven out of thermodynamic equilibrium. The essence of EPC lies in the fact that perturbation of the electronic state leads to an exchange of energy and momentum between electrons and phonons, and therefore results in elastic stress. Ultrafast optical excitation can induce such transient states, in which a large population of hot carriers is generated and relaxes its excess energy to the cold lattice. Therefore, atomic-scale measurements of structural changes in relevant timescales potentially allow us to explore fine details of the coupling between the electronic states and the lattice.

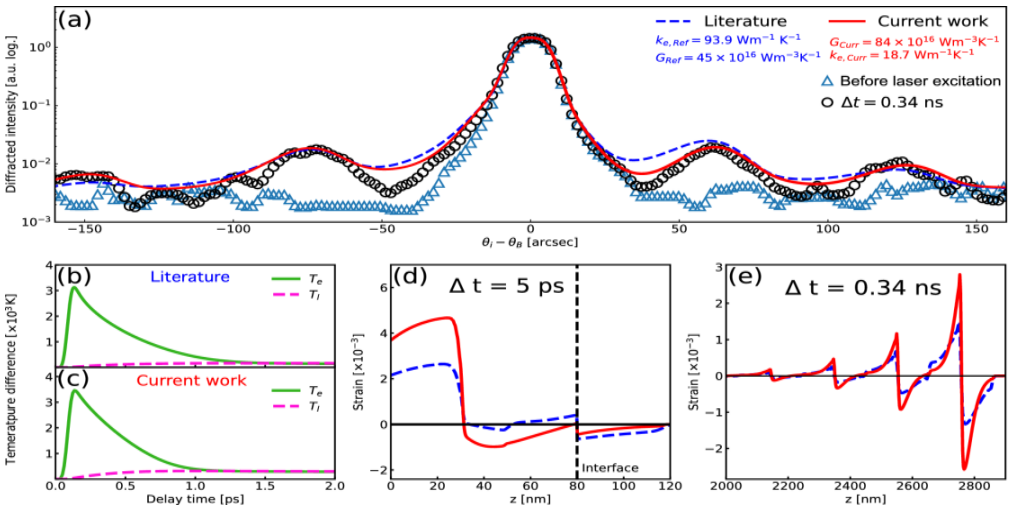

Fig. 2. *(**a**) Si (004) rocking curve (**black circle**) and calculation result of dynamical diffraction theory (blue dashed and red solid lines based on the literature values). The two temperature model for electron temperature and lattice temperature following laser excitation are shown for the literature values (**b**) and the current work (**c**). The calculated strain profiles for both the literature values (dashed blue) and current work (red solid) were solved at Δt = 5 ps (**d**) and at Δt = 0.34 ps (**e**).*

The capability to deliver femtosecond laser pulses on metallic surfaces provides a systematic means to induce strong non-equilibrium between electron and phonon subsystems. Typically, the EPC coefficients can be measured by using time-domain thermo-reflectance methods [6-9] where the sample's surface reflectively is monitored after the incidence of femtosecond laser pulses. The time-dependent reflectance is compared with the two-step thermal relaxation model [10] that assumes the linear relation between the reflectivity and temperature.

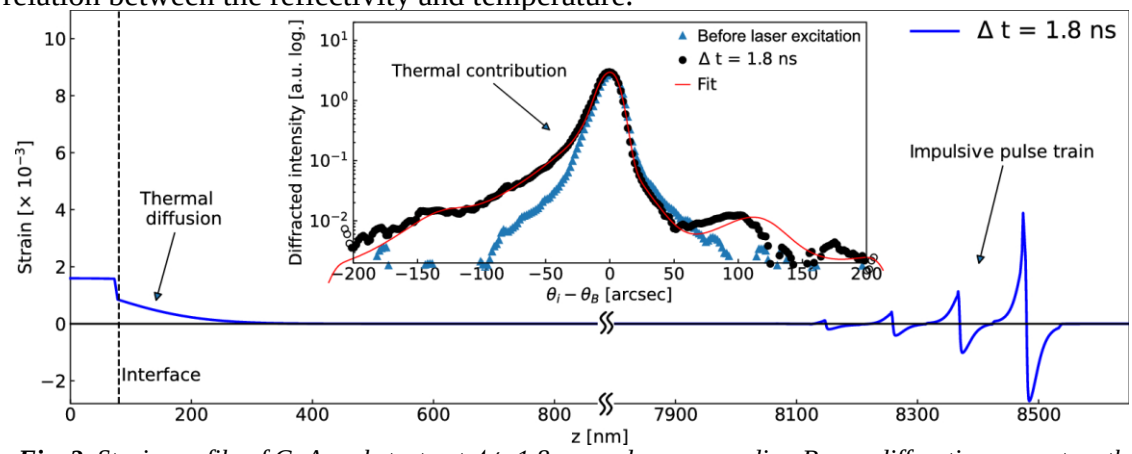

Fig. 3*. Strain profile of GaAs substrate at Δt=1.8 ns, and corresponding Bragg diffraction curve together with a fit result **(inset)**. The non-homogeneous temperature distribution near the interface gives rise to the asymmetry of the curve to the part of the lower angle.*

However, the experimentally acquired values have often shown considerable variation likely due to the complex interplay between electrons and phonons as well as multiple scattering mechanisms. To mitigate such experimental challenges, first principle calculations have been conducted on metals and semiconductors to confirm the EPC coefficients [11]. Nevertheless, the availability of such results is still limited and their ability to account for discrepancies between the simulation and the experiments remains questionable [12].

References

[1] C. W. Siders, A. Cavalleri, K. Sokolowski-Tinten, Cs. Tóth, T. Guo, M. Kammler, M. Horn von Hoegen, K. R. Wilson, D. von der Linde C. P. J. BartySiders, *Science* **286**, 1340 (1999).
[2] A. Rousse, C. Rischel, S. Fourmaux,I. Uschmann, S. Sebban, G. Grillon, Ph. Balcou, E. Förster, J.P. Geindre, P. Audebert, J.C. Gauthier D. Hulin, *Nature* **410**, 65 (2001).
[3] J. Bardeen, L.N. Cooper, J.R. Schrieffer, *Physical Review* **108**, 1175 (1957).
[4] A. Lanzara, P. V. Bogdanov, X. J. Zhou, S. A. Kellar, D. L. Feng, E. D. Lu, T. Yoshida, H. Eisaki, A. Fujimori, K. Kishio, J.-I. Shimoyama, T. Noda, S. Uchida, Z. Hussain Z.-X. Shen, *Nature* **412**, 510 (2001).
[5] H. Luo, Q. Gao, H.Liu, Y.Gu, D.Wu, C.Yi, J. Jia, S.Wu, X.Luo, Y.Xu,L.Zhao, Q.Wang, H.Mao, G.Liu, Z.Zhu, Y.Shi, K.Jiang, J.Hu, Z.Xu X. J. Zhou, *Nature Communications* **13**, 273 (2022).
[6] A. Giri, J. T.Gaskins, B.M. Foley, R. Cheaito, P.E. Hopkins, *Journal of Applied Physics* **117**, 044305 (2015).
[7] Y. Hu, L. Zeng, A.J. Minnich, M.S. Dresselhaus, G. Chen, *Nature Nanotechnology* **10**, 701 (2015).
[8] S. M. Oommen, S. Pisana, *Journal of Physics: Condensed Matter* **33**, 085702 (2020).
[9] K. Kang, G.-M. Choi, *Materials* **14**, 2755 (2021).
[10] K. Katayama, Y. Inagaki, T. Sawada, *Physical Review B* **61**, 7332 (2000).
[11] Z. Lin, L.V. Zhigilei, V. Celli, *Physical Review B* **77**, 075133 (2008).
[12] U. De Giovannini, H. Hübener, S.A. Sato, A. Rubio, *Physical Review Letters* **125**, 136401 (2020).

* Acknowledgements: This research used resources of the Advanced Photon Source, a U.S. Department of Energy (DOE) Office of Science User Facility operated for the DOE Office of Science by Argonne National Laboratory under Contract No. DE-AC02-06CH11357. E.C.L. was supported by a DePaul CSH FSRG and URC SRG. This research was supported by the National Research Foundation of Korea under contract No. NRF-2019K1A3A7A09033397, NRF-2020R1A2C1009597, NRF-2021R1A6A1A10044154, and NRF-2019K1A3A7A09033387. Preliminary sample characterization at 1C PAL-KRISS beamline at PLS-II were supported in part by MSIT and POSTECH.

Ultrasmall and tunable THz surface plasmon cavities in the deep Plasmonic regime

I. Aupiais[1], R.Grasset[1], T. Guo[1], D. Daineka[1], J. Briatico[2], S. Houver[3], L. Perfetti[1], J.-P. Hugonin[4]
J.-J. Greffet[4], Y. Laplace[1]
[1]*École Polytechnique -Institut Polytechnique de Paris, 91120 Palaiseau, France*
[2]*Unité Mixte de Physique CNRS/Thales, 91767 Palaiseau, France*
[3]*Université Paris Cité, 75006, Paris, France*
[4]*Université Paris-Saclay, 91127 Palaiseau, France*

The ability to confine THz photons into highly subwavelength volumes is a major goal towards the realization of ultrastrong light-matter coupling at low energy in quantum materials, with possible far reaching implications for the cavity control of material properties [1]. In optics, surface plasmons can provide an efficient confinement of light at visible/infrared frequencies, i.e. in the range of the plasma frequency of noble metals. On the other hand, the use of noble metals in most of the THz cavity architectures realized to date does not harness the potential of THz surface plasmons for photon confinement. In this talk, I will present our approach for making THz cavities which exploit the resonance of localized THz surface plasmon modes [2]. These THz plasmonic cavities achieve extreme plasmonic confinement of the EM-field in mode volumes V_{cav} as small as $V_{cav}/\lambda_0^3 \sim 10^{-8}$ ($\lambda_0 =$ free space wavelength) together with a large tunability as compared to more conventional architectures. Deep inside the plasmonic regime of light-matter interaction, the THz cavities exhibit strong signatures of electromagnetic nonlocality as the length scales involved become comparable to that of the microscopic degrees of freedom of the plasma.

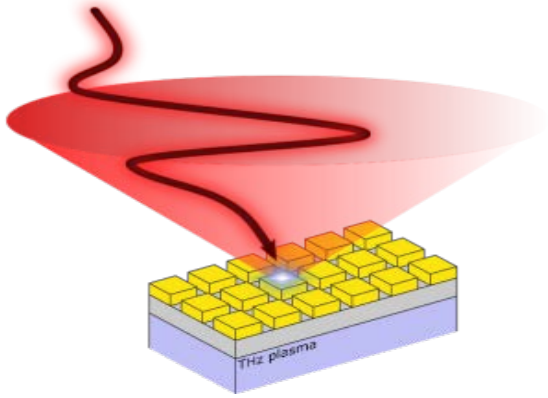

***Fig. 1**. Sketch of THz photons entering a deeply sub-wavelength THz plasmonic cavity*

These results demonstrate a new path towards the realization of ultrastrong, tunable and potentially exotic forms of light-matter coupling with cavities in the THz frequency range.

References

[1] F. Schlawin, D. M. Kennes, M. A. Sentef, *Applied Physics Reviews*, **9**, 011312 (2022).
[2] I. Aupiais, R. Grasset, T. Guo, D. Daineka, J. Briatico, S. Houver, L. Perfetti, J.-P. Hugonin, J.-J. Greffet, Y. Laplace (in preparation), (2023)

* Acknowledgement(s): this work was supported by Agence Nationale de la Recherche (grant n° ANR- 17-CE30-0011-11) and Labex PALM (grant n° ANR-10-LABX-0039-PALM).

Distilling the nonlinearity of a cuprate superconductor using 2-D Terahertz Spectroscopy

A. Liu[1], D. Pavicevic[1], M. Fechner[1], A. Cavalleri[1,2]
[1]*Max Planck Institute for the Structure and Dynamics of Matter, 22761 Hamburg, Germany*
[2]*University of Oxford, Oxford OX1 3PU, UK*

Quantum materials, systems in which quantum effects lead to unique macroscopic phenomena with tremendous technological potential, comprise the forefront of condensed matter physics research. In particular, collective excitations associated with broken-symmetry phases have attracted tremendous attention as powerful windows into their microscopic physics and dynamics. However, spectroscopy of these collective excitations has been hindered by the so-called 'terahertz gap', which refers to difficulties in generation and detection of radiation in the terahertz frequency range, where many relevant modes of quantum materials are found. In response to this challenge, we translate a technique known as 2-D spectroscopy [1], an optical analogue of multi-dimensional NMR spectroscopy, into the terahertz frequency range. We implement, for the first time, 2-D Terahertz Spectroscopy in a non-collinear, reflection geometry, enabling study of opaque materials and isolation of their constituent terahertz nonlinearities. We apply this technique to the Josephson plasma resonance [2] in $La_{2-x}Sr_xCuO_4$, a layered high-temperature superconductor, to distill the underlying plasmon correlations.

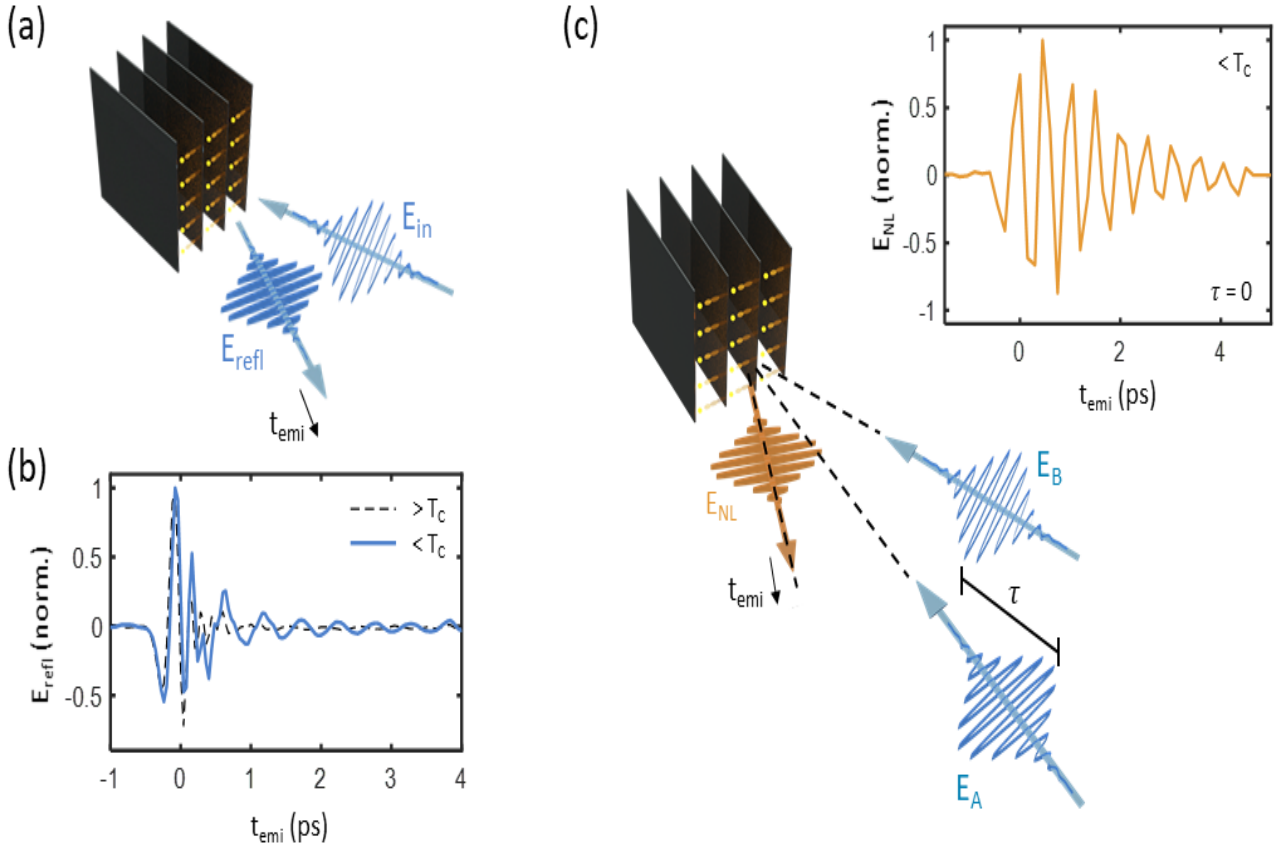

***Fig. 1. a**: Linear reflectivity experiment, involving an incident field E_{in} and a reflected field E_{refl}. **b**: Terahertz pulse reflected from optimally-doped $LSCO_{0.16}$, which exhibits long-lived oscillations from the Josephson plasma resonance at temperatures below T_c. **c:** Schematic of 2-D terahertz spectroscopy in a non-collinear and reflection geometry. Exemplary nonlinear terahertz emission E_{NL} is shown inset for $\tau = 0$ and below T_c.*

Measurements of the superconducting transition provide evidence of an unconventional phase-disordering transition without pair breaking.

References
[1] S. T. Cundiff, S. Mukamel, *Physics Today* **66,** 44 (2013).
[2] Y. Laplace, A. Cavalleri, *Advances in Physics X* **1**, 3(2016).
* A. Liu acknowledges support from the Alexander von Humboldt Foundation

Artificial quantum states of light from Single photons

P. Steindl[1], H. Snijders[1], J. A. Frey[2], J. Norman[2], J. E. Bowers[2]
D. Bouwmeester[1], W. Löffler[1]
[1]*Leiden University, 2333 CA Leiden, the Netherlands*
[2] *University of California, Santa Barbara, CA 93106, USA*

Multi-photon entanglement is an important resource for applications in quantum information, from measurement-based quantum information processing [1] to photonic quantum repeaters [2]. Recently, high-quality and high-rate single photon sources have been developed [3-6] which enable the production of multi-photon entanglement directly from single photons – from photon number superpositions [7] over GHZ states [8] to linear cluster states [9].Here we show engineering of artificial states of light based on single photons, in particular we show that light which reproduces the Poissonian statistics of coherent laser light can be synthesized [10]. We use a free-space optical Sagnac loop [11] to manipulate a continuous random stream of true single photons stream. The photons are produced using a single self-assembled InGaAs quantum dot in an optical micropillar cavity [4] using resonant laser excitation and cross-polarization laser filtering [12]. The photons are sent into the delay loop where photons in the loop act as a quantum memory leading to quantum correlations in the photon stream, by inducing quantum interference of photons produced at different times. We demonstrate experimentally that this leads to light with a second-order photon correlation function $g^{(2)}(0) \rightarrow 0$ as expected for coherent light, and from a model fit we derive indeed a Poissonian photon-number distribution. In contrast to text-book coherent states, photons in our artificial coherent states are quantum entangled in the form of linear cluster states – possibly shedding new light on an old discussion about realistic coherent states [13].

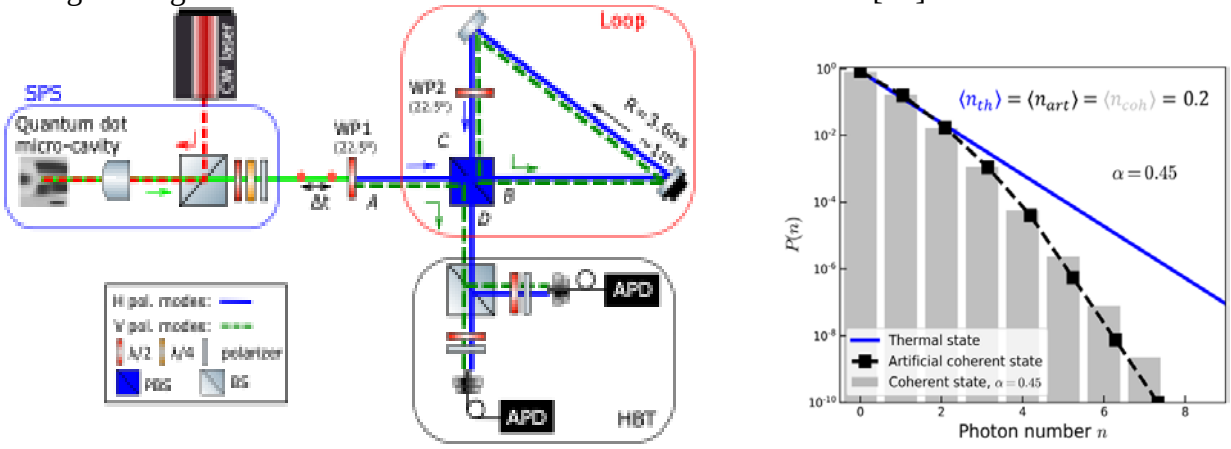

***Fig. 1 Left**: Sketch of the experimental setup. **Right**: Photon number distribution of the output light, the statistics of thermal, coherent, and our artificial coherent light is compared.*

This is manifested by a certain amount of squeezing – which might possibly find use in continuous-variable quantum information.

References

[1] R. Raussendorf, H. J. Briegel, *Physical Review Letters* **86**, 5188 (2001).
[2] K. Azuma, K. Tamaki, H.-K. Lo, *Nature Communications* **6**, 6787 (2015).
[3] N. Somaschi, V. Giesz, L. De Santis, J. C. Loredo, M. P. Almeida, G. Hornecker, S. L. Portalupi, T. Grange, C. Antón, J. Demory, C. Gómez I. Sagnes, N. D. Lanzillotti-Kimura, A. Lemaître, A. Auffeves, A. G. White, L. Lanco, P. Senellart, *Nature Photonics* **10**, 340 (2016).
[4] H. Snijders, J. A. Frey, J. Norman, V. P. Post, A. C. Gossard, J. E. Bowers, M. P. van Exter, W. Löffler, D. Bouwmeester, *Physical Review Applied* **9**, 031002 (2018)
[5] N. Tomm, A. Javadi, N. O. Antoniadis, D. Najer, M. C. Löbl, A.R. Korsch, R. Schott, S. R. Valentin, A. D. Wieck, A. Ludwig, R. J Warburton Nature Nanotechnology **16**, 399 (2021)
[6] S. E. Thomas, M. Billard, N. Coste, S. C. Wein, Priya, H. Ollivier, O. Krebs, L. Tazaïrt, A. Harouri, A. Lemaitre, I. Sagnes, C. Anton, L. Lanco N. Somaschi, J. C. Loredo, P. Senellart, *Physical Review Letters* **126**, 233601 (2021)
[7] S. C. Wein, J. C. Loredo, M. Maffei, P. Hilaire, A. Harouri, N. Somaschi, A. Lemaître, I. Sagnes, L. Lanco, O. Krebs, A. Auffèves, C.Simon P. Senellart, C. Antón-Solanas, *Nature Photonics* **16**, 374 (2022).
[8] M. Pont, G. Corrielli, A. Fyrillas, I. Agresti, G. Carvacho, N. Maring, P.-E. Emeriau, F. Ceccarelli, R. Albiero, P. H. D. Ferreira, N. Somaschi J. Senellart, I. Sagnes, M. Morassi, A. Lemaitre, P. Senellart, F.Sciarrino, M. Liscidini, N. Belabas, R. Osellame, *arXiv:2211.15626* (2022).
[9] D. Istrati, Y. Pilnyak, J. C. Loredo, C. Antón, N. Somaschi, P. Hilaire, H. Ollivier, M. Esmann, L. Cohen, L. Vidro, C. Millet, A. Lemaître I. Sagnes, A. Harouri, L. Lanco, P. Senellart, H. S. Eisenberg, *Nature Communications* **11**, 5501 (2020).
[10] P. Steindl, H. Snijders, G. Westra, E. Hissink, K. Iakovlev, S. Polla, J. A. Frey, J. Norman, A. C. Gossard, J. E. Bowers, D. Bouwmeester W. Löffler, *Physical Review Letters* **126**, 143601 (2021).
[11] E. Megidish, T. Shacham, A. Halevy, L. Dovrat, H. S. Eisenberg, *Physical Review Letters* **109**, 080504 (2012).
[12] P. Steindl, J.A. Frey, J. Norman, J.E. Bowers, D. Bouwmeester, W. Löffler, *arXiv:2302.05359* (2023).
[13] C. Noh, H. J. Carmichael, *Physical Review Letters* **100**, 120405 (2008).

Long-lived valley polarization in dichalcogenide monolayer and Heterostructure systems

P. H.M. van Loosdrecht
University of Cologne, 50937 Cologne, Germany

The two-dimensionality of monolayers and heterostructures of transition-metal dichalcogenides lead to a reduced dielectric screening and consequently to relatively strongly bound excitons. Not surprisingly, these systems show a wealth of interesting exciton and optical physics phenomena, including the formation of trions, strong luminescence, and multi-exciton phenomena. One of the most intriguing phenomena is that the lack of inversion symmetry in these systems, combined with a strong spin-obit coupling yields a novel quantum mechanical degree of freedom, the valley pseudospin, which is interesting from a fundamental point of view and even has some application potential.

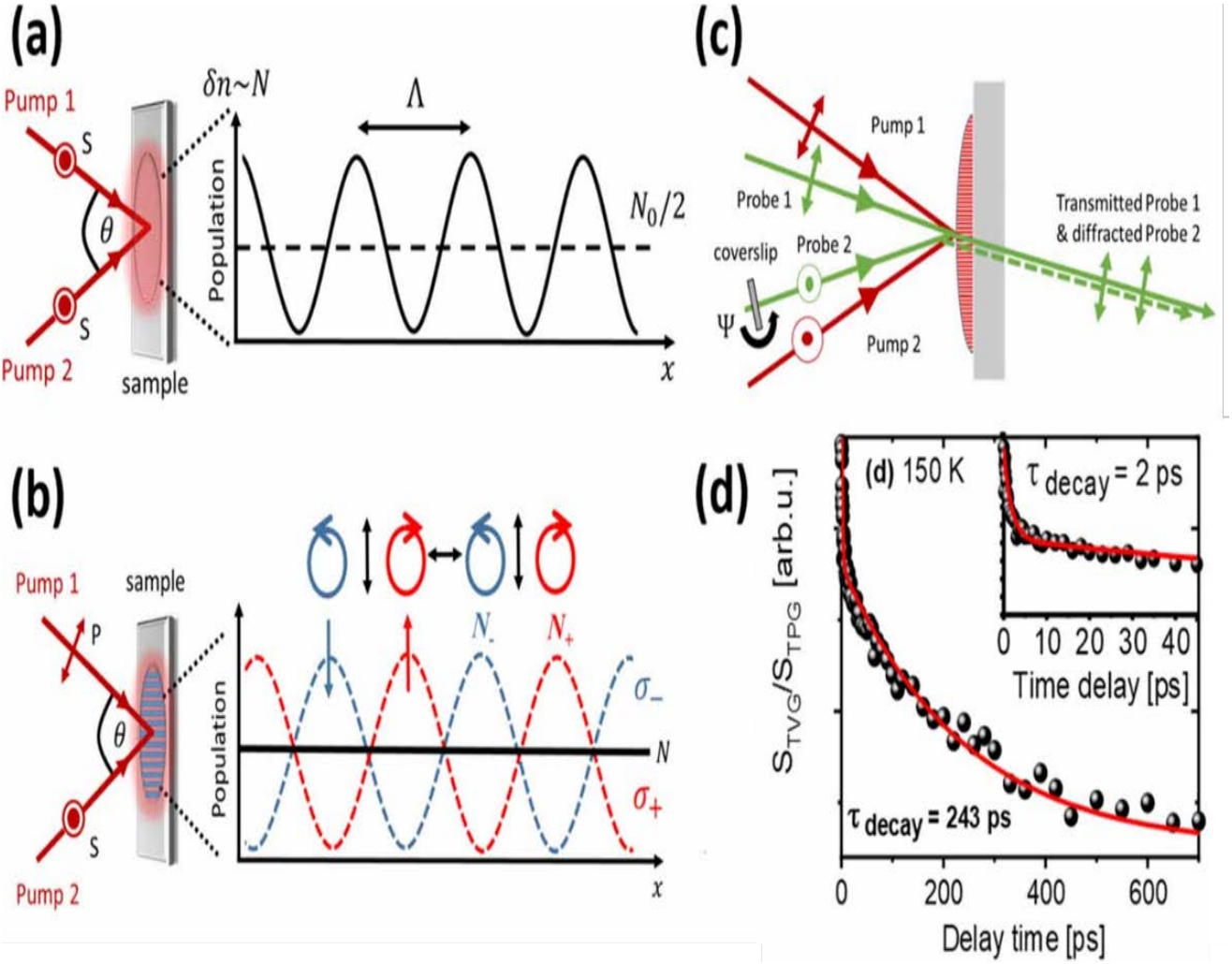

Fig. 1. *Principles of polarization selective heterodyned transient grating spectroscopy.*
(a) *Illustration of the population grating with parallel polarized pump excitation beams;*
(b) *Illustration of the spin or valley grating with cross polarized pump excitation beams;*
(c) *Optical scheme for heterodyne detection of both population and grating signals.*
(d) *Intervalley scattering dynamics in a low-pressure CVD grown WSe_2 monolayer at T=150 K.*
Open circles*: data;* ***red solid lines****: bi-exponential fits.*
The inset *shows the dynamics on the short time scales.*
Adopted from [1].

The current contribution will highlight some recent work on the nature and dynamics of excitons in these systems, with some focus on the valley degree of freedom as probed using transient absorption and 4-wave mixing (transient grating) spectroscopies.

References

[1] J. Wagner , H. Kuhn, R. Bernhardt, J. Zhu, P.H M van Loosdrecht, *2D Materials* **8**, 035018 (2021).

How to activate and detect the Higgs mode in superconductors

D. Manske
Max Planck Institute for Solid State Research, 70569 Stuttgart, Germany

Higgs spectroscopy is a new and emergent field [1-3] that allows to classify and determine the superconducting order parameter by means of ultra-fast optical spectroscopy. There are two established ways to activate the Higgs mode in superconductors, namely a single-cycle 'quench' or an adiabatic, multicycle 'drive' pulse, both illustrated in Figure 1. In the talk I will review and report on the latest progress on Higgs spectroscopy, in particular on the role of the third-harmonic-generation (THG) [4-6] and the possible IR-activation of the Higgs mode by impurities or external dc current [7,8]. I also provide new predictions for time-resolved ARPES experiments in which, after a quench, a continuum of Higgs mode is observable and a phase information of the superconducting gap function would be possible to extract [9].

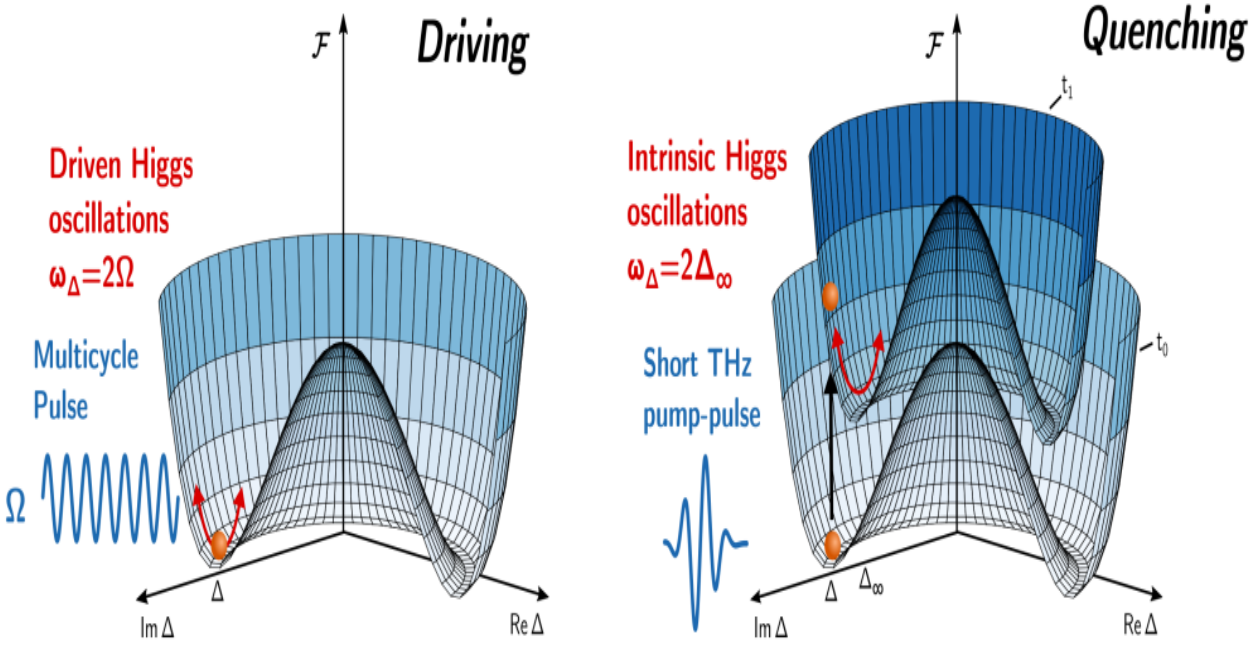

Fig. 1. *Two ways to activate the Higgs mode in superconductors: 'Driving' or 'Quenching'.* ***(left)*** *A driven superconductor in steady-state non-equilibrium becomes resonant at the eigen-frequency of the Mexican hat and leads to third harmonic generation (THG).*
(right) *In the non-adiabatic case, in which a single-cycle THz pulse shrinks suddenly the Mexican hat, one can observe Higgs oscillations directly in various quantities.*

Interestingly, I argue that the Higgs mode can solve the 25-years-old A_{1g}-puzzle in equilibrium Raman scattering on high-Tc cuprates [10]. Finally, I review all possibilities for activating the Higgs mode in superconductors known so far.

References

[1] L. Schwarz, L. Schwarz, B. Fauseweh, N. Tsuji, N. Cheng, N. Bittner, H. Krull, M. Berciu, G. S. Uhrig, A. P. Schnyder, S. Kaiser**,** *Nature Communications* **11**, 287 (2020).
[2] L.Schwarz, D. Manske, *Physical Review* B **101**, 184519 (2020).
[3] H.Chu, M.-J.Kim, K.Katsumi,S. Kovalev, R.D. Dawson, L.Schwarz, N.Yoshikawa, G.Kim, D Putzky, Z. Z. Li, H.Raffy, S.Germanskiy, J.-C. Deinert, N.Awari, I.Ilyakov, B.Green, M.Chen, M. Bawatna, G.Cristiani, G. Logvenov, Y.Gallais, A. V. Boris, B.Keimer, A. P. Schnyder D. Manske, M.Gensch, Z.Wang, R. Shimano, S. KaiserS.,*Nature Communications* **11**, 1793 (2020).
[4] L. Schwarz, R. Haenel, D. Manske, *Physical Review* B **104**, 174508 (2021).
[5] H.Chu, S. Kovalev, Z. X. Wang, L.Schwarz, T.Dong, L. Feng, R.Haenel, M.-J. Kim, P. Shabestrari, H.L. Phuong, K. Honasoge R. D. Dawson, D.Putzky, G.Kim, M.Puviani, M. Chen, N. Awari, A.N. Ponomaryov, I.Ilyakov, M. Blushke, F. Boshini, M. Zonno S. Zhdanovich, M. Na, G. Christiani, G. Logvenov, D. J. Jones, A. Damascelli, M.Minola, B. Keimer, D. Manske, N. Wang, J.-C. Deinert S. Kaiser, *Nature Communications* **14**, 1343 (2023).
[6] M.-J. Kim, S. Kaiser, D. Manske, (submitted to *Nature Materials*) (2023).
[7] M. Puviani, L. Schwarz, X.-X. Zhang, S. Kaiser, D. Manske, *Physical Review* B **101**, 220507 (2020).
[8] R. Haenel, P. Froese, D. Manske, L. Schwarz, *Physical Review* B **104**, 134504 (2021).
[9] L.Schwarz, B. Fauseweh, D. Manske, *Physical Review* B **101**, 224510 (2020).
[10] M. Puviani, A. Baum, S. Ono, Y. Ando, R. Hackl, D. Manske , *Physical Review Letters* **127**, 197001 (2021).

Spin-driven optical nonlinearities for detection and generation of Spin currents

M. Matsubara
Tohoku University, Sendai 980-8578, Japan

Future spintronics will require a portfolio of techniques for manipulating electron spins in functional nanodevices. Especially, the establishment of the methods to control spin current is the key ingredient essential for the transfer and processing of information, enabling faster and low-energy operation. In this talk, I will show that spin-driven optical nonlinearities are useful to detect and generate spin currents [1-3]. (1) I will show that photo-driven ultrafast spin currents can be generated in a magnetic metamaterial (MM) at room temperature via the magneto-photogalvanic effect (Fig. 1) [1]. By tuning the polarization state of the excitation light, spin currents can be directed with tunable magnitude along an arbitrary direction in the two-dimensional plane of the MM.

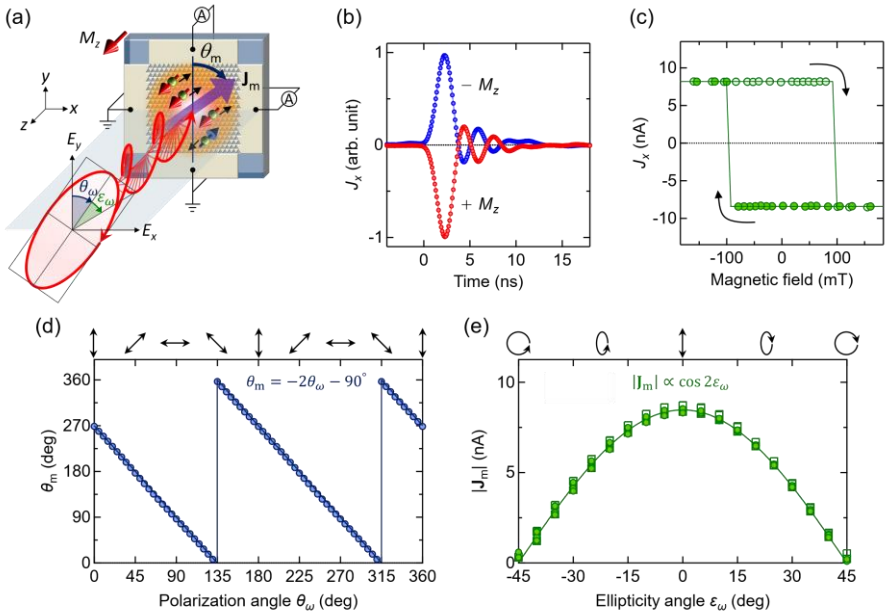

Fig. 1. ***(a)****: Schematic of the experimental setup for generating spin-driven photocurrents* $\boldsymbol{J}_m$*. A normally incident light with an arbitrarily polarized state (polarization angle , ellipticity angle) excites a magnetic metamaterial (MM) with threefold rotational symmetry and out-of-plane magnetization* M_z*.* ***(b)****: Dynamical responses of spin-driven photocurrent for* $\pm M_z$*.* ***(c)****: Magnetic-field dependence of spin-driven photocurrent.* ***(d)****: The flow direction* $_m$ *of spin-driven photocurrent as a function of .* ***(e)****: The magnitude* $|\boldsymbol{J}_m|$ *of spin-driven photocurrent as a function of* ε_ω*.*

(2) The manipulation of domains by external fields in ferroic materials is of major interest for applications. In multiferroics with strongly coupled magnetic and electric order, however, the magnetoelectric coupling on the level of the domains is largely unexplored. By using spin-driven optical second harmonic generation (SHG) microscopy we visualized what happened to the multiferroic domains in the archetypal spin-spiral $TbMnO_3$ under the application of electric, magnetic, and optical fields (Fig. 2) [2,3]. The results show the deterministic ferroelectric polarization flop by magnetic field, which leads to the transformation of neutral into nominally charged domain walls, and the reversible optical switching of multiferroic domains.

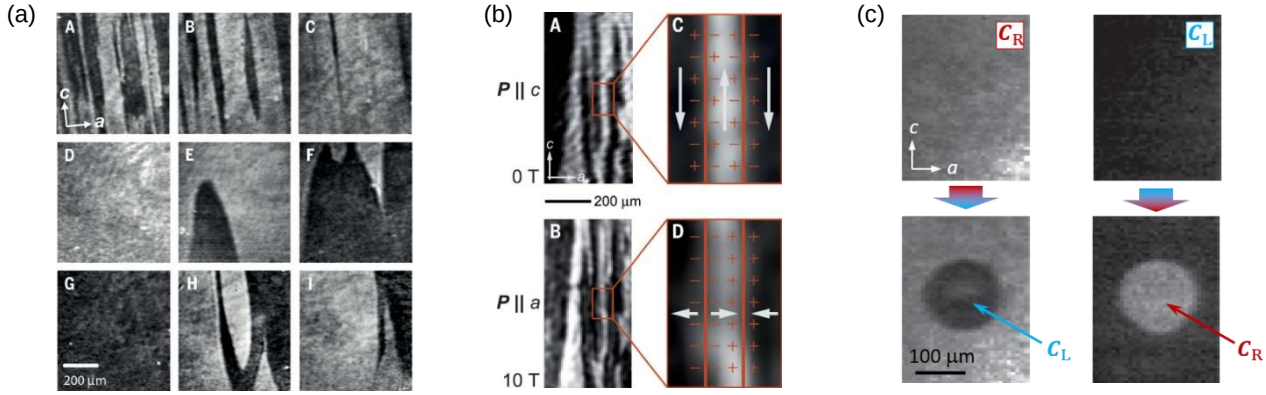

Fig. 2. *Control of multiferroic domains in* $TbMnO_3$ *revealed by spin-driven SHG microscopy.* ***(a)****: Electric-field control.* ***(b)****: Magnetic-field flop.* ***(c)****: Optical switching.*

References

[1] M. Matsubara, T. Kobayashi, H. Watanabe, Y. Yanase, S. Iwata, T. Kato, *Nature Communications* **13**, 6708 (2022).
[2] M. Matsubara, S. Manz, M. Mochizuki, T. Kubacka, A. Iyama, N. Aliouane, T. Kimura, S. Johnson, D. Meier, M. Fiebig, *Science* **348**, 1112 (2015).
[3] S. Manz, M. Matsubara, T. Lottermoser, J. Büchi, A. Iyama, T. Kimura, D. Meier, M. Fiebig, *Nature Photonics* **10**, 653 (2016).

Challenging space-time-energy limits of magnetism by Harnessing fluctuations

J.H. Mentink
Radboud University, 6525 Nijmegen, the Netherlands

Findings ways to switch between magnetically ordered states at the smallest possible length and time scale, while simultaneously dissipating the least amount of energy is a major challenge in magnetism. One of the most appealing routes to achieve this goal is by bringing a magnetic system strongly out of equilibrium, after which the dynamics is driven by exchange interaction, the strongest force in magnetism, which due to its short-rage nature also directly acts on nanometer length scales. Ferromagnets multilayers are very interesting model systems to explore exchange driven switching at the nanoscale, since they host magnetic skyrmions as (meta-) stable states, which can have nanoscale dimensions and feature an energy barrier for nucleation that is defined by the exchange interaction itself. Moreover, ultrafast optical skyrmion nucleation has been recently demonstrated in ferromagnetic multilayers [1-3]. Interestingly, despite the high energy barrier in equilibrium, X-ray studies [3] revealed that the switching was completed in less than 300ps, which is significantly faster than the characteristic timescale of skyrmions dynamics.In this contribution, we will present our efforts to gain understanding of the mechanism of ultrafast skyrmion nucleation. Based on atomistic spin dynamics simulations, we show that that the nucleation mechanism can stem from a transient topological fluctuation state [3]. By simulating the relaxation at fixed temperature and magnetic field, we demonstrate that the properties of the fluctuation state are governed by thermal fluctuations giving rise to spontaneous nucleation and decay of skyrmions (see figure 1), consistent with Arrhenius-like activation over a potential barrier. Stable textures can freeze out of such fluctuations when the effective temperature of the system relaxes faster than the decay time of the skyrmion textures [4].

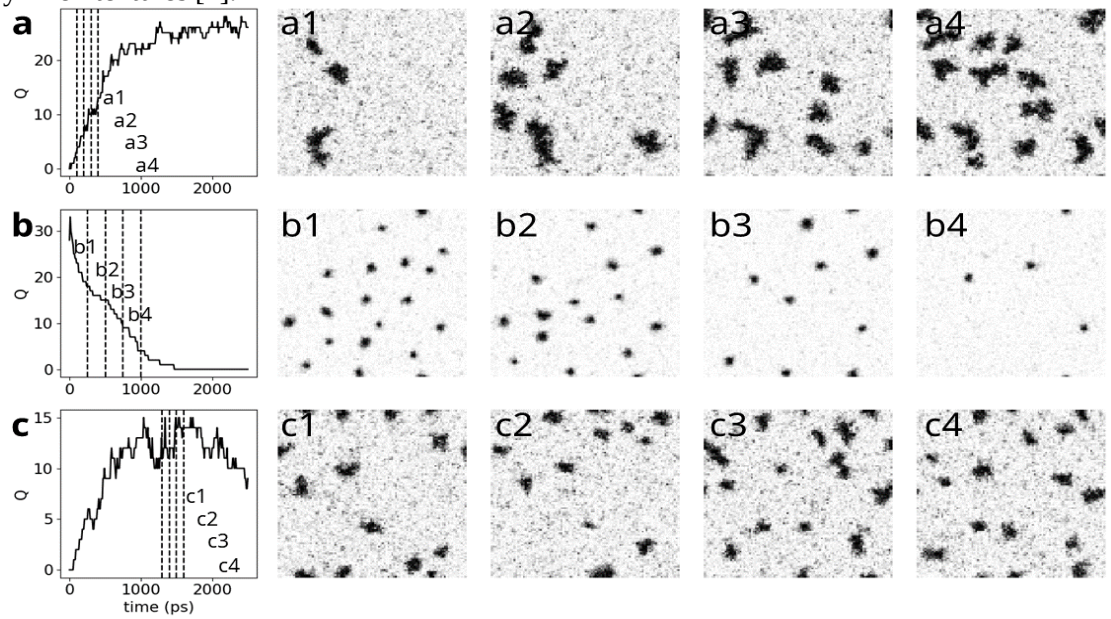

Fig.1*: Time evolution of the topological charge Q (number of skyrmions) and selected snapshots of the out-of-plane magnetization at different constant temperatures and fields in the atomistic simulations. The timestamps of the snapshots are shown as dashed vertical lines and encoded 1-4. Row (**a**) corresponds to a regime with spontaneous formation of skyrmions. The starting configuration was the ferromagnetic state. Row (**b**) shows a regime where skyrmions spontaneously decay, starting from completely randomly aligned spins. Row (**c**) represents the regime featuring both nucleation and decay, with an initial ferromagnetic state.*

Hence, our results show that fluctuations can be harnessed instead of considering them as a nuisance, suggesting a new route towards ultimately fast, small and more energy-efficient writing of stable magnetic bits.

References

[1] G. Berruto, I. Madan, Y. Murooka, G. M. Vanacore, E. Pomarico, J. Rajeswari, R. Lamb, P. Huang, A. J. Kruchkov, Y. Togawa, T. LaGrange, D. McGrouther, H. M. Rønnow, F. Carbone, *Physical Review Letters* **120**, 117201 (2018).

[2] S. -G. Je, P. Vallobra, T. Srivastava, J.-C. Rojas-Sańchez, T.H. Pham, M. Hehn, G. Malinowski, C. Baraduc, S. Auffret, G. Gaudin, S. Mangin H. Beá, O. Boulle, *Nano Letters* **18**, 7362 (2018).

[3] F. Büttner, B. Pfau, M. Böttcher, M. Schneider, G. Mercurio, C. M. Günther, P. Hessing, C. Klose, A. Wittmann, K. Gerlinger, L.-M. Kern C. Strüber, C. von Korff Schmising, J. Fuchs, D. Engel, A. Churikova, S. Huang, D. Suzuki, I. Lemesh, M. Huang, L. Caretta, D. Weder, J.H. Gaida, M. Möller, T.R. Harvey, S. Zayko, K. Bagschik, R. Carley, L. Mercadier, J. Schlappa, A. Yaroslavtsev, L. Le Guyarder N. Gerasimova, A. Scherz, C. Deiter, R. Gort, D. Hickin, J. Zhu, M. Turcato, D. Lomidze, F. Erdinger, A. Castoldi, S. Maffessanti, M. Porro, A. Samartsev, J. Sinova, C. Ropers, J.H. Mentink, B. Dupé, G.S.D. Beach, S. Eisebitt, *Nature Materials* **20**, 30 (2021).

[4] K. Gerlinger, R. Liefferink, M. Schneider, L.-M. Kern, C. Klose, D. Metternich, D. Engel, F. Capotondi, D. De Angelis, M. Pancaldi, E. Pedersoli, F. Büttner, S. Eisebitt, J.H. Mentink, B. Pfau, *arXiv 2212.03143 (*2022).

Optical manipulation of Rashba-split 2-dimensional electron gas

M. Michiardi[2], F. Boschini[3], H.-H. Kung[1], M. X. Na[1], S. K. Y. Dufresne[1], A. Currie[1], G. Levy[1]
S. Zhdanovich[1], A. K. Mills[1], D. J. Jones[1], J. L. Mi[4], B. B. Iversen[4], Ph. Hofmann[4], A. Damascelli[1]
[1]*University of British Columbia, Vancouver, BC, V6T 1Z1, Canada*
[2] *Max Planck Institute for Chemical Physics of Solids, 01187 Dresden, Germany*
[3]*Institut National de la Recherche Scientifique, Varennes, QC, J3X 1S2, Canada*
[4]*Aarhus University, 8000 Aarhus C, Denmark*

In spintronic devices, the two main approaches to actively control the electrons' spin degree of freedom involve either static magnetic or electric fields. An alternative avenue relies on the use of optical fields to generate spin currents, which promises to bolster spin-device performance allowing for significantly faster and more efficient logic. To date, research has mainly focused on the optical injection of spin currents through the photogalvanic effect, and little is known about the direct optical control of the intrinsic spin splitting. Here, to explore the all-optical manipulation of a material's spin properties: we consider the Rashba effect at a semiconductor interface. The Rashba effect has long been a staple in the field of spintronics owing to its superior tunability, which allows the observation of fully spin-dependent phenomena, such as the spin-Hall effect, spin-charge conversion, and spin-torque. In this work, by means of time and angle-resolved photoemission spectroscopy (TR-ARPES), we demonstrate that an ultrafast optical excitation can be used to manipulate the Rashba-induced spin splitting of a two-dimensional electron gas (2DEG) engineered at the surface of the topological insulator Bi_2Se_3.

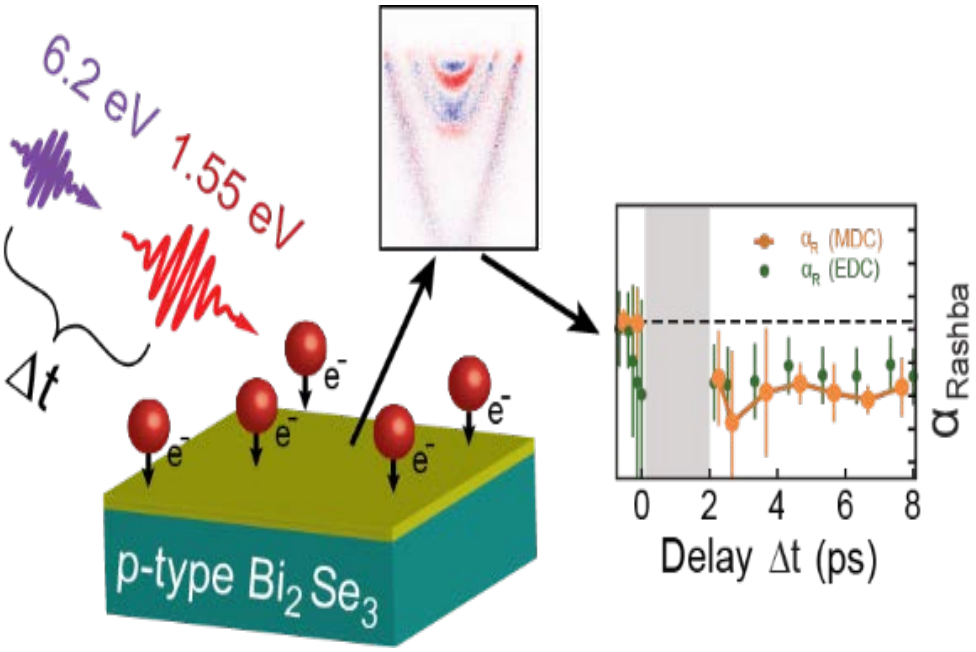

Fig. 1. *TR-ARPES experimental setup and all-optical switch of the Rashba splitting in a 2DEG. An infrared pulse impinges on an engineered 2DEG, inducing a reduction of its spin-splitting on a picosecond timescale, which is directly observed via photoemission.*

We establish that light-induced photovoltage and charge carrier redistribution modulate the spin-orbit coupling strength of the 2DEG on a sub-picosecond timescale. The charge diffusion governs the return to equilibrium on a nanosecond timescale. The all-optical switching of the Rashba states can offer an unprecedented platform for achieving THz spin logic devices.

References

[1] M.Michiardi, F. Boschini,H.-H. Kung, M.X. Na, S.K.Y, Dufresne , A. Currie , G. Levy, S. Zhdanovic, A.K. Mills, D.J. Jones, J.L Mi, B.B Iversen P. Hofmann, A. Damascelli, *Nature Communications* **13**, 3096 (2022).

* Authors acknowledge support from: the Max Planck-UBC-UTokyo Centre for Quantum Materials and the Canada First Research Excellence Fund, Quantum Materials and Future Technologies Program; the Gordon and Betty Moore Foundation's EPiQS Initiative, Grant GMBF4779 to A.D. and D.J.J.; the Killam, Alfred P. Sloan, and Natural Sciences and Engineering Research Council of Canada's (NSERC's) Steacie Memorial Fellowships (A.D.); the Alexander von Humboldt Foundation (A.D.); the Canada Research Chairs Program (A.D.); NSERC, Canada Foundation for Innovation (CFI); the British Columbia Knowledge Development Fund (BCKDF); the Department of National Defence (DND), the VILLUM FONDEN via the Centre of Excellence for Dirac Materials (Grant No. 11744); and the CIFAR Quantum Materials Program.

Fluctuation dynamics in the fractionally charged spatial fabric of a Polaronic Wigner crystal lattice

D. Mihailovic[1], J. Vodeb[1], V. Kabanov[1], I. Vaskivskyi[1], E. Božin[2], J. Ravnik[1]
[1]*Jozef Stefan Institute, 1000 Ljubljana, Slovenia*
[2]*Brookhaven National Laboratory, Upton, NY 11973, USA*

Ultrafast techniques give us useful a wealth of information on the behavior of single particle and collective excitations in systems undergoing transitions on the timescales from femtoseconds to picoseconds. However, the dynamics of many-body systems evolves over a much larger span of timescales. In particular, in the aftermath of a phase transition many-body systems display very rich mesoscopic self-assembly into metastable states that requires new techniques, beyond current optical, x-ray and electron diffraction techniques. Of particular interest are materials close to the Wigner crystal limit can exhibit very unusual metastable orders. A good example are the layered dichalcogenides which exhibit complex chiral domain states [1] and an amorphous Wigner glass [2], both of which appear after an external perturbation that forces the system through a symmetry breaking transition. New experimental evidence of characteristic polaronic local structural distortions well above CDW ordering temperatur es from X-ray local structure analysis of 1T-TaS_2 (Fig. 1 left), implies that the complex charge ordering in this material is better described in terms of a polaronic Wigner crystal than a conventional CDW [3].
The application of the Wigner crystal paradigm leads to significant progress in understanding its complex metastable state dynamics. In particular, optical charge injection is shown to lead to the charge fractionalization and entanglement with strong non-local effects that explains the remarkable robustness of the metastable state to local perturbations (Fig.1, middle and right).

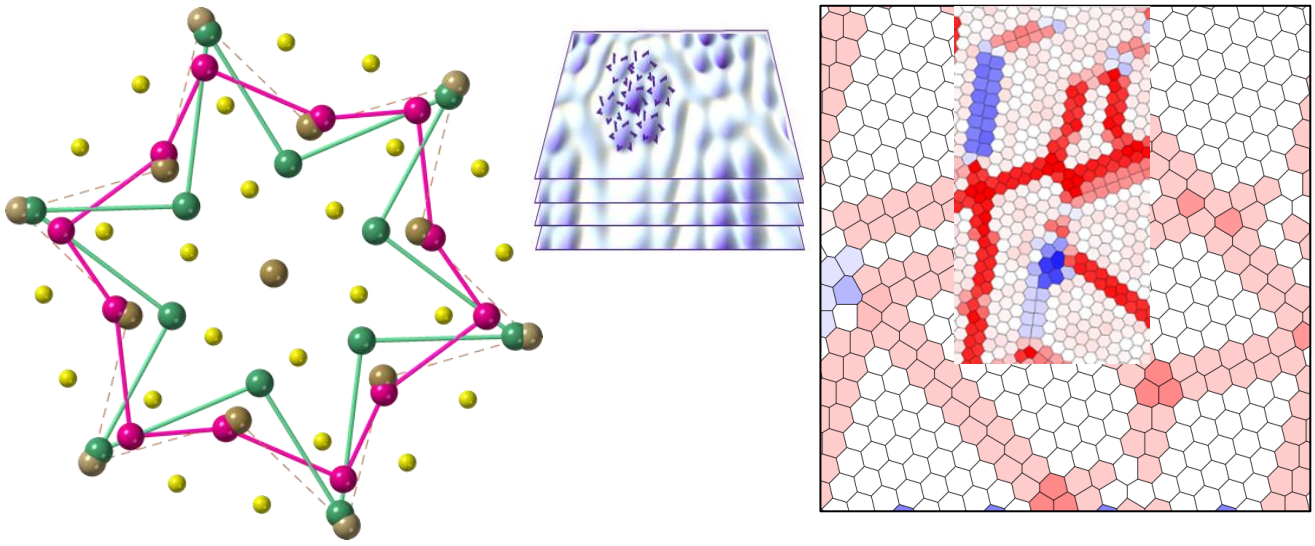

***Fig 1. Left**: Local displacement of atoms within a polaron measured in the different ordered phases of 1T-TaS_2. Chiral atomic distortions appear in the ordered phases. **Middle**: a schematic representation of the domains of polarons in the discommensurate phase. **Right**: Experimental STM data (left panel) and modeling (**right panel**) of the electronic charge density in the after charge injection shows fractionally charged sites on domain walls and their junctions within the charged lattice gas model, calculated with Monte-Carlo simulations.*

The entangled fractionally charged network that results upon charge injection presents a topologically robust gapless space-time fabric for the propagation of single particle excitations that are measured by conventional transport measurements. On the other hand, new fast STM scanning techniques reveal unusual and hitherto unobserved mesoscopic polaron dynamics. Remarkably, at low temperatures, the topological protection is overcome by incoherent tunneling between domain configurations which is very slow, but observable with STM. The domain dynamics is confirmed by simulations on a noisy superconducting quantum processor (NSQP) which uses direct mapping of NSQP qubits onto the crystal lattice sites of 1T-TaS_2, and dynamics within the transverse field Ising model. The noise in the superconducting qubit system and the electronic crystal both have similar spectral characteristics, enabling quantitative simulations of the domain dynamics based solely on microscopic interactions without need for error correction.

References

[1] Y. A. Gerasimenko, P. Karpov, I. Vaskivskyi, I.Brazovskii, D. Mihailovic, *Npj Quantum Materials* **4**, 1(2019).
[2] Y. A. Gerasimenko, I. Vaskivskyi, M. Litskevich, J. Ravnik, J. Vodeb, M. Diego, V. Kabanov, D. Mihailovic, *Naure Materials* **317**, 505 (2019).
[3] E. S. Bozin M. Abeykoon, S. Conradson, G. Baldinozzi, P. Sutar, D. Mihailovic, *arxiv 2301.05670* (2023).

Terahertz and infrared-driven spin dynamics in iron oxides

R.V. Mikhaylovskiy
Lancaster University, Lancaster LA1 4YB, United Kingdom

Understanding the physics of ultrafast angular momentum transfer between light and magnetic materials is a one of the key unresolved problems in magnetism. Its importance arises from the fact that light-driven control of magnetization may lead to revolutionary all-optical magnetic recording technology. Recently we demonstrated that in the iron oxides the terahertz and mid-infrared electric field triggers large amplitude deflection of the spins [1] that leads to transient switching of the net magnetization [2,3]. Revealing the microscopic mechanisms of THz-driven spin response to the terahertz pumping will allow to optimize the discovered spin switching mechanism and thereby open unforeseen routes to enable ultrafast magnetic recording.

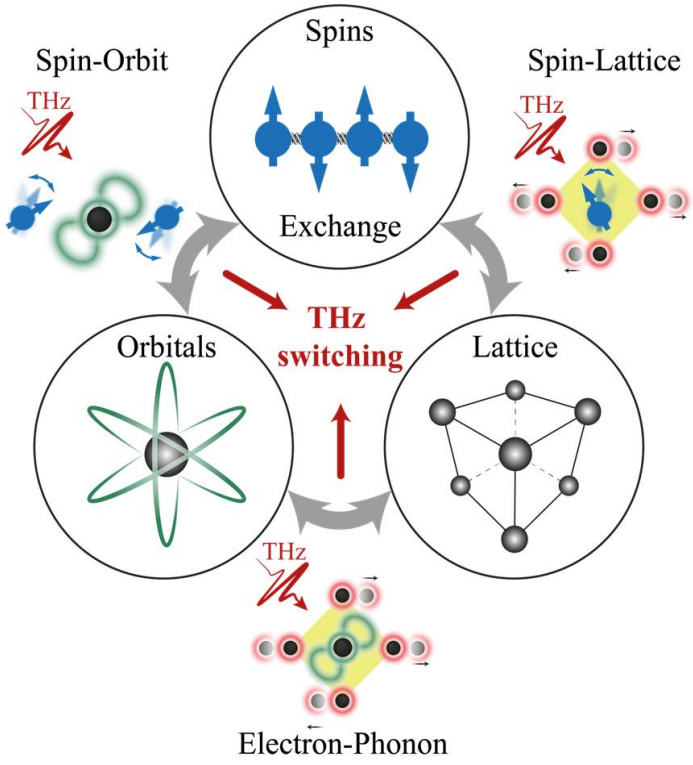

Fig. 1. *The intricate interplay between the spins, the lattice and the orbitals in transition metal oxides enables different pathways for manipulation of the material properties. As the spin-orbit, spin-lattice, electron-phonon and magnetic exchange interactions have meV energy scales, the THz-driven strong perturbation of them enables different pathways for spin control.*

In my talk I shall discuss most recent experiments performed in my group on antiferromagnetic iron oxides (e.g. iron borate and orthoferrites), which represent a very large group of magnetic materials at the heart of current condensed matter and materials science. While some of the most important fundamental processes of light-spin interactions on ultrafast time scales have been demonstrated in these compounds in the last decade they are particularly interesting for THz photonics, thanks to their high-frequency spin dynamics and wide bandgap. The intricate low-energy (~1-10 meV) interactions between lattice, orbital and spin degrees of freedom offer a rich playground for the THz manipulation of their properties (Fig. 1).

References

[1] S. Baierl, M. Hohenleutner, T. Kampfrath, A. K. Zvezdin, A. V. Kimel, R. Huber, and R. V. Mikhaylovskiy, *Nature Photonics* **10**, 715 (2016)
[2] S. Schlauderer, C. Lange, S. Baierl, T. Ebnet, C. P. Schmid, D. C. Valovcin, A. K. Zvezdin, A. V. Kimel, R. V. Mikhaylovskiy, R. Huber, *Nature* **569**, 383 (2019).
[3] D. Afanasiev, J. R. Hortensius, B. A. Ivanov, A. Sasani, E. Bousquet, Y. M. Blanter, R. V. Mikhaylovskiy, A. V. Kimel, A. D. Caviglia, *Nature Materials* **20**, 607 (2021).
* Acknowledgement(s): this work is supported by ERC Grant Starting Grant 852050 MAGSHKE and Horizon 2020 ITN 861300 COMRAD.

Ultrafast lasers based on transition metal doped chalcogenides

S. Vasilyev[1], S. Mirov[2]
[1] *IPG Photonics Southeast Technology Center, Birmingham, AL 35211, USA*
[2] *University of Alabama at Birmingham, Birmingham AL 35294, USA*

Femtosecond (fs) middle-IR (MIR, 2–20 μm, 500–5000 cm^{-1}) lasers have many applications in science, technology, industry, medicine. In particular, fs MIR frequency combs combining high brightness of laser beams with high temporal coherence of mode-locked laser oscillators and few-optical-cycle pulses are appealing because they significantly improve precision and sensitivity of conventional Fourier-transform spectroscopy [1] and enable various regimes of dual-comb spectroscopy [2]. Ultrafast MIR lasers based on transition-metal-doped II-VI chalcogenides (TM:II-VI, [3]) attract growing attention because they provide direct access to peak- and average-power scalable few-optical-cycle pulses in the 2 – 6 μm range. The progress in TM:II-VI lasers has been further accelerated by the development of new methods of laser material fabrication. Specifically, the technology based on a post-grown thermal diffusion doping of ZnS and ZnSe [3] has enabled large-scale production of large-size polycrystalline gain elements with high optical quality and high dopant concentration. This, in turn, has dramatically simplified the development of ultrafast amplifiers and

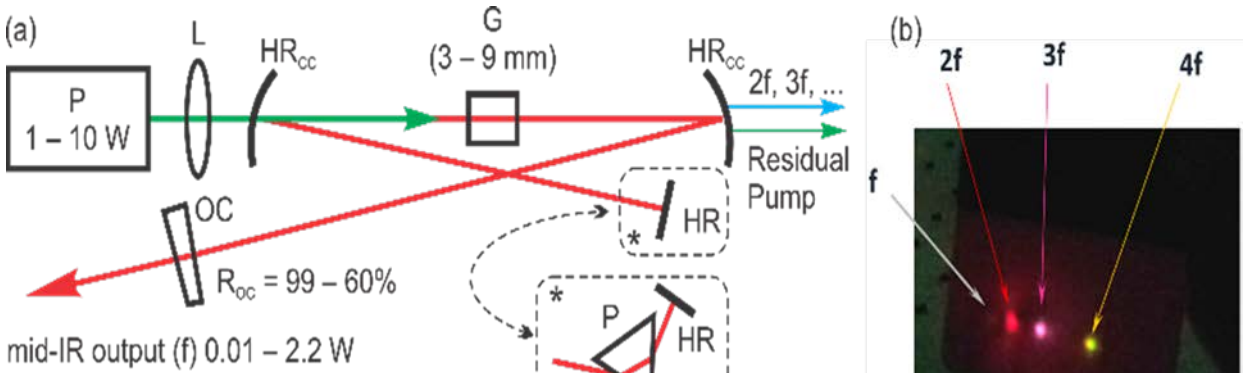

Fig.1 (a) *Design of Kerr-lens mode-locked polycrystalline Cr:ZnS(Se) oscillator (not to scale). P, pump laser at 1.5–2.1 μm; L, pump focusing lens; G, AR coated polycrystalline gain element at normal incidence; HR, high reflectors; HR_{CC}, concave high reflectors; OC, output coupler; f, main output of the oscillator and the fundamental wavelength; 2f, 3f, … optical harmonics of the main signal; *, optionally, the oscillator can be equipped with a dispersive prism (P) for the wavelength tuning. For simplicity, only the end mirrors HR and OC are shown in the resonator; additional HR mirrors can used to fold the laser beams for footprint reduction.* ***(b)*** *Output of a Kerr-lens mode-locked polycrystalline oscillator. Mid-IR fundamental band and optical harmonics, generated directly in the laser medium via RQPM process, are dispersed with a prism and visualized with a laser viewing card.*

enabled the development of fs oscillators with unique output parameters.Cr:ZnS is a typical cavity is representative of a large TM:II-VI family. It combines superb ultrafast laser capabilities with broad IR transparency and high nonlinearity of wide-bandgap II-VI semiconductors, and supports all mode-locking regimes from active, to passive, to Kerr-lens mode-locking. Extensive experimental studies of Kerr-lens mode-locking in polycrystalline Cr:ZnS(Se) have resulted in the development of a dedicated laser design, which is illustrated in Fig. 1. A prominent distinctive feature of this design is the normal incidence mounting of the polycrystalline gain element in an X-folded asymmetric optical cavity formed by two curved mirrors (HR_{CC}) and two plane mirrors (HR and OC). Depending on the desired fundamental repetition frequency f_R, and, hence, the required cavity length, the radii of the curved mirrors can be as large as 200 mm or as small as 10 mm. The curved mirrors are typically set at small incidence angles (2 – 10°, depending on the f_R). The asymmetry of the cavity is defined by its unequal legs with the typical ratio of 2:5, while the radii of the curved mirrors are typically equal. Thus, in contrast to classical designs of Kerr-lens mode-locked laser oscillators, the non-polarizing and astigmatic. The described unconventional design of polycrystalline oscillator allows to: -operate the laser at increased pump power; -obtain shorter output pulses with higher energy at a given repetition rate f_R; - utilize gain elements with extended length and, hence, enhance the non-linear interactions inside the optical cavity; - generate few-cycle vector solitons directly in the mid-IR [4]. Other distinctive features of the developed design are the utilization of the output

couplers with high transmission (up to 60%) and exclusive use of multilayer mirrors for dispersion control. Further, a part of the fundamental mid-IR laser radiation (f) is converted to second harmonic (2f) and higher harmonics (3f, 4f, 5f) via random-quasi-phase-matched (RQPM) process in polycrystal. Usually, the harmonics are out-coupled together with the residual pump light via a curved mirror with high near IR transmission, as illustrated in Fig.1. In most cases, the polycrystalline Cr:ZnS(Se) oscillators are optically pumped by the radiation of Er-doped fiber lasers at the wavelength 1.56 μm. However, the pumping by the radiations of Tm-doped fiber lasers (1.9 μm) and laser diodes (1.65 μm,) is possible too. The pump sources with low-intensity noise are utilized for demanding applications related to the generation and stabilization of the mid-IR frequency combs [5]. The Kerr-lens mode-locking with high temporal purity of the pulse train can be obtained in a wide range of relative air humidifies (from 0 to 60%, at temperatures up to 22 C). The spectra of pulses of selected Kerr-lens mode-locked polycrystalline oscillators hold the world records in terms of (i) instantaneous spectral span [6], (ii) average power, and (iii) pulse repetition frequency [7]. In general, few-cycle Kerr-lens mode-locked polycrystalline Cr:ZnS(Se) oscillators developed during the past years are efficient, compact, and reliable. The typical optical-to-optical conversion from CW pump light to few-cycle mid-IR pulses is 20–25%, and the typical size of the oscillator's package is 75×100×400 mm^3 (for the fundamental pulse repetition frequency f_R=80 MHz and excluding the pump laser). The initiation of mode-locked regime is now fully automated. The oscillators can operate for thousands of hours without maintenance, including continuous laser operation in mode-locked regime for hundreds of hours. More details about fs polycrystalline Cr:ZnS(Se) oscillators can be found in [3].Advanced applications of ultrafast mid-IR lasers impose stringent requirements on the parameters of output pulses. For instance, dual-comb spectroscopy requires fs pulse trains with stabilized carrier-envelope offset frequency and ultra-low, attosecond-level, timing jitter [8]. On the other hand, the experiments on the generation of isolated attosecond pulses via high harmonic generation require CEP-stable single-cycle mid-IR sources that combine high energy and high repetition rate. A fruitful approach to those very demanding laser regimes is provided by a combination of a few-cycle polycrystalline oscillator described above with simple, and hence robust, single-pass polycrystalline Cr:ZnS(Se) amplifier, as illustrated in Fig. 2(a) and described in detail in [6, 9, 10].

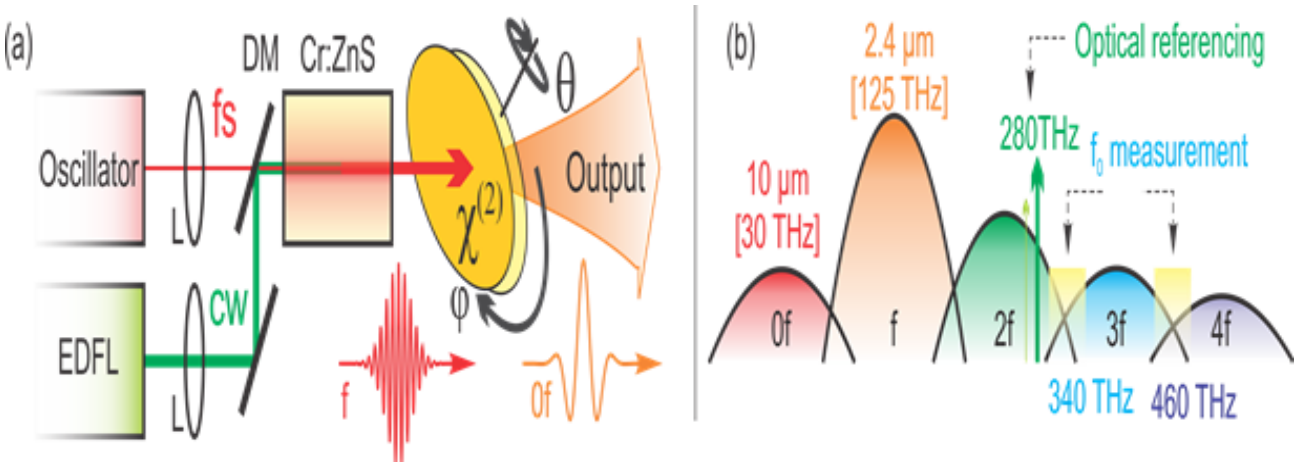

Fig. 2. (a) *Single-pass polycrystalline amplifier and supercontinuum generator. L, lenses; DM, dichroic mirror. For simplicity, only the transmissive imaging components (L) are shown; actual setups may also include reflective imaging components.* ***(b)*** *Supercontinuum spectrum and frequency comb referencing scheme.*

In short, the output of the oscillator is superimposed with CW or pulsed radiation from a pump laser using a dichroic mirror. Two co-propagating radiations are then coupled to a specially tailored polycrystalline Cr:ZnS(Se). During their propagation through the laser and non-linear medium, fs pulses simultaneously experience amplification and non-linear broadening to an optical octave.Further, RQPM process with ultra-broad bandwidth results in a multitude of intrapulse three-wave mixings. Thus, pulses' spectrum is extended to a continuum spanning many octaves from the bandgap edge of the material to its phonon cut-off. The structure of the continuum is illustrated in Fig. 2 (b). It consists of the specially broadened fundamental (f), optical harmonics (2f, 3f, …), and a long-wave component (0f) generated in the polycrystalline material via the optical rectification [11]. It consists of several superimposed frequency combs (0f, f, 2f, 3f, …) with different offset frequencies (0, f_0, $2f_0$, $3f_0$) but precisely the same tooth spacing (which is equal to the pulse repetition rate f_R = 80 MHz). An offset-free longwave IR comb 0f spanning from 5 μm to 12 μm and beyond is generated either directly in the polycrystalline material [6] or in an additional $\chi^{(2)}$ medium (e.g. ZGP

or GaSe, [12]) via optical rectification.Single-pass amplifiers combine simplicity of implementation with the complexity of laser and non-linear interactions. Therefore, they provide a lot of flexibility in terms of the achievable output laser parameters. Simple and robust single-pass Cr^{2+}:ZnS(Se) fs amplifiers allow for power scaling of the few-cycle pulse trains up to 30 W, while the kHz CPAs provide access to fs pulses with up to 68 GW peak power. Ultrafast Cr^{2+}:ZnS(Se) lasers are uniquely suited for generation of the optical frequency combs with ultra-low, attosecond-level, timing jitter of the pulse trains.The available optical spectra of the Cr:ZnS-based frequency combs are illustrated in Fig. 3. Depending on the application, one can utilize a direct output of a single-pass polycrystalline Cr:ZnS amplifier (Fig. 3 (a)).

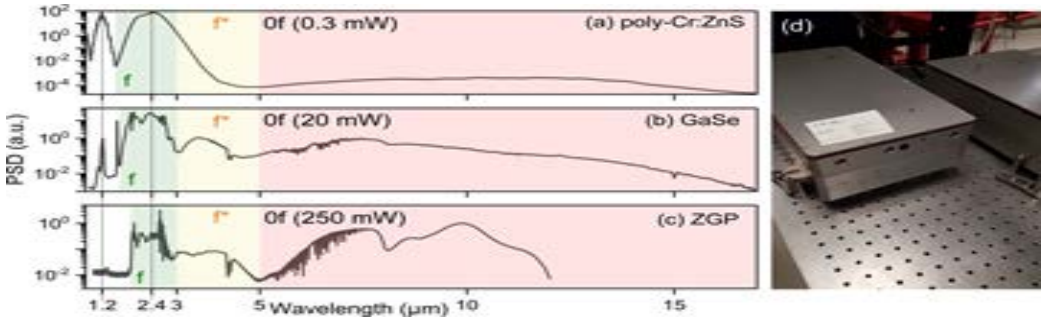

Fig. 3 (a, b, c) *Spectra of Cr:ZnS-based frequency combs. Numbers near spectra show optical power in the offset-free 0f band.* ***(d)*** *A photo of Cr:ZnS frequency comb with a business card shown for scale (excluding the EDFL pump and locking electronics).*

In this case, the optical power will be primarily concentrated in the fundamental comb f (2-cycle pulses with 4-W power spanning 60 THz at -20 dB level with respect to the main peak). Alternatively, one can equip the system with an additional optical rectification stage to enhance the optical power in the offset free longwave IR spectral band (Fig. 3 (b, c)). For instance, ZGP crystal allows the record-breaking efficiency of optical rectification. It generates super-octave longwave IR combs with Watt-level power. Remarkably, optical rectification of 2-cycle MIR pulses at 2.4 μm initiates secondary three-wave mixings between 0f and f combs that, in turn, results in a red-shift of the fundamental comb. Therefore, f and 0f combs merge in a continuum. The additional red-shifted spectral components of the fundamental comb are highlighted in Fig. 2 as f*.

The key advantage of Cr:ZnS ultrafast laser and frequency comb technology is high efficiency: 20 – 25% optical-to-optical conversion from low-cost CW EDFL light to 2-cycle MIR pulses and 10 – 12% conversion of 2-cycle pulses at 2.4 μm to single-cycle electromagnetic transients in the longwave IR. Further, the system's complexity is significantly reduced because all the optical signals required for stabilizing the MIR comb with the large lever arm are generated directly inside the polycrystalline Cr:ZnS laser and nonlinear medium. Those advantages, in turn, allowed us to implement shoe-box-sized, light-weight, fs frequency combs with the brightness exceeding the brightness of a synchrotron by orders of magnitude in a broad spectral range. The developed MIR frequency combs open new avenues in imaging, sensing, and spectroscopy. Our preliminary evaluations confirm the applicability ultrafast Cr:ZnS lasers for dual-comb spectroscopy with the optical-to-rf mapping factors in excess of 10^6 and the adequate time of coherent averaging time from seconds to tens of seconds, to minutes.

References

[1] L. Rutkowski, P.Masłowski, A.C.Johansson, A.Khodabakhsh, A.Foltynowicz, *J. Quantitative Spectroscopy& Radiative Transfer* **204**, 63 (2018).
[2] A. S. Kowligy, H. Timmers, A. J. Lind, U. Elu, F. C. Cruz, P. G. Schunemann, J. Biegert, S. A. Diddams, *Sciience Advances* **5**, eaaw8794 (2019).
[3] S. Mirov, I. Moskalev, S. Vasilyev, V. Smolski, V. Fedorov, D. Martyshkin, J. Peppers, M. Mirov, A. Dergachev, V. Gapontsev, *IEEE Journal Selective Topics. Quantum Electronics* **24**, 1601829 (2018).
[4] S. Vasilyev, M. Y. Sander, J. Gu, V. Smolski, I. Moskalev, M. Mirov, Y. Barnakov, J. Peppers, M. Kolesik, S. Mirov, V. Gapontsev, *Journal Optical Society of America -JOSA B* **38,** 1625 (2021).
[5] S. Vasilyev, V. Smolski, J. Peppers, I. Moskalev, M. Mirov, Y. Barnakov, S. Mirov, V. Gapontsev, *Optical Express* **27**, 35079 (2019).
[6] S. Vasilyev, I. Moskalev, V. Smolski, J. Peppers, M. Mirov, Y. Barnakov, V. Fedorov, D. Martyshkin, S. Mirov, V. Gapontsev, *Optical Express* **29,** 2458 (2021).
[7] V. Smolski, S. Vasilyev, I. Moskalev, M. Mirov, Q. Ru, A. Muraviev, P. Schunemann, S. Mirov, V. Gapontsev, K. Vodopyanov, *Applied Physics* B **124**, 101 (2018).
[8] I. Coddington, N. Newbury,W. Swann, *Optica* **3**, 414 (2016).
[9] S. Vasilyev, I. Moskalev, M. Mirov, S. Mirov, V. Gapontsev, *Optical Express* **24,** 1616 (2016).
[10] S. Vasilyev, I. Moskalev, V. Smolski, J. Peppers, M. Mirov, V. Fedorov, D. Martyshkin, S. Mirov, and V. Gapontsev, *Optica* **6(2),** 126(2019).
[11] J. Zhang, K. Fritsch, Q. Wang, F. Krausz, K.-F. Mak, O. Pronin, *Optics Letters* **44**, 2986 (2019).
[12] S. Vasilyev, I.S. Moskalev, V.O. Smolski, J.M. Peppers, M. Mirov, A.V. Muraviev, K. Zawilski, P.G. Schunemann, S.B. Mirov, K.L. Vodopyanov, V.P. Gapontsev, *Optica*, **6(1),** 111 (2019).

* Acknowledgement(s) : authors acknowledge support from IPG Photonics Corporation, S.M. also acknowledges support from DARPA (grant W31P4Q-15-1-0008), DOE (grant DE-SC0018378) and NIEHS (grant)P42ES027723.

Ultrafast x-ray spectroscopy of light-driven quantum materials

D. Baykusheva[1], I-T. Lu[2], H. Jang[3], S. F. R. TenHuisen[1], F. Glerean[1], C. Weber[4], T. Meng[1]
H. Padmanabhan[1], W. He[5], Y. Shen[5], G. D. Gu[5], D. M. Kennes[2,4], M. Claassen[6], M. P. M. Dean[5], A. Rubio[2]
M. Mitrano[1]
[1]*Harvard University, Cambridge, MA 02138, USA*
[2]*Max Planck Institute for the Structure and Dynamics of Matter, 22761 Hamburg, Germany*
[3]*Pohang Accelerator Laboratory, Gyeongbuk 37673, Republic of Korea*
[4]*Aachen University, 52056 Aachen, Germany*
[5]*Brookhaven National Laboratory (BNL), Upton, NY 11973 USA*
[6] *University of Pennsylvania, Philadelphia, PA 19104*

[7]The last two decades have witnessed a remarkable progress in the use of ultrafast lasers pulses as a tool to realize and control nontrivial dynamical states of matter, e.g., transient superconductivity and Floquet topological phases. Among a variety of nonthermal excitation pathways, a particularly intriguing route is represented by the direct light-engineering of effective many-body interactions, such as electron hopping amplitudes and electron-electron repulsion. Achieving control over these parameters in strongly correlated electron systems gives us the opportunity to tune their microscopic physics in ways akin to what achieved in quantum simulators. Here, I will discuss recent developments in our capability to manipulate electronic interactions in light-driven quantum materials and to accurately quantify these effects by using time-resolved x-ray spectroscopy. I will focus on quasi-one-dimensional and two-dimensional copper oxides as model systems to investigate the light-matter interaction in presence of intense electromagnetic fields.

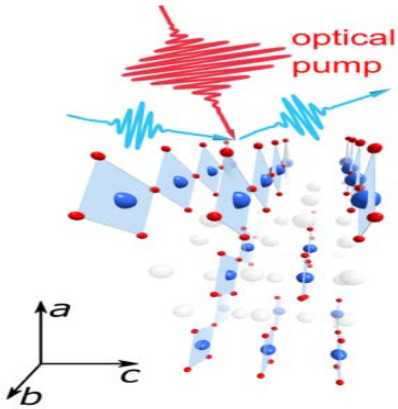

Fig. 1*. Crystal structure of quasi-1D cuprate Sr_2CuO_3. Cu atoms are shown in blue, O in red, Sr in white. The compound is driven by an intense pump field, and probed with delayed soft x-ray pulses.*

In the quasi-2D $La_{2-x}Ba_xCuO_4$, MV/cm laser fields are shown to dynamically renormalize the screened onsite Coulomb repulsion ("Hubbard *U*") [1]. In the quasi-1D ott insulator Sr_2CuO_3, a different picture emerges. Combining time-resolved optical and x-ray spectroscopy measurements with advanced theoretical modeling, we map out the transient electronic states giving rise to the light-dressed band structure as well as the renormalized electronic interactions [2].
We discuss the role of dimensionality in the light-matter interaction and the implications for the control of superconductivity, magnetism, as well as to the realization of other long-range-ordered phases such as spin liquidity [3,4] and η-pairing correlations [5,6] in light-driven quantum materials.

References

[1] D. R. Baykusheva, H. Jang, A. A. Husain, S. Lee, S. F. R. TenHuisen, P. Zhou, S. Park, H. Kim, J.-K. Kim, H. D. Kim, M. Kim, S.-Y. Park, P. Abbamonte, B. J. Kim, G. D. Gu, Y. Wang, M. Mitrano, *Physical Review X* **12**, 011013 (2022).
[2] D. R. Baykusheva, I-T. Lu, H. Jang, S. F. R. TenHuisen, F. Glerean, C. Weber, T. Meng, H. Padmanabhan, W. He, Y. Shen, G. D. Gu, D. M. Kennes, M. Claassen, M. P. M. Dean, A. Rubio, M. Mitrano, (submitted) (2023).
[3] M. Claassen, H.-C. Jiang, B. Moritz, T. P. Devereaux *Nature Communications* **8**, 1192 (2017).
[4] A. Szasz, J. Motruk, M. P. Zaletel, J. E. Moore, *Physical Review* X **10**, 021042 (2020).
[5] T. Kaneko, T. Shirakawa, S. Sorella, S. Yunoki, *Physical Review Letters* **122**, 077002 (2019).
[6] F. Peronaci, O. Parcollet, M. Schiró, *Physical Review* B **101**, 161101 (2020).

* Acknowledgement(s): *This work is primarily supported by the U.S. Department of Energy, Office of Basic Energy Sciences, Early Career Award Program, under Award No. DE-SC0022883. M. M. further acknowledges support by the Aramont Fellowship Fund for Emerging Science Research at Harvard University. D. R. B. was supported by the Swiss National Science Foundation through Project No. P400P2_194343. M. C. acknowledges support by NSF Grant No. DMR-2132591. D. M. K. acknowledges funding by the Deutsche Forschungsgemeinschaft (DFG, German Research Foundation) via Germany's Excellence Strategy—Cluster of Excellence Matter and Light for Quantum Computing (ML4Q) EXC 2004/1—390534769 and within the RTG 1995. We also acknowledge support from the Max Planck-New York City Center for Non-Equilibrium Quantum Phenomena.*

Transient Enhancement of the Ferroelectricity in the Rashba Semiconductor α-GeTe

G. Kremer[1], J. Maklar[2], L. Nicolaï[3], C.W. Nicholson[1], C. Silva[2], C. Yue[1], P. Werner[1], J.H. Dil[4]
J. Krempaský[5], G. Springholz[6], R. Ernstorfer[2], J. Minár[3], L. Rettig[2], C. Monney[1]
[1]*Université de Fribourg, CH-1700 Fribourg, Switzerland*
[2]*Fritz Haber Institute of the Max Planck Society, 14195 Berlin, Germany*
[3]*University of West Bohemia, 306 14Plzen, Czech Republic*
[4]*École Polytechnique Fédérale de Lausanne, 1015 Lausanne, Switzerland*
[5]*Photon Science Division, Paul Scherrer Institut, 5232 Villigen PSI, Switzerland*
[6]*Johannes Kepler Universität, A-4040 Linz, Austria*

α-GeTe(111) is a bulk ferroelectric Rashba semiconductor that exhibits the largest known Rashba-type spin splitting of so-far known materials. It has been recently demonstrated that it is possible to reversibly manipulate the spin polarization of its low-energy electronic structure by an external electric field in α-GeTe(111) [1], a promising behavior for spintronics applications. A stimulating direction of research is to investigate whether it is possible to coherently modify the ferroelectric properties of GeTe with light pulses.Using a 800 nm photoexcitation, we drive α-GeTe(111) out-of-equilibrium and probe its transient low-energy electronic structure with time-resolved angle-resolved photoemission spectroscopy (ARPES). We reveal that the Rashba splitting of its bulk states is *enhanced* after 200 fs. We show that this change of the electronic structure is driven by a shift of the Ge atomic layer towards the Te atomic layer, meaning a transient *increase* of the ferroelectric distortion [2].

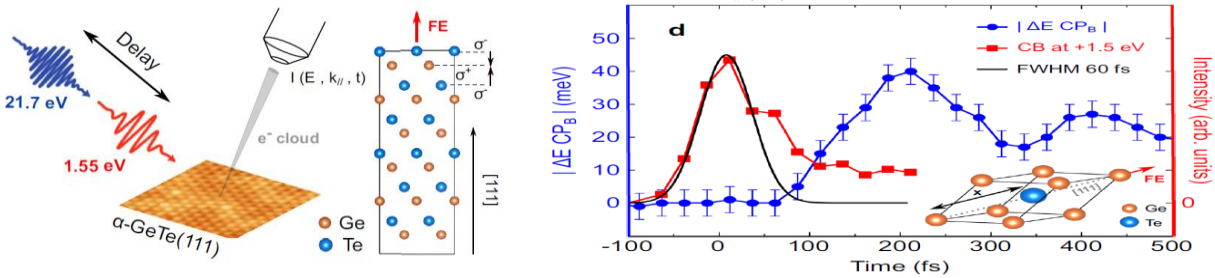

***Fig. 1. Left**: we performed time-resolved ARPES on the ferroelectric Rashba semiconductor GeTe. **Right**: temporal evolution of the Rashba splitting (blue curve) showing enhancement and a coherent modulation, following the photoexcitation populating the conduction band (red curve). See Ref. [2] for more details.*

We identify a surface photovoltage effect as the mechanism responsible for this transient enhancement of the ferroelectricity at the surface of GeTe and link it to a delayed displacive excitation of the coherent phonon of the ferroelectric distortion. Our work potentially opens the route for the control of the ferroelectric polarization in α-GeTe(111).

References

[1] J. Krempaský, S. Muff, J. Minár, N. Pilet, M. Fanciulli, A.P. Weber, E.B. Guedes, M. Caputo, E. Müller, V.V. Volobuev, M. Gmitra, C.A.F. Vaz V. Scagnoli, G. Springholz, J.H. Dil, *Physics Review* X **8**, 021067 (2018).
[2] G. Kremer, J. Maklar, L. Nicolaï, C.W. Nicholson, C. Yue, C. Silva, P. Werner, J.H. Dil, J. Krempaský, G. Springholz, R. Ernstorfer, J. Minár, L. Rettig, C. Monney, *Nature Communications* **13**, 6396 (2022).

Reliability and performance improvement in femtosecond lasers and Amplifiers, and their components

J. Henrich, M. Arrigoni, L. Moog, P. Vogt, S. Mosquera
Coherent Corporation, Santa Clara, CA95054, USA

In the last decades, femtosecond laser-based experiments have become increasingly complex. Multidimensional spectroscopy or Attosecond physics are examples of this evolution where the laser source is just the starting point of an extremely sophisticated optical train leading to the final experiment and data production. With these stringent boundary conditions, the main added value of an ultrafast laser source is the production of consistent, reliable and high-performance pulses of light. While ultimate laser performance in term of pulse duration, energy per pulse and mode quality is and has been the enabling point of experimental success, the reliability of the laser source has a dramatic impact on data productivity and ultimately technical paper throughput. Following this demand for performance and reliability, we took a series of steps towards the design and manufacturing of femtosecond laser sources that match performance ("technical specification") improvement with demanding reliability and environmental testing based on rugged industrial protocols. Many applications in advanced spectroscopy require pulses shorter than 100 femtoseconds and with energies achievable only with Chirped Pulsed Amplification (CPA) of the laser pulses. This process requires one or multiple stages of amplification of the initial pulses provided by the "seed" laser, as shown in the figure below. Multiple active and passive optical components are needed, and managing their interplay is critical for safe and reliable operation, often close to the limit of optical damage.

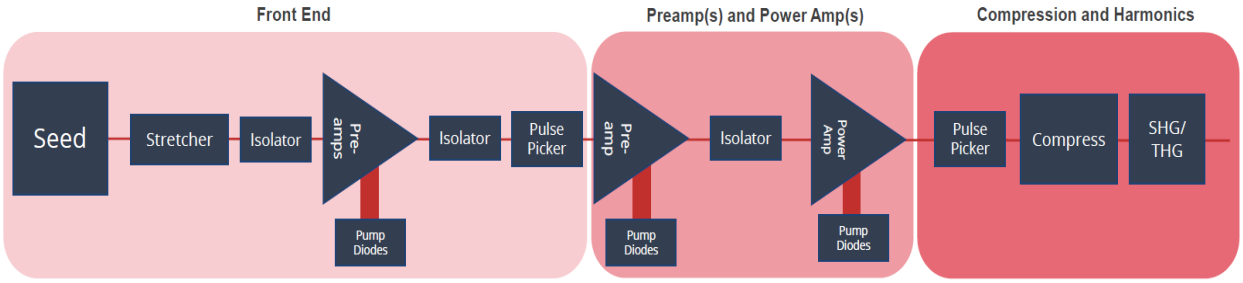

Fig.1 *Key optical elements in a fiber or bulk ultrafast amplifier*

We determined that an important pathway to improved performance and reliability is to control the design and manufacturing of as many critical elements of the supply chain as possible. This control is exercised by assessing the ultimate limitations of these components using testing tools not available to outside manufacturers or by provide extensive and proprietary feedback to the in-house component design and manufacturing teams [1]. To this end, we provide a review of recent improvements in component technology and performance that enable the scaling of ultrafast amplified systems in reliability, performance and efficiency.
Finally, we will present some examples of applications that are significant for this audience and that used ultrafast amplifiers from Coherent to produce high-quality data.

References

[1] M. Arrigoni, T. McComb, Presentation at NATO SET-308 workshop at Photonics West (2022)

Multi-mode-mixing Deep-strong light-matter interaction

J. Mornhinweg[1], L. Diebel[1], M. Halbhuber[1], M. Prager[1], J. Riepl[1]
T. Inzenhofer[1], D. Bougeard[1], R. Huber[1], C. Lange[2]
[1] *Department of Physics, University of Regensburg, 93040 Regensburg, Germany*
[2] *Department of Physics, TU Dortmund University, 44227 Dortmund, Germany*

Dressing quantum states of matter with virtual photons can drive non-perturbative light-matter dynamics on time scales even faster than the oscillation cycle of light. Ultrastrong coupling of light and matter features an exotic vacuum ground states hosting a significant number virtual excitations. Their fluctuating vacuum fields allows for spectacular cavity-QED effects ranging from vacuum-field induced charge transport [1], polaritonic chemistry [2], strong nonlinearities [3] and coherent polariton scattering [4]. With deep-strong coupling (DSC), the coupling strength defined as the ratio of the vacuum Rabi frequency Ω_R and the carrier frequency of light ω_c, even exceeds unity, $\Omega_R/\omega_c \geq 1$ [5,6]. Non-adiabatic switching of Ω_R [7] is expected to release the virtual ground state population in the form of vacuum radiation – a scenario which is becoming more realistic as coupling strengths are further increased. Despite impressive progress made in this direction, new research has found fundamental constraints caused by light-matter decoupling [8] or dissipation [9]. Moreover, the commonly used principle of resonant interaction of two modes [10] is intrinsically limited by the oscillator strength of a single electronic excitation.

Here [11], we overcome this limitation and present a conceptually novel regime of deep-strong light-matter coupling, making use of the fact that even strongly detuned electronic modes can significantly boost the vacuum ground state population of an optical mode. Going beyond single pairs of coupled modes (Fig. 1a), we cooperatively couple multiple, highly non-resonant modes (Fig. 1b) – magnetoplasmons specifically tailored by our maximally compact metasurface (Fig. 2a,b). We test our concept with several GaAs multi-quantum well (QW) heterostructures which host Landau-quantized two-dimensional (2D) electron gases, featuring a cyclotron resonance (CR) with a tunable frequency ν_c. Multiple discrete plasmon resonances formed by our metasurface hybridize with the CR and couple to the optical modes j of the resonator structure with an individual vacuum Rabi frequency $\Omega_{R,j,\alpha}$. We investigate 6 samples with n_{QW} = 1, 3, 6, 12, 24 and 48 QWs (Fig. 1c-h), displaying an evolution of the fan of upper polaritons, $UP_{j,\beta}$ from a tightly packed ensemble to multiple, clearly separated resonances. This ultrabroadband spectrum of more than 20 cavity polaritons spans up to 6 optical octaves, clearly evidencing the multi-mode character and the extreme coupling. We created a multi-mode theory of DSC based on the Hopfield Hamiltonian to properly characterize these spectra. Since the notion of the anti-crossing where the coupling strength is maximized becomes irrelevant for off-resonant, multi-mode coupling, we highlight the number of virtual photons in the vacuum ground state $\langle N_j \rangle$ of each photonic mode j as the figure of merit. Applying our theory to our experimental results, we reach up to $\langle N_1 \rangle = 1.00$ and $\langle N_2 \rangle = 0.18$, corresponding to $\Omega_{R,j=1}/\omega_{j=1} = 2.83$ and $\Omega_{R,j=2}/\omega_{j=2} = 0.93$ for the more than 20 unique, strongly coupled resonances of the sample with $n_{QW} = 48$. The combined vacuum ground state population is more than 2 times higher than previously achieved [5,6], and, for the first time, exceeds unity.

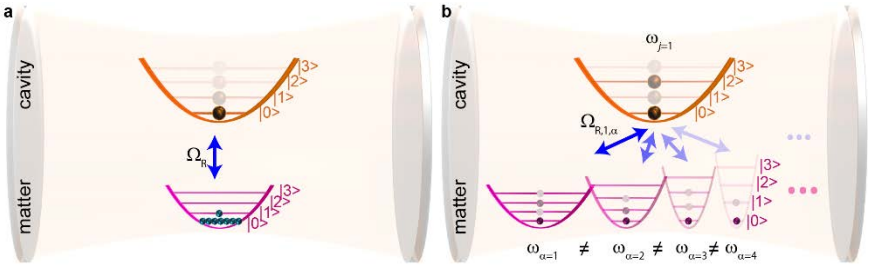

***Fig. 1. a**, Resonant ultrastrong coupling of a single cavity mode (upper parabola) to a single matter excitation (bottom parabola) with a vacuum Rabi frequency Ω_R. The weak population by virtual excitations in the vacuum ground state is indicated by semi-transparent spheres. **b,** Non-resonant DSC of one light mode (upper parabola) to multiple matter excitations (bottom parabolas) with vacuum Rabi frequencies $\Omega_{R,j,\alpha}$ under off-resonant conditions. Owing to the extremely large light-matter coupling, a significant number of virtual excitations are present.*

The extreme interaction results in a strongly subcycle exchange of vacuum energy between the multiple bosonic modes akin to high-order nonlinearities otherwise reserved to strong-field physics. This is also evident in the properties of the extreme vacuum ground state – equivalent to a record coupling strength of $\Omega_R/\omega_c = 3.19$ – resulting in strong two-mode squeezing, a highly non-classical

Fock-state probability distribution and the emission of correlated photon pairs, which is expected for non-adiabatic modulation [7].

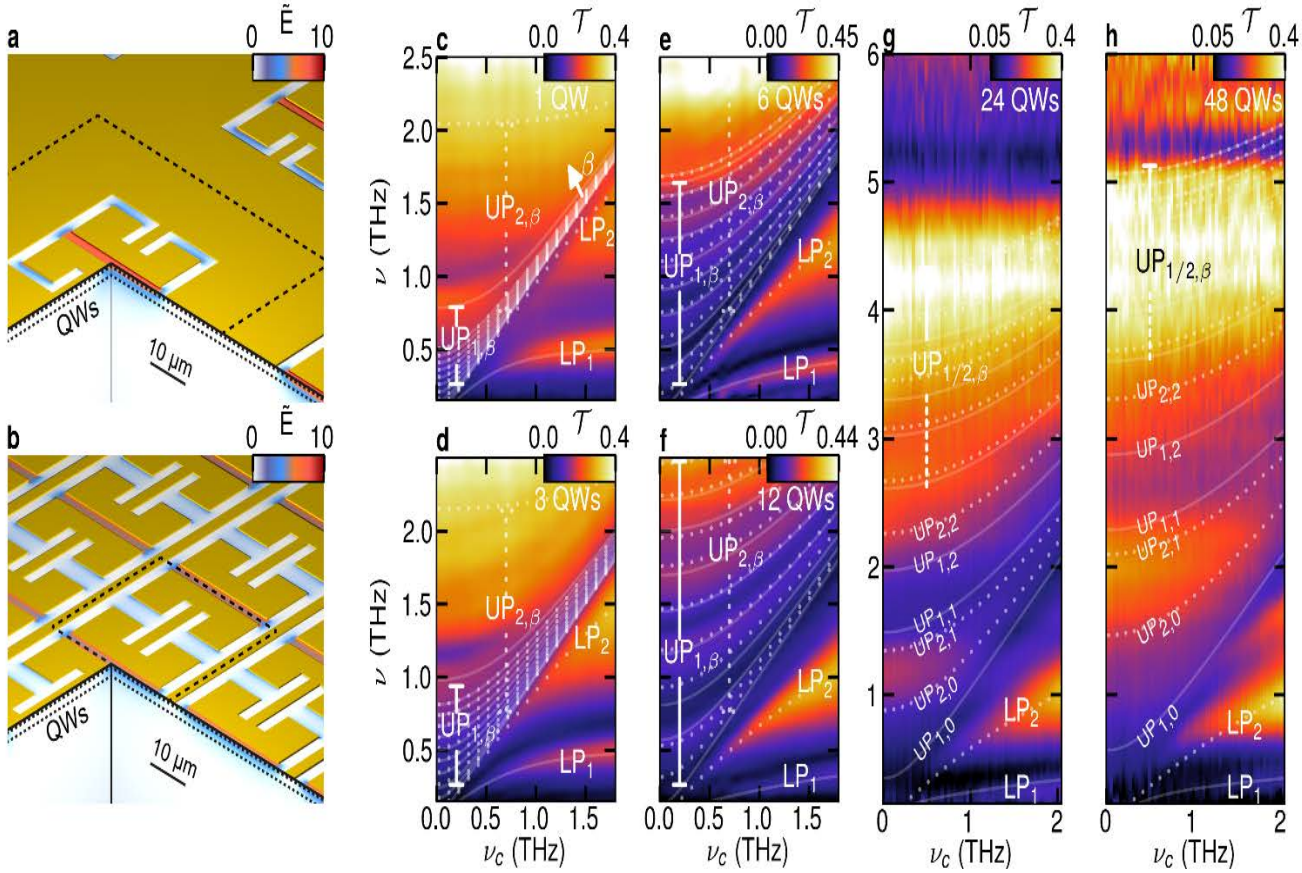

Fig. 2. a, *Conventional metasurface (gold) and its electric near-field $\tilde{E}$, for the fundamental mode at ν_c = 0.52 THz. The unit cell (size: 60 µm × 60 µm) is indicated by the dashed line. QW: quantum well stack.* ***b****, Electric field $\tilde{E}$ and unit cell for the maximally compact metasurface.* ***c-h****, THz transmission for 1, 3, 6, 12, 24, 48-QWs. White curves: polariton modes for the first resonator mode. Dashed curves: polaritons linked to the higher mode ν_2.* ***c,*** *1 QW, coupling strength: $\Omega_{R,1}/\omega_1$ = 0.55.* ***d****, 3-QWs ($\Omega_{R,1}/\omega_1$ = 0.76).* ***e****, 6-QWs ($\Omega_{R,1}/\omega_1$ = 1.34).* ***f****, 12-QWs ($\Omega_{R,1}/\omega_1$ = 2.32).* ***g****, 24-QWs ($\Omega_{R,1}/\omega_1$ = 2.65, $\Omega_{R,2}/\omega_2$ = 0.87).* ***h****, 48-QWs ($\Omega_{R,1}/\omega_1$ = 2.67, $\Omega_{R,2}/\omega_2$ = 0.88).*

In conclusion, our work [11] represents a leap forward in c-QED by overcoming the limitations of resonant light-matter coupling with our novel concept of cooperative, multi-mode hybridization, allowing to increase the total vacuum photon population almost arbitrarily by adding electronic oscillator strength within a wide spectral window. This even facilitates hybridization of otherwise orthogonal matter states purely through vacuum fields of a common cavity mode and can be applied to interactions between a variety of systems such as magnons, phonons or Dirac electrons, including the mixing of entirely different excitations. Combined with the resulting sizeable virtual populations of light and matter modes, our concept offers new flexibility and an unprecedented level of control of, for example, electronic transport [1], light-induced phase transitions [12] or chemical reactions [2], by merely shaping the dielectric environment with vacuum fields.

References

[1] G. L.Paravicini-Bagliani, F. Appugliese, E. Richter, F. Valmorra, J. Keller, M. Beck, N. Bartolo, C. Rössler, T. Ihn, K. Ensslin, C.Ciuti, G. Scalari J. Faist. *Nature Physics* **15**, 186 (2019).
[2] A. D. Dunkelberger, B. S. Simpkins, I. Vurgaftman, J. C. Owrutsky. *Annual Review of Physical Chemistry* **73**, 429 (2022).
[3] J. Mornhinweg, M. Halbhuber, C. Ciuti, D. Bougeard, R. Huber, C. Lange. *Physical Review Letters* **126**, 177404 (2021).
[4] M. Knorr, J. M. Manceau, J. Mornhinweg, J. Nespolo, G. Biasiol, N. L. Tran, M. Malerba, P. Goulain, X. Lafosse, M. Jeannin, M. Stefinger I. Carusotto, C. Lange, R. Colombelli, R. Huber. *Physical Review Letters* **128**, 247401 (2022).
[5] A. Bayer, M. Pozimski, S. Schambeck, D. Schuh, R. Huber, D. Bougeard, C. Lange. *Nano Letters* **17**, 6340 (2017).
[6] N. S. Mueller, Y. Okamura, B. G. M. Vieira, S. Juergensen, H. Lange, E. B. Barros, F. Schulz, S. Reich. *Nature* **583**, 780 (2020).
[7] M. Halbhuber, J. Mornhinweg, V. Zeller, C. Ciuti, D. Bougeard, R. Huber, C. Lange. *Nature Photonics* **14**, 675 (2020).
[8] S. De Liberato, *Physical Review Letters* **112**, 16401 (2014).
[9] S. Rajabali, E. Cortese, M. Beck, S. De Liberato, J. Faist, G. Scalari. *Nature Photonics* **15**, 690 (2021).
[10] E. Cortese, J. Mornhinweg, R. Huber, C. Lange, S. De Liberato. *Optica*, **10**, 11 (2023).
[11] J. Mornhinweg, L. Diebel, M. Halbhuber, M. Prager, J. Riepl, T. Inzenhofer, D. Bougeard, R. Huber, C. Lange, (*submitted)* (2023).
[12] F. Schlawin, A. Cavalleri, D. Jaksch., *Physical Review Letters* **122**, 133602 (2019).

* Acknowledgements: The authors thank Dieter Schuh and Imke Gronwald for valuable discussions and technical support. We gratefully acknowledge support by the Deutsche Forschungsgemeinschaft through Project IDs 231111959 and 422 31469 5032-SFB1277 (Subproject A01), grants no. LA 3307/1-2, and HU 1598/2, as well as by the European Research Council (ERC) through Future and Emerging Technologies (FET) grant no. 737017 (MIR-BOSE).

Subcycle dynamics of quantum light

A. S. Moskalenko
Korea Advanced Institute of Science and Technology, Daejeon 34141, Korea

Quantum properties of light play one of the central roles for emerging quantum technologies. Usually they are characterized in the frequency domain in a vicinity of a well-defined carrier frequency. In this picture the Wigner function is frequently used for a phase-space visualization of the states as well as for accessing their physical properties via the classical averaging of the corresponding quantities over the phase space. Extending this approach to a pulsed ultrabroadband quantum light would lead to a quite involved description in terms of a large set of single-frequency or shaped temporal modes, where each mode has to be characterized separately while keeping the intermode phase relation fixed, or would require an *a priori* knowledge about the shape of a smaller number of the localized temporal modes in which the state of the light can be expanded. An alternative approach is to consider the quantum fields directly in the time domain [1-3]. For example, we have shown that it is possible to formulate a time-domain theory of the generation and time-resolved detection of ultrabroadband pulsed squeezed vacuum states [4] and that it should be possible to get access to arbitrary rotated generalized quadratures of the field [5,6]. In this contribution, we discuss how to define and retrieve then the corresponding subcycle-resolved Wigner function.

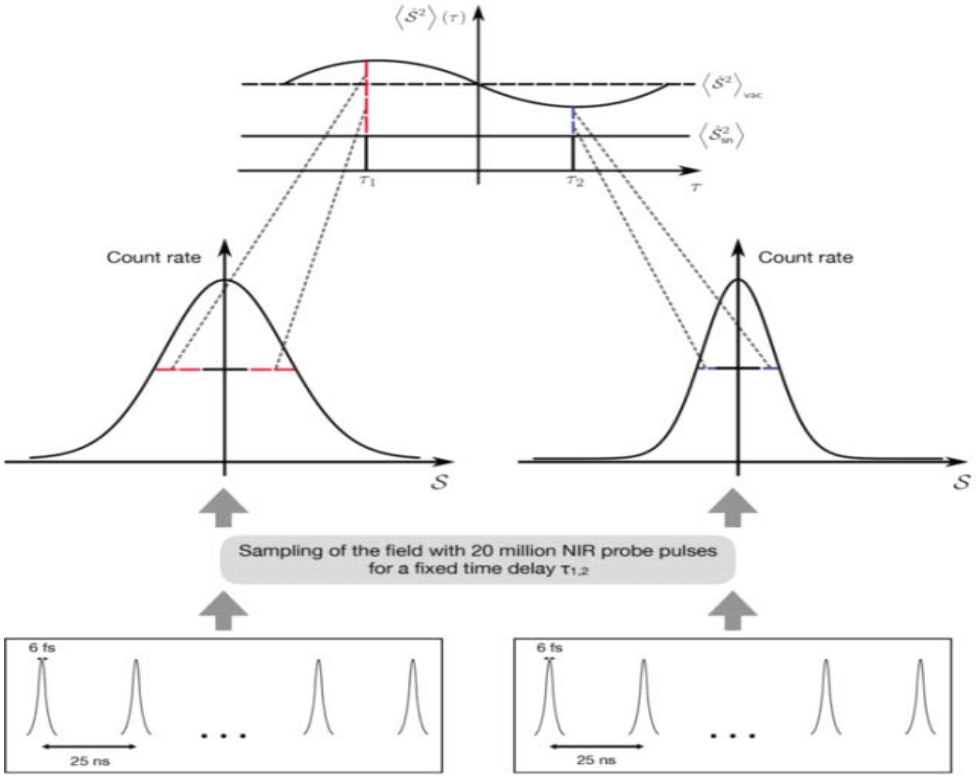

Fig.1. *Scheme of the statistical readout capable to trace the quantum statistics of the signal, containing the (quantum) shot-noise contribution and the part originated from the sampled quantum field .*

In the corresponding setup a few-femtosecond near-infrared (NIR) probe pulse is sent through a thin electro-optic crystal where it interacts with a quantum field in the mid-infrared (MIR) range and then analyzed via a statistical readout (see Fig. 1). We show that a slightly modified version of the setup enables the detection of the probability distribution of the analyzed probe field for arbitrary phase shifts, thus enabling a full quantum tomography of its state [5]. In order to extract phase-space distributions of the sampled MIR field, a procedure to disentangle the contributions of the MIR field from the NIR quantum shot noise has still to be found.

Assuming that this procedure is accomplished, we can demonstrate a way to reconstruct the phase-space distributions of the MIR field with an extreme (subcycle) temporal resolution. In order to avoid the complications connected with the shot noise, in this contribution we also show how to retrieve the subcycle-resolved Wigner function based on the homodyne detection with phase-controlled half-cycle pulses.

We illustrate the obtained theoretical results for the case of the pulsed squeezed vacuum states and derived from them photon-subtracted states (see Fig. 2).We have developed a new tomography scheme to completely resolve the instantaneous structure of quantum ultrabroadband light in the time domain. The function reconstructed from the tomography protocol represents a joint quasi-probability distribution of the sampled instantaneous electric field and its conjugated generalized quadrature. It is capable to visualize the dynamics of the field state, providing direct access to the ultrafast evolution of its characteristic features, such as photon content, squeezing and negativity.

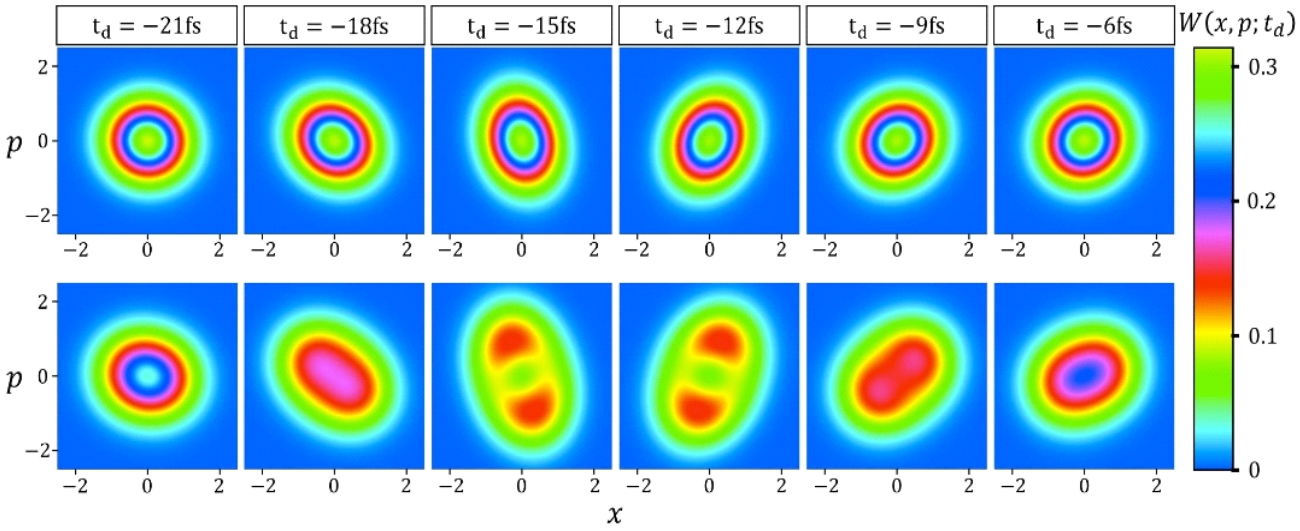

Fig. 2. *Snapshots of the subcycle-resolved Wigner function are shown for several values of the delay time* t_d *for the pulsed squeezed vacuum state (corresponding photon-subtracted state) in the* ***upper (lower)*** *row.*

This achievement paves the ways to further advances towards ultrafast quantum spectroscopy capable to probe femtosecond dynamics of correlations and entanglement in many-body systems, hidden to probing by methods of classical ultrafast photonics.

References

[1] C. Riek, D.V. Seletskiy, A.S. Moskalenko, J.F. Schmidt, P. Krauspe, S. Eckart, S. Eggert, G. Burkard, A. Leitenstorfer, *Science* **350**, 420 (2015).
[2] A. S. Moskalenko, C. Riek, D. V. Seletskiy, G. Burkard, A. Leitenstorfer, *Physical Review Letters* **115,** 263601 (2015).
[3] C. Riek, P. Sulzer, M. Seeger, A.S. Moskalenko, G. Burkard, D.V. Seletskiy, A. Leitenstorfer, *Nature* **541**, 376 (2017).
[4] M. Kizmann, T.L.M. Guedes, D.V. Seletskiy, A.S. Moskalenko, A. Leitenstorfer, G. Burkard., *Nature Physics* **15**, 960 (2019).
[5] M. Kizmann, A.S. Moskalenko, A. Leitenstorfer, G. Burkard, S. Mukamel, *Laser and Photonics Reviews* **16**, 2100423 (2022).
[6] S. Gündoğdu, S. Virally, M. Scaglia, D.V. Seletskiy, A.S. Moskalenko, *Laserand Photonics Reviews*, DOI:10.1002/lpor.202200706 (2023).

* Acknowledgement(s): the author acknowledges support from the National Research Foundation of Korea (NRF) grant funded by the Korea government (MSIT) (2020R1A2C1008500) and from the Deutsche Forschungsgemeinschaft (DFG), Project No. 425217212 - SFB 1432, via the Mercator Fellowship.

Ultrafast spectroscopy of optical and electrical properties of Dirac semimetal driven by periodic light field

Y. Murotani, R. Matsunaga
The University of Tokyo, Chiba 277-8581, Japan

Floquet engineering provides an efficient protocol to manipulate the states and properties of matter using external fields periodic in time. Interesting examples include the Floquet-Weyl semimetal (FWSM), which has been predicted to emerge in three-dimensional Dirac semimetals (DSMs) irradiated by circularly polarized light [1]. However, manifestations of such Floquet-engineered states to experimental probes remain largely unclear. We have studied optical and electrical properties of a three-dimensional DSM, Cd_3As_2, exposed to an intense multi-terahertz light field [2, 3]. Figure 1(a) shows the transient broadband absorption spectrum under the driving field at 120 meV (30 THz) [2].

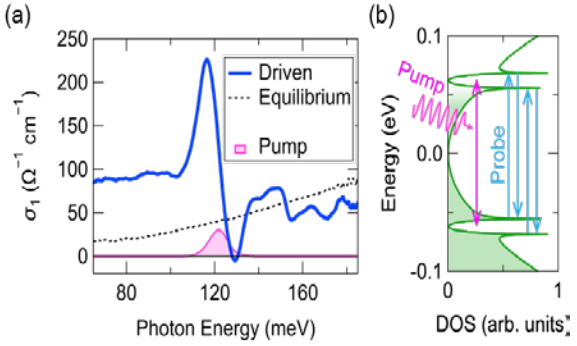

Fig. 1*. *(a) *Transient optical conductivity during irradiation by linearly polarized pump pulse.*
(b) *Schematic of the formation of Floquet states and the resulting stimulated Rayleigh scattering.*

The spectrum is characterized by a large dispersive structure with net optical gain around the driving frequency. Microscopic calculations revealed this drastic change to arise from optical transitions among the Floquet subbands (Fig. 1(b)), which take the form of stimulated Rayleigh scattering enhanced by the longitudinal plasma mode [2]. We next examined the anomalous Hall effect (AHE) of Cd_3As_2 under circularly polarized light, using time-resolved terahertz Faraday rotation spectroscopy [3]. Though a light-induced AHE has been proposed as an indication of the FWSM, we observed an anomalous Hall conductivity larger than, and with a sign opposite to, the theoretical prediction for a FWSM (Fig. 2(a)).

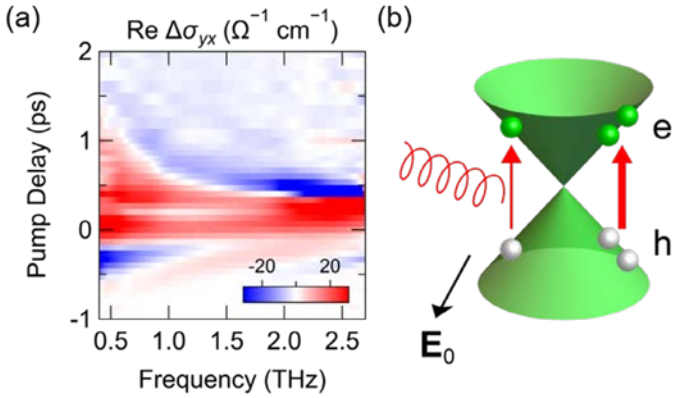

Fig. 2. (a) *Anomalous Hall conductivity during irradiation by left circularly polarized pump pulse.*
(b) *Schematic of the field-induced injection current, allowed by the terahertz electric field,* $\boldsymbol{E_0}$.

Microscopic analysis shows that this phenomenon originates from "field-induced injection current," i.e., a transverse photocurrent generation in the presence of an electric field (Fig. 2(b)). This result clarifies the essential role of photoexcited carriers under a bias field, and suggests that materials transparent to the driving field are better to observe the AHE by a FWSM.

References

[1] H. Hübener, M. A. Sentef, U. De Giovannini, A. F. Kemper, A. Rubio, *Nature Communications* **8**, 13940 (2017).
[2] Y. Murotani, N. Kanda, T. N. Ikeda, T. Matsuda, M. Goyal, J. Yoshinobu, Y. Kobayashi, S. Stemmer, R. Matsunaga, *Physical Review Letters* **129**, 207402 (2022).
[3] Y.Murotani, N.Kanda, T.Fujimoto, T.Matsuda, M.Goyal, J.Yoshinobu, Y.Kobayashi, T.Oka, S.Stemmer, R. Matsunaga, *arXiv:2211*.02229 (2022).

ALBATROSS – a single-cycle infrared light source with unique Waveform Stability

N. Nagl[3], P. Steinleitner[1], M. Kowalczyk[4], N. Karpowicz[1], A. Sebesta[4], A. Paudel[2]
D. Potamianos[4], M. Stadter[1], S. Gröbmeyer[2], A. Głuszek[5], A. Hudzikowski[5]
V. Pervak[2], J. Sotor[5], K. F. Mak[1], F. Krausz[1], A. Weigel[1]
[1]*Max Planck Institute of Quantum Optics, 85748 Garching, Germany*
[2]*Ludwig Maximilian University Munich, 85748 Garching, Germany*
[3]*PULSED GmbH, 85748 Garching, Germany*
[4]*Center for Molecular Fingerprinting, 1093 Budapest, Hungary*
[5]*Wrocław University of Science and Technology, 50-370 Wrocław, Poland*

Waveform-controlled single-cycle light sources lay the foundation for manipulating the nonlinear polarization of matter on a sub-femtosecond time scale. Due to their precisely controllable carrier-envelope phase (CEP), they have paved the way for ground-breaking research in the past, including the ultrafast manipulation of electric currents in solids [1] and the generation of isolated attosecond pulses [2]. In particular, strong-field processes in condensed matter, such as the tunneling through nanoscopic gaps [3], can already be induced at moderate, sub-nano-joule-level pulse energies.
Until recently, Ti:sapphire systems have been the gold standard for providing laser pulses with high waveform stability [4] and pulse durations approaching a single optical cycle [5]. Yet, their application has been constrained by their near-infrared emission spectrum at around 800 nm, requiring complex and inefficient frequency down-conversion to directly address light wave-driven carrier dynamics in low-bandgap semiconductors. Laser oscillators based on Cr^{2+}-doped II-VI gain media have evolved as promising alternatives, providing emission wavelengths around 2-3 µm — ideal for direct frequency-comb spectroscopy [6] and efficient down-conversion to the mid-infrared region [7]. In this contribution we present a unique CEP-stable single-cycle source at 2.2 µm with unprecedented waveform stability. The system is based on a diode-pumped Cr:ZnS laser oscillator combined with subsequent extreme nonlinear spectral broadening in a single thin TiO_2 bulk plate. Efficient frequency down-conversion can further extend the spectral coverage towards longer wavelengths and allows to generate single-cycle mid-infrared pulses with CEP-controlled waveforms [7]. For the wider proliferation of this new technology, a compact and monolithic platform has been developed: *ALBATROSS*. The heart of the experimental system, i.e. the precursor of *ALBATROSS*, constitutes a diode-pumped Cr:ZnS oscillator, delivering 28-fs short pulses at a repetition rate of 22.9 MHz (Fig. 1a).

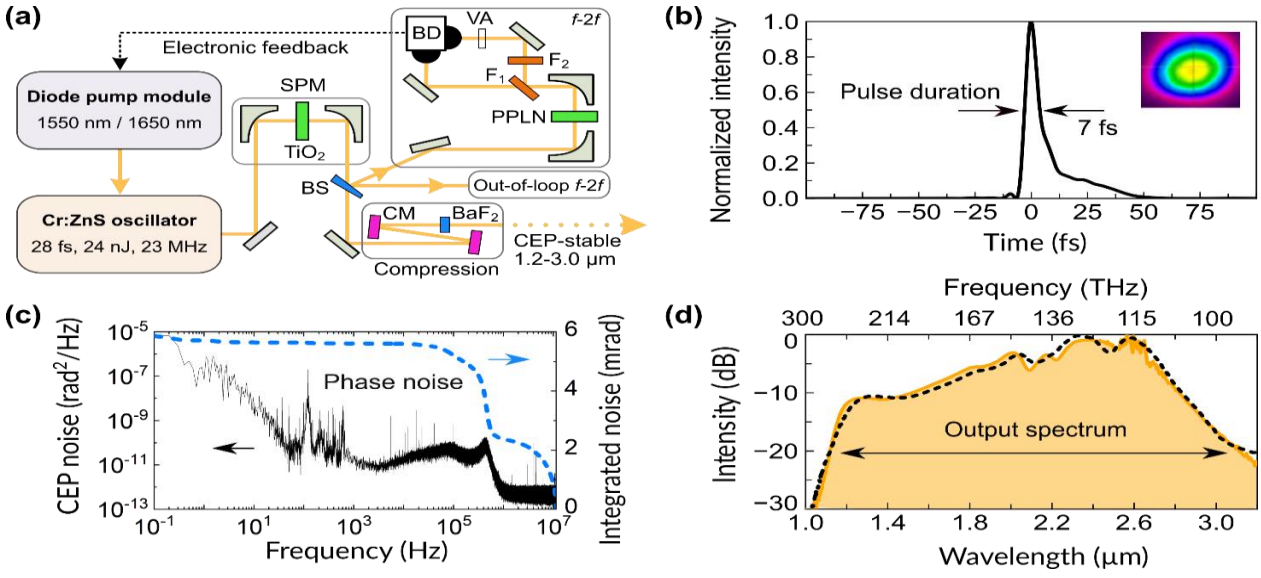

***Fig. 1. a**: **CEP-stable single-cycle pulse generation.** Schematic of the CEP-stabilized Cr:ZnS laser system. **b**: Temporal profile of the single-cycle output pulses and beam profile (inset). The pulse duration was measured with the SHG-FROG technique. **c**: CEP noise power spectral density and the corresponding integrated phase noise of the CEP-stabilized laser system **d**: Measured (orange) and simulated (black, dashed) supercontinuum spectrum after spectral broadening in TiO_2.*

The output of the laser is focused into a single 0.5-mm-thick TiO_2 plate and broadened to a supercontinuum spanning from 1.2 to 3.0 µm at -20 dB and 360 mW of output power (Fig. 1d). By using custom dispersive optics, the super-octave-spanning pulses are compressed to pulse durations down to 6.9 fs, which corresponds to a single oscillation cycle of the electric field at the spectral centroid of 2.2 µm (Fig. 1b). Detailed insights into the broadening mechanism in TiO_2 are obtained through numerical simulations, which closely reproduce the output spectrum of the broadening stage (Fig. 1d). To generate a feedback signal for active CEP stabilization, a fraction of the broadened output is sent into a highly compact common-path *f*-2*f* interferometer. Absolute CEP stability, i.e. with the carrier-envelope-offset frequency f_{ceo} set to zero, has been achieved with a residual phase noise of only 5.9 mrad in the range between 0.1 Hz to 11.45 MHz (Fig. 1c). This corresponds to the lowest value ever shown for single or few-cycle laser sources.Efficient down-conversion by cascaded intra-pulse difference frequency generation (IPDFG) in a $ZnGeP_2$ (ZGP) crystal allows to create CEP-controlled mid-IR waveforms across more than three optical octaves from 0.9 µm to 12 µm at -30 dB (Fig. 2a) [7].

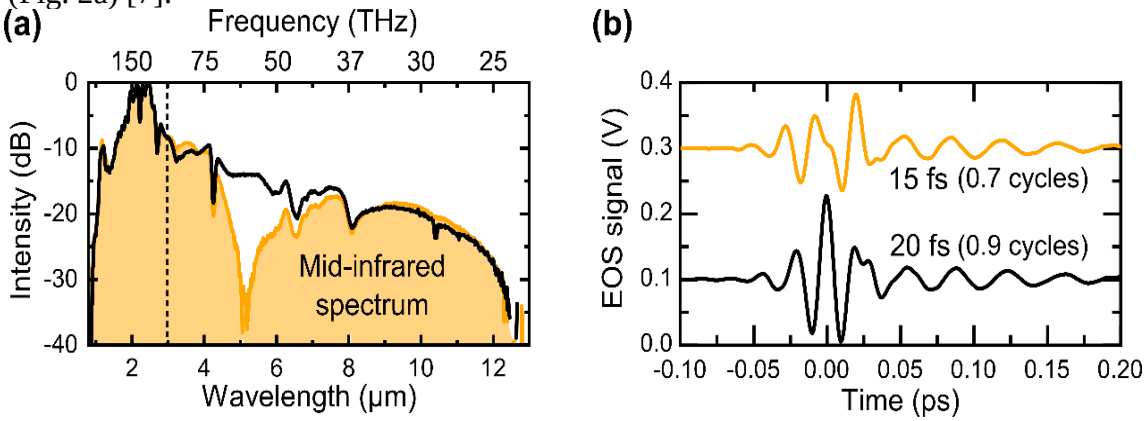

Fig. 2. CEP-controlled single-cycle mid-infrared-pulse generation. a*: Mid-infrared spectrum from cascaded intra-pulse difference frequency generation (IPDFG), shown for the extreme cases of constructive (black) and destructive (orange) interference between the even and odd cascaded IPDFG orders. The dashed line indicates the detection limit of the EOS measurement technique when using a 7-fs gate pulse.* ***b****: EOS time-domain data for the two different CEP-settings of the driver laser pulse. For better comparison, the two traces are offset by a constant factor (0.2 V). The pulse durations correspond to the full-width at half-maxima (FWHM) of the intensity envelopes. For calculating the number of optical cycles, the spectral centroids of the waveforms are considered.*

The adjustment of the waveforms is achieved by tuning the CEP of the driver laser pulse. In the two extreme cases shown, this leads to fully constructive (black curve in Fig. 2a) or destructive (orange curve in Fig. 2a) interference between the even and odd cascaded IPDFG orders, correspondingly modulating the spectral intensity around 5 µm. The average power of the mid-infrared part of the supercontinuum (>3.6 µm) for the case of constructive interference is 31 mW, corresponding to an IPDFG power conversion efficiency of 14%. To observe changes of the mid-infrared waveform induced by varying the CEP of the driving laser, the technique of electro-optic sampling (EOS) was used. It confirmed excellent temporal confinement of the waveforms to single-cycle durations (Fig. 2b). In conclusion, we demonstrate a compact and coherent infrared laser source, *ALBATROSS*, for delivering single-cycle pulses with ultra-high waveform stability – the ideal frontend for future field-resolved femtosecond experiments including light wave-driven control of charge carriers in low-bandgap semiconductor materials, and for generating controllable mid-infrared waveforms spanning multiple octaves. With regard to infrared-based biosensing and life science applications, we expect to achieve a new level in specificity and sensitivity, when combined with field-resolved detection (EOS) and dual-oscillator scanning techniques [8].

References

[1] S. Sederberg, D. Zimin, S. Keiber, F. Siegrist, M. S. Wismer, V. S. Yakovlev, I. Floss, C. Lemell, J. Burgdörfer, M. Schultze, F. Krausz N. Karpowicz, *Nature Communications* **11**, 430 (2020).

[2] M. Hentschel, R. Kienberger, C. Spielmann, G. A. Reider, N. Milosevic, T. Brabec, P. Corkum, U. Heinzmann, M. Drescher, F. Krausz, *Nature* **414**, 509 (2001).

[3] T. Rybka, M. Ludwig, M. F. Schmalz, V. Knittel, D. Brida, A. Leitenstorfer, *Nature Photonics* **10**, 667 (2016).

[4] R. Liao, H. Tian, T. Feng, Y. Song, M. Hu, G. Steinmeyer, *Optics Letters*. **44**, 1060 (2019).

[5] S. Rausch, T. Binhammer, A. Harth, J. Kim, R. Ell, F. X. Kärtner, U. Morgner, *Optics Express* **16**, 9739 (2008).

[6] S. Vasilyev, V. Smolski, J. Peppers, I. Moskalev, M. Mirov, Y. Barnakov, S. Mirov, V. Gapontsev, *Optics Express* **27**, 35079 (2019).

[7] P. Steinleitner, N. Nagl, M. Kowalczyk, J. Zhang, V. Pervak, C. Hofer, A. Hudzikowski, J. Sotor, A. Weigel, F. Krausz, K. F. Mak, *Nature Photonics* **16**, 512 (2022).

[8] A. Weigel, T. Buberl, P. Jacob, T. Amotchkina, C. Hofer, M. Trubetskov, P. Sulzer, S. A. Hussain, W. Schweinberger, V. Pervak, F. Krausz, I. Pupeza, *2021 Conference on Lasers and Electro-Optics Europe and European Quantum Electronics Conference*, Paper Cf_9_5, (2021).

New methods for driving and monitoring quantum materials

Z. Zhang[1], Z.-J. Liu[1], F. Y. Gao[2], E. Baldini[2], Y.-C. Chien[1], J. Deschamps[1], J. Lem[1], Y. Kai[1], I. Chaban[1]
T. Pezeril[3], K. A. Nelson[1]
[1]*Massachusetts Institute of Technology, Cambridge, MA 02135*
[2]*The University of Texas at Austin, Austin, TX 78705*
[3] *Institut de Physique de Rennes, 35042 Rennes, France*

There have been striking advances in recent years in our understanding of quantum materials, their transformations across complex multiphase landscapes, and the underlying interactions among their coupled modes. There also remain experimental challenges that must be overcome in order to provide further key insights and to guide progress from fundamental understanding to practical applications. Here we discuss recent methodological progress and results.

The first advance is aimed at using both optical and terahertz-frequency (THz) probes for time-resolved measurements of ultrafast material transformations that are irreversible or slowly reversible. Since the samples under study do not return to their initial states after photoexcitation, such transformations cannot be monitored through conventional methods that require many repetitions of a pump-probe pulse sequence with variable temporal delays between the pump and probe pulses. We have developed [1] and refined [2,3] a method for single-shot, real-time monitoring of ultrafast dynamics in which the usual variably delayed probe pulse is replaced by hundreds of probe pulses that all arrive at the pumped sample location with different time delays, covering a total temporal range of about 10 ps with approximately 25-fs intervals between successive pulses. For optical monitoring of the photoinduced response, the pulses are all measured in different regions of a camera after reflection from or transmission through the sample. We recently have extended the method to permit measurement at THz probe frequencies as well [4]. In this case, the sample is irradiated by a THz probe pulse and the resulting time-dependent THz field that is either transmitted through or reflected from the sample is measured through electro-optic (EO) sampling, i.e. through the change in optical polarization that the THz field induces. This is ordinarily measured with an optical "readout" pulse that is variably delayed to overlap temporally with different parts of the THz field profile. We have instead used several hundred readout pulses to measure the entire THz signal field profile in a single laser shot. We recently studied ultrafast metastable phase formation in the quasi-2D charge-density wave (CDW) crystal TaS_2 using both optical reflection and THz transmission measurements to probe ultrafast lattice and electronic responses [5]. Because the photoinduced collective transformation is irreversible at low temperatures (the initial commensurate CDW phase can be recovered by temperature cycling, which is extremely slow), conventional ultrafast measurement methods with many pump-probe repetitions cannot be used. Single-shot measurements clearly revealed ultrafast nonthermal collapse of the initial CDW ordering and formation of a far more highly conducting (H) state which showed its own CDW ordering signature (amplitude-mode oscillations) on subsequent shots after the first. See Fig. 1. The results also showed further collective evolution and conductivity increase when the excitation pulse fluence was raised further on subsequent shots. The results yielded greatly improved understanding of the nature of the photoinduced metastable state and the dynamics of its formation.

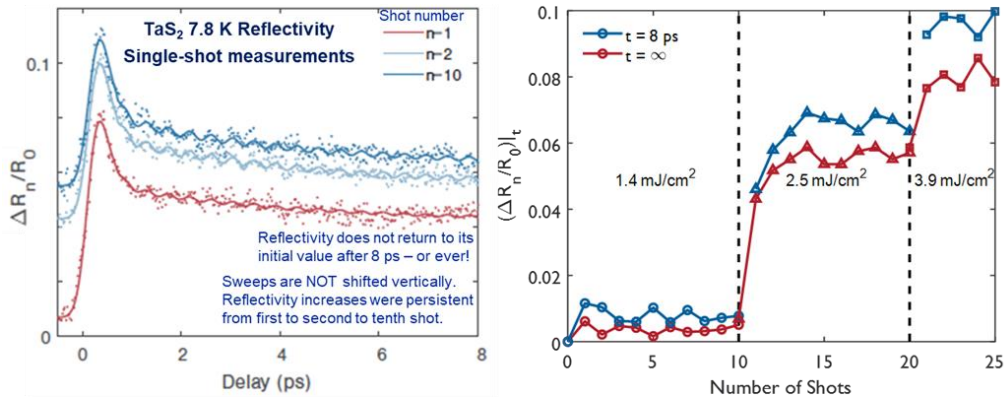

Fig. 1. *Dynamics of the emergent hidden phase formed after photoexcitation in 1T-TaS_2.* ***Left****: Single-shot transient reflectivity measurements (**dots**) at 7.8 K following irradiation with 2.5 mJ/cm^2 1.55-eV pump pulses are shown along with the corresponding fits to biexponential decays and oscillatory responses (**solid lines**). Ten shots were recorded at this fluence but only the 1st, 2nd, and 10th are reproduced here for clarity. Each irradiation was separated by more than 10 s.* ***Right****: The corresponding shot-to-shot change in steady-state reflectivity (**red**) and 8-ps reflectivity (**blue**) over the full sequence of irradiations. Note that n = 1 (**left**)) corresponds to the 11th shot (**right**).*

In samples that do not undergo long-lived photoinduced transformations, the single-shot measurement approach may still provide great advantages in data acquisition times and signal/noise (S/N) ratios, especially in experiments that are conducted using amplified laser systems with repetition rates that are comparable to the rate at which several hundred multi-time signals can be downloaded from the camera. We have realized these advantages in two-dimensional THz spectroscopy, which involves two distinct time delays – the time between two THz excitation pulses and the time at which the nonlinear THz signal is read out through EO sampling – that must be scanned. We earlier reported 2D THz electron spin resonance (ESR) spectra from magnon modes [6] as well as 2D THz rotational spectra from polar molecules in the gas phase [7,8]. In this work, each 2D spectrum required several days of uninterrupted data acquisition. We have recently adopted the single-shot EO sampling measurement approach described above to 2D THz spectroscopy conducted at a 1-kHz repetition rate [9]. This has resulted in dramatic improvement in both data acquisition times and S/N ratios, enabling systematic ESR study of antiferromagnetic crystals with slightly canted sublattice spin orientations that yield a nonzero net magnetization **M** [10,11]. In crystals among this broad class, there are two collective spin wave (magnon) branches formed from in-phase or out-of-phase precessions of the sublattice magnetic moments. In the ferromagnetic (F) magnon mode, the net magnetization direction undergoes precession about its unperturbed orientation, while in the antiferromagnetic (AF) mode, the magnetization direction remains unchanged but its magnitude is modulated. Linear ESR spectra recorded using weak THz fields polarized perpendicular or parallel to **M** reveal the F or AF mode respectively. We used THz pump pulse pairs to excite erbium orthoferrite ($ErFeO_3$, EFO) and yttrium orthoferrite ($YFeO_3$, YFO) with the crystal orientations adjusted so the incident THz polarization could drive either the F mode, the AF mode, or both modes. 2D ESR spectra were recorded from each crystal with different orientations relative to the incident THz polarization, rotating a full 360 degrees in 5-degree increments while detecting the coherent nonlinear THz signal with polarizations either parallel or perpendicular to the incident polarization. These *2D THz polarimetry* studies, with 144 2D spectra from each sample, would have been inconceivable earlier since each one would have required more than one year of uninterrupted data acquisition. The fully automated polarimetry measurements from each sample were completed in less than 24 hours! Additional measurements were conducted as a function of sample temperature and THz field strength. The results showed second-order signals including 2-quantum coherences (radiating at magnon sum and difference frequencies) that revealed mode-mode couplings that had never before been observed for different magnon modes. In one unusual example [10], an off-diagonal peak was observed due to unidirectional nonlinear coupling in which pumping only the ferromagnetic magnon mode yielded signals (with polarization perpendicular to that of the incident THz fields) from the antiferromagnetic mode. It occurs because driving the precessional F mode nonlinearly reduces the projection of the magnetization along the original **M** direction, thereby coupling to the AF mode. Driving the AF mode alone does not similarly couple to the F mode (although there may be other coupling mechanisms) because even a large-amplitude modulation of the amplitude |**M**| does not induce any precessional (F mode) response.

Many quantum material (and other crystalline) transformations involve changes in the lattice parameters. In such cases, strain can play a key role in controlling which phase is present. We have developed a facile method for laser generation of compressional or surface acoustic wave (SAW) shocks [12] that focus in the plane of a sample to reach multi-GPa stresses sufficient to cause material fracture, chemical decomposition, phase transitions, and other effects [13-17]. In that work, as in other laser shock generation methods, the sample is damaged by the optical excitation pulse even if it is not damaged by the shock. Thus is it not practical to repeat shock generation and delivery to the same sample region many times. This is also not practical in conventional shock generation by mechanical impact. In very recent work, we have developed a method for non-destructive generation of large-amplitude acoustic waves [18]. The approach permits repeated shocks to be delivered to the same sample region, and has been used to observe cumulative effects (i.e. fatigue) caused by thousands of shocks. See Fig. 2. The shocks also may be used to drive phase transitions by themselves or in conjunction with THz or optical excitation. More generally, shock can be used as a component of multimodal excitation of samples that could be probed in any spectral range from THz to x-ray at kHz repetition rates. A duration of >1 ns makes the shock quasi-static on the time scale of many fs-ps spectroscopy measurements, permitting such measurements to be conducted on a single sample as a function of strain. The possibility for repeated shock excitation in pump-probe measurements greatly broadens the parameter space across which searches for hidden phases including metastable phases may be conducted. This development offers novel prospects for fundamental study and potential practical applications of collective quantum dynamics.

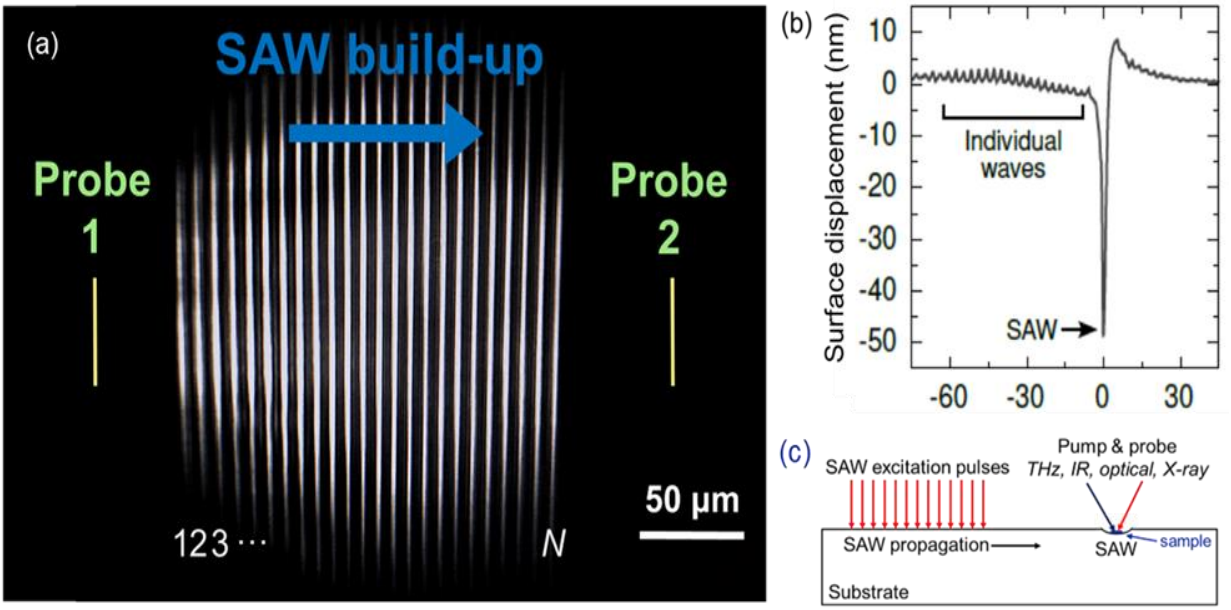

Fig. 2. *Generation of large-amplitude acoustic waves without optical damage to the sample.* ***(a)****: Build-up of SAW amplitude by a sequence of cylindrically focused excitation pulses that irradiate parallel linear regions of a $SrTiO_3$ (STO) sample that is doped with 0.7% Nb in order to absorb the 800-nm light. The image was recorded in reflection mode. The left-most pulse arrives first, then the next one to the right, and so on, with successive pulses shifted spatially and temporally to match the SAW velocity. The thermoelastic responses to all the pulses superpose coherently to reach a large amplitude.* ***(b)****: Displacement of a Nb:STO sample surface measured interferometrically after excitation with 1.0 J/cm^2 laser fluence. The superposed SAW was measured at the "Probe 2" location in (a). The SAW responses that propagated leftward from each excitation pulse did not superpose, giving rise to the small individual signals measured at the "Probe 1" location. The superposed SAW has a longitudinal strain of 1.0% at the free surface, corresponding to a stress of about 3 GPa. SAW amplitudes up to 3x larger than that shown were generated without optical damage to the irradiated region of the sample.* ***(c)****: Schematic illustration of multimodal excitation involving acoustic/shock and THz, IR, or optical pump pulses. The SAW (or bulk compressional wave) propagates to a pristine sample region at which a fs-ps time-resolved pump-probe (or 2D) measurement takes place.*

The doped $SrTiO_3$ sample absorbed the pump light in a penetration depth of only 15 μm, yielding a thermoelastic response that matched the SAW strain profile. In a more lightly doped material with a longer optical penetration depth, a bulk-like compressional wave will be generated. Either wave can be transduced into a sample of interest, including SAW propagation into a thin sample deposited onto the substrate surface or bulk shock propagation into a thicker sample.

The combination of strain and THz, IR, optical, or UV pumping makes possible the excitation of multiple, coupled degrees of freedom that play central roles in material transformations. This will advance our fundamental understanding and our ability to control material traversal across complex multiphase free energy landscapes.

References

[1] P. R. Poulin, K. A. Nelson, *Science* **313**, 1756 (2006).
[2] T. Shin, J.W. Wolfson, S.W. Teitelbaum, M. Kandyla, K.A. Nelson, *Review of Scientific Instru*ments **85**, 083115 (2014).
[3] S. W. Teitelbaum, T. Shin, J. W. Wolfson, Y.-H. Cheng, I. J. Porter, M. Kandyla, K. A. Nelson, *Physical Review X* **8**, 031081 (2018).
[4] S.M. Teo, B.K. Ofori-Okai, C.A. Werley, K.A. Nelson, *Review of Scientific Instru*ments **86**, 051301 (2015).
[5] F. Y. Gao, Z. Zhang, Z. Sun, L. Ye, Y.-H. Cheng, Z.-J. Liu, J. G. Checkelsky, E. Baldini, K. A. Nelson, *Science Advances* **8**, eabp9076 (2022).
[6] J. Lu, X. Li, H. Y. Hwang, B. K. Ofori-Okai, T. Kurihara, T. Suemoto, K. A. Nelson, *Physical Review Letters* **118**, 207204 (2017).
[7] J. Lu, Y. Zhang, H.Y. Hwang, B.K. Ofori-Okai, S. Fleischer, K.A. Nelson, *PNAS* **113**, 11800 (2016).
[8] Y. Zhang, J. Shi, X. Li, S. L. Coy, R. W. Field, K. A. Nelson, *PNAS* **118**, e2020941118 (2021).
[9] F. Y. Gao, Z. Zhang, Z.-J. Liu, and K. A. Nelson, *Optics Letters* **47**, 3479 (2022).
[10] Z. Zhang, F. Y. Gao, Y.-C. Chien, Z.-J. Liu, J. B. Curtis, E. Sung, X. Ma, W. Ren, S. Cao, P. Narang, A. von Hoegen, E. Baldini, K. A. Nelson, *arXiv*:2207.07103 (2022).
[11] Z. Zhang, F. Y. Gao, J. B. Curtis, Z.-J. Liu, Y.-C. Chien, A. von Hoegen, T. Kurihara, T. Suemoto, E. Sung, P. Narang, E. Baldini, K. A. Nelson, *arXiv*:2301.12555 (2023).
[12] T. Pezeril, G. Saini, D. Veysset, S. Kooi, R. Radovitzky, K.A. Nelson, *Physical Review Letters* **106**, 214503 (2011).
[13] D. Veysset, T. Pezeril, S. Kooi, A. Bulou, K.A. Nelson, *Applied Physics Letters* **106**, 161902 (2015).
[14] D. Veysset, U. Gutiérrez-Hernández, L. Dresselhaus-Cooper, F. De Colle, S. Kooi, K. A. Nelson, P. A. Quinto-Su, T. Pezeril, *Physical Review E* **97**, 053112 (2018).
[15] D. Veysset, A.A. Maznev, I.A. Veres, T. Pezeril, S. Kooi, A. Lomonosov, K.A. Nelson, *Applied Physics Letters* **111**, 031901 (2017).
[16] D. Veysset, S. E. Kooi, R. Haferssas, M. Hassani-Gangaraj, M. Islam, A. A. Maznev, Y. Chernukha, X. Zhao, K. Nakagawa, D. Martynowych X. Zhang, A. M. Lomonosov, C. A. Schuh, R. Radovitzky, T. Pezeril, K. A. Nelson, *Scripta Materialia* **158**, 42 (2019).
[17] L. Dresselhaus-Cooper, D. J. Martynowych, F. Zhang, C. Tsay, J. Ilavsky, S. G. Wang, Y.-S. Chen, L. Leninger, K. A. Nelson, *Journal of Physical Chemistry A* **124**, 3301 (2020).
[18] J. Deschamps, Y. Kai, J. Lem, I. Chaban, A. Lomonosov, A. Anane, S. E. Kooi, K. A. Nelson, T. Pezeril, *arXiv*:2209.13897 (2022).

* Acknowledgement: *Work at MIT was supported by the DOE Office of Basic Energy Sciences, under Award Number DE-SC0019126.*

Sub-diffusive topological defects of a charge density wave Probed by an x-ray laser

G. Orenstein[1], R.A. Duncan[1], G. A. de la Peña Muñoz[1], Y. Huang[1], V. Krapivin[1], Q. L. Nguyen[1]
S. Teitelbaum[2], A. G. Singh[3], R. Mankowsky[4], H. Lemke[4], M.Sander[4], Y. Deng[4], C.Arrell[4], I. R. Fisher[1]
D.A. Reis[1], M. Trigo[1]
[1] *SLAC National Accelerator Laboratory, Menlo Park, CA 94025, USA*
[2]*Arizona State University, Tempe, AZ 85281, USA*
[3]*Stanford University, Stanford, CA 94305, USA*
[4]*Paul Scherrer Institut, 5232 Villigen, Switzerland*

Excitation of materials with ultrafast light pulses has led to the discovery of novel states of matter out of equilibrium and represents a promising avenue to control their functional properties (1). Understanding and manipulating these emergent properties requires a deeper insight into how the photoinduced states evolve away from and towards equilibrium. In many photoexcited systems the evolution of these transient states is characterized by the formation of metastable, inhomogeneous regions and self-organization on mesoscopic length-scales (2–5). However, most ultrafast probes are only sensitive to the average structure and consequentially afford only limited insight into the transient emergent properties of the photoexcited materials (6). In this work we use the high wavevector and time resolution afforded by an x-ray free electron laser (XFEL), combined with a new scaling analysis, to gain unprecedented access to the dynamics on the relevant mesoscopic length-scales. We study the ultrafast dynamics of the charge density wave (CDW) in $LaTe_3$, a quantum material which has attracted attention for its competing charge ordered phases and exotic collective excitations (4,7-9). Our findings reveal unconventional subdiffusive dynamics which is governed by topological vortex strings of the CDW.In a material undergoing a symmetry breaking phase transition under nonequilibrium conditions, the low-symmetry phase develops independently in separate regions of space, leaving behind disconnected domains. This leads to the formation of topological defects (TDs) by the Kibble-Zurek mechanism (10, 11). As the system evolves towards equilibrium, these defects annihilate and the independently ordered domains coalesce. Generally, this coarsening process is characterized by a single length scale, $L(t) \propto t^{\beta}$, where β is the growth exponent (12,13). Here $L(t)$ corresponds to a mean domain size, or an average distance between TDs.

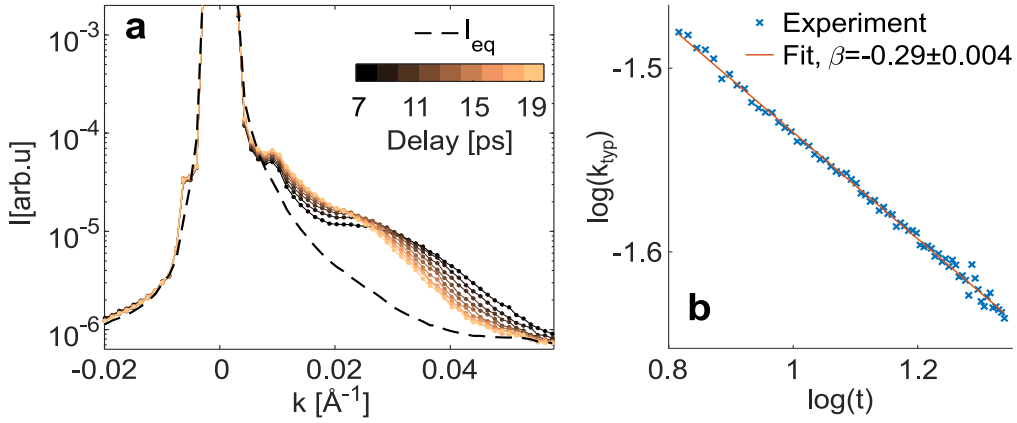

Fig. 1. (a)*: X-ray intensity of the* ***G*** *= (2/a, 2/b, (1 − q_{CDW})/c) CDW Bragg peak of $LaTe_3$ on a logarithmic scale versus wavevector along* ***G***+ ***k****, for* ***k*** *≈ (0, k, 0), where a, b and c are the respective standardized cell parameters and $q_{CDW} \approx 2/7$. The different colors represent different pump-probe delays starting from 6.5 ps. The dashed black line is the equilibrium intensity. The narrowing of the peak is the hallmark of coarsening of spatially inhomogeneous regions as the system recovers towards equilibrium.* ***(b)****: Log of the typical scattering wavevector, $k_{typ}(t)$, versus log of the pump-probe delay, where $k_{typ}(t) \propto L^{-1}(t)$. The red solid straight line is a fit to the data giving $\beta = 0.29$.*

We probed the dynamics of the lattice component of the CDW following an ultrafast optical excitation by using femtosecond total x-ray scattering at the Bernina instrument (14) of the SwissFEL facility (15). The high brightness of the XFEL, together with its exceptional temporal and wavevector resolution, allow subtle details of the dynamics of the diffuse intensity on the tails of the CDW Bragg peak to be captured. This enabled us to directly observe the coarsening process and extract the growth exponent of $\beta = 0.29$ (Fig. 1).A growth exponent of $\beta = 0.29$ is an intriguing result. Extensive studies (13,16,17) concluded that in systems with a non-conserved order parameter, the recovery of long range order at long times follows a diffusive process with $\beta = 0.5$. Subdiffusive

behavior, indicated by $\beta < 0.5$, is a manifestation of restricted microscopic motion of the system and suggests that the dynamics are constrained by additional conserved quantities.

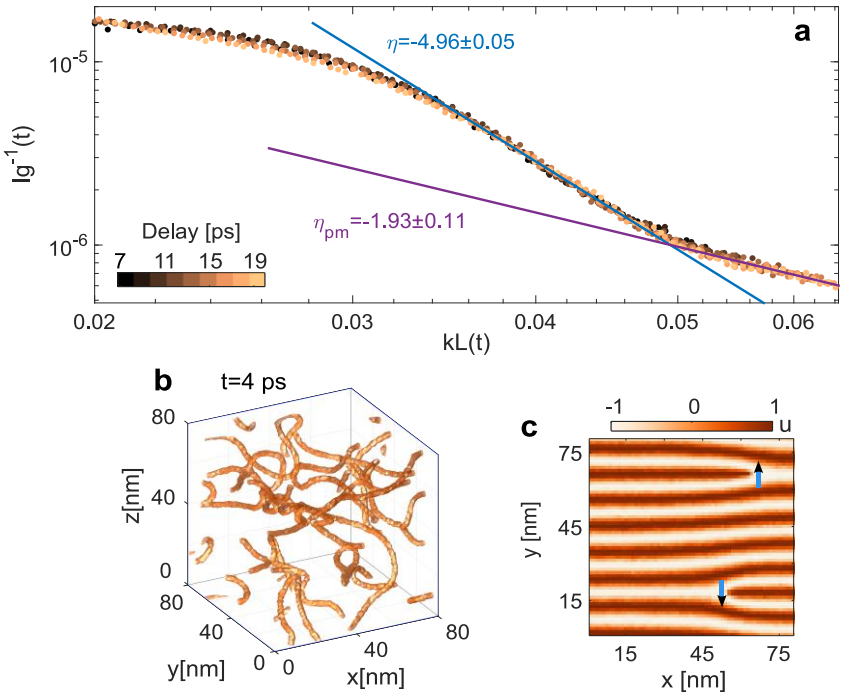

Fig. 2. ***(a)***: *Data collapse of the $LaTe_3$ CDW Bragg peak intensity at various delays to the universal function $Ig^{-1}(t)=F[kL(t)]$ (12,13), for $kL(t)>0.02Å^{-1}$. The data shows an asymptotic power law of $\sim k^{-5}$ (blue solid line), a clear signature of vortex strings (18). At larger kL(t) the power law changes to $\sim k^{-2}$ (purple solid line) which is typical to phase fluctuations of the CDW (16).* ***(b)***: *Ginzburg-Landau simulation (12) of a complex order parameter, $\psi(x, t)$, in three spatial dimensions following a sudden quench to the low symmetry potential energy. The isosurface plot of $|\psi(x, t)|^2 = 0.5$, 4 ps after the quench, shows that the initial random configuration quickly breaks down into topological vortex strings.* ***(c)***: *Illustration of a CDW lattice distortion on a single plane at a delay of 22 ps. Two vortices with opposite winding numbers correspond to two dislocations of the CDW with opposite Burgers vectors (19), indicated by blue arrows.*

Our scaling analysis of the diffuse scattering's asymptotic wavevector behavior reveals compelling evidence that photoinduced topological vortex strings (18), which are dislocations of the CDW, dominate the coarsening process (Fig. 2). The subdiffusive behavior is likely a signature of the restricted mobility of these dislocations (20,21).Our results constitute a clear measurement of photoinduced topological defects of the prototypical CDW in LaTe3 on ultrafast time scales. We show that shortly after photoexcitation the evolution of the highly nonequilibrium state is dominated by vortex strings. The observed subdiffusive dynamics is indicative of the strings' restricted mobility, which crucially impacts the system's thermalization and broken ergodicity. Our methods as well as the implications of our findings extend well beyond LaTe3, as formation of topological defects is expected to be ubiquitous in symmetry breaking phase transitions under nonequilibrium conditions (10, 11). Thus, the high resolution XFEL measurements, combined with scaling and data collapse analysis, establish an incisive approach to probe the mesoscopic, out-of-equilibrium behavior of intertwined orders in quantum materials.

References

[1] D. N. Basov, R. D. Averitt, D. Hsieh, *Nature Materials* **16**, 1077 (2017).
[2] J. Ravnik, *Nature Communications* **12**, 2323 (2021).
[3] L. Stojchevska, *Science* **344**, 177 (2014).
[4] A. Kogar, *Nature Physics* **16**, 159 (2020).
[5] S. Wandel, *Science* **376**, 860 (2022).
[6] S. Wall, *Science* **362**, 572 (2018).
[7] A. Zong, *Nature Physics* **15**, 27 (2019).
[8] F. Schmitt, *Science* **321**, 1649 (2008).
[9] Y. Wang, *Nature* **606,** 896 (2022).
[10] T. W. B. Kibble, *Journal of Physics A: Mathematical and General* **9**, 1387 (1976).
[11] W. H. Zurek, *Nature* **317**, 505 (1985).
[12] M. Mondello, N. Goldenfeld, *Physical Review* A **45**, 657 (1992).
[13] A. J. Bray, A. D. Rutenberg, Physical Review E **49**, R27 (1994).
[14] G. Ingold, *Journal of Synchrotron Radiation* **26**, 874 (2019).
[15] E. Prat, *Nature Photonics* **14**, 748 (2020).
[16] G. F. Mazenko, M. Zannetti, Physical Review B **32,** 4565 (1985).
[17] S. Vogelgesang, *Nature Physics* **14,** 184 (2018).
[18] A. J. Bray, K. Humayun, Physical Review E **47,** R9 (1993).
[19] F. Nabarro, *Oxford University Press* (1967).
[20] M. Pretko, L. Radzihovsky, Physical Review Letters **120,** 195301 (2018).
[21] A. Gromov, A. Lucas, R. M. Nandkishore, *Physical Review. Research* **2**, 033124 (2020).

* Acknowledgement(s): We acknowledge the Paul Scherrer Institute, Villigen, Switzerland for provision of free-electron laser beamtime at the Bernina instrument of the SwissFEL ARAMIS branch. Funding: G.O., R.A.D, G.A.P.M., Y.H., V.K., D.A.R., and M.T. were supported by the US Department of Energy, Office of Science, Office of Basic Energy Sciences through the Division of Materials Sciences and Engineering under Contract No. DE-AC02-76SF00515. For crystal growth and characterization, A.G.S. and I.R.F. were supported by the Department of Energy, Office of Basic Energy Sciences, under contract DE-AC02-76SF00515. G.O. acknowledges support from the Koret Foundation. R.A.D. acknowledges support through the Bloch Postdoctoral Fellowship in Quantum Science and Engineering from the Stanford University Quantum Fundamentals, Architectures, and Machines initiative (Q-FARM), and the Marvin Chodorow Postdoctoral Fellowship from the Stanford University Department of Applied Physics.

Extreme ultraviolet metaoptics

M. Ossiander[1], H. K. Hampel[2], M. L. Meretska[1], S. W. D. Lim[1]
N. Knefz[2], T. Jauk[2], F. Capasso[1], M. Schultze[2]
[1]*Harvard University, Cambridge, MA 02138 USA*
[2]*Graz University of Technology, 8010 Graz, Austria*

Modern attosecond science and state-of-the-art semiconductor lithography require extreme ultraviolet (EUV) light. However, the unavailability of optics for this spectral regime halts progress. Here, we realize the first metalenses for EUV radiation with 50 nm vacuum wavelength, which is less than a quarter of the current low wavelength cutoff of dielectric metasurfaces. The technology constitutes the first universal approach for achieving EUV optics, and devices can be manufactured using only semiconductor-foundry-compatible processes. To achieve the EUV metaoptics, we exploit that holes etched in a Silicon membrane have a considerably higher index (n = 1) than the surrounding Silicon (n = 0.77), allowing us to guide light and shift the phase of transmitted EUV radiation by varying the diameter of the holes. To design a metalens, we first digitize the phase profile of an aspheric lens and then match the required position-dependent transmission phase with the correct hole diameter.Via electron beam lithography and reactive ion etching, we fabricated a metalens with 10 mm focal length and 1 mm diameter from the device layer of a Silicon on insulator wafer. Fig. 1a shows a light image of the final optics. To characterize this metalens, we generated EUV radiation using high-harmonic generation and focused the 21st harmonic of the driving laser (49 nm wavelength). Fig. 1b presents the waist evolution of the focused EUV light beam using a knife-edge measurement. Focusing by the metalens is proved by the clear beam size minimum along the propagation direction.

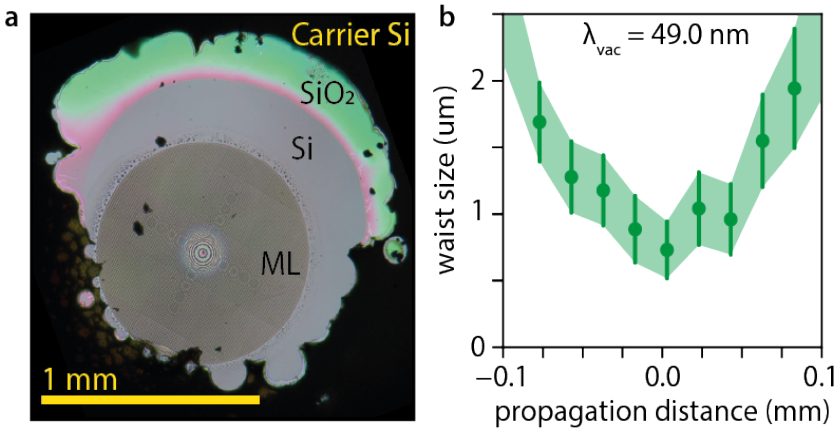

Fig. 1. *Experimental knife-edge characterization of a meta-lens focusing extreme ultraviolet light.* ***a)*** *Light microscope picture of a fabricated metalens (ML, focal length f = 10 mm, optics diameter 1 mm, λ_{vac} = 49 nm).*
b) *Position-dependent waist size (**green dots**) of the metalens-focused light beam around the focus located at z = 0 mm. The error bars mark 95% confidence.*

The meta-lens achieves a minimum beam waist of $w_0^{metalens}$ = (0.7 ± 0.3) um, which is only 1.6 times the diffraction limit determined by the nominal lens parameters and the incoming beam profile.

References

[1] M. L. Tseng, M. Semmlinger, M. Zhang, C. Arndt, T.-T. Huang, J. Yang, H. Y. Kuo, V.-C. Su, M. K. Chen, C. H. Chu, B. Cerjan , D. P. Tsai P. Nordlander. N. J. Halas. *Science Advances* **8**. 5644 (2022).
[2] Y. Deng, X. Wang, Z. Gong, K. Dong, S. Lou, N. Pégard, K. B. Tom, F. Yang, Z. You, L. Waller, J. Yao, *Advanced Materials* **30**, 1802632 (2018).
[3] K. Huang, J. Deng, H. S. Leong, S. L. K. Yap, R. B. Yang, J. Teng, H. Liu, *Laser Photonics Review* **13**, 1800289 (2019).
[4] C. Zhang, S. Divitt, Q. Fan, W. Zhu, A. Agrawal, Y. Lu, T. Xu, H. J. Lezec, *Light Science Applications* **9**, 55 (2020).

Using heterostructure engineering to tailor Two-photon absorption in nanomaterials

A. Alo, C.A. Sousa, J.C. Lemus, L.A. Padilha
Instituto de Fisica "Gleb Wataghin", Campinas, SP 13083, Brazil

Significant advances on synthesis methods and on the understanding of the photo-physics in colloidal semiconductor nanocrystals (NCs) have been achieved in the last decades. By controlling shape, composition, dimensions, and even by heterostructure engineering, now a days, it is possible to control multi-exciton, electron-phonon, and light-matter interactions to unprecedented levels. All these advances have allowed these NCs to move from laboratories bench top to real world applications, including luminescent solar concentrators, LEDs, among others. Within the several interesting properties presented by these quantum-confined materials, their nonlinear optical response has been subject of intense study in the last two decades. Much of the initial studies of nonlinear absorption and nonlinear refraction in NCs has been fueled by predictions of quantum confinement induced enhancement of the oscillator strength for nonlinear optical transitions in semiconductors [1-2]. Nevertheless, as it has been shown for a number of different nanomaterials,[3-5] quantum confinement does not enhance the overall nonlinear optical response of semiconductors because, despite the fact that the oscillator strength of a given nonlinear optical transition is enhanced due to quantum confinement, this results also on a drastic reduction on the density of states, spoiling the expected enhancement. [3, 6] In fact, considering NCs with confinement on all three directions (called here quantum dots), it has been shown that two-photon absorption (2PA) cross-section grows linearly with the QD volume and, at least for visible emitting nanomaterials, the trend seems to be independent of the composition, forming a universal volume scaling. [5] A consequence of this direct dependence of the 2PA cross-section on the QD volume (and radius) is that increasing the 2PA cross-section is directly associated with increasing the QD size, resulting on a red-shift of the NC bandgap. One way to reduce the coupling between 2PA cross-section and the NC bandgap energy is to change the nanomaterial shape. For example, in nanorods type of NCs, one can increase the 2PA cross-section by changing their length, while the bandgap energy is defined by the NC diameter. [6] Nevertheless, elongated nanostructures are typically less stable than their spherical counterparts, and the questions that arises is how much one can decouple the magnitude of the 2PA cross-section and the emission wavelength for spherically shaped NCs, by band structure engineering. Motivated by this, here we investigate the influence of different heterostructures on the 2PA cross-section of CdSe-based core/shell quantum dots. To do so, we have studied the 2PA cross-section for series of type-I CdSe/CdZnS, quasi-type-II CdSe/CdS, and core only CdSe QDs. Our results indicate that the volume dependence of the 2PA cross-section in core/shell heterostructures differs from that of core only QDs and follow a sublinear dependence on the total nanoparticle volume. Fig. 1a shows how the 2PA cross-section depends on the NC volume for a series of type-I CdSe/CdZnS NCs and two series of quasi-type-II CdSe/CdS.

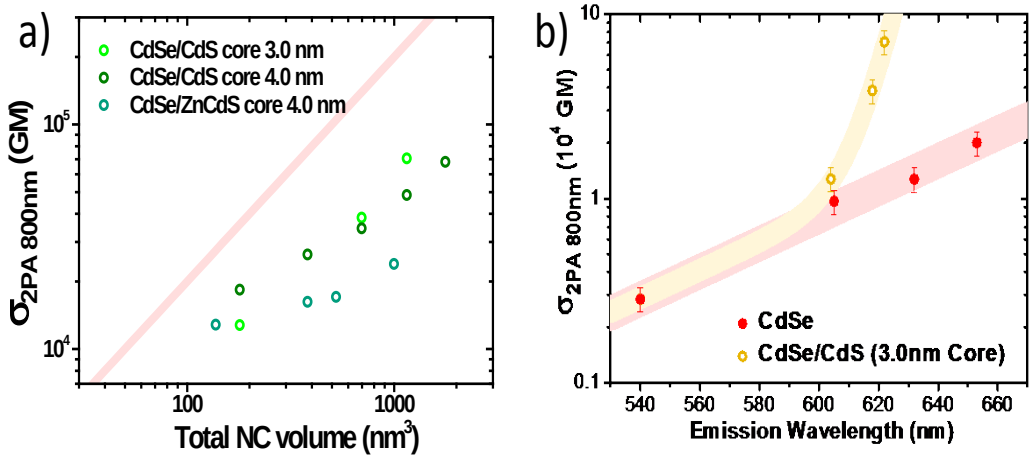

Fig. 1. a) *2PA cross section measured at 800 nm for three series of heterostructured CdSe-based NCs. The line represents the volume dependence of the 2PA cross-section at 800 nm for core only CdSe QDs.* ***(b)*** *2PA cross section as a function of the emission wavelength for quasi-type-II CdSe/CdS NCs compared to core only CdSe QDs.*

For each series, the core diameter is kept constant and the shell thickness is changed. It is interesting to note that for all series, for a given total volume, the 2PA cross-section is smaller for the heterostructures than for core only. This is a result of the reduced density of final states in core/shell nanoparticles when compared to core only systems. Furthermore, when comparing different types of core/shell structures with thick shell, one can see that the 2PA cross section reaches the largest values for the quasi-type-II system with smaller core. Reducing the core size favors the NC's band structure to be aligned as a type-II system. Consequently, our data suggests that, for NCs containing thick shells, the more the type-II aspect of the band alignment the larger the 2PA cross section. Finally, Figure 1b compares the 2PA cross section as a function of the wavelength of the peak emission for core only and the series of quasi-type-II with 3.0 nm core. One can see that, by employing engineered NCs it is possible to enhance the 2PA cross section by almost one order of magnitude without drastically shifting the emission wavelength.

In conclusion, our results indicate a clear path to decouple the magnitude of 2PA cross-section from the emission properties of semiconductor NCs. Despite the bandgap engineered NCs do not show 2PA cross-section larger than for core only systems, they offer a solution for two-photon absorption on demand, in which one is able to obtain high two-photon absorbing NCs without paying the price of drastically changing the emission spectra

.

References

[1] S. Schmitt-Rink, D. Miller, D.S. Chemla, *Physical Review B* **35**, 8113 (1987)

[2] P. Roussignol, D. Ricard, C. Flytzanis, *Applied Physics B* **51**, 437 (1990).

[3] L.A. Padilha, J.Fu, D.J.Hagan, E.W.Van Stryland, C.L.Cesar, L.C.Barbosa, C.H.B.Cruz, D.Buso, AMartucci, *Physical Review B* **75** 075325 (2007)

[4] N.S. Makarov, P.C. Lau, C. Olson, K.A. Velizhanin, K. M. Solntsev, K. Kieu, S. Kilina, S. Tretiak, R.A. Norwood, N. Peyghambarian, *ACS Nano* **8**, 12572 (2014)

[5] G. Nagamine, J.O. Rocha, L.G. Bonato, A.F. Nogueira, Z. Zaharieva, A.A. Watt, C.H. de Brito Cruz, L.A. Padilha, *Journal Physical Chemistry Letters* **9**, 3478 (2018)

[6] M. Allione, A. Ballester, H. Li, A. Comin, J.L. Movilla, J.I. Climente, L. Manna, I. Moreels, *ACS Nano* **7**, 2443 (2013).

* Acknowledgement: This work has been funded by the Sao Paulo Research Foundation (FAPESP)under the grants 2018/15574-6, 2018/25339-4, 2019/22823-5.

Spin and charge current dynamics in Spintronic THz emitters

E. Th. Papaioannou[2], B. Das-Mohapatra[1], N. Kanistras[1],T. Kehagias[2], G Schmidt[1]
[1] *Martin-Luther University Halle-Wittenberg, 06120 Halle, Germany*
[2] *Aristotle University of Thessaloniki, 54124 Thessaloniki, Greece*

Ultrafast spin-to-charge conversion in heterostructures composed of ferromagnetic (FM)/non-magnetic (NM) thin films can give rise to the emission of THz electromagnetic waves [1]. The experimental scheme involves the use of femtosecond (fs) laser pulses to trigger ultrafast spin and charge dynamics in FM/NM bilayers, where the NM layer features a strong spin-orbit coupling. Via the inverse spin Hall effect (ISHE), the spin current generated in the FM layer by the fs-laser pulse is converted to an ultrashort charge current burst that gives rise to the THz radiation. In this presentation, we explore the potential of spintronic THz emitters (STE) for stronger THz radiation and adjustable bandwidth by studying the spin and the subsequent charge current dynamics after the laser illumination. We first show the influence of the FM/NM interface engineering on the strength of the spin current, Figure 1a). We grow Fe/Pt bilayers and we induce at the interface the $L1_0$-FePt alloyed phase. Our findings show that the presence of 1-2 nm thick $L1_0$-FePt interlayer promotes the interface transmission of the spin current and amplifies the THz emission [2]. The unique result of the increased THz emission in Fe/$L1_0$-FePt/Pt structure opens new perspectives in the direction of application of spintronic THz emitters. Next, we reveal that not only the spin current dynamics but also the charge redistribution is important for the properties of the THz signal. The charge relaxation leads to a current backflow with a delay and a time constant that mainly depends on the conductivity and the dielectric properties of the emitter Figure b) [3]. We show that to extract and quantify the spin current from the detected THz signal we need to take into consideration the charge redistribution in the spintronic layers [3].

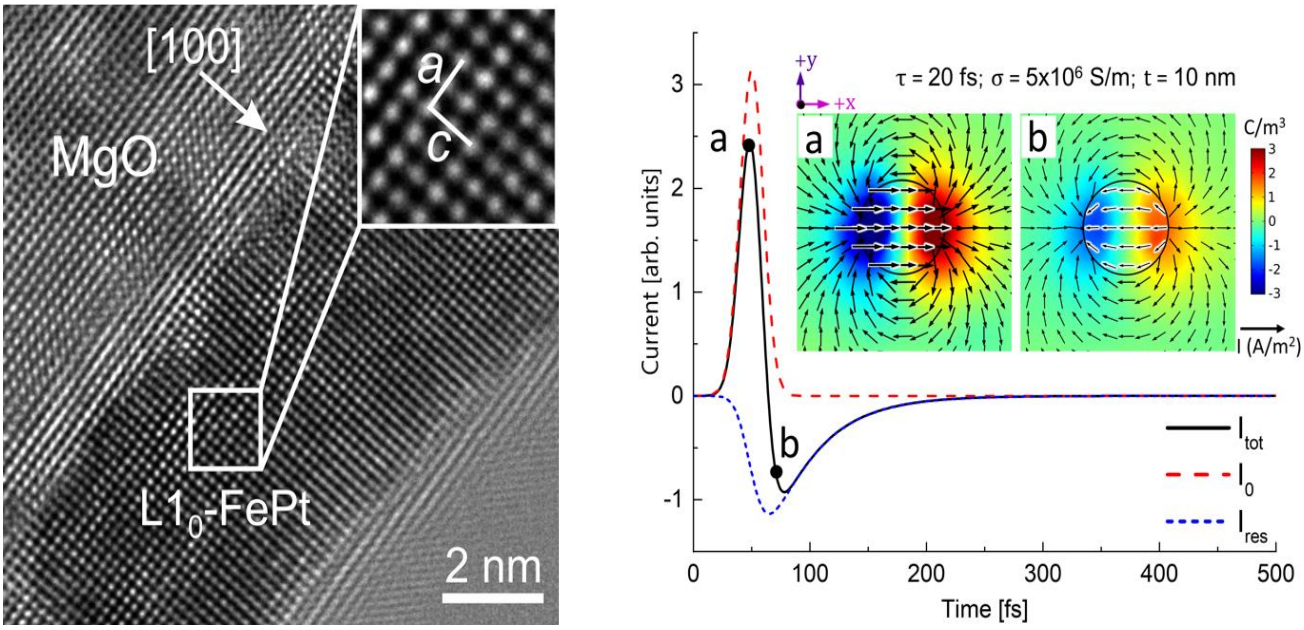

Fig. 1. a)*: Cross-sectional high-resolution transmission electron microscopy of a Fe/L10-FePt/Pt trilayer with a few monolayers thickness. The structure promotes the THz emission after fs-laser illumination.* ***b)****: Current over time for the original excitation pulse I_0 (**dashed red**), the total current I_{tot} (**solid black**) and the response of the system I_{res} (**dotted blue**) for a 10 nm thick spintronic THz emitter.* ***Insets*** *show the current and charge distribution at two different times, respectively, marked a and b in the black curve.*

We further discuss how the ultrafast charge redistribution accounts for significantly changes of profile in time of the THz pulse. We indicate that the time constant of the system reduces the lower frequency part of the spectrum but not the higher frequencies and the corresponding cutoff frequency becomes higher with increasing conductivity of the emitter.

References

[1] E. Th. Papaioannou, R. Beigang, *Nanophotonics* **10,** 1243(2021).
[2] L. Scheuer, M. Ruhwedel, D. Karfaridis, I. Vasileiadis, D. Sokoluk, G. Torosyan, G. Vourlias, G. Dimitrakopoulos, M. Rahm, B. Hillebrands T. Kehagias, R. Beigang, E.Th. Papaioannou, *iScience* **25**, 104319, (2022).
[3] G. Schmidt, B. Das-Mohapatra, E. Th. Papaioannou, *Physical Review Applied* **19**,L041001 (2023).

Revealing the pseudospin texture of Dirac states using Circular dichroism in photoemission

E. Papalazarou, J. Zhang, Z. Chen, N. Nilforoushan, M. Marsi
Université Paris-Saclay , 91405 Orsay, France

Angle-resolved photoemission spectroscopy (ARPES) is an indisputable tool to have an insight into the quantum properties of materials using polarized light. For instance, using circularly polarized light (CPL) one can retrieve dichroic photoelectron intensity maps that reflect the material's electron chirality and the pseudospin properties. Moreover, when the latter is combined with time-resolution it can provide unprecedented insights of out-of-equilibrium states. In the present work, we focus our attention on quasi two-dimensional materials bounded to Dirac surface states. We perform a comparative study of the momentum transfer from polarized low-energy photons to Dirac surface states in various Dirac compounds such as Bi_2Se_3, Bi_2Te_2Se and $BaNiS_2$. Analysis of the circular dichroism (CD) in the photoemission yield of photo-excited Dirac states reveals the spin-vector state. Our experimental approach based on out-of-equilibrium time-of-flight multidimensional ARPES is able to disentangle experimental geometry and matrix element effects allowing extracting qualitatively the pseudospin texture of excited surface states [1]. In the case of the topological insulators Bi_2Se_3 and Bi_2Te_2Se, the analysis of the CD-ARPES evolution as a function of the electron's binding energy from the Dirac point to the bulk conduction band indicates (Fig 1a) that the Dirac surface states of Bi_2Te_2Se present a strong out-of-plane spin polarization compared to those of Bi_2Se_3 [2]. $BaNiS_2$ has generated increasing attention because of its peculiar properties related to the combined effects of crystal field and strong spin-orbit coupling [3, 4], resulting in hidden Rashba-split spin-polarized bands Dirac states. Here, we reveal the orbital character and the spin-texture of the various bulk and surface states (Fig 1b). Moreover, we show that Dirac states can be tuned in momentum space by acting on the charge transfer from hybridized orbitals [5].

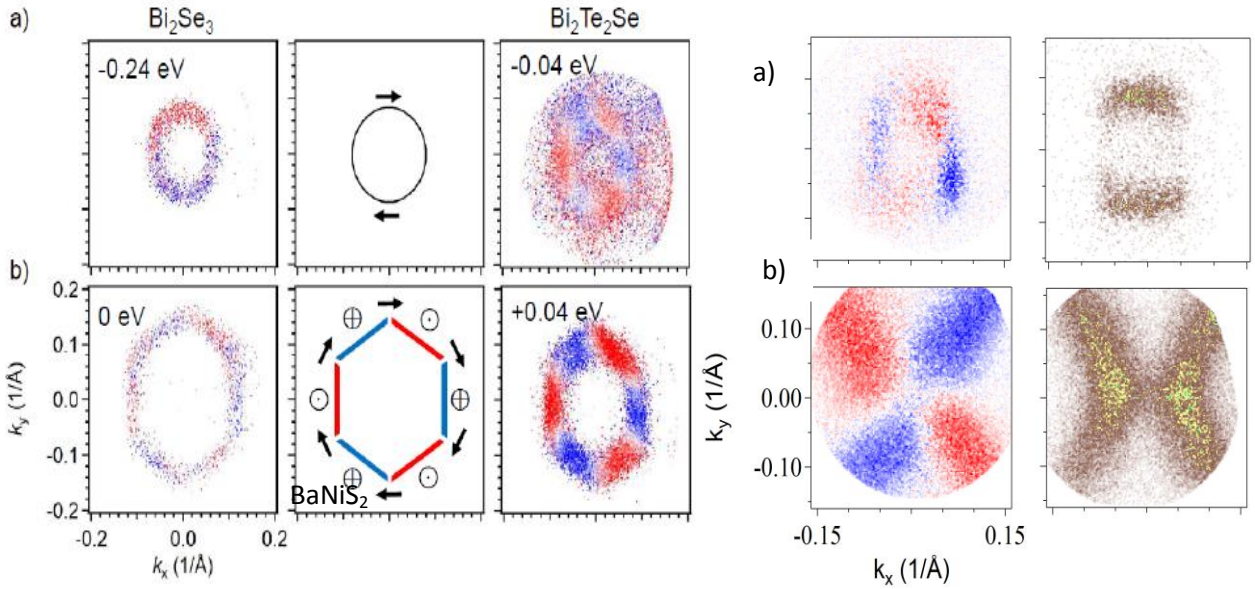

***Fig. 1.a**. Isoenergy contours of Bi_2Se_3 (**left**) and Bi_2Te_2Se (**right**) for energies close to Dirac point using CD and **b**: CD (**left**) and p-polarized (**right**) isoenergy contours of $BaNiS_2$ around Γ.*

Moreover, we show that Dirac states can be tuned in momentum space by acting on the charge transfer from hybridized orbitals [5].

References

[1] Y.H. Wang, D. Hsieh, D. Pilon, L. Fu, D.R. Gardner, Y.S. Lee, N. Gedik, *Physical Review Letters*, **107**, 207602 (2011).
[2] J. Zhang, J. Caillaux, Z. Chen, M. Konczykowski, A. Hruban A. Wołoś, A. Materna, L. Perfetti E. Papalazarou, M. Marsi, *Journal of Electron Spectroscopy and Related Phenomena*, **253**, 147125 (2021).
[3] D. Santos-Cottin, M. Casula, G. Lantz, Y. Klein, L. Petaccia, P. Le Fèvre, F. Bertran, E. Papalazarou, M. Marsi, A. Gauzzi, *Nature Comm*unications **7**, 11258 (2016).
[4] N. Nilforoushan, M. Casula, A. Amaricci, M. Caputo, J. Caillaux, L. Khalil, E. Papalazarou, P. Simon, L. Perfetti, I. Vobornik, P.K. Das, J. Fujii, A. Barinov, D. Santos-Cottin, Y. Klein, M. Fabrizio, A. Gauzzi, M. Marsi, *Proceedings National Academy of Sciience*. **118**, e2108617118, (2021).
[5] J. Zhang, Z. Chen, J. Caillaux, Y. Klein, A. Gauzzi, A. Bendounan, A. Taleb-Ibrahimi, L. Perfetti, E. Papalazarou, M. Marsi. *Europen Phyical Journal Special Topics* (2022). https://doi.org/10.1140/epjs/s11734-022-00746-9.
* Acknowledgement(s): authors (E. Papalazarou, M. Marsi) acknowledge support from "Investissement d'avenir Labex Palm" (Grant No. ANR-10-LABX-0039-PALM.

Imaging the constituent electron and hole of a Moiré localized interlayer exciton

O. Karni[1], E. Barré[2,], V. Pareek[3], J. D. Georgaras[1], M. K. L. Man[3], C. Sahoo[3], D. R. Bacon[3], X. Zhu[3]
H. B. Ribeiro[1], A. L. O'Beirne[1], J. Hu[1], A. Al-Mahboob[3], M. M. M. Abdelrasoul[3], N S. Chan[3]
A. Karmakar[3], A. J. Winchester[3], B. Kim[4], K. Watanabe[5], T. Taniguchi[5], K. Barmak[4], J. Madéo[3]
F. H. da Jornada[1], T F. Heinz[1], K. M. Dani[3]
[1]*Stanford University, Stanford, CA 94305, USA*
[2]*SLAC, Menlo Park, CA 94025, USA*
[3]*Okinawa Institute of Science and Technology, Onna-son 904-0495, Japan*
[4]*Columbia University, New York, NY 10027, USA*
[5]*Naional Institute for Material Science, Tsukuba 305-0044, Japan*

Heterostructure made by stacking two distinct van der Waals monolayer (1L) semiconductors, such as transition metal dichalcogenides (TMDCs, e.g., MoS_2), has attracted attention owing to their novel and tunable optoelectronic properties[1]. One of these properties includes hosting interlayer excitons (ILXs) such that electrons in one layer are bound to holes in another layer of the heterostructure by coulomb interaction. This results in the ILXs having long lifetimes, making them an attractive platform to study many-body exciton physics and various device applications. On top of that, the two 1L semiconductors in the heterostructure can be put together with a small twist angle between them, giving rise to moiré superlattices that modulate its electronic structure and various novel phenomena such as superconductivity. However, a deeper understanding of the properties of ILXs, such as their size, valley configuration, and the effect of the moiré confinement, is still largely lacking. Several optical spectroscopic studies on various heterostructure systems provide only partial information regarding the nature of ILXs[2–4]. For instance, optical studies can access only a limited portion of the momentum distribution of the ILX and thus cannot provide complete information about its size or valley configuration reliably. One must access the full momentum space distribution of its constituent-bound electrons and holes for a complete understanding.

Recently, our group was able to directly image the size of the excitons in 1L WSe_2 by capturing the momentum distribution of the exciton-bound electrons through time-resolved and angle-resolved photoemission spectroscopy (Tr-ARPES)[5,6].

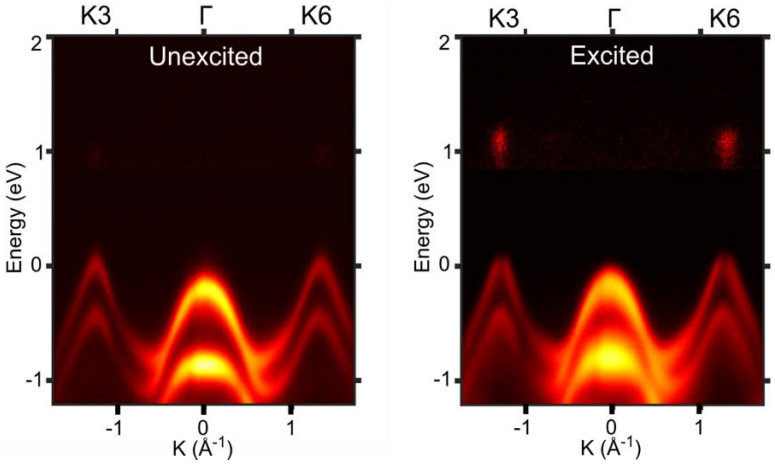

Fig. 1. Left: *Unexcited band structure of WSe_2/MoS_2 heterostructure.*
Right*: Interlayer exciton at 25ps time delay following 1.67eV excitation.*

However, capturing the momentum distribution of the exciton-bound holes has not been possible so far. In this talk, I will discuss our recent study on ILXs in WSe_2/MoS_2 heterostructure using Tr-ARPES[7]. I will discuss the advancement made by our group in resolving the momentum distribution of the ILX's electrons and its constituent holes. I will also discuss the impact of moiré potential on the ILX and show that one does not require a large moiré lattice to confine ILXs, contrary to the current assumptions.

References

[1] P. Rivera, H. Yu, K. L. Seyler, N. P. Wilson, W. Yao, X. Xu, *Nature Nanotechnology* **13**, 1004 (2018).
[2] K. Tran, G. Moody, F. Wu, X. Lu, J. Choi, K. Kim, A. Rai, D. A. Sanchez, J. Quan, A. Singh, J. Embley, A. Zepeda, M. Campbell, T. Autry T. Taniguchi, K. Watanabe, N. Lu, S. K. Banerjee, K. L. Silverman, S. Kim, E. Tutuc, L. Yang, A. H. MacDonald, X. Li, *Nature* **567**, 71 (2019).
[3] K. L. Seyler, P. Rivera, H. Yu, N. P. Wilson, E. L. Ray, D. G. Mandrus, J. Yan, W. Yao, X. Xu, *Nature* **567**, 66 (2019).
[4] O. Karni, E. Barré, S. C. Lau, R. Gillen, E. Y. Ma, B. Kim, K. Watanabe, T. Taniguchi, J. Maultzsch, K. Barmak, R. H. Page, T. F. Heinz *Physical Review Letters.* **123**, 247402 (2019).
[5] M. K. L. Man, J. Madéo, C. Sahoo, K. Xie, M. Campbell, V. Pareek, A. Karmakar, E. L. Wong, A. Al-Mahboob, N. S. Chan, D. R. Bacon, X. Zhu, M. M. M. Abdelrasoul, X. Li, T. F. Heinz, F. H. da Jornada, T. Cao, K. M. Dani, *Science Advances* **7**, eabg0192 (2021).
[6] J. Madéo, M. K. L. Man, C. Sahoo, M. Campbell, V. Pareek, E. L. Wong, A. Al-Mahboob, N. S. Chan, A. Karmakar, B. M. K. Mariserla, X. Li T. F. Heinz, T. Cao, K. M. Dani, *Science* **370**, 1199 (2020).
[7] O. Karni, E. Barré, V. Pareek, J. D. Georgaras, M. K. L. Man, C. Sahoo, D. R. Bacon, X. Zhu, H. B. Ribeiro, A. L. O'Beirne, J. Hu A. Al-Mahboob, M. M. M. Abdelrasoul, N. S. Chan, A. Karmakar, A. J. Winchester, B. Kim, K. Watanabe, T. Taniguchi, K. Barmak, J. Madéo F. H. da Jornada, T. F. Heinz, and K. M. Dani, *Nature* **603**, 247 (2022).

The role of current fluctuations in the creation of Light-matter entanglement

G. Passetti[1], C. J. Eckhardt[2] , C. S. Weber[3]
M. Claassen[3], M. A. Sentef[4], D. M. Kennes[1]
[1] *Aachen University, 52056 Aachen, Germany*
[2] *Max Planck Institute for the Structure and Dynamics of Matter, 22761 Hamburg, Germany*
[3] *University of Pennsylvania, Philadelphia, PA 19104, USA*
[4] *University of Bristol, Bristol BS8 1TL, United Kingdom*

Driving quantum materials is a promising route for potential future applications in the engineering of quantum properties, such as superconductivity and topologically protected edge states [1].
First, we are going to discuss how to control superconducting properties in ultrafast transient phenomena [2, 3] by the transient steering of symmetries. Then we will switch gears and discuss potential routes to manipulate quantum properties in the emerging field of cavity quantum electrodynamics. The latter aims at controlling material properties via the coupling with the quantized photon modes in a cavity. Through the hybridization of light and matter we explore to which extent it is possible to tailor properties of extended solids, realizing what was coined "cavity quantum materials" [4, 5]. The entanglement entropy between light and matter is a direct measure of the degree of hybridization, but a clear understanding on what are the necessary conditions for this to be generated in the emergent field of cavity coupled band electrons [6, 7, 8] is still missing. We consider a paradigmatic model of interacting spinless fermions coupled with the first resonant mode of a cavity. We derive an analytic expression, exact in the cavity high frequency limit, that relates the cavity-matter entanglement to the quantum fluctuations of the current operator.
This relation establishes that the presence of such fluctuations is a necessary condition for non-zero light-matter entanglement. Furthermore, we solve numerically *exactly* the model, showing that the qualitative behavior predicted by our analytic expansion holds in a wide range of parameters.
We also discuss problematic aspects of mean field approaches to this model- Fig. 1.

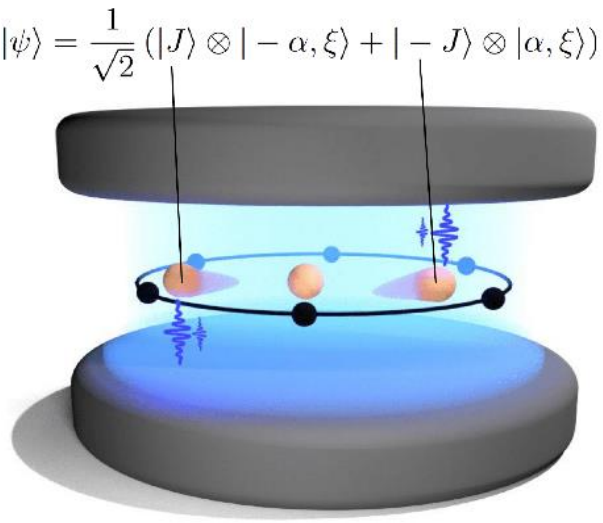

Fig. 1. *Cartoon picture of the mechanism generating light-matter entanglement, a superposition of Bloch states is responsible for the insurgence of entanglement between light and matter degrees of freedom.*

The results presented in this work are expected to hold in more general settings than the particular model discussed, providing a first fundamental condition for the realization of true light-matter hybridized band electrons in a cavity [9].

References

[1] A. de la Torre, D. M. Kennes, M. Claassen, S. Gerber, J. W. McIver, M. A. Sentef, *Review of Modern Physics* **93**, 041002 (2021).
[2] M. Claassen, D. M. Kennes, M. Zingl, M. A. Sentef, A. Rubio, *Nature Physics.* **15**, 766-770 (2019).
[3] C. S. Weber, S. Gassner, D. M. Kennes, M. Claassen, (to be submitted).
[4] F. Schlawin, D. M. Kennes, M. A. Sentef, *Applied Physics Reviews* **9**, 011312 (2022).
[5] A. Frisk Kockum, A. Miranowicz, S. De Liberato, S. Savasta, F. Nori, *Nature Review Physics* **1,** 19 (2019).
[6] F. Schlawin, A. Cavalleri, D. Jaksch, *Physical Review. Letters* **122**, 133602 (2019).
[7] H. Gao, F. Schlawin, M. Buzzi, A. Cavalleri, D. Jaksch, *Phyical Review Letters* **125**, 053602 (2020).
[8] A. Chakraborty, F. Piazza, *Physical Review Letters* **127**, 177002 (2021).
[9] G. Passetti, C. J. Eckhardt, M. A. Sentef, D. M. Kennes, *a*rxXiv: 2212.03011 (2022).

Using ultrafast disorder to control a Photo-induced phase transition

A. S. Johnson[1], E. Pastor[2], S. B. Porro[3], H. Benzidi[4], T. Katayama[5], G, A. de la Peña Muñoz[6], V. Krapivin[6]
N. López[4], M. Trigo[6], S. E. Wall[7]
[1] *IMDEA Nanoscience, 28049 Madrid, Spain*
[2] *Université de Rennes, 35000 Rennes, France*
[3] *ICFO—Institut de Ciencies Fotòniques, 08860 Castelldefels, Barcelona, Spain*
[4] *Institute of Chemical Research of Catalonia, 43007 Tarragona, Spain*
[5] *Japan Synchrotron Radiation Research Institute, Hyogo 679-5198, Japan.*
[6] *SLAC - National Accelerator Laboratory,Menlo Park, CA 94025, USA.*
[7] *Aarhus University, 8000 Aarhus, Denmark*

A solid can exist in different crystal forms with unique chemical and physical properties. Interchange between such forms or polymorphs is known as a solid-solid phase transition and is a ubiquitous process in nature that can be induced by changes in temperate and pressure. From a technological viewpoint, the capacity to stabilise solid phases is paramount to harness their properties and generate new applications. Indeed, control over how solids transform is central for the development of energy conversion or high-speed data storage technologies. For example, phase control is essential to guarantee the stability of high performing solar cells and is an integral part of the mechanism of different non-volatile electronics [1]. Light excitation offers an alternative way to pressure and temperature to control a phase transition by exploring non-equilibrium dynamics. In this framework, the excitation of the solid in one of the phases can launch coherent motion of atoms in multiple unit cells [2, 3]. Re-excitation of the sample alongside the period of the relevant vibrational modes that connect the two phases can potentially modulate the energy required to drive the transition. Recently ground-breaking studies have shown that phase transitions in low-dimensional systems can be coherently controlled [4,5]. Inspired by the demonstration of coherent control of solids, herein we explore routes to control the solid-solid phase transition in (3D) VO_2, a prototypical material that undergoes an insulator to metal transition accompanied by a dramatic change in structure from monoclinic to rutile. We perform double pump experiments in which one laser beam weakly interacts with the sample to generate an excited monoclinic state and launch coherent phonons. Subsequently a second laser beam re-excites the sample (Fig 1). We assess how the dividing the total energy between the two pulses affects the energy required to initiate the phase transition, namely the transition's fluence threshold.

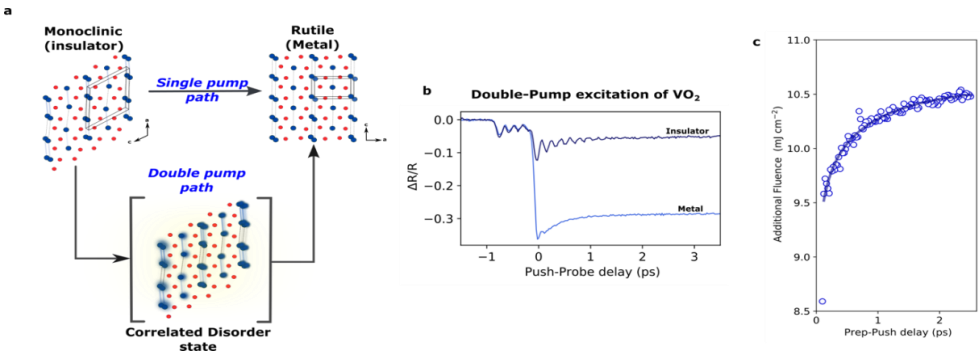

Fig.1*.(**a**)Representation of the VO_2 structure and the transformation pathways we monitor.*
(b) *Double pump experiment and* ***(c)*** *the reduction in the fluence threshold as a function of the delay between the two excitation pumps*
.

We find that we are unable to exert coherent control over the sample and observe that, despite a measurable coherent phonon signal, the fluence threshold does not oscillate with the phonon response. However, our data reveals a large incoherent decrease in the fluence threshold at early times. No effect is observed at long times. To understand this effect, we conducted time-resolved diffraction measurements at the SACLA XFEL to monitor Bragg and diffuse scatter simultaneously. Our results, indicate that excitation of the monoclinic structure results in the population of incoherent phonons within 50fs that manifest as specific 2D patterns of the diffuse scatter. These data, alongside DFT calculations, suggest that photoinduced correlated disorder can provide a path to control the phase transition. In this presentation I will discuss the supporting data and observations and its possible implications in our ability to control solids on demand.

References

[1] T. Y. Teo, X. Ma, E. Pastor,H. Wang, J.K. George, J.K.W. Yang, S. Wall, M.Miscuglio, R.E. Simpson, V.J.Sorger, *Nanophotonic* **11**, 4073 (2022)
[2] A.S. Johnson, D. Moreno-Mencía E.B. Amuah, M. Menghini, J.-P. Locquet, C. Giannetti, E. Pastor, S.E. Wall,. *Physical Review Letters* **129** 255701 (2022).
[3] E. Pastor, D. Moreno-Mencía, M. Monti, A.S. Johnson, N. Fleischmann, C. Wang, Y. Shi, X. Liu, D.G. Mazzone, M.P.M Dean, S. Wal, *Physical. Review.* B, **105**, 064409 (2022).
[4] J.G. Horstmann, H. Böckmann, B. Wit, F. Kurtz, G. Storeck, C. Ropers, *Nature* **583**, 232 (2020).
[5] J. Maklar, S. Dong, J. Sarkar,Y.A. Gerasimenko, T. Pincelli, S.Beaulieu, P.S.Kirchmann, J.A. Sobota, S.-L. Yang, D. Leuenberger, R.G Moore Z.-X.Shen, M. Wolf, ,D. Mihailovic, R. Ernstorfer,L. Rettig, *arxiv.org/abs/2206.03788* (2022)..

Tomography of light–controlled Superconductivity by using Phase and amplitude of two THz E&M pulses

I. E. Perakis
University of Alabama at Birmingham, Birmingham, AL 35294-1170, USA

Quantum Science relies on correlations between elementary excitations. These correlations are measured imperfectly with existing experimental tools. Multi-dimensional Coherent Terahertz (THz-MDCS) spectroscopy is a new tool when studying quantum materials. It allows sensing of the changes in the collective modes arising from nonlinear couplings and THz driving of coherence and high-order correlation in ways not seen in conventional materials. However, establishing this experimental technique in correlated condensed matter systems such as superconductors and topological materials requires solving a non-equilibrium many-body problem that spans across several fields of current interest, including light-induced superconductivity, parametric driving of metastable phases, and quantum entanglement of supercurrent qubits. In this talk, I will review the recent theoretical and experimental advancements [1-6] that establish THz multi-dimensional coherent spectroscopy as a quantum correlation tomography tool achieving "super" resolution of highly driven quantum states. In particular, I will show how THz-MDCS monitors directly the field-induced changes in the collective modes that uniquely characterize strongly driven non-equilibrium quantum states not realized close to equilibrium. While conventional THz spectroscopy enables ultrafast time-resolved studies of quantum states of matter, with intense electromagnetic field pulses, several nonlinear excitation pathways can occur. This complicates the interpretation of the conventional one-dimensional pump-probe spectroscopies applied so far in superconductors, as different processes contribute at the same frequencies. By taking advantage of both amplitude and relative phase of two phase-locked THz field pulses to excite a superconductor, I will discuss how to separate in two-dimensional frequency space various light-induced higher order signals from those arising from previously studied pump–probe, four-wave–mixing, high-harmonic generation and Raman processes. The level of imaging and visualization of higher correlation in driven states achieved with THz-MDCS is not possible with conventional single-particle or pump–probe spectroscopy measurements or seen in previously studied conventional materials. I will demonstrate how to create and visualize in this way long-lived light-induced superconductivity states with finite momentum and order parameter phases not seen in equilibrium.

Superconducting materials are being considered for quantum computing, and superconducting quantum bits, or qubits, are the heart of the new technology. One strategy to control supercurrent flows in qubits is to use strong light-wave pulses to accelerate the electrons. I will discuss how this can be achieved via nonlinear quantum transport phenomena resulting from acceleration of superconducting condensates in thin superconducting films by the effective field resulting from the interplay between electromagnetic propagation and nonlinearity. In this way, persistent dynamical symmetry breaking is achieved by THz driving of long-lived finite-momentum-pairing states stabilized well after the THz pulse. I will also discuss how the interplay between such long-lived Cooper pairs with finite momentum with parametric driving of superconductivity by persistent oscillations of the relative phase of the order parameters between electron and hole bands in iron-based superconductors leads to new quantum states characterized by amplitude-phase collective modes that differ drastically from the Higgs and Leggett collective modes. In particular, this parametric driving results in Floquet-like sidebands at twice the Higgs frequency, which have been observed experimentally in iron pnictide superconductors. I will compare iron pnictides with strong inter-band Coulomb interaction with those of BCS multi-band superconductors where intraband Coulomb interactions dominate over inter-band ones to demonstrate the crucial role of the interband interaction. I will present direct experimental evidence of transitions between different non-equilibrium states achieved above a critical THz field that show the breakdown of the conventional susceptibility description of nonlinear responses and Raman processes. I will interpret such experiments in terms of parametric driving of superconductivity by coherent modulation of order parameter amplitude and phase that is controlled experimentally by THz pulse-pairs. The emergence of parametrically-driven superconductivity is witnessed directly by the drastic transition from THz-MDCS spectra dominated by the nonlinear peaks predicted by third-order responses and Raman processes to THz-MDCS spectra dominated by the Higgs peak to a drastically different 2D-frequency profile dominated by high-order nonlinear peaks located at high frequencies. In particular, I will show the emergence of Floquet-like superconducting states witnessed directly through the

development of new THz-MDCS peaks above critical driving. These new high-frequency peaks, absent at low excitation, are located at twice the Higgs mode frequency and dominate over the Higgs mode peaks which are suppressed. Finally, I will discuss the THz-control of soliton non-equilibrium states achieved by tuning THz pulse-pair superconductor excitation.

Parametric Driving of Fe-SC Non-equilibrium State

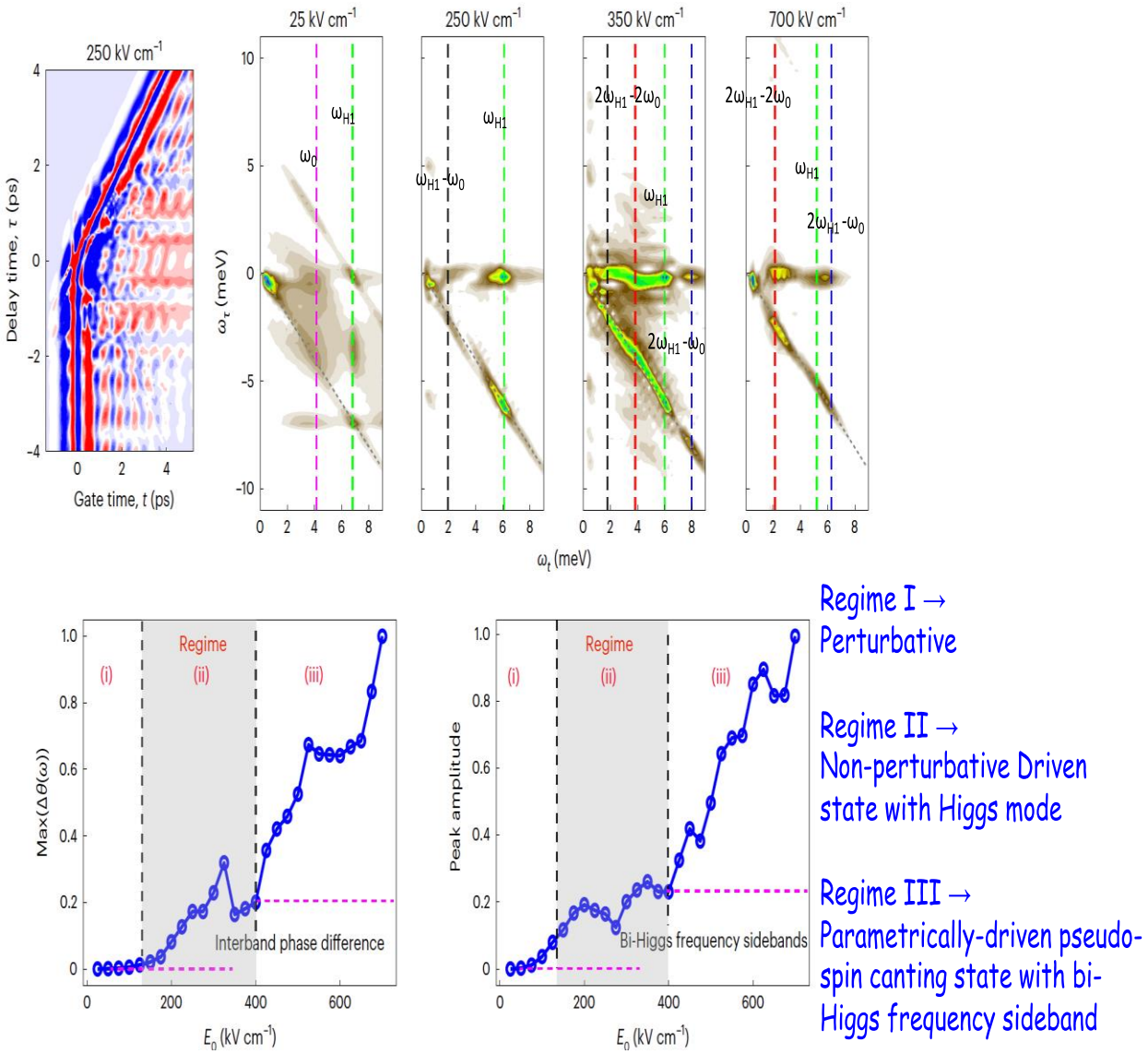

***Fig. 1**. Transition between different driven superconductivity states in iron-based superconductors, characterized by different collective modes controlled by phase coherent THz-pulse-pair excitation (from reference **[1]**)*

In conclusion, the recent application of THz-MDCS to quantum materials provides the basis of a more general quantum tomography tool useful for quantum information science and engineering. This multi-dimensional phase coherent spectroscopy technique enables quantum sensing and control of complex superconducting and topological order parameters controlled by utilizing both the phase and the amplitude of a pair of intense phase-locked THz electromagnetic fields.

References

[1] L. Luo, M. Mootz, J. H. Kang, C. Huang, K. Eom, J. W. Lee, C. Vaswani, Y. G. Collantes, E. E. Hellstrom, I. E. Perakis, C. B. Eom, J. Wang *Nature Physics* **19**, 201(2023) https://doi.org/10.1038/s41567-022-01827-1

[2] M. Mootz, L. Luo, J. Wang, I. E. Perakis *Communications Physics* **5**, (2022).

[3] C Vaswani, J. H Kang, M Mootz, L. Luo, X Yang, C Sundahl, D. Cheng, C. Huang, R. H.J Kim, Z. Liu, Y.G. Collantes, E.E. Hellstrom I. E Perakis, C.B Eom, J. Wang, *Nature Communications* **12**, 258(2021).

[4] C Vaswani, M Mootz, C. Sundahl, D. H. Mudiyanselage, J. H. Kang, X. Yang, D. Cheng, C. Huang, R. H. J. Kim, Z. Liu, L. Luo,I. E Perakis J. Wang, *Physical Review Letters* **124**, 207003 (2020).

[5] M. Mootz, J. Wang, I. E. Perakis, *Physical Review* B **102**, 054517 (2020).

[6] X. Yang, C. Vaswani, C. Sundahl, M. Mootz, L. Luo, J. H. Kang, I. E. Perakis, C. B. Eom, J. Wang, *Nature Photonics* **13**, 707 (2019).

Theoretical and experimental results in ultrafast dynamics and Ultrafast bandgap photonics

J. Dong[1], D. Shin[2], E. Pastor[3], T. Ritsche[4], L. Cario[5], Z. Chen[6], W. Qi[1], R. Grasset[1], M. Marsi[6], A. Taleb-Ibrahimi[7], N. Park[8], A. Rubio[9], E. Papalazarou[6], L. Perfetti[1]

[1] *Institut Polytechnique de Paris, 91128 Palaiseau, France*
[2] *Gwangju Institute of Science and Technology (GIST), Gwangju 61005, Republic of Korea*
[3] *Universitat Jaume I, 12006 Castello, Spain*
[4] *Technische Universitat Dresden, 01069 Dresden, Germany*
[5] *Université de Nantes, 44000 Nantes , France*
[6] *Université Paris-Saclay, 91405 Orsay, France*
[7] *France Société Civile Synchrotron SOLEIL, 91192 Gif-sur-Yvette, France*
[8] *Ulsan National Institute of Science and Technology (UNIST), Ulsan 44919, Korea*
[9] *Max Planck Institute for the Structure and Dynamics of Matter, 22761 Hamburg, Germany*

The transition metal 1T-TaS_2 is a layered insulator with a rich phase diagram aSoci\'{e}t\'{e} civile Synchrotron SOLEIL, L'Orme des Merisiers, Saint-Aubin - BP 48, 91192 GIF-sur-YVETTE, Frances a function of pressure and temperature. Its broken symmetry phases include incommensurate, nearly commensurate, and commensurate Charge Density Waves (CDWs). Within each layer, the Ta lattice undergoes a periodic distortion in which 13 Ta ions form clusters with the motif of a Star-of-David (SD). These clusters have an odd filling and lock-in to a Commensurate CDW (C-CDW) below 180 K. The observed insulating behavior of the C-CDW phase is generally attributed to the Mott localization of the electron in the highest occupied state of SDs. Recent calculations revised the strength of Coulomb repulsion in this family of compounds and highlighted the strong effects that electronic interactions have on the band structure of 1T-TaS_2.Although widely believed to be a Mott insulator, the commensurate CDW phase also features an interlayer stacking with SDs dimerization. The stacking of two adjacent layers can be of three different kinds: Top Aligned (*A*) and Laterally displaced (*L*) with a vector of magnitude *2a*. The dimerized geometry of 1T-TaS_2 is formed by alternating stacking between *A* and *L* configurations, called *AL* stacking. By hosting an even number of electrons, the dimerized unit cell of the commensurate CDW cannot be a pure Mott phase. This duality gave origin to several works, addressing the Slater-towards-Mott character of the ground state.This work reports time-resolved ARPES measurement on high-quality single crystals of 1T-TaS_2 in the insulating C-CDW phase. By making use of different polarizations of the probe pulse, we are able to visualize the dispersion of electronic states below and above the chemical potential. The experimental data are compared with state-of-the-art Density Functional Theory calculations with the Generalized Orbital U (DFT+GOU). The Coulomb U of a SD cluster is self-consistently calculated via the ACBN0 method.

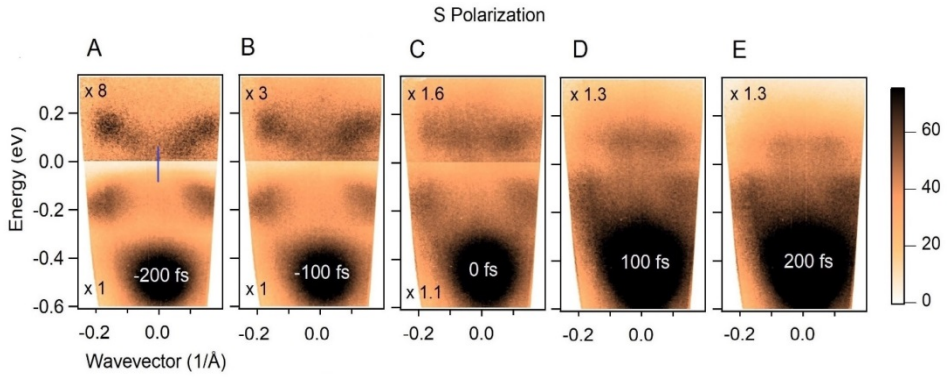

Fig.1.A-E)*:Photoelectron intensity map acquired with* ***S*** *probe polarization along the Γ-M direction for different pump-probe delays. The intensities above and below the Fermi level have been multiplied by rescaling factors in order to better visualize the electronic states with respect to a fixed color scale. The blue line in panel A stands for the electronic gap size.*

Our results indicate that both stacking order and electronic correlations are essential to reproduce the correct gap size. Moreover, time-resolved ARPES data acquired with S polarized probe disclose novel aspects of the photoinduced phase transition. The pump pulse erases the band dispersion and halves the gap magnitude within half a period of the coherent CDW motion. Besides the oscillations of CDW amplitude,we propose that photoexcitation also engenders local variations of dimerization, orbital filling, and U potential. The combination of these effects triggers the melting of the Mott-Peierls gap.

References

[1] D. Shin, N. Tancogne-Dejean, J. Zhang, M. S. Okyay, A. Rubio, N. Park, *Physical Review Letters* **126**, 196406 (2021).
[2] J. Dong, D. Shin, E. Pastor, T. Ritschel, L. Cario, Z. Chen, W. Qi, R.Grasset, M.Marsi, A.Taleb, N. Park, A. Rubio, L. Perfetti, E. Papalazarou *arXiv:2210.11052.*

Terahertz lightwave-driven control of magnetism

I. Radu
European X-ray Free-Electron Laser, 22869 Schenefeld, Germany

Harnessing order parameters in solids, as e.g. magnetism, ferroelectricity, superconductivity etc, using ultrashort light pulses is a key science driver in condensed matter research. This is particularly true for the field of magnetism and spintronics [1-4] where besides a fundamental scientific interest there is an exciting potential for technological applications in, e.g., high-speed magnetic logic and magnetic storage devices. A long sought-after and yet to be realized phenomenon is the coherent and deterministic control of a macroscopically ordered spin ensemble on the sub-cycle timescales of the photo-exciting light field [4].

Here, I will showcase the latest developments in our projects on ultrafast magnetism by employing strong-field THz and mid-IR excitations on ferrimagnetic materials to (i) demonstrate an ultrafast and fully deterministic magnetization switching process upon single-shot THz pulse exposure and (ii) photo-drive the generation of a coupled spin-lattice quasiparticle at THz frequencies with ultralong coherence lifetimes – see Fig. 1.

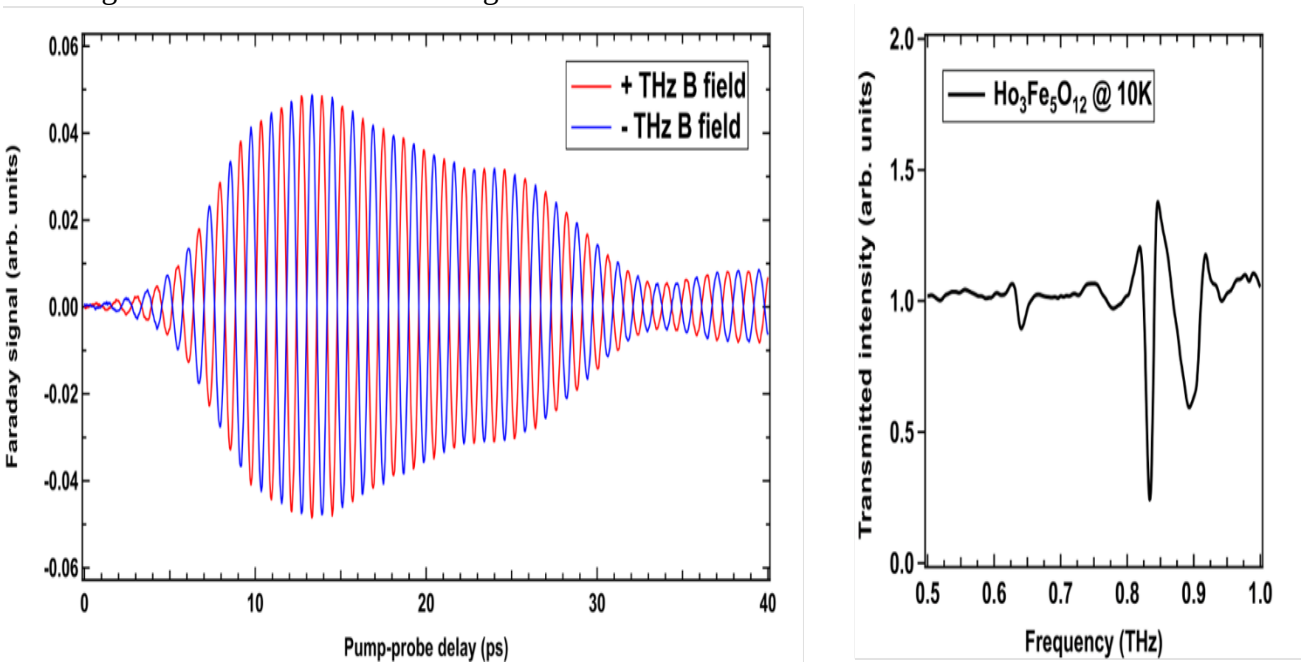

***Fig. 1. Left**: Time-resolved magneto-optical Faraday signal measured on a ferrimagnetic $Ho_3Fe_5O_{12}$ sample upon flipping the B field component of the pumping THz pulse. The narrowband THz pulse centered at 0.83 THz resonantly excites an IR-allowed spin-lattice mode generating a long-lived precession of the macroscopic magnetization. **Right**: FTIR spectrum measured at 10 K on the $Ho_3Fe_5O_{12}$ sample showing the spectral signature of the coupled spin-lattice mode below 1 THz.*

I will conclude with our future plans on highly brilliant THz light sources to be implemented at the European XFEL.

References

[1] A. Kirilyuk, A.V. Kimel, Th. Rasing, *Review Modern Physics* **82**, 2731 (2010).
[2] K. Carva, P. Balasz, I. Radu, *Handbook of Magnetic Materials* **26**, 29 (2017).
[3] I. Radu, K. Vahaplar, C. Stamm, T. Kachel, N. Pontius, H. A. Dürr, T. A. Ostler, J. Barker, R. F. L. Evans, R. W. Chantrell, A. Tsukamoto A. Itoh, A. Kirilyuk, Th. Rasing, A. V. Kimel, *Nature* **472**, 205 (2011).
[4] I. Radu, Journal Physics Condensed Matter **33**, 353001 (2021).

All optical control of magnetism for energy efficient and Brain inspired computing

Th. Rasing
Radboud University, 6525 Nijmegen, the Netherlands

The ability to switch magnets between two stable bit states is the main principle of digital data storage technologies since the early days of the computer. However, the explosive growth of digital data and its related energy consumption is pushing the need to develop fundamentally new physical principles and materials for faster and more energy-efficient processing and storage of data [1]. Since our demonstration of magnetization reversal by a single 40 femtosecond laser pulse, the manipulation of spins by ultra-short laser pulses has developed into an alternative and energy efficient approach to magnetic recording [2.3]. Plasmonic antennas have allowed us to push this optical control even down to nanometer length scales [4], while photonic networks allow the development of an optically switchable MRAM [5].

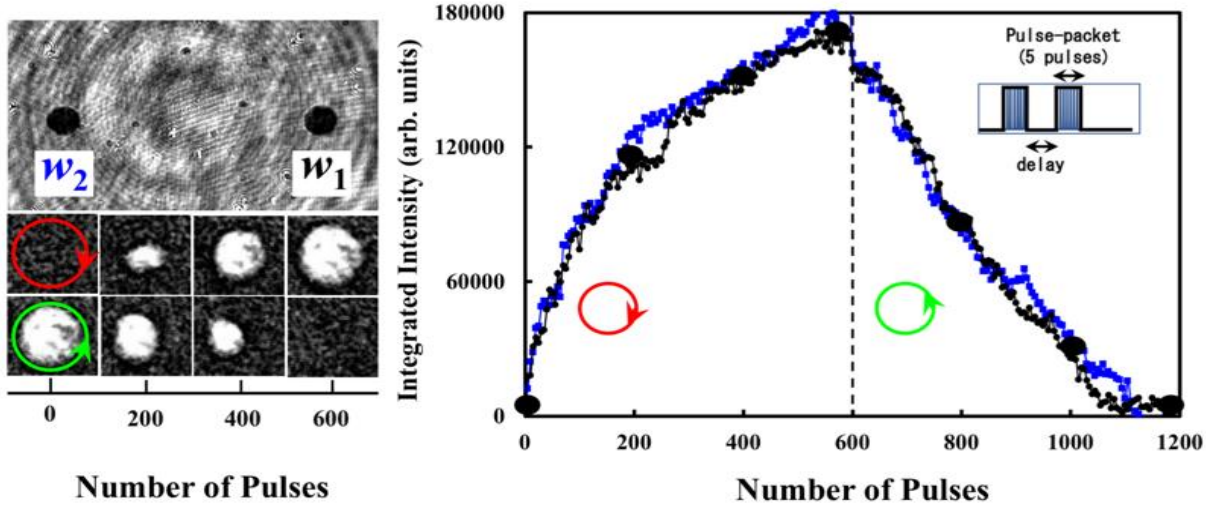

***Fig. 1**. (**Left**): Magneto-optical image of two physically-separated laser-written synaptic weights, w_1, w_2 (**dark spots**); the bottom shows eight background subtracted images illustrating evolution of the magnetization changes due to the right (**top row**) and left (**bottom row**) circularly-polarized fs laser pulses irradiating the Co/Pt sample. (**Right**): Extracted intensity changes as function of the number of laser pulses, demonstrating continuously-controllable weights, shown in **black** (**blue**) for w_1 (w_2). Black solid disks correspond to the images in the bottom rows of **(a)**. The inset shows the pulse packets used for learning.*

However, new ICT technologies, such as Artificial Intelligence push the exponentially increasing energy requirement of data manipulation even more [6]. Therefore, the development of radically new physical principles that combine energy-efficiency with high speeds and high densities is crucial for a sustainable future. One of those is neuromorphic computing, that is inspired by the notion that our brain uses a million times less energy than a supercomputer while, at least for some tasks, it even outperforms the latter [7]. Ultimately, future brain-inspired technology should provide room temperature operation down to picosecond timescales, nanoscale dimensions and at an energy dissipation as low as the Landauer limit (~zJ). In this talk, I will discuss the state of the art in ultrafast manipulation of magnetic bits and present some first results [8,9,10] to implement brain-inspired computing concepts in magnetic materials that operate close to these ultimate limits.

References

[1] T. Becker, R. Haas, J. Schemmel, S. Furber, S. Dolas, S,https://www.etp4hpc.eu/white-papers.html#unconv (2022).
[2] A. Kirilyuk, A. V. Kimel, Th. Rasing, *Review Modern Physics* **82**, 2731(2010).
[3] A. V. Kimel, M. Li, *Nature Reviews Materials* **4**, 189 (2019).
[4] T.-M. Liu, T. Wang, A. H. Reid, M. Savoini, B. Koene, P. Granitzka, C.E. Graves, D.J. Higley, Z. Chen G. Razinskas, M. Hantschmann, A. Scherz, J. Stohr, A. Tsukamoto, B. Hecht, A.V. Kimel, A. Kirilyuk, Th. Rasing H. Durr, *Nano Letters*, 15, 6862 (2015).
[5] L. Avilés-Félix, L. Alvaro-Gomez, G. Li, C.S. Davies, A. Olivier, M. Rubio-Roy, S. Auffret, A. Kirilyuk, A.V. Kimel, Th. Rasing, L.D. Buda-Prejbeanu, R.C. Sousa, B. Dieny, I.L. Prejbeanu, *AIP Advances* **9**, 125328 (2019).
[6] A. Mehonic, A.J. Kenyon, *Nature* **604**, 255 (2022).
[7] D. J. Kösters, B. A. Kortman, I.Boybat, E. Ferro, S.Dolas, R.Ruiz de Austri, J.Kwisthout, H.Hilgenkamp, T. Rasing, H.Riel,A.Sebastian S. Caron J.H. Mentink, *APL Machine Learning* **1**, 016101 (2023)
[8] A. Chakravarty, J.H. Mentink, C. S. Davies, K. Yamada, A.V. Kimel, Th. Rasing, *Applied Physics Letters* **114** 192407 (2019).
[9] A. Chakravarty, J.H. Mentink, S. Semin, Th. Rasing, *Applied Physics Letters* **120,** 022403 (2022).
[10] K. Raab, M.A. Brems, G. Beneke, T. Dohi, J. Rothörl, F.Kammerbauer, J.H. Mentink, M. Kläui, *Nature Communications* **13**, 6982 (2022).
* Acknowledgement(s): Support from the Dutch Research Council (NWO) and the European Research Council ERC grant agreement no.856538 (3D-MAGiC) is acknowledged.

Towards imaging optically induced charge density with atomic resolution

C. Ornelas-Skarin[1], T. Bezriadina[3], M. Fuchs[4], S. Ghimire[2], J. B. Hastings[2], N. N. Hua [5], L. Leroy [5]
Q. Nguyen[2], G. de la Peña[2], D. Popova-Gorelova[3],S. Shwartz[6], M. Trigo[2], T. Sato[2], D. Zhu[2]
D. A. Reis[1]

[1] *Stanford University, Stanford, CA 94305, USA*
[2]*SLAC National Accelerator Laboratory, Menlo Park, CA 94025, USA*
[3]*University of Hamburg, D-20355 Hamburg, Germany*
[4]*University of Nebraska, Lincoln, NE, 68588, USA*
[5]*Paul Scherrer Institut, 5232 Villigen PSI, Switzerland*
[6]*Bar-Ilan University, Ramat Gan 5290002, Israel*

The nonlinear interaction of x-ray and optical photons in materials can be used to image the atomic-scale local optically induced charge density [1, 2]. This method can be thought of as x-ray and optical sum and difference frequency generation, or equivalently x-ray diffraction from the optically modulated charge density, $\delta\rho(\vec{r},t)$. By measuring energy and momentum sidebands to ordinary Bragg diffraction gives direct information about the local induced charges (and thus currents) that would otherwise be invisible because of the long wavelength at optical frequencies. Similar to conventional crystallography which ideally measures $\rho(\vec{r})$ information about $\delta\rho(\vec{r},t)$. is obtained through the nonlinear diffracted intensity. This intensity depends on the spatial and temporal Fourier components, $\delta\rho_{\vec{G}}^{(\omega)}$ since

$$I_{\vec{G}}^{(\omega)} \propto \left|\delta\rho_{\vec{G}}^{(\omega)}\right|^2 = \left|\int \delta\rho(\vec{r},t)e^{i\vec{G}\cdot\vec{r}}e^{-i\omega t}\, d\vec{r}\, dt\right|^2,$$

where $\vec{G}$ is a reciprocal lattice vector. The feasibility of imaging the linear optical response with atomic resolution was first demonstrated in [3]. In that experiment, the mixing of single photons from an x-ray free-electron laser (FEL) and a Ti:sapphire laser was reported in single crystal diamond. Higher-order wave-mixing, involving more than one optical photon with one x-ray photon is expected due to the nonlinear interaction of the optical beam with the material. The higher-order Fourier components of the nonlinear induced charge density, $\delta\rho_{\vec{G}}^{(\omega=n\omega_{opt.})}$ (where $|n| > 1$), can have nontrivial dependence on polarization compared to the first-order optical response,

$$\delta\rho_{\vec{G}}^{(\omega=n\omega_{o.})} \propto |\vec{\epsilon}\cdot\vec{G}|,$$

where $\vec{\epsilon}$ is the laser polarization and ω_o is the optical frequency. An atomic-scale image of the linear much less nonlinear response to optical excitation would be an enormous advance. Measurements of the nonlinear response would be useful for Floquet engineering of novel states in quantum materials [4] and imaging the nonperturbative currents in solid-state high-harmonic generation [5, 6]. Here we discuss recent measurements of XOM for $n = \pm 1$ and $n = 2$, corresponding to oscillations at $\omega_o$and $2\omega_o$ inside silicon. Particularly the $2\omega_o$ component is an example of how XOM can be used to observe details of the electron dynamics invisible to longer wavelength probes, such as purely optical measurements, due to the inversion symmetry in bulk silicon. The experimental challenges of measuring XOM stem from its relatively small efficiencies and large elastic back-grounds. The mixing signal is concentrated in an extremely small solid-angle and phase-matching conditions about the elastic Bragg peaks. This requires high precision and stable mechanics as well as a relatively narrow monochromator and analyzer with high rejection in angle and energy. We have designed and constructed a suitable multi-channel cut (CC) Si 311 dispersive monochromator (CCM) and analyzer (CCA). The proposed setup is shown in Fig. 1.

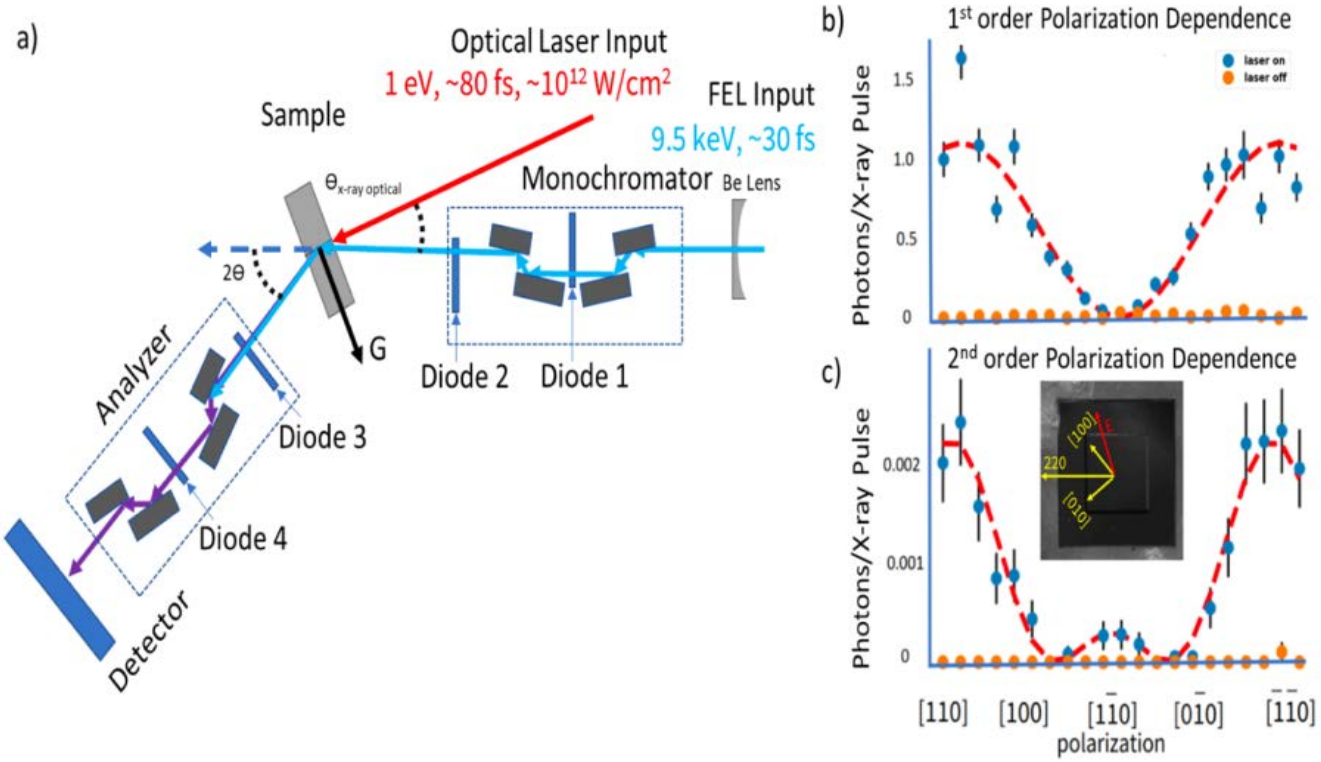

Fig. 1. a) *Schematic of the setup used to measure the sum frequency generation signal, ω_{SFG} . The x rays ($\omega_x = 9.5$ keV) from the LCLS FEL then pass through a beryllium lens and the monochromator, which reduces the bandwidth and collimates the x rays. The x rays then diffract from the optically pumped sample (ω_o= 1eV). The sum frequency photons are collected while the elastically diffracted photons are rejected by the analyzer. The diodes act as intensity monitors to track any drift in the optics. In* ***b)*** *and* ***c)*** *we show the polarization dependence of the signal corresponding to oscillations at* ***b)*** *$\omega_{SFG} = \omega_x + \omega_o$1ωoptical and* ***c)*** *2ωoptical in the plane containing [100] and [010] as pictured in the inset image of the sample in* ***c)****. The red dashed line is a fit to the form given the text.*

We measured the sum and difference frequency signals about the (220) Bragg peak, $I_{(220)}^{(\pm\omega_o)}$, in a 40 μm thick silicon crystal, as well as the second-order sum frequency ($I_{(220)}^{(2\omega_o)}$), at LCLS using our double CCM/CCA pairs. Even though silicon is inversion symmetric at the macroscopic scale, both the diffraction geometry and the local bonding environment break in- version symmetry; this allows us to measure sidebands associated with the anharmonic charge density oscillations at laser second-harmonic of the laser. We measured a relative efficiency $I_{(220)}^{(\omega_o)}/I_{(220)}^{(0)} \sim 10^{-6}$and $I_{(220)}^{(2\omega_o)}/I_{(220)}^{(0)} \sim 10^{-9}$ for an incident intensity of a few 10^{12}W/cm^2 at a 1eV optical photon energy. The polarization dependence of the 2nd-order sideband for the symmetric 220 peak of the (001) cut crystal is shown in Fig. 1 c). The 2nd-order charge density is proportional to the product of two-optical fields, $\delta\rho_{\vec{G}}^{(2\omega_o)} \propto G_i\, \tilde{\chi}^{(2)}{}_{G,ijk} E_j E_k \equiv F_{G,jk}\, E_j E_k$. Due to the crystal cut, we were constrained to measuring two of the four independent components of $\tilde{\chi}^{(2)}{}_{(220)}$, such that $I_{(220)}^{(\omega_o)} \propto |F_{(220),xx} + F_{(220),xy} \cos 2\theta_{\vec{\varepsilon}\cdot\vec{G}}|^2$as shown in Fig. 1 c). We find $F_{(220),xy} \approx 2F_{(220),xx}$, and the measured background is less than 5 10^{-6} photons/x-ray pulse, orders of magnitude below the measured signal. We will discuss future directions including crystallographic reconstruction of optically induced charge density, including by direct phasing, extension to lower quality crystalline samples and extension to sub-cycle time-domain measurements at FELs.

References

[1] P. Eisenberger, S. McCall. Mixing of x-ray and optical photons. *Physical Review* A **3,** 1145 (1971).
[2] I. Freund, B. F. Levine. Optically modulated x-ray diffraction. *Physical Review Letters* **25, 1**241 (1970).
[3] T.E. Glover, D. M. Fritz, M. Cammarata, T.K. Alison, S. Coh, J. M. Feldcamp, H. Lemke, D. Zhu, Y. Feng, R. N. Coffee, M. Fuchs S. Ghimire, J. Chen, S. Shwartz, D A. Reis, S. E. Harris, J. B. Hastings, *Nature* **488**, 603(2012).
[4] D. Basov, R. Averitt, D. Hsieh, *Nature Materials* **16,** 1077 (2017).
[5] D. Popova-Gorelova, D. A. Reis, R. Santra, *Physical Review* B **98 ,** 224302 (2018).
[6] S. Ghimire, D. A. Reis, *Nature Physics* **15,** 10(2011).

* This work is supported by the US Department of Energy, Office of Science, Office of Basic Energy Sciences, Chemical Sciences, Geosciences, and Biosciences Division through the AMOS program and performed on the LCLS. We thank X. Huang for the fabrication and advice on the design of the Si 311 channel cut crystals. We thank S. Gerber, H. Lemke, R. Mankowsky, M. Sander and C. Svetina for help with preliminary experiments on SwissFEL.

Observing quantum materials in real time by Pump-probe Raman scattering

D. Reznik
University of Colorado-Boulder, Boulder, CO 80309, USA

In this talk I describe the time-resolved Raman scattering work at the University of Colorado. The Raman lab shares an ultrafast laser system with an angle-resolved photoemission (ARPES) setup, which allows investigation of bosonic and fermionic excitations under the same driven nonequilibrium conditions. I will discuss new physics that was uncovered in three recent projects.
We combined ultrafast pump-probe Raman scattering and ARPES to directly follow electron-hole excitations as well as the G-phonon in graphite after an excitation by an intense laser pulse. This phonon is known to couple relatively strongly to electrons. Cross-correlating effective electronic and phonon temperatures places new constraints on model-based fits. The accepted two-temperature model predicts that G-phonon population should start to increase as soon as excited electron-hole pairs are created and that the rate of increase should not depend strongly on the pump fluence. Instead we found that the increase of the G-phonon population occurs with a delay of ~65 fs. This time-delay is also evidenced by the absence of the so-called self-pumping for G phonons. The time-delay decreases with increased pump fluence. These observations imply a new relaxation pathway: Instead of hot carriers transferring energy to G-phonons directly, the energy is first transferred to optical phonons near the zone boundary K-points, which then decay into G-phonons via phonon-phonon scattering. Our work demonstrates that phonon-phonon interactions must be included in any calculations of hot carrier relaxation in optical absorbers even when only short timescales are considered [1].

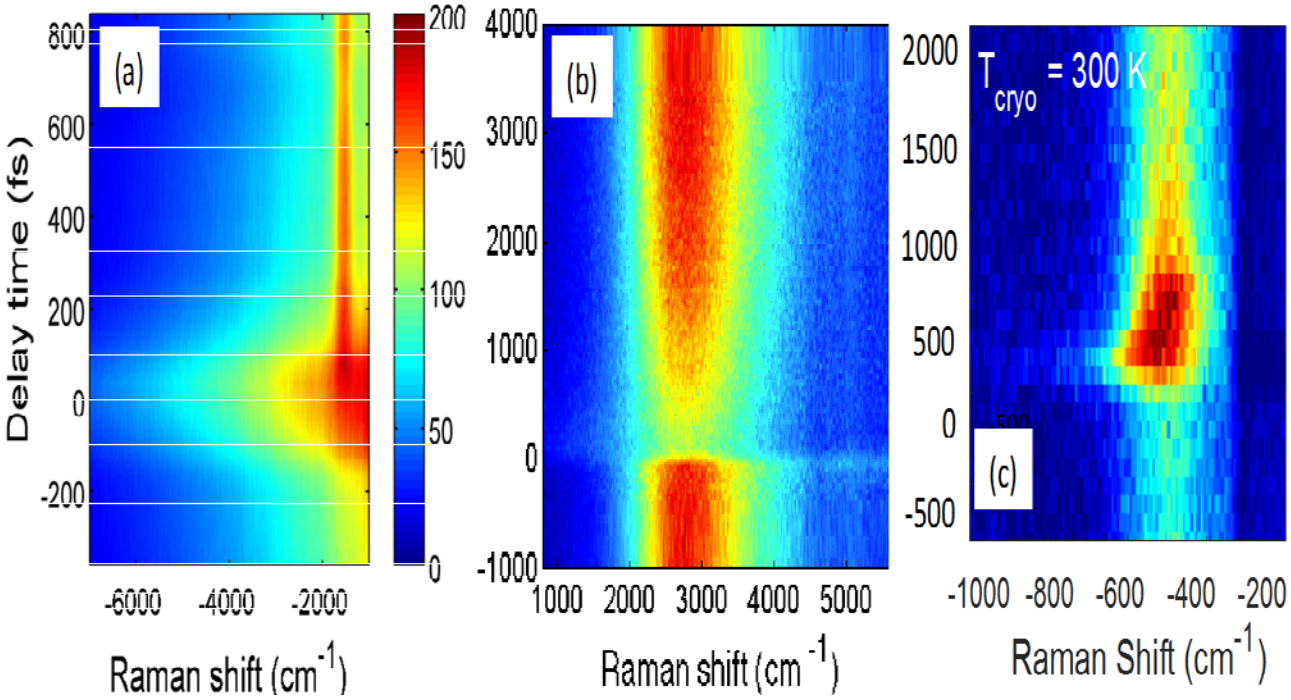

***Fig. 1. (a)**: Anti-Stokes Raman scattering in graphite as a function of the time delay between the pump and the probe. G-phonon at 1580 cm^{-1} emerges at positive times [1]. **(b)**: Stokes 2-magnon Raman spectrum of antiferromagnetic YBCO with intensity suppression at short delay times clearly visible [2]. **(c)**: Anti-Stokes Raman scattering in nearly optimally-doped YBCO (superconducting T_c=90K) dominated by the apical oxygen phonon at 500 cm^{-1} as a function of the pump-probe time delay [3].*

The second project focused on the time-evolution of the two-magnon Raman scattering in an insulating antiferromagnetic sample of $YBa_2Cu_3O_{6+x}$ (YBCO). These experiments demonstrated that time-resolved 2M Raman scattering is a powerful probe of ultrafast demagnetization in antiferromagnetic Mott/charge transfer insulators. It can be applied to a variety of materials where 2M Raman scattering has been observed. Electron-spin coupling plays an important role in photo-carrier relaxation as evidenced by a radical disturbance of the magnon spectrum. In YBCO the maximum effect occurred within our experimental resolution of 90 fs of photoexcitation, which is much faster than demagnetization timescales in itinerant

ferromagnets. Slower timescales characterizing subsequent relaxation to thermal equilibrium are of the same order of magnitude or greater than phonon-driven relaxation in conventional materials (e.g., graphite). We have proposed a simple explanation of these results in terms of slow relaxation of the charge sector and fast relaxation of the magnetic sector. Our results demonstrate strong coupling between charge and spin degrees of freedom, which potentially accounts for high-Tc superconductivity. The coupling between spin and phonon degrees of freedom remains to be understood. In the future tuning pump laser energy to resonate with particular dipole-active phonons may allow using these measurements to provide new insights [2].We also used pump-probe Raman scattering to investigate the apical oxygen vibration in strongly doped superconducting $YBa_2Cu_3O_{6+x}$ under nonequilibrium conditions. We have demonstrated quantitative agreement with theory of the time-varying apical phonon frequency as the electronic system loses its excess energy to the broader phonon bath. This results highlights that the dynamics of energy transfer are responsible for the temporal behavior of the electrons and phonons, as well as the disparity between interactions in and out of equilibrium. Although in strongly correlated materials such as YBCO there are strong Coulomb processes and impurity scattering that dominate the electronic spectra, when it comes to time domain these processes rapidly come to an internal equilibrium and effectively shut off. Our results provide a new, phonon-centered, perspective on previous experiment in $Bi_2Sr_2CaCu_2O_8$ with both time-resolved ARPES and ultrafast electron diffraction that both observed a similar quantitative agreement [3].This work provides new insights into photoinduced superconductivity. Its signatures were recently reported in the optical spectra of underdoped YBCO up to time-delays of about 1ps when pumping with 790 nm near-IR pulses as well as with pulses that resonated with IR-active apical oxygen phonons. Our experiments reproduced the former pumping condition and showed that optimally-doped and underdoped superconducting YBCO behave similarly. We found that hot and cold phonons were out of thermal equilibrium, but electrons and hot phonons were at or near thermal equilibrium at time delays below 1ps. At these time-delays electronic temperatures were always well above room temperature. We plan to determine transient heating while pumping the IR-active phonons in future experiments [3].

References

[1] J.A. Yang, S. Parham, D. Dessau, and D. Reznik, *Scientific Reports* 7, 40876 (2017).

[2] J.A. Yang, N. Pellatz, T. Wolf, R. Nandkishore, D. Reznik, *Nature Communications* **11**, 2548 (2020).

[3] N. Pellatz, S. Roy, J.W. Lee, J.L. Schad, H. Kandel, N. Arndt, C.-B. Eom, D. Reznik, *Physical Review* B **104**, L180505 (2021).

* Raman experiments at the University of Colorado were supported by the NSF under Grant No. DMR-1709946 and laboratory upgrade that made these experiments possible by DARPA through the DRINQS program. The time-resolved ARPES work was supported by NSF grant DMR-1508785, with the equipment purchased in part through NSF MRI-1546961. The work at University of Wisconsin-Madison (thin film synthesis and structural and electrical characterizations) was supported by the US Department of Energy (DOE), Office of Science, Office of Basic Energy Sciences (BES), under award number DE-FG02-06ER46327 as well as by the National Science Foundation under Grant No. DMR-1752713. The work at the University of Wisconsin-Parkside was supported by WiSys and UW System Applied Research Grant award number 102-4-812000-AAH1775.

Optically induced avoided crossing in Graphene studied by MIR pump/ Raman probe spectroscopy

M. Rübhausen
University of Hamburg, 22761 Hamburg, Germany

Spontaneous time-resolved Raman scattering in a pump-probe configuration is a novel tool that has essentially four important parameters that can be tuned to be used for different types of research.[1] Firstly, the incident photon energy of the probe can be tuned into resonance with the desired quasiparticle excitation of interest.[2] Resonant Raman scattering has been used to amplify excitations such as phonons, magnons, and inelastic scattering from order parameters in condensed matter. Secondly, in pump-probe configuration, the pump wavelength and corresponding energy can address different degrees of freedom by pumping resonantly phonons, charge-transfer excitations or transitions between lower and upper Hubbard bands. Both photon pulses, thus, benefit from a substantial tunability of pump and probe energies. Thirdly, we have time resolution that allows to disentangle the impact of the pump on the spontaneous probe spectra as a function of time. And, finally, fluence is important, in particular, for scenarios where coherent pumping is required. With this in mind, we designed, constructed, and put into operation a pump-probe setup for spontaneous Raman scattering that allows to tune the incident energy of the probe laser beams between 1 eV and 6 eV utilizing a fully reflective coupling of the scattered photons combined with a frequency and also spatially filtered bandpass operation of a custom-made spectrometer as shown in Fig. 1[3]. We have embedded this setup with a laser system that allows pumping of various degrees of freedom continuously from the mid-infrared spectral range up to the deep UV (0.1 eV to 6 eV) – see Fig. 1.

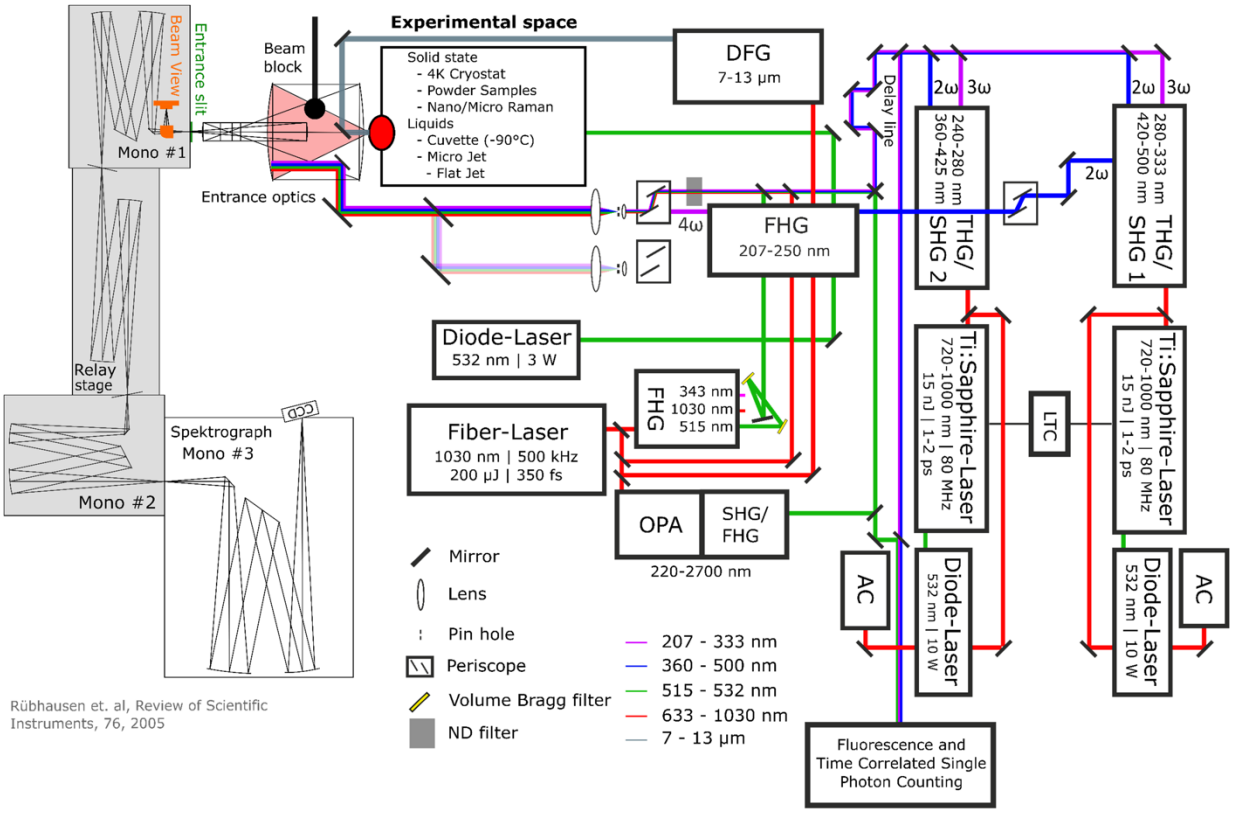

Fig. 1.: *General outline of the time-resolved spontaneous Raman setup at the CFEL. Three main laser sources (two diode-pumped TiSa lasers, one fiber amplified laser) serve as general sources for the following steps of flexible harmonic generation, optical parametric amplification followed by second and third harmonic generation, as well as difference frequency generation. By these means laser pulses with pulse durations between 300 fs and 5 ps can be obtained. Focusing and signal collection is done by a fully reflective Cassegrain type objective with a numerical aperture of 0.52 featuring parabolic on-axis mirrors for diffraction limited imaging of the source into the UT-3 Raman spectrometer. Straylight rejection of the instrument is amplified by a beam block implemented in the objective and the premonochromator stage made of off-axis parabolic mirrors with embedded spatial filtering to suppress edge diffraction effects occurring at the blades of the slits. The spectral range of the detection system covers 1 eV – 6 eV. The spectral range of the pump covers 0.1 eV to 6 eV.*

The temporal width of the probe pulse can vary between 800 fs to 5 ps and the temporal width of the pump can vary between 300 fs to 1.2 ps. Delays between pump and probe can reach up to the ns range. We have utilized this setup for studies of the superconducting order parameter in cuprates in the past revealing the response of the pair-breaking peak after a charger-transfer pump.[1] However, the extension into the mid-infrared spectral range allows to study the coherent anharmonic coupling between two orthogonal phonon modes generating a new vibronic state. Furthermore, only few theories to calculate the Raman response function under non-equilibrium conditions exist. Frequently, the observed line shape is dominated by the pulse broadening of the probe. However, upon proper tuning of pump and probe pulse durations it is possible to derive a spontaneous Raman signal that is dominated in its spectral response by the intrinsic behavior of the sample making it useful to analyze the changes of the line shape of the transient Raman results with varying pump conditions. I am going to show the application of this approach to the degenerate Raman and IR active modes in bi- and multilayer graphene and discuss how to analyze the changes in line shape upon tuning the pump wavelength through the IR mode.[4] Due to the strong anharmonic coupling of these degenerate modes a new vibronic state appears with distinct spectral features and properties that I am going to discuss in my presentation. Most notable is a line shape sharpening of the transient spontaneous Raman scattering compared to the equilibrium, a frequency change upon tuning of the IR pump and an ultra-sharp resonance of the transient Raman response that matches the width of the pumped IR phonon. I will be utilizing an equation of motion approach using a Greens-function method calculating the transient Raman response of two degenerate harmonic oscillators [5]. Overall a good agreement with the experimental observation can be found. In an outlook I will briefly address the possibility to study in-gap excitations of high TC superconductors that will be in contrast to our previous work studying the temporal evolution of the pair-breaking excitation in superconductors [6,7].

References

[1] R. P. Saichu, I. Mahns, A. Goos, S. Binder, P. May, S. G. Singer, B. Schulz, A. Rusydi, J. Unterhinninghofen, D. Manske, P. Guptasarma M. S. Williamsen, M. Rübhausen, *Physical Review Letters* **102**, 177004 (2009).

[2] D. Budelmann, B. Schulz, M. Rübhausen, M. V. Klein, M. S. Williamsen, P. Guptasarma, *Physical Review. Letters* **95,** 057003 (2005).

[3] B. Schulz, J. Bäckström, D. Budelmann, R. Maeser**,** M. Rübhausen, M. V. Klein, E. Schoeffel, A. Mihill, S. Yoon, *Review of Scientific Instruments* **76**, 073107 (2005).

[4] S.Buchenau, J. Reichstetter, B.Grimm-Lebsanft, F Biebl, M.Fechner, S.Herres-Pawlis, D.Manske, A. Cavalleri, M. Rübhausen,(submitted) 2023.

[5] M. Rübhausen, J. Reichstettet, D. Manske, (submitted) 2023.

[6] L. Schwarz, B. Fauseweh, N. Tsuji,D. Manske, S. Kaiser, *Nature Communications* **11**, 287 (2020).

[7] M. Puviani, A. Baum, S. Ono, Y. Ando, R. Hackl, D. Manske, Phys. Rev. Lett. 127, 197001 – 2021.

* Acknowledgement(s): I would like to thank the numerous researchers who have helped to set up this unique instrument over the past years. For the new particular research that I am addressing in my presentation I would like to thank S. Buchenau, T. Glier, B. Grimm-Lebsanft, F. Biebl L. Westphal, M. Rerrer, M. v. Heek. For many discussions on the physics I would also like to acknowledge D. Manske, J. Reichstetter, M. Fechner, A. Cavalleri. S. Kaiser. This work was financially support by the BMBF (05K19GU5) and the DFG (RU773/7, RU773/8).

Time-resolved photoelectron diffraction: mapping atomic motion in Bi_2Se_3 Phonon Oscillations

C. E. Sanders[1], D. Curcio[2], K. Volckaert[2], D. Kutnyakhov[3], S. Y. Agustsson[2], K. Bühlmann[5], F. Pressacco[3]
M. Heber[3], S. Dziarzhytski[3], Y. Acremann[5], J. Demsar[4], W. Wurt[6], Ph. Hofmann[2]
[1] *STFC Central Laser Facility, Didcot OX11 0QX, UK*
[2] *Aarhus University, 8000 Aarhus-C, Denmark*
[3] *Deutsches Elektronen-Synchrotron DESY, 22607 Hamburg, Germany*
[4] *Johannes Gutenberg-Universität, 55099 Mainz, Germany*
[5] *ETH Zürich, 8093 Zürich, Switzerland*
[6] *Hamburg University, 22761 Hamburg, Germany*

X-ray photoelectron diffraction (XPD) is a powerful technique, based on the tools of X-ray photoelectron spectroscopy (XPS). It combines chemical sensitivity with the power to elucidate local geometric order [1]. It can be used to determine the global surface lattice of a crystal [2,3], and can also reveal the local structural order around individual adsorbates on crystalline surfaces [4]. Free-electron lasers (FELs) can deliver ultra-short X-ray pulses in an energy range suitable for XPD study. The fact that FEL pulse trains can be synchronized with those of secondary, lower-photon-energy laser sources means that XPD can potentially be adapted to pump-probe, time-resolved studies. This would expand the technique's scope in some of the most important research areas in the chemistry and physics of out-of-equilibrium systems. One can imagine using it to probe the excitation and detailed evolution of complex phonon modes in crystals, or to visualize surface catalysis in action.The fundamental principle of XPD is that photoelectrons travel to a photoelectron detector both by direct paths and by paths that involve multiple scattering from surrounding atoms. The intensity at the detector is the coherent sum of all these partial waves, and a diffraction pattern arises as a function of emission angle (or parallel momentum), as measured at the detector. An example of such a pattern is shown in Fig. 1(b).

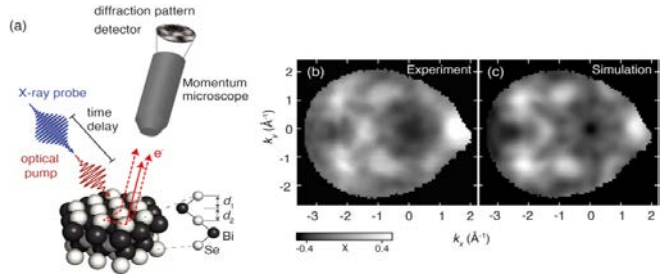

Fig. 1. ***(a)*** *Schematic of experimental setup.* ***(b)*** *Measured static (unpumped) XPD pattern.* ***(c)*** *Simulated XPD pattern obtained from the optimized structural model. Figure reproduced from [5].*

In post-analysis, one simulates diffraction patterns for assumed structures, and then refines the structural parameters of the models, so as to cause the simulated diffraction pattern to converge to the measurement. Such a simulation is shown in Fig. 1(c).We have now used pump-probe techniques at the PG2 beamline of the FLASH free-electron laser (FEL) to demonstrate time-resolved XPD measurements of the "simple" model system Bi_2Se_3 [5]. Key to the success of this experiment is the HEXTOF experimental station, which is based on a time-of-flight (ToF) momentum microscope (MM). The ToF-MM allows the entire XPD pattern to be probed simultaneously, without the need to rotate or tilt the sample. The experimental setup is shown in Fig. 1(a). The symmetric A_{1g} coherent optical phonon modes can be excited with ultrashort laser pulses [6,7]. In the present experiment, we pumped the A_{1g}^1 mode with a tabletop laser system. The pumping power was 4.2 mJ cm^{-2} with 1.55-eV photon energy. The pump beam was synchronized with the pulse train generated by the FEL. FEL photon energy of 113 eV was chosen, so as to photoemit from the Se 3d core levels. With our approach, we can successfully observe—with temporal and spatial resolution of 140 fs and 1 pm, respectively—the pumping of oscillations in the first interlayer spacings d_1 and d_2 (see Fig. 1[a]). The results are consistent with previous reports based on other techniques [8,9], and pave the way for studies of more complex dynamical systems by XPD, with improved statistics at higher repetition rates and at time scales down to tens of fs.

References

[1] D. P Woodruff, *Journal of Electron Spectroscopy and Related Phenomena* **126,** 55, (2002).
[2] W. Auwärter, T. J. Kreutz, T. Greber, J. Osterwalder, *Surface Science* **429,** 229 (1999).
[3] H. Bana, E. Travaglia, L. Bignardi, P. Lacovig, C. E. Sanders, M. Dendzik, M. Michiardi, M. Bianchi, D. Lizzit, F. Presel, D. De Angelis N. Apostol, P. K. Das, J. Fujii, I. Vobornik, R. Larciprete, A. Baraldi, P. Hofmann, S. Lizzit, *2D Materials* **5,** 035012 (2018).
[4] Ph. Hofmann, K.-M. Schindler, S. Bao, A. M. Bradshaw, D. P. Woodruff, *Nature* **368,** 131 (1994).
[5] D. Curcio, K. Volckaert, D. Kutnyakhov, S. Y. Agustsson, K. Bühlmann, F. Pressacco, M. Heber, S. Dziarzhytski, Y. Acremann, J. Demsar W. Wurth, C. E. Sanders, P. Hofmann, *Physical Review B* **106,** L201409, (2022).
[6] J. Qi, X. Chen, W. Yu, P. Cadden-Zimansky, D. Smirnov, N. H. Tolk, I. Miotkowski, H. Cao, Y. P. Chen, Y. Wu, S. Qiao, Z., Jiang, *Applied Physics Letters* **97,** 182102, (2010).
[7] N. Kumar, B. A. Ruzicka, N. P. Butch, P. Syers, K. Kirshenbaum, J. Paglione, H. Zhao, *Physical Review B* **83,** 235306, (2011).
[8] J. Hu, K. Igarashi, T. Sasagawa, K. G. Nakamura, O. V. Misochko, *Applied Physics Letters* **112,** 031901, (2018).
[9] J. A. Sobota, S.-L. Yang, D. Leuenberger, A. F. Kemper, J. G. Analytis, I. R. Fisher, P. S. Kirchmann, T. P. Devereaux, Z.-X. Shen, *Physical Review Letters* **113,** 157401, (2014).

* Acknowledgements: the authors acknowledge funding from VILLUM FONDEN via the Centre of Excellence for Dirac Materials (Grant No.11744) and the Independent Research Fund Denmark (Grant No. 1026-00089B). This research was carried out at FLASH at DESY. The research has been supported by the project CALIPSOplus under Grant Agreement No.30872 by the Deutsche Forschungsgemeinschaft (DFG)within project B2), and within TRR 173-268565370 (Project No.A05). We thank Holger Meyer, Sven Gieschen, and Harald Redlin for experimental support, as well as Gerd Schönhense, Davide Campi,Anton Tamögl, and Wolfgang Ernst for helpful discussions.

Extremely high average power THZ sources for Nonlinear THz spectroscopy at high repetition rate

T. Vogel, C. Millon,M. Khalili, Y. Wang, S. Mansourzadeh C. J. Saraceno
Ruhr University Bochum, 44801, Bochum, Germany

Terahertz Time Domain Spectroscopy (THz-TDS) has become a ubiquitous tool in many scientific fields and is also increasingly deployed in industrial settings. While these systems become more and more mature, efficient and lab-based THz generation methods combining broad bandwidth and high dynamic range (e.g., as provided by high THz average power and correspondingly high repetition rate) remain rare. Most industrial THz-TDS systems make use of semiconductor-based photoconductive emitters and receivers; these offer high dynamic range operation at very high repetition rates of hundreds of MHz, and the corresponding emitters provide high conversion efficiencies with low power excitation, driven by compact ultrafast fiber-lasers. For applications where strong-fields are desired, for example for nonlinear THz spectroscopy, the most commonly used technique is optical rectification in nonlinear crystals, for instance zinc telluride (ZnTe), gallium phosphide (GaP), lithium niobate (LiNbO3) or organic crystals (e.g., BNA, DAST, DSTMS). Whereas all these techniques have seen continuous performance progress in the last few years driven by different application fields, their average power has mostly remained low. A promising route of current great interest is simply to increase the average power of the driving lasers using state-of-the-art, high-average power ultrafast Yb-gain based lasers providing multi-100-W to kilowatt average-power levels as excitation sources, which are increasingly available both in laboratory setting and commercially. This new excitation regime for THz generation in various schemes has become an active area of research in the last few years, and current results have allowed to reach power levels in the THz domain in the multi-ten to multi-hundred milliwatts in different repetition rate regions [1,2,3] – which was previously restricted to accelerator facility-type THz sources. This progress opens the door to a multiplicity of new and old research areas to be re-visited.

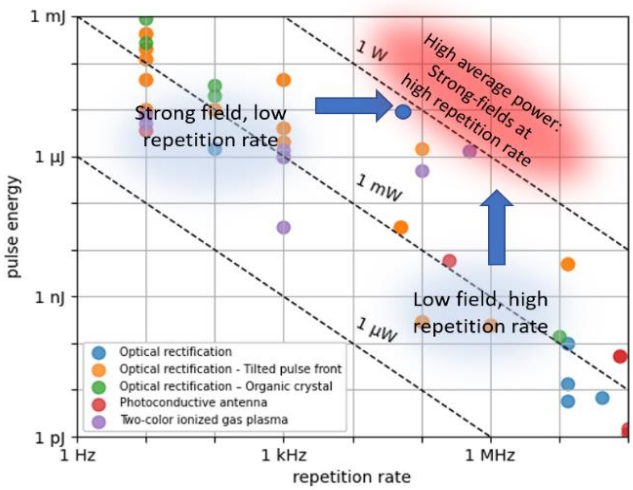

Fig. 1. Left *Overview of lab-based THz-TDS sources showing current trend towards higher average powers – both increasing the pulse energy at very high repetition rates but also making strong-field sources available at very high repetition rate.*

In this presentation, we will review recent progress in the generation of high-average power THz-TDS. We will present a record-holding THz-TDS with 643 mW of average power at 40 kHz repetition rate. We will present the state-of-the-art of high-power ultrafast laser sources with potential for driving THz sources, current technological challenges in scaling THz average power, and applications areas that could potentially benefit from these novel lab-based sources; in particular areas in ultrafast spectroscopy that could be greatly advanced by the availability of these unique sources.

References

[1] F. Meyer, T. Vogel, S. Ahmed, C. Saraceno, *Optics Letters* **45**,2494 (2020).
[2] P. L. Kramer, M. K. R. Windeler, K. Mecseki, E. G. Champenois, M. C. Hoffmann, F. Tavella, *Optics Express* **28**, 169512 (2020).
[3] J. Buldt H. Stark, M. Müller, C. Grebing, C.Jauregui,J. Limpert *Optics Letters* **46**, 5256 (2021),

Polariton condensate lattices: novel Quantum Simulator Platform

P.G. Savvidis
Westlake University, Hangzhou, Zhejiang 310030, China

Exciton-polaritons, are mixed light-matter quasiparticles resulting from the strong coupling of photons confined in a microcavity and quantum well excitons. Being bosons, polaritons can condense into macroscopically coherent many-body state and have thus emerged as prime candidates for the study of non-equilibrium systems of interacting bosons. Our recent studies, exploit non-equilibrium nature of polariton condensates, showing that polariton condensates can spontaneously magnetize [1,2], and how their spin can be controlled both optically and electrically[3]. Direct coupling of polaritons to leaking microcavity photons provides on-the-fly information of all characteristics of the polariton condensates such as energy, momentum, spin, and their phase. We employ spatially patterned external laser excitation to create arbitrary potential landscapes for polaritons and demonstrate ferromagnetic and antiferromagnetic coupling between neighbouring condensates[4].

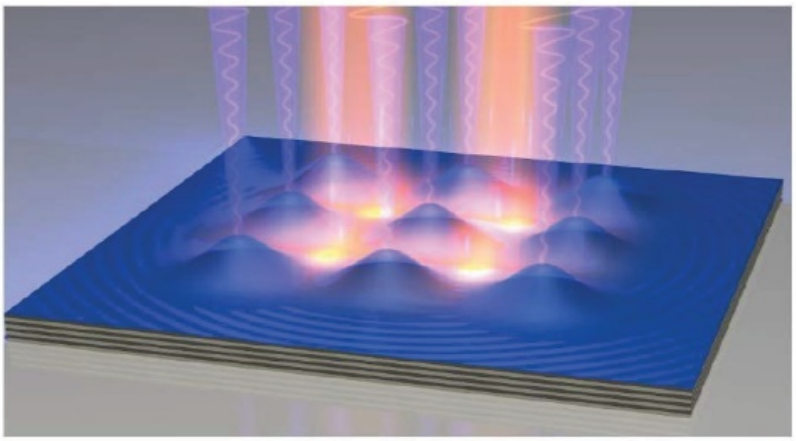

Fig.1. *Optically controlled magnetized polariton lattices.*

Furthermore, using such techniques, polariton condensates can now be imprinted into arbitrary two dimensional lattices with tunable intra[5]- and inter-site interactions providing exciting opportunities for devising novel and versatile quantum simulation platforms[6]**.**

References

[1] H. Ohadi, A. Dreismann, Y. G. Rubo, F. Pinsker, Y. del Valle-Inclan Redondo, S. I. Tsintzos, Z. Hatzopoulos, P. G. Savvidis, J. J. Baumberg *Physical Review X* **5**, 031002 (2015).
[2] Y. C. Balas, E. S. Sedov, G. G. Paschos, Z. Hatzopoulos, H. Ohadi, A. V. Kavokin, P. G. Savvidis, *Physical Review Letters* 128, 117401 (2022).
[3] A. Dreismann, H. Ohadi, Y. del Valle-Inclan Redondo, R.Balili, Y. G. Rubo, S.I. Tsintzos, G.Deligeorgis, Z.Hatzopoulos, P.G. Savvidis J. J. Baumberg, *Nature Materials* **15**, 10741078 (2016).
[4] A. Dreismann, H.Ohadi, Y. del Valle-Inclan Redondo, R.Balili, Y. G. Rubo, S.I. Tsintzos, G. Deligeorgis, Z.Hatzopoulos, P. G. Savvidis J.J. Baumberg, *Physical Review Letters* **116**, 106403 (2016).
[5] S. I. Tsintzos, A. Tzimis, G. Stavrinidis, A. Trifonov, Z. Hatzopoulos, J. J. Baumberg, H. Ohadi, P. G. Savvidis, *Physical Review Letters* **121** 037401 (2018)
[6] H. Ohadi, Y. del Valle-Inclan Redondo, A. J. Ramsay, Z. Hatzopoulos, T. C. H. Liew, P. R. Eastham, P. G. Savvidis, J. J. Baumberg**,** *Physical Review* B **97**, 195109 (2018).

Giant photoelasticity of polaritons for detecting Coherent phonons with quantum sensitivity

A. V. Scherbakov[1], M. Kobecki[1], D. D. Yaremkevich[1], T. Henksmeier[2], A. Trapp[2]
D. Reuter[2], S. M. Kukhtaruk[3], V. E. Gusev[4], A. V. Akimov[5], M. Bayer[1]
[1] *Technische Universität Dortmund, 44227 Dortmund, Germany*
[2] *Universität Paderborn, 33098 Paderborn, Germany*
[3] *V.E. Lashkaryov Institute, 03028 Kyiv, Ukraine*
[4] *Le Mans Universite, 72085 Le Mans, France*
[5] *University of Nottingham, Nottingham NG7 2RD, UK*

Coherent acoustic phonons of sub-THz frequencies are attractive information carriers for quantum communications and nanoscopic imaging due to their nanometer wavelengths [1]. Up to now, the generation and detection of coherent acoustic phonons in this frequency range exploit ultrashort laser pulses [2]. Generation is based on ultrafast optical excitation of an opaque material with the following energy transfer to the lattice on the sub-picosecond time scale. The detection operates with the ultrafast phonon-induced modulation of the optical properties of a media. The spectroscopic effects; which accompany this modulation, are fascinating in structures with narrow optical resonances. We have demonstrated chirping of exciton resonances in semiconductor quantum well [3], THz modulation of light emission from a microcavity [4], picosecond switching of polariton condensate [5]. Here we focus on our recent experiments on detecting coherent acoustic phonons in GaAs/AlAs superlattice [6]. We exploit the giant photoelasticity of polaritons [7] to detect phonons in the transient reflectivity signal with extremely high sensitivity. The demonstrated reflectivity modulation by the phonon-associated dynamical strain owned by the polariton resonance is sufficient for detecting single phonon quanta in pump-probe setups. Fig. 1(a) shows the experimental scheme.

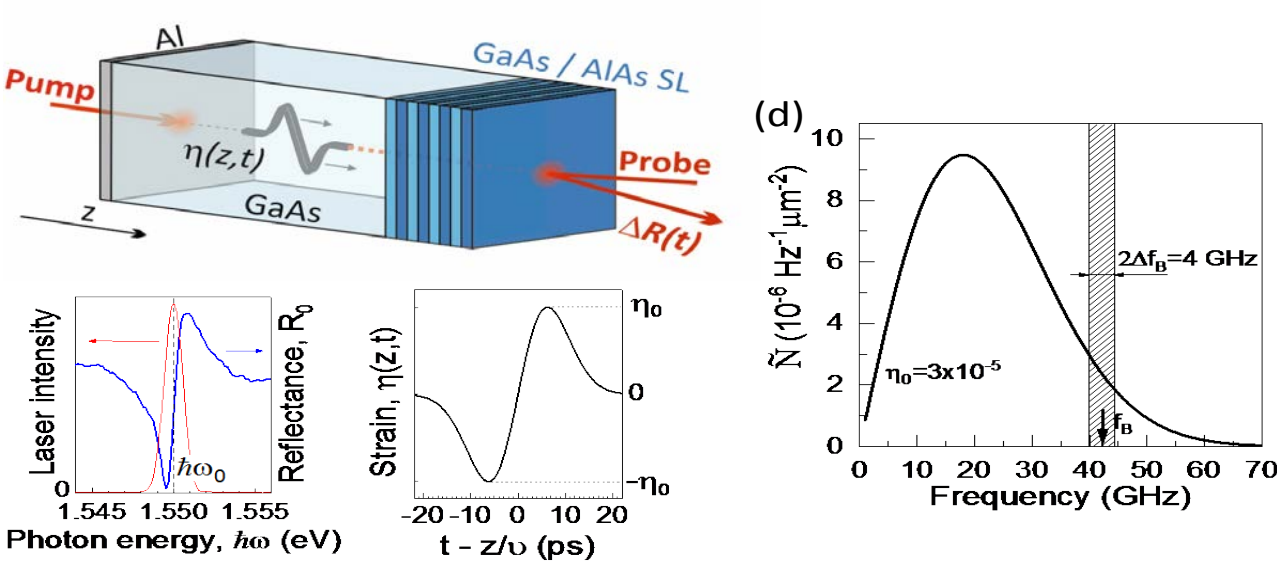

Fig. 1. (a) *Experimental scheme. (**b**) Reflectivity spectrum in the vicinity of the polariton resonance (**blue curve**). Dashed red curve shows the spectrum of the spectrally narrow probe pulse centered at the polariton resonance. (**c**) Simulated temporal profile of the strain pulse injected into the GaAs substrate from the Al optoacoustic transducer. (**d**) Spectral-spatial density of phonons in the coherent phonon wave packet for the pump power density J = 0.5 mJ/cm^2. Shaded area shows the spectral range of detected phonons.*

The studied structure is a short-period superlattice with 30 pairs of GaAs(12 nm)/AlAs(14.2 nm) grown on a GaAs substrate. The SL polariton resonance shown in Fig. 1(b) is centered at $\hbar\omega_0$ =1.55 eV and has a spectral width of 0.7 meV. For generating and detecting coherent phonons, we use 200-fs pulses of a Ti:Sapphire regenerative amplifier (100-kHz repetition rate, central photon energy of 1.55 eV). The pump pulses hit the Al film deposited on the substrate's backside. The film serves as an optoacoustic transducer: it expands due to the optically induced heating and generates a coherent phonon wave packet in the form of a bipolar strain pulse with ~10 ps duration and amplitude η_0, as shown in Fig 1(c). Its spectrum with a maximum at f = 20 GHz is shown in Fig. 1(d). The wave packet propagates in the structure with the velocity of longitudinal sound, υ =4.8 km/s. The coherent phonons are detected in the SL by measuring the transient reflectivity changes, $\Delta R(t)$, using the probe pulses split from the same laser source, and delayed on the propagation time

of the phonon wave packet through the substrate. Scanning the time delay between the probe and pump pulses by a mechanical delay line provides the sub-ps time resolution. To study the effect of the SL polariton resonance on the efficiency of phonon detection, we extend the duration of the probe pulse up to 1.35 ps with a corresponding narrowing of its spectral width down to 1.4 meV by using a tunable filter and measure the signal $\Delta R(t)$ for different central photon energy $\hbar\omega$.
Fig. 2(a) shows the transient reflectivity signal measured at the probe photon energy $\hbar\omega = \hbar\omega_0$ =1.55 eV It possesses the oscillatory behavior known as time domain Brillouin scattering (TDBS) [8]. The oscillations begin at t = –150 ps and last until t = +150 ps. During this time interval, coherent phonons propagate through the SL toward the free surface and after reflection at t = 0 ps, in the opposite direction toward the substrate. The fast Fourier transform of $\Delta R(t)$ shown in Fig. 2(b) demonstrates an intense line at f_B= 42 GHz. The oscillation frequency at the normal incidence of the probe beam is set by the selection rule:

$$f_B = vq_B/2\pi\,;\, q_B = 2k_1$$

where q_B is the wave vector of detected phonons and k_1 is the wave vector of the probe light in the media. The main parameters of the transient reflectivity signal, i.e., its amplitude, frequency, phase, and decay rates, depend on the probe photon energy. Fig. 2(c) demonstrates the dependence of the TDBS amplitude A_B on $\hbar\omega$. It is seen that $A_B(\hbar\omega)$ has a maximum at the spectral position of the polariton resonance and rapidly decreases with the increase of the detuning of $\hbar\omega$ from $\hbar\omega_0$. It leads us to the conclusion that the TDBS signal is governed by the polariton resonance when the probe photon energy $\hbar\omega$ is close to $\hbar\omega_0$. The most spectacular observation is the huge amplitude $A_B \sim 10^{-2}$ for the used pump fluence $J \sim 0.1$ mJ/cm^2 at $\hbar\omega = \hbar\omega_0$. The amplitude of the TDBS signal in a material without a narrow optical resonance for a similar phonon wave packet would be 3 orders of magnitude smaller [9,10].

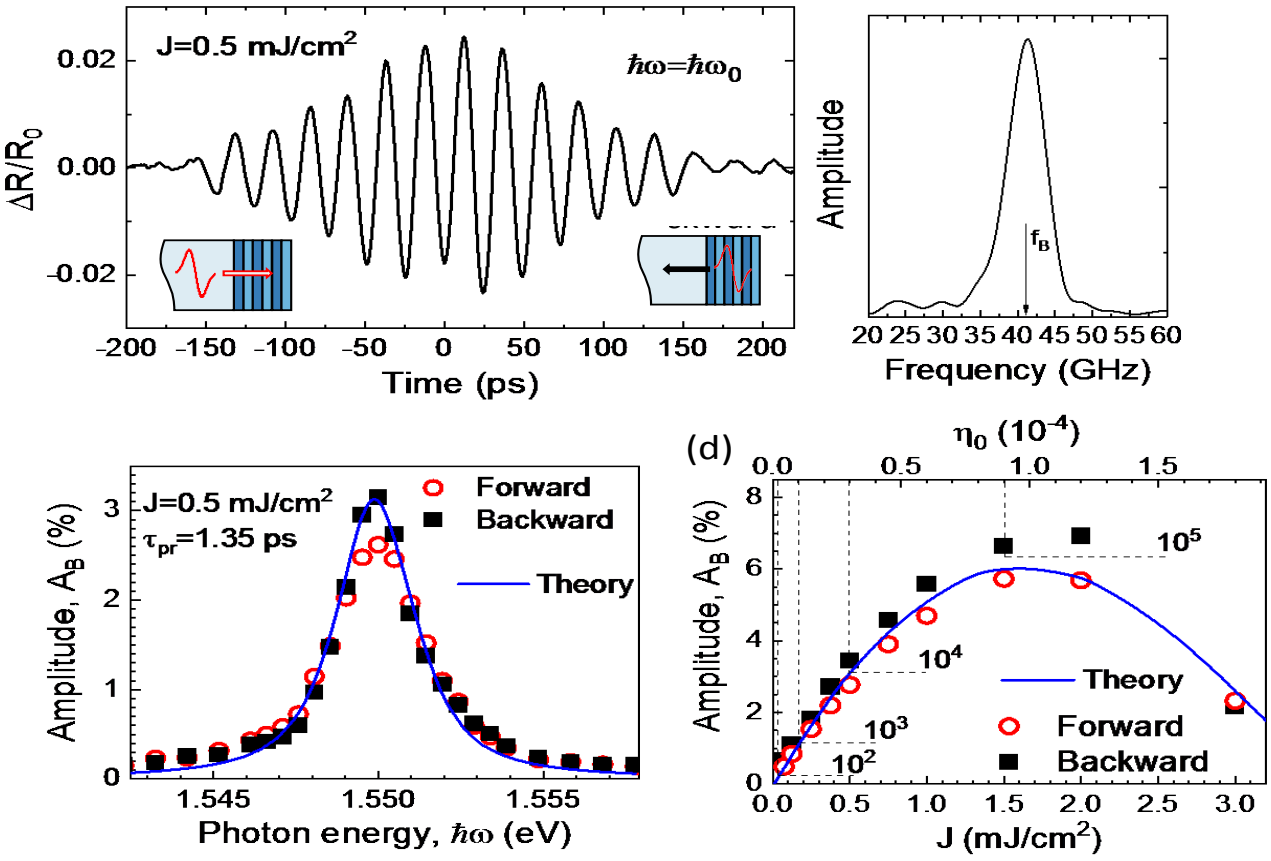

Fig. 2. *(a) TDBS signals measured at $\hbar\omega = \hbar\omega_0$ and its FFT spectrum (b). (c) Dependence of the TDBS signal amplitude $A_B$on the probe photon energy. (d) (a) Dependence of the TDBS signal amplitude on the optical excitation. The dashed lines indicate the estimated number of detected phonons per pulse per square micron N_B for the corresponding strain amplitudes. In (c) and (d) the experimental data is shown by symbols, and solid lines show the results of numerical modelling.*

We propose a simplified model for a qualitative explanation of the TDBS signal and its dependence on the probe photon energy. With an assumption that the spectral width of the probe pulse is much smaller than the spectral width of the polariton resonance, we show analytically that the detection sensitivity is determined by the derivative of the complex refractive index $\tilde{n}(\hbar\omega)$ on the strain. It has a sharp extremum at the spectral position of the polariton resonance, and the spectral shift of the polariton resonance due to the phonon-induced strain [11] results in strong reflectivity modulation. The qualitative conclusions are supported by comprehensive numerical modelling, in which we take into account the finite spectral width of the probe pulse and its Stokes/anti-Stokes spectral shifts due to the scattering process. The numerical modelling demonstrates perfect agreement with the experiment. The large amplitude of the transient reflectivity signal allows us to achieve quantum sensitivity of phonon detection. The number of phonons responsible for the TDBS is determined by their spectral density in the phonon wave packet in the frequency interval $f_B \pm \Delta f_B$ The finite spectral width $2\Delta f_B = 4$ GHz shown by dashed rectangular in Fig. 1(d) is due to the finite size of the SL and the limited penetration of the probe light, which determine the rise-decay rate of the TDBS signal. The number of phonon in the detected frequency interval is determined by the spatial-temporal profile of the generated phonon wave packet. Figure 2(d) shows the power dependence of the TDBS amplitude measured at $\hbar\omega = \hbar\omega_0$. The minimal density of detected phonons, proportional to J^2, is $N_B \approx 10^2$ μm^{-2} and corresponds to the pump fluence, at which the TDBS amplitude exceeds the noise level. In the experiments with a high repetition rate laser, the sensitivity limit can be easily lowered to $N_B \approx 10^{-2}$ μm^{-2} ($A_B \sim 10^{-5}$). This enables the detection of phonon wave packets with one phonon quantum at the Brillouin frequency. At the same time, increasing the number of phonons in the wavepacket results in decreased detection sensitivity. The decrease of $A_B(J)$ at large pump excitation density is due to the large phonon-induced shift of the polariton resonance, which becomes comparable with the polariton spectral width. In this case, $\tilde{n}(\hbar\omega)$ becomes dependent on the coordinate and time. It is equivalent to the spectral broadening of the polariton resonance and, thus, decreases the TDBS sensitivity. The demonstrate quantum sensitivity of the optical detection of coherent acoustic phonons paves the way for applications in phononics with extremely low-density phonon fluxes. For instance, this technique could be used for the detection of phonons emitted from single nanoobjects and the nanoscopy of such delicate nanoobjects as biological cells [12].

References

[1] P. Delsing, A. N. Cleland, M. J. A. Schuetz, J. Knörzer, G. Giedke, J. I. Cirac, K. Srinivasan, M. Wu, K. C. Balram, C. Bäuerle, *Journal of Physics* D **52**, 353001 (2019).

[2] O. Matsuda, M. C. Larciprete, R. Li. Voti, O. B. Wright, *Ultrasonics* **56**, 3 (2015).

[3] A. V. Scherbakov, A.S. Salasyuk, A.V. Akimov, X. Liu, M. Bombeck, C. Bruggemann, D.R. Yakovlev, V.F. Sapega, J.K. Furdyna M. Bayer, *Physical Review Letters* **105**, 117204 (2010).

[4] C. Brüggemann, A. V. Akimov, A. V. Scherbakov, M. Bombeck, C. Schneider, S. Höfling, A. Forchel, D. R. Yakovlev, M. Bayer, *Nature Photonics* **6**, 30 (2012).

[5] A. A. Demenev, D. D. Yaremkevich, A. V. Scherbakov, S. M. Kukhtaruk, S. S. Gavrilov, D. R. Yakovlev, V. D. Kulakovskii, M. Bayer *Physical. Review* B **100**, 100301(R) 2019.

[6] M. Kobecki, A. V. Scherbakov ,S. M. Kukhtaruk, D. D. Yaremkevich, T. Henksmeier, A. Trapp, D. Reuter, V. E. Gusev, A. V. Akimov M. Bayer, *Physical Review Letters* **128**, 157401(2022).

[7] A. N. Poddubny, A. V. Poshakinskiy, B. Jusserand, A. Lemaître, *Physical Review* B **89**, 235313 (2014).

[8] C. Thomsen, H. T. Grahn, H. J. Maris, J. Tauc, *Optical Communications* **60**, 55 (1986).

[9] A. Huynh, B. Perrin, N. D. Lanzillotti-Kimura, B. Jusserand, A. Fainstein, A. Lemaître, *Physical Review* B **78**, 233302 (2008).

[10] A. V. Scherbakov, M. Bombeck, J. V. Jäger, A. S. Salasyuk, T. L. Linnik, V. E. Gusev, D. R. Yakovlev, A. V. Akimov, M. Bayer, *Optics Express* **21**, 16473 (2013).

[11] A. V. Akimov, A. V. Scherbakov, D. R. Yakovlev, C. T. Foxon, M. Bayer, *Physical Review Letters* **97**, 037401 (2006).

[12] F. Prez-Cota1, R. Fuentes-Domnguez, S. La Cavera, W. Hardiman, M. Yao, K. Setchfield, E. Moradi, S. Naznin, A. Wright, K. F. Webb A. Huett, C. Friel, V. Sottile, H. M. Elsheikha, R. J. Smith, M. Clark, Journal Appled. Physics **128**, 160902 (2020).

* Acknowledgement(s) : authors acknowledge support by the Deutsche Forschungsgemeinschaft (Grant No. TRR 142 Project A06 and Grant No. TRR160 Project A01) and the Volkswagen Foundation (Grant No. 97758).

Ultrafast lattice dynamics during singlet Exciton fission in pentacene single crystals

H. Schwoerer[1], H. Seiler[2], R. Ernstorfer[2], S. Hammer[4], M. Rossi[1]
[1] *Max Planck Institute for the Structure and Dynamics of Matter, 22761 Hamburg, Germany*
[2] *Fritz Haber Institute of the Max Planck Society, 14195 Berlin, Germany*
[3] *Julius-Maximilian University, 97074 Würzburg, Germany*

Singlet exciton fission SEF is an electronic process occurring in certain photoexcited organic molecular solids, where one exciton (bound electron hole pair) of spin zero spontaneously decays into two excitons of spin 1 each. In the context of organic photovoltaics, this provides the possibility of generating two free electrons and two holes (after separation at a boundary) per one absorbed photon, rather than one, of course of maximum half the energy each. The (not immediately obvious) efficiency benefit for photovoltaics sparks the continuous attention to SEF since its first observation more than half a centure ago, and will be explained in the introductory part of the talk. As a process of high yield in an electronically excited state, it has to be ultrafast; and since fission of an exciton eventually leads to two spin and electronically independent and spatially separated excitons, it requires strong correlation in the crystal beyond the molecular entities, mediated by overlap of the (intramolecularly delocalized) π molecular orbitals. Hence, it is intriguing to learn, whether and which intra- and/or intermolcular structural motions accompany SEF or even positively or negatively affect its yield. The current understanding assumes singlet exciton fission to be a three step process, with an initial ultrafast fission into two electronically and spin coupled triplet excitons, a subsequent loss of their electronic coherence, and eventually loss of their spin coherence and spatial separation of the two triplets. For recent reviews see [1,2]. So far, fission dynamics have almost exclusively been investigated by femtosecond laser spectroscopic means (transient absorption or two-dimensional spectroscopy etc.), observing electronic populations and interactions thereof and indirectly inferring atomic and molecular structural dynamics.

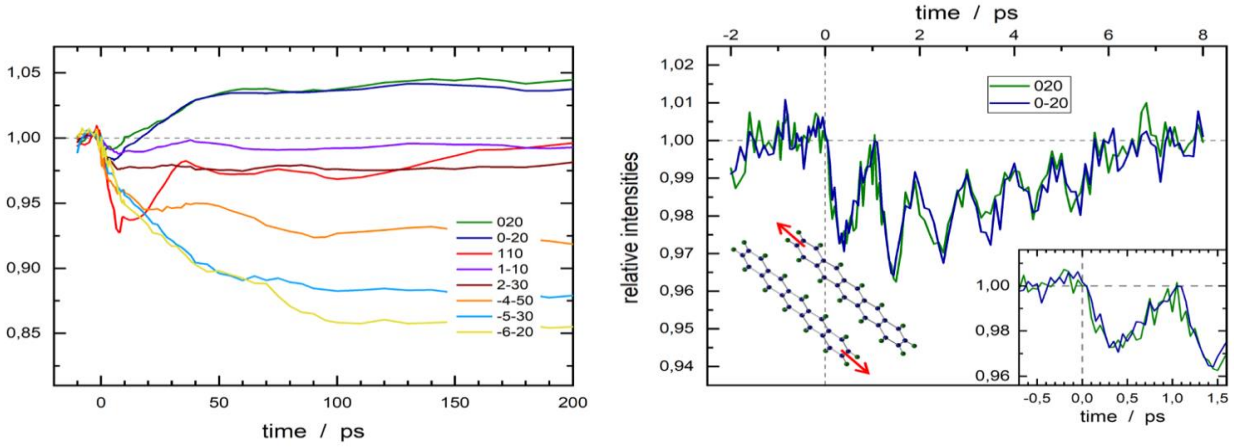

***Fig. 1.**: Ploted are changes of diffraction peak intensity of different orders as a function of time after pahoto excitation of pentacene single crystals. These changes are manifestation of incoherent and coherent structural dynamics of photoexcited during singlet exciton fission, such as the slip sliding motion of the two pentacene molecules in the unit cell or the lattice reorganisation due to the final plaronic nature of the triplet excitons [3].*

Here, we apply ultrafast electron diffraction being sensitive to structural dynamics of periodc lattices with a high spatial resolution and a temporal resolution sufficient to detect coherent motion and reorganization on a subpicosecond scale. We will discuss the present state of the art of UED experiments, its current limitations and promising directions of improvements. We investigate single crystalline pentacene with the initial (exothermic) fission shorter than 100 fs and a 100% fission yield. Pentacene is one of the most thoroughly investigated SEF materials, also due to its substantial balance of complexity and simplicity on both, the molecular and the crystalline level. Despite pentacene, as pure hydrocarbon material, being a bad scatterer, we could identify oscillatory coherent and incoherent dynamics with three distinct and characteristic time constants, present in various diffraction orders, see Fig, 1. By combining analysis of diffraction symmetries, time dependent density function theory and molecular dynamics simulations, we assign the observations to coherent intermolecular motion and lattice reorganisations during the exciton fission evolution towards the free triplets [3].

References

[1] M. Smith, J. Michl, *Annual Review of Physical Chemistry* **64**, 361, (2019).
[2] K. Miyata, F. Conrad-Burton, F. Geyer, X.-Y. Zhu, *Chemical Reviews* **119**, 4261, (2019).
[3] H. Seiler, M. Krynski, D. Zahn, S. Hammer, Y. Windsor, T. Vasileiadis, J. Pflaum, R. Ernstorfer, M. Rossi, H. Schwoerer, *Science Advances* **7**, eabg0869, (2021).

Light-induced coherent c-axis charge carrier responses in stripe-ordered cuprate superconductors

R. Shimano
The University of Tokyo, 113-0033 Tokyo, Japan

Light-induced superconductivity in cuprate superconductors has been reported in stripe-ordered phases of $La_{1.675}Eu_{0.2}Sr_{0.125}CuO_4$ [1] and $La_{2-x}Ba_xCuO_4$ [2], and also in underdoped $YBa_2Cu_3O_y$[3]. In particular for the stripe-ordered system, the mechanism is interpreted as the revival of inter-layer Josephson coupling which is vanished in equilibrium because of the π phase shift of superconducting order between neighbouring stripes within a plane [4]. To have a deeper understanding on the competition between the charge/spin stripes and the superconductivity, we investigated another archetypical stripe-ordered superconductor, $La_{2-x-y}Nd_ySr_xCuO_4$ (x=0.12) where the correlation length of stripes is shown to be short-ranged compared to that of $La_{2-x}Ba_xCuO_4$ [5]. Upon the irradiation of ultrafast near-infrared (800 nm) light pulse, a clear plasma edge and the corresponding loss function peak were identified in the c-axis terahertz reflectivity above T_c(=3.2 K) until the onset temperature of the charge stripe T_{co} (=67 K) as represented in Fig.1. On the other hand, the $1/\omega$ divergence of the imaginary part of the optical conductivity, which has been identified as an optical fingerprint of the light-induced superconductivity, was not observed and the spectrum was mostly reproduced by the Drude model with unusually small scattering rate [6].

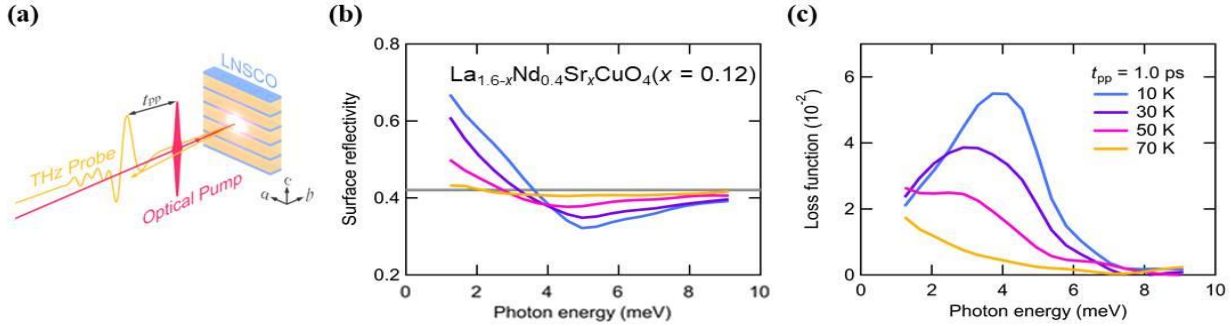

Fig. 1. (a)*: Schematic setup of optical pump-terahertz probe spectroscopy in $La_{2-x-y}Nd_ySr_xCuO_4$ (LNSCO)(x=0.12) with T_c=3.2 K.* ***(b)****: Reflectivity and* ***(c)*** *loss function spectrum at 1 ps after the photoexcitation at the indicated temperatures.*

To reconcile these results, we discuss the possibility of short-ranged (or fluctuating) superconductivity in the NIR pump-induced states and its relevance to the charge stripes. We will also compare the results with that of $YBa_2Cu_3O_{7-\delta}$ under the NIR pumping studied by the observation of THz nonlinear responses [7].

References

[1] D. Fausti, R. I. Tobey, N. Dean, S. Kaiser, A. Dienst, M. C. Hoffmann, S. Pyon, T. Takayama, H. Takagi, A. Cavalleri, *Science* **331**, 189 (2011).
[2] D. Nicoletti, E. Casandruc, Y. Laplace, V. Khanna, C. R. Hunt, S. Kaiser, S. S. Dhesi, G. D. Gu, J. P. Hill, and A. Cavalleri, *Physical Review* B **90**, 100503(R) (2014).
[3] S. Kaiser, C. R. Hunt, D. Nicoletti, W. Hu, I. Gierz, H. Y. Liu, M. Le Tacon, T. Loew, D. Haug, B. Keimer, A. Cavalleri, *Physical Review* B **89** 184516 (2014).
[4] E. Berg, E. Fradkin, E.-A. Kim, S. A. Kivelson, V. Oganesyan, J. M. Tranquada, S. C. Zhang, *Physical Review Letters* **99**, 127003 (2007).
[5] S. B. Wilkins, M. P. M. Dean, Jörg Fink, Markus Hücker, J. Geck, V. Soltwisch, E. Schierle, E. Weschke, G. Gu, S. Uchida, N. Ichikawa J. M. Tranquada, J. P. Hill, *Physical Review* B **84**, 195101 (2011).
[6] M. Nishida, K. Katsumi, D. Song, H.i Eisaki, R. Shimano, *arXiv*:2303.01961 (2023).
[7] K. Katsumi, M. Nishida, S. Kaiser, S. Miyasaka, S. Tajima, R. Shimano, *arXiv*:2209.01633 (2022).

Ultrafast surface melting of electronic phase transition

K.Siddiqui, M. Monti, S.Wall
Aarhus University, 8000 Aarhus-C, Denmark

Our understanding of ultrafast phase transitions has been shaped by the assumption that the ordered bulk order properties are prevalent and represent a homogeneous system as a whole. However, recent studies have unveiled the role of disorder and heterogeneity with the latter being a ubiquitous feature of many considered quantum materials [1,2]. Moreover, the equilibrium surface properties can be very different from that of the bulk [3,4], but studies that clarify how surface affects the non-equilibrium properties during a phase transition are lacking but are important in improving our understanding of the ultrafast phase transitions. In this talk, we will report on our results in which we probe the ultrafast dynamics of the layered manganite, $L_{0.5}Sr_{1.5}MO_4$ which displays an orbital ordering (OO) phase transition below T_{OO} = 220 K accompanied by a structural phase transition leading to quadrupling of the unit cell. Using grazing incidence x-ray diffraction at a femtosecond x-ray free-electron laser facility (SwissFEL), we measure the surface orbital ordering peak (orbital truncation rod, OTR) and the bulk orbital order Bragg peak and compare their dynamics induced by an intense femtosecond near-infrared laser pulse at 800 nm. We find that the melting threshold for OTR peak is significantly lower (Fig 1) than the suppression of the structural distortions. In addition, we perform reciprocal space mapping of both peaks to clarify how disorder contributes to the phase transition by analysis of diffuse scattering and via extraction of the corresponding correlation lengths. In the talk, we will reveal the details of the analysis and discuss the implication of our observations for the description of phase transition in quantum materials.

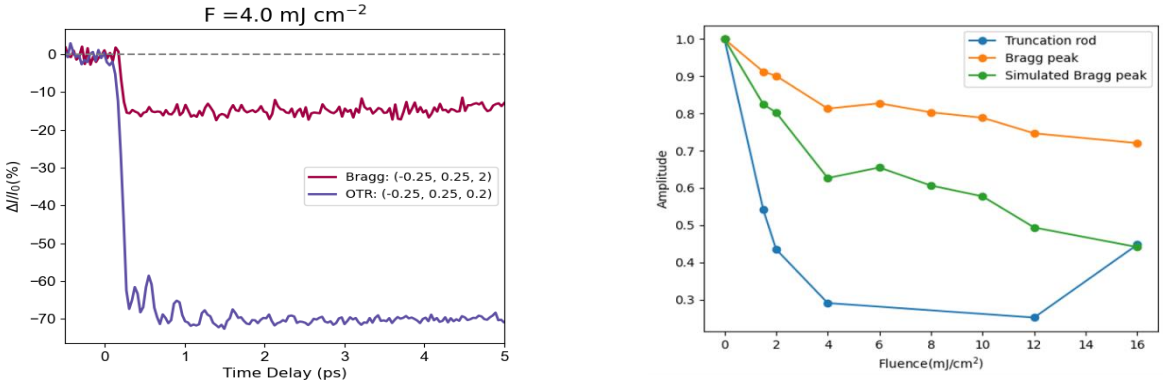

***Fig. 1. Left**: Temporal response of ORT (**blue**) and Bragg peak (**red**) following 800 nm photoexcitation.*
***Right**: Plot comparing the magnitude of reduction of the respective peaks as a function of fluence.*
These plots reflect that the melting threshold for the surface order is much lower than the bulk order.

In addition, we perform reciprocal space mapping of both peaks to clarify how disorder contributes to the phase transition by analysis of diffuse scattering and via extraction of the corresponding correlation lengths. In the talk, we will reveal the details of the analysis and discuss the implication of our observations for the description of phase transition in quantum materials.

References

[1] S. Wall, S.Yang, L.Vidas, M. Chollet, J. M. Glownia, M. Kozina, T. Katayama, T. Henighan, M. Jiang, T. A. Miller, D. A. Reis, L. A. Boatner, O. Delaire M. Trigo, *Science* **362**, 572 (2018).
[2] D. Perez-Salina, A. S. Johnson, D. Prabhakaran and S. Wall, *Nature Communications* **13**, 238 (2022).
[3] S. B. Wilkins, X. Liu, Y. Wakabayashi, J.-W. Kim, P. J. Ryan, H. Zheng, J. F. Mitchell, and J. P. Hill, *Physical Review* B **84**, 165103 (2011).
[4]. Y. Wakabayashi, M. H. Upton, S. Grenier, J. P. Hill, C. S. Nelson, J.-W. Kim, P. J. Ryan, A. I. Goldman, H. Zheng , J. F. Mitchell, *Nature Materials* **6**, 972 (2007).

Picosecond Volume Expansion in a Nano-textured Mott Insulator

A. Singer
Cornell University, Ithaca, New York, 14853, USA

Technology is moving towards ever faster switching between different electronic and magnetic states of a material. Manipulating properties at terahertz rates requires accessing the natural timescales of the electrons (fs) and phonons (sub-ps to few ps) in condensed matter, possible with short-pulse photoexcitation. Yet, in Mott insulators featuring abrupt, volume-changing insulator-to-metal (IMT) phase transitions, such as in VO_2 and V_2O_3, the nucleation and growth of percolating domains often hamper the ultrafast dynamics [1, 2]. Here, using time-resolved x-ray diffraction, we show a ~1.2 ps photoinduced volume expansion in an epitaxially strained Mott insulator Ca_2RuO_4 (see Figure). The diffraction data from the strained thin films display a transient nano-texture in the low-temperature ground state. X-ray imaging elucidates that the satellite peaks in diffraction form due to strain-induced ferroelastic domains emerging transiently during the metal-insulator transition (the nano-texture disappears when heated above the transition). Instead of homogeneously transforming into a low-temperature structure (like in bulk), the strained Mott insulator splits into nanodomains with alternating lattice constants, as confirmed by cryogenic scanning transmission electron microscopy[3]. Time-resolved x-ray reciprocal space mapping reveals dynamic nano-texture, proposing a mechanism where the photoinduced phase heterogeneously nucleates at inclusions of the incipient long-bond phase stabilized through epitaxial strain. The structure factor and lattice spacing analysis reveals a structure absent in equilibrium. Photoexcitation also launches lateral domain dynamics centered at a frequency of ~ 0.2 THz, consistent with the strain-induced heterogeneity.

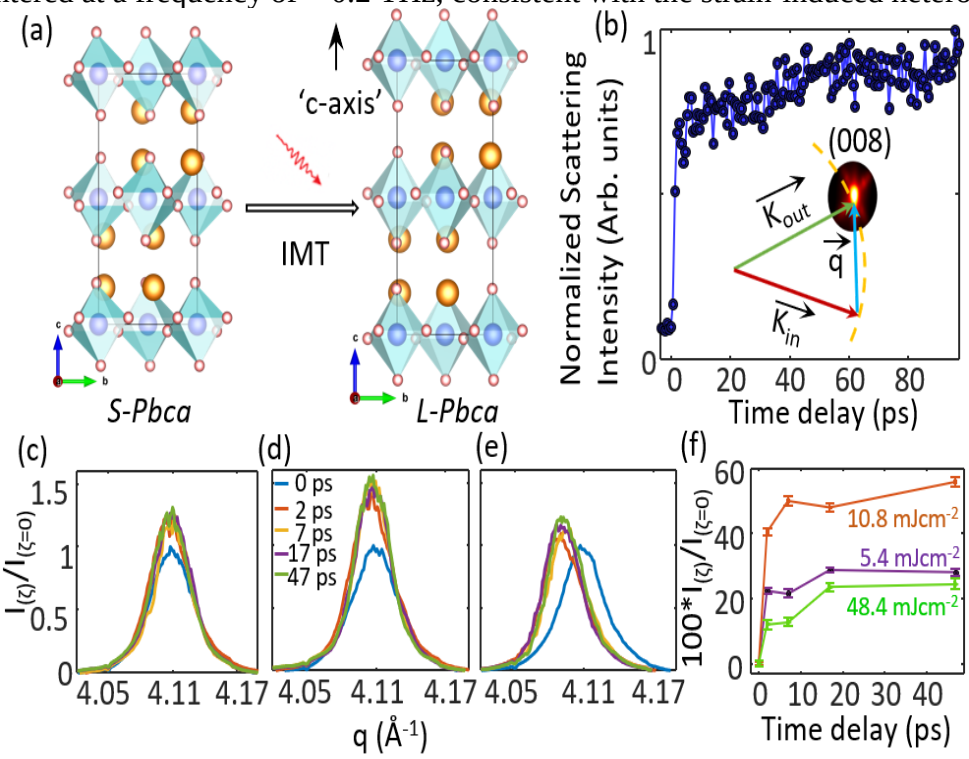

Fig.1 . (a) *Ca_2RuO_4 unit cell diagram for insulating (**S-Pbca**) and metallic (**L-Pbca**) phases where calcium ions are shown in red, ruthenium ions in blue, and oxygen ions in peach color, **(b)** Time-resolved normalized scattering intensity of 008 Bragg peak plotted against the time-delay. **(c)** Normalized scattering intensity plot with a series of time delays at fix fluence, where **(c)** 5.4 mJcm^{-2}, **(d)** 10.4 mJcm^{-2}, and **(e)** 48.4 mJcm^{-2} and extracted characteristics parameters of the peak at various pump fluence and time delays, these are fitted by the Gauss function, where **(f)** Peak height as a function of time-delay at pump fluences 5.4 mJcm^{-2}, 10.4 mJcm^{-2}, and 48.4 mJcm^{-2}*

This work highlights the use of strain for tuning the timescales in photoinduced transitions, potentially offering opportunities for terahertz technologies.

References

[1] E. Abreu, S. Wang, J.G. Ramírez, M. Liu,J. Zhang,K. Geng,I.K. Schuller,R.D. Averitt, *Physical Review* B **92** 085130 (2015).
[2] A. Singer, J.G. Ramirez, I. Valmianski, D. Cela, N. Hua, R. Kukreja, J. Wingert, O. Kovalchuk, J.M. Glownia M. Sikorski, M. Chollet,M. Holt,I.K. Schuller,O.G. Shpyrko, *Physical Review Letters* **120**, 207601 (2018).
[3] Z. Shao, N. Schnitzer, J. Ruf, O.Y. Gorobtsov, C. Dai, B.H. Goodge, T. Yang, H. Nair, V.A. Stoica, J.W. Freeland, J. Ruff, L.-Q. Chen D.G. Schlom,K.M. Shen,L.F. Kourkoutis,A. Singer *arXiv* ***2211.01506*** (2022).

En route to next generation high energy high repetition rate Ultrafast laser sources in the mid-IR

I. T. Sorokina[1], V. L. Kalashnikov[1], A.Rudenkov[1], M.Demesh[1], C. Grivas[1], N. Gusakova[1], E. Sorokin[2]
[1]*Norwegian University of Science and Technology, 7034 Trondheim, Norway*
[3] *Technische Universität Wien, A-1040 Vienna, Austria*

The solid-state lasers based on the Cr^{2+}-doped crystals of the II-VI family [1-3] operate at room temperature, possess the widest among existing solid-state lasers bandwidth of up to 45% of the central wavelength, provide tens of Watts power levels, and deliver few-cycle femtosecond pulses [2,4], recently also in diode-pumped setups [5]. The output peak powers reaching 1 MW and pulse durations as short as 28 fs, direct generation of CEP-stable mid-infrared pulses became a reality. The works on power scaling have enabled the generation, via nonlinear frequency conversion, of mid-IR light that spans the entire "molecular fingerprint" region between 4.5 and 14 μm [4,5]. Despite the rapid development of ultrafast lasers based on Cr^{2+}- crystals during the last two decades, both with respect to applications and sources, the interaction of these ultra-short pulses with matter are mostly limited by the relatively low nanojoule pulse energies obtainable directly from the oscillator. Currently, the highest pulse energy was obtained from the Cr:ZnS chirped-pulse oscillator (CPO), amounting to about 50 nJ [6]. In turn, development of energetic 0.1-10 μJ ultrafast mid-IR sources would pave the way for additional interesting industrial applications such as e.g. sub-wavelength 3-D sub-surface processing of silicon and other semiconductor materials [7,8].

In this talk we review the state-of-the art in the field with a particular emphasis on our recent advances towards the challenging goal of development of compact high-energy ultrashort-pulsed laser systems in the 2–3 μm wavelength range. We will discuss approaches for generating high laser peak power and energy scaling in a hybrid mid-IR chirped pulse oscillator-amplifier (CPO-CPA) system and discuss ways to achieve stable operation in fluctuating environment. We also present the results of our feasibility study of spatiotemporal mode-locking in a mid-IR Cr:ZnS waveguide laser based on the nonlinear spatial mode coupling, providing a route to the energy-scalable waveguide lasers. In our latest report in Optics Express we proposed a novel technique to provide hybrid CPO-CPA pulse energy scaling, preserving the output spectrum's high-fidelity compression. In the following, we describe the first steps in this direction, both experimentally and theoretically, demonstrating the viability of the proposed concept.

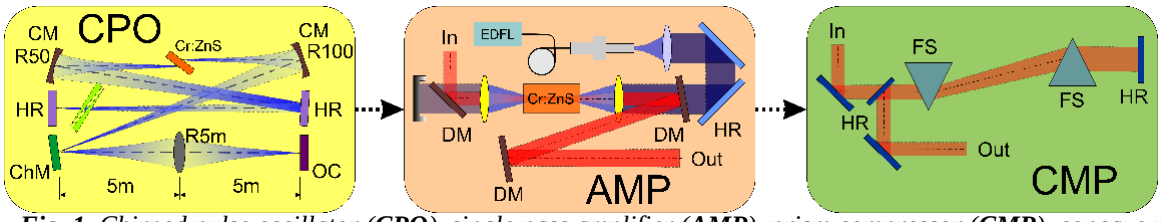

Fig. 1. *Chirped pulse oscillator (**CPO**), single pass amplifier (**AMP**), prism compressor (**CMP**), concave mirror (**CM**), chirped mirror (**ChM**), output coupler (**OC**), dichroic mirrors (**DM**), erbium doped fiber laser (**EDFL**), fused silica prisms (**FS**), highly reflective mirrors (**HR**).*

The classical route of obtaining the high-energy pulses incorporates a small-power ultrashort seed oscillator, pulse picker, stretcher, amplifier and compressor, which might be too complex for many possible uses. Another way is to employ a travelling-wave amplifier. This approach has been demonstrated with ultrashort pulses [4], showing that the obtainable energy is limited by the strong nonlinear interactions in the gain medium if no stretching is used. We propose and demonstrate using a hybrid reduced-nonlinearity scheme, which incorporates a reduced repetition rate chirped-pulse oscillator (CPO) directly followed by an amplifier, which thus operates in a chirped pulse regime as well (Fig. 1) [9]. The system produces pulses of 1.5-3 ps duration which can be compressed below 200 fs using a simple prism compressor (Fig. 2).

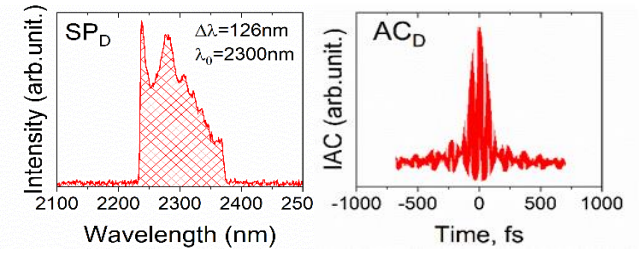

Fig. 2. *Amplified pulse spectrum **(left)** and autocorrelation trace **(right)** after compression from 3 ps.*

There are more advantages in using such a scheme than just saving on pulse picker and stretcher. First, the CPO oscillator has a well-confined spectrum with sharp edges (Fig. 2), which in the case of Cr:ZnS helps to stay away from air humidity (see Section 3). Another CPO advantege is the possibility of pulse energy scalability, which allows reducing the oscillator repetition rate even further. In this regime, called dissipative resonance, the higher pulse energy increase is accommodated by chirp growth without spectral broadening. Reaching this regime [9] allows anticipating higher energies for low repetition rate systems in basically the same simple setup.
For practical applications of ultrashort pulses in the spectral regions with significant atmospheric absorption and dispersion it is important to provide a reliable operation of the system which would not be subject to humidity, pressure or other fluctuations. To avoid cumbersome evacuation or continuous purging, one would need a way to compensate for the atmospheric changes. Using the Cr:ZnS ultrashort-pulsed laser as a test-bed, we demonstrated the air influence on a femtosecond and chirped-pulse oscillator performance and showed that the humidity GVD is the main factor [10]. The GVD due to the molecular absorbers can be readily calculated to provide wildly oscillating by ps^2 features even in the transparency windows (Fig. 3a). We have shown that it is the slowly varying *average* GVD that matters (Fig. 3b) and provided methods to calculate it for given humidity, temperature and pressure.

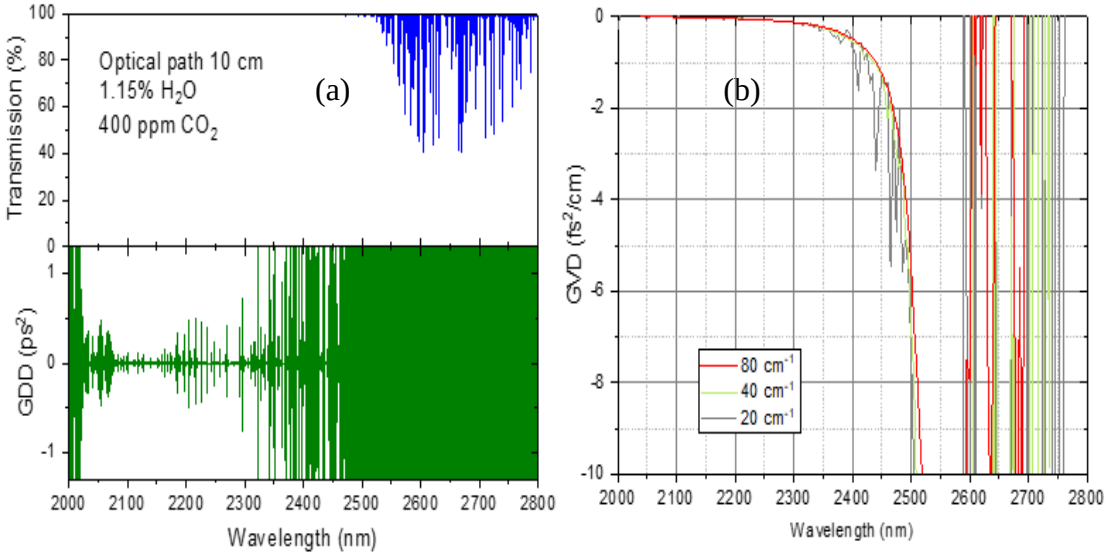

Fig. 3. ***(a)*** *Transmission of the atmosphere and corresponding GDD for the 10 cm optical path at 40% relative humidity (r.h.) at $T = 296$ K and $p = 1$ atm. Note the scale of the GDD, which is in picoseconds squared.* ***(b)*** *Slowly varying GVD due to water vapour using different spectral windowing.*

.

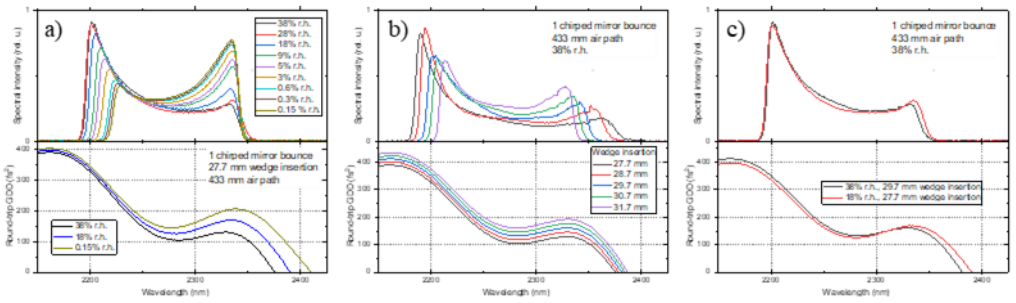

Fig. 4. ***(a)*** *CPO oscillator spectra under nitrogen purging.* ***(b)*** *CPO oscillator spectra at open air with different YAG wedge insertions.* ***(c)*** *Approximate compensation of higher humidity by increased YAG wedge insertion. For all graphs, the lower plot shows the calculated round-trip GDD.*

Knowing the dispersion associated with the humidity, CO_2 or other atmospheric absorbers allows compensating for its changes. We have demonstrated the feasibility of this approach using a Cr:ZnS CPO with a four-meter long cavity round-trip. The CPO is a good test-bed as it is very sensitive to dispersion changes (Fig. 4a). As it is shown in Fig. 4b, by changing the wedge insertion by mere 2 mm it is possible to nearly completely compensate for the humidity change of 20% r.h. This result

demonstrates the possibility to operate mid-IR oscillators in a wide range of laboratory conditions without evacuation or purging the whole setup. The high nonlinearity of the II-VI materials opens the way to realizing the concept of spatio-temporal mode-locking [11]. We demonstrate the feasibility of implementing this concept in a Cr:ZnS waveguide laser operating in the regime of *distributed Kerr-lens mode-locking* [12] when the nonlinear coupling between the spatial modes causes the formation of an ultrashort pulse by only a transversely profiled pump beam.

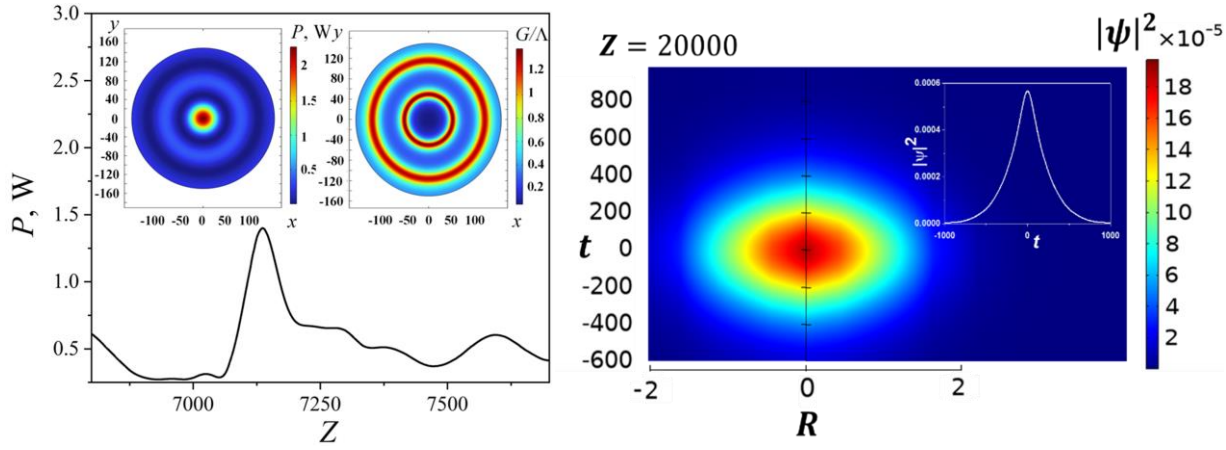

Fig. 5. (left) *Evolution of the beam power with waveguide rounf-trip Z for wavegude radius 30 μm and pump beam radius 40 μm. The left inset shows the dimensionless power profile near the power peak. The right inset demonstrates the corresponding relative gain profile.* ***(right)*** *Spatiotemporal contour plots of the dimesionless dissipative soliton intensity* $|\psi|^2$ *on the dimensionless (radial coordinate, time)-plane at the noted waveguide roundtrip Z for the anomalous group-delay dispersion.*

Below the mode-locking threshold defined by a pump power, waveguide, and pump beam radii, the field consists of many spatial modes (Fig. 5, left), which compete through the gain saturation (see insets). As a result, the laser operates in a Q-switched regime. When the nonlinear coupling between the modes sets on, the modes of the most intensive field spike relax to the ground mode, which experiences the maximum gain. Thus, a spatio-temporal dissipative soliton develops (Fig. 5, right).

Our most recent experiments and numerical simulations [13] demonstrate that pump beam forming a soft aperture could provide an effective spatial mode control in a nonlinear multimode waveguide which, through nonlinear spatial inter-mode coupling, enables formation of a spatiotemporal dissipative soliton - a ‘light bullet’. This novel approach paves the way to the next generation compact MIR laser sources - distributed Kerr-Lens Mode-locked energy-scalable solid-state waveguide lasers. Our most recent experiments and numerical simulations [13] demonstrate that pump beam forming a soft aperture could provide an effective spatial mode control in a nonlinear multimode waveguide which, through nonlinear spatial inter-mode coupling, enables formation of a spatiotemporal dissipative soliton - a ‘light bullet’. This novel approach paves the way to the next generation compact MIR laser sources - distributed Kerr-Lens Mode-locked energy-scalable solid-state waveguide lasers

References

[1] I. T. Sorokina, *Optical Materials*, **26**, 395 (2004).
[2] I. T. Sorokina, E. Sorokin, *IEEE Journal of Selected Topics in Quantum Electronics* **21,** 1601519 (2015).
[3] . S. B. Mirov, D. Martyshkin; I. S. Moskalev; M.Mirov; S. Vasilyev, *IEEE Journal Selective Topics. Quantum Electronics* **21,** 292 (2015).
[4] S. Mirov, I. Moskalev, S. Vasilyev, V. Smolski, V. Fedorov, D. Martyshkin, J. Peppers, M. Mirov, A. Dergachev, V. Gapontsev, *IEEE Journal Selective Topics. Quantum Electronics* **24**, 1601829 (2018).S. Mirov, et al., *IEEE JSTQE* **24,** 1601829 (2018).
[5] N. Nagl, “A New Generation of Ultrafast Oscillators for Mid-Infrared Applications”. PhD thesis. Springer (2021).
[6] N. Tolstik, C. S. J. Lee, E. Sorokin, I.T. Sorokina, *Proceedings: Conference on Lasers and Electro- Optics*", CLEO SF1N.2(2018) .
[7] N. Tolstik, E. Sorokin, J.C. Mac-Cragh, R. Richter, I. T. Sorokina *Proceedings: Conference Lasers and Electro-Optics*", CLEO AM41.8 (2022).
[8] I. T. Sorokina, OPIC’2022, Japan (2022).
[9] A. Rudenkov V. L. Kalashnikov, E.Sorokin, M. Demesh, I.T. Sorokina , *arxiv.org/abs/2212.00626*.
[10] E. Sorokin, Alexander Rudenkov, Vladimir Kalashnikov, Irina Sorokina, *arxiv.org/abs/2212.00909*.(2022).
[11] W. Fu, L. G. Wright, P. Sidorenko, S. Backus, F.W. Wise, Optics. Express **268**, 9432 (2018).
[12] J. Zhang, . Pötzlberger, Q. Wang, J. Brons, M. Seidel D.Bauer, D Sutter, V. Pervak, A. Apolonski, K.F. Mak, V.Kalashnikov, Z. Wei, F. Krausz O. Pronin, *Ultrafast Science* **2022,** 9837892 (2022).
[13] M. Demesh, (submitted to JOSA B) (2023).

* Acknowledgement(s) : authors ITS, VLK, AR, MD, CG, and NG acknowledge support from the Norwegian Research Council projects #303347 (UNLOCK), 326503 (MIR) and #326241(LAMMO-3D).

Ultrafast dynamics in quantum materials

P. Padmanabhan[1], Y. Huang[1], N. S. Sirica[1], F. L. Buessen[2], R. V. Aguilar[3], R. Tutchton[1]
K. W. C. Kwoc[4], S. Gilinsky[1], M. C. Lee[1], M. A. McGuire [5], S. R. Singamaneni[6], A. Paramekanti[2]
J.-X. Zhu[1], S. A. Trugman[1],S.-W. Cheong[7], L. Yuan[7], D. A. Yarotski[1], A. Azad[1], R. P. Prasankumar[1]
A. J. Taylor[1]

[1]*Los Alamos National Laboratory, Los Alamos, NM 87545 , USA*
[2]*University of Toronto, Toronto,* ON M5S *Canada*
[3]*Ohio State University, Columbus, OH43210, USA*
[4]*Columbia University, New York, NY 10027, USA*
[5]*Oak Ridge National Laboratory, Oak Ridge, TN 37830, USA*
[6]*The University of Texas at El Paso, El Paso, TX 79968*
[7]*Rutgers University, Piscataway, NJ 08854, USA*

Quantum materials exhibit a wide range of properties resulting from the intricate interplay of the charge, spin, lattice, and orbital degrees of freedom. Unraveling their underlying interactions enables the development of an understanding of emergent properties in quantum materials. In this context, ultrafast optical spectroscopy has provided many valuable insights into the study of competing many-body interactions. Quantum material systems hosting novel intrinsic magnetic order represent an exciting new playground to study the transient interactions between photons and spin excitations in ordered phases, uncovering the nature of the mechanisms that underlie these processes and exploiting them to harness new magnetic phenomena. In this talk, we focus on ultrafast dynamics in emerging magnetic materials.The enormous potential of van der Waals (vdW) magnets in nanoscale information storage and spintronic technologies has stimulated a great deal of research into their equilibrium magnetic and structural properties. Nevertheless, comparatively little is known about their behavior under non-equilibrium conditions or the nature of magneto-structural coupling in this material class on its intrinsic ultrafast timescale. This talk will discuss our recent studies of non-equilibrium lattice and spin dynamics in vdW magnets using ultrafast spectroscopy. In the prototypical 2D magnet, CrI_3, we observe strong light-driven coherent lattice oscillations, commensurate with phonon modes of A_{1g} symmetry. Intriguingly, the amplitude of the c-axis A_{1g} mode shows a strong pump helicity dependence below the magnetic ordering temperature. The correlation between magnetic order and vibrational amplitude of this mode is indicative of a strong coherent coupling between the spin and lattice degrees of freedom [1]. Simulations suggest that this coupling originates from the modulation of exchange interactions through the distortion of the lattice (Fig. 1).

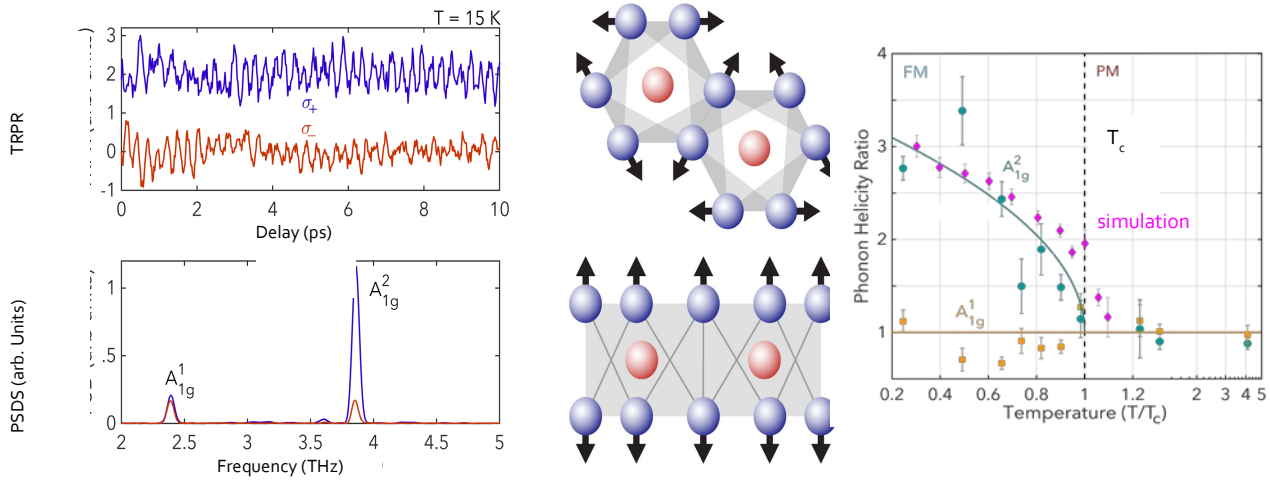

***Fig. 1. Left**: Oscillations in the time-resolved polarization signal at T=15K in the ferromagnetic phase, after subtraction of the demagnetization background, for left circularly polarized σ_+ (blue) and right circularly polarized σ_- (red) pump helicities (**upper** panel) and their corresponding power spectral densities **(lower** panel) **Middle**: Schematic of the eigenvectors of the two phonon modes, A^1_{1g} (top) and A^1_{1g} (bottom). **Right**: The ratio of σ_+/σ_- of the integrated Fourier transform peaks of the measured signal at the A^1_{1g} (orange and A^2_{1g} green) mode frequencies, and the simulated helicity-dependent ratio at the A^2_{1g} frequency (pink) versus normalized temperature. The solid green line is a fit using an FM order-parameter-like function and the solid orange line is a guide to the eye.*

This work highlights the strong interplay between the lattice and spin structure in layered magnetic materials, providing crucial insight for the realization of the next generation of high-speed nanoscale magneto-optic technologies.

Understanding and controlling the antiferromagnetic order in multiferroic materials on an ultrafast time scale underpins potential applications of these materials in magnetic data storage and ultrafast magnetoelectric switching. In the second half of the talk, we present an optical pump-THz probe study of the multiferroic $Eu_{0.75}Y_{0.25}MnO_3$. The pump energy of 1.55eV was chosen to match the dominant d-d transitions of the Mn^{3+} ions and the temporal evolution of the pump-induced transient conductivity was recorded via electro-optic sampling of the THz probe [2]. Our measurement found two clear relaxation times due to: (1) spin-lattice thermalization and (2) magnetic order-related electron-hole recombination. While the spin-lattice thermalization shows a power law relationship with temperature from the melting of spin order, the temperature dependence of the electron-hole recombination suggests a channel opening below the Néel temperature. Suppression of electromagnon modes was observed within the spin-lattice thermalization time and potentially results from the melting of the magnetic order. These measurements reveal the dynamic functionality of quantum materials by directly probing low-energy excitations such as electromagnons, offering a powerful approach to understanding the coupling between their different degrees of freedom.

References

[1] P. Padmanabhan, F. Buessen, R. Tutchton, K.W.C. Kwock, S. Gilinsky, M.C. Lee, M.A. McGuire, S.R Singamaneni, D.A. Yarotski A. Paramekanti, J-X. Zhu, R.P. Prasankumar, *Nature Communication*s **13**, 4473 (2022).

[2] Y. Huang, R. V. Aguilar, S.A. Trugman, S.-W. Cheong, L. Yuan, M.-C. Lee, A. Azad, A.J. Taylor, N.S. Sirica R. P. Prasankumar, D.A.Yarotski, (in preparation) (2023).

* Acknowledgement: This work was supported, in part, by the Center for Integrated Nanotechnologies, an Office of Science User Facility operated for the U.S. Department of Energy.

Mesoscale structure in nonequilibrium Charge density wave systems visualized with X-ray free electron lasers

A. Miller[1], G. Orenstein[3], V. Krapivin[3], Y. Huang[2], Jade Stanton[1], Matthew Hurley[1], Ryan Duncan[3], Q. Nguyen[2]
G. De la Pena[3] , M. Sander[4], R. Mankowsky[4], Y. Deng[4], H. Lemke[4], M. Trigo[2], S. W. Teitelbaum[1]
[1]*Arizona State University, Tempe AZ 85287, USA*
[2]*SLAC National Accelerator Laboratory, Menlo Park, CA 94025, USA*
[3]*Stanford University, Stanford, CA 94305, USA*
[4]*Paul Scherrer Institut, 5232 Villigen, Switzerland*

Heterogeneous dynamics are both a well-known to mediate phase competition in systems with complex phase diagrams near equilibrium, and heterogeneity is a well-known consequence of systems entering an ordered phase far from equilibrium (e.g. the Kibble-Zurek mechanism for formation of topological defects) [1]. And yet, in light-driven systems far from equilibrium on very fast timescales, we are just beginning to use tools such as ultrafast electron microscopy and x-ray free electron lasers to reveal the role intrinsic heterogeneity plays at very fast timescales. These early studies reveal the role of topological defects in mediating the superconductivity/CDW order competition in cuprates [2,3], stabilization of the so-called "hidden" charge density (CDW) phase in 1T-TaS_2 [4] to the importance of phase competition in the rare-earth tritellurides [5,6].X-ray free electron lasers (XFELs) are particularly incisive tools to probe these critical yet complex heterogeneous dynamics due to their combination of high brightness, high momentum resolution, and high temporal resolution. All three parameters key for observing the relatively weak, rapidly evolving scattering signals from mesoscale (~10 nm) optically generated domains and defects. In two distinct quasi-two dimensional systems with CDW order, Pd-intercalated $ErTe_3$, a prototypical charge density wave (CDW) system, and 1T-$TiSe_2$, an excitonic insulator candidate, we observe complex dynamics near the CDW ordering wavevector due to the intrinsic heterogeneity of phase transitions system. In the rare-earth tritelluride CDW system Pd:$ErTe_3$, we observe scattering along the b-axis (surface normal) direction after optical excitation with 800 nm light strong enough to quench the CDW order near the surface. This scattering is due to the formation of an antiphase domain wall [7,8]. In metal-intercalated tritellruides, these defects are observed to persist for hundreds of picoseconds, much longer than the lifetime of the excited electronic state. We attribute the mechanism of domain wall relaxation to its decay into vortex strings, which are topologically protected defects in the material. The slow relaxation of these defects is key to the long-lived suppression of long-range CDW order. We model the melting and recovery of the CDW order with a time and spatially dependent Ginzburg-Landau model that accounts for both thermal fluctuations and impulsive optical excitation, and produces the expected topologically protected states. The Hamiltonian of the system can be described by a complex order parameter ψ with the effective (local) free energy U given by

$$U(\boldsymbol{r},t) = \big(1-\eta(\boldsymbol{r},t)\big)|\psi|^2 + \frac{1}{2}|\psi|^4 + \xi^2|\nabla\psi|^2,$$

where $\eta(\boldsymbol{r},t)$ represents a temporally and spatially dependent optical excitation density that decays away from the surface, and over time as hot electrons thermalize with the lattice. The finite lifetime of the hot carriers generates a fast quench of the potential on the timescale of the CDW response.
The finite penetration depth of the laser leads to a quench that inverts the sign of the CDW at the surface, generating domains throughout the material.

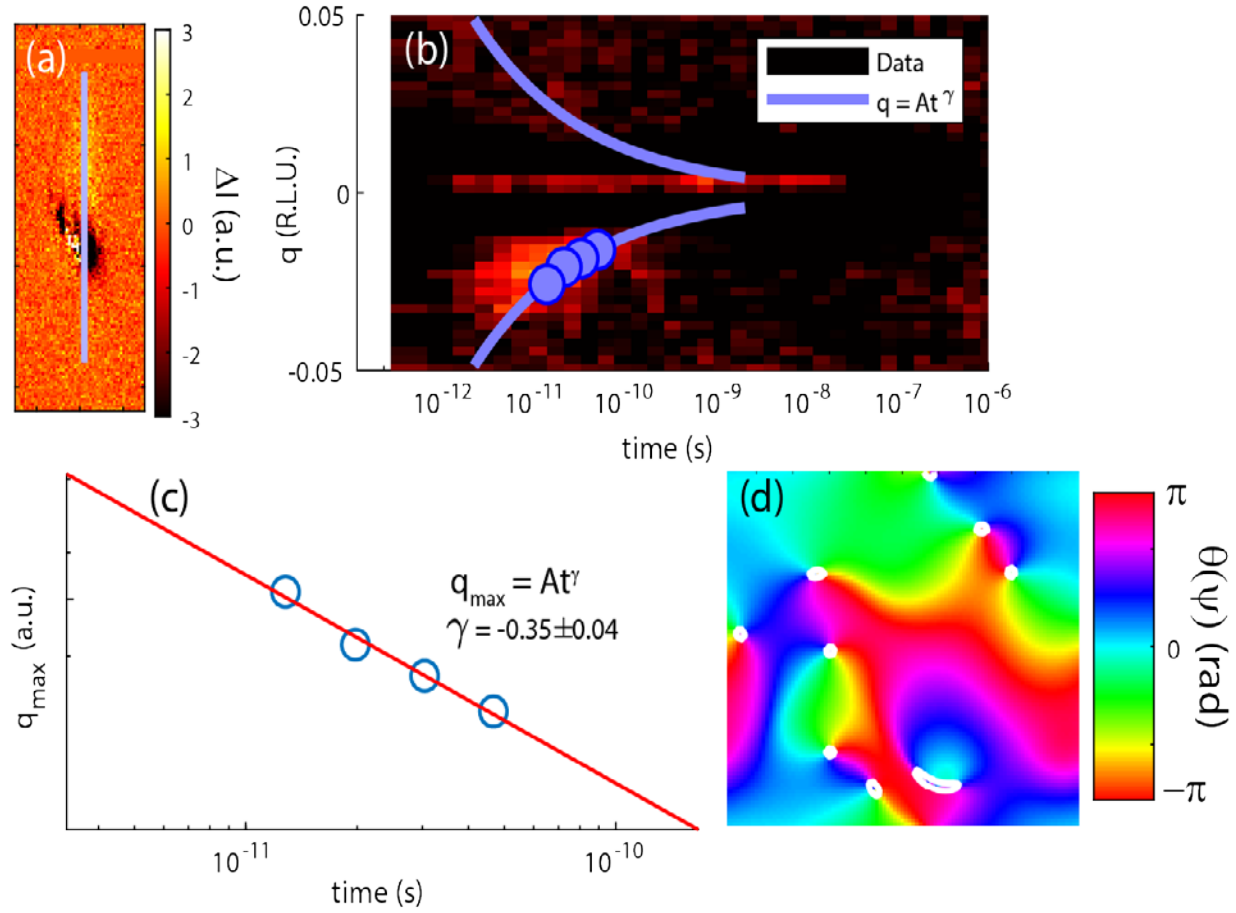

Fig. 1*: Time-domain x-ray scattering of charge density wavesreveals dislocation formation after a quench.* ***(a)*** *Differential intensity I(q) near the CDW peak of ErTe3 10 ps following photoexcitation by 800 nm light. The bright region near the top is a satellite peak from domain wall scattering. The blue line shows the linocut along the [0 1 0] out of plane direction.* ***(b)*** *Intensity I(q,t) along the linecut as a function of time. The time axis is logarithmically scaled to show the range of timescales observed in the experiment. The blue dots represent the maximum scatted intensity of the satellite peak.*
(c) *Position of the satellite peak maximum as a function of time, fit to a power law, which reveals a power-law scaling of* $q \propto t^{-1/3}$*, indicating the presence of a conserved quantity in the relaxation.* ***(d)*** *The phase of the order parameter of a time-dependent Ginzburg-Landau model following a quench. Singularities in the phase (topological defects) are shown in white.*

Our simulations reproduce the production of topological defects after a light-driven quench at finite temperature, and produce the power-law scaling of the fundamental length scale that we observe experimentally.

References

[1] T. W. B. Kibble, *Journal of Physics A: Mathematical and General Topology of cosmic domains and strings* **9,** 1387 (1976).
[2] S. Wandel, F Boschini , E H da Silva Neto, L Shen, M X Na, S Zohar, Y Wang, S B Welch, M H Seaberg, J D Koralek, G L Dakovski, W Hettel M-F Lin, S P Moeller, W F Schlotter, A H Reid, M P Minitti, T Boyle, F He, R Sutarto, R Liang, D Bonn, W Hardy, R A Kaindl, D G Hawthorn J.-S. Lee, A F Kemper, A Damascelli, C Giannetti, J J Turner, G Coslovich, *Science* **376**, 860 (2022).
[3] M. Mitrano, S. Lee, A. A. Husain, L. Delacretaz, M. Zhu, G. de la Peña Munoz, S. X.-L. Sun, Y. I. Joe, A. H. Reid, S. F. Wandel, *Science Advances* **5** , 3346 (2019).
[4] Y. A. Gerasimenko, P. Karpov, I. Vaskivskyi, S. Brazovskii, D. Mihailovic, *Npj Quantum Materials* **4**, 1 (2019).
[5] A. Kogar A. Zong, P. E. Dolgirev, X.Shen, J.Straquadine, Y.-Q. Bie,X. Wang, T.Rohwer, I-C. Tung, Y.Yang, Li, J.Yang, S.Weathersby, S.Park M. E. Kozina, E. J. Sie, H.Wen, P. Jarillo-Herrero, I. R. Fisher, X.Wang, N. Gedik , *Nature Physics* **16**, 159 (2020).
[6] A. Zong, M. Huber, Y. Lin, N. G Dale, R.Sailus, S.Tongay, R. A. Kaindl, A. Lanzara, *Nature Physics* **15**, 27 (2019).
[7] M. Trigo, P. Giraldo-Gallo, M. E. Kozina, T. Henighan, M. P. Jiang, H. Liu, J. N. Clark, M. Chollet, J. M. Glownia, D. Zhu, T. Katayama D. Leuenberger, P. S. Kirchmann, I. R. Fisher, Z. X. Shen, D. A. Reis, *Physical Review* B **99**, 104111 (2019).
[8] M. Trigo, P. Giraldo-Gallo, J. N. Clark, M. E. Kozina, T. Henighan, M. P. Jiang, M. Chollet, I. R. Fisher, J. M. Glownia, T. Katayama P. S. Kirchmann, D. Leuenberger, H. Liu, D. A. Reis, Z. X. Shen, D. Zhu, *Physical. Review* B **103**, 054109 (2021).

In-gap spectral weight of the optical conductivity induced by a strong Subcycle pulse in low-dimensional Mott insulators

T. Tohyama
Tokyo University of Science, Tokyo 125-0051, Japan

Electric pulse applied to the Mott insulators induces insulator-to-metal transitions. Not only low-energy Drude component but also in-gap excitations emerge in the optical conductivity after the transitions. Strong subcycle (mono- or half-cycle) pulses with zero frequency induce quantum tunneling in the low-dimensional Mott insulators. It is interesting to know how in-gap spectral weights behave when quantum tunneling occurs. We calculate time-resolved optical conductivity for one-dimensional and two-leg ladder Mott insulators driven by strong subcycle pulses. The time-dependent Lanczos method and time-dependent density-matrix renormalization group are used for the calculation of the optical conductivity in the half-filled extended Hubbard model. In a one-dimensional Mott insulator, subcycle pulses with zero frequency suppress spectral weights contributing to the Drude weight and enhance in-gap spectral weights with increasing the strength of the pulses (see Fig. 1).

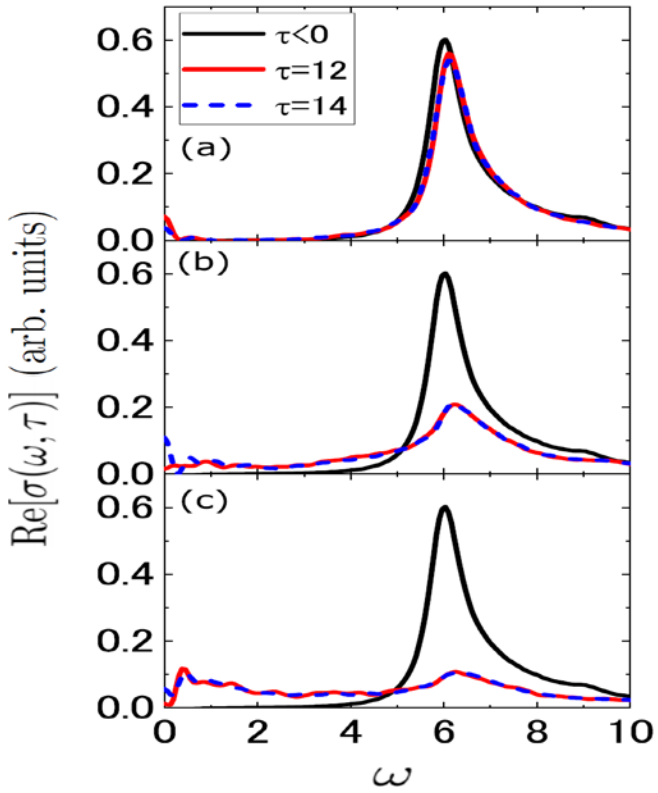

Fig.1. *Time-dependent optical conductivity excited by a zero-frequency mono-cycle pulse for a half-filled one-dimensional extended Hubbard lattice with 32 sites and on-site (nearest-neighbor) Coulomb interaction U=10 (V=3) in the unit of hopping energy.* ***(a)****: electric-field strength* E_0*=1.5.* ***(b)****:* E_0*=1.8.* ***(c)****:* E_0*=2.1. Black, red, and blue-dashed lines are for time* $\tau<0$ *(before pumping),* $\tau=12$*, and* $\tau=14$*, respectively.*

This is in contrast to a metallic behavior induced by photon absorption and chemical doping. The strong suppression of the Drude weight and the enhancement of in-gap weights in the quantum tunneling regime are a result of the emergence of the Hilbert-space fragmentation, which makes pulse-excited states glassy [1]. The glassy state is accompanied by electric polarization that breaks inversion symmetry [2]. We also demonstrate that, using an ultrashort subcycle pulse, one can generate a steady electric current because of an Aharonov-Bohm flux instantaneously introduced through the phase of an electric field. Consequently, time-reversal symmetry is broken [2]. Both symmetry breakings can be monitored by second harmonic generation. These findings propose a new methodology for designing the symmetries of electronic states and open up a new field of subcycle-pulse engineering. In a two-leg ladder, on the other hand, in-gap spectral weights are strongly suppressed and show negative values [3]. A similar behavior is obtained in pumping an absorption peak just above on-site Coulomb energy. Since the absorption peak is related to the presence of magnetic dimer in the ground state, the negative in-gap weights are due to a magnetic origin.

These works were done in collaboration with Kazuya Shinjo, Shigetoshi Sota, and Seiji Yunoki.

References

[1] K. Shinjo, S. Sota, and T. Tohyama, *Physical Review Research* **4**, L032019 (2022).
[2] K. Shinjo, S. Sota, S. Yunoki, T. Tohyama, *arXiv*:2211. 08694, (submitted to *Physical Review B)*, (2022).
[3] K. Shinjo, S. Sota, S. Yunoki, T. Tohyama, (to be submitted), (2023).

Measuring everything you've ever wanted to know about an Ultrashort laser pulse

R. Trebino[1], E.Grace[2], R.Jafari[1], P.Zhu[1], Z. Guang[1], P.Bowlan[1]
[1]*Georgia Institute of Technology, Atlanta, GA 30332 USA*
[2]*Lawrence Livermore National Lab, Livermore, CA 94550 USA*

Because ultrashort laser pulses are the shortest events ever created, their measurement has been challenging, and, as a result, mismeasurements have been common and remain so even today[1]. Many poorly developed pulse-measurement techniques have been introduced and even widely implemented, often yielding anomalously short pulse lengths and anomalously simple pulse shapes[2]. Worse, they have even masked the presence of instability of pulse shapes in trains of pulses. Fortunately, a few techniques and devices (and only a few!) have been shown, over many years, to yield essentially unambiguous results and that are quite reliable[3,4]. The main issue, widely misunderstood for decades, has been the effect of *pulse-shape instability* in trains of pulses measured using techniques that scan a delay or another parameter and so yield measurements that average over many, potentially quite different pulses, a very common case. In early measurements using autocorrelation techniques, this yielded the infamous *coherent artifact*—basically, a measure of only the shortest spike of an often much more complex pulse. This resulted in numerous claims of erroneously short pulses. Even today, this problem remains common (See Fig. 1).

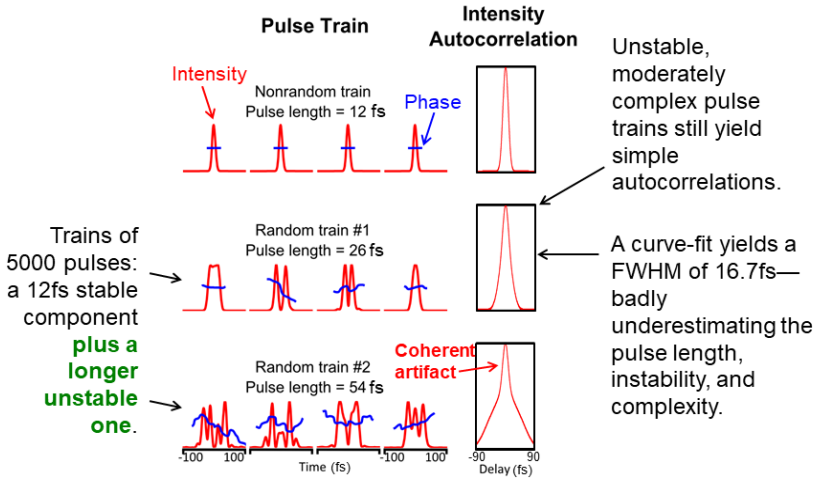

Fig. 1. *Intensity autocorrelations of trains of stable* ***(top row)*** *and unstable* ***(middle and bottom rows)*** *pulses. Note that the unstable, moderately complex pulse train appears to yield a smooth short pulse, but this assumption yields an erroneously short pulse length and no indication of the presence of the pulse-shape instability. Figure reprinted from frog.gatech.edu.*

This problem is particularly severe in many recently introduced *interferometric* techniques, most of which operate in the frequency domain, where the coherent artifact appears in a less familiar form: specifically, a linear spectral phase[2]. This is because a complex spectral phase, which contains the specific complex temporal pulse structure, washes out when averaging over many different pulses. Some of these methods, including the most popular ones, measure *only* the coherent artifact and, worse, provide no information about the presence or absence of the pulse train's pulse-shape instability (See Fig. 2). As a result, they cannot distinguish a train of short, simple, stable pulses from the diametrically opposite case of a train of long, complex, unstable pulses. They have likely achieved popularity due to a combination of a desire to claim the shortest pulses and humankind's penchant for self-deception. On the other hand, *spectrographic* methods, the first class of methods shown to be able to measure the complete pulse intensity and phase vs. time, do not suffer from these issues. Their reliability and power have now been convincingly demonstrated for a wide range of pulse intensities, rep rates, wavelengths, and even complexities[3, 4] (See Fig. 2). Unfortunately, their adoption has been hampered by their reporting of longer—albeit accurate—pulse lengths and also the resulting discrepancies between measured and retrieved traces when pulse-shape instability is present. In addition, their use of novel iterative algorithms for pulse retrieval, which has often been blamed for such discrepancies, when in fact such discrepancies indicate pulse-shape instability, have also slowed their adoption. Finally, a poor understanding by many researchers of the role of unstable pulse trains, in general, has played a role, as well. And finally, admittedly, until recently, iterative pulse-retrieval algorithms have not been reliable, having had a tendency to stagnate, that is, not converge. But these latter problems have been solved with the recent introduction of a modified algorithm that has been shown, not only to be fast, but also 100% reliable, even for extremely complex pulses [5]. This latter algorithm reliably retrieves even extremely complex pulses with time-bandwidth products as large as 100 and likely even higher even in the presence of significant noise.

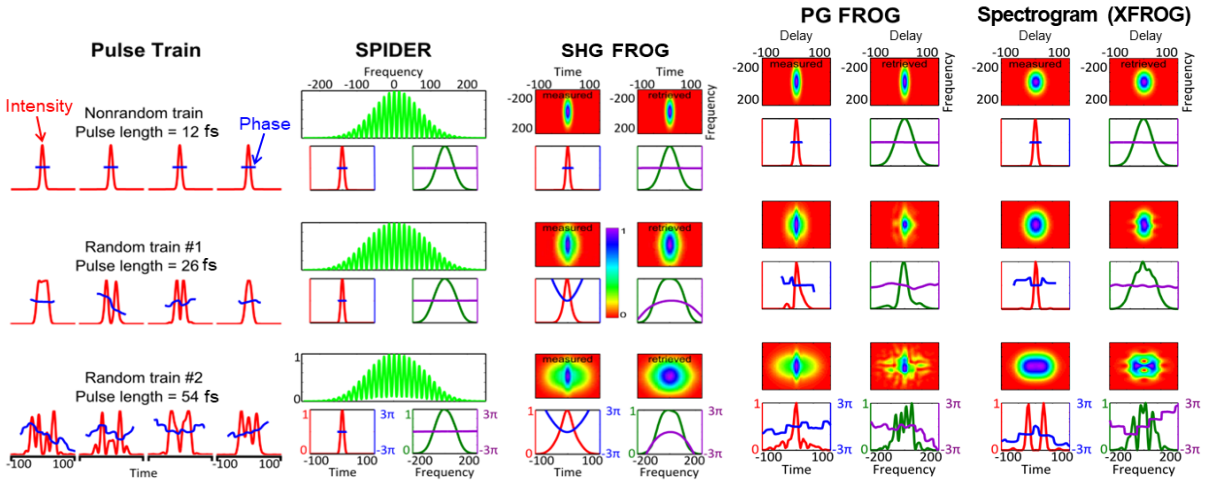

Fig. 2*. The same trains of stable (**top row**) and unstable (**middle and bottom rows**) pulses and their SPIDER and FROG traces and retrieved pulses. Note that SPIDER yields the same measured trace and only the coherent artifact for all three pulse trains, even the highly unstable train of long comple pulses, severely under-estimating the pulse length when pulse-shape instability is present. This occurs for SPIDER measurements for all types of pulse-shape instability. Also, there is no indication of instability in SPIDER. The various versions of FROG, on the other hand, yield more realistic pulses and pulse lengths, and their rertieved traces reveal the presence of instability via obvious discrepancies between the measured and retrieved traces. Figure reprinted from frog.gatech.edu.*

It also definitively distinguishes between stable and unstable pulse trains, finally also solving this long-standing problem[6] (Fig. 3).In addition, once a reliable measurement has been made of a pulse directly from a laser, such a measured pulse can act as a reference pulse to assist additional (even interferometric) methods to measure even more complex quantities, such as the complete *spatiotemporal* intensity and phase—that is, the complete electric field—of an arbitrary ultrashort laser pulse[7-10]. We recently used such a method to measure even a single extremely complex terawatt laser pulse completely in space and time at Lawrence Livermore National Lab[11]. This was the first ever single-shot complete spatiotemporal pulse measurement of any pulse.

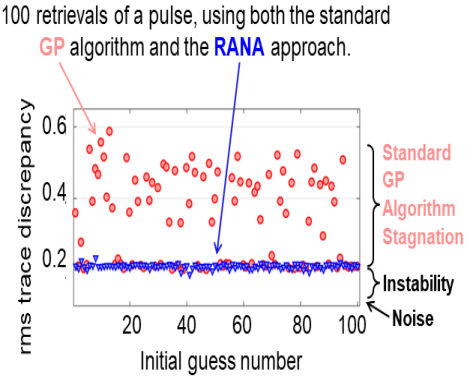

Fig.3. Plots of the rms trace discrepancy between simulated measured and retrieved SHG FROG traces for different initial guesses for an unstable pulse train. Because the measured trace is the sum of many different traces due to the many different pulses, it cannot correspond to a single pulse, and so there will necessarily be discrepancies between it and the retrieved trace. Plotted here are the rms trace discrepancies for 100 different initial guesses for the same trace (of a moderately complex pulse) using the standard GP pulse-retrieval algorithm and also for the new, ultra-reliable RANA approach. Note that the RANA approach converges to the lowest possible trace discrepancy for all initial guesses (yielding a true estimate of the pulse-shape instability), whereas the GP algorithm often stagnates and so over-estimates the discrepancy. As a result, the RANA approach reliably indicates the presence of stability or instability. Figure reprinted from frog.gatech.edu.

Our conclusion is that the field of pulse measurement is essentially solved—unless we count the need to eradicate the remaining misconceptions and misleading methods. The next step is to use these existing *reliable* methods to measure important pulses.

References

[1] R. Trebino, *Optics and Photonics News* **31**, 46 (2020).
[2] M. Rhodes, G. Steinmeyer, J. Ratner, R. Trebino, *Laser & Photonics Reviews* **7**, 557 (2013).
[3] R. Trebino, R. Jafari, S. A. Akturk, P. Bowlan, Z. Guang, P. Zhu, E. Escoto, G. Steinmeyer, *SRC Handbook of Laser Technology and Applications* **1**, 487 (2021).
[4] R. Trebino, R. Jafari, S. A. Akturk, P. Bowlan, Z. Guang, P. Zhu, E. Escoto, G. Steinmeyer, Journal Applied Physics **128**, 171103 (2020).
[5] R. Jafari, R. Trebino, IEEE Journal. of Quantum Electronics **56**, 1(2020).
[6] S. D. K. R. Jafari, R. Trebino, *Nature Scientific Reports* **12,** (2022).
[7] P. Zhu, R. Jafari, T. Jones, R. Trebino, *Optics Express* **25**, 24015 (2017).
[8] Z. Guang, M. Rhodes, R. Trebino, *Applied Optics* **56**, 3319 (2017).
[9] Z. Guang, M. Rhodes, R. Trebino, *Journal Optical Society of. America-JOSA* B **33**, 1955 (2016).
[10] P. Bowlan, U. Fuchs, R. Trebino, U. D. Zeitner, *Optics Express* **16**, 13663 (2008).
[11] E. Grace, T. Ma, Z. Guang, R. Jafari, J. Park, J. Clark, E. Kemp, J. Moody, M. Rhodes, Y. Ping, R. Shepherd, B. Stuart, R. Trebino, *Journal of Optics* **23**, 075505 (2021).

* Rick Trebino owns a company that sells pulse-measurement devices, and Rana Jafari consults for it.

Ionisation dynamics and surface plasmon excitation in Dielectrics irradiated with Mid-Infrared femtosecond pulses

G. D. Tsibidis[1], E. Stratakis[2]
[1]*Institute of Electronic Structure and Laser (IESL), 70013 Heraklion, Greece*
[2]*University of Crete, 71003 Heraklion, Greece*

The employment of ultrashort laser sources at the mid-IR spectral region for dielectrics is expected to open innovative routes for laser patterning and a wealth of exciting applications in optics and photonics. To elucidate the material response to irradiation with mid-IR laser sources, a consistent analysis of the interaction of long wavelength femtosecond pulses with dielectric materials is presented (Fig.1a). The influence of the pulse duration is particularly emphasized in specifying the laser parameters for which photoionization and impact ionization are important [1]. Simulation results using pulses at 2.2 μm, 3.2 μm (Fig.1b) and 5 μm are conducted to illustrate the optimum conditions for the onset of damage on the solid that is related to the occurrence of the optical breakdown. Results predict that the damage threshold scales as $\sim\tau_p^a$ $(0.31 \leq a \leq 0.37)$ at all laser wavelengths (Fig.1c). Given the significant effect of the induced excitation level on the excitation of Surface Plasmons (SP) which account for the formation of laser-induced periodic structures (LIPSS) [2] oriented perpendicular to the laser polarization, a correlation of the produced electron densities with SP and the threshold of SP excitation ($\sim\tau_p^\beta$, $0.33 \leq \beta \leq 0.39$) are also discussed in this as yet unexplored spectral region (Fig.1d). These periodic structures are just one category of LIPSS in addition to other topographies predicted and observed at this spectral region [2].

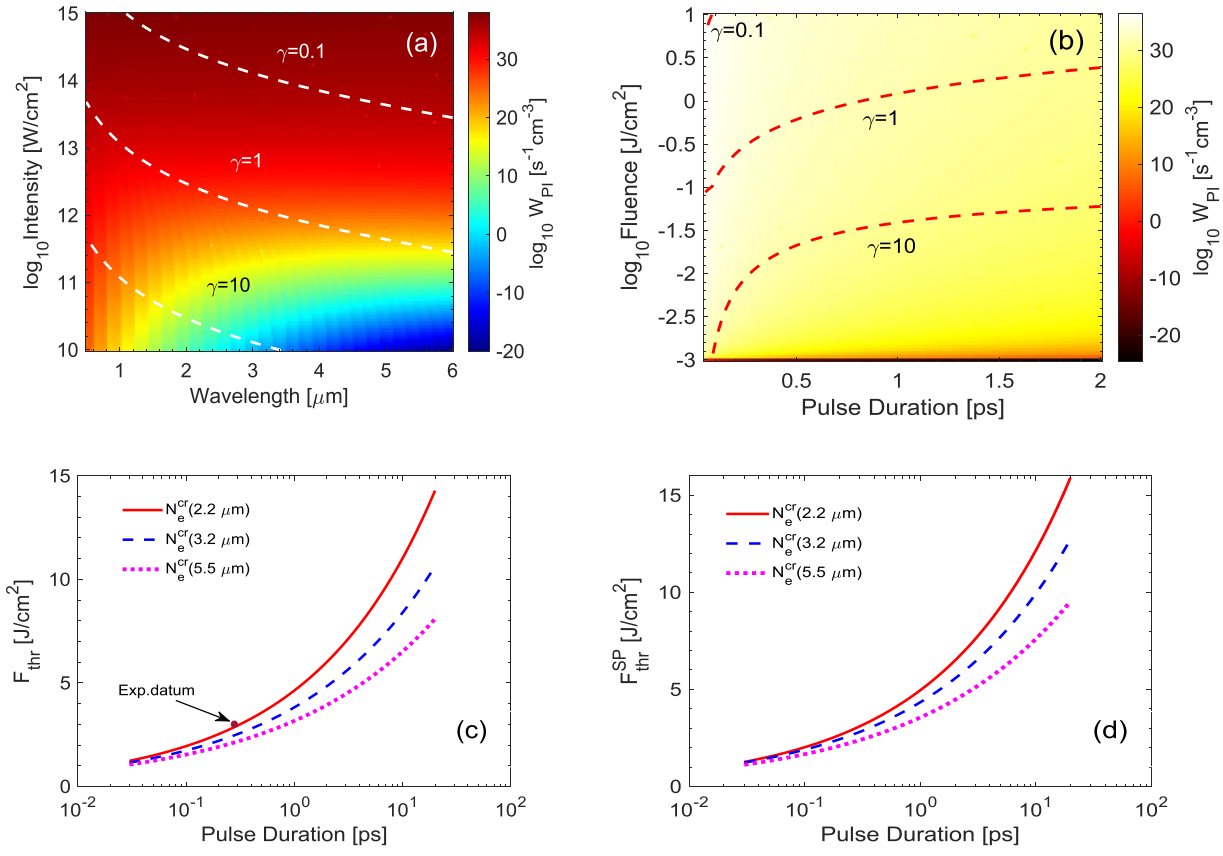

Fig. 1 *Photoionization rates W_{PI} as a function of* ***(a)*** *laser wavelength and (peak) intensity,* ***(b)*** *laser (peak) fluence and pulse duration ($\lambda_L = 3.2\ \mu m$).* ***(c)*** *Minimum fluence to reach OBT as a function of laser pulse duration (for $\lambda_L = 2.2\ \mu m$, 3.2 μm, 5 μm); Brown coloured filled circle corresponds to experimental data at 2 μm for 150 fs,* ***(d)*** *Threshold for SP excitation as a function of laser pulse duration (for $\lambda_L = 2.2\ \mu m$, 3.2 μm, 5 μm).*

Results are expected to guide development of an innovative approach to surface patterning using strong mid-IR pulses for advanced applications.

References

[1] G. D. Tsibidis, E. Stratakis, *Applied Physics Letters* **122**, 04350 (2023).
[2] G. D. Tsibidis, E. Stratakis, *Scientific Reports* **10**, 8675 (2020).

Two-mode excitations with terahertz light pulses: from phonons to Superconducting plasmons

M. Udina[1], M. Basini[2], J. Fiore[1], F. Gabriele[1], M. Pancaldi [3], N. Sellati[1], V. Unikandanunni [2], S. Bonetti [4]
L. Benfatto[1]
[1] "Sapienza" University of Rome, 00185 Rome, Italy
[2] Stockholm University, 10691 Stockholm, Sweden
[3] Elettra-Sincrotrone Trieste S.C.p.A, 34149 Basovizza, Trieste, Italy
[4] Ca' Foscari University of Venice, 30172 Venice, Italy

The technical improvements in the generation of intense and phase-stable terahertz (THz) pulses considerably enlarged the possibilities to design experiments aimed at coherently driving low-energy excitations of complex systems on ultrafast time scales. The general idea is that one can take advantage of the quadratic coupling of light to Raman-active modes to drive large amplitude fluctuations of the corresponding degrees of freedom, ranging from lattice vibrations [1] to collective-modes of broken-symmetry states, as for magnetic or superconducting (SC) transitions [2]. Within this picture, the largest response occurs when twice the pump frequency of the THz light matches the mode resonance, i.e. $2\Omega = \omega_{res}$, highlighting the underlying two-photon sum-frequency nature of the excitation process [3-4]. On the other hand, a related but different possibility is that strong pulses can drive simultaneously two modes. In this case, one would expect the response to be larger when the pump frequency directly matches the mode resonance at ω_{res}.

So far, such a possibility has been mainly discussed within the context of the so-called non-linear phononics [5]. Indeed, thanks to anharmonic couplings among lattice vibrations, the simultaneous excitation of two infra-red (IR) active phonon modes acts as a driving process for exciting Raman-active phonons [3], opening in principle a pathway to drive materials towards metastable states which may not be accessible at thermal equilibrium and leading to interesting effects like e.g. the observation of silent phonon modes [6]. On the other hand, the very same mechanism underlies also the non-linear driving of plasma waves in superconductors [7]. Below T_c the emergence of a complex SC order parameter leads to two collective electronic modes related to its amplitude (Higgs) and phase fluctuations, respectively, with the latter carrying information on the spectrum of SC plasma modes. While in ordinary, isotropic superconductors this is usually a large energy scale, around hundreds of THz, in layered superconductors, as e.g. high-T_c cuprates, the weak coupling among layers leads to a soft out-of-plane plasma mode at few THz, depending on the cuprate family, well described by a discrete Josephson-like model for inter-layer phase fluctuations. Due to the large value of the SC gap, such a soft Josephson plasma mode (JPM) is pushed below the optical gap and leads to the appearance of a well-defined plasma edge in the out-of-plane reflectivity at THz frequencies.In this talk I will discuss the possibility of driving simultaneously multiple collective modes using intense THz pulses, starting from the more conventional case of IR active phonons in wide-band insulators, to the resonant excitation of JPMs in superconducting cuprates. In particular, we have recently shown that two-phonon excitations give a sizable contribution to the THz Kerr response in insulating $SrTiO_3$ [8]. While the conventional electronic Kerr effect, probing a change in the refractive index proportional to the square of the applied electric field, is associated with off-resonant electronic transitions, such a ionic contribution, named ionic Kerr effect (IKE), relies on the resonant excitations of multiple infrared modes as an intermediate step (see Fig. 1a), thus providing an alternative mechanism to modulate the refractive index on ultrashort time-scales. Given the capability of terahertz-driven phonons to couple to different order parameters and to drive materials towards metastable states which may not be accessible at thermal equilibrium [5], the IKE can be used to investigate the electron-phonon coupling across various phase transitions.A similar theoretical description can be extended to describe the excitation of SC Josephson plasmons, which has been intensively studied in cuprate families with both one and two layers per unit cell. In the first case, experiments have shown that the nonlinear response at THz frequencies has a well-defined resonance at $2\omega_p$ [9-10], where ω_p is the energy of the soft plasmon, supporting the idea that THz pulses can simultaneously excite two JPMs with opposite momentum (see Fig. 1b).

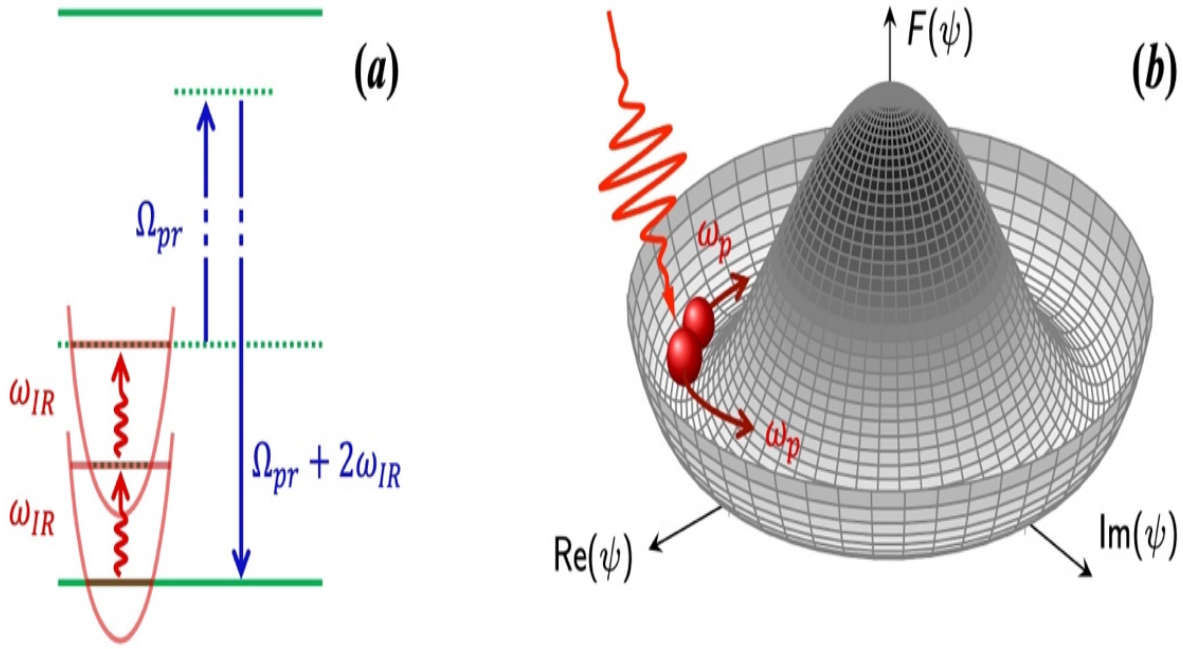

Fig. 1. (a)*: Schematic representation of the ionic Kerr effect in a THz pump-optical probe experiment. When the pump pulse is resonant with an IR-active phonon at ω_{IR}, two modes can be excited to reach a virtual electronic state. The time-delayed probe field then couples to this virtual excitation, leading to a modulation of the emitted light at $2\omega_{IR}$.* ***(b)****: Schematic view of the mexican-hat potential for the free energy $F(\psi)$, with ψ the complex order parameter of a superconductor below T_c. A phase-gradient excitation corresponds to a longitudinal shift along the minima. An intense light pulse with almost zero momentum can excite simultaneously two plasma waves with frequency ω_p and opposite momenta.*

The resonant excitation occurs when the pump frequency matches the energy of the soft out-of-plane plasmon measured by linear reflectivity [7]. In contrast to the single-layer case, recent experiments [11] suggest instead that no resonances are present when the pumping frequency matches the value of the reflectivity plasma edge in double-layer YBCO. In a recent work [12], we have provided a comprehensive derivation of the nonlinear optical response in layered superconductors, accounting for the full momentum dispersion of the two plasma modes simultaneously excited by the THz pump pulse. We have shown that the unavoidable entanglement between in-plane and out-of-plane plasma waves in a layered system represents a crucial ingredient to understand what marks the difference between the single-layer and the bilayer case, and to fully reproduce the existing experimental results.

References

[1] S. Maehrlein, A, Paarmann, M.Wolf, T.Kampfrath**,** *Physical Review Letters* 119, 127402, (2017).
[2] R. Matsunaga, Y. I. Hamada, K.Makise, Y. Uzawa, H.Terai, Z.Wang, R.Shimano, *Physical Review Letters* 111, 057002, (2013).
[3] D. M. Juraschek, S. Maehrlein, *Physical Review B* **97,** 174302, (2018).
[4] M. Udina, T. Cea, L. Benfatto, *Physical Review B* **100,** 165131, (2019).
[5] D. Nicoletti, A. Cavalleri, *Advances in Optics and Photonics* **8**, 401-464 (2016).
[6] M. Kozina, M. Fechner,P. Marsik, T. van Driel, J. M. Glownia, C. Bernhard, M. Radovic, D. Zhu, S. Bonetti,U. Staub ,M. C. Hoffmann, *Nature Physics* **15**, 387 (2019).
[7] F. Gabriele, M. Udina, L. Benfatto, *Nature Communications* **12**, 752 (2021).
[8] M.Basini,M. Udina, M. Pancaldi, V. Unikandanunni, S. Bonetti, *arXiv:2210.14053* (2022).
[9] S. Rajasekaran, S. Rajasekaran, E. Casandruc, Y. Laplace, D. Nicoletti, G. D. Gu, S. R. Clark, D. Jaksch, A. Cavalleri, *Nature Physics* **12**, 1012 (2016).
[10] K. Kaj,*K.A. Cremin. I.Hammock. J.Schalch. D. N. Basov. R. D. Averitt*, ***arXiv:2211.17184 (2022*****)**
[11] K. Katsumi,, M.Nishida, S.Kaiser, S.Miyasaka, S. Tajima, R. Shimano, *arXiv:2209.01633* (2022).
[12] J. Fiore, M. Udina, (*to be submitted)* (2023).
* Acknowledgement(s): M. Udina acknowledge support from EU under program MORE-TEM ERC-SYN (grant agreement No 951215).

High-precision high-resolution spectroscopy with frequency combs: from Mid-IR to THz

D. Konnov[1], S. Vasilyev[2], A. Muraviev[1], K. Vodopyanov[1]
[1]*University of Central Florida, Orlando, FL 32816, USA*
[2] *IPG Photonics Corporation, Oxford, MA 01752, USA*

We present our new approach to the creation of ultra-broadband frequency combs in the whole mid-IR to terahertz range (1-100 THz) enabled by a new laser technology: Kerr-lens mode-locked solid-state Cr:ZnS lasers producing sub-3-cycle pulses at λ=2.4 μm as a driving source. This allowed conducting dual-comb spectroscopy of molecular gases in a wide spectral range, and at a record high resolution and speed according to the following 3 scenarios for different spectral bands:
In our **first approach**, the dual-comb spectroscopy (DCS) system is based on a pair of subharmonic optical parametric oscillators (OPOs) pumped by either a pair of phase-locked 1.93-μm Tm-laser combs that produce mid-IR combs spanning 3.1-5.4 μm [1], or by two 2.4-μm Cr:ZnS laser combs that produce combs spanning two octaves, 3-12 μm [2]. The beam from the first OPO comb passes through a multipass gas cell with a mixture of gases and serves as a 'sensing' comb, while the output of the second OPO serves as a 'sampling' comb. The beams are coherently combined and sent to a fast mid-IR detector to produce DCS interferograms. This approach allowed massively parallel and ultrasensitive detection of molecules and their isotopologues in a mixture of gases with sub-part-per-billion sensitivity [1]. Also, the line list produced by our high-resolution DCS measurements of carbon disulfide (CS_2) at 4-5 μm [3] is now part of the HITRAN database.

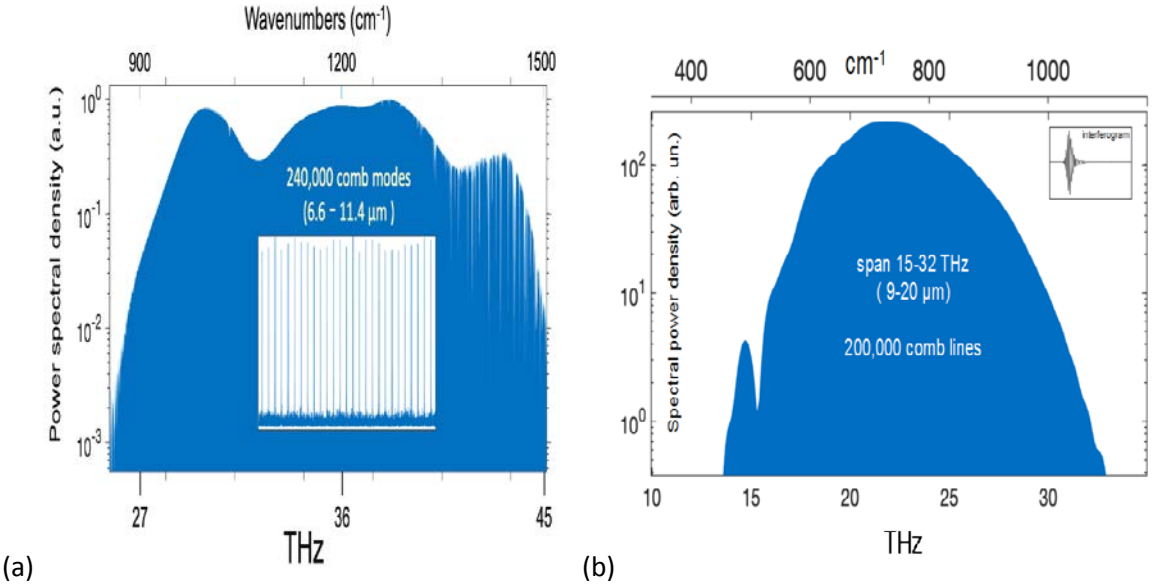

***Fig. 1. (a)**: Comb-mode-resolved spectrum of the longwave IDFG output achieved in ZGP crystal. **(b)**: IDFG comb spectrum achieved in GaSe crystal (the dip at ~15 THz is due to 2-phonon absorption in GaSe).*

In our **second approach**, both 'sensing' and 'sampling' combs are produced in the long-wave infrared (LWIR) region (4–20 μm) via intrapulse difference frequency generation (IDFG) in ZGP or GaSe nonlinear crystals with 2.4-μm pulses serving as a pump. A comparatively long-wavelength pump at 2.4 μm allows generating IDFG outputs with a record high conversion efficiency reaching 10% in ZGP crystal. Thanks to the high average power of the combs (300 mW per each comb, span 6.6–11.4 μm, >1 μW per comb mode, Fig 1a), we were able to acquire DCS data in this wavelength range corresponding to 240,000 comb-mode resolved spectral points at 80-MHz spacing, with acquisition speeds up to video rate (10 Hz). Also, metrological-grade LWIR absorption spectra of nitrous oxide (N_2O) and methanol (Figs. 2-3) were obtained in just 12 seconds [4].
In our **third approach**, Cr:ZnS pumping creates a long wavelength output via IDFG in a GaSe crystal that can cover the entire range from 1 to 50 THz (6-300 μm) with an instantaneous comb span that can reach 2 octaves (e.g. 10-40 THz, 7.5-30 μm). Another Cr:ZnS laser comb generates the second harmonic pulse at 1.2 μm serving as a probe for electrooptic sampling (EOS); here the electric field of the mid-IR/THz transient is detected via induced change of the polarization state of the probe pulse inside an electrooptic crystal using ellipsometry and a balanced InGaAs detector. Fig. 1b shows the span of the comb we used to obtain the high resolution long wavelength spectrum of the low pressure mixture of carbon dioxide (CO_2) and acetylene (C_2H_2) shown in Fig.3.

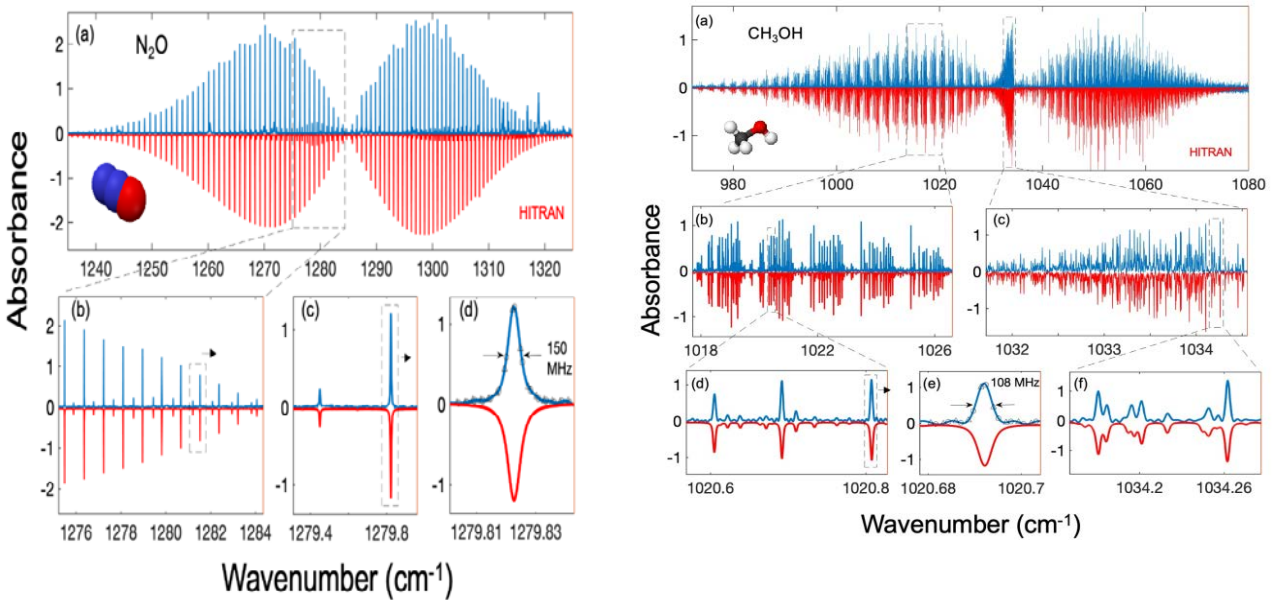

a) b)

Fig. 2. (a) *High-resolution DCS spectrum of low pressure nitrous oxide (N_2O) and* ***(b)*** *methanol (CH_3OH) – both obtained in just 12 seconds.*

The expanded views of separately CO_2 and C_2H_2 spectra and their comparison with the HITRAN simulation are depicted in Figs. 3c-d. We will also discuss our DCS measurements with tuning the combs' repetition rate that provides spectral resolution well below the spacing between the comb lines (80 MHz in our case), as well as our pilot long wavelength EOS measurements at 2-4 THz.

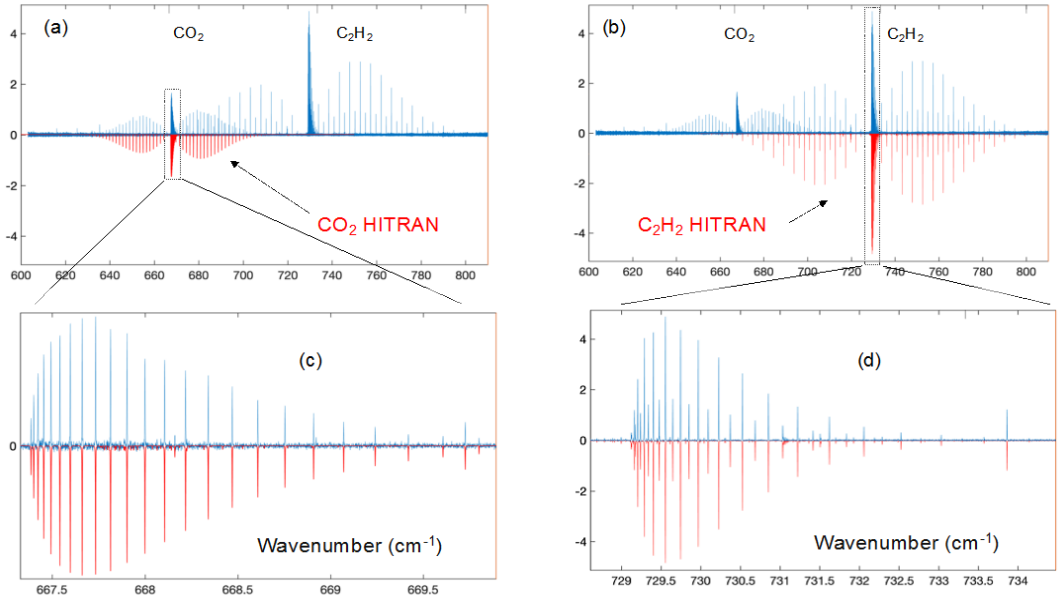

Fig. 3. (a,b)*: High-resolution LWIR spectrum of a mixture of two molecules (CO_2 and C_2H_2) with buffer gas N_2 at few mbar) pressure.* ***(c)*** *Expanded view of the CO_2 spectrum and its comparison with the HITRAN simulation.* ***(d)*** *Expanded view of the C_2H_2 (acetylene) spectrum and its comparison with the HITRAN simulation.*

In summary, we report a novel approach to dual-comb spectroscopy based on a 2.4-μm Cr:ZnS laser platform. To our knowledge, we have demonstrated for the first time all the advantages of the DCS technique achievable simultaneously in the longwave IR region (λ>8 μm): broadband coverage (> 500 cm^{-1}), Doppler spectral resolution, absolute frequency referencing and data acquisition speeds up to video rate with 240,000 comb lines resolved.

References

[1] A. V. Muraviev, V. O. Smolski, Z. E. Loparo, K. L. Vodopyanov, *Nature Photon.* **12**, 209 (2018).
[2] Q. Ru, T. Kawamori, P. G. Schunemann, S. Vasilyev, S. B. Mirov, K. L. Vodopyanov, *Optics Letters* **46**, 709 (2021)
[3] A. V. Muraviev, D. Konnov, K. L. Vodopyanov, *Scientific Report* **10**, 18700 (2020).
[4] S. Vasilyev, A. Muraviev, D. Konnov, M. Mirov, V. Smolski, I. Moskalev, S. Mirov, K.L. Vodopyanov, *Optics Letters* **48**, (in print) (2023)
* We acknowledge support from the ONR, DARPA, DOE and AFOSR grants.

Light induced metastable magnetization in a 2D antiferromagnet

B. Ilyas[1], T. Luo[1], A. von Hoegen[1], E. V. Boström[2], A. Rubio[2], N. Gedik[1]
[1] *Massachusetts Institute of Technology, 02139 Cambridge, United States*
[2] *Max Planck for the Structure and Dynamics of Matter, 22607 Hamburg, Germany*

The XPS3 (X=Mn, Ni, Fe, Co) family of van der Waals antiferromagnets has recently attracted a lot of attention due to their strongly coupled spin, lattice and electronic degrees of freedom[1-4]. They offer a rich testing ground for 2D magnetism and provide an opportunity to explore its interplay with other correlated order parameters and their ultrafast control. In particular, the perturbation of the electronic degrees of freedom via resonant pumping of specific electronic transitions in these materials was explored to find new ways to control spins and lattice at an ultrafast timescale[5]. In our work we go along a different avenue, by using intense THz light pulses, we resonantly drive the fundamental eigenmodes of the spin and lattice degrees of freedom, i.e., magnons and phonons, in $FePS_3$ directly. This way, the electronic degrees of freedom remain unperturbed and we can study the low energy physics associated with the magnetism along non-thermal pathways. Our THz excitation launches spin and lattice dynamics in the form of coherent magnons and phonons, which we follow as a function of temperature by recording the polarization rotation (dichroism) and ellipticity (birefringence) of a transmitted 800-nm wavelength ultra-short laser pulse (see Fig.1,left). Besides these fast dynamics, we also observe the emergence of a slow component close to the Neel temperature T_N = 118 K (see Fig. 1, right).

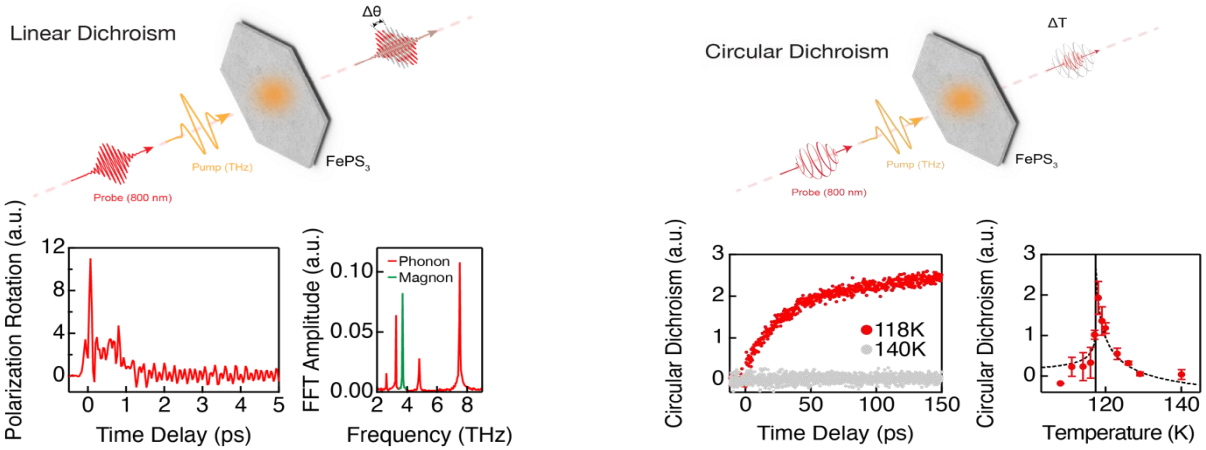

***Fig. 1. Left**: Schematic of the ultrafast linear dichroism measurement with THz pump (**orange**) and 800-nm probe pulse (**red**) together with an example time-trace and fast Fourier transform featuring coherent magnon (**green**) and phonon (**red**) oscillations. **Right**: Schematic of the ultrafast circular dichroism measurement with an example time-trace at 118K (**red**) and 140K (**grey**) and the full temperature dependence close to the transition temperature.*

These slow dynamics are concomitant with the appearance of a long-lived circular dichroism (CD), strongly suggesting a finite out-of-plane magnetization inside the sample. This CD signal shows a nonlinear dependence on the excitation field strength, appears only when the THz pump spectrally covers the relevant long-energy modes and has a lifetime of about 1.4 ms. To understand our results, we employed first principles calculations to evaluate the spin-lattice coupling. We found that one lattice vibrational mode, which is strongly hybridized with the AF-magnon at zero field[2], distorts the lattice in such a way that the exchange coupling between first-, second-, and third-nearest neighbor Fe atoms favors a ground state with a finite magnetization. These findings demonstrate how the magnetic ground state in 2D van der Waals magnets can be efficiently manipulated along non-thermal pathways using THz light. The long lifetime of the light-induced magnetization in $FePS_3$ promises possible applications in micro- and optoelectronic devices and impacts the field of spintronics in general.

References

[1] E. Ergeçen, B. Ilyas, Ju. Kim, J. Park, M. B. Yilmaz, T. Luo, D. Xiao, S. Okamoto, J.-G., N. Gedik, *PNAS* **120** (12), (2023)
[2] D. Vaclavkova, M. Palit, J. Wyzula, S. Ghosh, A. Delhomme, S. Maity, P. Kapuscinski, A. Ghosh, M. Veis, M. Grzeszczyk, C. Faugeras, M. Orlita, S. Datta, M. Potemski, *Physical Review B* **104**, 134437 (2021)
[3] K. Hwangbo, Q. Zhang, Q. Jiang, Y. Wang, J. Fonseca, C. Wang, F. M. Diederich, D. R. Gamelin, D. Xiao, J.-H. Chu, W. Yao,X. Xu, *Nature Nanotechnology* **16**, 655 (2021).
[4] C. A. Belvin, E. Baldini, I. O. Ozel, D. Mao, H. C. Po, C. J. Allington, S. Son, B. H. Kim, J. Kim, I. Hwang, J. Hoon Kim, J.-G. Park, T. Senthil N. Gedik , *Nature Communications* **12**, 4837 (2021).
[5] D. Afanasiev, J. R. Hortensius, M. Matthiesen, S. Mañas-Valero, M. Šiškins, M. Lee, E. Lesne, H. S. J. van der Zant, P. G. Steeneken, B. A. Ivanov, E. Coronado, A. D. Caviglia, *Science Advances* **7**, 23, (2021)

* Acknowledgement(s) : Alexander von Hoegen acknowledges support from the Alexander von Humboldt foundation. We acknowledge support from the US Department of Energy and Gordon and Betty Moore Foundation's EPiQS Initiative grant GBMF9459.

Probing nonlinear transport in a non-equilibrium Superconductor

E. Wang, J. D. Adelinia, M. Chavez-Cervantes, T. Matsuyama, M. Fechner, M. Buzzi
G. Meier, A. Cavalleri
Max Planck Institute for the Structure and Dynamics of Matter, 22761 Hamburg, Germany

Optically driven quantum materials exhibit a variety of non-equilibrium functional phenomena [1-12], which to date have been primarily studied with ultrafast optical, photoemission, X-Ray scattering and spectroscopy methods. However, little has been done to characterize their transient electrical responses, which are directly associated with the functionality of these materials. Especially interesting are linear and nonlinear current-voltage characteristics at frequencies below 1 THz, which are not easily measured at picosecond temporal resolution. Here, we report on ultrafast transport measurements in photo-excited K_3C_{60}, in which a transient phase with superconducting like optical properties has been recently documented [13-17]. Nonlinear transport measurements are executed by connecting thin films of this compound to photo-conductive switches with co-planar waveguides. We observe characteristic signatures of a photo-induced granular superconductivity, including characteristic nonlinear current-voltage responses that reveal the presence of excited weak links between transiently superconducting grains.

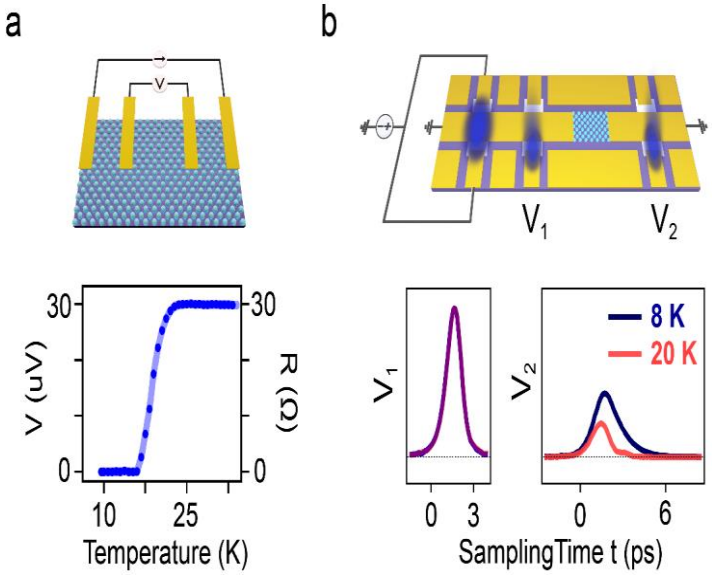

Fig. 1. *Conventional DC four-point transport measurement and on-chip ultrafast transport measurement.* ***a****,* ***Upper****: Schematic of a DC four-point transport measurement on a K_3C_{60} thin film.* ***Lower:*** *Measured resistance versus temperature of the K_3C_{60} thin film with 1 μA current bias.* ***b****, Upper: Schematic of on-chip ultrafast transport device. The MBE grown K_3C_{60} thin film* ***(cyan)*** *and three pairs of photo-conductive switches* ***(white)*** *were incorporated within a coplanar waveguide* ***(yellow)*** *on a sapphire substrate* ***(purple)****. Ultrashort electrical pulses were launched by illuminating laser pulses onto the left pair of photo - conductive switches, which were simultaneously biased by a voltage source. The launched pulse $V_1(t)$ was sampled by illuminating one switch of the middle pair and by changing the mutual delay between the launching and sampling laser pulses. Similarly, the transmitted pulse $V_2(t)$ was sampled with one switch of the right pair.* ***Lower****: $V_1(t)$ and $V_2(t)$ measured at 8 K and 20 K. Both measurements were normalized by the peak value of $V_1(t)$.*

Ultrafast nonlinear transport provides access to the physics of driven quantum materials and will enable integration of non-equilibrium functionalities into ultrafast optoelectronic platforms.

References

[1] I. Radu, K Vahaplar, C Stamm, T Kachel, N Pontius, H A Dürr, T A Ostler, J Barker, R F L Evans, R W Chantrell, A Tsukamoto, A Itoh A Kirilyuk, Th Rasing, A V Kimel,. *Nature* **472**, 205 (2011).
[2] T F Nova, A S Disa, M Fechner, A Cavalleri, *Science* **364**, 1075 (2019).
[3] X.Li T.Qiu, J.Zhang,, E.Baldini, J.Lu, A. M. Rappe, K.A. Nelson, *Science* **364**,1079 (2019)
[4] A. S. Disa, M. Fechner, T.F. Nova, B.Liu, M.Först, D.Prabhakaran, P.G. Radaelli,A.Cavalleri, *Nature Physics* **16,** 937 (2020).
[5] Y.H. Wang, Y.H., Y. H. Wang, H. Steinberg, P. Jarillo-Herrero, N. Gedik, *Science* **342**, 453 (2013).
[6] J. W. McIver.B. Schulte. F.-U. Stein, T. Matsuyama.G. Jotzu, G. Meier.A. Cavalleri, *Nature Physics* **16**, 38 (2020).
[7] S.Zhou, C. Bao, B. Fan, H. Zhou. Q. Gao, H. Zhong, T.Lin, H.Liu, P. Yu, P. Tang, S. Meng, W. Duan. S.Zhou, *Nature* **614**, 75 (2023).
[8] X Wang, C.Xiao, H.Park, J. Zhu, C.Wang, T. Taniguchi, K. Watanabe, J.Yan, D.Xiao, D. R Gamelin, W.Yao, X. Xu, **Nature 604**, 468 (2022).
[9] D. Fausti , R. I. Tobey, N. Dean, S. Kaiser, A. Dienst, M. C. Hoffmann, S. Pyon, T. Takayama, H. TakagI, A. Cavalleri, *Science* **331**,189 (2011).
[10] W. Hu, S. Kaiser, D. Nicoletti, C. R. Hunt, I. Gierz, M. Hoffmann, M. Le Tacon,T.Loew, B.Keimer,A.Cavalleri, *Nature Materials* **13,** 705 (2014).
[11] K.A. Cremin, J. Zhang, C. C. Homes, G. D. Gu, Z.Sun, M. M. Fogler, A.J. Millis, D. N. Basov, R. D. Averitt, *Proceedings of the National Academy of Sciences* **116,** 19875 (2019).
[12] K.Isoyama, N.Yoshikawa, K.Katsumi, J.Wong, N.Shikama, Y.Sakishita, F.Nabeshima, A.Maeda, R.Shimano, *Communications Physics* **4** 160(2021).
13] M.Mitrano, A.Cantaluppi, D.Nicoletti, S Kaiser, A,Perucchi, S Lupi, P.Di Pietro, D.Pontiroli, M Riccò, S. Clark, D.Jaksch, A.Cavalleri, *Nature* **530**.461(2016)
[14] A.Cantaluppi,M. Buzzi, G. Jotzu, D. Nicoletti, M. Mitrano, D. Pontiroli,M. Riccò, A. Perucchi, P. Di Pietro,A. Cavalleri, Nature Physics 14, 837 (2018)
[15] M.Buzzi, D. Nicoletti, M. Fechner, N. Tancogne-Dejean, M. A. Sentef, A. Georges, T. Biesner, E. Uykur, M. Dressel, A. Henderson, T. Siegrist, J. A. Schlueter, K. Miyagawa, K. Kanoda, M.-S. Nam, A. Ardavan, J. Coulthard, J. Tindall, F. Schlawin, D. Jaksch, A. Cavalleri, *Physical Review* X **10,** 031028 (2020).
[16] M.Budden, T. Gebert, M. Buzzi, G. Jotzu, E. Wang, T. Matsuyama, G. Meier, Y. Laplace, D. Pontiroli, M. Riccò, F. Schlawin, D. Jaksch A.Cavalleri, *Nature Physics* **17**, 611 (2021).
[17] M.Buzzi, D. Nicoletti, S. Fava, G. Jotzu, K. Miyagawa, K. Kanoda, A. Henderson, T. Siegrist, J. A. Schlueter, M.-S. Nam, A. Ardavan A.Cavalleri, Physical Review Letters 127, 197002 (2021).

Spontaneous symmetry breaking by geometric motive force at Topological instability

J. Wang
Iowa State University, Ames, IA 50011, USA

An emerging light-induced symmetry and topology switch is breaking new ground in quantum science and technology [1-5]. Symmetry is at the heart of defining order parameters and classifying matter phases. Topology provides a beyond-symmetry classification and reveals a class of matter states which are symmetrically identical but topologically distinguishable. For a long time, topology-symmetry interplay has been studied "one-way", i.e., topological states are examined subject to a specific fixed symmetry. This work demonstrates that their interplay could be mutual. We show that crystalline symmetries (e.g., inversion symmetry) and time-reversal symmetry may turn fragile when topological phase transitions are triggered, which are manifested by the excitation of IR phonon mode off-resonantly, the generation of strong non-field-driven photocurrents and geometric charge pumping [6]. Such observations apply broadly and can establish a generic link between symmetry and topological transitions.

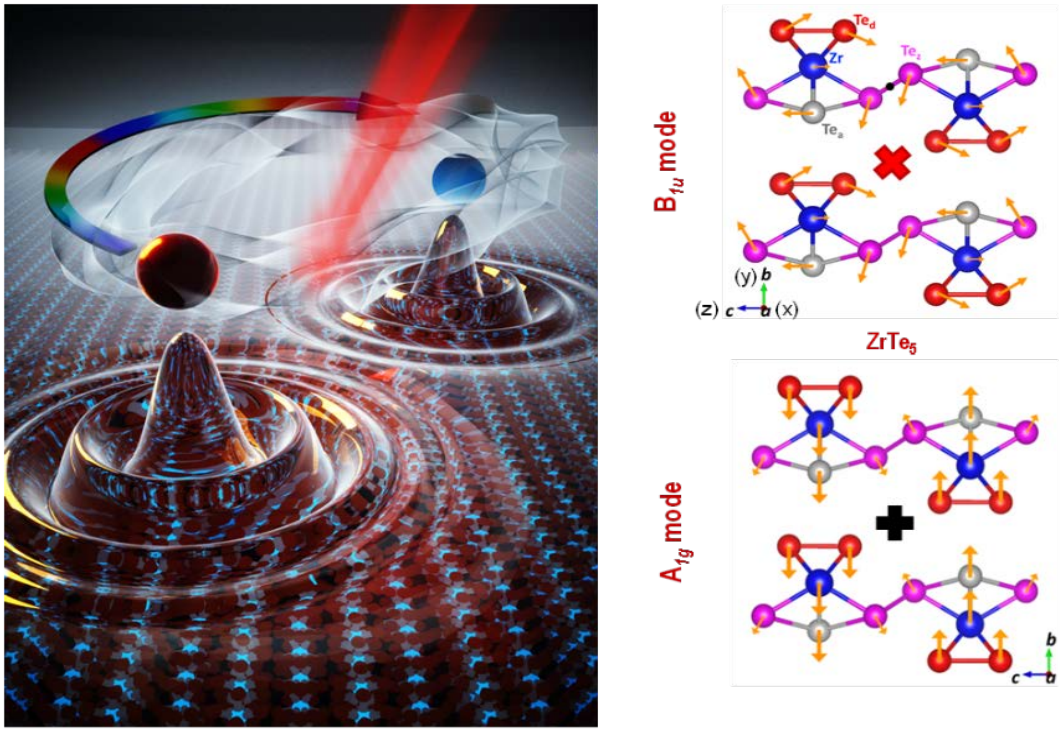

Fig. 1: *Light-induced of symmetry breaking at topological instability (**left**) in a Dirac material of $ZrTe_5$. Inversion symmetry and time-reversal symmetry breaking are manifested by the excitation of IR phonon mode off-resonantly (**right**), the generation of strong non-field-driven photocurrents and geometric charge pumping.*

On the other side, light engineering of correlation gaps in broken-symmetry ground states of topological materials provides a new avenue of achieving exotic topological phases inaccessible by conventional tuning methods. Here we demonstrate a light-controllable topological phase switching in a model CDW and polaron insulator [7]. Our ultrafast terahertz photocurrent spectroscopy reveals a topological phase switching from an axion insulator phase to a hidden Weyl phase with chirality controlled by light helicity.

References

[1] L. Luo, D.Cheng, B. Song, L.-L. Wang, C.Vaswani, P. M. Lozano, G. Gu, C. Huang, R. H. J. Kim, Z.Liu, J.-M. Park, Y. Yao, K.Ho, I. E. Perakis, Q.Li, J,Wang , *Nature Materials* **20**, 329 (2021).
[2] C. Vaswani, C. Vaswani, L.-L. Wang, D. H. Mudiyanselage, Q. Li, P. M. Lozano, G. D. Gu, D. Cheng, B. Song, L. Luo, R. H. J. Kim, C. Huang Z. Liu, M. Mootz, I. E. Perakis, Y. Yao, K. M. Ho, J. Wang, *Physical Review* X **10,** 021013 (2020).
[3] R. H. J. Kim, C.Huang,Y.Luan,L.-L. Wang,Z. Liu, J.-M. Park,L.Luo,P. M. Lozano,G. Gu,D. Turan,N. T. Yardimci,M.Jarrahi,I.E. Perakis Z. Fei,Q. Li,J. Wang, *ACS Photonics* **8**, 1873 (2021).
[4] X. Yang X. Yang, L.Luo, C. Vaswani, X.Zhao, Y.Yao, D.Cheng, Z.Liu, R. H. J. Kim, X.Liu, M. Dobrowolska-Furdyna, J.K. Furdyna, I. E. Perakis, C. Wang, K. Ho,J. Wang, *Quantum Materials* **5,** 13 (2020).
[5] C. Vaswani, C. Vaswani, J. H. Kang, M. Mootz, L. Luo, X. Yang, C. Sundahl, D. Cheng, C. Huang, R. H. J. Kim, Z. Liu, Y. G. Collantes E. E. Hellstrom, I. E. Perakis, C. B. Eom, J. Wang, *Nature Communications* **12**, 258 (2021).
[6] L. Luo, preprint(2023).
[7] B. Cheng, preprint (2023)

Nonlinear terahertz spectroscopy study on the interplay between Superconductivity and pseudogap in cuprate superconductor

N.-L. Wang
Peking University, Beijing 100871, China

We present nonlinear terahertz third harmonic generation (THG) measurement on different doping YBa2Cu3O6+x thin films and electron-doped LCCO thin films. Different from conventional superconductors [1], the THG signal starts to appear in the normal state, which is consistent with the crossover temperature T^* of pseudogap over broad doping levels. Upon lowering temperature, the THG signal shows anomaly just below Tc. Strikingly, we observe a beat pattern directly in the measured real time waveform of THG signal, as shown below in Fig. 1 [2]. We elaborate that the Higgs mode, which develops below Tc, couples to the mode already developed below T^*, resulting in an energy level splitting. The strong coupling effect offers new insight into the interplay between superconductivity and pseudogap. The result suggests that the pseudogap phase is not likely a precursor of superconductivity but represents a distinct order.

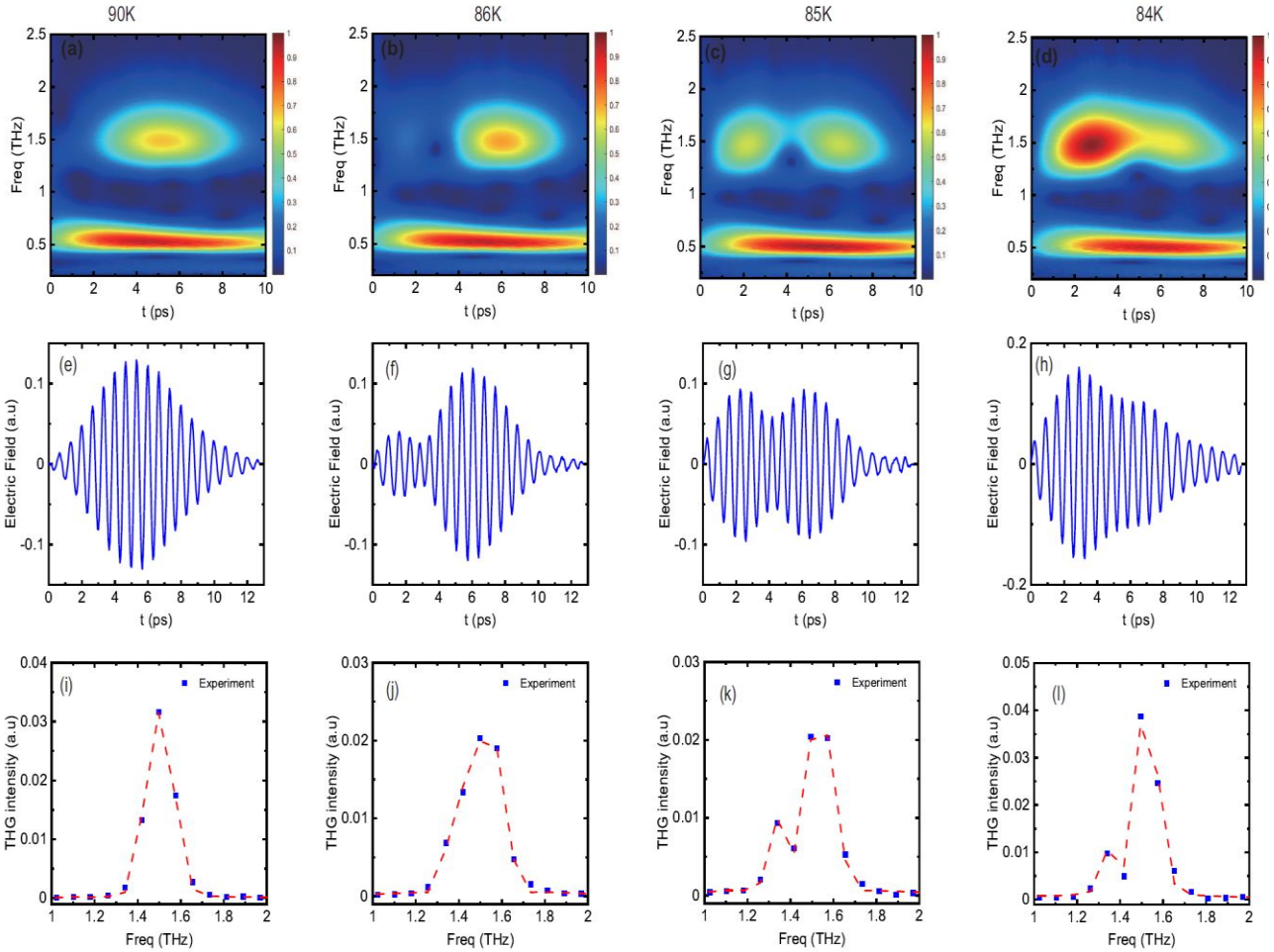

Fig. 1: ***(a)-(d)****, THG intensity continuous wavelet transformation chronograms in optimal doped YBCO thin film driven by 0.5 THz pulse for (a) 89 K, (b) 86 K, (c) 85 K and (d) 84 K. (e)-(h) The real time waveforms of THG signal after a digital 1THz high pass filter. The beating pattern in the waveform is corresponding to the dip in CWT chronogram.* ***(i)-(i)*** *The THG spectrum for 89 K, 86 K, 85 K and 84 K after the global FFT. The splitting is caused by the dynamical strong coupling between Higgs mode and pseudogap collective mode.*

Work done in collaboration with Tao Dong, Jia-Yu Yuan and other team members in Peking University.

References:

[1] Z.-X. Wang, J.-R. Xue, H.-K. Shi, X.-Q. Jia, T. Lin, L.-Y. Shi, T. Dong, F. Wang, N.-L. Wang, *Physical Review B* **105**, L100508 (2022).
[2] J. Y. Yuan, L. Y. Shi, L. Yue, B. H. Li, Z. X. Wang, S. X. Xu, T. Q. Xu, Y. Wang, Z. Z. Gan, F. C. Chen, Z. F. Lin, X. Wang, K. Jin, X. B. Wang, J. L. Luo, S. J. Zhang, Q. Wu, Q. M. Liu, T. C. Hu, R. S. Li, X. Y. Zhou, D. Wu, T. Dong, N. L. Wang, *arXiv:*2211.06961.

* Acknowledgement: This work was supported by the National Science Foundation of China and the National Key Research and Development Program of China.

Controlling magnetic excitations and entanglement using Ultrafast laser

Y. Wang
Clemson University, Clemson, SC 29634

The rapidly evolving quantum science calls for precise and predictive control of collective electronic properties beyond the classical realm. Among various control knobs, an ultrafast laser pump is a promising approach due to its rich degrees of freedom. Together with the laser's capability of influencing electronic structure comes the necessity to track the instantaneous status of a time-dependent nonequilibrium material. Novel pump-probe spectral techniques play a critical role in bridging experiments and theory and quantifying the nonequilibrium state of materials.

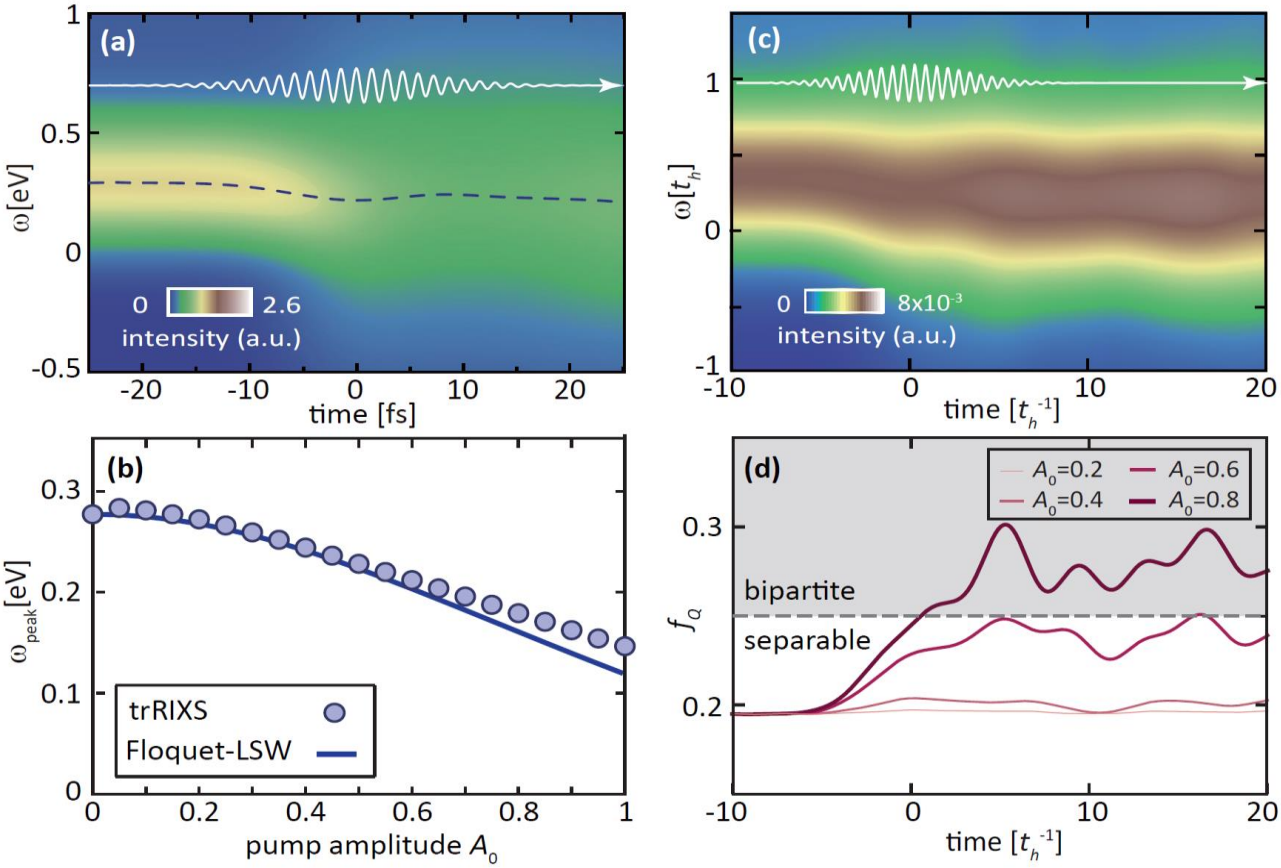

Fig. 1. (a)*: Collective spin excitations measured by trRIXS in a 2D doped Mott insulator, reflecting the light-induced softening of paramagnons. The dashed line tracks the evolution of the peak position in time, following the pump pulse (white line).* ***(b)*** *The comparison of the transient paramagnon energy (circles) at the center of pump pulse with the Floquet-linear-spin wave theory (solid line).* ***(c)*** *The trRIXS measurement of a quarterly filled 1D cuprate chain.* ***(d)*** *Dynamics of quantum Fisher information revealed from trRIXS, witnessing a bipartite-entangled state induced by laser.*

In this talk, I will discuss the application of time-resolved resonant inelastic x-ray scattering (trRIXS) in magnetic materials [see Fig.1(a)]. By comparing the trRIXS for antiferromagnetic materials, we find that the instantaneous paramagnon excitations can be manipulated by pulsed laser in a predictive manner, following the Floquet theory in the center of the pulse [see Fig.1(b)]. Such a Floquet engineering works only at doped Mott insulators without long-range order, while the trRIXS study of an undoped Mott insulator violates the Floquet approximation. Leveraging the light-engineered magnetic excitations, we further study the nonequilibrium dynamics of a 1D cuprate chain [see Fig.1(c)]. Through a self-consistent iteration, trRIXS can probe the transient entanglement of wavefunctions in nonequilibrium materials via the quantum Fisher information. Via this approach, we reveal the possibility of enhancing entanglement in a cuprate chain using an ultrafast laser pulse [see Fig.1(d)].

References

[1] M. Mitrano, Y. Wang. *Communications Physics* **3**, 184 (2020).
[2] Y. Wang, Y. Chen, T.P. Devereaux, B. Moritz, M. Mitrano, *Communications Physics* **4**, 212 (2021)
[3] J. Hales, U. Bajpai, T. Liu, D.R. Baykusheva, M. Li, M. Mitrano, Y. Wang, *arXiv:2209.02283* (2022)
* Acknowledgement(s) : Y.W. acknowledges support from U.S. Department of Energy, Office of Science, Basic Energy Sciences, under Early Career Award No. DE-SC0022874.

Ultrafast spin excitations in 3d and 4f metals

M. Weinelt
Freie Universität Berlin, 14195 Berlin, Germany

Understanding ultrafast spin dynamics is not only a complex and fascinating challenge in fundamental physics, but carries the potential for magnetic recording based on all-optical switching (AOS) of the magnetic order [1]. AOS triggered by a single fs laser pulse was first observed in the ferrimagnetic alloy FeCoGd and more recently in Pt/Co/Gd stacks [2-4]. The key to AOS is exchange of angular momentum between the oppositely aligned magnetic moments of the transition metal and rare earth sublattices [5,6]. Spin transport and exchange scattering are discussed as microscopic processes responsible for spin dynamics and all-optical switching. However, it remains debated to what extent ultrafast magnetization dynamics generates spin currents and vice versa. We will highlight a few examples of the signature of spin dynamics in the electronic structure in 3d and 4f metals and the role of spin transport. In particular, we use time- and spin-resolved photoemission spectroscopy to study an antiferromagnetically coupled Gd/Fe bilayer, a prototype system for all-optical switching. Spin transport leads to an ultrafast drop of the spin polarization at the Gd surface demonstrating angular-momentum transfer over several nanometers. Thereby Fe acts as spin filter, absorbing spin majority but reflecting spin minority electrons. Spin transport from Gd to Fe was corroborated by an ultrafast increase of the Fe spin polarization in a reversed Fe/Gd bilayer. In contrast, for a pure Gd film spin transport into the tungsten substrate can be neglected as spin polarization stays constant.

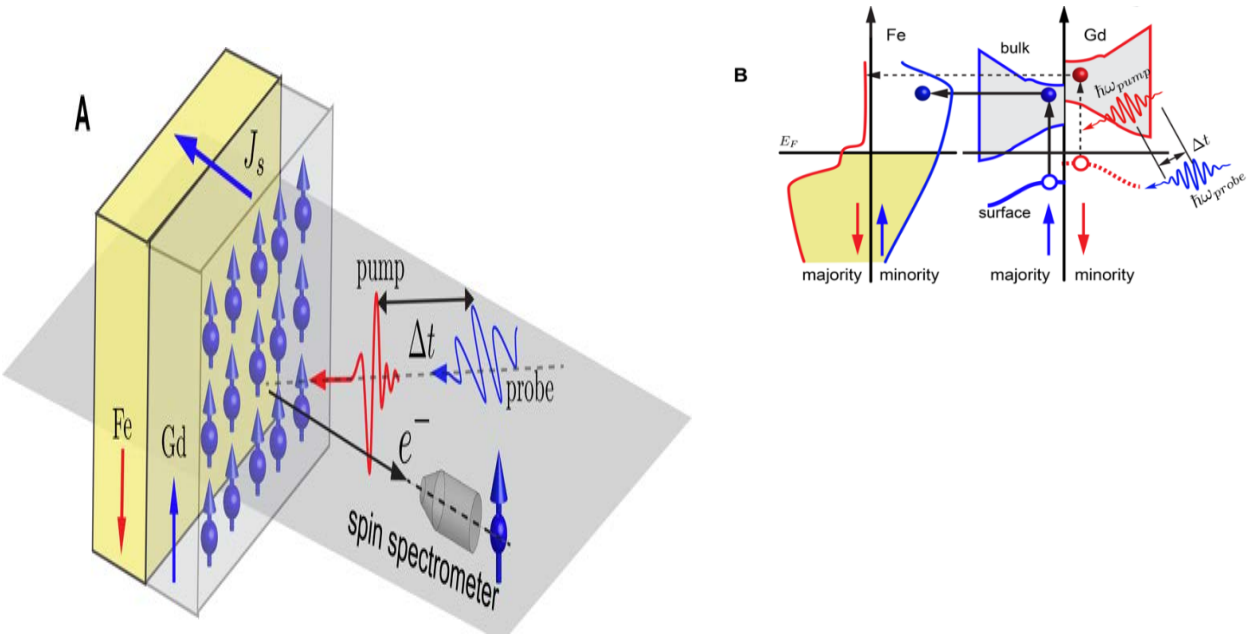

Fig. 1. A) *Spin transport in Gd|Fe on W(110) and Fe|Gd on W(110) revealed by spin- and time-resolved photoelectron spectroscopy.* ***B)*** *Spin-filter effect.*

Our results suggest that ultrafast spin transport drives the magnetization dynamics in Gd/Fe and reveal microscopic insights into ultrafast spin dynamics [8].

References

[1] V. Kimel, M.Li, *Nature Review Materials* **4**, 189 (2019).
[2] C. D. Stanciu F. Hansteen, A. V. Kimel, A. Kirilyuk, A. Tsukamoto, A. Itoh, Th. Rasing, Physical Review Letters **99**, 047601 (2007);
[3] T. A. Ostler, J. Barker, R. F. L. Evans, R. W. Chantrell, U. Atxitia, O. Chubykalo-Fesenko, S. El Moussaoui, L. Le Guyader E. Mengotti, L. J. Heyderman, F. Nolting, A. Tsukamoto, A. Itoh D. Afanasiev, B. A. Ivanov, A. M. Kalashnikova K. Vahaplar, J. Mentink, A. Kirilyuk, Th. Rasing, and A. V. Kimel, *Nature Communications* **3**, 666 (2012).
[4] M. Beens M. Beens, M. L. M. Lalieu, A. J. M. Deenen, R. A. Duine, B. Koopmans, *Physical Review* B **100**, 220409 (2019).
[5] I. Radu, K. Vahaplar, C. Stamm, T. Kachel, N. Pontius, H. A. Dürr, T. A. Ostler, J. Barker, R. F. L. Evans, R. W. Chantrell A. Tsukamoto, A. Itoh, A. Kirilyuk, Th. Rasing, A. V. Kimel, *Nature* **472**, 205 (2011).
[6] C. E. Graves, A. H. Reid, T. Wang, B. Wu, S. de Jong, K. Vahaplar, I. Radu, D. P. Bernstein, M. Messerschmidt, L. Müller R. Coffee, M. Bionta, S. W. Epp, R. Hartmann, N. Kimmel, G. Hauser, A. Hartmann, P. Holl, H. Gorke, J. H. Mentink A. Tsukamoto, A. Fognini, J. J. Turner, W. F. Schlotter, D. Rolles, H. Soltau, L. Strüder, Y. Acremann, A. V. Kimel A. Kirilyuk, Th. Rasing, J. Stöhr, A. O. Scherz, H. A. Dürr, *Nature Materials* **12,** 293 (2013).
[7] B. Frietsch, A. Donges, R. Carley, M. Teichmann, J. Bowlan, K. Döbrich, K. Carva, D. Legut, P. M. Oppeneer, U. Nowak M. Weinelt, *Science Advances* **6**, eabb 1601 (2020).
[8] B. Liu, H. Xiao, M. Weinelt, *Science Advances*, (submitted) (2023).
* Acknowledgement: author acknowledges support from Deutsche Forschungsgemeinschaft, CRC/TRR 227 - *Ultrafast Spin Dynamics*, Project A01, and from Bundesministerium für Bildung und Forschung, grant: 05K22KE2

Ultrafast electron and spin dynamics in NiO upon above Bandgap excitation

K. Gillmeister[1], D. Golez[2], Y. Pavlyukh[3], J. Berakdar[1], P. Werner[2], W. Widdra[1]
[1] *Martin-Luther-Universität Halle-Wittenberg, Halle, Germany*
[2] *University of Fribourg, Fribourg, Switzerland*
[3] *Technische Universität Kaiserslautern, Kaiserslautern, Germany*

Charge excitation across an electronic band gap plays an important role in optoelectronics and light harvesting. In strongly correlated materials, such as NiO, studies of above-band-gap photoexcitation are still in their infancy, despite their use in spintronics. Here we present a combined scanning tunnelling microscopy (STM), scanning tunnelling spectroscopy (STS), and time-resolved two-photon photoemission (2PPE) study for ultrathin films of NiO(001) to address the electronic response upon optical excitation [1-4].

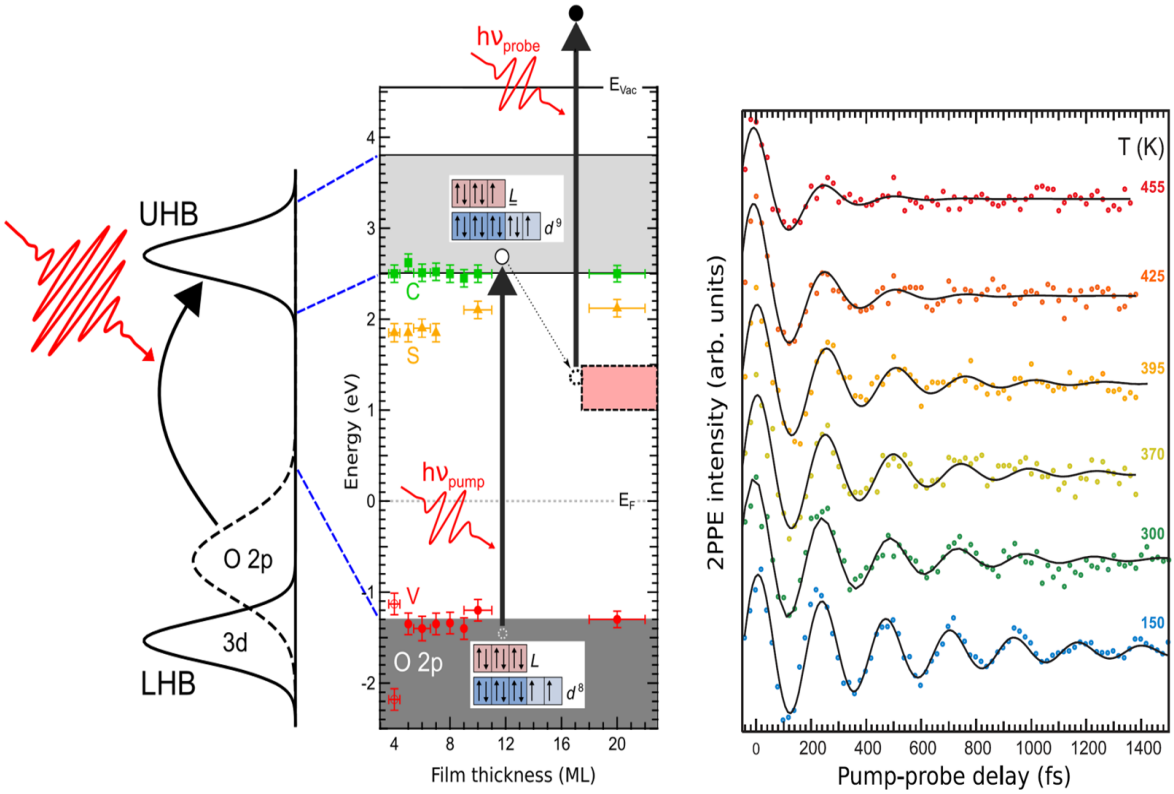

***Fig. 1. Left**: NiO band structure and excitation scheme. **Right**: Time-resolved 2PPE intensity of the in-gap states upon excitation across the bandgap. The frequency of the oscillations corresponds to the Ni-O-Ni super-exchange energy.*

At the surface of epitaxial NiO(001) films grown on Ag(001), we find series of well-defined image potential states below the vacuum level with film thickness dependent lifetimes in the range from 30 to 120 fs [2]. In contrast to these rather long lifetimes, we find an ultrafast (<10 fs) relaxation for electrons that are excited just across the charge-transfer gap into the conduction band. The latter forms the upper Hubbard band of a charge-transfer insulator NiO as sketched in Fig. 1 [3]. We identified the initial optical excitation into the upper Hubbard band which is followed by an ultrafast relaxation into long-lived many-body in-gap states. Remarkably, the spectral weight of these in-gap states displays coherent THz oscillations up to 2 ps at low temperature as shown in the right part of Fig.1 [3]. The frequency of these oscillations corresponds to the strength of the antiferromagnetic superexchange interaction in NiO and their lifetime vanishes slightly above the Néel temperature. These observations indicate a strong coupling of the excited states to the antiferromagnetic spin system and pave the way for addressing antiferromagnetic spin-spin correlation in oxides on the ultrafast time scale [3].

References

[1] K. L. Kostov, F. O. Schumann, S. Polzin, D. Sander, W. Widdra, *Physical Review* B **94**, 075438 (2016).
[2] K. Gillmeister, M. Kiel, W. Widdra, *Physical Review* B **97**, 085424 (2018).
[3] K. Gillmeister, D. Golež, C.-T. Chiang, N. Bittner, Y. Pavlyukh, J. Berakdar, P. Werner, W. Widdra, *Nature Communications* **11**, 4095 (2020).
[4] Y. W. Windsor, D. Zahn, R. Kamrla, J. Feldl, H. Seiler, C.-T. Chiang, M. Ramsteiner, W. Widdra, R. Ernstorfer, L. Rettig, *Physical Review Letters* **126**, 147202 (2021).

* Support by the Sonderforschungsbereich SFB/TRR-227 “Ultrafast spin dynamics” is gratefully acknowledged

Ultrafast dynamics probed by time-resolved and local Spectroscopy at the nanoscale

M. Wolf
Fritz-Haber Institut der Max-Plank-Gesellschaft, 14195 Berlin, Germany

Interaction of many-body systems with ultrashort light pulses may lead to emergent phenomena away from equilibrium. Recent advances in time-resolved photoemission spectroscopy (trARPES) combined with momentum microscopy allow direct probing of excited states throughout the complete Brillouin zone. 2D materials and their heterostructures provide a vast playground to obtain a mechanistic understanding of exciton dynamics and energy transfer into nuclear motions. Here we extend these studies and investigate the primary step of singlet fission in crystalline pentacene using orbital tomography. Knowledge about the localization and orbital character of the exciton wave functions allows to decompose energetically overlapping states on the basis of their orbital character [1]. Our results indicate a charge-transfer mediated mechanism with a hybridization of Frenkel and charge transfer states in the lowest bright singlet exciton.
Using scanning probe microscopy, extreme spatial resolution can be obtained by atomic-scale light confinement in plasmonic "picocavities". We show that inelastic light scattering is dramatically enhanced by forming a quantum point contact (QPC) on a single adatom in a well-defined picocavity controlled precisely by low-temperature scanning tunneling microscopy (STM). Tip enhanced Raman spectra from a single silver atom on Ag(111) in the QPC regime exhibit spectral features originating from the interaction with both vibrations and electrons in the STM junction. The atomic-scale light confinement is reproduced by TDDFT simulations including the vibrational dynamics of the atomistic structures. Coherent phonons can provide microscopic insight into ultrafast lattice dynamics and coupling to other degrees of freedom. We implement ultrafast laser-induced STM applied to coherent phonon spectroscopy (see Fig.1). Excitation and relaxation of coherent phonons may be susceptible to the local nanoscale environment, calling for real-space observation of ultrafast lattice dynamics. We demonstrate nanoscale local coherent phonon spectroscopy employing time-resolved STM in a plasmonic junction, and unveil spatial inhomogeneities of coherent phonon dynamics in ultrathin zinc oxide (ZnO) films with few nanometer spatial and femtosecond temporal resolution. The coherent phonons in ZnO are locally excited by the tightly-confined gap plasmon, and are probed via the photoinduced tunneling current through an electronic resonance of the ZnO film.

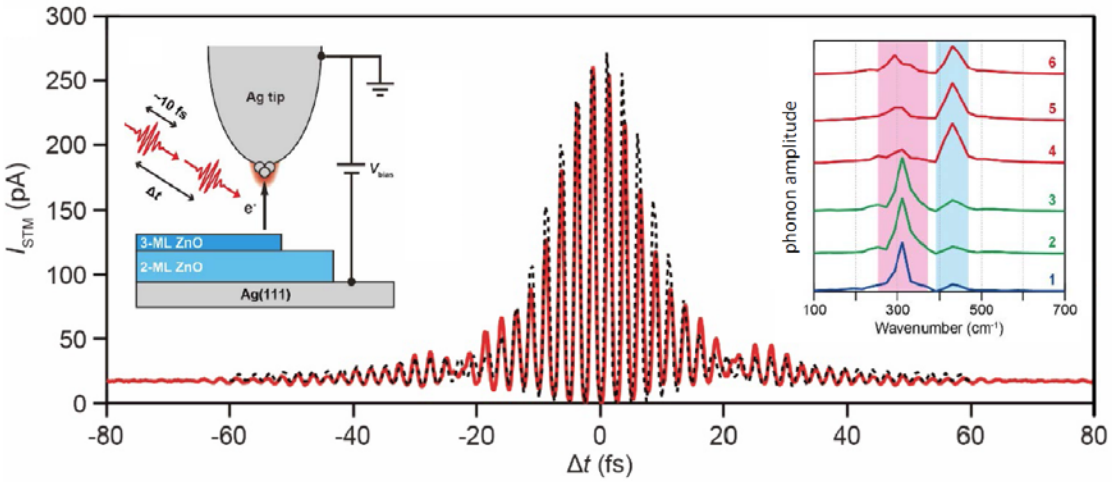

Fig. 1. *Ultrashort pulsed laser-induced STM in a plasmonic junction on Ag(111), 2-ML and 3-ML ZnO, respectively. Main panel: Interferrometric autocorrelation (IAC) trace of the photocurrent for a Ag tip–Ag(111) junction. The right inset shows FT spectra of the IAC traces at different sample positions on ZnO (with 2 nm steps).*

In combination with tip-enhanced Raman spectroscopy and scanning tunneling spectroscopy, we reveal the involved phonon modes and a correlation of the local electronic structure with the coherent phonon dynamics [2].

References

[1] A. Neef, S. Beaulieu, S. Hammer, S. Dong, J. Maklar, T. Pincelli, P. Xian, M. Wolf, L. Rettig, J. Pflaum, R. Ernstorfer, *Nature* **616**, 275 (2023).
[2] S. Liu, A. Hammud, I. Hamada, M. Wolf, M. Müller, T. Kumagai, *Science Advances* **8**, eabq5682 (2022).
* Acknowledgements: This work was performed in collaboration with Alexander Neef, Samuel Beaulieu, Sebastian Hammer, Shuo Dong, Julian Maklar, Tommaso Pincelli, R. Patrick Xian, Laurenz Rettig, Jens Pflaum, Ralph Ernstorfer and Shuyi Liu, Takashi Kumagai, Melanie Müller, Franco Bonafe, Heiko Appel, Angel Rubio

Propagation of extreme pulsed light: First-principles computational study

K. Yabana
University of Tsukuba, Tsukuba 305-8577, Japan

When describing the interaction between intense ultrashort laser pulses and solids theoretically, two aspects need to be considered: The strong electric field of the light pulse induces highly nonlinear and transient electron dynamics in the solid that cannot be described by perturbation theory. This nonlinear electron motion then manifests itself as nonlinear polarization on a macroscopic scale and dominates the propagation of intense pulsed light. Therefore, to understand the interaction between significantly intense pulsed light and matter, especially its propagation, it is necessary to consider the coupling between the dynamics of the optical electromagnetic field and the nonlinear dynamics of the electrons. The spatial scale of the two dynamics also needs to be taken into account: for interactions with two-dimensional atomic layer materials and very thin films, microscopic electromagnetics that varies on the atomic scale is effective, while for sufficiently thick films and bulk surfaces, macroscopic electromagnetics with coarse-graining is required. Based on the first-principles time-dependent density functional theory (TDDFT), we have developed a theoretical and computational method for the interaction of intense ultrashort pulsed light with solids [1,2], which we call the Maxwell - TDDFT calculation method. This method has been implemented in the open-source software SALMON developed by the authors' group [3].

Figure 1(a) summarizes the Maxwell-TDDFT calculation method with coarse-graining for the case of pulsed light propagating through a thin film. One-dimensional light propagation in the thin film is described by the wave equation for a vector potential using uniform grid points in the Z-axis coordinates; electron motion is considered at each grid point in Z and described by a time-dependent Bloch orbital function. The time evolution of that Bloch orbital is described by the time-dependent Kohn-Sham equation, which is the fundamental equation of TDDFT. Thus, by solving the Maxwell equations and the fundamental equations of TDDFT jointly and simultaneously, light propagation and electron dynamics can be described simultaneously. This method with coarse-graining is called the Maxwell-TDDFT multiscale

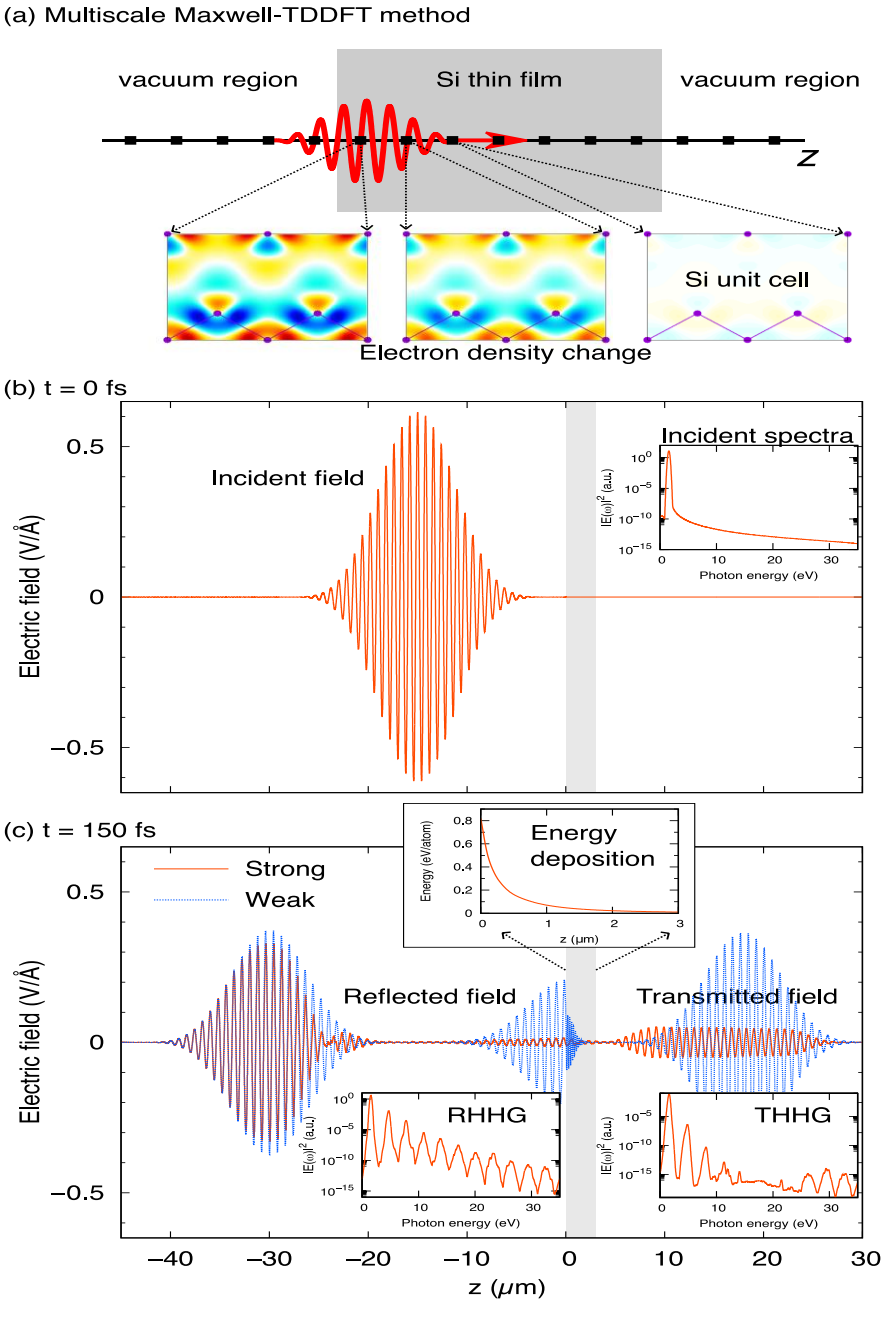

Fig. 1. *Overview of the theoretical method*

method because it uses two lattice systems with different resolutions [1]. We have also developed a method for the microscopic Maxwell equations using a single lattice, which we call the Maxwell-TDDFT single-scale method [2]. Figures 1(b) and 1(c) show typical calculations of pulsed light propagating through a 3μm-thick silicon (Si) thin film. Figure 1(b) shows the electric field of the initial pulse located in front of the thin film; the thin film is shown as a light gray area. The average frequency of the pulse was set to 1.55 eV, which is below the direct band gap of Si.
The maximum intensity of the incident pulse was set to $5\text{x}10^{12}$ W/cm^2. Figure 1(c) shows a snapshot of the electric field at 150 fs. The results corresponding to the initial pulses of two different maximum intensities are shown here: the $5\text{x}10^{12}$ W/cm^2 is shown by the solid red line, and the much weaker pulse is shown by the dotted blue line. The latter is multiplied by a factor so that the difference between the two lines manifests the nonlinear effect of the stronger pulse. It is observed that the nonlinear effects are more pronounced in the transmitted pulse than in the reflected pulse. The stronger transmitted pulse undergoes strong nonlinear effects with an almost flat envelope. From these calculations, various physical information can be extracted. For example, as shown in the inset of Fig. 1(c), the energy transfer from the light field to the electrons in the unit cell as a function of Z provides useful information for understanding the initial stages of non-thermal laser processing [4]. Fourier spectra of reflected and transmitted pulses (RHHG and THHG) for strong incident pulses are shown in the inset of Figure 1(c). These show spectra of higher-order harmonic generation, a typical nonlinear phenomenon [5,6]. The light response of a material varies significantly with light intensity. The response to weak light is described by the dielectric constant, which varies greatly depending on whether the material is a dielectric or a metal, and in the case of dielectrics, on the band gap and the frequency of light. On the other hand, for very intense pulsed light, it is well known that all materials exhibit plasma reflections. Using the Maxwell-TDDFT multiscale method, we present the results of a systematic analysis of how the optical response of various materials changes as the maximum intensity of the pulsed light increases. Figure 2 shows the calculated reflectance, absorption, and transmittance of a 200 nm thick Si thin film normally irradiated with linearly polarized pulsed light of various intensities, with the maximum intensity of the pulse on the horizontal axis. At sufficiently low intensities, the optical response is linear and is described by a dielectric function, as expected.

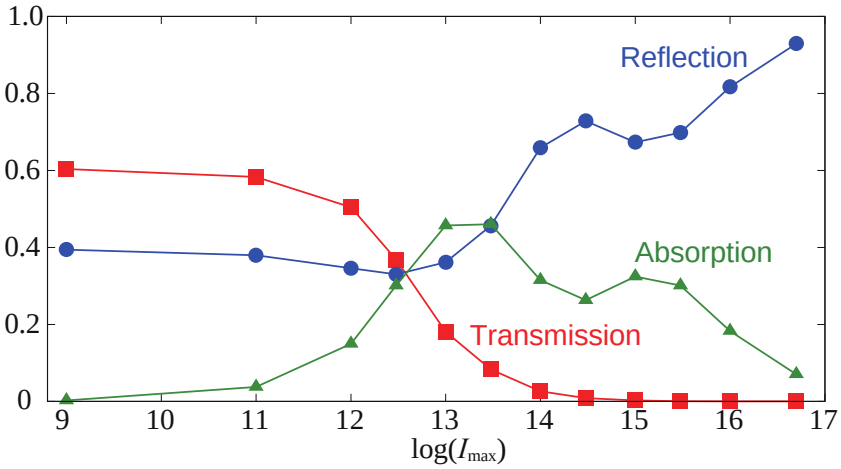

Fig. 2. *Reflection, absorption, and transmission rates of a Si thin film of 200nm thickness are plotted against the maximum intensity of the pulsed light.*

As the intensity increases, multiphoton absorption occurs, with the absorption showing a maximum at about 10^{13} W/cm^2. Above 10^{14} W/cm^2, more electrons are excited at the leading edge of the pulse and plasma reflection becomes dominant. However, the process from multiphoton absorption to plasma reflection is not monotonous, and complex changes are observed at intensities around 10^{15} W/cm^2. At this intensity, the plasma frequency of the excited electrons coincides with the fundamental frequency of the incident pulse, resulting in the appearance of a minimum in the reflection. Such an analysis can be performed for any material understood by the band structure.

References

[1] K. Yabana, T. Sugiyama, Y. Shinohara, T. Otobe, G.F. Bertsch, *Physical Review* B **85**, 045134 (2012).
[2] S. Yamada, M. Noda, K. Nobusada, K. Yabana, *Physical Review* B**98**, 245147 (2018).
[3] M. Noda, S.A. Sato, Y. Hirokawa, M. Uemoto, T. Takeuchi, S. Yamada, A. Yamada, Y. Shinohara, M. Yamaguchi, K. Iida, I. Floss, T. Otobe K.-M. Lee, K. Ishimura, T. Boku, G.F. Bertsch, K. Nobusada, K. Yabana, *Computer Physics Communications* **235**, 356 (2019).
[4] A. Yamada, K. Yabana, *The European Physical Journal* D**73,** 1 (2019).
[5] S. Yamada, K. Yabana, *Physical Review* B**103**, 155426 (2021).
[6] S. Yamada, T. Otobe, D. Freeman, A. Kheifets, K. Yabana, *Physical Review* B**107**, 035132 (2023).

Ultrafast intrinsic optical-to-electrical conversion dynamics in Graphene investigated using on-chip THz spectroscopy

K. Yoshioka
NTT Corporation, 243-0198 Atsugi, Japan

With the anticipated exponential growth of data traffic, there is an imminent need for optical receivers that enable the conversion of optical signals into electrical signals while maintaining ultrahigh bandwidth and low power consumption. Graphene-based photodetectors (PDs) utilizing the photothermoelectric (PTE) effect have gained significant attention due to their potential to outperform existing semiconductor devices [1]. However, despite their promising potential, the demonstrated operational speed of these devices is limited to approximately 70 GHz [2], which falls far short of the theoretical expectation of 200 GHz. Despite the crucial role of optical-to-electrical (O-E) conversion on the intrinsic timescale for the design of ultrafast graphene optoelectronic devices, achieving this capability and understanding its underlying mechanism have yet to be realized.

Here, we showcase the ability to perform ultrafast electrical readout of PTE current in high-quality graphene that is encapsulated in hexagonal boron nitride (hBN). By employing on-chip terahertz (THz) spectroscopy [3] and a zinc oxide (ZnO) gate structure that eliminates high-frequency capacitive coupling [4], we successfully overcome the limitations imposed by the bandwidth of readout electronics and the large RC time constant of the device. Fig. 1(a) shows a schematic of our on-chip THz spectroscopy setup

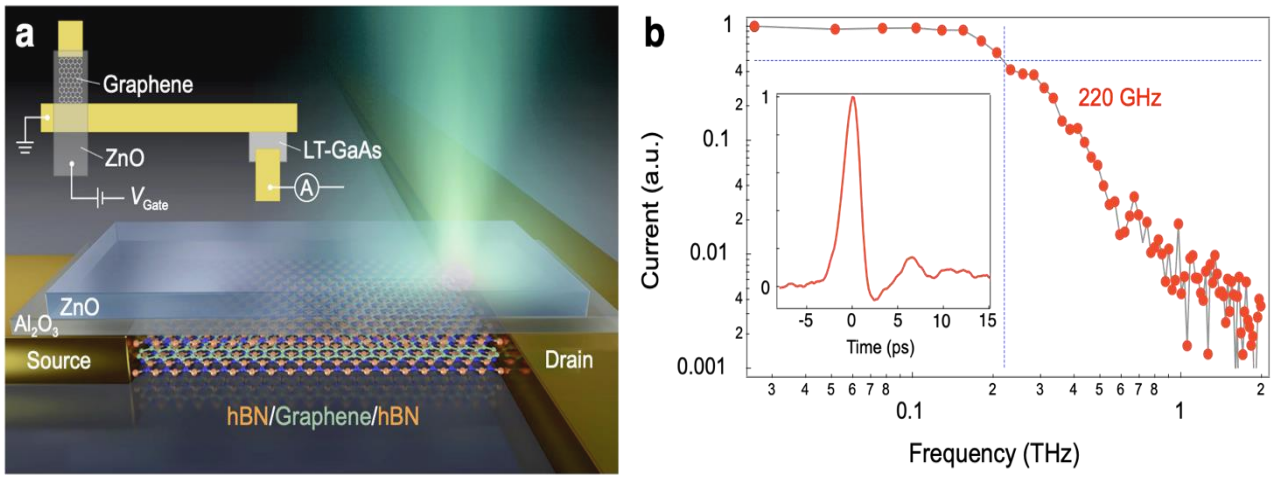

***Fig. 1. a**: Schematic of on-chip THz spectroscopy with ZnO gate structure to investigate intrinsic O-E conversion dynamics in graphene. **b**: Fourier spectrum of obtained photocurrent with the 3 dB bandwidth of 220 GHz. Inset shows a time-domain waveform.*

Our graphene FET is connected to a photoconductive switch with the terahertz (THz) waveguide to read out photocurrent with sub-picosecond time resolution. To exclude the dominant RC time constant from the large gate capacitance, we used the ZnO gate, which is transparent above the GHz frequency range [4]. This enables us to operate graphene PD with its intrinsic timescale. As shown in Fig. 1(b), the 3 dB bandwidth of our graphene PD reaches 220 GHz, which indicates that our methodology is suitable for tracking the O–E conversion mechanisms in graphene.Furthermore, we comprehensively explore the nonlocal ultrafast dynamics of the PTE current by adjusting parameters such as V_{Gate}, pump position, channel length, and graphene mobility. As a result, we have achieved a quantitative understanding of the O-E conversion processes [5]. We are convinced that our on-chip ultrafast electrical readout approach removes the obstacle between device engineering and ultrafast optical science by showing how to bring out the functionality based on a fundamental understanding of carrier dynamics in quantum materials.

References

[1] M. Romagnoli, V. Sorianello, M. Midrio, F. H. L. Koppens, C. Huyghebaert, D. Neumaier, P. Galli, W. Templ, A. D'Errico, A. C. Ferrari, *Nature Review Materials* **3**, 392 (2018).
[2] S. Marconi, M. A. Giambra, A. Montanaro, V. Mišeikis, S. Soresi, S. Tirelli, P. Galli, F. Buchali, W. Templ, C. Coletti, V. Sorianello M. Romagnoli, *Nature Communications* **12**, 806 (2021).
[3] K. Yoshioka, N. Kumada, K. Muraki, M. Hashisaka, *Applied Physics Letters* **117**, 161103 (2020).
[4] N. H. Tu, K. Yoshioka, S. Sasaki, M. Takamura, K. Muraki, N. Kumada, *Communications Materials* **1**, 7 (2020).
[5] K. Yoshioka, T. Wakamura, M. Hashisaka, K. Watanabe, T. Taniguchi, N. Kumada, *Nature Photonics* **16**, 718 (2022).

MILESTONES 2016-2023

Ultrafast Dynamics and Metastability
Ultrafast Bandgap Photonics

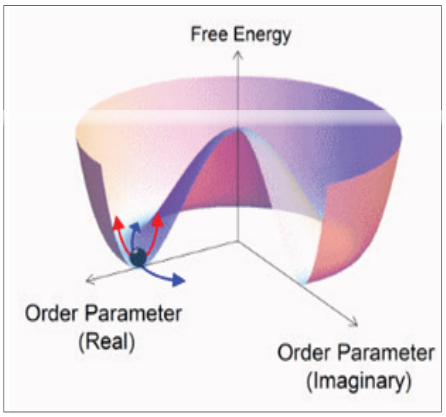

Physica Scripta – 2017

Focus: Ultrafast Bandgap Photonics
Guest Editors: Michael K. Rafailov and Luca Perfetti, 2017
http://iopscience.iop.org/journal/1402-4896/page/Focus-issue-on-Ultrafast-Bandgap-Photonics

Ultrafast Bandgap Photonics

Baltimore, 2016
http://spie.org/Publications/Proceedings/Volume/9835

Anaheim, 2017
http://spie.org/Publications/Proceedings/Volume/10193

Orlando, 2018
https://spie.org/Publications/Proceedings/Volume/10638

Ultrafast Dynamics and Metastability 2017 Workshop
Washington, DC, 2018
https://sites.google.com/a/georgetown.edu/ultrafast-dynamics-and-metastability-archive-2017/

Ultrafast Dynamics and Metastability & Ultrafast Bandgap Photonics 2019
V International Workshop
Washington, DC, April 2019

Ultrafast Bandgap Photonics: Dynamics and Metastability of Transient States
VI International Conference
St. Petersburg, 2019

Ultrafast Bandgap Photonics: Dynamics and Metastability of Transient States 2020
VII International Symposium
Hersonissos, Crete, Greece June 2022

Ultrafast Dynamics and Metastability & Ultrafast Bandgap Photonics 2021
VIII International Workshop
Washington, DC, November 2021

Ultrafast Dynamics and Metastability & Ultrafast Bandgap Photonics 2022
IX International Workshop
Washington, DC, November 2022

Ultrafast Bandgap Photonics: Dynamics and Metastability of Transient States 2023
X International Symposium
Hersonissos,Crete, June 04-10 2023

Ultrafast Bandgap Photonics & Ultrafast Dynamics 2023
XI International Workshop 2023